EMERGING INFECTIOUS DISEASES®

CDC
Centers for Disease Control and Prevention

Zoonoses

June 2019

Francisco de Goya y Lucientes (1746–1828). *Don Manuel Osorio Manrique de Zuniga* (1784–1792). Oil on canvas, 50 in x 40 in/127 cm x 101.6 cm. The Metropolitan Museum of Art, New York, NY, USA; The Jules Bache Collection, 1949 (49.7.41). Image copyright © The Metropolitan Museum of Art. Image source: Art Resource, NY.

EMERGING INFECTIOUS DISEASES®

EDITOR-IN-CHIEF
D. Peter Drotman

ASSOCIATE EDITORS
Paul Arguin, Atlanta, Georgia, USA
Charles Ben Beard, Fort Collins, Colorado, USA
Ermias Belay, Atlanta, Georgia, USA
David Bell, Atlanta, Georgia, USA
Sharon Bloom, Atlanta, Georgia, USA
Richard Bradbury, Atlanta, Georgia, USA
Mary Brandt, Atlanta, Georgia, USA
Corrie Brown, Athens, Georgia, USA
Charles Calisher, Fort Collins, Colorado, USA
Benjamin J. Cowling, Hong Kong, China
Michel Drancourt, Marseille, France
Paul V. Effler, Perth, Australia
Anthony Fiore, Atlanta, Georgia, USA
David Freedman, Birmingham, Alabama, USA
Peter Gerner-Smidt, Atlanta, Georgia, USA
Stephen Hadler, Atlanta, Georgia, USA
Matthew Kuehnert, Edison, New Jersey, USA
Nina Marano, Atlanta, Georgia, USA
Martin I. Meltzer, Atlanta, Georgia, USA
David Morens, Bethesda, Maryland, USA
J. Glenn Morris, Gainesville, Florida, USA
Patrice Nordmann, Fribourg, Switzerland
Johann D.D. Pitout, Calgary, Alberta, Canada
Ann Powers, Fort Collins, Colorado, USA
Didier Raoult, Marseille, France
Pierre Rollin, Atlanta, Georgia, USA
Frank Sorvillo, Los Angeles, California, USA
David Walker, Galveston, Texas, USA
J. Todd Weber, Atlanta, Georgia, USA
Jeffrey Scott Weese, Guelph, Ontario, Canada

Managing Editor
Byron Breedlove, Atlanta, Georgia, USA

Copy Editors Kristina Clark, Dana Dolan, Karen Foster, Thomas Gryczan, Amy Guinn, Michelle Moran, Shannon O'Connor, Jude Rutledge, P. Lynne Stockton, Deborah Wenger

Production Thomas Eheman, William Hale, Barbara Segal, Reginald Tucker

Journal Administrator Susan Richardson

Editorial Assistants Kelly Crosby, Kristine Phillips

Communications/Social Media Sarah Logan Gregory, Tony Pearson-Clarke

Founding Editor
Joseph E. McDade, Rome, Georgia, USA

EDITORIAL BOARD
Timothy Barrett, Atlanta, Georgia, USA
Barry J. Beaty, Ft. Collins, Colorado, USA
Martin J. Blaser, New York, New York, USA
Christopher Braden, Atlanta, Georgia, USA
Arturo Casadevall, New York, New York, USA
Kenneth C. Castro, Atlanta, Georgia, USA
Vincent Deubel, Shanghai, China
Christian Drosten, Charité Berlin, Germany
Isaac Chun-Hai Fung, Statesboro, Georgia, USA
Kathleen Gensheimer, Silver Spring, Maryland, USA
Rachel Gorwitz, Atlanta, Georgia, USA
Duane J. Gubler, Singapore
Richard L. Guerrant, Charlottesville, Virginia, USA
Scott Halstead, Arlington, Virginia, USA
David L. Heymann, London, UK
Keith Klugman, Seattle, Washington, USA
Takeshi Kurata, Tokyo, Japan
S.K. Lam, Kuala Lumpur, Malaysia
Stuart Levy, Boston, Massachusetts, USA
John S. Mackenzie, Perth, Australia
John E. McGowan, Jr, Atlanta, Georgia, USA
Jennifer H. McQuiston, Atlanta, Georgia, USA
Tom Marrie, Halifax, Novia Scotia, Canada
Nkuchia M. M'ikanatha, Harrisburg, Pennsylvania, USA
Frederick A. Murphy, Bethesda, Maryland, USA
Barbara E. Murray, Houston, Texas, USA
Stephen M. Ostroff, Silver Spring, Maryland, USA
Ann Powers, Fort Collins, Colorado, USA
Mario Raviglione, Prévessin-Möens, France
David Relman, Palo Alto, California, USA
Guenael R. Rodier, Saône-et-Loire, France
Connie Schmaljohn, Frederick, Maryland, USA
Tom Schwan, Hamilton, Montana, USA
David Swayne, Athens, Georgia, USA
Rosemary Soave, New York, New York, USA
P. Frederick Sparling, Chapel Hill, North Carolina, USA
Robert Swanepoel, Pretoria, South Africa
David E. Swayne, Athens, Georgia, USA
Phillip Tarr, St. Louis, Missouri, USA
Duc Vugia, Richmond, California, USA
John W. Ward, Atlanta, Georgia, USA
Mary E. Wilson, Cambridge, Massachusetts, USA

Emerging Infectious Diseases is published monthly by the Centers for Disease Control and Prevention, 1600 Clifton Rd NE, Mailstop H16-2, Atlanta, GA 30329-4027, USA. Telephone 404-639-1960, fax 404-639-1954, email eideditor@cdc.gov.

The conclusions, findings, and opinions expressed by authors contributing to this journal do not necessarily reflect the official position of the U.S. Department of Health and Human Services, the Public Health Service, the Centers for Disease Control and Prevention, or the authors' affiliated institutions. Use of trade names is for identification only and does not imply endorsement by any of the groups named above.

All material published in Emerging Infectious Diseases is in the public domain and may be used and reprinted without special permission; proper citation, however, is required.

Use of trade names is for identification only and does not imply endorsement by the Public Health Service or by the U.S. Department of Health and Human Services.

EMERGING INFECTIOUS DISEASES is a registered service mark of the U.S. Department of Health & Human Services (HHS).

∞ Emerging Infectious Diseases is printed on acid-free paper that meets the requirements of ANSI/NISO 239.48-1992 (Permanence of Paper)

EMERGING INFECTIOUS DISEASES®

Zoonoses **June 2019**

On the Cover

Francisco de Goya y Lucientes (1746–1828). *Don Manuel Osorio Manrique de Zuniga* (1784–1792). Oil on canvas, 50 in x 40 in/127 cm x 101.6 cm. The Metropolitan Museum of Art, New York, NY, USA; The Jules Bache Collection, 1949 (49.7.41). Image copyright © The Metropolitan Museum of Art. Image source: Art Resource, NY.

About the Cover p. 1256

Perspectives

Using Big Data to Monitor the Introduction and Spread of Chikungunya, Europe, 2017
J. Rocklöv et al. **1041**

Related material available online: https://wwwnc.cdc.gov/eid/article/25/6/18-0138_article

West Nile and Usutu Virus Infections and Challenges to Blood Safety in the European Union
D. Domanović et al. **1050**

Related material available online: https://wwwnc.cdc.gov/eid/article/25/6/18-1755_article

Synopses

Immunopathology of Fatal Human Variegated Squirrel Bornavirus 1 Encephalitis, Germany, 2011–2013
D. Tappe et al. **1058**

Related material available online: https://wwwnc.cdc.gov/eid/article/25/6/18-1082_article

Medscape EDUCATION ACTIVITY

Epidemiologic and Clinical Features of Lassa Fever Outbreak in Nigeria, January 1–May 6, 2018
The outbreak, which included 423 confirmed cases and caused 106 deaths, was the largest recorded Lassa fever outbreak.
E.A. Ilori et al. **1066**

Related material available online: https://wwwnc.cdc.gov/eid/article/25/6/18-1035_article

Medscape EDUCATION ACTIVITY

Nontuberculous Mycobacterial Musculoskeletal Infection Cases from a Tertiary Referral Center, Colorado, USA
Vigilance is needed for patients with these infections, particularly those who are immunosuppressed or have had musculoskeletal sugery.
N. Goldstein et al. **1075**

Related material available online: https://wwwnc.cdc.gov/eid/article/25/6/18-1041_article

Research

Phenotypic and Genomic Analyses of *Burkholderia stabilis* Clinical Contamination, Switzerland
H.M.B. Seth-Smith et al. **1084**

Related material available online: https://wwwnc.cdc.gov/eid/article/25/6/17-2119_article

Patterns of Abundance, Host Use, and Everglades Virus Infection in *Culex* (*Melanoconion*) *cedecei* Mosquitoes, Florida, USA
I.J. Hoyer et al. **1093**

Related material available online: https://wwwnc.cdc.gov/eid/article/25/6/18-0338_article

Assessment of Economic Burden of Concurrent Measles and Rubella Outbreaks, Romania, 2011–2012
J. Njau et al. **1101**

Related material available online: https://wwwnc.cdc.gov/eid/article/25/6/18-0339_article

Novel Orthobunyavirus Causing Severe Kidney Disease in Broiler Chickens, Malaysia, 2014–2017
V. Palya et al. **1110**

EMERGING INFECTIOUS DISEASES®
June 2019

Joint Estimation of Relative Risk for Dengue and Zika Virus Infections, Colombia, 2015–2016
D.A. Martínez-Bello et al. **1118**
Related material available online: https://wwwnc.cdc.gov/eid/article/25/6/18-0392_article

Respiratory Syncytial Virus Seasonality, Beijing, China, 2007–2015
J. Yu et al. **1127**

Enhancement of Risk for Lyme Disease by Landscape Connectivity, New York, New York, USA
M.C. VanAcker et al. **1136**
Related material available online: https://wwwnc.cdc.gov/eid/article/25/6/18-1741_article

Use of Single-Injection Recombinant Vesicular Stomatitis Virus Vaccine to Protect Nonhuman Primates Against Lethal Nipah Virus Disease
C.E. Mire et al. **1144**
Related material available online: https://wwwnc.cdc.gov/eid/article/25/6/18-1620_article

Performance of 2 Commercial Serologic Tests for Diagnosis of Zika Virus Infection
A. Matheus et al. **1153**

Sequential Emergence and Wide Spread of Neutralization Escape Middle East Respiratory Syndrome Coronavirus Mutants, South Korea, 2015
Y.-S. Kim et al. **1161**
Related material available online: https://wwwnc.cdc.gov/eid/article/25/6/18-1722_article

Mass Die-Off of Saiga Antelopes, Kazakhstan, 2015
S. Fereidouni et al. **1169**
Related material available online: https://wwwnc.cdc.gov/eid/article/25/6/18-0990_article

Survey of Crimean-Congo Hemorrhagic Fever Enzootic Focus, Spain, 2011–2015
A. Negredo et al. **1177**

Historical Review

Equine Influenza Virus—A Neglected, Reemergent Disease Threat
A. Sack et al. **1185**
Related material available online: https://wwwnc.cdc.gov/eid/article/25/6/16-1846_article

Dispatches

Outbreak of Vaccinia Virus Infection from Occupational Exposure, China, 2017
B. Lu et al. **1192**
Related material available online: https://wwwnc.cdc.gov/eid/article/25/6/17-1306_article

Pertactin-Negative and Filamentous Hemagglutinin-Negative *Bordetella pertussis*, Australia, 2013–2017
Z. Xu et al. **1196**
Related material available online: https://wwwnc.cdc.gov/eid/article/25/6/18-0240_article

Increase in Enterovirus D68 Infections in Young Children, United Kingdom, 2006–2016
E. Kamau et al. **1200**
Related material available online: https://wwwnc.cdc.gov/eid/article/25/6/18-1759_article

Multirecombinant Enterovirus A71 Subgenogroup C1 Isolates Associated with Neurologic Disease, France, 2016–2017
S.T. Ngangas et al. **1204**
Related material available online: https://wwwnc.cdc.gov/eid/article/25/6/18-1460_article

New Delhi Metallo-β-Lactamase 5–Producing *Klebsiella pneumoniae* Sequence Type 258, Southwest China, 2017
X. Zhang et al. **1209**
Related material available online: https://wwwnc.cdc.gov/eid/article/25/6/18-1939_article

Scrub Typhus in Continental Chile, 2016–2018
T. Weitzel et al. **1214**

Research Letters

National Surveillance of Legionnaires' Disease, China, 2014–2016
T. Qin et al. **1218**
Related material available online: https://wwwnc.cdc.gov/eid/article/25/6/17-1431_article

Molecular Evidence of Human Monkeypox Virus Infection, Sierra Leone
F. Ye et al. **1220**
Related material available online: https://wwwnc.cdc.gov/eid/article/25/6/18-0296_article

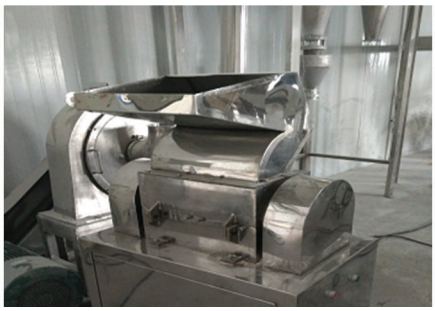

EMERGING INFECTIOUS DISEASES®
June 2019

Leishmaniasis in Norway Rats in Sewers, Barcelona, Spain
M.T. Galán-Puchades et al. **1222**

Related material available online: https://wwwnc.cdc.gov/eid/article/25/6/18-1027_article

Influenza D Virus Infection in Dromedary Camels, Ethiopia
S. Murakami et al. **1224**

Absence of *Neospora caninum* DNA in Human Clinical Samples, Spain
R. Calero-Bernal et al. **1226**

Reemergence of Classical Swine Fever, Japan, 2018
A. Postel et al. **1228**

Related material available online: https://wwwnc.cdc.gov/eid/article/25/6/18-1578_article

African Swine Fever Virus in Pork Brought into South Korea by Travelers from China, August 2018
H.-J. Kim et al. **1231**

Hepatitis E Virus Infection in European Brown Hares, Germany, 2007–2014
V.M. Corman et al. **1233**

Sarcoptic Mange of Fox Origin in Multiple Farm Animals and Scabies in Humans, Switzerland, 2018
S.R.R. Pisano et al. **1235**

Suboptimal Handling of Piccolo Samples or Reagent Discs for Consideration in Ebola Response
J.R. Spengler et al. **1238**

Infection with New York Orthohantavirus and Associated Respiratory Failure and Multiple Cerebral Complications
R. Fernando et al. **1241**

***Rickettsia japonica* Infection after Land Leech Bite, Japan**
E. Sando et al. **1243**

Related material available online: https://wwwnc.cdc.gov/eid/article/25/6/18-1985_article

Schistosome Interactions within the *Schistosoma haematobium* Group, Malawi
B.L. Webster et al. **1245**

Related material available online: https://wwwnc.cdc.gov/eid/article/25/6/19-0020_article

Hepatitis Rebound after Infection with Yellow Fever Virus
B. Denis et al. **1248**

Comparative Analysis of Whole-Genome Sequence of African Swine Fever Virus Belgium 2018/1
J.H. Forth et al. **1249**

Related material available online: https://wwwnc.cdc.gov/eid/article/25/6/19-0286_article

Highly Pathogenic Swine Getah Virus Infecting Blue Foxes, Eastern China, 2017
N. Shi et al. **1252**

Related material available online: https://wwwnc.cdc.gov/eid/article/25/6/18-1983_article

About the Cover

The Red Boy, the Black Cat
B. Breedlove **1256**

Etymologia

Neospora caninum
R. Henry **1228**

Corrections

Vol. 25 No. 5 **1254**
The affiliation for Marie E. Killerby was listed incorrectly in Risk Factors for MERS-CoV Seropositivity among Animal Market and Slaughterhouse Workers, Abu Dhabi, United Arab Emirates, 2014–2017 (A. Khudhair et al.).

Vol. 25 No. 3 **1255**
Figures 2 and 4 were incomplete in Donor-Derived Genotype 4 Hepatitis E Virus Infection, Hong Kong, China, 2018 (S. Sridhar et al.).

The World Unseen:
Intersections of Art and Science
May 20–August 30, 2019

Amie Esslinger, *Collisions*, mixed media, 2016

The World Unseen: Intersections of Art and Science gathers the work of 10 international artists who draw upon microbiology, biotechnology, anatomy, and texts in their investigations of microbes and cells, DNA, history of disease and science, the body, and beauty. Through paintings, drawings, installations, and videos, these artists ponder the humanistic and scientific implications of knowing and seeing what we normally cannot see.

DAVID J. SENCER
CDC MUSEUM
History·Legacy·Innovation

The David J. Sencer CDC Museum, a Smithsonian Affiliate, uses award-winning exhibitions, dynamic educational programming, and physical and web archives to educate visitors about the value of public health, while presenting the rich heritage and vast accomplishments of CDC.

Hours

Monday–Wednesday: 9 a.m.–5 p.m.
Thursday: 9 a.m.–7 p.m.
Friday: 9 a.m.–5 p.m.
Closed weekends and federal holidays

Location

1600 Clifton Road, NE
Atlanta, GA
30329-4021
Phone (404) 639-0830

Admission and parking free
Vehicle inspection required
Government-issued photo ID required for adults over the age of 18
Passport required for non-U.S. citizens

Using Big Data to Monitor the Introduction and Spread of Chikungunya, Europe, 2017

Joacim Rocklöv, Yesim Tozan, Aditya Ramadona, Maquines O. Sewe, Bertrand Sudre, Jon Garrido, Chiara Bellegarde de Saint Lary, Wolfgang Lohr, Jan C. Semenza

With regard to fully harvesting the potential of big data, public health lags behind other fields. To determine this potential, we applied big data (air passenger volume from international areas with active chikungunya transmission, Twitter data, and vectorial capacity estimates of *Aedes albopictus* mosquitoes) to the 2017 chikungunya outbreaks in Europe to assess the risks for virus transmission, virus importation, and short-range dispersion from the outbreak foci. We found that indicators based on voluminous and velocious data can help identify virus dispersion from outbreak foci and that vector abundance and vectorial capacity estimates can provide information on local climate suitability for mosquitoborne outbreaks. In contrast, more established indicators based on Wikipedia and Google Trends search strings were less timely. We found that a combination of novel and disparate datasets can be used in real time to prevent and control emerging and reemerging infectious diseases.

Many sectors of society have taken full advantage of new opportunities provided by big data, but public health has not (*1*). Although electronic health records have long been used in surveillance, novel applications of big data are rare. Internet search query data from Google or Wikipedia have been applied to anticipate influenza epidemics but are hampered by several limitations, including specificity and granularity (*2–4*). More recently, crowdsourcing of symptoms through emails, text messages, or tweets has been explored, and outbreaks have been tracked by scanning high-volume surveillance systems (*5*,*6*). However, when it comes to fully harvesting the potential of big data, public health still lags behind other fields. Using chikungunya as a case study, we illustrate how big data can help tackle emerging infectious diseases through prevention, detection, and response.

Author affiliations: Umeå University, Umeå, Sweden (J. Rocklöv, A. Ramadona, M.O. Sewe, W. Lohr); New York University, New York, New York, USA (Y. Tozan); European Centre for Disease Prevention and Control, Stockholm, Sweden (B. Sudre, J. Garrido, C.B. de Saint Lary, J.C. Semenza)

DOI: https://doi.org/10.3201/eid2506.180138

A key driver of the emergence and spread of vectorborne diseases is human mobility (*7–10*), yet little is known about the epidemiologic consequences of mobility patterns at different spatial scales within the context of vectorborne diseases. A main obstacle to studying the complex interactions between human hosts, pathogens, and vectors has been the limited availability of spatiotemporal datasets for analyzing human mobility patterns. Prior research relied on low-resolution mobile phone records, such as call and messaging logs from mobile phone networks (*11–13*), for which biases were notable (*14*,*15*). Furthermore, use of mobile phone data for tracking human mobility is likely to be fraught with privacy concerns and data access restrictions (*15*).

Recently, social media has emerged as an alternative source of real-time, high-resolution geospatial data on a large scale (*1*,*15*). Use of this unique aspect of publicly available social media data to study the human dimensions of the introduction and spread of emerging infectious diseases has not been explored to its fullest extent. In areas where risk for virus importation and onward transmission is heightened, such knowledge can inform outbreak preparedness and response planning by pinpointing receptive areas where proactive countermeasures should be implemented in a timely fashion (*16*,*17*).

The impediments to using big data in public health are not only the size of the databases but also the complexity of their processing. The challenges include 3 main dimensions: volume, velocity, and variety (*18–20*). Volume calls for statistical sampling; velocity, for instant access to near real-time transaction data; and variety, for management of nonaligned data structures. We illustrate how big data can be used to monitor the introduction and spread of the 2017 chikungunya outbreak in Europe by tackling these challenges (*18–20*).

To assess risk for virus importation from international areas with active chikungunya transmission, we extracted air passenger volume from large-scale aviation data. To quantify the risk for short-range dispersion (defined as the potential for onward transmission and spread of chikungunya virus from

the initial outbreak foci to other areas during transmission season), we used a mining algorithm to process quasi–real-time, geolocated Twitter activity data and computed mobility patterns of users. We have previously shown that mobility data from Twitter users is predictive of disease spread (*21*). We then estimated the seasonal vectorial capacity of *Aedes albopictus* mosquitoes to transmit chikungunya virus and linked it with human mobility patterns. We further complemented these data with Internet and information search activities related to chikungunya infection, vectors, and clinical signs and symptoms collected from Wikipedia and Google Trends. Last, we estimated the empirical basic reproduction number (R_0) from the outbreaks and compared these numbers with our model predictions of epidemic potential based on climate conditions. More detail on our methods is provided in Appendix 1 (https://wwwnc.cdc.gov/EID/article/25/6/18-0138-App1.pdf).

Climate Suitability: Vectorial Capacity

The vectorial capacity of *Ae. albopictus* mosquitoes to transmit chikungunya virus in areas of Europe where the vector is established (*17*), such as the outbreak zones in France and Italy, was estimated to be high in July and August but lower in September and October. Estimates of suitability were low in October for most areas, except those in southern Italy and Greece and southeastern Spain (Figure 1). Overall, warmer than average temperatures led to a substantial increase in vectorial capacity during the study period (June–October 2017) (Appendix 2 Figure 1, https://wwwnc.cdc.gov/EID/article/25/6/18-0138-App2.pdf). Using empirical data from the outbreaks in Italy (*22*), we estimated R_0 to be 2.28 (95% CI 2.01–2.59) for the Anzio region, 3.54 (95% CI 2.62–4.97) for the Rome region, and 3.11 (95% CI 2.16–4.79) for the Calabria region (Figure 2).

Long-Range Importation: Air Passenger Volume

On average, ≈50,000 air passenger-journeys (1 passenger flight, including all legs of travel) were taken each month from areas with active chikungunya transmission worldwide to the outbreak zones (Figure 3). Specifically, in August, 56,300 passengers from outbreak zones were estimated to arrive in Rome, 6,484 in Nice, and 5,629 in Marseille. The passenger-journey volume into Europe when the outbreak started in June is shown in Appendix 2 Figure 2. The countries with the highest number of departing passengers in August were Thailand (352,332 passengers), Brazil (255,439 passengers), and India (301,298 passengers). According to molecular epidemiology, the genome sequence of a chikungunya virus isolate from the Lazio region of Italy revealed the East/Central/South African lineage, Indian Ocean sublineage, which is similar to that of recent sequences from Pakistan and India (*23*). We also extracted air passenger-journey data for flights from the outbreak zones in southeastern France and central Italy to other areas in Europe (Figure 3). The top 5 destinations with the highest volume were the larger metropolitan areas of Europe, most of which were outside

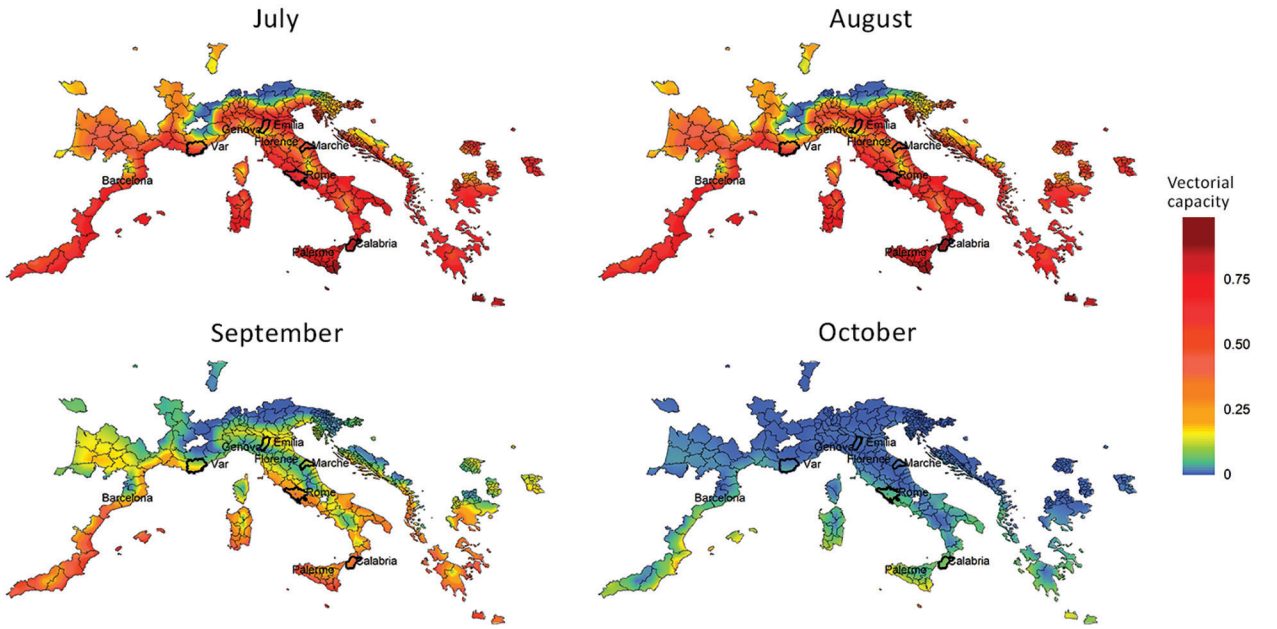

Figure 1. Vectorial capacity estimates based on average temperature conditions in Europe with stable populations of *Aedes albopictus* mosquitoes around chikungunya outbreak zones, Italy and France, July–October 2017. Heavy outlines indicate the outbreak areas. The vectorial capacity translates to an average basic reproduction number in the range of 2–3 in Anzio and Rome and in the range of 3–4 in Calabria during the months of July and August for an infectious period of 4 days.

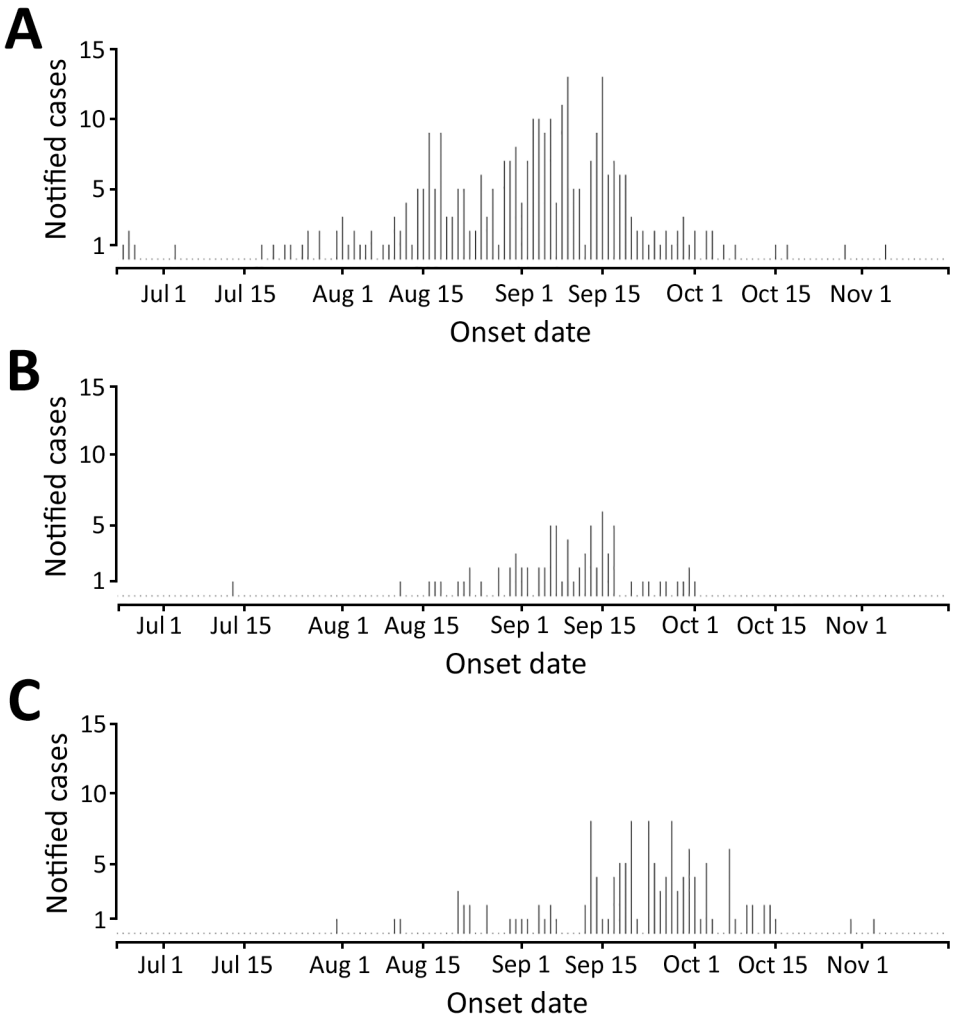

Figure 2. Notified chikungunya cases in the Anzio (A), Rome (B), and Calabria (C) regions and basic reproduction number (R_0) estimates of outbreaks, June–October 2017, Italy.

the boundaries of areas where the vector is known to be present (Figure 4). However, high flight connectivity was observed from the outbreak zones to Barcelona (Spain) and Catania and Palermo (Italy).

Short-Range Dispersion: Geocoded Tweets

The spatiotemporal analysis of geocoded Twitter data showed strong human mobility from Lazio (Figure 4) and the Var department in France (Appendix 2 Figure 3) toward several larger cities where *Ae. albopictus* mosquitoes are present. The top 10 estimates of mobility out of the 2 outbreak zones of Var and Lazio showed the strongest pattern for potential dispersion of chikungunya virus not only into the areas geographically close to the outbreak zones but also to several relatively large cities in Italy, France, and Spain (Table). The monthly mobility patterns during the study period varied between months; for example, the vacation month of August showed a stronger mobility pattern out of Var to areas not in direct connectivity, most notably to Rome (Appendix 2 Figure 4). When we contrasted the mobility proximities between the 2 outbreak zones, we observed the highest proximities within countries (Figure 4; Appendix 2 Figure 3). Although the Var and Lazio outbreak zones experienced high mobility proximity to Barcelona, Lazio was also highly connected to southern Italy (e.g., Catania and Palermo), in close proximity to the chikungunya outbreak in the Calabria area, which was also observed in the International Air Transport Association (IATA) flight passenger data (Figures 3, 4). In Italy, cases were first notified in Anzio at the end of June, followed by notifications in Rome later in July, and in Calabria in early August in order of temporal appearance (Figure 2). In our mobility analysis, we identified the mobility links to all outbreak regions (Figure 4), with the exception of the Emilia-Romagna region, although the region neighboring Emilia-Romagna was positive in our analysis. The mobility patterns correlated more strongly to the outbreak regions in July and August.

A closer look at the Lazio outbreak zone in Italy revealed strong connectivity between Anzio (where the first

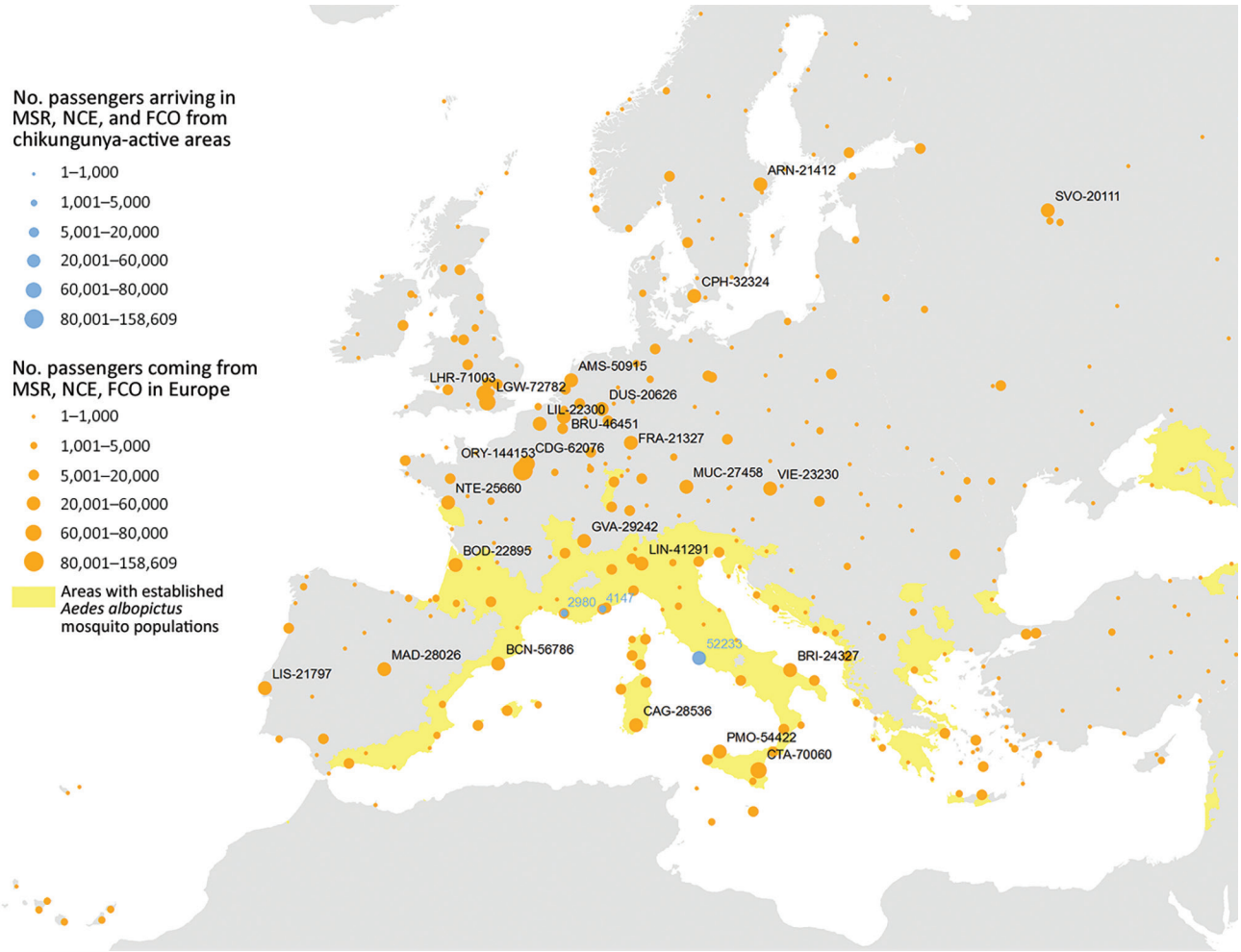

Figure 3. Incoming passengers from chikungunya active transmission areas and outgoing passengers to other airports in Europe from Rome (FCO), Marseille (MRS), and Nice (NCE) airports, August 2017. The stable vector presence area is highlighted in yellow.

cases in Italy were confirmed) and Rome (where a higher number of cases were notified) (Figure 5). We compiled the top 10 mobility proximity areas from the outbreak zones of Anzio and Rome in August and September (Table). Although the highest mobility proximity from Anzio was to Rome in August and September, the mobility proximity from Rome to Anzio was also found among the top 10 destinations. Overall, Rome had higher connectivity to many more areas than Anzio.

Synergistic Effects: Human Mobility and Transmission Suitability

We derived risk maps for autochthonous chikungunya transmission by combining the vectorial capacity and mobility proximity estimates for the Lazio region in Italy and Var department in France for August–October 2017 (Appendix 2 Figure 4). The areas at risk because of the outbreak in Var were identified to be located along the French and northern Spanish Mediterranean coastlines, Mallorca, and Rome in August (Appendix 2 Figure 4); the risk regions for the Lazio outbreak in August included large parts of Italy as well as areas in France, Spain, and Greece (Figure 6). In general, the size of the area at risk contracted in September and more so in October because of less favorable climate conditions, except in the most southern region of Italy (Figure 6), such as the Calabria region, where the outbreak also empirically continued longer in the fall (Figure 2).

In the Lazio region, an analysis of the combination of vectorial capacity (Appendix 2 Figure 5) and mobility proximity revealed a higher transmission potential in August (Appendix 2 Figure 6), with implications for targeting surveillance and outbreak control activities to this region. The largest area of risk for spread from Anzio was Rome, but the risk for spread from Rome was more widespread in the region (Appendix 2 Figures 6, 7). The areas at risk for spread in the Lazio region differed during August compared with September and October.

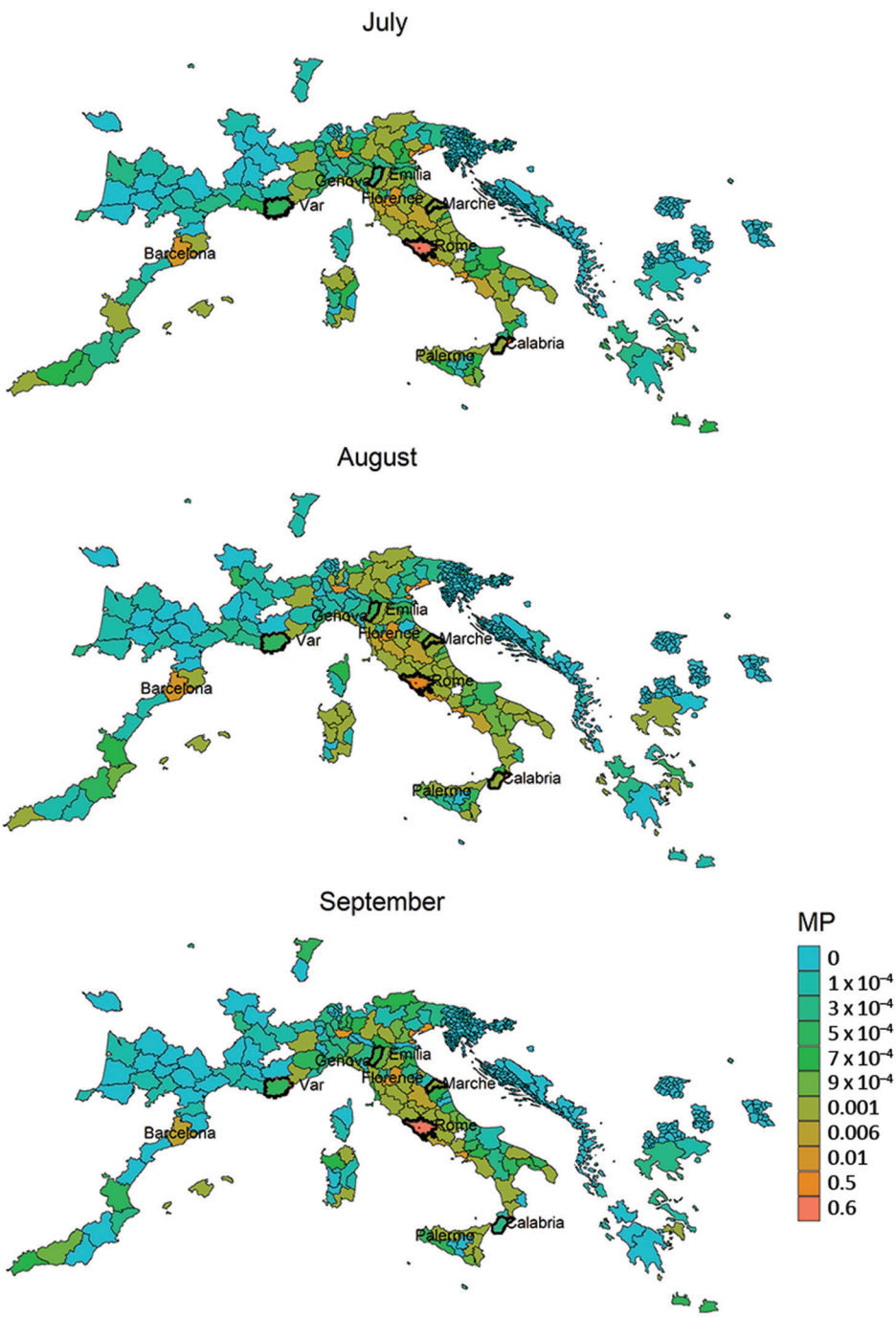

Figure 4. MP estimates from the Lazio region, Italy, to areas in Europe with stable populations of *Aedes albopictus* mosquitoes, July–September 2017. Heavy outlines indicate the chikungunya outbreak areas. MP, mobility proximity.

Wikipedia and Google Trend Indicators

For the outbreaks in Italy, several pathogen and vector-related Wikipedia and Google Trend search pattern anomalies are illustrated (Appendix 2 Figure 8). The peaks in these abnormalities coincided with the peak of the outbreak and therefore are not useful for early detection and response activities. Detailed information about Wikipedia and Google Trend indicators are provided in Appendix 3 (https://wwwnc.cdc.gov/EID/article/25/6/18-0138-App3.pdf).

Big Data and Emerging Infectious Diseases

In light of the arrival and explosive expansion of chikungunya in the Americas in 2013 through *Ae. aegypti* moquitoes (*24*), big data offer the opportunity to monitor the introduction and spread of chikungunya in Europe. An

Table. Top 10 areas where mobility proximity to the 2 chikungunya outbreak zones was highest, Europe, August 2017

	Southern Europe		Lazio region	
Rank	From Var department, France	From Lazio region, Italy	From Anzio	From Rome
1	Alpes-Maritimes	Florence	Roma	Vatican
2	Bouches-du-Rhône	Milano	Nettuno	Fiumicino
3	Torino	Napoli	Sabaudia	Sabaudia
4	Paris	Venezia	Ardea	Civitavecchia
5	Alpes-de-Haute-Provence	Paris	Civitavecchia	Santa Marinella
6	Rhone	Barcelona	Pomezia	Tivoli
7	Hérault	Perugia	Aprilia	Anzio
8	Vaucluse	Latina	Cisterna Di Latina	Ladispoli
9	Barcelona	Siena	Fondi	Pomezia
10	Baeleares	Salerno	Amatrice	Valmontone

outbreak can be divided, broadly speaking, into 2 distinct phases. The first phase is importation of the virus via a viremic person into a virus-naive population. For this phase, we used big data (volume) to estimate air passenger-journeys from areas with active chikungunya transmission as a measure of the force of introduction of the virus into the outbreak zones in Europe. To identify areas with onward transmission risk, we also considered the volume of air passengers leaving these outbreak zones. For the second phase, the establishment of autochthonous transmission in Europe is a function of virus importation, population density, vector activity, climate conditions, exposure patterns, and several other factors that are more difficult to quantify (*17*). Our study addressed some of these epidemiologic challenges by using big data. Rather than a Twitter content analysis, which has been performed for several outbreaks (*25–28*), we used near–real-time geocoded Twitter data (velocity) to quantify human mobility patterns and disentangled connectivity between populations. Mobility estimates also reflect population density and indirectly take into account exposure patterns because such populations on the move are occasionally susceptible to exposure and are also a source of exposure. The ecology of the virus and the human-vector transmission cycle were captured by vectorial capacity (variety), which quantified transmission risk on the basis of climate conditions. Thus, we were able to quantify the trajectory of an arbovirus outbreak by dissecting and better understanding its phases.

Our analysis of big data revealed distinct mobility patterns between the outbreak zones in France and Italy, between Rome and Anzio, and between Rome and most of the local outbreak clusters in Italy. However, the potential effects of these mobility patterns on local spread need to be confirmed epidemiologically by phylogenetic analyses. Although the sensitivity of our risk maps based on mobility and climate data to identify areas at risk for virus spread was good, the specificity needs to be further improved, for example, by including local contextual factors such as land use and vector activity. Wikipedia page hits and Google Trends have been proposed as resources for disease surveillance and outbreak detection. However, our analysis demonstrates that these sources seemed to mainly indicate public awareness of the chikungunya outbreaks as they peaked. For such reasons, they seem to be of little use for early response.

The combination of short-distance air passenger-journeys (within Europe, as opposed to overseas) and geocoded Twitter data lends itself to cross-validation. We found that the 2 approaches consistently identified several cities with established vector populations at a heightened risk for virus importation, reflecting the potential for spread between countries and cities in Europe. Some of these regions had previously encountered autochthonous transmission (*29*).

The R_0 estimates, which were derived by using epidemiologic data, were in accordance with the vectorial capacity predictions for the outbreak zones based on local climate conditions. Based on the vectorial capacity, R_0 can be derived by multiplication with the infectious period. For chikungunya, an infectious period of 3–7 days was reported (*30*). The vectorial capacity of ≈0.7 would give rise to an R_0 of ≈2–3. This range is within that which we observed in the Rome and Anzio regions in July and August, but the vectorial capacity was estimated to be higher (≈0.8) in the Calabria region, translating into an R_0 of just over 3–4, which is in agreement with the epidemiologic analysis of the outbreak data (Figure 2).

Although our mobility analysis showed that the local mobility from Var was considerable, no autochthonous chikungunya cases were reported from other identified risk regions along the Mediterranean coast of France and in northern Spain. However, the vectorial capacity of *Ae. albopictus* mosquitoes to transmit the virus is lower in Var than in Lazio, which may explain this discrepancy. Previous studies assessing the risk for local outbreaks after outbreaks outside of Europe found that inbound flight traveler frequencies correlated strikingly well with local reports of virus importation frequencies into Europe (*9*). However, most of these studies evaluated these risks independently and did not attempt to estimate the combined risk for virus importation and climate suitability (*31*,*32*). Moreover, they did not assess local dispersion patterns from airports or outbreak areas. We analyzed big data for long- and short-distance mobility. A major strength of this big data approach is the near real-time availability of mobility patterns based

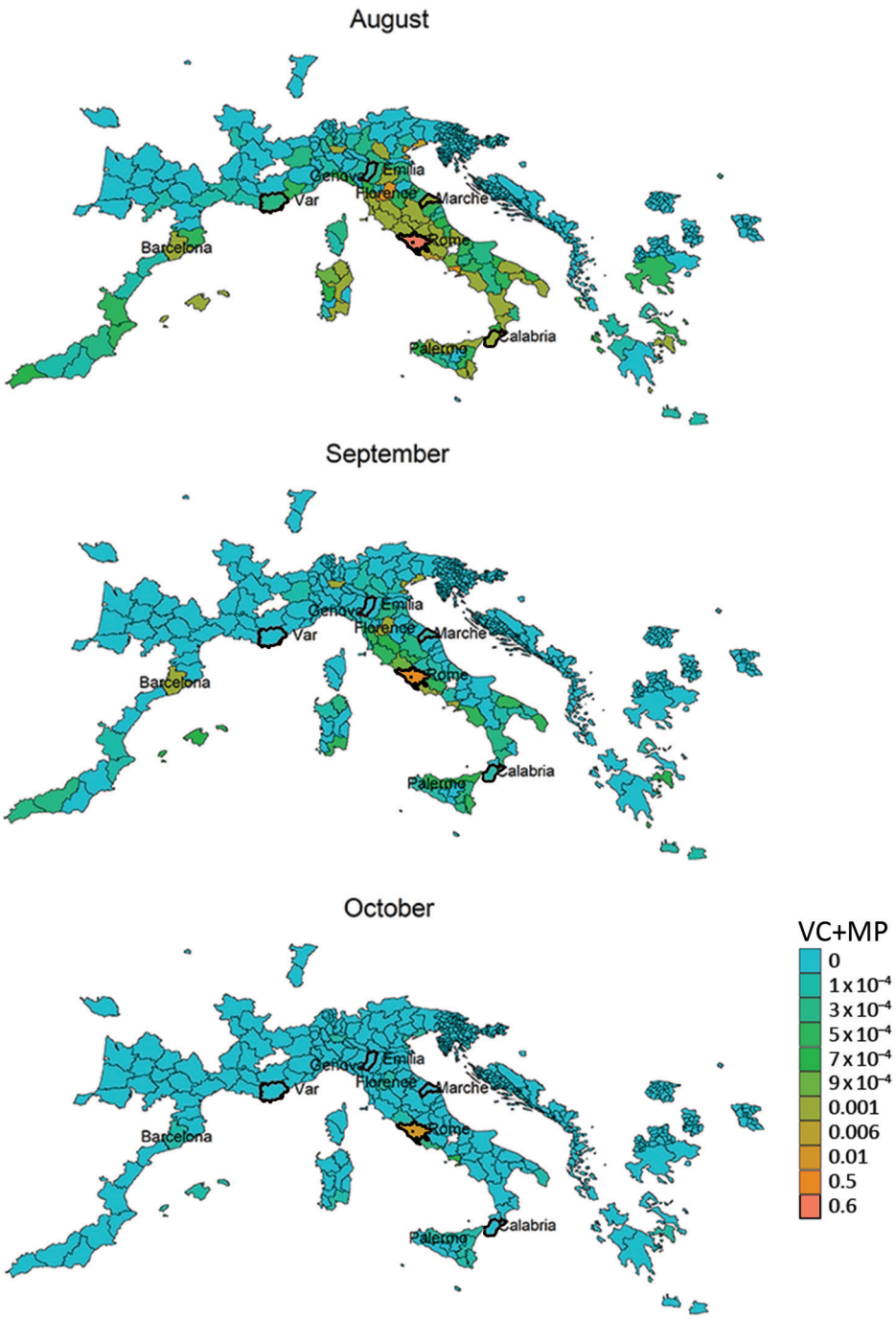

Figure 5. Estimated areas of risk for chikungunya spread from the outbreak areas of Anzio and Rome in the Lazio region, Italy, based on combined VC and MP estimates, August–October 2017. Heavy outlines indicate the outbreak areas. MP, mobility proximity; VC, vectorial capacity.

on social media, which are timelier and more accessible and less costly than air passenger data available from commercial providers, such as the IATA. This approach can identify areas of heightened mobility that are potentially at risk for onward transmission, as we have shown in this analysis. Geocoded Twitter data can be a good proxy for human mobility (*15*), but prior research did not explore how such data can be a timely resource for preparedness and response to infectious disease outbreaks.

Similar to others who have used IATA and Twitter data in their studies, we found these novel data sources to be reliable and useful. However, we note that Twitter data can potentially be biased because Twitter users may represent a select population whose mobility patterns differ from those of the general population; more specifically, they represent a population of Twitter users who have allowed Twitter to follow their geolocations. Future studies need to validate the use of social media data in such applications.

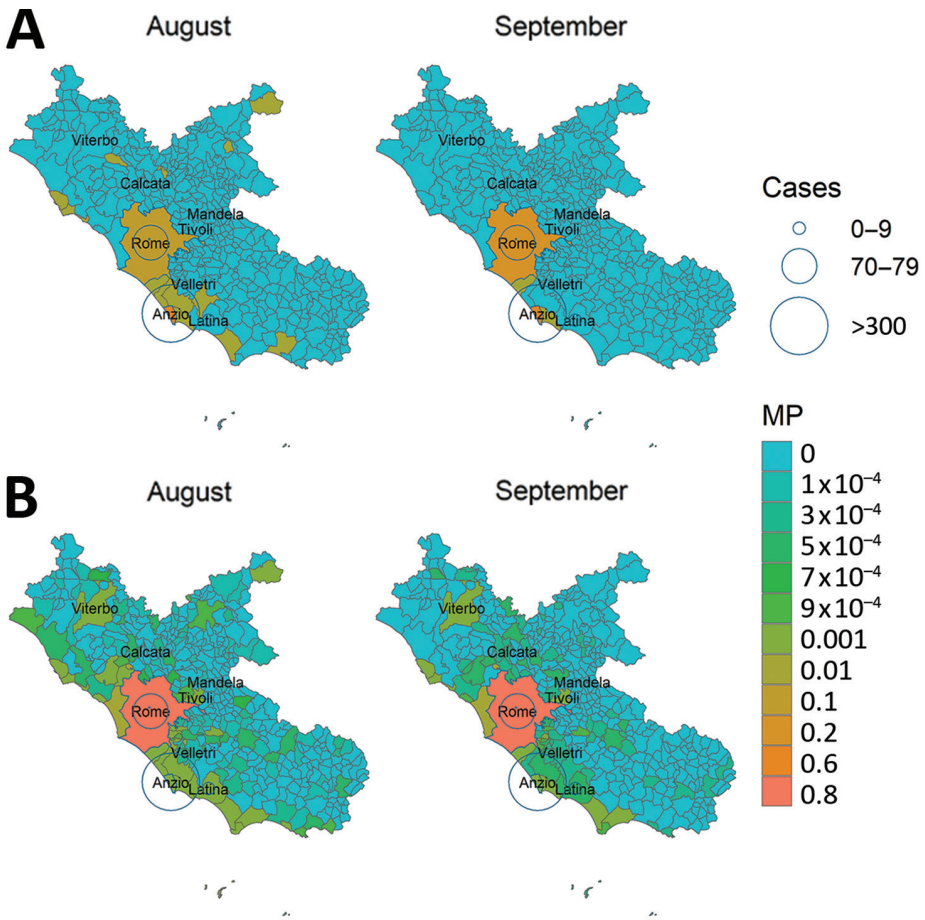

Figure 6. Estimated areas of risk for chikungunya spread from the outbreak areas in Lazio region, Italy, based on MP estimates, August–September 2017. A) Anzio; B) Rome. Circles indicate number of reported cases. MP, mobility proximity.

These methods are an improvement over mobile telephone tracking data because they do not rely on a single provider network and are a less costly data source to acquire.

Seasonal weather forecasts may have provided better input into the assessment of vectorial capacity, specifically for the fall of 2017. Moreover, autochthonous transmission risk may also be related to local proliferation of vectors and local environmental, social, and behavioral characteristics, such as awareness about the symptoms of chikungunya (Appendix 3). Such factors have been found to be associated with the local transmission risk for dengue (*33*). Last, because of the paucity and underreporting of chikungunya cases, we may have potentially underestimated the passenger volume from active transmission areas in Africa.

This study illustrates the potential value of using big data (*18–20*) to pinpoint areas at risk for the introduction and dispersion of emerging infectious diseases. The analysis identified that the areas at greatest risk were those in close proximity to the original outbreaks and several larger metropolitan areas. The trajectory and sustained spread of emerging infectious diseases can be anticipated with predictive modeling in real time. This study suggests that big data can be an indispensable tool for the prevention and control of emerging infectious diseases.

J.R. received partial funding from the Swedish Research Council for Sustainable Development (FORMAS) (no. 2017-01300). The funder had no influence on the research conducted.

About the Author

Dr. Rocklöv is professor of epidemiology and public health at Umeå University. His research interests focus on how climate, environmental, biological, medical, and social information can benefit preparedness and control of infectious diseases and be applied to early warning and response systems.

References

1. Simonsen L, Gog JR, Olson D, Viboud C. Infectious disease surveillance in the big data era: towards faster and locally relevant systems. J Infect Dis. 2016;214(suppl 4):S380–5.
2. Butler D. When Google got flu wrong. Nature. 2013;494:155–6. http://dx.doi.org/10.1038/494155a
3. Ginsberg J, Mohebbi MH, Patel RS, Brammer L, Smolinski MS, Brilliant L. Detecting influenza epidemics using search engine query data. Nature. 2009;457:1012–4. http://dx.doi.org/10.1038/nature07634
4. McIver DJ, Brownstein JS. Wikipedia usage estimates prevalence of influenza-like illness in the United States in near real-time. PLOS Comput Biol. 2014;10:e1003581. http://dx.doi.org/10.1371/journal.pcbi.1003581

5. Health HSoP. HealthMap. 2016 [cited 2017 Jan 5]. http://www.healthmap.org
6. World Health Organization [cited 2017 Jan 5]. http://www.who.int/csr/alertresponse/epidemicintelligence
7. Semenza JC, Lindgren E, Balkanyi L, Espinosa L, Almqvist MS, Penttinen P, et al. Determinants and drivers of infectious disease threat events in Europe. Emerg Infect Dis. 2016;22:581–9. http://dx.doi.org/10.3201/eid2204.151073
8. Semenza JC, Rocklöv J, Penttinen P, Lindgren E. Observed and projected drivers of emerging infectious diseases in Europe. Ann N Y Acad Sci. 2016;1382:73–83. http://dx.doi.org/10.1111/nyas.13132
9. Semenza JC, Sudre B, Miniota J, Rossi M, Hu W, Kossowsky D, et al. International dispersal of dengue through air travel: importation risk for Europe. PLoS Negl Trop Dis. 2014;8:e3278. http://dx.doi.org/10.1371/journal.pntd.0003278
10. Stoddard ST, Morrison AC, Vazquez-Prokopec GM, Paz Soldan V, Kochel TJ, Kitron U, et al. The role of human movement in the transmission of vector-borne pathogens. PLoS Negl Trop Dis. 2009;3:e481. http://dx.doi.org/10.1371/journal.pntd.0000481
11. Bengtsson L, Gaudart J, Lu X, Moore S, Wetter E, Sallah K, et al. Using mobile phone data to predict the spatial spread of cholera. Sci Rep. 2015;5:8923. http://dx.doi.org/10.1038/srep08923
12. Finger F, Genolet T, Mari L, de Magny GC, Manga NM, Rinaldo A, et al. Mobile phone data highlights the role of mass gatherings in the spreading of cholera outbreaks. Proc Natl Acad Sci U S A. 2016;113:6421–6. http://dx.doi.org/10.1073/pnas.1522305113
13. Wesolowski A, Metcalf CJ, Eagle N, Kombich J, Grenfell BT, Bjørnstad ON, et al. Quantifying seasonal population fluxes driving rubella transmission dynamics using mobile phone data. Proc Natl Acad Sci U S A. 2015;112:11114–9. http://dx.doi.org/10.1073/pnas.1423542112
14. Bansal S, Chowell G, Simonsen L, Vespignani A, Viboud C. Big data for infectious disease surveillance and modeling. J Infect Dis. 2016 ;214(suppl 4):S375–9.
15. Jurdak R, Zhao K, Liu J, AbouJaoude M, Cameron M, Newth D. Understanding human mobility from Twitter. PLoS One. 2015;10:e0131469. http://dx.doi.org/10.1371/journal.pone.0131469
16. Semenza JC, Zeller H. Integrated surveillance for prevention and control of emerging vector-borne diseases in Europe. Euro Surveill. 2014 ;19:pii:20757.
17. Semenza JC, Suk JE. Vector-borne diseases and climate change: a European perspective. FEMS Microbiol Lett. 2018;365. http://dx.doi.org/10.1093/femsle/fnx244
18. Laney D. 3D data management: controlling data volume, velocity, and variety [cited 2019 Apr 3]. https://blogs.gartner.com/doug-laney/files/2012/01/ad949-3D-Data-Management-Controlling-Data-Volume-Velocity-and-Variety.pdf
19. Heitmueller A, Henderson S, Warburton W, Elmagarmid A, Pentland AS, Darzi A. Developing public policy to advance the use of big data in health care. Health Aff (Millwood). 2014;33:1523–30. http://dx.doi.org/10.1377/hlthaff.2014.0771
20. Gandomi AHM, Haider M. Beyond the hype: big data concepts, methods, and analytics. Int J Inf Manage. 2015;35:137–44. http://dx.doi.org/10.1016/j.ijinfomgt.2014.10.007
21. Ramadona A, Tozan Y, Lazuardi L, Rocklöv J. A combination of incidence data and mobility proxies from social media predicts the intra-urban spread of dengue in Yogyakarta, Indonesia. Plos Negl Trop Dis. In press 2019.
22. Istituto Superiore di Sanita. Italy: autochtonous cases of chikungunya virus [cited 2019 Mar 21] http://www.salute.gov.it/portale/temi/documenti/chikungunya/bollettino_chikungunya_20171221.pdf
23. Carletti F, Marsella P, Colavita F, Meschi S, Lalle E, Bordi L, et al. Full-length genome sequence of a chikungunya virus isolate from the 2017 autochthonous outbreak, Lazio region, Italy. Genome Announc. 2017;5:e01306-17. http://dx.doi.org/10.1128/genomeA.01306-17
24. Leparc-Goffart I, Nougairede A, Cassadou S, Prat C, de Lamballerie X. Chikungunya in the Americas. Lancet. 2014;383:514. http://dx.doi.org/10.1016/S0140-6736(14)60185-9
25. Chew C, Eysenbach G. Pandemics in the age of Twitter: content analysis of Tweets during the 2009 H1N1 outbreak. PLoS One. 2010;5:e14118. http://dx.doi.org/10.1371/journal.pone.0014118
26. Signorini A, Segre AM, Polgreen PM. The use of Twitter to track levels of disease activity and public concern in the U.S. during the influenza A H1N1 pandemic. PLoS One. 2011;6:e19467. http://dx.doi.org/10.1371/journal.pone.0019467
27. Kim EK, Seok JH, Oh JS, Lee HW, Kim KH. Use of Hangeul Twitter to track and predict human influenza infection. PLoS One. 2013;8:e69305. http://dx.doi.org/10.1371/journal.pone.0069305
28. Broniatowski DA, Dredze M, Paul MJ, Dugas A. Using social media to perform local influenza surveillance in an inner-city hospital: a retrospective observational study. JMIR Public Health Surveill. 2015 Jan–Jun;1:e5.
29. Italy Ministry of Health. National plan of surveillance and response to arbovirus transmitted by mosquitoes (*aedes* sp.), with particular reference to chikungunya, dengue and zikaviruses–2017 [cited 2019 Apr 3]. http://www.salute.gov.it/portale/temi/documenti/chikungunya/bollettino_chikungunya_20171221.pdf
30. Centers for Disease Control and Prevention. Travelers health. Chapter 3. Infectious diseases related to travel: chikungunya [cited 2018 Oct 16]. https://wwwnc.cdc.gov/travel/yellowbook/2018/infectious-diseases-related-to-travel/chikungunya
31. Rocklöv J, Quam MB, Sudre B, German M, Kraemer MUG, Brady O, et al. Assessing seasonal risks for the introduction and mosquito-borne spread of Zika virus in Europe. EBioMedicine. 2016;9:250–6. http://dx.doi.org/10.1016/j.ebiom.2016.06.009
32. Faria NR, Azevedo RDSDS, Kraemer MUG, Souza R, Cunha MS, Hill SC, et al. Zika virus in the Americas: early epidemiological and genetic findings. Science. 2016;352:345–9. http://dx.doi.org/10.1126/science.aaf5036
33. Reiter P, Lathrop S, Bunning M, Biggerstaff B, Singer D, Tiwari T, et al. Texas lifestyle limits transmission of dengue virus. Emerg Infect Dis. 2003;9:86–9. http://dx.doi.org/10.3201/eid0901.020220

Address for correspondence: Joacim Rocklöv, Umeå University, Department of Public Health and Clinical Medicine, 901 87 Umeå, Sweden; email: joacim.rocklov@umu.se

West Nile and Usutu Virus Infections and Challenges to Blood Safety in the European Union

Dragoslav Domanović, Celine M. Gossner, Ryanne Lieshout-Krikke, Wolfgang Mayr, Klara Baroti-Toth, Alina Mirella Dobrota, Maria Antonia Escoval, Olaf Henseler, Christof Jungbauer, Giancarlo Liumbruno, Salvador Oyonarte, Constantina Politis, Imad Sandid, Miljana Stojić Vidović, Johanna J. Young, Inês Ushiro-Lumb, Norbert Nowotny

West Nile virus (WNV) and Usutu virus (USUV) circulate in several European Union (EU) countries. The risk of transfusion-transmitted West Nile virus (TT-WNV) has been recognized, and preventive blood safety measures have been implemented. We summarized the applied interventions in the EU countries and assessed the safety of the blood supply by compiling data on WNV positivity among blood donors and on reported TT-WNV cases. The paucity of reported TT-WNV infections and the screening results suggest that blood safety interventions are effective. However, limited circulation of WNV in the EU and presumed underrecognition or underreporting of TT-WNV cases contribute to the present situation. Because of cross-reactivity between genetically related flaviviruses in the automated nucleic acid test systems, USUV-positive blood donations are found during routine WNV screening. The clinical relevance of USUV infection in humans and the risk of USUV to blood safety are unknown.

Author affiliations: European Centre for Disease Prevention and Control, Solna, Sweden (D. Domanović, C.M. Gossner, J.J. Young); European Blood Alliance, Amsterdam, the Netherlands (R. Lieshout-Krikke); Austrian Red Cross, Vienna, Austria (W. Mayr, C. Jungbauer); National Competent Authority for Blood, Budapest, Hungary (K. Baroti-Toth); National Competent Authority for Blood, Bucharest, Romania [external expert] (A.M. Dobrota); National Competent Authority for Blood, Lisbon, Portugal (M.A. Escoval); Paul Ehrlich Institute, Langen, Germany (O. Henseler); Italian National Blood Centre, National Institute of Health, Rome, Italy (G. Liumbruno); National Competent Authority for Blood, Madrid, Spain (S. Oyonarte); Hellenic Center for Disease Control and Prevention (KEELPNO), Athens, Greece (C. Politis); National Competent Authority for Blood, Paris, France (I. Sandid); Croatian Institute for Transfusion Medicine, Zagreb, Croatia (M.S. Vidović); National Health Service Blood and Transplant (NHSBT), London, UK (I. Ushiro-Lumb); University of Veterinary Medicine, Vienna, Austria (N. Nowotny); Mohammed Bin Rashid University of Medicine and Health Sciences, Dubai, United Arab Emirates (N. Nowotny)

DOI: https://doi.org/10.3201/eid2506.181755

West Nile virus (WNV) and Usutu virus (USUV) are arthropod-borne flaviviruses that belong to the Japanese encephalitis serocomplex. Their natural life cycle involves ornithophilic mosquitoes (predominantly *Culex* spp.) as vectors and birds as amplifying hosts. Mammals, including horses and humans, may act as accidental hosts. In temperate climate zones, WNV and USUV usually circulate from late spring to mid-autumn, when competent mosquitoes are active.

WNV was detected in Europe in 1958 (*1*). Among its 9 evolutionary lineages (*2*), WNV lineages 1 and 2 are the most notable. Most recent outbreaks of WNV infections in the European Union (EU) are caused by the central European lineage 2 WNV, which was introduced to southeastern Hungary in 2004 (*3*) and has spread to other countries in Europe since 2008 (*4*,*5*). Another (eastern European) lineage 2 WNV was independently introduced to the Volgograd area of Russia at approximately the same time (*6*) and spread from there to Romania (*7*) and Italy (*8*). In addition, lineage 1 WNV strains are still circulating in Europe, partly overlapping with lineage 2 strains (*8*,*9*). Around 80% of WNV infections in humans are asymptomatic (*9*,*10*). Most clinical WNV infections present with mild, influenza-like symptoms, and ≈1% of infected persons, most often the elderly or immunosuppressed, develop West Nile neuroinvasive disease (WNND), which causes variable rates of illness and death (*9*,*10*).

In humans, transmission of WNV through blood transfusion, organ transplantation, breast-feeding, and intrauterine means has been reported (*11*–*14*). WNV poses a risk to blood safety because an asymptomatic donor may donate infectious blood, which, if transfused, may cause a serious clinical illness in the recipient. To mitigate such risk, EU countries apply measures described in the EU Directives (*15*), professional guidelines (*16*), and the European Centre for Disease Prevention and Control (ECDC) coordinated blood safety preparedness plan (*17*). As part of these actions, blood banks should apply blood safety measures

directed to donors residing in or visiting areas affected by WNV (*17*). An area with ≥1 confirmed case of autochthonous WNV transmission to humans is considered affected (*18*). To support EU countries in applying legislation related to travelers visiting affected areas, the ECDC has developed web-based maps indicating areas at Nomenclature of Territorial Units for Statistics (NUTS) level 3 in the EU where confirmed cases of WNV infections in humans have been reported (*19*).

USUV is a mosquitoborne flavivirus closely related to WNV that was reported in Europe as a cause of death in birds (mainly blackbirds) in and around Vienna, Austria, in 2001 (*20*). It was also retrospectively identified as the etiologic agent of blackbird die-off in the Tuscany region of Italy in 1996 (*21*). Since then, the virus has spread across Europe (*22*,*23*). Clinically manifested cases of USUV infection in humans are rarely detected. In 2003, USUV-specific nucleic acid was identified in the blood of a young man with a rash in a USUV-endemic area around Vienna (*24*). In 2009, two human cases of USUV-related neuroinvasive illness were reported in Italy (*25*,*26*), and in 2013, three other human cases were reported in Croatia (*27*). USUV has also been recently associated with a clinical diagnosis of idiopathic facial paralysis in France (*28*). Transfusion-transmitted USUV infection has not been reported.

We evaluated the safety of the blood supply during WNV outbreaks in the EU by summarizing the preventive strategies applied, the functional use of WNV infection distribution maps by blood banks and responsible blood safety authorities, the occurrence of WNV infections among blood donors, and cases of transfusion-transmitted WNV (TT-WNV) infection. Because USUV circulates or cocirculates with WNV in certain EU countries (*29*) and current virus RNA detection systems show cross-reactivity between these viruses, we also discuss the threat posed by USUV to blood safety.

Materials and Methods

ECDC organized an expert meeting in Vienna in March 2018. Experts and representatives of the National Competent Authorities for blood and blood components from 11 countries in Europe presented relevant data, which we used in this evaluation. The European Blood Alliance provided data on preventive measures from the other EU member states. We also reviewed the scientific literature on blood donation and transfusion-related WNV and USUV infections, and retrieved data on reported cases of WNV infection in the EU population from The European Surveillance System (TESSy) of ECDC.

Results

According to data reported to TESSy during 2009–2017, a total of 1,757 cases of WNV infection, with an annual range from 30 to 356 cases, were reported in the EU countries (Figure). Most cases (1,695) were reported to be locally acquired; only 62 cases were imported (*30*). We summarized data on WNV infection among blood donors, which were

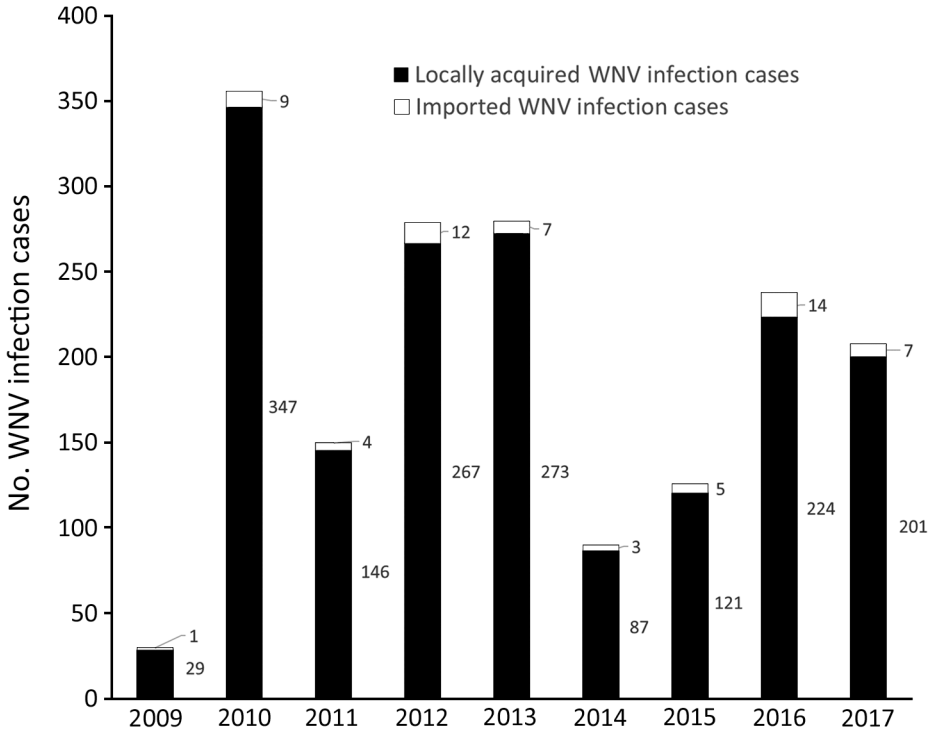

Figure. Annual number of locally acquired and imported WNV infection cases in the European Union reported to the European Surveillance System during 2009–2017. WNV, West Nile virus.

not consistently reported. Detailed descriptions of blood safety measures and frequencies of WNV-and USUV-positive blood donations in the EU are provided in the Appendix (https://wwwnc.cdc.gov/EID/article/25/6/18-1755-App1.pdf).

Preventive Strategies

As of August 31, 2018, most EU countries (15/17; 88%) without local WNV transmission to humans apply a 28-day deferral of asymptomatic blood donors after they leave an area with ongoing transmission of WNV to humans. These countries defer donors with a travel history to WNV-affected areas within EU at NUTS 3 level or at a country level in affected non-EU countries such as the United States, Canada, and countries in the tropical zone (delimited by latitudes 23°26′12.5″ in the Northern and Southern Hemispheres). The minimum time spent in an affected area that countries consider as a deferral criterion varies from 1 night to 2 consecutive days. As alternatives to the 28-day deferral, the United Kingdom uses a minipool (MP) of 6 samples and Ireland performs individual donation (ID) WNV screening using nucleic acid testing (NAT) of blood donations from traveling donors who have visited a WNV-affected country in the previous 28 days during the mosquito season (May–November). These methods are used to avoid donor shortages resulting from deferral and the cost incurred to maintain an adequate donor base by recruiting new donors. Some blood banks in Germany perform either MP or ID-NAT screening of donations from travelers to affected areas.

As of August 31, 2018, a total of 11 of 28 (39%) EU countries have reported local autochthonous transmission of WNV; 9 (81%) of those countries implemented NAT screening of blood donations (Table 1). For purposes of implementation of local blood safety measures, geographic determination of an area in which a vectorborne disease is present is based on epidemiologic analysis and risk assessment (*18*).

ECDC's WNV Maps

All blood banks in the EU use WNV maps to assess the travel-related risk of WNV infection among blood donors. Although the weekly updated maps are publicly available, some National Competent Authorities for Blood use ECDC WNV maps and supporting tables to produce national instructive documents for blood banks. Upon detection of a WNV NAT-reactive donor, blood banks retrieve and quarantine blood components derived from whole blood donated by the involved donor 120 days before the date of collection of the reactive donation and initiate a retrospective (lookback) analysis of recipients of potentially implicated blood components. There have been instances of observed differences between data on confirmed and probable human cases shown in the maps and reported by other sources (e.g., Rapid Alert System for Blood and Blood Components [RAB]), which is partially the result of occasional delays of longer than 10 days in reporting of cases to ECDC by some member states. These discrepancies could cause uncertainties for the map users and delays in the implementation of blood safety measures.

WNV Infections among Blood Donors

During 2010–2017, blood banks in the affected areas of 7 EU countries (Austria, France, Greece, Italy, Portugal, Romania, and Spain) detected 152 WNV RNA–reactive donations among 2,636,653 donated blood units, corresponding to a mean frequency of 0.60 (range 0–2.95) positive donations/10,000 donations tested (Table 2). This estimation of WNV-positive donations in the EU is biased by the small amount of data from countries with sporadic outbreaks. In countries with established continuous WNV circulation

Table 1. Occurrence of locally transmitted or imported cases of West Nile virus infection and blood safety measures by country in the European Union as of August 31, 2018*

Country	Affected areas with local transmission cases (measure)	Nonaffected areas with imported cases (measure)
Austria	+ (MP-NAT)	0 (D/MP-NAT†)
Belgium	0	0 (D)
Bulgaria	+ (D)	0 (D)
Croatia	+ (ID-NAT‡)	0 (D)
Cyprus	0	0 (D)
Czech Republic	0	0 (D)
Denmark	0	0 (D)
Estonia	0	0 (D)
Finland	0	0 (D)
France	+ (ID-NAT)	0 (D)
Germany	0	0 (D/MP/ID-NAT†)
Greece	+ (ID-NAT/D/TSD)	+ (D)
Hungary	+ (D)	0 (D)
Ireland	0	+ (ID-NAT
Italy	+ (ID-NAT)	+ (D/ID-NAT†)
Latvia	0	0 (D)
Lithuania	0	0 (D)
Luxembourg	0	0 (D)
Malta	0	0 (D)
Netherlands	0	+ (D)
Poland	0	0 (D)
Portugal	+ (ID-NAT)	0 (D)
Romania	+ (2D-NAT†/D/TSD)	+ (D)
Slovakia	0	0 (D)
Slovenia	+ (ID-NAT‡)	0 (D)
Spain	+(ID-NAT)	0(D)
Sweden	0	+(D)
United Kingdom	0	+(MP-NAT)

*D, 28-d deferral of donors coming from affected areas; ID-NAT, individual donation NAT; 2D-NAT, 2 donations NAT; MP-NAT, minipool NAT; NAT, nucleic acid testing; TSD, temporary stop of donations in the area; +, presence of cases; 0, absence of cases. More information about data collection in the different European Union countries is provided in the Appendix (https://wwwnc.cdc.gov/EID/article/25/6/18-1755-App1.pdf).
†NAT screening in some blood banks.
‡NAT screening began in the end of summer 2018.

in humans, such as Greece and Italy, the number of WNV-positive blood donations is proportional to the number of reported clinical cases in the general population, showing correlation coefficients of, for instance, R = 0.92 for Greece and R = 0.69 for Italy. Consequently, during the peak years, the positivity rate per 10,000 donations was 2.95 in Greece and 1.20 in Italy. In Austria, France, Spain, and Portugal, no positive blood donation was observed when only 1–3 autochthonous human WNV infections were detected in the population.

Transfusion-Transmitted WNV Infection

One report of WNV infectious blood donation noted that this donation resulted in TT-WNV infections in 2 patients (*31*). In 2012, the Greek Haemovigilance Centre reported these 2 TT-WNV infections: 1 patient received a platelet transfusion and developed WNND, and another patient received fresh frozen plasma and became positive for WNV but remained asymptomatic. Both blood components, including nontransfused erythrocytes, were prepared from a single whole blood donation and tested positive for WNV RNA after notification. These erythrocytes were discarded. The implicated donor, who retrospectively received a diagnosis of WNV infection, donated blood 8 days before a case of WNV infection in Greece was reported and preventive measures initiated (*31*).

Threat to Blood Safety Posed by Emerging USUV

Because of NAT cross-reactivity, USUV-infected donations in the EU blood supply have been detected during routine screening of blood donations for WNV RNA. A USUV RNA–positive blood donor in the EU was detected in Germany in 2016 (*32*). In 2017, the follow-up investigation of 7 donors among 12,047 donations from eastern Austria whose blood tested positive by NAT (Cobas WNV assay; Roche Diagnostics, https://diagnostics.roche.com), showed by virus-specific NATs and sequencing that 6 of them had USUV infection, not WNV (*33*). Retrospective analyses of 4 blood donations among 70,864 donations from eastern Austria diagnosed as WNV-positive in 2016 showed 1 USUV-positive sample (*33*). In the 2018 transmission season, the highest-ever number of WNV

Table 2. Autochthonous and imported cases of WNV infection and WNV-positive blood donations by country in the European Union, 2009–2017*

Country and year	No. cases of WNV infection, autochthonous (imported)	No. WNV-positive blood donations	No. blood donations screened	WNV-positive blood donations/10,000 donations
Austria†				
2014	2	0	67,800	0.00
2015	6	5	74,677	0.67
2016	5	3	70,864	0.42
2017	6	2	67,544	0.30
France†				
2015	1	0	30,900	0.00
2017	2	0	4,044	0.00
Greece				
2010	262	8	27,108	2.95
2011	99 (1)	5	105,610	0.47
2012	160 (2)	4	36,911	1.08
2013	86	1	26,910	0.37
2014	15	0	6,662	0.00
2017	48	0	3,779	0.00
Italy				
2009	18	2	59,815	0.33
2010	11	6	118,295	0.51
2011	32	4	148,255	0.27
2012	73	14	116,255	1.20
2013	126 (3)	19	284,564	0.67
2014	24	4	334,356	0.12
2015	61(1)	16	322,196	0.50
2016	76 (5)	31	455,930	0.68
2017	57 (1)	25	338,900	0.74
Portugal				
2015	1	0	4,247	0.00
Romania‡				
2016	17	1	10,694	0.94
2017	16	1	11,390	0.88
Spain				
2010	2	0	10,768	0.00
2016	3	0	9,457	0.00

*USUV, Usutu virus; WNV, West Nile virus.
†Austria corrected numbers of WNV-positive cases and donations by excluding USUV-positive donations in 2016 and 2017. Other affected countries did not make corrections related to possible USUV positivity.
‡Data from affected areas where blood donations were screened.

and USUV NAT-positive blood donations were identified in eastern Austria (5 WNV NAT–positive, 17 USUV NAT–positive, and 1 WNV/USUV double infection among 31,598 blood donations) (*34*). Similarly, in the Lazio region of Italy, all 5 WNV NAT–reactive blood donations in 2017 and 2018 turned out to contain USUV, and not WNV, RNA (*35*). USUV antibodies in blood donors had been detected earlier. In 2009, four of 359 healthy blood donors were positive for USUV IgG in Italy (*36*), and in 2012, one of 4,200 screened blood donations tested positive for USUV IgG and IgM in southwest Germany (*37*).

Discussion

The differences in the applied WNV blood safety measures in the EU countries with autochthonous human WNV transmission probably reflect the fact that the EU Blood Directives define measures only for donors returning from WNV-affected areas but not for donors residing in affected areas (*15*,*38*). Therefore, in the affected areas, each EU country applies blood safety interventions consistent with its national epidemiologic situation, economic capabilities, and experiences, as well as the EU preparedness plan for the prevention of TT-WNV (*17*), the European blood guide (*16*), recommendations from the US Food and Drug Administration (*39*), the American Association of Blood Banks standards (*40*), and other sources. Because of the smaller magnitude of outbreaks in affected EU countries, various blood safety measures are applied only locally. Conversely, driven by a continuous high number of WNV infection cases, an all-year universal donor screening has been implemented nationwide in the United States, but in Canada, donor screening is done only during the summer. Both countries switch from MP to ID-NAT depending on WNV activity levels (*39*,*41*). As predicted by models of environmental and climatic drivers (*42*), and after a substantial increase in human cases in 2018 (*43*), it is likely that WNV activity and the prevalence of infection in the donor population will increase across the EU in the future, which will inevitably call for greater screening of blood donations.

Changes in the epidemiology of existing infections and increasingly frequent emerging and reemerging infections may challenge the relevance of the current EU legislation on blood, tissues, and cells. Because the affected area at NUTS 3 level, which is currently used by EU countries in the donor selection procedure for travelers, could be considerably broader than the geographic area with ongoing transmission to humans, a new term should be developed for such affected areas to avoid misinterpretations. The role of ECDC in coordination of the development of common preparedness plans at the EU level (e.g., EU preparedness plans for the prevention of transfusion-transmitted WNV and Zika virus infections and safety of substances of human origin [*17*,*44*]) is to identify gaps in measures mandated through existing legislation and to achieve a high consistency and efficacy of implemented measures.

The mean frequency of 0.60 WNV RNA–positive donations/10,000 blood donations at the EU level is similar to data from the United States, where the American Red Cross detected 1,576 WNV-positive donations among 27 million donations during 2003–2012 (0.59 [range 0.18–1.49] positive/10,000 donations) (*45*). Observed data in the EU and United States show that the mean frequencies of WNV-positive blood donations in affected areas are low but not negligible. These data and experiences from the EU countries suggest that, in newly affected areas, initial cases of WNV transmission to humans tend to be sporadic, posing a low risk to potential blood donors, especially travelers. Such risk increases when more clinical cases are reported in the population, indicating that continuous transmission of WNV to humans has been established. However, in previously affected or endemic areas in Greece and Italy, WNV-positive donations had been reported before clinical cases were diagnosed in the general population (*46*–*48*). In Greece, lookback studies in 2010 of possible TT-WNV among patients with thalassemia revealed that some WNV-positive blood units might have been donated before the criteria used for initiating the implementation of blood screening with NAT were met (*48*). In Italy, circulation of the virus between birds and mosquitoes or a single case of transmission to a human or animal host are considered indicators of an increased risk of virus transmission to humans, and screening of blood donation starts even before the first case in humans is confirmed. Conversely, the absence of WNV-positive blood donated by travelers returning from affected areas calls for reevaluating triggers for implementation of traveler risk-related safety interventions because increased deferrals may have an effect on donor availability, especially during summer months.

Only 1 case of fully documented WNV transmission from a single donation to 2 recipients has been reported in the EU (*31*), which suggests that the current blood safety measures effectively prevent WNV infectious blood donations from entering the blood supply in the EU. However, besides blood safety interventions, other factors that constitute the risk of TT-WNV infection also contribute to the current situation. Considering that the projected incidence of WNV-positive donations generally correlates with WNND case frequencies (*49*), it is possible that the number of WNV-positive donations associated with the annual number of 30–356 cases of WNV infection in the EU (*30*) is too low for the occurrence of low-viremic donations that might escape safety interventions. In the United States, where substantially more WNV cases are reported annually, some breakthrough transfusion-transmitted cases

occurred because of low-level viremia that escaped detection by MP-NAT (*50*). It is also believed that, despite the implemented surveillance and hemovigilance protocols and improvements in diagnostic tests, many WNV-like symptoms were undiagnosed, or the routes of infection were not investigated. Thus, a certain level of underrecognition and underreporting certainly contributes to the lack of TT-WNV cases.

Recent molecular and serologic surveillance studies in Germany, Austria, and Italy identified USUV infections in blood donors (*32*,*33*,*36*,*37*). USUV is currently circulating more widely than WNV in the EU (*22*,*23*,*33*). Historically, USUV was introduced to Europe decades after WNV, although WNV activity was low in Europe before 2008. Because of the similar environmental requirements, mosquito vectors, and amplifying cycle in birds, USUV has easily been introduced in areas where WNV was present, resulting in a substantial geographic overlap in the circulation of these 2 viruses. USUV is currently spreading more intensively into new areas than WNV (*22*). Consequently, USUV but not WNV is currently circulating in the Netherlands, Belgium, and Switzerland (*33*). Furthermore, in Germany, only a few cases of WNV infections in birds were identified in 2018, whereas USUV is endemic throughout the country. No transfusion-associated USUV infection has been reported. However, the occurrence of USUV among blood donors is not fully determined because countries with USUV but without WNV circulation are not required to screen blood donations for flavivirus RNA. Assessing the risk of USUV transmission through blood transfusion and the clinical relevance of USUV infections in humans is therefore crucial. The currently used ID-NATs for blood screening are highly sensitive. The cross-reactivity of these test systems with USUV (*33*,*34*) and potentially with other members of the Japanese encephalitis virus complex can contribute to the detection of these flaviviruses in donated blood. WNV NAT–reactive donations should therefore undergo virus-specific confirmatory tests to determine the actual flavivirus present in donated blood.

In summary, the paucity of reported TT-WNV cases provides reassurance about the efficacy of WNV blood safety interventions in the EU. However, the cocirculation of WNV and USUV in several EU countries, together with the yet unknown transfusion risk and clinical relevance of human USUV infections, needs further attention.

About the Author

Dr. Domanović is a senior expert in the vigilance and traceability of substances of human origin at the European Centre for Disease Prevention and Control, Stockholm, Sweden. His research interests are donor-derived infections, emerging infections, and risk of infectious diseases transmission though substances of human origin.

References

1. Hubálek Z, Halouzka J. West Nile fever—a reemerging mosquito-borne viral disease in Europe. Emerg Infect Dis. 1999;5:643–50. http://dx.doi.org/10.3201/eid0505.990505
2. Pachler K, Lebl K, Berer D, Rudolf I, Hubalek Z, Nowotny N. Putative new West Nile virus lineage in *Uranotaenia unguiculata* mosquitoes, Austria, 2013. Emerg Infect Dis. 2014;20:2119–22. http://dx.doi.org/10.3201/eid2012.140921
3. Bakonyi T, Ivanics E, Erdélyi K, Ursu K, Ferenczi E, Weissenböck H, et al. Lineage 1 and 2 strains of encephalitic West Nile virus, central Europe. Emerg Infect Dis. 2006;12:618–23. http://dx.doi.org/10.3201/eid1204.051379
4. Bakonyi T, Ferenczi E, Erdélyi K, Kutasi O, Csörgő T, Seidel B, et al. Explosive spread of a neuroinvasive lineage 2 West Nile virus in Central Europe, 2008/2009. Vet Microbiol. 2013;165:61–70. http://dx.doi.org/10.1016/j.vetmic.2013.03.005
5. Papa A, Bakonyi T, Xanthopoulou K, Vazquez A, Tenorio A, Nowotny N. Genetic characterization of West Nile virus lineage 2, Greece, 2010. Emerg Infect Dis. 2011;17:920–2. http://dx.doi.org/10.3201/eid1705.101759
6. Platonov AE, Karan' LS, Shopenskaia TA, Fedorova MV, Koliasnikova NM, Rusakova NM, et al. Genotyping of West Nile fever virus strains circulating in southern Russia as an epidemiological investigation method: principles and results [in Russian]. Zh Mikrobiol Epidemiol Immunobiol. 2011;2:29–37.
7. Sirbu A, Ceianu CS, Panculescu-Gatej RI, Vazquez A, Tenorio A, Rebreanu R, et al. Outbreak of West Nile virus infection in humans, Romania, July to October 2010. Euro Surveill. 2011;16:19762.
8. Ravagnan S, Montarsi F, Cazzin S, Porcellato E, Russo F, Palei M, et al. First report outside eastern Europe of West Nile virus lineage 2 related to the Volgograd 2007 strain, northeastern Italy, 2014. Parasit Vectors. 2015;8:418. http://dx.doi.org/10.1186/s13071-015-1031-y
9. Sambri V, Capobianchi M, Charrel R, Fyodorova M, Gaibani P, Gould E, et al. West Nile virus in Europe: emergence, epidemiology, diagnosis, treatment, and prevention. Clin Microbiol Infect. 2013;19:699–704. http://dx.doi.org/10.1111/1469-0691.12211
10. Barzon L, Papa A, Lavezzo E, Franchin E, Pacenti M, Sinigaglia A, et al. Phylogenetic characterization of central/southern European lineage 2 West Nile virus: analysis of human outbreaks in Italy and Greece, 2013–2014. Clin Microbiol Infect. 2015;21:1122.e1–10. http://dx.doi.org/10.1016/j.cmi.2015.07.018
11. Harrington T, Kuehnert MJ, Kamel H, Lanciotti RS, Hand S, Currier M, et al. West Nile virus infection transmitted by blood transfusion. Transfusion. 2003;43:1018–22. http://dx.doi.org/10.1046/j.1537-2995.2003.00481.x
12. Hinckley AF, O'Leary DR, Hayes EB. Transmission of West Nile virus through human breast milk seems to be rare. Pediatrics. 2007;119:e666–71. http://dx.doi.org/10.1542/peds.2006-2107
13. Centers for Disease Control and Prevention (CDC). Intrauterine West Nile virus infection—New York, 2002. MMWR Morb Mortal Wkly Rep. 2002;51:1135–6.
14. Pealer LN, Marfin AA, Petersen LR, Lanciotti RS, Page PL, Stramer SL, et al.; West Nile Virus Transmission Investigation Team. Transmission of West Nile virus through blood transfusion in the United States in 2002. N Engl J Med. 2003;349:1236–45. http://dx.doi.org/10.1056/NEJMoa030969
15. European Commission. Commission Directive 2014/110/EU of 17 December 2014 amending Directive 2004/33/EC as regards temporary deferral criteria for donors of allogeneic blood donations 2014 [cited 2018 Mar 11]. http://eur-lex.europa.eu/legal-content/EN/TXT/?uri=OJ%3AJOL_2014_366_R_0011
16. European Directorate for the Quality of Medicines and Healthcare. Guide to the preparation, use and quality assurance of blood components, 19th ed. Strasbourg (France): Council of Europe; 2016.

17. European Commission. West Nile virus and blood safety—introduction to a preparedness plan in Europe 2012 [cited 2018 Mar 11]. https://ec.europa.eu/health/sites/health/files/blood_tissues_organs/docs/wnv_preparedness_plan_2012.pdf
18. Domanovic D, Giesecke J. How to define an area where transmission of arthropod-borne disease is occurring? Euro Surveill. 2012;17:20171.
19. European Center for Disease Prevention and Control (ECDC). West Nile fever maps 2012 [cited 2012 Feb 22]. http://ecdc.europa.eu/en/activities/diseaseprogrammes/emerging_and_vector_borne_diseases/pages/west_niles_fever_risk_maps.aspx
20. Weissenböck H, Kolodziejek J, Url A, Lussy H, Rebel-Bauder B, Nowotny N. Emergence of Usutu virus, an African mosquito-borne flavivirus of the Japanese encephalitis virus group, central Europe. Emerg Infect Dis. 2002;8:652–6. http://dx.doi.org/10.3201/eid0807.020094
21. Weissenböck H, Bakonyi T, Rossi G, Mani P, Nowotny N. Usutu virus, Italy, 1996. Emerg Infect Dis. 2013;19:274–7. http://dx.doi.org/10.3201/eid1902.121191
22. Cadar D, Lühken R, van der Jeugd H, Garigliany M, Ziegler U, Keller M, et al. Widespread activity of multiple lineages of Usutu virus, western Europe, 2016. Euro Surveill. 2017;22:30452. http://dx.doi.org/10.2807/1560-7917.ES.2017.22.4.30452
23. Bakonyi T, Erdélyi K, Brunthaler R, Dán Á, Weissenböck H, Nowotny N. Usutu virus, Austria and Hungary, 2010-2016. Emerg Microbes Infect. 2017;6:e85.
24. Weissenböck H, Chvala-Mannsberger S, Bakonyi T, Nowotny N. Emergence of Usutu virus in central Europe: diagnosis, surveillance and epizootiology. In: Takken W, Knols BGJ, editors. Emerging pests and vector-borne diseases in Europe—ecology and control of vector-borne diseases. Wageningen (the Netherlands): Wageningen Academic Publishers; 2007. p. 153–68.
25. Pecorari M, Longo G, Gennari W, Grottola A, Sabbatini A, Tagliazucchi S, et al. First human case of Usutu virus neuroinvasive infection, Italy, August–September 2009. Euro Surveill. 2009;14:19446.
26. Cavrini F, Gaibani P, Longo G, Pierro AM, Rossini G, Bonilauri P, et al. Usutu virus infection in a patient who underwent orthotropic liver transplantation, Italy, August–September 2009. Euro Surveill. 2009;14:19448.
27. Santini M, Vilibic-Cavlek T, Barsic B, Barbic L, Savic V, Stevanovic V, et al. First cases of human Usutu virus neuroinvasive infection in Croatia, August–September 2013: clinical and laboratory features. J Neurovirol. 2015;21:92–7. http://dx.doi.org/10.1007/s13365-014-0300-4
28. Simonin Y, Sillam O, Carles MJ, Gutierrez S, Gil P, Constant O, et al. Human Usutu virus infection with atypical neurologic presentation, Montpellier, France, 2016. Emerg Infect Dis. 2018;24:875–8. http://dx.doi.org/10.3201/eid2405.171122
29. Nikolay B. A review of West Nile and Usutu virus co-circulation in Europe: how much do transmission cycles overlap? Trans R Soc Trop Med Hyg. 2015;109:609–18. http://dx.doi.org/10.1093/trstmh/trv066
30. European Center for Disease Prevention and Control. The European surveillance system 2018 [cited 2018 Aug 31]. https://ecdc.europa.eu/en/publications-data/european-surveillance-system-tessy
31. Pervanidou D, Detsis M, Danis K, Mellou K, Papanikolaou E, Terzaki I, et al. West Nile virus outbreak in humans, Greece, 2012: third consecutive year of local transmission. Euro Surveill. 2014;19:20758. http://dx.doi.org/10.2807/1560-7917.ES2014.19.13.20758
32. Cadar D, Maier P, Müller S, Kress J, Chudy M, Bialonski A, et al. Blood donor screening for West Nile virus (WNV) revealed acute Usutu virus (USUV) infection, Germany, September 2016. Euro Surveill. 2017;22:30501. http://dx.doi.org/10.2807/1560-7917.ES.2017.22.14.30501
33. Bakonyi T, Jungbauer C, Aberle SW, Kolodziejek J, Dimmel K, Stiasny K, et al. Usutu virus infections among blood donors, Austria, July and August 2017—raising awareness for diagnostic challenges. Euro Surveill. 2017;22:17-00644. http://dx.doi.org/10.2807/1560-7917.ES.2017.22.41.17-00644
34. Aberle SW, Kolodziejek J, Jungbauer C, Stiasny K, Aberle JH, Zoufaly A, et al. Increase in human West Nile and Usutu virus infections, Austria, 2018. Euro Surveill. 2018;23:1800545. http://dx.doi.org/10.2807/1560-7917.ES.2018.23.43.1800545
35. Carletti F, Colavita F, Rovida F, Percivalle E, Baldanti F, Ricci I, et al. Expanding Usutu virus circulation in Italy: detection in the Lazio region, central Italy, 2017 to 2018. Euro Surveill. 2019;24:1800649. http://dx.doi.org/10.2807/1560-7917.ES.2019.24.3.1800649
36. Gaibani P, Pierro A, Alicino R, Rossini G, Cavrini F, Landini MP, et al. Detection of Usutu-virus-specific IgG in blood donors from northern Italy. Vector Borne Zoonotic Dis. 2012;12:431–3. http://dx.doi.org/10.1089/vbz.2011.0813
37. Allering L, Jöst H, Emmerich P, Günther S, Lattwein E, Schmidt M, et al. Detection of Usutu virus infection in a healthy blood donor from south-west Germany, 2012. Euro Surveill. 2012;17:20341.
38. European Commission. Commission Directive 2004/33/EC of 22 March 2004 implementing Directive 2002/98/EC of the European Parliament and of the Council as regards certain technical requirements for blood and blood components, 2004 [cited 2018 Apr 25]. http://eur-lex.europa.eu/LexUriServ/LexUriServ.do?uri=OJ:L:2004:091:0025:0039:EN:PDF</eref>
39. US Department of Health and Human Services, Food and Drug Administration, Center for Biologics Evaluation and Research. Guidance for industry, use of nucleic acid tests to reduce the risk of transmission of West Nile virus from donors of whole blood and blood components intended for transfusion. 2009 [cited 2018 Apr 25]. https://www.fda.gov/downloads/BiologicsBloodVaccines/GuidanceComplianceRegulatoryInformation/Guidances/Blood/UCM189464.pdf
40. American Association of Blood Banks. Standards for blood banks and transfusion services. 31st edition. Bethesda (MD): The Association; 2018.
41. Vamvakas EC, Kleinman S, Hume H, Sher GD. The development of West Nile virus safety policies by Canadian blood services: guiding principles and a comparison between Canada and the United States. Transfus Med Rev. 2006;20:97–109. http://dx.doi.org/10.1016/j.tmrv.2005.11.001
42. Semenza JC, Tran A, Espinosa L, Sudre B, Domanovic D, Paz S. Climate change projections of West Nile virus infections in Europe: implications for blood safety practices. Environ Health. 2016;15(Suppl 1):28. http://dx.doi.org/10.1186/s12940-016-0105-4
43. Haussig JM, Young JJ, Gossner CM, Mezei E, Bella A, Sirbu A, et al. Early start of the West Nile fever transmission season 2018 in Europe. Euro Surveill. 2018;23:1800428. http://dx.doi.org/10.2807/1560-7917.ES.2018.23.32.1800428
44. European Center for Disease Prevention and Control. Zika virus and safety of substances of human origin: a guide for preparedness activities in Europe 2017 [cited 2018 Aug 31]. https://ecdc.europa.eu/en/publications-data/zika-virus-and-safety-substances-human-origin-guide-preparedness-activities-0
45. Dodd RY, Foster GA, Stramer SL. Keeping blood transfusion safe from West Nile virus: American Red Cross experience, 2003 to 2012. Transfus Med Rev. 2015;29:153–61. http://dx.doi.org/10.1016/j.tmrv.2015.03.001
46. Rizzo C, Napoli C, Venturi G, Pupella S, Lombardini L, Calistri P, et al.; Italian WNV surveillance working group. West Nile virus transmission: results from the integrated surveillance system in Italy, 2008 to 2015. Euro Surveill. 2016;21:30340. http://dx.doi.org/10.2807/1560-7917.ES.2016.21.37.30340

47. Politis C, Tsoukala A, Hatzitaki M, Pappa A, Englezou A, Zafeiriou C, et al. West Nile virus (WNV) outbreak in Greece and blood safety measures. Vox Sang. 2011;101(Suppl1):42.
48. Politis C, Pappa A, Hassapopoulou H, Pantelidou D, Perifanis V, Teli A, et al. Transfusion transmitted West Nile virus (WNV) infection in thalassaemic patients in Greece. Vox Sang. 2011;101(Suppl2):236.
49. Betsem E, Kaidarova Z, Stramer SL, Shaz B, Sayers M, LeParc G, et al. Correlation of West Nile virus incidence in donated blood with West Nile neuroinvasive disease rates, United States, 2010–2012. Emerg Infect Dis. 2017;23:212–9. http://dx.doi.org/10.3201/eid2302.161058
50. Stramer SL, Fang CT, Foster GA, Wagner AG, Brodsky JP, Dodd RY. West Nile virus among blood donors in the United States, 2003 and 2004. N Engl J Med. 2005;353:451–9. http://dx.doi.org/10.1056/NEJMoa044333

Address for correspondence: Dragoslav Domanović, European Centre for Disease Prevention and Control, Gustav III:s Boulevard 40 Solna, Stockholm 16973 Sweden; email: Dragoslav.Domanovic@ecdc.europa.eu

EMERGING INFECTIOUS DISEASES®

February 2018

Zoonoses

- Increase in Ocular Syphilis Cases at Ophthalmologic Reference Center, France, 2012–2015
- Adenovirus Type 4 Respiratory Infections among Civilian Adults, Northeastern United States, 2011–2015
- Ecologic Features of Plague Outbreak Areas, Democratic Republic of the Congo, 2004–2014
- Hypervirulent *Klebsiella pneumoniae* in Cryptogenic Liver Abscesses, Paris, France
- *Echinococcus* spp. Tapeworms in North America
- *Borrelia miyamotoi* Infections in Humans and Ticks, Northeastern China
- Plasmid-Encoded Transferable *mecB*-Mediated Methicillin Resistance in *Staphylococcus aureus*
- Multiplex PCR–Based Next-Generation Sequencing and Global Diversity of Seoul Virus in Humans and Rats
- Clinical and Molecular Epidemiology of Staphylococcal Toxic Shock Syndrome in the United Kingdom
- Lethal Respiratory Disease Associated with Human Rhinovirus C in Wild Chimpanzees, Uganda, 2013
- Spread of Meropenem-Resistant *Streptococcus pneumoniae* Serotype 15A-ST63 Clone in Japan, 2012–2014
- Role of Environmental Factors in Shaping Spatial Distribution of *Salmonella enterica* Serovar Typhi, Fiji
- *Yersinia pestis* Survival and Replication in Potential Ameba Reservoir
- New Parvovirus Associated with Serum Hepatitis in Horses after Inoculation of Common Biological Product
- Development of a Pediatric Ebola Predictive Score, Sierra Leone
- Trends in Infectious Disease Mortality, South Korea, 1983–2015
- Use of Pristinamycin for Macrolide-Resistant *Mycoplasma genitalium* Infection
- Risk Communication and Ebola-Specific Knowledge and Behavior during 2014–2015 Outbreak, Sierra Leone
- Macacine Herpesvirus 1 Antibody Prevalence and DNA Shedding among Invasive Rhesus Macaques, Silver Springs State Park, Florida, USA
- Co-circulation of Influenza A H5, H7, and H9 Viruses and Co-infected Poultry in Live Bird Markets, Cambodia
- Effects of Culling on *Leptospira interrogans* Carriage by Rats
- Scrub Typhus Outbreak in Chonburi Province, Central Thailand, 2013
- Epidemic Varicella Zoster Virus among University Students, India
- Fly Reservoir Associated with *Wohlfahrtiimonas Bacteremia* in a Human
- Containment of Highly Pathogenic Avian Influenza A(H5N1) Virus, Lebanon, 2016
- *Emergomyces africanus* in Soil, South Africa

To revisit the February 2018 issue, go to:
https://wwwnc.cdc.gov/eid/articles/issue/24/2/table-of-contents

SYNOPSIS

Immunopathology of Fatal Human Variegated Squirrel Bornavirus 1 Encephalitis, Germany, 2011–2013

Dennis Tappe, Jonas Schmidt-Chanasit, Jessica Rauch, Petra Allartz, Christiane Herden

Variegated squirrel bornavirus 1 (VSBV-1) is a zoonotic virus that causes fatal encephalitis in humans who are infected after contact with exotic squirrels. We analyzed the brain lesions and the immune responses in all 4 known human cases that showed panencephalitis. Inflammatory infiltrates in areas positive for VSBV-1 RNA and antigen consisted of CD4+ and CD8+ T cells, with perivascular B-cell accumulation. Strong microglial response and bizarre astroglial expansion were present. Areas of malacia contained neutrophils and foamy microglia and macrophages. Immunopathologic examination during infection showed cleavage of caspase 3 in brain cells adjacent to CD8+ cells and widespread p53 expression, hallmarks of apoptosis. Cerebrospinal fluid analyses over time demonstrated increasing protein concentrations and cell counts, paralleled by pathologic lactate elevations in all patients. The most severe cerebrospinal fluid and histologic changes occurred in the patient with the highest viral load, shortest duration of disease, and most medical preconditions.

Variegated squirrel bornavirus (VSBV-1; family *Bornaviridae*, species *Mammalian 2 orthobornavirus*) is a new zoonotic virus that causes severe and eventually fatal encephalitis in humans. VSBV-1 was discovered retrospectively in 2015 in a cluster of 3 fatal encephalitis cases among private breeders of exotic variegated squirrels (*Sciurus variegatoides*) in eastern Germany (*1*). Phylogenetic analyses showed that this virus forms a separate lineage within the *Bornaviridae* family. VSBV-1 is related to, but distinct from, the classical Borna disease virus 1 (BoDV-1; species *Mammalian 1 orthobornavirus*). Recently, also in retrospect, VSBV-1 was shown to be responsible for fatal limbic encephalitis in a zoo animal caretaker after contact with an exotic Prevost's squirrel (*Callosciurus prevostii*) in northern Germany (*2*). The virus is of unknown origin (*3*) and most likely transmitted by bites and scratches of infected exotic squirrels of the subfamilies *Sciurinae* from Central America and *Callosciurinae* from Southeast Asia (*1*,*2*) in holdings in Europe. The animals are asymptomatic and show high viral RNA loads, not only in the brain but also in organs capable of secretion and excretion, such as the kidney, urinary bladder, skin, and oropharynx (*1*,*3*,*4*). The distribution of viral RNA and antigen in the human brain has been described only in 1 patient (the patient with limbic encephalitis) (*2*). The pathophysiology of human VSBV-1 infection and the immune response toward the virus in humans is unknown.

We here summarize clinical data of all 4 known human VSBV-1 encephalitis cases and describe the distribution of VSBV-1 in different brain areas as determined by real-time reverse transcription PCR (RT-PCR) and immunohistochemical (IHC) analysis in the initial encephalitis cluster. We focus on the characterization of the central nervous system (CNS) immunologic response to VSBV-1 by IHC analyses of immune cells in the brain of all patients, as well as by examination of cerebrospinal fluid (CSF) reactions over time during the disease.

Patients, Materials, and Methods

Encephalitis Cases

Three patients were male private breeders (62–72 years of age) of exotic squirrels (*1*), and 1 patient was a female zoo animal caretaker (45 years of age) who had occupational contact with exotic squirrels (*2*). All 4 patients had had subacute, slow-onset, progressive, and eventually fatal encephalitis. Duration of their illnesses ranged from 2 to 4 months. In all 4 patients, fever or chills, initial abdominal symptoms, and later respiratory problems occurred, in addition to signs of CNS involvement, such as confusion and psychomotor slowing. Myoclonus occurred in 2 patients and ataxia in 3 patients. Illnesses progressed to coma and death. Changes in the brain or meninges were visible by magnetic resonance imaging late in the course of the disease, >4 weeks after onset of the first symptoms (Table 1).

Author affiliations: Bernhard Nocht Institute for Tropical Medicine, Hamburg, Germany (D. Tappe, J. Schmidt-Chanasit, J. Rauch, P. Allartz); German Centre for Infection Research, Hamburg (J. Schmidt-Chanasit); University of Giessen, Giessen, Germany (C. Herden)

DOI: https://doi.org/10.3201/eid2506.181082

Table 1. Characteristics of patients with fatal variegated squirrel bornavirus 1 encephalitis, Germany

Characteristic	Patient 1	Patient 2	Patient 3	Patient 4
Year of illness (reference)	2011 (*1*)	2013 (*1*)	2013 (*1*)	2013 (*2*)
Age, y/sex	63/M	62/M	72/M	45/F
Duration of illness, mo.	3	2	4	3
Medical preconditions	Hypertension	Hypertension, type 2 diabetes, renal insufficiency	Hypertension, obesity	None
Predominant symptoms	Myoclonus, tetraparesis, coma	Myoclonus, ataxia, coma	Ocular paresis, ataxia, coma	Ataxia, coma
Geographic area (state) of infection	East Germany (Saxony-Anhalt)	East Germany (Saxony-Anhalt)	East Germany (Saxony-Anhalt)	North Germany (Schleswig-Holstein)
Squirrel contact	Private breeder of variegated squirrels	Private breeder of variegated squirrels	Private breeder of variegated squirrels	Zoo animal caretaker, contact with a Prevost's squirrel

From all 4 patients, formalin-fixed paraffin-embedded (FFPE) brain tissue was available; from patient 1, only a brain biopsy sample was available because no autopsy was granted. However, FFPE blocks from internal organs of patients 2–4 (myocardium, lungs, liver, kidney, spleen, bone marrow, intestine) were also available for analyses. Ethics clearance was obtained from the local ethics board (Medical Board of Hamburg, no. PV5616).

Molecular Assays

VSBV-1–specific quantitative real-time RT-PCR was performed from FFPE tissues as previously described (*1*,*2*). Tissue samples from different brain areas from patients 1–3 and samples of internal organs from patients 2 and 3 were analyzed in this study. For patient 4, real-time RT-PCR analyses for VSBV-1 RNA in different brain areas and internal organs had been performed previously (*2*).

Histologic and IHC Analyses

Standard hematoxylin and eosin staining was performed from FFPE CNS tissues of all 4 patients and from FFPE internal organs of patients 2–4. IHC for VSBV-1 antigen was performed for patients 1–3 on different CNS tissue samples and for patients 2–4 on internal organ samples. For patient 4, IHC for VSBV-1 only from brain has been performed previously (*2*). For VSBV-1 IHC, polyclonal rabbit antiserum against viral N and P proteins was used (*2*).

Further IHC studies were performed for all 4 patients in CNS tissue samples to demonstrate glial fibrillary acidic protein (GFAP, 1:100; Zytomed Systems, https://www.zytomed-systems.de), CD3 (1:400; Epitomics Abcam, https://www.abcam.com), CD20 (1:150; Agilent, https://www.agilent.com), CD4 (1:30; Cell Marque, http://www.cellmarque.com), CD8 (1:20; Cell Marque), CD68 (1:100; Agilent), CD177 (1:33; Zytomed Systems), HLA-DR (1:50; DakoAgilent, https://www.agilent.com/en/dako-products), inducible nitric oxide synthase (iNOS, 1:100; Zytomed Systems), cleaved caspase-3 (CC3, 1:300; Cell Signaling Technology, https://www.cellsignal.de), TdT-mediated dUTP-biotin nick end labeling (TUNEL assay, 1:10; SigmaAldrich/Merck, https://www.sigmaaldrich.com), granzyme B (1:50; Agilent), Ki67 (1:20; DakoAgilent), and p53 (1:50; DakoAgilent). After pretreatment with buffers containing Trilogy (medac diagnostika, http://www.medac-diagnostika.de) at 95°C for CD177, EDTA (pH 8 for CD4 and p53), or citrate (pH 6 for CD3, CD20, CD8, CD68, HLA-DR, iNOS, TUNEL, and Ki67) and endogenous peroxidase blocking, the FFPE tissue sections were incubated with the respective antibodies in Antibody Diluent Solution (Zytomed) at 4°C overnight. This step was followed by incubation with the DCS-AEC 2 Component Detection Kit and 3-amino-9-ethylcarbazole substrate (DCS, http://www.dcs-diagnostics.de) for immunoperoxidase staining or the DCS AP Detection Kit and Fast Blue substrate (DCS) for immunophosphatase staining. Brain tissue from 5 patients without encephalitis served as negative controls and human lymphatic tissue as a positive control for immunologic staining of immune cells.

CSF Analyses

Total CSF protein and lactate concentrations and cell counts were performed following standard procedures from all 4 patients over time while the patients were still alive. Patients were seen in different hospitals with an initially unknown disease and CSF analyses were performed in different time intervals. Intrathecal antibody synthesis was demonstrated by testing for oligoclonal bands (isoelectric focusing and immunofixation of IgG parallel in serum and CSF) and by calculation of the IgM, IgA, and IgG index (ratio between CSF and serum immunoglobulin class after correcting for albumin concentrations in the CSF and serum).

Results

Real-time RT-PCR Detection of VSBV-1 RNA

Real-time RT-PCR for VSBV-1 RNA was positive in different brain areas in all patients but negative in all internal organs. The highest viral loads were detected in midbrain regions, hippocampus, and temporal cerebral cortex (Table 2).

Table 2. Real-time RT-PCR results for variegated squirrel bornavirus 1 RNA in different brain areas and internal organs, Germany*

Sample	Cycle threshold		
	Patient 1	**Patient** 2	Patient 3
Cortical biopsy	31.2	30.8	N/A
Cortex frontal	NA	31.1	29.9
Cortex temporal	NA	27.9	28.9
Striatum	NA	28.9	29.7
Hippocampus	NA	28.3	29.4
Midbrain/substantia nigra	NA	26.4	29.4
Cerebellum	NA	34.6	29.9
Olfactory bulb	NA	NA	29.7
Myocardium	NA	Neg	Neg
Lungs	NA	Neg	Neg
Kidney	NA	Neg	Neg
Liver	NA	Neg	Neg
Spleen	NA	Neg	Neg

*All materials tested were formalin-fixed paraffin-embedded tissue specimens. Not all tissues were available from all patients because no autopsy was performed on patient 1 and no biopsy sample was taken from patient 3. From patient 4, real-time RT-PCR analyses for variegated squirrel bornavirus 1 RNA in different brain areas and internal organs were performed earlier (*2*). NA, not available; neg, negative; RT-PCR, reverse transcription PCR.

Histologic and IHC Analyses of Brain Tissue and Internal Organs in VSBV-1 Infection

In general, tissue analyses showed the histologic picture of a panencephalitis. Most commonly, the temporal and insular lobes and the basal ganglia and midbrain were affected. Areas of tissue necrosis (malacia), edema, perivascular lymphocyte cuffing, parenchymal lymphocyte infiltration, and glial activation were found in the brains of all patients in the white and gray matter in a random distribution (Figure 1, panel A). Astrocytes appeared bizarre and enlarged (Figure 1, panel B). The most severe changes were found in the brain tissue of patient 2. Furthermore, satellitosis, occasional neuronophagia, single-cell necrosis of Purkinje cells (patients 2 and 4), loss of hippocampal pyramidal cell layer (patient 2), focally extensive hemorrhage (patient 2), and lipofuscin deposition were found. No Histopathologic analyses of the internal organs in the patients showed no inflammatory or degenerative changes (data not shown). GFAP reactivity (Figure 1, panel C) confirmed the strong astroglial activation consisting of variably enlarged protoplasmic astrocytes which could be binucleated or multinucleated up to a bizarre appearance. Compared with negative control brains, patient brain tissues showed strong HLA-DR and CD68+ reactivity throughout the inflamed regions in predominantly foamy cells, which represent either lipid-laden microglia or macrophages, and in a few bushy microglia (Figure 1, panels D, E). In contrast, little iNOS production was seen (Appendix Figure 1, https://wwwnc.cdc.gov/EID/article/25/6/18-1082-App1.pdf).

Invasion by neutrophils showed infiltration of the brain parenchyma from blood vessels in areas of malacia

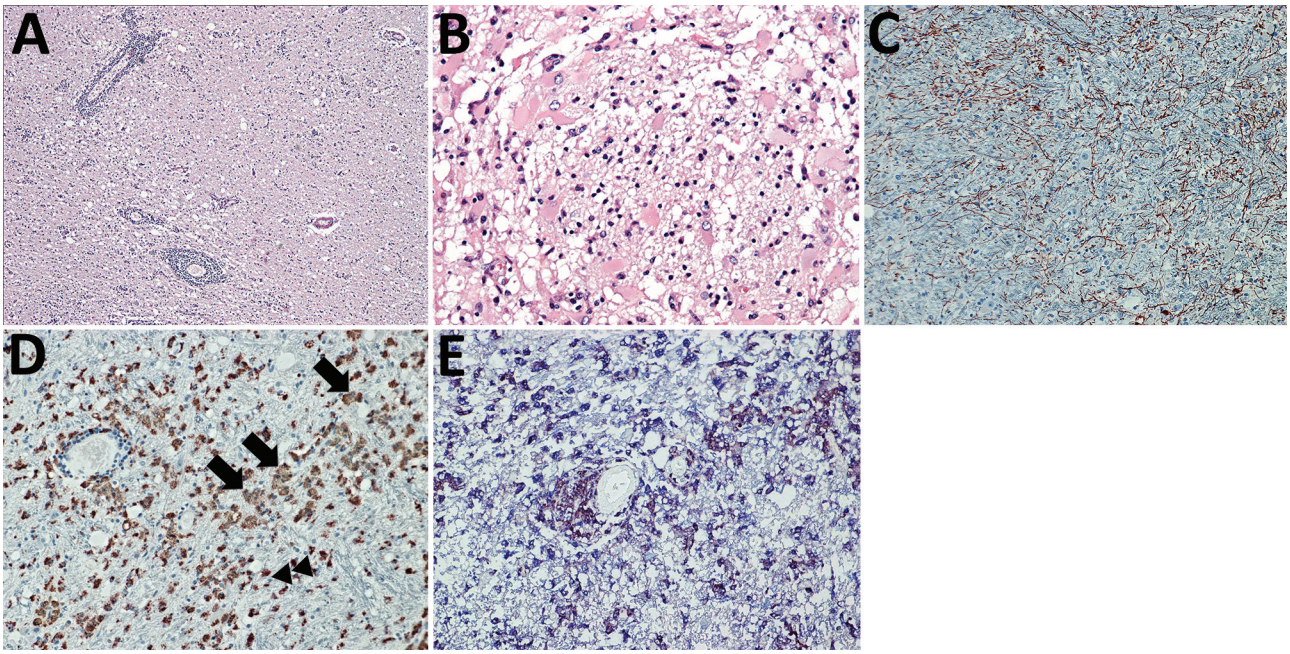

Figure 1. Brain inflammation in patients with fatal variegated squirrel bornavirus 1 encephalitis. A) Brain section showing mononuclear cell infiltration and tissue edema. Hematoxylin and eosin stain; original magnification ×100. B) Depiction of glial cell activation in a brain biopsy sample of malacia. Astrocytes appear bizarre and enlarged. Hematoxylin and eosin stain; original magnification ×400. C) Demonstration of glial fibrillary acidic protein (GFAP). Immunoperoxidase stain with hematoxylin counterstain; original magnification ×200. D) Predominantly foamy cells (lipid-laden microglia or macrophages [arrows]) and a few bushy microglia (arrowheads) as shown by marked CD68 positivity throughout the inflamed regions. Immunoperoxidase stain with hematoxylin counterstain; original magnification ×200. E) HLA-DR (brown) and CD68 positivity (blue) indicating many reactive microglia and macrophages. Immunoperoxidase and immunophosphatase stains; original magnification ×200.

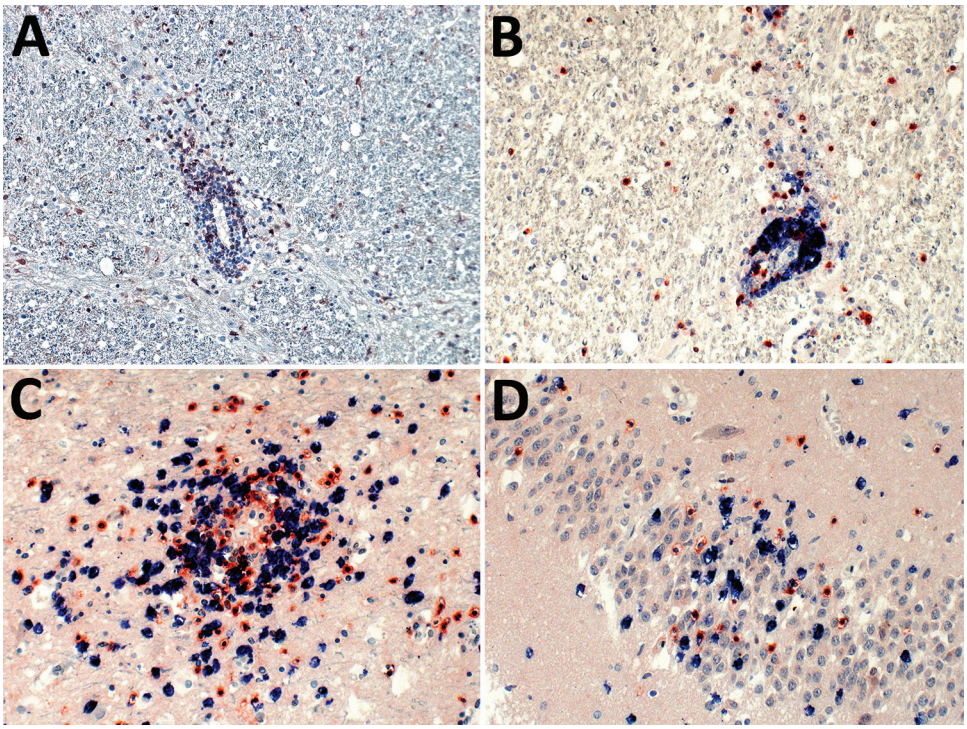

Figure 2. Demonstration of neutrophils, B cells, and CD4+ and CD8+ T-lymphocyte infiltration of the brain parenchyma during variegated squirrel bornavirus 1 infection. A) Demonstration of CD177+ neutrophils infiltrating the brain parenchyma from a blood vessel. Neutrophils are also seen scattered throughout the tissue during the infection. Immunoperoxidase stain with hematoxylin counterstain; original magnification ×200. B) Depiction of B cells (CD20, blue) and T cells (CD3, red) around a blood vessel. B cells showed mainly perivascular cuffing, and only a few were found in the brain parenchyma, whereas T cells were also seen in high numbers infiltrating the brain parenchyma. Immunoperoxidase and immunophosphatase stains; original magnification ×200. C, D) Mixed CD4+ (red) and CD8+ (blue) T-cell infiltrates around a blood vessel and invading adjacent tissue (C), and the hippocampus (D). Immunoperoxidase and immunophosphatase stains; original magnification ×400.

(Figure 2, panel A); these CD177+ cells were also scattered throughout the brain tissue in such regions. CD20+ B cells were mainly seen as perivascular cuffing, and only a few were found in the tissue otherwise (Figure 2, panel B). In contrast, CD3+ T cells also occurred in high numbers in the brain parenchyma. The T-cell infiltrates consisted of CD4+ helper cells and CD8+ cytotoxic cells; neither type predominated (Figure 2, panels C and D). In control brain tissues, CD4+ cells were sparse in the parenchyma, but no CD8+ cells or granulocytes were present (data not shown).

In all patients, IHC analysis for VSBV-1 antigen showed areas of widespread neuropil, cytoplasmic, and nuclear staining (Figure 3, panel A). Antigen was found in neurons and astrocytes (Figure 3, panels B–D), mainly with enlarged appearance, and oligodendrocytes (Figure 3, panel E). Endothelial cells were always spared. IHC analysis detected VSBV-1 antigen in the brain areas that were also positive for VSBV-1 RNA. No positive VSBV-1 immunostaining was detected in the internal organs (data not shown).

Staining for granzyme B showed immune cells adjacent to large neurons and glia cells (Figure 4, panels A, B) during VSBV-1 infection. Widespread apoptosis was shown by positive CC3 staining and shrinkage of brain cells in close association with CD8+ T lymphocytes and granzyme B positivity (Figure 4, panels C, D), as well as positive TUNEL assays (not shown). In addition, widespread p53 positivity was seen mainly in perivascular mononuclear inflammatory cells, some neurons, astrocytes, and rod cells throughout the affected areas (Figure 4, panel E) but only sparse Ki67 positivity in perivascular inflammatory mononuclear cells (Appendix Figure 2). In control brain tissues, no CC3, TUNEL, p53, or Ki67 positivity was seen (data not shown).

CSF Changes During VSBV-1 Infection

Standard clinical CSF analyses of the patients over time showed lymphocytic pleocytosis (range 11–361 cells/μL, median 142 cells/μL [reference <5/μL]) (Figure 5, panel A), markedly elevated protein concentrations (range 824–6,092 mg/L, median 1,976 mg/L [reference <500 mg/L]) (Figure 5, panel B), lactate level elevation (range 2.9–8.47 mmol/L, median 5.1 mmol/L [reference <2.1 mmol/L]) (Figure 5, panel C), and blood–brain barrier dysfunction. All patients showed increasing CSF protein concentrations over time. Patients 1, 3, and 4 demonstrated slow decreases of pathologic lactate concentrations during the observation period. In contrast, patient 2 exhibited a drastic increase of lactate levels and CSF cell counts. In patient 1, cell counts were only very mildly elevated; in patients 3 and 4, cell counts changed in an undulating manner over time. In all patients, increased intrathecal concentrations of IgM, IgA, and IgG were found, with positive IgM and IgG indices and oligoclonal IgG bands that demonstrated intrathecal antibody production.

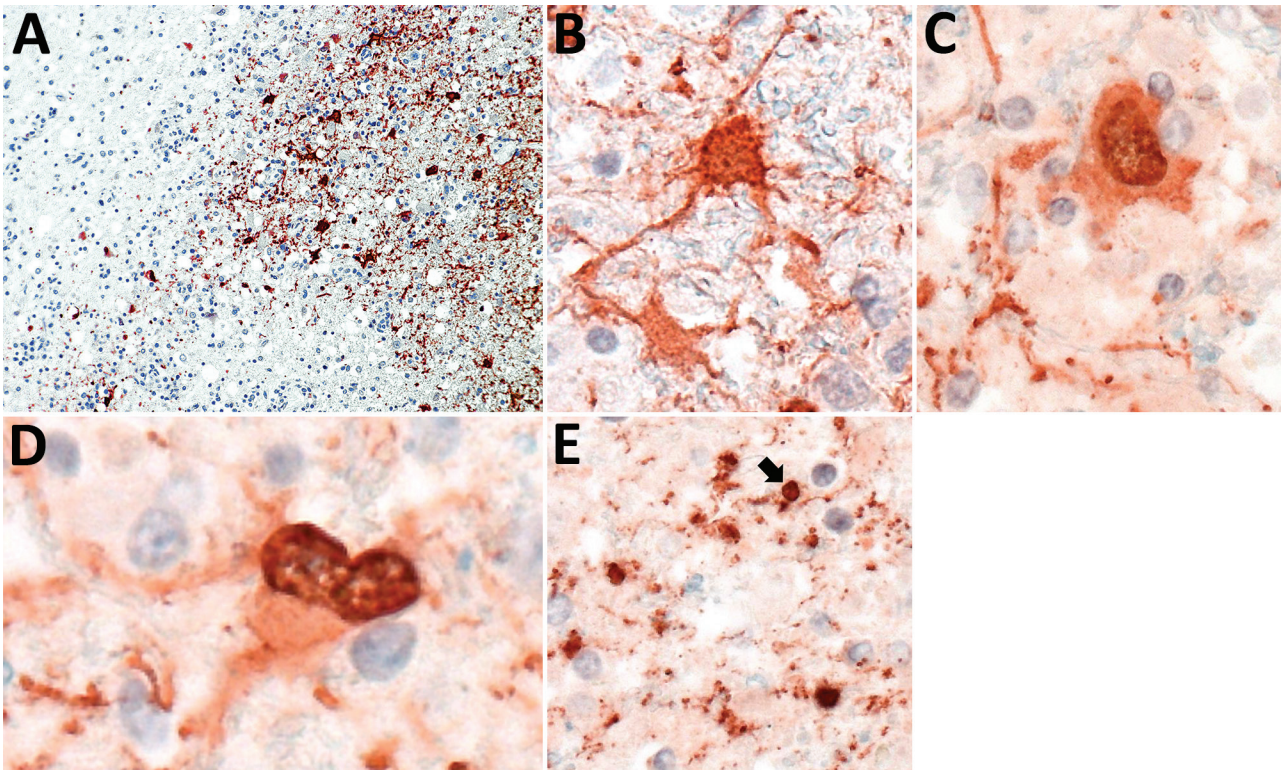

Figure 3. Presence of variegated squirrel bornavirus 1 (VSBV-1) antigen in neurons, astrocytes, and oligodendrocytes. A) Widespread presence of VSBV-1 antigen in brain tissue. Endothelial cells show no viral antigen. Immunoperoxidase stain with hematoxylin counterstain; original magnification ×200. B, C) Demonstration of VSBV-1 antigen in neurons. Immunoperoxidase stain with hematoxylin counterstain; original magnification ×600. D) VSBV-1 antigen in an astrocyte. Immunoperoxidase stain with hematoxylin counterstain; riginal magnification ×600. E) VSBV-1 antigen in an oligodendrocyte (arrow). Immunoperoxidase stain with hematoxylin counterstain; original magnification ×600.

Discussion

In this study, we analyzed VSBV-1 distribution in the brains of human patients. We focused on the local immune response in brain tissue, as well as CSF reactions during infection. We broadly expanded previously published scarce general histologic descriptions of fatal human VSBV-1 infection and initial CSF laboratory findings.

In patients 1–3, we found VSBV-1 RNA in all brain regions that were available: cerebral cortex, basal ganglia, hippocampus, midbrain, cerebellum, and olfactory bulb. In patient 4, VSBV-1 RNA has been shown in the limbic system, basal ganglia, and cerebellum, but not in the cerebral cortex (*2*). The highest viral loads were found in midbrain regions, hippocampus, and temporal cortex, whereas the lowest viral loads were seen in the cerebellum. These findings are in line with previous findings for natural and experimental infections of animals with BoDV-1 (*5*,*6*). Viral loads in our study were determined by quantitative real-time RT-PCR from FFPE sections known to have higher cycle thresholds than native samples because of the formalin fixation. In addition to tissue, CSF has been shown to be RT-PCR positive in patients from whom CSF had been stored (patients 3 [*1*] and 4 [*2*]). In concordance with previous results of patients 1 (*1*) (biopsy only) and 4 (*2*) (different brain regions), we showed that viral nucleic acid could be demonstrated in every brain area that was also positive for viral antigen by IHC in all patients. This finding also fits with the simultaneous detection in animals experimentally or naturally infected with BoDV-1. Patients with cerebral cortex infection as shown by RT-PCR and IHC analysis had myoclonus (patients 1 and 2), and those with cerebellar and basal ganglia infection showed ataxia (patients 2–4). In none of the patients was viral RNA or antigen detected in the internal organs. This finding does not exclude an infection of other organs that could not be analyzed in our study. However, experimental infection of immunocompetent rats is also strictly neurotropic and did not result in any peripheral organ spread of BoDV-1 (*7*,*8*).

For unknown reasons, all patients had initial abdominal and later respiratory signs or symptoms. Involvement of the peripheral nervous system, which we did not examine because of lack of preserved material, could be possible. The only cranial nerve available for analysis, the olfactory bulb of patient 3, was positive for viral RNA and antigen. Whether the infection of the olfactory bulb implies a potential intranasal entry route or resulted

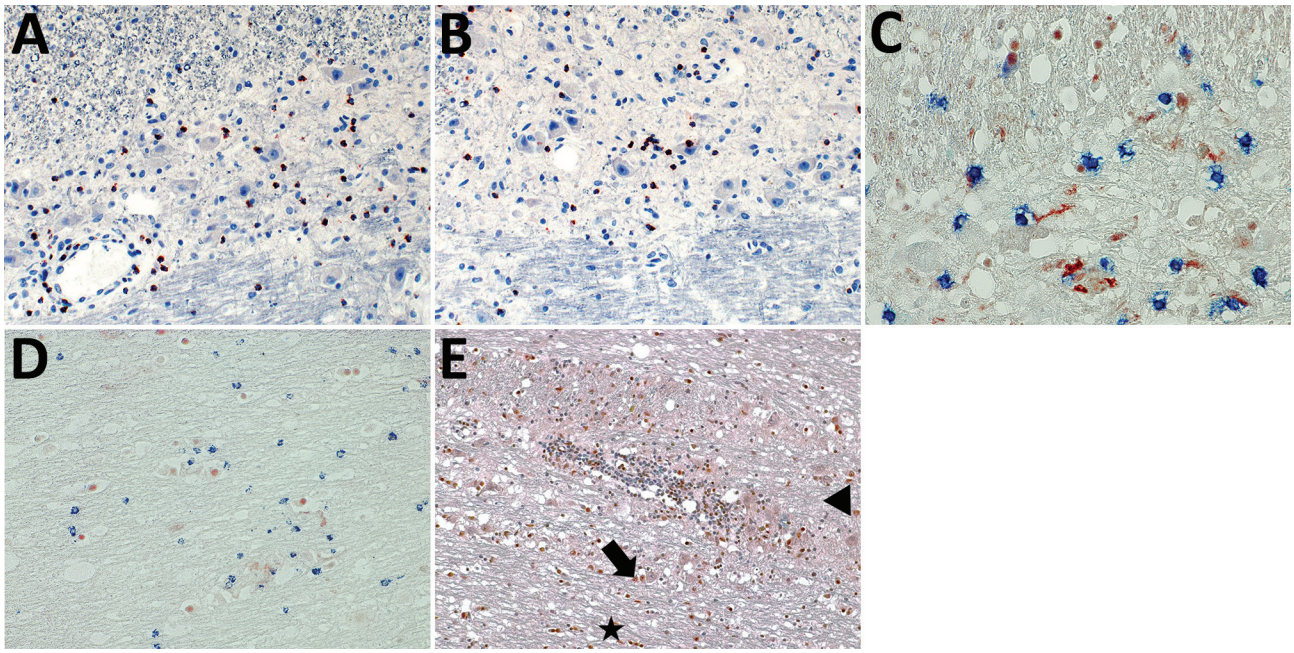

Figure 4. Induction of apoptosis in brain cells through association with granzyme B+/CD8+ cells, formation of cleaved caspase 3 and p53 up-regulation. A, B) Granzyme B+ cells in association with neurons and astrocytes during variegated squirrel bornavirus 1 infection. Immunoperoxidase stain with hematoxylin counterstain; original magnification ×400. C) Demonstration of brain cell apoptosis by shrinkage and positivity for cleaved caspase 3 (red) in close contact with CD8+ T cells (blue). Immunoperoxidase and immunophosphatase stains; original magnification ×600. D) Apoptotic cells positive for cleaved caspase 3 (red) in spatial association with granzyme B+ cytotoxic cells (blue). Immunoperoxidase and immunophosphatase stains; original magnification ×400. E) Widespread positivity for the p53 protein. Marked staining of perivascular mononuclear inflammatory cells, neurons (arrow), astrocytes (arrowhead), and rod cells (star) is shown. Immunoperoxidase stain with hematoxylin counterstain; original magnification ×200.

from centrifugal spread of VSBV-1 from the brain remains unclear.

The histologic features of VSBV-1 infection of the brain in the 4 patients consisted of multifocal malacia, edema, inflammatory perivascular, and parenchymal cell infiltration, as well as strong microglial and astroglial activation. The enlarged astrocytes seen in our study resemble the bizarre appearance of astrocytes in JC virus–induced progressive multifocal leukencephalopathy cases where they tend to undergo apoptosis and might be misdiagnosed as tumor cells (*9*). The inflammatory infiltrates in the brain parenchyma of the VSBV-1 encephalitis patients mainly consisted of CD4+ and CD8+ T cells, accompanied by neutrophils and macrophages, and a few B cells. The pronounced infiltration by CD8+ T cells and the close association of CD8+ T cells with neuronal cells and granzyme B+ cells with astrocytes are signs of a prominent cytotoxic response of the human immune system to the VSBV-1 infection. Orthobornaviruses cause nonlytic infections of CNS cells; clinical disease and histopathologic lesions in animals after infection with BoDV-1 are caused by a T-cell–mediated immunopathology and not by the viral replication itself (*10*–*12*). The presence of CD4+ and CD8+ T cells were already demonstrated in horses naturally infected with BoDV-1 (*12*) and in experimentally infected rats and mice (*8*,*13*–*16*). In horses and rats, CD4+ cells dominated the perivascular inflammatory infiltrates, and CD8+ T cells were found in parenchymal infiltrates. In our study of human VSBV-1 infections, we did not observe this effect; rather, CD4+ and CD8+ cells were equally distributed around blood vessels and in the brain parenchyma. Such effects, however, might be due to different time points of histologic examination as horses and experimental animals are euthanized early in the course of disease. Similar to findings for equine BoDV-1 infections (*15*), a predominance of CD3+ cells and rarity of neutrophils and B cells in the parenchymal infiltrates was seen in the human VSBV-1 infections.

The hypothesis of a T-cell–mediated immunopathogenesis causing clinical signs and symptoms during human VSBV-1 infection is highlighted by the detection of CC3- and TUNEL-positive cells as apoptotic markers in close association with the infiltrating cytotoxic immune cells. Caspase 3 is a member of the cysteine protease family and, in its activated cleaved form, CC3, a key mediator of neuronal apoptosis. CC3 is affected by both the cell surface receptor-mediated and the mitochondrial apoptosis pathways and thus plays an important role in the final common pathway of apoptosis (*17*,*18*). In neonatal rats infected with BoDV-1, hippocampal caspase 3 activation has been observed (*19*), and neuronal apoptosis has been

shown in the neocortex, hippocampus, and cerebellum (*20*). However, these animals were immune incompetent at the time of infection. Caspase 3 inhibitors were experimentally neuroprotective in rodents during cerebral ischemia and necrosis (*18*,*21*) but are not licensed as medical therapeutics. Caspase inhibitors repressed apoptosis in a BoDV-1–infected nonneuronal cell line but could not block viral transcription (*22*). For experimental BoDV-1 infections in rodents, infected neurons were not lysed by cytotoxic T cells (*6*,*23*). Thus, further investigation is needed on whether the immunopathologic mechanisms during human VSBV-1 infection differ from those observed in animal BoDV-1 infection or might instead result from a potential proinflammatory state of the CNS. A longer duration of inflammation and clinical disease in human infections also could be a reason. The observed p53 up-regulation in our study seems to be associated with the inflammatory process, but whether this represents an enhancement of the aforementioned apoptotic processes or is a beneficial event remains to be elucidated. For BoDV-1, the viral phosphoprotein can interfere with p53 indirectly through host HMBG1 and it was therefore suggested that BoDV-1 inhibits p53 activity (*24*). Viral interference with the p53 system in the CNS is also seen in JC virus infections (*25*); however, the proliferation marker Ki67 that is overexpressed in progressive multifocal leukencephalopathy (*26*) was only sparsely demonstrated in our study.

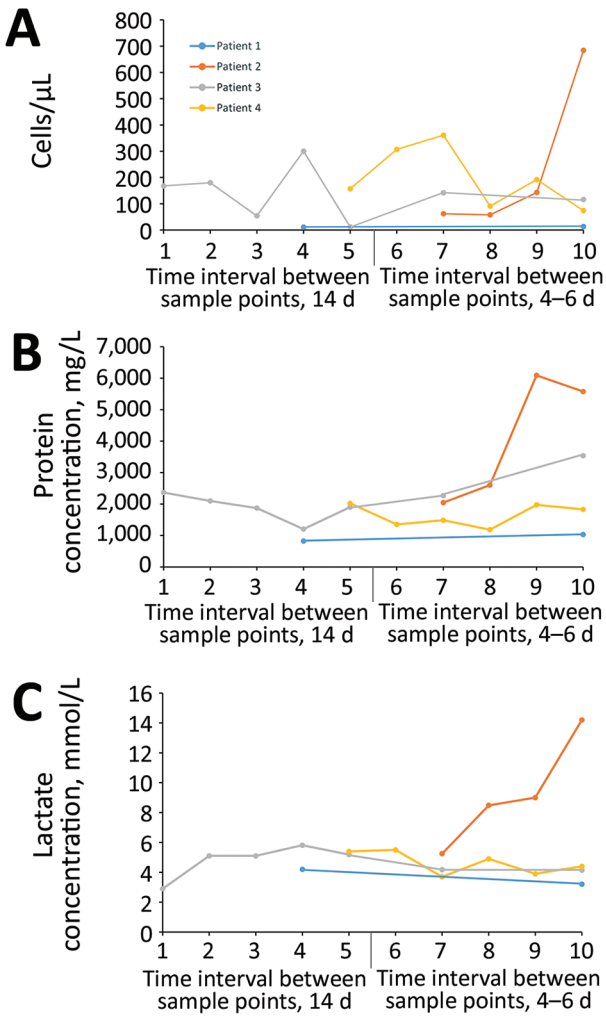

Figure 5. Cerebrospinal fluid (CSF) parameter changes over time during human infection with variegated squirrel bornavirus 1 (VSBV-1) encephalitis. CSF analyses were performed at different time intervals (every 14 days or every 4–6 days) because the patients were seen in different hospitals. Patients had different durations of the disease (2–4 months), including a nonspecific prodromal phase during which no lumbar puncture was performed. A) Changes in CSF cell counts during the course of disease. An undulating lymphocytic pleocytosis is seen in patients 3 and 4, whereas in patient 1 only a mild cell count elevation is visible. In contrast, patient 2 shows a very prominent cell increase. B) Constantly increasing CSF protein levels during infection. A marked increase is demonstrated for patient 2. C) Lactate concentration changes in the CSF. Although pathologic levels decreased slowly over time in patients 1, 3, and 4, levels in patient 2 increased prominently.

The CSF changes in the patients in our study (lymphocytic pleocytosis, protein elevation, blood–brain barrier dysfunction, and local antibody production) are typical for a viral infection of the CNS. The lactate concentration elevations in the CSF of all patients are most likely reflecting the severe inflammation and necrosis. Especially in patient 2, the person with the most severe histologic changes (inflammation and presence of viral antigen) and the shortest duration of disease (2 months vs. a 3- to 4-month course of disease in the other patients), the prominent increases of lactate levels, protein concentrations, and cell counts that were seen over time may serve as a marker for a rapid VSBV-1 disease progression. This patient also had the most medical preconditions and the highest viral load in central brain areas. In the other patients, the protein concentration elevations were paralleled by a rather moderate pleocytosis. All patients showed markedly elevated CSF protein levels that further increased over time and intrathecal antibody production. In patient 4, the specificity of such CSF IgG antibodies for VSBV-1 was demonstrated recently (*2*).

In conclusion, our results strongly demonstrate a severe inflammatory response pointing toward a T-cell–mediated immunopathology in human VSBV-1 infection. This process involves immune cells also seen in BoDV-1–associated lesions in natural and experimental infection, accompanied by evidence of brain cell apoptosis. A rapid clinical course in 1 patient could be linked to higher viral load and more severe inflammation.

This study was supported by the Federal Ministry of Education and Research within the Zoonotic Bornavirus Consortium (ZooBoCo), a project of the National Network of Zoonotic Infectious Diseases, Germany.

About the Author

Dr. Tappe is a clinical microbiologist and infectiologist at the National Reference Center for Tropical Pathogens, based at the Bernhard Nocht Institute, Hamburg. His research interests comprise the detection and epidemiology of new pathogens, the respective clinical disease, and immunology.

References

1. Hoffmann B, Tappe D, Höper D, Herden C, Boldt A, Mawrin C, et al. A variegated squirrel bornavirus associated with fatal human encephalitis. N Engl J Med. 2015;373:154–62. http://dx.doi.org/10.1056/NEJMoa1415627
2. Tappe D, Schlottau K, Cadar D, Hoffmann B, Balke L, Bewig B, et al. Occupation-associated fatal limbic encephalitis caused by variegated squirrel bornavirus 1, Germany, 2013. Emerg Infect Dis. 2018;24:978–87. http://dx.doi.org/10.3201/eid2406.172027
3. Schlottau K, Hoffmann B, Homeier-Bachmann T, Fast C, Ulrich RG, Beer M, et al. Multiple detection of zoonotic variegated squirrel bornavirus 1 RNA in different squirrel species suggests a possible unknown origin for the virus. Arch Virol. 2017;162: 2747–54. http://dx.doi.org/10.1007/s00705-017-3432-z
4. Schlottau K, Jenckel M, van den Brand J, Fast C, Herden C, Höper D, et al. Variegated squirrel bornavirus 1 in squirrels, Germany and the Netherlands. Emerg Infect Dis. 2017;23:477–81. http://dx.doi.org/10.3201/eid2303.161061
5. Carbone KM, Duchala CS, Griffin JW, Kincaid AL, Narayan O. Pathogenesis of Borna disease in rats: evidence that intra-axonal spread is the major route for virus dissemination and the determinant for disease incubation. J Virol. 1987;61:3431–40.
6. Herden C, Herzog S, Richt JA, Nesseler A, Christ M, Failing K, et al. Distribution of Borna disease virus in the brain of rats infected with an obesity-inducing virus strain. Brain Pathol. 2000; 10:39–48. http://dx.doi.org/10.1111/j.1750-3639.2000.tb00241.x
7. Ludlow M, Kortekaas J, Herden C, Hoffmann B, Tappe D, Trebst C, et al. Neurotropic virus infections as the cause of immediate and delayed neuropathology. Acta Neuropathol. 2016;131:159–84. http://dx.doi.org/10.1007/s00401-015-1511-3
8. Stitz L, Bilzer T, Planz O. The immunopathogenesis of Borna disease virus infection. Front Biosci. 2002;7:d541–55. http://dx.doi.org/10.2741/A793
9. Berger JR, Aksamit AJ, Clifford DB, Davis L, Koralnik IJ, Sejvar JJ, et al. PML diagnostic criteria: consensus statement from the AAN Neuroinfectious Disease Section. Neurology. 2013; 80:1430–8. http://dx.doi.org/10.1212/WNL.0b013e31828c2fa1
10. Lipkin WI, Briese T, Hornig M. Borna disease virus—fact and fantasy. Virus Res. 2011;162:162–72. http://dx.doi.org/10.1016/j.virusres.2011.09.036
11. Tizard I, Ball J, Stoica G, Payne S. The pathogenesis of bornaviral diseases in mammals. Anim Health Res Rev. 2016;17:92–109. http://dx.doi.org/10.1017/S1466252316000062
12. Rott R, Herzog S, Richt J, Stitz L. Immune-mediated pathogenesis of Borna disease. Zentralbl Bakteriol Mikrobiol Hyg [A]. 1988; 270:295–301. http://dx.doi.org/10.1016/S0176-6724(88)80166-4
13. Kramer K, Schaudien D, Eisel UL, Herzog S, Richt JA, Baumgärtner W, et al. TNF-overexpression in Borna disease virus-infected mouse brains triggers inflammatory reaction and epileptic seizures. PLoS One. 2012;7:e41476. http://dx.doi.org/10.1371/journal.pone.0041476
14. Bilzer T, Planz O, Lipkin WI, Stitz L. Presence of CD4+ and CD8+ T cells and expression of MHC class I and MHC class II antigen in horses with Borna disease virus-induced encephalitis. Brain Pathol. 1995;5:223–30. http://dx.doi.org/10.1111/j.1750-3639.1995.tb00598.x
15. Caplazi P, Ehrensperger F. Spontaneous Borna disease in sheep and horses: immunophenotyping of inflammatory cells and detection of MHC-I and MHC-II antigen expression in Borna encephalitis lesions. Vet Immunol Immunopathol. 1998;61:203–20. http://dx.doi.org/10.1016/S0165-2427(97)00128-1
16. Hausmann J, Hallensleben W, de la Torre JC, Pagenstecher A, Zimmermann C, Pircher H, et al. T cell ignorance in mice to Borna disease virus can be overcome by peripheral expression of the viral nucleoprotein. Proc Natl Acad Sci U S A. 1999;96: 9769–74. http://dx.doi.org/10.1073/pnas.96.17.9769
17. Khan S, Ahmad K, Alshammari EM, Adnan M, Baig MH, Lohani M, Somvanshi P, Haque S. Implication of caspase-3 as a common therapeutic target for multineurodegenerative disorders and its inhibition using nonpeptidyl natural compounds. Biomed Res Int. 2015;2015:379817.
18. Sun Y, Xu Y, Geng L. Caspase-3 inhibitor prevents the apoptosis of brain tissue in rats with acute cerebral infarction. Exp Ther Med. 2015;10:133–8. http://dx.doi.org/10.3892/etm.2015.2462
19. Williams BL, Hornig M, Yaddanapudi K, Lipkin WI. Hippocampal poly(ADP-Ribose) polymerase 1 and caspase 3 activation in neonatal bornavirus infection. J Virol. 2008;82:1748–58. http://dx.doi.org/10.1128/JVI.02014-07
20. Weissenböck H, Hornig M, Hickey WF, Lipkin WI. Microglial activation and neuronal apoptosis in bornavirus infected neonatal Lewis rats. Brain Pathol. 2000;10:260–72. http://dx.doi.org/10.1111/j.1750-3639.2000.tb00259.x
21. Han BH, Xu D, Choi J, Han Y, Xanthoudakis S, Roy S, et al. Selective, reversible caspase-3 inhibitor is neuroprotective and reveals distinct pathways of cell death after neonatal hypoxic-ischemic brain injury. J Biol Chem. 2002;277:30128–36. http://dx.doi.org/10.1074/jbc.M202931200
22. Mizutani T, Inagaki H, Tada M, Hayasaka D, Murphy M, Fujiwara T, et al. The mechanism of actinomycin D-mediated increase of Borna disease virus (BDV) RNA in cells persistently infected by BDV. Microbiol Immunol. 2000;44:597–603. http://dx.doi.org/10.1111/j.1348-0421.2000.tb02539.x
23. Hausmann J, Schamel K, Staeheli P. CD8(+) T lymphocytes mediate Borna disease virus-induced immunopathology independently of perforin. J Virol. 2001;75:10460–6. http://dx.doi.org/10.1128/JVI.75.21.10460-10466.2001
24. Zhang G, Kobayashi T, Kamitani W, Komoto S, Yamashita M, Baba S, et al. Borna disease virus phosphoprotein represses p53-mediated transcriptional activity by interference with HMGB1. J Virol. 2003;77:12243–51. http://dx.doi.org/10.1128/JVI.77.22.12243-12251.2003
25. Delbue S, Comar M, Ferrante P. Review on the role of the human polyomavirus JC in the development of tumors. Infect Agent Cancer. 2017;12:10. http://dx.doi.org/10.1186/s13027-017-0122-0
26. Ariza A, Mate JL, Isamat M, Calatrava A, Fernández-Vasalo A, Navas-Palacios JJ. Overexpression of Ki-67 and cyclins A and B1 in JC virus-infected cells of progressive multifocal leukoencephalopathy. J Neuropathol Exp Neurol. 1998;57:226–30. http://dx.doi.org/10.1097/00005072-199803000-00003

Address for correspondence: Dennis Tappe, Bernhard Nocht Institute for Tropical Medicine, Bernhard-Nocht-Str. 74, 20359 Hamburg, Germany; email: tappe@bnitm.de

Epidemiologic and Clinical Features of Lassa Fever Outbreak in Nigeria, January 1–May 6, 2018

Elsie A. Ilori,[1] Yuki Furuse,[1] Oladipupo B. Ipadeola,[1] Chioma C. Dan-Nwafor,[1] Anwar Abubakar, Oboma E. Womi-Eteng, Ephraim Ogbaini-Emovon, Sylvanus Okogbenin, Uche Unigwe, Emeka Ogah, Olufemi Ayodeji, Chukwuyem Abejegah, Ahmed A. Liasu, Emmanuel O. Musa, Solomon F. Woldetsadik, Clement L.P. Lasuba, Wondimagegnehu Alemu, Chikwe Ihekweazu, Nigeria Lassa Fever National Response Team[2]

Medscape EDUCATION ACTIVITY

In support of improving patient care, this activity has been planned and implemented by Medscape, LLC and Emerging Infectious Diseases. Medscape, LLC is jointly accredited by the Accreditation Council for Continuing Medical Education (ACCME), the Accreditation Council for Pharmacy Education (ACPE), and the American Nurses Credentialing Center (ANCC), to provide continuing education for the healthcare team.

Medscape, LLC designates this Journal-based CME activity for a maximum of 1.00 ***AMA PRA Category 1 Credit(s)***™. Physicians should claim only the credit commensurate with the extent of their participation in the activity.

Successful completion of this CME activity, which includes participation in the evaluation component, enables the participant to earn up to 1.0 MOC points in the American Board of Internal Medicine's (ABIM) Maintenance of Certification (MOC) program. Participants will earn MOC points equivalent to the amount of CME credits claimed for the activity. It is the CME activity provider's responsibility to submit participant completion information to ACCME for the purpose of granting ABIM MOC credit.

All other clinicians completing this activity will be issued a certificate of participation. To participate in this journal CME activity: (1) review the learning objectives and author disclosures; (2) study the education content; (3) take the post-test with a 75% minimum passing score and complete the evaluation at http://www.medscape.org/journal/eid; and (4) view/print certificate. For CME questions, see page 1260.

Release date: May 17, 2019; Expiration date: May 17, 2020

Learning Objectives

Upon completion of this activity, participants will be able to:

- Describe epidemiological characteristics of the Lassa fever (LF) outbreak between January 1, 2018, and May 6, 2018, in Nigeria
- Determine clinical characteristics and mortality in the LF outbreak between January 1, 2018, and May 6, 2018, in Nigeria
- Explain factors associated with mortality in the LF outbreak between January 1, 2018, and May 6, 2018, in Nigeria.

CME Editor

Jude Rutledge, BA, Technical Writer/Editor, Emerging Infectious Diseases. *Disclosure: Jude Rutledge has disclosed no relevant financial relationships.*

CME Author

Laurie Barclay, MD, freelance writer and reviewer, Medscape, LLC. *Disclosure: Laurie Barclay, MD, has disclosed no relevant financial relationships.*

Authors

Disclosures: ***Elsie Ilori, MSc; Yuki Furuse, MD, PhD; Oladipupo Ipadeola, MPH; Chioma Dan-Nwafor, MPH; Michael Onoja Amedu, MSC; Akanimo Iniobong, BSc; Ayodele Adeyemo, BTech; Anwar Abubakar, BS; Saliu Oladele, MBA; Esther Namukose Muwanguzi, DVM, MPH; Tanyth de Gooyer, PhD, MPhil (Appl.Epi), MPH; Oboma Eteng Womi-Eteng, MSc; Samuel Kitgakka Mutbam, MD, MPH; Emmanuel Onuche Musa, MD, MPH; Solomon F. Woldetsadik, MD; Lugala Peter Clement, MBBS, MPH; Wondimagegnehu Alemu, MD, MPH&TM, FAIPH;*** *and* ***Chikwe Ihekweazu, MBBS, MPH, FFPH,*** *have disclosed no relevant financial relationships.*

Author affiliations: Nigeria Centre for Disease Control, Abuja, Nigeria (E.A. Ilori, O.B. Ipadeola, C.C. Dan-Nwafor, A. Abubakar, O.E. Womi-Eteng, C. Ihekweazu); Kyoto University, Kyoto, Japan (Y. Furuse); World Health Organization, Abuja (Y. Furuse, E.O. Musa, S.F. Woldetsadik, C.L.P. Lasuba, W. Alemu); US Centers for Disease Control and Prevention, Abuja (O.B. Ipadeola); African Field Epidemiology Network, Abuja (C.C. Dan-Nwafor); Irrua Specialist Teaching Hospital, Irrua, Nigeria (E. Ogbaini-Emovon, S. Okogbenin); Federal Teaching Hospital, Abakaliki, Nigeria (U. Unigwe, E. Ogah); Federal Medical Centre, Owo, Nigeria (O. Ayodeji, C. Abejegah, A.A. Liasu)

DOI: https://doi.org/10.3201/eid2506.181035

[1]These first authors contributed equally to this article.

[2]Other members of the Nigeria Lassa Fever National Response Team are listed at the end of this article.

Lassa fever (LF) is endemic to Nigeria, where the disease causes substantial rates of illness and death. In this article, we report an analysis of the epidemiologic and clinical aspects of the LF outbreak that occurred in Nigeria during January 1–May 6, 2018. A total of 1,893 cases were reported; 423 were laboratory-confirmed cases, among which 106 deaths were recorded (case-fatality rate 25.1%). Among all confirmed cases, 37 occurred in healthcare workers. The secondary attack rate among 5,001 contacts was 0.56%. Most (80.6%) confirmed cases were reported from 3 states (Edo, Ondo, and Ebonyi). Fatal outcomes were significantly associated with being elderly; no administration of ribavirin; and the presence of a cough, hemorrhaging, and unconsciousness. The findings in this study should lead to further LF research and provide guidance to those preparing to respond to future outbreaks.

Lassa fever (LF) is a febrile infectious disease caused by Lassa virus. The disease was first described in Nigeria in 1969 (*1*). Rodents, particularly *Mastomys natalensis*, are considered the natural hosts of the virus (*2*). The disease is mainly spread to humans through contamination with the urine or feces of infected rats (*3*,*4*). Human-to-human transmission can occur through contact with the body fluids of infected persons; therefore, healthcare workers (HCWs) are at high risk for infection when the standard precautions for infection prevention and control are inadequate (*5*,*6*). The incubation period of the disease is 3–21 days. The clinical manifestation of the disease is nonspecific and includes fever, fatigue, hemorrhaging, gastrointestinal symptoms (vomiting, diarrhea, and stomachache), respiratory symptoms (cough, chest pain, and dyspnea), and neurologic symptoms (disorientation, seizures, and unconsciousness) (*3*). The observed case-fatality rate (CFR) among patients hospitalized for severe LF is 15%–50% (*7*,*8*). However, ≈80% of infections are considered to cause mild or no symptoms in humans and are undiagnosed (*8*).

In Nigeria, laboratory-confirmed LF patients are treated in isolation units, according to national guidelines, to prevent community and nosocomial human-to-human infections (*9*). The country has 3 main LF treatment centers: the Irrua Specialist Teaching Hospital (Edo State), the Federal Medical Centre Owo (Ondo State), and the Federal Teaching Hospital Abakaliki (Ebonyi State) (*10*). Isolation units are also located in tertiary-care centers in other states. Ribavirin has been shown to reduce the CFR for LF (*11*); Nigeria national guidelines recommend that parenteral ribavirin be administered over a 10-day period for patients with confirmed LF (*9*).

Lassa fever is endemic to the West Africa countries of Benin, Ghana, Guinea, Liberia, Mali, Sierra Leone, and Nigeria (*7*); an estimated 300,000 LF cases occur each year in this region, resulting in ≈5,000 deaths (*8*). The annual peak of LF cases in Nigeria is observed in the dry season (December–April), and the number decreases around May (*3*). The increased likelihood of humans encountering *Mastomys* rodents and their excreta inside houses during the dry season (when these animals are seeking food) is thought to play a role in the seasonality of disease incidence (*12*). Transmission risk might be exacerbated by enhanced survival of the virus at decreased relative humidity (*13*).

During 2014–2016, around 100 laboratory-confirmed LF cases were reported annually in Nigeria (*14*,*15*). From the end of 2017 through May 2018, the country experienced its largest recorded LF outbreak. On January 22, 2018, the Nigeria Centre for Disease Control (NCDC) activated its Emergency Operations Centre to coordinate the outbreak response (*16*). During January 1–May 6, 2018, a total of 423 laboratory-confirmed cases were reported (*17*). On May 10, 2018, NCDC announced the end of the emergency phase of the outbreak because the LF case count had consistently declined in the preceding 6 weeks and had dropped below levels considered to be a national emergency, based on historical trends in LF incidence (*10*). Here we describe the epidemiologic and clinical aspects of this LF outbreak.

Methods

Ethics Considerations

This investigation was performed as a part of the LF public health response in Nigeria in 2018. The investigation was not considered to be research on human subjects, as per the US Department of Health and Human Services' Federal Policy for the Protection of Human Subjects (*18*).

Case Definition and Laboratory Confirmation

A suspected case of LF was defined as illness meeting 1 of the following criteria: 1) ≥1 signs/symptoms (e.g., malaise, fever, headache, sore throat, cough, nausea, vomiting, diarrhea, myalgia, central chest pain or retrosternal pain, and hearing loss) and a history of contact with excreta or urine of rodents; 2) ≥1 signs/symptoms and a history of contact with a person with probable or confirmed LF within 21 days of symptom onset; or 3) inexplicable bleeding or hemorrhaging (*9*). Probable LF cases were defined as any suspected case in a patient who died without the collection of a specimen for laboratory testing (*9*). Confirmed LF cases were defined as any suspected case with a laboratory confirmation (positive for IgM antibody, reverse transcription PCR [RT-PCR], or virus isolation) (*9*).

During the study period, blood samples from patients with suspected cases were sent to 1 of 4 laboratories: the Central Research Laboratory at College of Medicine of the University of Lagos–Lagos University Teaching Hospital (Lagos State), the Federal Teaching Hospital Abakaliki (Ebonyi State), the Institute of Lassa Fever Research and Control at the Irrua Specialist Teaching Hospital (Edo

State), or the National Reference Laboratory (Federal Capital Territory). Laboratory confirmation was performed by using RT-PCR by means of the RealStar Lassa Virus RT-PCR Kit (Altona Diagnostics, https://www.altona-diagnostics.com), the LF diagnosis protocol developed by Nikisins et al. (*19*), or both. More than 95% of samples were tested by using both protocols to ensure greater sensitivity for the heterogeneous Lassa virus in Nigeria (*20*). A positive result in either or both of the protocols was regarded as positive for LF.

Contact Tracing

Persons who had contact with patients with confirmed LF were recorded and followed up daily for 21 days by Disease Surveillance and Notification Officers (DSNOs). If contacts had symptoms, blood samples were collected and tested for LF as described.

Data Collection and Report

All suspected LF cases were immediately reported to the DSNO for each Local Government Area and the State Epidemiologist for each state by using a surveillance reporting form developed for integrated disease surveillance and response in Nigeria (*21*). Samples were collected and tested for all suspected cases as long as the case-patient was alive (*9*). If the test was positive, detailed demographic (age, sex, and residential address), clinical (symptoms, outcome, and administration of ribavirin), and epidemiologic (occupation, onset date, and exposure history) information were collected by using a national case investigation form (CIF). All suspected, probable, and confirmed cases were line listed, and the information in the CIFs was submitted weekly by the state epidemiologists to NCDC. A summary of the figures was published weekly in a situation report (*17*); the compiled reports of the outbreak are provided in the Appendix (https://wwwnc.cdc.gov/EID/article/25/6/18-1035-App1.pdf). The projected population figures of each state were obtained from a report based on data from the National Population Commission of Nigeria and the National Bureau of Statistics (*22*). Anonymized clinical and epidemiologic data of case-patients are available by request, contingent on the recipient agreeing to appropriate guidelines for their use.

Statistical Analyses

We conducted binomial logistic regression analyses to determine the age- and sex-adjusted odds ratio (aOR) among survived and deceased patients with laboratory-confirmed LF. Likewise, we used aORs to compare the presence of each symptom and the administration of ribavirin among these cases, adjusted for age and sex. We conducted the Mantel-Haenszel test to see the statistical trend of CFR through the outbreak. We conducted chi-square tests to detect the statistical difference in exposure history between HCWs and non-HCWs.

We performed statistical tests using SPSS version 24 (IBM, https://www.ibm.com). We computed 95% CIs and p values to test statistical significance and adjusted p values by the Bonferroni correction for multiple comparisons. A p value of <0.05 was considered statistically significant.

Results

During the study period (January 1–May 6, 2018), a total of 1,893 suspected LF cases were reported, including 10 probable cases and 423 laboratory-confirmed cases. The laboratory-confirmed cases were reported from 20 states and the Federal Capital Territory. Most (80.6%) of the laboratory-confirmed cases were reported from the 3 states with a dedicated LF treatment center: Edo (178 cases), Ondo (99 cases), and Ebonyi (64 cases) (Figure 1, panel A). LF incidence was highest in these 3 states (Table 1). Edo and Ondo also had the largest number of laboratory-negative suspected cases. The positive rate (i.e., the proportion of the number of laboratory-confirmed cases among all persons with suspected cases tested) was 22.5% (423/1,883) nationally, ranging from 3.4% (Lagos) to 70.0% (Delta). Among the 3 states with the highest number of cases, the positive rates were 16.5% (Edo), 31.6% (Ondo), and 69.6% (Ebonyi).

CFR among the laboratory-confirmed cases was 25.1% (106/423 [95% CI 20.9%–29.2%]). Among the 3 most affected states, CFR was 14.6% (Edo), 24.2% (Ondo), and 23.4% (Ebonyi) (Table 1). Among the 423 cases, a total of 414 CIFs with detailed information, including demographic information, onset date, symptoms, exposure history, and ribavirin administration, were collected (collection rate 97.9%). However, the data in some fields of the CIFs were incomplete. For example, the onset date was unknown in 2.4% (10/414) of cases, and symptom information was missing in 12.8% (53/414). An epidemic curve based on the onset date for laboratory-confirmed cases peaked at epidemiologic week 5 in 2018 (Figure 1, panel B). No statistically significant change was observed in the national CFR throughout the outbreak (p value for trend = 0.41).

We analyzed the age and sex distribution of the 414 patients with laboratory-confirmed cases (Table 2). Median age was 32 years (interquartile range 20–44 years); 157 (37.9%) were female and 257 (62.1%) male. CFR was lowest in children ≤10 years of age (11.1%) and highest in adults ≥61 years of age (38.2%); the aOR of fatal outcomes in the elderly group was 4.9 (95% CI 1.5–15.6) compared with children ≤10 years of age. Adults 41–60 years of age also had statistically higher CFRs compared with children ≤10 years of age (Table 2). CFR was higher for male patients (26.6%) than female patients (21.8%) but was not significantly different;

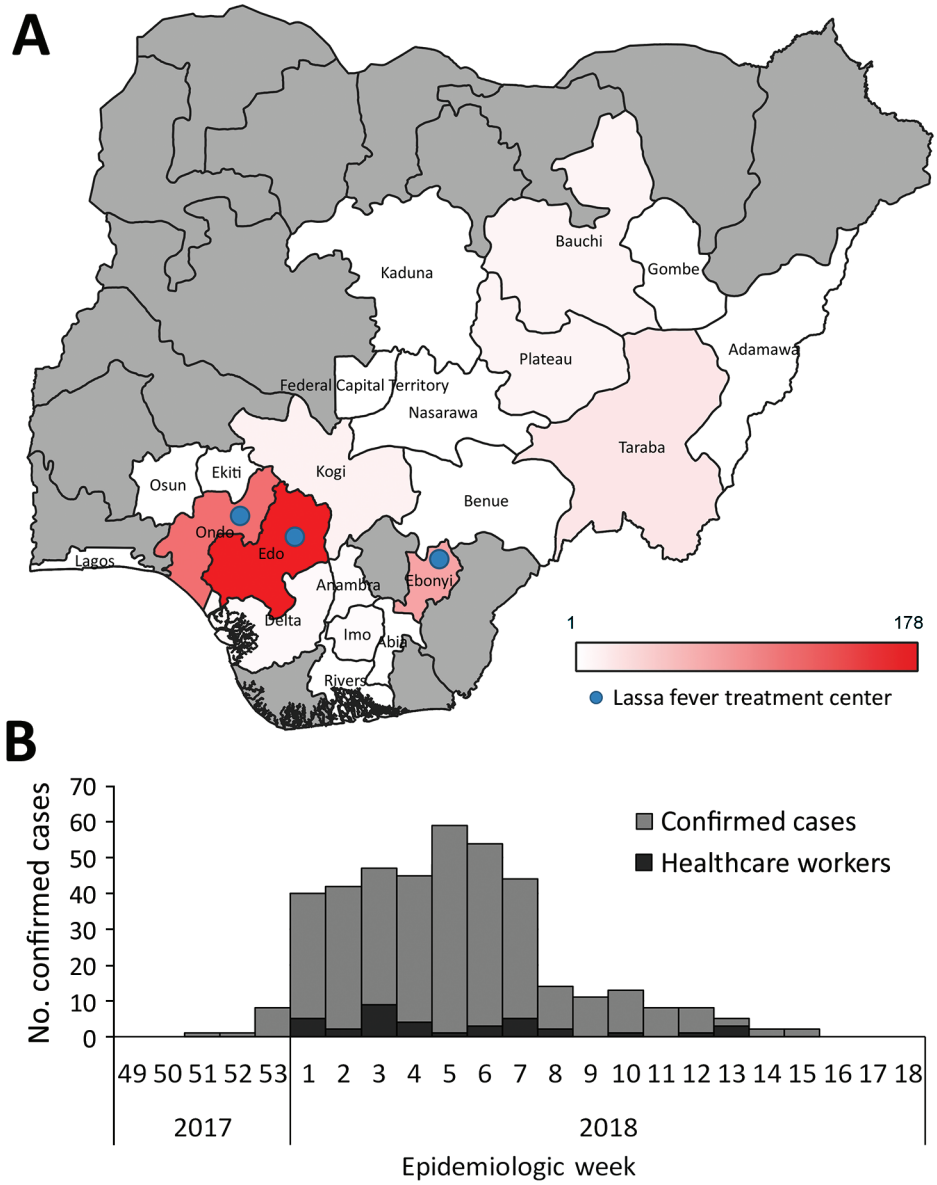

Figure 1. Geographic and temporal distribution of laboratory-confirmed Lassa fever cases, Nigeria, January 1–May 6, 2018. A) Geographic distribution of laboratory-confirmed cases by state. Gray shading indicates states reporting no laboratory-confirmed cases. Locations of Lassa fever treatment centers are indicated. B) Epidemic curve of laboratory-confirmed Lassa fever cases. Epidemiologic week numbers are based on the date of symptom onset.

the aOR of fatal outcomes in male patients compared with female patients was 1.3 (95% CI 0.81–2.1).

The most common signs and symptoms among patients with laboratory-confirmed LF were fever (96.4%, 348/361), headache (58.7%, 210/358), vomiting (49.4%, 177/358), fatigue (43.3%, 155/358), and abdominal pain (40.2%, 144/358) (Table 3). Hemorrhaging was observed in 17.0% (61/358) of these patients. Cough (p = 0.0050), hemorrhaging (p<0.001), and unconsciousness (p = 0.0018) were significantly more prevalent in fatal than nonfatal cases.

During the 3 weeks before symptom onset, 17.7% (62/350) of case-patients reported contact with patients who had known suspected or confirmed LF, 17.0% (56/330) reported contact with rodents or their urine or feces, and 2.9% (9/315) reported attendance at a burial ceremony (Figure 2, panel A). During the study period, 5,012 persons were determined to have had contact with confirmed case-patients; follow-up was conducted for 5,001 of them. During the 21-day follow-up period, 81 contacts experienced onset of symptoms, and 28 were found to have laboratory-confirmed LF. The positive rate among symptomatic contacts was 34.6% (28/81), and the secondary attack rate was 0.56% (28/5,001; 95% CI 0.35%–0.77%).

During the study period, 37 HCWs were infected, resulting in 8 deaths (CFR 21.6%). The incidence of HCW infections was distributed throughout the outbreak period (Figure 1, panel B). A significantly high proportion of HCWs (55.9%, 19/34) reported contact with patients with known suspected or confirmed LF compared with non-HCWs (p<0.001) (Figure 2, panel A).

Table 1. Number and incidence of Lassa fever cases, by state or territory, Nigeria, January 1–May 6, 2018

State or territory	Population, ×1,000*	No. confirmed cases (deaths)	Case-fatality rate, %	No. confirmed cases/100,000 population	No. laboratory-negative suspected cases	No. probable cases	Positive rate, %
Abia	3,727	1 (1)	100.0	0.027	11	1	8.3
Adamawa	4,248	1 (1)	100.0	0.024	2	1	33.3
Anambra	5,528	4 (2)	50.0	0.072	3	0	57.1
Bauchi	6,537	10 (5)	50.0	0.153	50	0	16.7
Benue	5,742	1 (1)	100.0	0.017	6	1	14.3
Delta	5,663	7 (3)	42.9	0.124	3	0	70.0
Ebonyi	2,880	64 (15)	23.4	2.222	28	4	69.6
Edo	4,236	178 (26)	14.6	4.202	901	0	16.5
Ekiti	3,271	2 (1)	50.0	0.061	10	0	16.7
Federal Capital Territory	3,564	3 (2)	66.7	0.084	38	0	7.3
Gombe	3,257	2 (2)	100.0	0.061	13	0	13.3
Imo	5,409	4 (1)	25.0	0.074	11	0	26.7
Kaduna	8,252	1 (1)	100.0	0.012	4	0	20.0
Kogi	4,474	11 (4)	36.4	0.246	15	2	42.3
Lagos	12,551	1 (1)	100.0	0.008	28	0	3.4
Nasarawa	2,523	3 (2)	66.7	0.119	34	0	8.1
Ondo	4,672	99 (24)	24.2	2.119	214	1	31.6
Osun	4,706	2 (1)	50.0	0.043	2	0	50.0
Plateau	4,200	9 (7)	77.8	0.214	39	0	18.8
Rivers	7,304	1 (1)	100.0	0.014	7	0	12.5
Taraba	3,067	19 (5)	26.3	0.620	41	0	31.7
Total	193,393	423 (106)	25.1	0.219	1,460	10	22.5

*Data source: National Bureau of Statistics (*22*).

Ribavirin was administered to 94.1% (334/355) of the patients with laboratory-confirmed cases. CFR for patients who received ribavirin was 20.7% (69/334), compared with 71.4% (15/21) for patients who did not receive ribavirin (Figure 2, panel B). We also analyzed the subset of patients who survived ≥7 days after symptom onset to account for the possible effect of the difference in clinical conditions. We further divided the patients who received ribavirin into 2 groups: patients who received the drug within 7 days after symptom onset and patients who received the drug after that point. Among case-patients who survived ≥7 days, CFR was significantly higher for patients who did not receive any ribavirin (66.7%, 12/18) compared with patients who received the drug ($p<0.01$), whether receipt of the drug occurred within 7 days of symptom onset or >7 days after onset (Figure 2, panel C). CFR was lower among patients who received the drug within 7 days of symptom onset (12.5%, 15/120) compared with patients who received the drug after that point (20.1%, 38/189), although this difference was not significant ($p = 0.095$). Because this reduction in CFR might have been attributable to not only ribavirin but also the other supportive treatments provided, the time between symptom onset date and the patient's arrival at a health facility was included in addition to age and administration of ribavirin as a covariable in the binomial logistic regression analysis for fatal outcomes. Although absence of ribavirin administration ($p<0.001$) and advanced age ($p = 0.025$) remained significant factors in fatal outcomes, delay in visiting health facility did not ($p = 0.19$).

Discussion

We describe the epidemiologic and clinical features of the LF outbreak in Nigeria during January 1–May 6, 2018. A total of 423 laboratory-confirmed cases were reported during the study period. Most of the laboratory-confirmed

Table 2. Distribution of age and sex among patients with laboratory-confirmed Lassa fever, Nigeria, January 1–May 6, 2018*

Characteristic	No. girls and women (deaths)	No. boys and men (deaths)	Total no. (deaths)	Case-fatality rate, %	aOR (95% CI)	p value
Age group, y						
0–10	19 (3)	26 (2)	45 (5)	11.1	Reference	
11–20	24 (4)	42 (10)	66 (14)	21.2	2.1 (0.71–6.4)	0.18
21–30	38 (5)	52 (13)	90 (18)	20.5	2.1 (0.71–6.0)	0.18
31–40	30 (7)	60 (16)	90 (23)	25.6	2.7 (0.95–7.6)	0.063
41–50	23 (5)	39 (15)	62 (20)	32.3	3.8 (1.3–11.0)	0.015
51–60	10 (4)	15 (4)	25 (8)	32.0	3.8 (1.1–13.2)	0.039
≥61	12 (5)	22 (8)	34 (13)	38.2	4.9 (1.5–15.6)	0.0074
Total	157 (34)	257 (68)	423 (106)			
Case-fatality rate, %	21.8	26.6				
aOR (95% CI)	Reference	1.3 (0.81–2.1)				
p value		0.26				

*aORs, 95% CIs, and p values calculated by using the binomial logistic regression model for fatal outcomes. Because information on age and sex was missing for some cases, the number of total cases is not equal to sum of the number of cases in all age groups. aOR, adjusted odds ratio.

Table 3. Prevalence of symptoms and outcomes among patients with laboratory-confirmed Lassa fever, Nigeria, January 1–May 6, 2018*

	Cases, % (no. positive/no. with data available)				
Sign/symptom	All cases	Fatal cases	Nonfatal cases	aOR (95% CI)	p value
Fever	96.4 (348/361)	97.8 (87/89)	96.3 (260/270)	1.5 (0.31–7.3)	1
Headache	58.7 (210/358)	64.0 (57/89)	56.6 (151/267)	1.4 (0.83–2.3)	1
Vomiting	49.4 (177/358)	56.2 (50/89)	47.6 (127/267)	1.5 (0.88–2.4)	1
Fatigue	43.3 (155/358)	55.1 (49/89)	39.7 (106/267)	1.5 (0.93–2.6)	1
Abdominal pain	40.2 (144/358)	49.4 (44/89)	37.1 (99/267)	1.7 (1.0–2.9)	0.68
Anorexia	33.0 (118/358)	39.3 (35/89)	31.1 (83/267)	1.4 (0.81–2.3)	1
Cough	30.4 (109/358)	46.1 (41/89)	25.5 (68/267)	2.6 (1.6–4.4)	0.0050
Diarrhea	26.8 (96/358)	39.3 (35/89)	22.8 (61/267)	2.2 (1.3–3.7)	0.068
Sore throat	22.1 (79/358)	32.6 (29/89)	18.7 (50/267)	2.0 (1.1–3.5)	0.33
Chest pain	21.3 (76/357)	26.1 (23/88)	19.9 (53/267)	1.4 (0.76–2.4)	1
Myalgia	18.5 (66/357)	28.4 (25/88)	15.0 (40/267)	2.1 (1.2–3.8)	0.28
Hemorrhaging	17.0 (61/358)	37.1 (33/89)	10.1 (27/267)	5.1 (2.8–9.3)	<0.001
Arthralgia	16.5 (59/357)	26.1 (23/88)	13.5 (36/267)	2.3 (1.2–4.3)	0.17
Dyspnea	14.8 (53/357)	25.0 (22/88)	11.6 (31/267)	2.6 (1.4–4.9)	0.061
Unconsciousness	4.8 (17/357)	13.6 (12/88)	1.9 (5/267)	9.4 (3.1–28.7)	0.0018
Conjunctivitis	4.5 (16/358)	6.7 (6/89)	3.7 (10/267)	2.1 (0.71–6.1)	1
Disorientation	4.2 (15/357)	8.0 (7/88)	3.0 (8/267)	2.8 (0.97–8.3)	1
Skin rash	3.6 (13/358)	6.7 (6/89)	2.6 (7/267)	3.0 (0.97–9.6)	1
Photophobia	3.4 (12/357)	6.8 (6/88)	2.2 (6/267)	3.0 (0.92–9.9)	1
Hiccup	2.5 (9/358)	6.7 (6/89)	1.1 (3/267)	6.6 (1.6–28.0)	0.22
Jaundice	2.2 (8/358)	4.5 (4/89)	1.5 (4/267)	3.7 (0.87–15.6)	1

*aORs and 95% CIs calculated by using a binomial logistic regression model for fatal outcomes adjusted for age and sex. p values calculated by using a binomial logistic regression model and adjusted by the Bonferroni correction. aOR, adjusted odds ratio.

cases were reported from the 3 states (Edo, Ondo, and Ebonyi) where dedicated LF treatment centers are located; disease incidence was also highest in these areas. However, the positive rate among suspected cases was not especially high for these 3 states. In addition to the high prevalence of LF in the areas, HCWs in these 3 states had a high suspicion of LF in patients with high-grade fevers, which might have led to increased testing. Conversely, suspicion of LF might be low in some areas other than these 3 states. Lack of LF expertise and diagnostic capacity in these other areas might have discouraged active detection of LF patients, leading to underreporting of the disease. Also, LF incidence and prevalence might actually be lower in some areas for epidemiologic and environmental reasons, such as low prevalence of the virus in rodents or good hygiene practices that help reduce contact between humans and rodents. To clarify different LF prevalence by areas, sensitization and strengthening of the surveillance system to detect suspected cases and obtain test samples are required, particularly in states other than Edo, Ondo, and Ebonyi. In addition, seroprevalence surveys and ecologic studies of LF in humans and rodents should give further insight on the actual burden of the disease.

We used 2 protocols for molecular diagnosis of LF to cover the heterogeneous Lassa virus in Nigeria (*20*), and we tested >95% of the samples by using both protocols during the outbreak. Further study is needed to reveal sensitivity and specificity of each protocol in this country. That

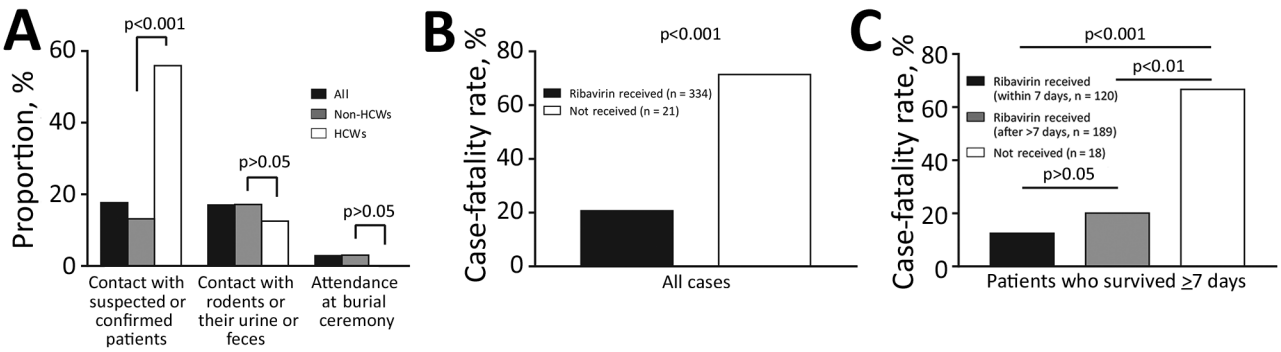

Figure 2. Exposure history and case-fatality rate among patients with laboratory-confirmed Lassa fever cases, Nigeria, January 1–May 6, 2018. A) Proportion of persons reporting Lassa fever exposure risks for all case-patients, HCWs, and non–HCWs. To assess differences in exposure risks between HCWs, and non–HCWs, p values were calculated by using the χ^2 test and adjusted by the Bonferroni correction. B) The case-fatality rate for case-patients who did or did not receive ribavirin. C) An investigation of the case-fatality rate in patients who survived ≥7 days after symptom onset. For panels B and C, p values were calculated by using binomial logistic regression analysis adjusted for age and sex and applying the Bonferroni correction. HCW, healthcare worker.

information would also give us further insight on genetic diversity of the virus in natural hosts in the country.

Although NCDC situation reports showed the peak of the outbreak at week 7 (*17*), our study found that the outbreak peaked at week 5. This difference occurred because the epidemic curve from the situation reports was based on the reporting date, whereas the epidemic curve in our study was based on symptom onset date. The difference can be explained by the time lag between symptom onset to health facility presentation and subsequent diagnosis and reporting. The median of the time lag between symptom onset to suspicion of LF was 7 days (interquartile range 4–11 days), and several additional days were required for a health facility to report through the DSNO for each Local Government Area and for the state epidemiologist in each state to report NCDC. Further strengthening of the surveillance system is required to shorten this time gap.

Girls and women accounted for a lower proportion of the laboratory-confirmed LF cases than boys and men (37.9% vs. 62.1%). Past studies have shown no or little difference in LF incidence between male and female patients (*23*–*25*). It is unclear whether the difference in this study came because men and boys were at higher risk for infection or more susceptible to the disease than women and girls or because ascertainment of cases in women and girls was low during this outbreak.

CFR among laboratory-confirmed cases during the study period was 25.1% and did not change substantially throughout the outbreak. CFR can reach 50% in hospitalized patients during epidemics (*8*), whereas the observed CFR among patients hospitalized with severe LF is 15% (*7*). CFR in this outbreak was especially high among elderly patients. Such difference in CFR among age groups was not observed in previous studies (*26*,*27*). The large number of cases in this outbreak might have increased the statistical power to detect the difference.

Gastroenteric symptoms, including vomiting, abdominal pain, and anorexia, were frequently observed among patients with laboratory-confirmed cases (>30%), whereas hemorrhaging was only observed in 17.0% of case-patients (Table 3). This observation is consistent with previous reports (*28*,*29*). Because some symptoms, such as cough, hemorrhaging, and unconsciousness, were more frequently observed for fatal cases than nonfatal cases, these symptoms might be predictors for fatal outcomes. Patients with such symptoms would require more attention to achieve better clinical outcomes.

Lassa virus is primarily transmitted to humans from rodents. The virus is also occasionally transmitted through the body fluids of infected persons (*3*). In this outbreak, ≈17% of patients reported a history of contact with rodents. A similar percentage reported contact with patients with suspected or confirmed LF. Because this information was obtained by patient interview, recall bias might have influenced the accuracy of exposure history. Although the secondary attack rate was as low as 0.56%, the positive rate for LF among person with suspected cases was higher for those who had contact with confirmed case-patients than that in the general population (34.6% vs. 22.5%). Contact tracing did not account for 34 LF patients, although they had reported contact with other confirmed or suspected case-patients. Some case-patients might have been targeted in the contact tracing whereas others were not because they reported contact with persons with suspected (but not confirmed) cases. Strengthening and expanding contact tracing is required but posed a challenge in resource-limited settings during the outbreak. A high rate of contact with suspected or confirmed LF case-patients among HCWs suggests the possibility of nosocomial infections, although we could not rule out another source of infection, such as rodents (*30*). Nevertheless, good infection prevention and control practices and readily available personal protective equipment are important to protect HCWs from infection with the virus (*5*,*6*).

The findings in this study support the effectiveness of ribavirin in reducing mortality rates from LF. CFR was lowest among patients who received treatment with ribavirin. Patients in severe conditions might have not received ribavirin because they died before reaching healthcare facilities where treatment was available; that is, the difference in CFRs between patients who did or did not receive ribavirin might be attributable not only to the ribavirin treatment but also to the patient's clinical condition before ribavirin administration (*6*,*28*). To explore this issue further, we analyzed a subset of patients who survived ≥7 days after symptom onset. The highest CFR was still observed among patients who did not receive ribavirin; CFR was lower even if provision of ribavirin was deferred to >7 days after symptom onset. Furthermore, the early commencement of ribavirin treatment reduced CFR compared with deferred administration of the drug, although this difference was not statistically significant. Therefore, the reduction in CFR was more likely attributable to ribavirin than to the other supportive treatments provided. These findings support Nigeria's national guidelines for clinical management of the disease, which advise that patient outcomes are more favorable when ribavirin treatment is commenced earlier (*9*).

This study has several limitations. Although we collected CIFs from 414 of the 423 patients with laboratory-confirmed cases, the data in some fields were incomplete. Availability of CIFs for patients with suspected cases whose laboratory tests were negative would have enabled us to conduct a case–control study to better determine the risk factors for the disease; however, collection of this information for 1,460 laboratory-negative suspected cases would have been burdensome to outbreak response staff. Also, our study did not provide any insights into why the 2018 LF outbreak was larger than those in previous years. Studies using viral genomic data have suggested that the outbreak

was not caused by ongoing human-to-human transmission from a single source but by multiple environmental sources (*31*). Better surveillance through increased availability of laboratory testing of suspected cases might have played a role in the larger number of laboratory-confirmed cases during this outbreak. Localized clusters, which were not investigated as part of this study, might have contributed to the inflation of case numbers in some areas.

LF is endemic in Nigeria. The LF surveillance data from Nigeria, even with their limitations, are arguably the best longitudinal data collected on LF globally. Although these data mostly relate to the 2018 outbreak, data collection has continued, and all aspects of surveillance are being continuously improved (e.g., educating HCWs on the case definition, increasing ease and efficiency of the transport of samples, and increasing capacity and quality of diagnosis). In this study, we described the epidemiologic and clinical features of the largest recorded LF outbreak, which had a high CFR. The investigation also revealed several risk factors for fatal outcomes and the contribution of early treatment in reduction of CFR. These findings should lead to further investigation of the disease. Our study also highlights the need for specific incidence and seroprevalence surveys to determine the actual burden of disease in Nigeria and West Africa. Although the emergency phase of this outbreak was declared over on May 10, 2018, a small number of cases in some areas continued to be reported thereafter (*10*). Ceaseless efforts to improve risk communication, surveillance, laboratory diagnosis, clinical management, infection prevention and control practices, logistics, and coordination could mitigate the impact of future outbreaks.

Additional members of the Nigeria Lassa Fever National Response Team: Michael Popoola, Anthony Ahumibe, Amedu M. Onoja, Akanimo Iniobong, Dike K. Ugochukwu, Favour M. Isi, Joy Musa (Nigeria Centre for Disease Control); Ayodele Adeyemo (eHealth Africa); Winifred Ukponu (University of Maryland Baltimore); Saliu Oladele, Esther N. Muwanguzi, Tanyth de Gooyer, Samuel K. Mutbam (World Health Organization); Demian U. Nwidi (Federal Teaching Hospital Abakaliki); Olumuyiwa B. Salu, Ayorinde B. James, and Sunday A. Omilabu (University of Lagos).

Acknowledgments

We thank all the staff working at the national and international organizations who fought against this outbreak, including personnel at the healthcare facilities, LF diagnostic laboratories, Nigeria Centre for Disease Control, World Health Organization, Alliance for International Medical Action, Médecins Sans Frontières, Robert Koch Institute, African Field Epidemiology Network, Public Health England, US Centers for Disease Control and Prevention, and numerous other partners. We also express our sincerest condolences to the family and friends of those who died during the outbreak.

About the Author

Ms. Ilori is an incident manager at the Nigeria Centre for Disease Control in Abuja, Nigeria. Her primary research interests include outbreak preparedness and response.

References

1. Frame JD, Baldwin JM Jr, Gocke DJ, Troup JM. Lassa fever, a new virus disease of man from West Africa. I. Clinical description and pathological findings. Am J Trop Med Hyg. 1970;19:670–6. http://dx.doi.org/10.4269/ajtmh.1970.19.670
2. Monath TP, Newhouse VF, Kemp GE, Setzer HW, Cacciapuoti A. Lassa virus isolation from *Mastomys natalensis* rodents during an epidemic in Sierra Leone. Science. 1974;185:263–5. http://dx.doi.org/10.1126/science.185.4147.263
3. Richmond JK, Baglole DJ. Lassa fever: epidemiology, clinical features, and social consequences. BMJ. 2003;327:1271–5. http://dx.doi.org/10.1136/bmj.327.7426.1271
4. Keenlyside RA, McCormick JB, Webb PA, Smith E, Elliott L, Johnson KM. Case-control study of *Mastomys natalensis* and humans in Lassa virus-infected households in Sierra Leone. Am J Trop Med Hyg. 1983;32:829–37. http://dx.doi.org/10.4269/ajtmh.1983.32.829
5. Fisher-Hoch SP, Tomori O, Nasidi A, Perez-Oronoz GI, Fakile Y, Hutwagner L, et al. Review of cases of nosocomial Lassa fever in Nigeria: the high price of poor medical practice. BMJ. 1995;311:857–9. http://dx.doi.org/10.1136/bmj.311.7009.857
6. Ajayi NA, Nwigwe CG, Azuogu BN, Onyire BN, Nwonwu EU, Ogbonnaya LU, et al. Containing a Lassa fever epidemic in a resource-limited setting: outbreak description and lessons learned from Abakaliki, Nigeria (January–March 2012). Int J Infect Dis. 2013;17:e1011–6. http://dx.doi.org/10.1016/j.ijid.2013.05.015
7. World Health Organization. Lassa fever fact sheet [cited 2018 May 13]. http://origin.who.int/mediacentre/factsheets/fs179
8. Centers for Disease Control and Prevention. Lassa fever [cited 2018 May 13]. http://www.cdc.gov/vhf/lassa
9. Nigeria Centre for Disease Control. Standard operating procedures for Lassa fever case management [cited 2018 May 13]. http://www.ncdc.gov.ng/themes/common/docs/protocols/30_1502277315.pdf
10. Nigeria Centre for Disease Control. Honourable Minister of Health announces end of emergency phase of Nigeria's Lassa fever outbreak [cited 2018 May 13]. http://ncdc.gov.ng/news/142/honourable-minister-of-health-announces-end-of-emergency-phase-of-nigeria%5C%27s-lassa-fever-outbreak
11. McCormick JB, King IJ, Webb PA, Scribner CL, Craven RB, Johnson KM, et al. Lassa fever. N Engl J Med. 1986;314:20–6. http://dx.doi.org/10.1056/NEJM198601023140104
12. Stephenson EH, Larson EW, Dominik JW. Effect of environmental factors on aerosol-induced Lassa virus infection. J Med Virol. 1984;14:295–303. http://dx.doi.org/10.1002/jmv.1890140402
13. Fichet-Calvet E, Lecompte E, Koivogui L, Soropogui B, Doré A, Kourouma F, et al. Fluctuation of abundance and Lassa virus prevalence in *Mastomys natalensis* in Guinea, West Africa. Vector Borne Zoonotic Dis. 2007;7:119–28. http://dx.doi.org/10.1089/vbz.2006.0520
14. Nigeria Centre for Disease Control. Weekly Epidemiological Report. Weekly updates on epidemics in Nigeria: as at 16th September, 2016 [cited 2018 May 13]. http://www.ncdc.gov.ng/reports/7/2016-september-week-37
15. Nigeria Centre for Disease Control. Weekly Epidemiological Report. Weekly updates on epidemics in Nigeria: as at 6th January, 2016 [cited 2018 May 13]. http://www.ncdc.gov.ng/reports/23/2017-january-week-1
16. Nigeria Centre for Disease Control. Weekly Epidemiological Report. Stopping spread of Lassa fever: instituting infection

prevention control measures in health facilities [cited 2018 May 13]. http://www.ncdc.gov.ng/reports/104/2018-january-week-3
17. Nigeria Centre for Disease Control. An update of Lassa fever outbreak in Nigeria for week 19 [cited 2018 May 13]. http://www.ncdc.gov.ng/themes/common/files/sitreps/473e68581953ff7e0d0b08445c1f6726.pdf
18. Otto JL, Holodniy M, DeFraites RF. Public health practice is not research. Am J Public Health. 2014;104:596–602.
19. Nikisins S, Rieger T, Patel P, Müller R, Günther S, Niedrig M. International external quality assessment study for molecular detection of Lassa virus. PLoS Negl Trop Dis. 2015;9:e0003793. http://dx.doi.org/10.1371/journal.pntd.0003793
20. Andersen KG, Shapiro BJ, Matranga CB, Sealfon R, Lin AE, Moses LM, et al.; Viral Hemorrhagic Fever Consortium. Clinical sequencing uncovers origins and evolution of Lassa virus. Cell. 2015;162:738–50. http://dx.doi.org/10.1016/j.cell.2015.07.020
21. Isere EE, Fatiregun AA, Ajayi IO. An overview of disease surveillance and notification system in Nigeria and the roles of clinicians in disease outbreak prevention and control. Niger Med J. 2015;56:161–8. http://dx.doi.org/10.4103/0300-1652.160347
22. National Bureau of Statistics. National population estimates [cited 2018 May 19] https://nigerianstat.gov.ng/download/474
23. Yalley-Ogunro JE, Frame JD, Hanson AP. Endemic Lassa fever in Liberia. VI. Village serological surveys for evidence of Lassa virus activity in Lofa County, Liberia. Trans R Soc Trop Med Hyg. 1984;78:764–70. http://dx.doi.org/10.1016/0035-9203(84)90013-0
24. Bausch DG, Demby AH, Coulibaly M, Kanu J, Goba A, Bah A, et al. Lassa fever in Guinea: I. Epidemiology of human disease and clinical observations. Vector Borne Zoonotic Dis. 2001;1:269–81. http://dx.doi.org/10.1089/15303660160025903
25. Fraser DW, Campbell CC, Monath TP, Goff PA, Gregg MB. Lassa fever in the Eastern province of Sierra Leone, 1970–1972. I. Epidemiologic studies. Am J Trop Med Hyg. 1974;23:1131–9. http://dx.doi.org/10.4269/ajtmh.1974.23.1131
26. Yinka-Ogunleye A, Ipadeola O, Saleh M, Ilori E, Dan-Nwafor C, Nwachukwu W, et al. 2016/2017 Lassa fever outbreak in Nigeria: age and sex have no effect on treatment outcome. Pan Afr Med J. 2018;8:3.
27. McCormick JB, King IJ, Webb PA, Johnson KM, O'Sullivan R, Smith ES, et al. A case-control study of the clinical diagnosis and course of Lassa fever. J Infect Dis. 1987;155:445–55. http://dx.doi.org/10.1093/infdis/155.3.445
28. Okokhere P, Colubri A, Azubike C, Iruolagbe C, Osazuwa O, Tabrizi S, et al. Clinical and laboratory predictors of Lassa fever outcome in a dedicated treatment facility in Nigeria: a retrospective, observational cohort study. Lancet Infect Dis. 2018; 18:684–95. http://dx.doi.org/10.1016/S1473-3099(18)30121-X
29. McCormick JB. Clinical, epidemiologic, and therapeutic aspects of Lassa fever. Med Microbiol Immunol (Berl). 1986;175:153–5. http://dx.doi.org/10.1007/BF02122438
30. Lo Iacono G, Cunningham AA, Fichet-Calvet E, Garry RF, Grant DS, Khan SH, et al. Using modelling to disentangle the relative contributions of zoonotic and anthroponotic transmission: the case of Lassa fever. PLoS Negl Trop Dis. 2015;9:e3398. http://dx.doi.org/10.1371/journal.pntd.0003398
31. Siddle KJ, Eromon P, Barnes KG, Mehta S, Oguzie JU, Odia I, et al. Genomic analysis of Lassa virus during an increase in cases in Nigeria in 2018. N Engl J Med. 2018;379:1745–53. http://dx.doi.org/10.1056/NEJMoa1804498

Address for correspondence: Chikwe Ihekweazu, Nigeria Centre for Disease Control, Plot 801 Ebitu Ukiwe, Jabi, Abuja, Nigeria; email: chikwe.ihekweazu@ncdc.gov.ng

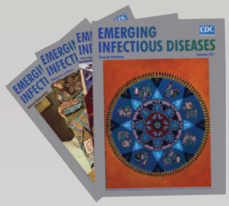

EMERGING INFECTIOUS DISEASES

December 2018

Zoonotic Infections

- Outbreak of HIV Infection Linked to Nosocomial Transmission, China, 2016–2017
- Autochthonous Human Case of Seoul Virus Infection, the Netherlands
- Reemergence of St. Louis Encephalitis Virus in the Americas
- Restaurant Inspection Letter Grades and Salmonella Infections, New York City
- Spatial Analysis of Wildlife Tuberculosis Based on a Serologic Survey Using Dried Blood Spots, Portugal
- Comparison of Highly Pathogenic Avian Influenza H5 Guangdong Lineage Epizootic in Europe (2016–17) with Previous HPAI H5 Epizootics
- *Capnocytophaga canimorsus* Capsular Serovar and Disease Severity, Helsinki, Finland, 2000–2017
- Rat Lungworm Infection in Rodents Across Post-Katrina New Orleans, Louisiana
- Crimean-Congo Hemorrhagic Fever Virus, Mongolia, 2013–2014
- Emerging Multidrug-Resistant Hybrid Pathotype Shiga toxin–producing *Escherichia coli* O80 and Related Strains of Clonal Complex 165, Europe
- Terrestrial Bird Migration and West Nile Virus Circulation, United States
- Substance Use and Adherence to HIV Prexposure Prophylaxis for Men Who Have Sex with Men
- Genomic Characterization of β-Glucuronidase–Positive *Escherichia coli* O157:H7 Producing Stx2a
- Highly Pathogenic Clone of Shiga Toxin–producing *Escherichia coli* O157:H7, England and Wales
- CTX-M-65 Extended-Spectrum β-Lactamase–Producing *Salmonella* Serotype Infantis, United States
- Novel Type of Chronic Wasting Disease Detected in Moose (*Alces alces*), Norway
- Survey of Ebola Viruses in Frugivorous and Insectivorous Bats in Guinea, Cameroon, and the Democratic Republic of the Congo, 2015–2017

To revisit the December 2018 issue, go to:
https://wwwnc.cdc.gov/eid/articles/issue/24/12/table-of-contents

Nontuberculous Mycobacterial Musculoskeletal Infection Cases from a Tertiary Referral Center, Colorado, USA

Noah Goldstein,[1] J. Benjamin St. Clair,[1] Shannon H. Kasperbauer, Charles L. Daley, Bennie Lindeque

Medscape EDUCATION ACTIVITY

In support of improving patient care, this activity has been planned and implemented by Medscape, LLC and Emerging Infectious Diseases. Medscape, LLC is jointly accredited by the Accreditation Council for Continuing Medical Education (ACCME), the Accreditation Council for Pharmacy Education (ACPE), and the American Nurses Credentialing Center (ANCC), to provide continuing education for the healthcare team.

Medscape, LLC designates this Journal-based CME activity for a maximum of 1.00 ***AMA PRA Category 1 Credit(s)***™. Physicians should claim only the credit commensurate with the extent of their participation in the activity.

Successful completion of this CME activity, which includes participation in the evaluation component, enables the participant to earn up to 1.0 MOC points in the American Board of Internal Medicine's (ABIM) Maintenance of Certification (MOC) program. Participants will earn MOC points equivalent to the amount of CME credits claimed for the activity. It is the CME activity provider's responsibility to submit participant completion information to ACCME for the purpose of granting ABIM MOC credit.

All other clinicians completing this activity will be issued a certificate of participation. To participate in this journal CME activity: (1) review the learning objectives and author disclosures; (2) study the education content; (3) take the post-test with a 75% minimum passing score and complete the evaluation at http://www.medscape.org/journal/eid; and (4) view/print certificate. For CME questions, see page 1260.

Release date: May 17, 2019; Expiration date: May 17, 2020

Learning Objectives

Upon completion of this activity, participants will be able to:

- Describe clinical characteristics of patients with nontuberculous mycobacterial (NTM) nonspinal musculoskeletal infections, according to a case series of 14 patients treated at University of Colorado Hospital (UCH) over a 6-year period
- Determine medical and surgical management of patients with NTM nonspinal musculoskeletal infections, based on a case series of 14 patients treated at UCH over a 6-year period
- Explain microbiological and histopathological findings and treatment outcomes of patients with NTM nonspinal musculoskeletal infections, based on a case series of 14 patients treated at UCH over a 6-year period

CME Editor

Dana C. Dolan, BS, Copyeditor, Emerging Infectious Diseases. *Disclosure: Dana C. Dolan, BS, has disclosed no relevant financial relationships.*

CME Author

Laurie Barclay, MD, freelance writer and reviewer, Medscape, LLC. *Disclosure: Laurie Barclay, MD, has disclosed no relevant financial relationships.*

Authors

Disclosures: ***Noah Goldstein, BS; J. Benjamin St Clair, MD, PhD;*** *and* ***Bennie Lindeque, MD, PhD,*** *have disclosed no relevant financial relationships.* ***Shannon H. Kasperbauer, MD,*** *has disclosed the following relevant financial relationships: served as an advisor or consultant for Insmed Incorporated; served as a speaker or a member of a speakers bureau for Insmed Incorporated; received grants for clinical research from Insmed Incorporated.* ***Charles L. Daley, MD,*** *has disclosed the following relevant financial relationships: served as an advisor or consultant for Horizon Pharma; Insmed Incorporated; Johnson & Johnson Pharmaceutical Research & Development, L.L.C.; Paratek Pharmaceuticals; Spero Therapeutics; received grants for clinical research from Insmed Incorporated.*

Author affiliations: University of Colorado, Aurora, Colorado, USA (N. Goldstein, J.B. St. Clair, S.H. Kasperbauer, B. Lindeque); University of Chicago, Chicago, Illinois, USA (J.B. St. Clair); National Jewish Health, Denver, Colorado, USA (S.H. Kasperbauer, C.L. Daley)

DOI: https://doi.org/10.3201/eid2506.181041

[1]These first authors contributed equally to this article.

Nontuberculous mycobacteria represent an uncommon but important cause of infection of the musculoskeletal system. Such infections require aggressive medical and surgical treatment, and cases are often complicated by delayed diagnosis. We retrospectively reviewed all 14 nonspinal cases of nontuberculous mycobacterial musculoskeletal infections treated over 6 years by orthopedic surgeons at a university-affiliated tertiary referral center. All patients

required multiple antimicrobial agents along with aggressive surgical treatment; 13 of 14 patients ultimately achieved cure. Four patients required amputation to control the infection. Half these patients were immunosuppressed by medications or other medical illness when they sought care at the referral center. Six cases involved joint prostheses; all ultimately required hardware removal and placement of an antimicrobial spacer for eradication of infection. Our findings highlight the importance of vigilance for nontuberculous mycobacterial musculoskeletal infection, particularly in patients who are immunosuppressed or have a history of musculoskeletal surgery.

Nontuberculous mycobacteria (NTM) are opportunistic pathogens found in soil and water and are the sources of an increasing number of infections and illness (*1*,*2*). Multiple recent studies have recognized this temporal trend of increasing annual prevalence of NTM disease; current prevalence is estimated at 2.6%–10% annually (*1*–*4*). NTM cause a broad range of clinical manifestations, depending on the immune competency of the host. Pulmonary disease is most common and is often seen in immunocompetent hosts. It is difficult to estimate the prevalence of extrapulmonary NTM infection in the United States because no system of national surveillance and reporting exists as for tuberculosis. Reported laboratory isolation data indicate that extrapulmonary disease may comprise up to one quarter of all NTM infections, although the best estimates are based on data that are 1–3 decades old. Data from the mid-1990s estimated the overall US incidence of NTM infection at 1.0%–1.8%, with ≈5% of isolates reported to the Centers for Disease Control and Infection at that time being of extrapulmonary origin. A population-based record review in Oregon that used data gathered during 2005–2006 found ≈22% of isolates originating from nonpulmonary specimens. Data from North Carolina gathered during 2006–2010 showed 16%–23% of total isolates originating from extrapulmonary specimens (*5*–*7*). Skin and soft tissue infections represent most extrapulmonary NTM disease, whereas bone and joint disease is less common. With increasing immunosuppression, NTM is more likely to manifest as disseminated disease, possibly including bone and joint involvement.

Previous case reports and series of NTM musculoskeletal infections have focused on the demographics, diagnosis, and treatment of patients with these difficult-to-manage infections (*8*–*24*). Patients were often immunocompetent persons who contracted an NTM disease after direct inoculation via traumatic skin puncture (*25*–*28*). In a series of 29 cases from South Korea, all patients required surgical intervention in addition to antimicrobial drugs; 3 patients failed to respond despite aggressive treatment, and an additional 4 were lost to follow-up. Of note, only 20 of the patients in this series received NTM-specific antimicrobial therapy; the remainder were treated with empirical antimicrobial therapy. A series of 28 cases of *M. marinum* musculoskeletal infections found that 93% of cases involved fingers or hands and 87% were related to aquatic exposure; two thirds progressed from cutaneous to invasive infection. Most cases were managed with multiple antimycobacterial agents in addition to surgery, and the series reported a 75% cure rate and 25% loss to follow-up. A study of 8 cases of prosthetic joint infection (PJI) caused by rapidly growing mycobacteria found that the median interval from prosthesis implantation to infection was 312 weeks and that all patients required either resection and explantation of infected prostheses or chronic suppressive antimicrobial therapy.

In these series, infections occurred throughout the musculoskeletal system but were particularly common in the hands and spine. Identification of NTM as the causative agent was often delayed due to the indolent course of the infection and lack of appropriate diagnostic testing. Once identified, the infections could be treated effectively with a combination of debridement and conventional antimycobacterial chemotherapy.

We reviewed all cases of nonspinal NTM musculoskeletal infection treated at the University of Colorado Hospital (UCH; Aurora, CO, USA) over a 6-year period by a multidisciplinary team of providers at UCH and National Jewish Health (NJH; Denver, CO, USA), a renowned center for mycobacterial research and treatment that receives referrals for difficult-to-treat NTM infections from across the United States. Our aim was to describe the clinical characteristics and treatment outcomes of patients with NTM musculoskeletal infections.

Materials and Methods

Study Design

We performed a retrospective study of patients with nonspinal NTM musculoskeletal infections treated at UCH during 2009–2015. The management of each case was directed by an orthopedic surgeon and infectious disease physicians at UCH and NJH. For patients with positive culture results at UCH, mycobacterial speciation and susceptibility data were identified by ARUP Laboratories (https://www.aruplab.com) using DNA sequencing or matrix-assisted laser desorption/ionization time-of-flight mass spectrometry.

Case Ascertainment

We identified all cases of nonspinal NTM musculoskeletal infections treated by orthopedic surgeons at UCH during the study period using a registry of NTM musculoskeletal infections. We omitted spinal cases because they are handled by a different department at UCH and so were not

part of the surgeons' personal registry. We reviewed the medical records of patients after approval from the Institutional Review Board.

Data Collection

We performed our review of the medical records using a standardized case report form. We collected demographic characteristics and data on concurrent conditions, laboratory values, surgical intervention, antimycobacterial chemotherapy, and outcomes.

Literature Review

We searched the Medline database to identify case reports and reviews of NTM musculoskeletal infections. We used both the PubMed and Ovid access tools.

Results

Patient Characteristics

Of the 14 patients in our series, 7 were receiving immunosuppressive medications at arrival, and 5 of those had chronic autoimmune disease. Twelve patients were referred from NJH. No predisposing host factor was identified for 6 patients. (Table 1).

Clinical Presentation and Diagnosis

The patients had a wide array of sites of infection when they sought care at UCH (5 knee, 2 hip, 1 thigh, 1 hand, 1 foot, 1 elbow, 3 with disseminated disease at multiple sites). The diagnosis at arrival was most commonly PJI (n = 6); the next most common diagnoses included septic

Table 1. Demographics of patients in retrospective study of nontuberculous mycobacterial musculoskeletal infections, Colorado, USA*

Patient no.	Age, y/sex	Immunocompromising conditions	Inciting or predisposing factor(s)	Time to symptom onset, mo	Reason care sought	Time from symptom onset to diagnosis, mo	Diagnostic procedure, source of microbiologic diagnosis
1	55/M	History of lymphoma, pseudogout, oral steroid use	Steroid injection, left ankle	UNK	Osteomyelitis, septic arthritis	12	Tissue sample from ankle debridement
2	53/F	None	Pedicure	0	Synovitis, osteomyelitis, cellulitis	4	UNK; diagnosis at another hospital
3	48/F	None	Second THA	UNK	PJI	UNK	Thigh fluid sampled during I&D
4	45/M	None	AKA	1	Draining wound at stump	2	Sample of fluid draining from AKA stump
5	64/F	None	Carpal tunnel release	0	Tenosynovitis, septic arthritis	8	Synovial fluid obtained during excision of synovitis
6	69/F	Diabetes mellitus	THA	6	PJI	9	Synovial biopsy obtained during explantation
7	23/F	Systemic lupus erythematosus, oral steroids, hydroxyl-chloroquine, mycophenolate mofetil	Avascular necrosis, ankle fusion	3	Septic arthritis, osteomyelitis, skin abscesses	1	UNK; diagnosis at another hospital
8	57/F	Polymyositis, oral steroids, azathioprine, rituximab,methotrexate	ACL repair, arthroscopy, steroid injection	UNK	Septic arthritis	UNK	Aspirate of left knee and right hip
9	76/M	Nonspecific autoimmune disease, oral steroids	Calcium pyrophosphate deposition disease, TKA	0	PJI	2	UNK; diagnosis at another hospital
10	58/M	None	Trauma, steroid injection	12	Septic arthritis	19	UNK; diagnosis at another hospital
11	77/F	Rheumatoid arthritis, prednisone, azathioprine	TKA	300	PJI	12	Synovial biopsy obtained during placement of antimicrobial spacer
12	83/M	Malnutrition, prednisone	TKA	168	PJI	8	Tissue obtained during TKA revision
13	49/F	None	TKA (revision)	14	PJI	2	UNK; diagnosis at another hospital
14	24/F	Crohn's disease, infliximab	Failed IV	0	Cellulitis, abscess	7	Skin biopsy

*AKA, above-knee amputation; I&D, irrigation and debridement; PJI, prosthetic joint infection, THA, total hip arthroplasty; TKA, total knee arthroplasty; UNK, unknown.

arthritis (n = 5), osteomyelitis (n = 3), tendon sheath infection (n = 2), skin abscess (n = 2), cellulitis (n = 2), and surgical-wound infection (n = 1). Several patients had complex local infections with multiple concurrent tissue diagnoses; case-patients 1, 7, and 8 had disseminated disease at multiple sites. Each patient had undergone ≥1 prior procedure at the site of infection, including 6 patients with infected prostheses, 4 with other surgical procedures, 2 with steroid injection, 1 with a failed intravenous (IV) placement, and 1 with a cosmetic pedicure. The median interval from symptom onset to diagnosis was 7.5 months (range 1–19 months).

Of 10 patients tested, the median erythrocyte sedimentation rate (ESR) was above the upper limit of normal (ULN) in 7 patients (70%) at arrival (ULN 15 mm/h in men, 20 mm/h in women). C-reactive protein level was elevated in 4/14 patients (29%) (ULN 10.0 mg/L). Blood leukocyte count was elevated in 2/14 patients (14%) (ULN 10.1×10^4 cells/μL). All 3 laboratory tests were within reference limits in 1 patient, and both C-reactive protein and leukocyte levels were within reference limits in an additional 2 patients without ESR data.

PJIs

Six patients arrived with PJI at the knee (4 patients) and hip (2 patients). The interval from prosthesis implantation to symptom onset ranged from the immediate aftermath of implantation to 25 years postimplantation; median duration was 6 months. Infected hardware was removed in all patients with PJI; the median period from symptom onset to explantation was 8.5 months (range <3–16 months). After explantation, 2-stage revision was undertaken, first with implantation of a temporary articulating prosthesis prepared with 1 g of antimicrobial-loaded polymethylmethacrylate bone cement, with drug selection based on sensitivity testing. This preparation, called an antimicrobial spacer, was subsequently replaced with a permanent prosthesis after several months without evidence of recurrent infection. Medication-loaded bone cement was also used for patients requiring intramedullary nailing. Patients with PJI were also treated with amikacin-containing calcium sulfate beads implanted within the surgical bed (1 g of amikacin per 10 cc packet of calcium sulfate mixture). These antimicrobial beads were used at initial explantation or when the antimicrobial spacer was replaced with a permanent prosthesis at the discretion of the surgeon as needed to fill dead space from aggressive debridement or the infection itself. The precise amount of amikacin used is not always clearly reflected in the surgical record; however, in our series, use of up to 5 g of amikacin has been recorded. Amikacin is used for its activity against mycobacteria and its ability to integrate with the calcium sulfate material to form beads. Such amikacin-laden beads were also used in 2 other patients with extensive soft-tissue involvement. A seventh patient with septic arthritis of her native knee (case-patient 8) underwent a total knee arthroplasty that was insufficient to eradicate the infection and ultimately required subsequent 2-stage revision.

Surgical Treatment

All patients required surgical treatment for control of infection, and all but 1 patient were ultimately cured by combined medical and surgical treatment. Seven patients had ≥1 procedure at outside hospitals before seeking treatment at UCH. Case-patients 4 and 5 required only a single surgical procedure at UCH for control of infection. Case-patients 6 and 12 underwent planned 2-stage revision and required no further surgeries. The remaining 10 case-patients had initial procedures at UCH that were intended to definitively treat infection but proved unsuccessful. Surgical treatment at UCH consisted of aggressive debridement of infected bone and soft tissue, as well as explantation of any infected hardware with 2-stage revision of infected prostheses. Four patients with infections involving the knee also required placement of intramedullary nails coated with antibiotic-loaded cement (case-patients 9, 10, 11, and 13). The median interval from initial diagnostic or therapeutic procedure to definitive surgical treatment was 14 months (range 4–52 months) in the patients who required multiple procedures. One patient with disseminated *M. abscessus* (case-patient 1) required a debridement of the femur, partial claviculectomy, synovectomy of an ankle and a knee, and a fasciectomy. The patient with disseminated *M. massiliense* in the setting of chronic immunosuppressive therapy (case-patient 7) required ≥12 procedures including multiple debridements and soft tissue excisions, removal of infected ankle fusion hardware, and osteotomy and arthrotomy of an infected elbow with extensive use of antimicrobial beads and bone cement. A patient with *M. intracellulare* infection disseminated to the left knee and right hip (case-patient 8) required multiple irrigations and debridements, total knee arthroplasty with antimicrobial spacer, and subsequent implantation of a tumor prosthesis. One patient with *M. fortuitum* infection (case-patient 5) had a debridement and eventually required amputation of her hand. One patient had cellulitis and abscess formation caused by *M. marinum* (case-patient 14) requiring a wide excision of the soft tissue around her elbow. One patient with a hip-prosthetic infection caused by *M. abscessus* (case-patient 3) required hemipelvectomy due to the progressive spread of the infection despite >1 year of intravenous therapy, prosthetic hip explantation, and multiple debridements (Table 2).

Histopathology and Microbiology

The species of NTM responsible for the musculoskeletal infection was known or identified in each patient. All patients had tissue specimens taken for culture during their

Table 2. Surgical treatment of patients with nontuberculous mycobacterial musculoskeletal infections, Colorado, USA*

Patient no.	Site	Previous surgeries	Symptom onset to first surgery, mo	Surgeries for control of infection at UCH		Time between surgeries, mo	First visit to definitive procedure, mo	Length of follow-up, mo
				First procedure(s)	Definitive procedure			
1	Multiple joints†	Multiple I&Ds, below-knee amputation	UNK	I&D, excision of soft-tissue masses, debridement, synovectomy, amikacin bead implantation	Wide excision of right calf	36	22	7
2	Left foot	Debridement, amputation L 5th toe, nodule excision	2	Debridement of dorsum of left foot	Excisional debridement of left foot	17	14	60
3	Left hip (PJI)	UNK	UNK	Debridement and polyethylene exchange	Hemi-pelvectomy	31	38	14
4	Left thigh	None	18	NA	Above-knee amputation stump revision	NA	14	1
5	Right hand	None	9	NA	Amputation of right hand and forearm	NA	3	37
6	Right hip (PJI)	None	9	Resection arthroplasty, tobramycin cement spacer	Revision THA	4	6	49
7	Multiple joints‡	I&D	1	Hardware removal, I&D, amikacin bead implantation, arthrotomy and osteotomy with amikacin cement, soft-tissue excisions	Excisional debridement of left forearm and right foot with amikacin bead placement§	51	51	2
8	Left knee, right hip	None	UNK	I&D, amikacin cement spacer	TKA with tumor prosthesis, gentamicin cement, amikacin beads	7	8	48
9	Left knee (PJI)	Explant with antimicrobial spacer, I&D	4	I&D, explantation, tobramycin spacer, intramedullary nail with tobramycin cement, revision of spacer	Revision TKA with tobramycin cement and amikacin beads	20	12	20
10	Left knee	Arthroscopic meniscectomy, synovial biopsy, aspirations, arthroscopic synovectomy	2	Radical synovectomy, amikacin bead implantation, resection arthroplasty, knee-spanning intramedullary nail with tobramycin cement	TKA with tumor prosthesis and tobramycin cement	40	12	4
11	Right knee (PJI)	None	12	Explantation, amikacin spacer, I&D, intramedullary nail with amikacin cement	Revision TKA with gentamicin cement and amikacin beads	7	11	17
12	Left knee (PJI)	I&D, polyethylene exchange	0	Explantation, gentamicin cement spacer	Revision TKA with tobramycin cement and amikacin beads	12	5	20
13	Right knee (PJI)	Explant, I&D, antimicrobial spacers	3	Revision TKA, I&D, intramedullary nail with amikacin cement	Revision TKA with amikacin cement and amikacin beads	14	6	1
14	Right elbow	None	8	Wide excision of right forearm, nodule excision	Wide excision of right forearm	4	10	47

*I&D, irrigation and debridement; NA, not applicable; PJI, prosthetic joint infection, THA, total hip arthroplasty; TKA, total knee arthroplasty; UNK, unknown.
†Infection was present in patient's left thigh and knee, and right talus, ankle joint, and subtalar joint.
‡Infection was present in patient's left elbow, buttock, forearm, calf, right ankle and thigh, and both feet.
§Because this patient is in treatment for chronic disseminated infection, definitive procedure is defined as the most recent surgical procedure.

procedure(s) at UCH. Eight patients had microbiologic diagnoses of NTM infection before transfer to UCH, and 6 of these patients were culture-negative at the time of surgery at UCH (case-patients 1, 2, 4, 8, 9, and 13). Antimicrobial therapy was initiated at outside hospitals in 6 of the 8 patients who came to UCH with established microbiologic diagnoses; the other 2 patients were referred directly to infectious diseases specialists at UCH, NJH, or both for treatment.

Seven patients were infected with a rapidly growing mycobacterial species, whereas the remaining 7 were infected with slowly growing species (Table 1). Ten patients had intraoperative biopsy specimens demonstrating granuloma formation, but only 2 of these had evidence of acid-fast bacilli on direct microscopy. Eight of 14 patients had intraoperative cultures that grew NTM, with speciation consistent with prior data when available. All patients had visual evidence of infection at the time of operation. One patient who had *M. marinum* worked at a pet store that sold fish and aquariums and frequently submerged her hands and arms in the water, and her infection originated at a failed IV site. In the 5 patients with *M. avium* complex, 3 had speciation available that identified *M. intracellulare*.

Antimicrobial Treatment

All patients were treated with combination antimycobacterial chemotherapy (Table 3) determined on the basis of antimicrobial drug sensitivities (Appendix Table, https://wwwnc.cdc.gov/EID/article/25/6/18-1041-App1.xlsx) and recommendations from NJH. Thirteen of 14 patients were receiving antimycobacterial therapy at the time of surgery based on previous culture and drug susceptibility test results. Antimicrobial therapy was not administered around the time of surgery for case-patient 7 because of adverse effects from these medications.

Table 3. Microbiology and antimicrobial treatment of patients with nontuberculous mycobacterial musculoskeletal infections, Colorado, USA*

Patient no.	Species	Oral therapy (duration, mo)	Intravenous therapy (duration, mo)	Total duration of therapy, mo	Time from last surgery to cessation of antimicrobial therapy, mo	Outcome
1	*M. abscessus*	Azithromycin (24)	Tigecycline + amikacin + imipenem (24)	24	0	Cured
2	*M. abscessus*	Azithromycin + linezolid (6)	Amikacin + imipenem (6)	6	0	Cured
3	*M. abscessus*	Azithromycin + clofazimine (20)	Imipenem + amikacin (15)	20	0	Cured
4	*M. abscessus*	Azithromycin + clofazimine (14)	Cefoxitin + amikacin (8)	14	0	Cured
5	*M. fortuitum*	Moxifloxacin (2)	Imipenem (2)	2	1	Cured
6	*M. fortuitum*	Doxycycline + ciprofloxacin + trimethoprim/ sulfamethoxazole (5)	Amikacin (3)	5	3	Cured
7	*M. massiliense*	Azithromycin, linezolid (4)	Cefoxitin, tigecycline, linezolid, amikacin, azithromycin (4)	4†	NA	Treatment failure
8	*M. intracellulare*	Azithromycin + ethambutol + rifabutin (14)	Amikacin (8)	14	1	Cured
9	MAC, speciation unavailable	Azithromycin + clofazimine + ethambutol + rifampin (39)	Amikacin (2)	39	11	Cured
10	*M. intracellulare*	Azithromycin + rifampin + clofazimine + ethambutol (27)	Amikacin (5)	27	7	Cured
11	*M. intracellulare*	Azithromycin + moxifloxacin + ethambutol (9)	None	9	5	Cured
12	MAC, speciation unavailable	Azithromycin + ethambutol + rifampin (7)	None	7	3	Cured
13	*M. gordonae*	Azithromycin + trimethoprim/ sulfamethoxazole + ethambutol (16)	Amikacin (2)	16	2	Cured
14	*M. marinum*	Azithromycin + ciprofloxacin (14)	Imipenem (10)	14	10	Cured

*All bacteria are *Mycobacterium* spp. MAC, *Mycobacterium avium* complex.
†Patient elected to discontinue antimicrobial treatment after experiencing intolerable side effects from multiple medications, despite ongoing disseminated infection.

Amikacin-related toxicity occurred in 3 patients. Ototoxicity occurred in 2 patients: case-patient 1 reported hearing loss after 9 months of parenteral amikacin and within 1 month of implantation of amikacin beads, and case-patient 6 experienced tinnitus after 3 months of parenteral amikacin. Kidney injury occurred in case-patient 7 after 3 months of parenteral amikacin and 1 month after implantation of amikacin beads (creatinine level increased from 0.71 to 2.37 mg/dL). Tigecycline was also discontinued in case-patient 7 due to intractable nausea and vomiting within 2 days of initiation, and cefoxitin was discontinued due to fever within 3 days of treatment. Clofazimine also caused intractable nausea and vomiting upon initiation in this patient and was discontinued after 1 month. Apart from case-patient 1, who experienced permanent hearing loss, toxicity resolved with discontinuation of medications. Two patients with *M. avium* complex infection did not receive amikacin due to history of *C. difficile* infection (case-patients 10 and 11).

The median duration of antimicrobial chemotherapy was 14 months (range 2–39 months). Among the 7 patients with rapidly growing NTM, the median duration was 6 months. The median duration was longer in patients with slow-growing NTM, at 14 months. Twelve patients received injectable antimicrobial drugs as part of their treatment regimen, whereas 2 patients had oral therapy alone. The median duration of therapy with injectable agents was 5 months; rapidly growing strains were treated for a median of 6 months and slow-growing strains for a median of 5 months. The median duration of antimicrobial drug therapy after definitive surgery was 2 months. Patients infected with slow-growing NTM received a more protracted course of postoperative antimicrobial therapy, with a median duration of 5 months, compared with <1 month in patients infected with rapidly growing strains.

Outcomes

During the follow-up period after surgical intervention (median duration 20 months, range 1–60 months), 13/14 patients did not develop clinical or microbiological relapse and were cured. One (case-patient 7) had clinical and microbiological relapse and was deemed to have failed treatment; the first relapse occurred 2 months after the first surgery to control the infection. The relapse, a disseminated infection distant from the original surgical site, was a likely result of the patient receiving multiple immunosuppressive medications to control systemic lupus erythematosus. She required 12 surgical procedures within the first year and subsequently required ≈1 procedure/year for control of chronic disseminated infection over the next 3 years, primarily in the form of debridement and excision of soft tissue mass. Of note, this patient chose to forgo antimicrobial therapy after the first 4 months of treatment because of intolerable side effects from multiple medications. Two instances of microbiologic relapse were documented for this patient.

Discussion

We present a series of cases of NTM musculoskeletal infections requiring surgical intervention and antimycobacterial chemotherapy that were managed at UCH and NJH over a 6-year period. NTM musculoskeletal infections have been reported in the literature sporadically due to their rare occurrence; 2 previous case series documented 29 cases over 13 years in South Korea (*27*) and 8 cases of PJI by NTM over 4 decades at the Mayo Clinic in the United States (*26*). In a 6-year period, we have identified 14 case-patients treated at our institutions with unique characteristics, in comparison to previous studies (*25–28*). Specifically, the cases we report indicate the importance of a low threshold for suspicion and testing for NTM in any patient who has an unidentified musculoskeletal infection, particularly with evidence of granuloma formation on pathology. Furthermore, for all of our case-patients, NTM infections developed at the site of a prior procedure (prosthetic joint or other intervention), raising the concept of early culture for mycobacteria in conjunction with or after negative results from conventional bacterial culture.

One of the most notable findings from the 3 previous case series studying NTM musculoskeletal infections was that, in all studies, the overwhelming majority of the patients were immunocompetent (*26–28*). In contrast, half the patients in our study were immunosuppressed as a result of either an underlying medical condition or a medication used to treat rheumatologic disease. While this may be a manifestation of the relationship between UCH and NJH, our report highlights the importance of hypervigilance for possible NTM in immunocompromised patients with musculoskeletal infections. The most severely immunocompromised patients in our series (case-patients 1, 7, and 8) had disseminated infection. Immunocompromised patients with a history of musculoskeletal surgery should receive a mycobacterial workup as a component of their care.

Another crucial aspect of our case series is the observation that 10/14 cases occurred at the site of a previous musculoskeletal surgery and 6 of these cases involved a joint prosthesis. Moreover, all 14 cases were preceded by an invasive procedure at the initial site of infection. In all but 3 of our surgery-associated cases, the onset of symptoms occurred ≥3 months after the preceding surgical procedure, suggesting hematogenous spread, possibly due to transient mycobacteremia, with seeding of surgically altered tissue as the likely mechanism of inoculation. This mechanism is particularly likely in case-patients 1, 7, 8, 11, and 12, which comprise 3 cases of disseminated infection in severely immunocompromised patients and 2 late prosthetic joint

infections with more than a decade between initial prosthetic joint surgery and eventual infection. The previous report from South Korea noted a minority of periprosthetic infections, but most cases were related to trauma or iatrogenic injections rather than surgery (*27*).

The report from the Mayo Clinic focused on PJIs but noted only 8 cases over 4 decades (*26*). A recent series of 6 cases of chronic trauma– or intervention-related joint infection not responding to empiric therapy reported no cases of periprosthetic NTM infection (*29*). Our relatively rapid accumulation of surgery-related cases over a 6-year period is due to the relationship between UHC and NJH and NJH's high volume of NTM cases; we cannot generalize this trend to the general US population, given the unique referral characteristics of our patient population. It is possible that improvements in detection and identification of NTM infections may contribute to this increased case volume, as has been suggested to explain the increasing incidence and prevalence of pulmonary NTM (*30*). Regardless, infections in our study were more likely to occur at the site of a previous orthopedic surgery and in ≥4 cases led to severe complications requiring partial or full amputation, with 1 patient requiring hemipelvectomy. Three of these patients were infected with *M. abscessus* and 1 with *M. fortuitum*. *M. abscessus* is highly drug resistant and therefore responds poorly to antimicrobial therapy. It is difficult to ascertain if these amputations could have been avoided with earlier diagnosis and aggressive surgical therapy. In several cases, patients with long delays in diagnosis ultimately required amputation; almost one third of patients in our series required amputation.

Given the importance in identifying NTM musculoskeletal infections in the immunocompromised or those with prior surgery, it is unfortunate that our data did not identify more substantial diagnostic criteria based upon inflammatory markers. Whereas the ESR in our patients was usually elevated, the C-reactive protein and leukocyte counts were typically normal. The patient who failed treatment had one of the highest ESRs in our patient group, nearly double the median value of 38 at intake, perhaps because of her chronic autoimmune condition.

All patients had positive mycobacterial cultures at time of initial diagnosis. Thirteen of 14 patients were receiving mycobacterial therapy at the time of surgery at our institution and only half of them were persistently positive for mycobacterial growth despite ongoing symptoms and intraoperative observation of sinus tract formation and suppuration. We are familiar with this phenomenon, and therefore do not require a positive culture to define failure of therapy. If a patient has ongoing signs of infection while receiving effective antimicrobial drugs (based on drug sensitivity testing), then they need more aggressive resection of infected tissue. The 3 patients with PJI and rapidly growing NTM infection all required prolonged courses of IV and oral antimicrobial therapy. One of the 3 patients with *M. avium* complex–related PJI also required 2 months of concomitant IV amikacin. All patients with PJIs required explantation of the infected hardware followed by antimicrobial spacer placement for ≥3 months in addition to ongoing postoperative oral or intravenous antimicrobial therapy to achieve a successful outcome. In ≥5 cases, microbiologic diagnosis of mycobacterial infection was only confirmed during the initial surgical intervention, and in each of these cases, prior or subsequent surgeries were required for ultimate control of infection. Ultimately, the fact that 10/14 cases required multiple surgeries for control of infection with long intervals from onset of symptoms and initial seeking of care to identification of the infectious agent and finally definitive surgical treatment underscores the need for early identification and aggressive treatment of NTM infection.

About the Author

Dr. Goldstein is a graduate of the University of Colorado School of Medicine, Aurora, CO. He will begin his residency in psychiatry at the University of North Carolina in July 2019.

References

1. Prevots DR, Shaw PA, Strickland D, Jackson LA, Raebel MA, Blosky MA, et al. Nontuberculous mycobacterial lung disease prevalence at four integrated health care delivery systems. Am J Respir Crit Care Med. 2010;182:970–6. http://dx.doi.org/10.1164/rccm.201002-0310OC
2. Adjemian J, Olivier KN, Seitz AE, Holland SM, Prevots DR. Prevalence of nontuberculous mycobacterial lung disease in U.S. Medicare beneficiaries. Am J Respir Crit Care Med. 2012;185:881–6. http://dx.doi.org/10.1164/rccm.201111-2016OC
3. Al-Houqani M, Jamieson F, Mehta M, Chedore P, May K, Marras TK. Aging, COPD, and other risk factors do not explain the increased prevalence of pulmonary *Mycobacterium avium* complex in Ontario. Chest. 2012;141:190–7. http://dx.doi.org/10.1378/chest.11-0089
4. Spaulding AB, Lai YL, Zelazny AM, Olivier KN, Kadri SS, Prevots DR, et al. Geographic distribution of nontuberculous mycobacterial species identified among clinical isolates in the United States, 2009–2013. Ann Am Thorac Soc. 2017;14:1655–61. http://dx.doi.org/10.1513/AnnalsATS.201611-860OC
5. Griffith DE, Aksamit T, Brown-Elliott BA, Catanzaro A, Daley C, Gordin F, et al.; ATS Mycobacterial Diseases Subcommittee; American Thoracic Society; Infectious Disease Society of America. An official ATS/IDSA statement: diagnosis, treatment, and prevention of nontuberculous mycobacterial diseases. Am J Respir Crit Care Med. 2007;175:367–416. http://dx.doi.org/10.1164/rccm.200604-571ST
6. Smith GS, Ghio AJ, Stout JE, Messier KP, Hudgens EE, Murphy MS, et al. Epidemiology of nontuberculous mycobacteria isolations among central North Carolina residents, 2006–2010. J Infect. 2016;72:678–86. http://dx.doi.org/10.1016/j.jinf.2016.03.008
7. Cassidy PM, Hedberg K, Saulson A, McNelly E, Winthrop KL. Nontuberculous mycobacterial disease prevalence and risk factors: a changing epidemiology. Clin Infect Dis. 2009;49:e124–9. http://dx.doi.org/10.1086/648443

8. Booth JE, Jacobson JA, Kurrus TA, Edwards TW. Infection of prosthetic arthroplasty by *Mycobacterium fortuitum.* Two case reports. J Bone Joint Surg Am. 1979;61:300–2. http://dx.doi.org/10.2106/00004623-197961020-00029
9. Horadam VW, Smilack JD, Smith EC. *Mycobacterium fortuitum* infection after total hip replacement. South Med J. 1982;75:244–6. http://dx.doi.org/10.1097/00007611-198202000-00036
10. Heathcock R, Dave J, Yates MD. *Mycobacterium chelonae* hip infection. J Infect. 1994;28:104–5. http://dx.doi.org/10.1016/S0163-4453(94)94533-0
11. Pring M, Eckhoff DG. *Mycobacterium chelonae* infection following a total knee arthroplasty. J Arthroplasty. 1996;11:115–6. http://dx.doi.org/10.1016/S0883-5403(96)80170-7
12. Luque AE, Kaminski D, Reichman R, Hardy D. *Mycobacterium szulgai* osteomyelitis in an AIDS patient. Scand J Infect Dis. 1998;30:88–91. http://dx.doi.org/10.1080/003655498750002376
13. Breda L, de Michele G, Nozzi M, De Sanctis S, Di Marzio D, Chiarelli F. Non-tuberculous mycobacterial osteomyelitis: an unusual cause of hip pain in immunocompetent children. Rheumatol Int. 2009;29:1487–9. http://dx.doi.org/10.1007/s00296-009-0844-4
14. Wang S-X, Yang C-J, Chen Y-C, Lay C-J, Tsai C-C. Septic arthritis caused by *Mycobacterium fortuitum* and *Mycobacterium abscessus* in a prosthetic knee joint: case report and review of literature. Intern Med. 2011;50:2227–32. http://dx.doi.org/10.2169/internalmedicine.50.5610
15. Garcia DC, Sandoval-Sus J, Razzaq K, Young L. Vertebral osteomyelitis caused by *Mycobacterium abscessus*. BMJ Case Rep. 2013;2013:cr2013009597. http://dx.doi.org/10.1136/bcr-2013-009597
16. Suy F, Carricajo A, Grattard F, Cazorla C, Denis C, Girardin P, et al. Infection due to *Mycobacterium thermoresistibile*: a case associated with an orthopedic device. J Clin Microbiol. 2013;51:3154–6. http://dx.doi.org/10.1128/JCM.00925-13
17. Bakhsh WR, Mesfin A. *Mycobacterium kansasii* infection of the spine in a patient with sarcoidosis: a case report and literature review. J Surg Orthop Adv. 2014;23:162–5. http://dx.doi.org/10.3113/JSOA.2014.0162
18. Hazara AM, Edey M, Roy A, Bhandari S. Rapidly growing non-tuberculous mycobacterial infection in a renal transplant patient after alemtuzumab induction. Transpl Infect Dis. 2014;16:847–52. http://dx.doi.org/10.1111/tid.12269
19. Kato S, Murakami H, Demura S, Yoshioka K, Hayashi H, Yokogawa N, et al. Vertebral osteomyelitis caused by *Mycobacterium abscessus* surgically treated using antibacterial iodine-supported instrumentation. Case Rep Orthop. 2014;2014:197061. http://dx.doi.org/10.1155/2014/197061
20. Nguyen HH, Fadul N, Ashraf MS, Siraj DS. Osteomyelitis infection of *Mycobacterium marinum:* a case report and literature review. Case Rep Infect Dis. 2015;2015:905920. http://dx.doi.org/10.1155/2015/905920
21. Sharma VK, Pai G, Deswarte C, Lodha R, Singh S, Kang LW, et al. Disseminated *Mycobacterium avium* complex infection in a child with partial dominant interferon gamma receptor 1 deficiency in India. J Clin Immunol. 2015;35:459–62. http://dx.doi.org/10.1007/s10875-015-0173-1
22. Silva JT, López-Medrano F, Fernández-Ruiz M, San-Juan R, Ruiz-Cano MJ, Delgado JF, et al. *Mycobacterium abscessus* pulmonary infection complicated with vertebral osteomyelitis in a heart transplant recipient: case report and literature review. Transpl Infect Dis. 2015;17:418–23. http://dx.doi.org/10.1111/tid.12381
23. Wood BR, Buitrago MO, Patel S, Hachey DH, Haneuse S, Harrington RD. *Mycobacterium avium* complex osteomyelitis in persons with human immunodeficiency virus: case series and literature review. Open Forum Infect Dis. 2015;2:ofv090. http://dx.doi.org/10.1093/ofid/ofv090
24. Kuntz M, Seidl M, Henneke P. Osteomyelitis because of *Mycobacterium xenopi* in an immunocompetent child. Pediatr Infect Dis J. 2016;35:110–3.
25. Marchevsky AM, Damsker B, Green S, Tepper S. The clinicopathological spectrum of non-tuberculous mycobacterial osteoarticular infections. J Bone Joint Surg Am. 1985;67:925–9. http://dx.doi.org/10.2106/00004623-198567060-00015
26. Eid AJ, Berbari EF, Sia IG, Wengenack NL, Osmon DR, Razonable RR. Prosthetic joint infection due to rapidly growing mycobacteria: report of 8 cases and review of the literature. Clin Infect Dis. 2007;45:687–94. http://dx.doi.org/10.1086/520982
27. Park JW, Kim YS, Yoon JO, Kim JS, Chang JS, Kim JM, et al. Non-tuberculous mycobacterial infection of the musculoskeletal system: pattern of infection and efficacy of combined surgical/antimicrobial treatment. Bone Joint J. 2014;96-B:1561–5. http://dx.doi.org/10.1302/0301-620X.96B11.33427
28. Johnson MG, Stout JE. Twenty-eight cases of *Mycobacterium marinum* infection: retrospective case series and literature review. Infection. 2015;43:655–62. http://dx.doi.org/10.1007/s15010-015-0776-8
29. Gundavda MK, Patil HG, Agashe VM, Soman R, Rodriques C, Deshpande RB. Nontuberculous mycobacterial infection of the musculoskeletal system in immunocompetent hosts. Indian J Orthop. 2017;51:205–12. http://dx.doi.org/10.4103/0019-5413.201718
30. Johnson MM, Odell JA. Nontuberculous mycobacterial pulmonary infections. J Thorac Dis. 2014;6:210–20.

Address for correspondence: Bennie Lindeque, University of Colorado, 12631 E 17th Ave, Academic Office 1, Rm 4602, Mailstop B202, Aurora, CO 80045, USA; email: bennie.lindeque@ucdenver.edu

RESEARCH

Phenotypic and Genomic Analyses of *Burkholderia stabilis* Clinical Contamination, Switzerland

Helena M.B. Seth-Smith, Carlo Casanova, Rami Sommerstein, Dominik M. Meinel,[1] Mohamed M.H. Abdelbary,[2] Dominique S. Blanc, Sara Droz, Urs Führer, Reto Lienhard, Claudia Lang, Olivier Dubuis, Matthias Schlegel, Andreas Widmer, Peter M. Keller,[3] Jonas Marschall, Adrian Egli

A recent hospital outbreak related to premoistened gloves used to wash patients exposed the difficulties of defining *Burkholderia* species in clinical settings. The outbreak strain displayed key *B. stabilis* phenotypes, including the inability to grow at 42°C; we used whole-genome sequencing to confirm the pathogen was *B. stabilis*. The outbreak strain genome comprises 3 chromosomes and a plasmid, sharing an average nucleotide identity of 98.4% with *B. stabilis* ATCC27515 BAA-67, but with 13% novel coding sequences. The genome lacks identifiable virulence factors and has no apparent increase in encoded antimicrobial drug resistance, few insertion sequences, and few pseudogenes, suggesting this outbreak was an opportunistic infection by an environmental strain not adapted to human pathogenicity. The diversity among outbreak isolates (22 from patients and 16 from washing gloves) is only 6 single-nucleotide polymorphisms, although the genome remains plastic, with large elements stochastically lost from outbreak isolates.

Burkholderia is a diverse genus of gram-negative bacteria, with isolates identified from a variety of environments, and ever more species being identified and classified. Whereas some *Burkholderia* species are associated with bioremediation potential and antimicrobial and antifungal production, others are animal and human pathogens that generally fall within the *B. cepacia* complex (Bcc) (*1*). *Burkholderia* bacteria have large, flexible, multi-replicon genomes, a large metabolic repertoire, various virulence factors, and inherent resistance to many antimicrobial drugs (*2*,*3*).

An outbreak of *B. stabilis* was identified among hospitalized patients across several cantons in Switzerland during 2015–2016 (*4*). The bacterium caused bloodstream infections, noninvasive infections, and wound contaminations. The source of the infection was traced to contaminated commercially available, premoistened washing gloves used for bedridden patients. After hospitals discontinued use of these gloves, the outbreak resolved.

Many instances of Bcc strain contamination of medical devices and solutions have been described (*4*), including an outbreak in Korea associated with a 0.5% chlorhexidine solution (*5*). *B. stabilis* also has been identified in nosocomial infections (*6*–*8*).

We conducted in-depth characterization of the *B. stabilis* strain from the Switzerland outbreak by using clinical methods and whole-genome sequencing (WGS). We generated a complete draft genome by combining short- and long-read genomic data and compared it to other outbreak isolates to provide a complete genomic assessment of this strain. We provide a thorough comparative genomic analysis of this outbreak strain.

Methods

Bacterial Isolate Collection

Isolates were collected from 22 patients (labeled 1–22) and 16 contaminated washing gloves (labeled A–P) across Switzerland during the outbreak (*4*). For comparison, we

Author affiliations: University Hospital Basel, Basel, Switzerland (H.M.B. Seth-Smith, D.M. Meinel, A. Widmer, A. Egli); University of Basel, Basel (H.M.B. Seth-Smith, D.M. Meinel, A. Egli); University of Bern, Bern, Switzerland (C. Casanova, S. Droz); Bern University Hospital, Bern (R. Sommerstein, J. Marschall); Lausanne University Hospital, Lausanne, Switzerland (M.M.H. Abdelbary, D.S. Blanc); Biel Hospital, Biel, Switzerland (U. Führer); ADMED, La Chaux-de-Fonds, Switzerland (R. Lienhard); Viollier AG, Allschwil, Switzerland (C. Lang, O. Dubuis); Cantonal Hospital St. Gallen, St. Gallen, Switzerland (M. Schlegel); Swissnoso, National Center for Infection Prevention, Bern (M. Schlegel, A. Widmer, J. Marschall); University of Zurich, Zurich, Switzerland (P.M. Keller)

DOI: https://doi.org/10.3201/eid2506.172119

[1]Current affiliation: Genetics and Genomics at Roche, Basel, Switzerland.

[2]Current affiliation: RWTH Aachen University Hospital, Aachen, Germany.

[3]Current affiliation: University of Bern, Bern, Switzerland

collected 14 unrelated *Burkholderia* spp. patient isolates in Switzerland (labeled O-1 through O-14; Appendix 1 Table 1, https://wwwnc.cdc.gov/EID/article/25/6/17-2119-App1.xlsx). We obtained a control strain, *B. stabilis* ATCC27515 BAA-67, isolated in 1993 from sputum of a patient with cystic fibrosis in Belgium, from the American Type Culture Collection (ATCC, https://www.atcc.org).

Clinical Diagnostics

We performed routine identification using matrix-assisted laser desorption/ionization time-of-flight (MALDI-TOF) mass spectrometry and biochemical species identification. For MALDI-TOF mass spectrometry, we used Biotyper MBT Smart (Bruker Corporation, https://www.bruker.com) with flexControl and MBT Compass version 4.1 software. We considered scores >2.0 high confidence identification and scores of 1.7–2.0 low confidence identification. We used VITEK 2 gram negative identification card (bioMérieux, https://www.biomerieux.com) for biochemical species identification. Phenotypic antimicrobial resistance profiles were determined using disk diffusion. We interpreted breakpoints according to Clinical and Laboratory Standards Institute (*9*) standards for Bcc (ceftazidime, trimethoprim/sulfamethoxazole, and meropenem) or *Enterobacteriaceae* (aminoglycosides, ciprofloxacin, piperacillin/tazobactam, and other β-lactams). We used *Xba*I to digest DNA before using previously described pulsed-field gel electrophoresis (PFGE) molecular typing principles (*10*). We used GelCompar (Applied Maths, http://www.applied-maths.com) to analyze PFGE results.

Cellular Fatty Acid Analysis

We prepared and derivatized cellular fatty acids from outbreak isolates 7, 13, and O, with control strain *Pseudomonas aeruginosa* strain ATCC27853, as previously described (*11*). We performed chromatography on an HP 6890 gas chromatograph (Hewlett Packard Enterprise, https://www.hpe.com) and analyzed data in SHERLOCK MIS version 6.2 (Midi Inc., http://midi-inc.com).

Genome Sequencing, Assembly, Annotation, and Mapping

We extracted DNA using EZ1 Advanced XL (QIAGEN, https://www.qiagen.com) or Wizard Genomic DNA Purification kit (Promega, https://www.promega.com) and then sequenced it on the Illumina MiSeq platform (https://www.illumina.com) following Nextera XT library creation within the Division of Clinical Microbiology, University Hospital Basel (300-bp paired-end reads) or the Unit of Genomics of the Institute of Microbiology, Lausanne University Hospital (150-bp paired-end reads). We mapped data against the genome of *B. cepacia* ATCC25416 (GenBank accession nos. CP007746–8) for quality control and coverage determination (Appendix 1 Table 1). We sequenced DNA from outbreak isolate 5 on a PacBio RS II platform (Pacific Biosciences, https://www.pacb.com) with 1 SMRT cell at the Functional Genomics Centre, Zurich. We submitted read data for all samples to the European Nucleotide Archive under project nos. PRJEB18658 and PRJEB19203 (data previously analyzed; *12*).

We used CLC Genomics Workbench 9 (https://clc-genomics-workbench.software.informer.com/9.0) to assemble Illumina reads from outbreak isolate E (1,736 contigs; assembly length 8,816,302 bp) and from unrelated isolates. We processed PacBio reads with CLC Genomics Workbench 9 using an error correction of 30 or 50 and assembled resulting reads or used them to correct the Illumina assembly of E. We used Spades version 3.10.0 (*13*) to assemble the PacBio reads with Illumina reads from isolates E or 5. We manually compared assemblies in Artemis and ACT (*14*,*15*) to circularize and split chromosomes 1 and 2 according to the genome of *B. stabilis* BAA-67 (GenBank accession nos. CP016442–4) (*16*). We found chromosome 3 is a single contig that was not obviously circularizable. We used Prokka version 1.11 (*17*) for automated annotation and manually curated coding sequences (CDSs) by using Artemis and ACT. We submitted the genome draft to ENA under accession no. ERZ480954.

We performed mapping in CLC Genomics Workbench 9, which we also used to generate k-mer trees (*18*) using default parameters. For single-nucleotide polymorphism (SNP) phylogenies, we used variant calling with 5× minimum coverage, 5 minimum count, and 70% minimum frequency and created SNP trees with 5× minimum coverage, 5% minimum coverage, 0 prune distance, and multinucleotide variants.

Database and Genome Comparisons

We used multilocus sequence typing (MLST; https://cge.cbs.dtu.dk/services/MLST) to identify alleles from assemblies of isolate E and unrelated *Burkholderia* spp. (*19*) and compared these against Bcc MLST databases (https://pubmlst.org/bcc) (*20*) for species designation. We performed average nucleotide identity (ANI) determination using the ANI calculator (http://enve-omics.ce.gatech.edu/ani) (*21*), and digital DNA-DNA hybridization (dDDH) with GGDC2.1 (http://ggdc.dsmz.de/distcalc2.php) (*22*). We used antiSMASH version 4.0.0 (https://antismash.secondarymetabolites.org) (*23*) to predict gene clusters involved in antimicrobial resistance and secondary metabolite production.

Results

Clinical and Major Fatty Acid Characterization

We analyzed outbreak and unrelated *Burkholderia* spp. isolates by PFGE (Appendix 2 Figure 1, https://wwwnc.

cdc.gov/EID/article/25/6/17-2119-App2.pdf). PFGE patterns of outbreak isolates from patients and washing gloves formed a cluster separate from the unrelated isolates. Outbreak isolates shared 75.7% similarity by Pearson correlation analysis; previous studies used a value of 80% for outbreak grouping (*24*).

We conducted MALDI-TOF mass spectrometry on 12 outbreak isolates and identified *B. cepacia* group (n = 4), *B. stabilis* (n = 4), *B. multivorans* (n = 2), *B. cenocepacia* (n = 1), and *B. pyrrocinia* (n = 1) with scores of 1.88–2.21. Because MALDI-TOF mass spectrometry is known to misidentify Bcc species (*25*), we used VITEK 2 to conduct biochemical testing on isolates from 3 patients and 1 washing glove and identified either Bcc group (scores of 91%–95%) or *Acinetobacter lwoffii* (scores of 86%–91%).

Our outbreak isolates and control strain shared a defining characteristic of *B. stabilis*, the inability to grow at 42°C (*26*). Using VITEK 2, we saw 2 other key characteristics of *B. stabilis* in the outbreak strain, absence of β-galactosidase activity and inability to oxidize sucrose (Table 1). In contrast to other *B. stabilis* strains, VITEK 2 showed our strain was negative for adonitol acidification, ornithine decarboxylase, and lysine decarboxylase. Phenotypic identification of *Burkholderia* spp. often is a tedious process (*26*), with high rates of misidentification because of false negative reporting by VITEK 2 (*29*). Clinical standard identification on the VITEK 2 runs up to 16 hours, but *Burkholderia* phenotypes can take up to 7 days to develop. Our subsequent genome analysis identified genes encoding ornithine decarboxylase and lysine decarboxylase in the outbreak strain.

Cellular fatty acid profiling of 3 outbreak isolates showed profiles highly similar to the reference strains *B. stabilis* and *B. cepacia* (*26*,*30*), and expectedly distinct from control strain *P. aeruginosa* strain ATCC27853 (Appendix 1 Table 2; Appendix 2 Figure 2). Together, these assays identified the outbreak strain as a member of the genus *Burkholderia* within Bcc but did not enable a firm species-level identification.

Table 1. Biochemistry of *Burkholderia stabilis* outbreak strain from 3 patient isolates and 1 environmental isolate collected from hospitals in Switzerland, 2015–2016*

Reaction	Result	No. outbreak strains with result	Expected *B. stabilis* result†
Saccharose, sucrose‡	–	4	–
β-galactosidase‡	–	4	–
Maltose acidification	+	3	+
Adonitol acidification	–	4	+
Ornithine decarboxylase	–	4	+
Lysine decarboxylase	–	4	+
D-mannitol	–	4	+
D-glucose	+	4	+
D-cellobiose	+	4	+
Malonate	–	4	+
D-sorbitol	–	4	+
Urease	–	4	+ or –

*Performed using VITEK 2.
†From (*26*,*28*).
‡Specific discriminatory test for *B. stabilis*.

Identification of Outbreak Isolate Clade in Bcc

We conducted WGS on 22 patient isolates and 16 isolates from washing gloves. We compared a full-length 16S rRNA gene sequence derived from the genome assembly of isolate E against the National Center for Biotechnology Information nucleotide sequence database using blastn (http://blast.ncbi.nlm.nih.gov). We identified 2 top hits, both sharing 1,520 out of 1,521 nt identities, *B. pyrrocinia* DSM10685, and *B. stabilis* BAA-67. Many other Bcc species shared >99% nucleotide identity, including *B. stagnalis* MSMB735WGS, *B. cenocepacia* AU1054, *B. cenocepacia* J2315, *B. ambifaria* AMMD, and *B. lata* 383. We mapped the WGS data of all outbreak isolates against a draft assembly of isolate E and found 99%–100% coverage from all isolates, but only 60%–75% coverage from unrelated isolate sequences (Appendix 1 Table 1). K-mer analysis of outbreak and unrelated *Burkholderia* isolates showed a separate cluster of outbreak isolates (Appendix 2 Figure 3).

Table 2. Genome comparisons of *Burkholderia stabilis* outbreak strain CH16 from Switzerland against *Burkholderia* reference strains*

Reference genome	Genomovar	GenBank accession nos.	ANI,† 1-way,%	dDDH,‡ formula 2	Probability dDDH ≥70%	% G+C difference
B. stabilis ATCC BAA-67	IV	CP016442–4	98.4	87.8	94.98	0.08
B. pyrrocinina DSM10685	IX	CP011503–6	92.9	49.4	17.44	0.17
B. stabilis LA20W§	IV	GCA_001685505.1	92.5	49.3	17.3	0.16
B. lata 383		NC_007509–11	91.4	44.7	7.72	0.12
B. cepacia ATCC25416	I	NZ_CP012981–3	91.3	44.5	7.52	0.37
B. cenocepacia J2315	III	AM747720–3	91.1	44	6.68	0.55
B. ambifaria AMMD	VII	NZ_CP009798–800	89.8	39.9	2.65	0.44
B. latens AU17928		CP013435–8	88.8	37	1.22	0.03
B. dolosa AU0158	VI	CP009793–5	88.8	37.2	1.27	0.66
B. vietnamensis LMG10929	V	CP009629–32	88.5	36.2	0.97	0.48
B. multivorans DDS 15A-1	II	CP008728–30	88.3	36	0.89	0.25
B. multivorans BAA247	II	CP009830–2	88.1	35.3	0.71	0.9

*ANI, average nucleotide identity; dDDH, digital DNA-DNA hybridization.
†Species cutoff 95%.
‡Species cutoff 70%.
§From these results, strain LA20W should not be classified as *B. stabilis*.

Identification of New *B. stabilis* Strain

We used MLST to extract alleles from the genome draft to obtain a new sequence type (ST), 1095, with the following genes: *atpD* (380, new), *gltB* (456), *gyrB* (213), *lepA* (70), *phaC* (348, new), *recA* (109), *trpB* (173). The top matches to this MLST profile are all *B. stabilis* isolates sharing ≤4 of the 7 alleles. The matching isolates are from Canada, which had 4 matching alleles; and Czechia, Serbia, China, France, Italy, and the United Kingdom, each with 2 matching alleles, including the *B. stabilis* type strain ATCC27515 BAA-67.

We used ANI calculations of genomic relatedness to compare the isolate E genome draft to a comprehensive panel of sequenced Bcc strains (Table 2). *B. stabilis* BAA-67 is the most closely related with an ANI of 98.4%, which is above the species cutoff of 95% (*31*). In addition, dDDH comparing the outbreak strain to the Bcc panel showed that the maximum score of the outbreak genome is with *B. stabilis* BAA-67 at 84.2%, with the classic species threshold at 70%. These genomic parameters currently are the most robust for species designation (*32–34*) and we are confident that the outbreak strain belongs to the species *B. stabilis*. The high dDDH score might reflect the high genome conservation within this species, giving it its name (*26*).

Description of Draft of *B. stabilis* Strain CH16

A hybrid assembly of PacBio and Illumina data resulted in an improved, high-quality genome draft (*35*) of the outbreak strain, named CH16 because it occurred in Switzerland in 2016. This draft comprises 1 contig for each of the 3 chromosomes. Comparison with the genome of *B. stabilis* BAA-67 (*16*) showed that the genomes are syntenic with the exception of a rearrangement on chromosome 1 between the rRNA operons, which might be a real inversion or an assembly artifact in 1 of the genomes (Figure 1). We detected a separate contig representing a predicted plasmid sequence, whereas none was found within strain BAA-67 (J. Bugrysheva, US Centers for Disease Control and Prevention, pers. comm., 2017 Jan 10) (Table 3).

In addition to being large and multireplicon, *Burkholderia* genomes are characterized by the presence of multiple phages, genomic islands, and insertion sequences (IS elements) (*3*). The draft genome CH16 contains many insertions of single or multiple genes relative to strain BAA-67: 16 on chromosome 1; 34 on chromosome 2; and 10 on chromosome 3 (Figure 1). Appendix 1 Table 3 lists regions of difference (RDs).

The *B. stabilis* CH16 genome has a paucity of IS elements. We have identified only 40, including 6 families with copy numbers of 3–12 (Appendix 1 Table 4), that cause disruption of 9 CDSs (Appendix 1 Table 5). CH16 did not appear to be experiencing IS element expansion, which is associated with genome rearrangements, large-scale genomic deletions, and niche adaptation (*36–38*), but it has the potential for IS element expansion if it goes through a population bottleneck.

Table 3. General properties of genome draft for *Burkholderia stabilis* strain CH16 from Switzerland*

Property	Value
Draft genome size, bp	8,505,958
Chromosomes	3
Chromosome sizes, bp	3,705,321; 3,499,410; 1,230,432
Plasmid size, bp	70,922
% G+C content	66.3
Predicted CDSs (per chromosome and plasmid)	7,629 (3,402; 3,068; 1,075; 84)
Coding density	86.40%
Average gene length	965 bp
Pseudogenes	20
rRNA operons	6
tRNAs	75
Insertion elements	40

*CDSs, coding sequences.

Frameshifts and premature stop codons have created 11 additional pseudogenes (Appendix 1 Table 5). The 20 pseudogenes of CH16 contrast with 142 annotated in the genome of strain BAA-67, indicating that most of the CH16 genome is required for survival in diverse environments and that this strain is not adapting to a pathogenic lifestyle.

RDs and Virulence Factors of *B. stabilis* Strain CH16

Using genome-wide blastn comparisons, we determined that the CH16 genome carries 973 novel CDSs relative to BAA-67 of the total 7,629 CDSs (12.7%; Appendix 1 Table 3), many of which are novel to all *Burkholderia* sequenced to date. Larger insertions containing >40 CDSs are putative phages or integrative and conjugative elements. Smaller insertions of <10 CDSs appear to represent deletions in the BAA-67 strain relative to their common ancestor.

Factors that might contribute to the virulence of CH16 include adhesins and hemaglutinins, including *BSTAB16_1184*, *_5825*, *_5829*, *_5874*, *_6110*, *_6684*, *_6804*, and *_6861*, of which most have homologs in other Bcc strains; and Type II and Type VI secretion systems (*BSTAB16_4657–74*, *_5069–91*, and *_5583–9*). The many regulators within the CH16 genome and the RDs provide additional layers of translational control necessary in a genome of this size. We saw no evidence of the known *Burkholderia* virulence factors cable pilus or *B. cepacia* epidemic strain marker (*36*). The toxins we identified, for example *BSTAB16_5843* containing the HipA domain, are antibacterial toxins rather than virulence factors.

The many efflux pumps found in the CH16 genome might explain its ability to grow in the wash solution, including members of the following families: resistance nodulation and cell division, ATP-binding cassette, small multidrug resistance, multidrug and toxic compound extrusion,

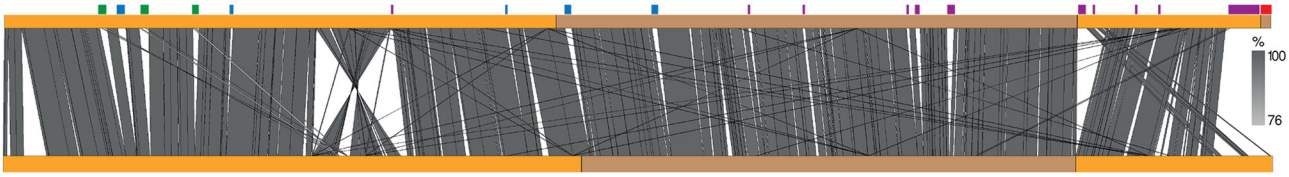

Figure 1. Comparison of the genome of *Burkholderia stabilis* strain CH16 from Switzerland (top bar) with that of *B. stabilis* reference strain BAA-67 (bottom bar). Alternating orange and brown bar sections represent chromosomes 1, 2, 3, and a plasmid. Scale bar indicates identity between the genomes (determined by blastn, http://blast.ncbi.nlm.nih.gov). Colors above the CH16 genome indicate the following: purple, regions of difference between the 2 strains; green, putative integrative and conjugative element; blue, phage; and red, the plasmid.

and major facilitator superfamily. Several secondary metabolite synthesis pathways are predicted: 4 on chromosome 1; 5 on chromosome 2; and 5 on chromosome 3 (Appendix 1 Table 6). Most of these are shared with the BAA-67 reference genome, encoding the ability to produce signaling molecules, siderophores, terpenes, and a bacteriocin, among others.

The plasmid comprises largely novel sequences not seen before within the *Burkholderia* or elsewhere. It carries genes predicted to be involved in conjugation, indicating that it might be a mobile plasmid, such as 1 recently hypothesized in *B. cenocepacia* (*39*). The rest of the plasmid largely comprises genes encoding hypothetical proteins.

Antimicrobial Drug Resistance of *B. stabilis* Strain CH16

We performed phenotypic antimicrobial drug susceptibility testing on a subset of outbreak isolates (Appendix 1 Table 7) and used genomic findings to interpret the results. Breakpoints are not established clinically and are not recommended to guide patient therapy (*40*).

All Bcc isolates are intrinsically resistant to aminoglycosides (*40*), which we confirmed in our isolates. Intrinsic resistance also is described against chloramphenicol and tetracycline (*40*) (not tested) through the presence of efflux pumps. We identified several efflux pumps within the CH16 genome (*BSTAB16_5335–6*, *_4605–6*, and *_7210–1*), none of which are unique to the outbreak strain. Sensitivity to trimethoprim/sulfamethoxazole was a feature of the outbreak isolates; we did not identify trimethoprim/sulfamethoxazole resistance determinants in the draft genome.

Bcc is considered to be intrinsically and clinically resistant to many β-lactams through impermeability and the presence of inducible β-lactamases (*40*). All Bcc isolates tested were resistant to aminopenicillins, carboxypenicillins, and first-generation cephalosporins. Phenotypic resistance to third-generation cephalosporins, ureidopenicillins, and carbapenems was more variable among Bcc. We identified several β-lactamases in the CH16 genome, representing class A (*BSTAB16_4862* and *_4440*), class C (*BSTAB16_6957*), class D (*BSTAB16_5918*), and metallo-β-lactamases (*BSTAB16_ 3974* and *_5115*), none of which are unique to this strain.

The outbreak isolates are sensitive to ciprofloxacin, in contrast to *B. stabilis* BAA-67, with sporadic resistance seen among other Bcc isolates. Resistance can be associated with efflux (*40*) or specific mutations in *gyrA* (*BSTAB16_1445*). The *gyrA* of CH16 differs from that of strain BAA-67 at I83T and A700S (numbered according to *E. coli*). In general, this strain does not display enhanced antimicrobial resistance compared with other clinical Bcc isolates or *B. stabilis* BAA-67 (*2*,*41*,*42*).

Of note, some of the outbreak isolates had anomalous antibiograms, which we confirmed through repeated testing (Appendix 1 Table 7). This finding might relate to colony morphology because several morphotypes were observed during clinical work on the outbreak isolates. This phenomenon is known to occur within *Burkholderia* (*43–46*), resulting from reversible colony morphotype switching (*44*) or stable mutations (*43*,*46*). Altered genes often are involved in exopolysaccharide production, also causing changes in biofilm production, virulence, resistance, and motility (*43–46*), and might result from stress (*44*,*45*).

Comparison of Outbreak Isolates

PFGE and k-mer analyses showed that the outbreak isolates cluster. We investigated how related the isolates are by comparing genomes using high-quality SNPs. The SNP phylogeny (Figure 2) indicates a maximum of 6 SNPs between isolates from the outbreak source, in agreement with Abdelbary et al. (*12*). The previously published core genome MLST (cgMLST) phylogeny used the same genome data but indicated up to 18 alleles difference between isolates (*4*), though these are likely artifacts of the methodology (*47*).

Washing glove isolates were located throughout the phylogeny; we observed diversity within a lot number (isolates E–F and L–O), and even within single packets (isolates A, B, and L–O). Patient samples also were found throughout the phylogeny, even those originating from the same city (isolates 5, 7, 9–13 are from a first city; 6, 8, 21,

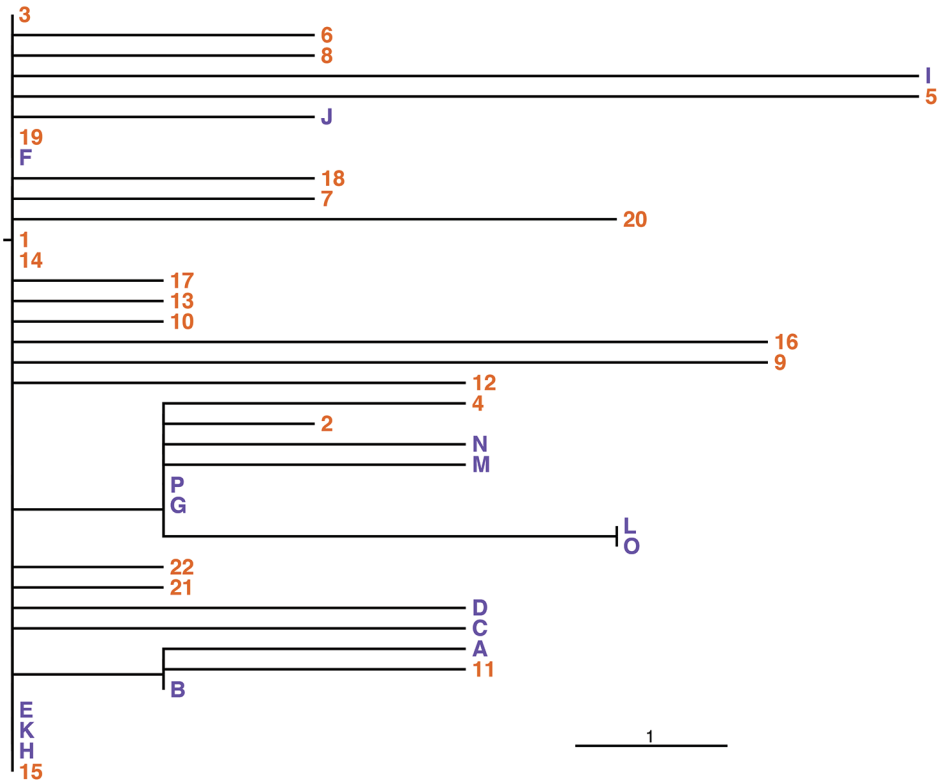

Figure 2. Phylogeny of outbreak isolates of *Burkholderia stabilis* strain CH16 from Switzerland based on high-quality single nucleotide polymorphisms (SNPs). This phylogeny of all sequenced outbreak isolates might represent a conservative estimate of SNP numbers. Given the large genome size and possible mismapping to repeats, it is difficult to determine the ultimate number of SNPs between samples. This phylogeny was confirmed using several parameters and manual checking of called SNPs. The root was arbitrarily chosen to give the fewest root to tip SNPs (n = 6). Numbers represent isolates from patients; letters represent isolates from washing gloves, located in the root position. Scale bar indicates 1 SNP.

and 22 are from a second city; and 14–20 are from a third city), reflecting trends seen from cgMLST data (*4*).

SNP locations (Appendix 1 Table 8) indicate that, of the 40 nonsynonymous SNPs, 15 are in genes predicted to encode regulators, 6 in transporters, and 3 in flagellin. We could not tell whether these are random mutations or have been subject to selective pressure, but all classes are represented in both glove and patient isolates.

In addition to the SNPs, we saw some large-scale genomic differences. By mapping read data against each individual replicon, we noted that isolates E and 20 do not carry the plasmid, which appears to be a stochastic event because the SNP phylogeny indicates that these isolates are not derived from a common ancestor. Isolates D and E have highly similar PFGE patterns (Appendix 2 Figure 1), suggesting that the plasmid does not affect the PFGE results or was lost during laboratory culture. Patient isolate 22 also shows the loss of the first 52.5 kb of chromosome 3, representing an RD, which this isolate apparently lost spontaneously during the course of the outbreak. Because of this genome plasticity, we hypothesize the CH16 genome was changing even during the course of the outbreak.

Discussion

We provide a thorough and detailed description of a *Burkholderia* sp. outbreak resolved by WGS (*4*) and illustrate various associated challenges, including morphotype differences, species designation, and a large genome with associated assembly, annotation, and interpretation issues. Defining species within Bcc is notoriously difficult (*26*), whether phenotypically by using biochemical or MALDI-TOF mass spectrometry profiles, genomically by using 16S rRNA gene sequences, or both. WGS provides the most thorough analysis and is increasingly cost and time effective, even compared with sequencing MLST loci, interpretation of which also is complex. We saw anomalies between the phenotype of this *B. stabilis* outbreak strain and those described in the literature (*26*,*27*) due to shorter than optimal test incubation times in standard clinical phenotyping (*29*).

Several techniques can be used on WGS data to provide phylogenies. K-mer analysis (Appendix 2 Figure 3) provides an indication of clustering, but the branch lengths cannot be relied on to provide a true phylogeny and do not truly reveal relationships within clades. With this technique, a lot of genomic information regarding the coding capacity of the genome is lost. cgMLST compares nucleotide sequences of CDSs common to a group of isolates, linking isolates with the highest numbers of identical alleles. During this process some genomic data necessarily are lost, with information from accessory genes and intergenic regions disregarded. However, both methods can be performed routinely with minimal training to enable rapid visualization of outbreak

clusters. Comparing reads from all outbreak isolates to an assembled draft genome to generate a SNP phylogeny includes all genomic information but requires more computation, time, and expertise.

WGS is the optimal way to determine the detailed relationships between isolates, giving insights into an outbreak and providing a basis from which to develop further typing methods. For future cases, we suggest rapid WGS, extraction of MLST alleles from assemblies for species identification as recommended by Mahenthiralingam et al. (*48*), and cgMLST typing for rapid outbreak identification. SNP detection can be a valuable subsequent step to determine accurate relatedness of isolates.

Bcc bacteria are known to survive in pharmaceutical and disinfectant materials (*1*,*48*,*49*). *B. stabilis* strains sharing MLST types can be isolated from the natural environment, hospitals, and patients (*50*), implicating the natural environment as a source of opportunistic *Burkholderia* and emphasizing the versatility of Bcc to survive and grow under diverse conditions. The CH16 genome displays features representative of *Burkholderia* in general; it is large, highly plastic, and contains many novel elements that might be involved in pathogenesis or environmental survival (*36*). The low number of pseudogenes and IS elements indicates that this strain has not undergone niche adaptation, and most likely is an opportunistic pathogen (*36*–*38*).

The cloud of diversity seen in the SNP phylogeny indicates that the source of the original contamination was not clonal or that several mutations occurred during the incubation of CH16 within the patient washing gloves. The loss of genomic elements, including the plasmid, from some of the isolates, also demonstrates the flexibility and the redundancy within such a large genome. Our study shows the importance of WGS in investigating and resolving this outbreak, which appears to have been caused by an environmental Bcc strain.

Acknowledgments

We thank Clarisse Straub, Elisabeth Schultheiss, and Christine Kiessling for excellent technical assistance in performing whole-genome sequencing; Andrea Patrignani for PacBio sequencing; Doris Hohler for performing the phenotypic and antimicrobial testing; and Peter Vandamme for advice on species definition. Assemblies were performed at sciCORE (http://scicore.unibas.ch) scientific computing facility at the University of Basel.

A.E. received a research grant from the Swiss National Science Foundation (Ambizione grant no. PZ00P3_154709/1). We used the *Burkholderia cepacia* complex Multi Locus Sequence Typing website (http://pubmlst.org/bcc) developed by Keith Jolley (*20*), located at the University of Oxford and funded by the Wellcome Trust.

About the Author

Dr. Seth-Smith works in clinical microbiology at University Hospital Basel, using whole-genome sequencing data to answer questions relating to emerging pathogens, outbreaks, and transmission.

References

1. Depoorter E, Bull MJ, Peeters C, Coenye T, Vandamme P, Mahenthiralingam E. *Burkholderia*: an update on taxonomy and biotechnological potential as antibiotic producers. Appl Microbiol Biotechnol. 2016;100:5215–29. http://dx.doi.org/10.1007/s00253-016-7520-x
2. Nzula S, Vandamme P, Govan JRW. Influence of taxonomic status on the in vitro antimicrobial susceptibility of the *Burkholderia cepacia* complex. J Antimicrob Chemother. 2002;50:265–9. http://dx.doi.org/10.1093/jac/dkf137
3. Burns J. Antibiotic resistance of *Burkholderia* species. In: Coenye T, Vandamme P, editors. *Burkholderia*: molecular microbiology and genomics. Wymondham, England, UK: Horizon Bioscience; 2006. p. 81–91.
4. Sommerstein R, Führer U, Lo Priore E, Casanova C, Meinel DM, Seth-Smith HM, et al. *Burkholderia stabilis* outbreak associated with contaminated commercially-available washing gloves, Switzerland, May 2015 to August 2016. Euro Surveill. 2017;22:pii:17-00213. http://dx.doi.org/10.2807/1560-7917.ES.2017.22.49.17-00213
5. Ko S, An HS, Bang JH, Park SW. An outbreak of *Burkholderia cepacia* complex pseudobacteremia associated with intrinsically contaminated commercial 0.5% chlorhexidine solution. Am J Infect Control. 2015;43:266–8. http://dx.doi.org/10.1016/j.ajic.2014.11.010
6. Otağ F, Ersöz G, Salcioğlu M, Bal C, Schneider I, Bauernfeind A. Nosocomial bloodstream infections with *Burkholderia stabilis.* J Hosp Infect. 2005;59:46–52. http://dx.doi.org/10.1016/j.jhin.2004.06.034
7. Heo ST, Kim SJ, Jeong YG, Bae IG, Jin JS, Lee JC. Hospital outbreak of *Burkholderia stabilis* bacteraemia related to contaminated chlorhexidine in haematological malignancy patients with indwelling catheters. J Hosp Infect. 2008;70:241–5. http://dx.doi.org/10.1016/j.jhin.2008.07.019
8. Wang L, Wang M, Zhang J, Wu W, Lu Y, Fan Y. An outbreak of *Burkholderia stabilis* colonization in a nasal ward. Int J Infect Dis. 2015;33:71–4. http://dx.doi.org/10.1016/j.ijid.2014.12.046
9. Clinical and Laboratory Standards Institute.Performance standards for antimicrobial susceptibility testing (M100–S27). Wayne (PA); The Institute; 2017.
10. Strandén A, Frei R, Widmer AF. Molecular typing of methicillin-resistant *Staphylococcus aureus*: can PCR replace pulsed-field gel electrophoresis? J Clin Microbiol. 2003;41:3181–6. http://dx.doi.org/10.1128/JCM.41.7.3181-3186.2003
11. Osterhout GJ, Shull VH, Dick JD. Identification of clinical isolates of gram-negative nonfermentative bacteria by an automated cellular fatty acid identification system. J Clin Microbiol. 1991;29:1822–30.
12. Abdelbary MMH, Senn L, Moulin E, Prod'hom G, Croxatto A, Greub G, et al. Evaluating the use of whole-genome sequencing for outbreak investigations in the lack of closely related reference genome. Infect Genet Evol. 2018 Apr;59:1–6. http://dx.doi.org/10.1016/j.meegid.2018.01.014
13. Bankevich A, Nurk S, Antipov D, Gurevich AA, Dvorkin M, Kulikov AS, et al. SPAdes: a new genome assembly algorithm and its applications to single-cell sequencing. J Comput Biol. 2012;19:455–77. http://dx.doi.org/10.1089/cmb.2012.0021
14. Carver TJ, Rutherford KM, Berriman M, Rajandream MA, Barrell BG, Parkhill J. ACT: the Artemis Comparison Tool.

Bioinformatics. 2005;21:3422–3. http://dx.doi.org/10.1093/bioinformatics/bti553
15. Rutherford K, Parkhill J, Crook J, Horsnell T, Rice P, Rajandream M-A, et al. Artemis: sequence visualization and annotation. Bioinformatics. 2000;16:944–5. http://dx.doi.org/10.1093/bioinformatics/16.10.944
16. Bugrysheva JV, Cherney B, Sue D, Conley AB, Rowe LA, Knipe KM, et al. Complete genome sequences for three chromosomes of the *Burkholderia stabilis* type strain (ATCC BAA-67). Genome Announc. 2016;4:e01294-16. http://dx.doi.org/10.1128/genomeA.01294-16
17. Seemann T. Prokka: rapid prokaryotic genome annotation. Bioinformatics. 2014;30:2068–9. http://dx.doi.org/10.1093/bioinformatics/btu153
18. Larsen MV, Cosentino S, Lukjancenko O, Saputra D, Rasmussen S, Hasman H, et al. Benchmarking of methods for genomic taxonomy. J Clin Microbiol. 2014;52:1529–39. http://dx.doi.org/10.1128/JCM.02981-13
19. Larsen MV, Cosentino S, Rasmussen S, Friis C, Hasman H, Marvig RL, et al. Multilocus sequence typing of total-genome-sequenced bacteria. J Clin Microbiol. 2012;50:1355–61. http://dx.doi.org/10.1128/JCM.06094-11
20. Jolley KA, Maiden MC. BIGSdb: Scalable analysis of bacterial genome variation at the population level. BMC Bioinformatics. 2010;11:595. http://dx.doi.org/10.1186/1471-2105-11-595
21. Goris J, Konstantinidis KT, Klappenbach JA, Coenye T, Vandamme P, Tiedje JM. DNA-DNA hybridization values and their relationship to whole-genome sequence similarities. Int J Syst Evol Microbiol. 2007;57:81–91. http://dx.doi.org/10.1099/ijs.0.64483-0
22. Auch AF, von Jan M, Klenk H-P, Göker M. Digital DNA-DNA hybridization for microbial species delineation by means of genome-to-genome sequence comparison. Stand Genomic Sci. 2010;2:117–34. http://dx.doi.org/10.4056/sigs.531120
23. Weber T, Blin K, Duddela S, Krug D, Kim HU, Bruccoleri R, et al. antiSMASH 3.0—a comprehensive resource for the genome mining of biosynthetic gene clusters. Nucleic Acids Res. 2015;43(W1):W237–43. http://dx.doi.org/10.1093/nar/gkv437
24. Chetoui H, Melin P, Struelens MJ, Delhalle E, Nigo MM, De Ryck R, et al. Comparison of biotyping, ribotyping, and pulsed-field gel electrophoresis for investigation of a common-source outbreak of *Burkholderia pickettii* bacteremia. J Clin Microbiol. 1997;35:1398–403.
25. Fehlberg LC, Andrade LH, Assis DM, Pereira RH, Gales AC, Marques EA. Performance of MALDI-ToF MS for species identification of *Burkholderia cepacia* complex clinical isolates. Diagn Microbiol Infect Dis. 2013;77:126–8. http://dx.doi.org/10.1016/j.diagmicrobio.2013.06.011
26. Vandamme P, Mahenthiralingam E, Holmes B, Coenye T, Hoste B, De Vos P, et al. Identification and population structure of *Burkholderia stabilis* sp. nov. (formerly *Burkholderia cepacia* genomovar IV). J Clin Microbiol. 2000;38:1042–7.
27. Henry DA, Mahenthiralingam E, Vandamme P, Coenye T, Speert DP. Phenotypic methods for determining genomovar status of the *Burkholderia cepacia* complex. J Clin Microbiol. 2001;39:1073–8. http://dx.doi.org/10.1128/JCM.39.3.1073-1078.2001
28. Vandamme P, Holmes B, Vancanneyt M, Coenye T, Hoste B, Coopman R, et al. Occurrence of multiple genomovars of *Burkholderia cepacia* in cystic fibrosis patients and proposal of *Burkholderia multivorans* sp. nov. Int J Syst Bacteriol. 1997;47:1188–200. http://dx.doi.org/10.1099/00207713-47-4-1188
29. Zbinden A, Böttger EC, Bosshard PP, Zbinden R. Evaluation of the colorimetric VITEK 2 card for identification of gram-negative nonfermentative rods: comparison to 16S rRNA gene sequencing. J Clin Microbiol. 2007;45:2270–3. http://dx.doi.org/10.1128/JCM.02604-06
30. Samuels SB, Moss CW, Weaver RE. The fatty acids of *Pseudomonas multivorans* (*Pseudomonas cepacia*) and *Pseudomonas kingii*. J Gen Microbiol. 1973;74:275–9. http://dx.doi.org/10.1099/00221287-74-2-275
31. Rodriguez-R L, Konstantinidis K. Bypassing cultivation to identify bacterial species. Microbe. 2014;9:111–8. http://dx.doi.org/10.1128/microbe.9.111.1
32. Peeters C, Meier-Kolthoff JP, Verheyde B, De Brandt E, Cooper VS, Vandamme P. Phylogenomic study of *Burkholderia glathei*-like organisms, proposal of 13 novel *Burkholderia* species and emended descriptions of *Burkholderia sordidicola, Burkholderia zhejiangensis*, and *Burkholderia grimmiae.* Front Microbiol. 2016;7:877. http://dx.doi.org/10.3389/fmicb.2016.00877
33. Meier-Kolthoff JP, Auch AF, Klenk H-P, Göker M. Genome sequence-based species delimitation with confidence intervals and improved distance functions. BMC Bioinformatics. 2013;14:60. http://dx.doi.org/10.1186/1471-2105-14-60
34. Vandamme P, Peeters C. Time to revisit polyphasic taxonomy. Antonie van Leeuwenhoek. 2014;106:57–65. http://dx.doi.org/10.1007/s10482-014-0148-x
35. Chain PS, Grafham DV, Fulton RS, Fitzgerald MG, Hostetler J, Muzny D, et al.; Genomic Standards Consortium Human Microbiome Project Jumpstart Consortium. Genomics. Genome project standards in a new era of sequencing. Science. 2009;326:236–7. http://dx.doi.org/10.1126/science.1180614
36. Holden MT, Seth-Smith HM, Crossman LC, Sebaihia M, Bentley SD, Cerdeño-Tárraga AM, et al. The genome of *Burkholderia cenocepacia* J2315, an epidemic pathogen of cystic fibrosis patients. J Bacteriol. 2009;191:261–77. http://dx.doi.org/10.1128/JB.01230-08
37. Parkhill J, Sebaihia M, Preston A, Murphy LD, Thomson N, Harris DE, et al. Comparative analysis of the genome sequences of *Bordetella pertussis, Bordetella parapertussis* and *Bordetella bronchiseptica*. Nat Genet. 2003;35:32–40 http://dx.doi.org/10.1038/ng1227
38. Stinear TP, Seemann T, Harrison PF, Jenkin GA, Davies JK, Johnson PD, et al. Insights from the complete genome sequence of *Mycobacterium marinum* on the evolution of *Mycobacterium tuberculosis.* Genome Res. 2008;18:729–41. http://dx.doi.org/10.1101/gr.075069.107
39. Fernández-González E, Bakioui S, Gomes MC, O'Callaghan D, Vergunst AC, Sangari FJ, et al. A Functional *oriT* in the Ptw Plasmid of *Burkholderia cenocepacia* Can Be Recognized by the R388 Relaxase TrwC. Front Mol Biosci. 2016;3:16. http://dx.doi.org/10.3389/fmolb.2016.00016
40. European Committee on Antimicrobial Susceptibility Testing. Antimicrobial susceptibility of *Burkholderia cepacia* complex (BCC). Stockholm: EUCAST; 2013 [cited 01 Dec 2017]. http://www.eucast.org/fileadmin/src/media/PDFs/EUCAST_files/General_documents/BCC_susceptibility_testing_130719.pdf
41. Peeters E, Nelis HJ, Coenye T. In vitro activity of ceftazidime, ciprofloxacin, meropenem, minocycline, tobramycin and trimethoprim/sulfamethoxazole against planktonic and sessile *Burkholderia cepacia* complex bacteria. J Antimicrob Chemother. 2009;64:801–9. http://dx.doi.org/10.1093/jac/dkp253
42. Tseng S-P, Tsai W-C, Liang C-Y, Lin Y-S, Huang J-W, Chang C-Y, et al. The contribution of antibiotic resistance mechanisms in clinical *Burkholderia cepacia* complex isolates: an emphasis on efflux pump activity. PLoS One. 2014;9:e104986. http://dx.doi.org/10.1371/journal.pone.0104986
43. Silva IN, Ferreira AS, Becker JD, Zlosnik JE, Speert DP, He J, et al. Mucoid morphotype variation of *Burkholderia multivorans* during chronic cystic fibrosis lung infection is correlated with changes in metabolism, motility, biofilm formation and virulence. Microbiology. 2011;157:3124–37. http://dx.doi.org/10.1099/mic.0.050989-0

44. Chantratita N, Wuthiekanun V, Boonbumrung K, Tiyawisutsri R, Vesaratchavest M, Limmathurotsakul D, et al. Biological relevance of colony morphology and phenotypic switching by *Burkholderia pseudomallei.* J Bacteriol. 2007;189:807–17. http://dx.doi.org/10.1128/JB.01258-06
45. Zlosnik JE, Hird TJ, Fraenkel MC, Moreira LM, Henry DA, Speert DP. Differential mucoid exopolysaccharide production by members of the *Burkholderia cepacia* complex. J Clin Microbiol. 2008;46:1470–3. http://dx.doi.org/10.1128/JCM.02273-07
46. Bernier SP, Nguyen DT, Sokol PA. A LysR-type transcriptional regulator in *Burkholderia cenocepacia* influences colony morphology and virulence. Infect Immun. 2008;76:38–47. http://dx.doi.org/10.1128/IAI.00874-07
47. Leekitcharoenphon P, Nielsen EM, Kaas RS, Lund O, Aarestrup FM. Evaluation of whole genome sequencing for outbreak detection of *Salmonella enterica.* PLoS One. 2014;9:e87991. http://dx.doi.org/10.1371/journal.pone.0087991
48. Mahenthiralingam E, Baldwin A, Dowson CG. *Burkholderia cepacia* complex bacteria: opportunistic pathogens with important natural biology. J Appl Microbiol. 2008;104:1539–51. http://dx.doi.org/10.1111/j.1365-2672.2007.03706.x
49. Haim MS, Mollerach M, Van Domselaar G, Teves SA, Degrossi J, Cardona ST. Draft Genome Sequences of *Burkholderia contaminans* FFI-28, a strain isolated from a contaminated pharmaceutical solution. Genome Announc. 2016;4:e01177-16. http://dx.doi.org/10.1128/genomeA.01177-16
50. Baldwin A, Mahenthiralingam E, Drevinek P, Vandamme P, Govan JR, Waine DJ, et al. Environmental *Burkholderia cepacia* complex isolates from human infections. Emerg Infect Dis. 2007;13:458–61. http://dx.doi.org/10.3201/eid1303.060403

Address for correspondence: Helena M.B. Seth-Smith or Adrian Egli, Universitätsspital Basel, Division of Clinical Bacteriology and Mycology, Petersgraben 4, Basel 4031, Switzerland; email: helena.seth-smith@usb.ch or adrian.egli@usb.ch

EMERGING INFECTIOUS DISEASES®

June 2018

Zoonoses

- Ferrets as Models for Influenza Virus Transmission Studies and Pandemic Risk Assessments
- Occupation-Associated Fatal Limbic Encephalitis Caused by Variegated Squirrel Bornavirus 1, Germany, 2013
- Use of Bead-Based Serologic Assay to Evaluate Chikungunya Virus Epidemic, Haiti
- Widespread *Treponema pallidum* Infection in Nonhuman Primates, Tanzania
- Genomic Epidemiology of Global Carbapenemase-Producing *Enterobacter* spp., 2008–2014
- Influenza D Virus Infection in Feral Swine Populations, United States
- Prion Disease in Dromedary Camels, Algeria
- Frequent Implication of Multistress-Tolerant *Campylobacter jejuni* in Human Infections
- Bioclinical Test to Predict Nephropathia Epidemica Severity at Hospital Admission
- Hepatitis E in Long-Term Travelers from the Netherlands to Subtropical and Tropical Countries, 2008–2011
- Novel Parvovirus Related to Primate Bufaviruses in Dogs
- Novel Poxvirus in Proliferative Lesions of Wild Rodents in East Central Texas, USA
- *Rickettsia parkeri* in Dermacentor parumapertus Ticks, Mexico
- Foot-and-Mouth Disease in the Middle East Caused by an A/ASIA/G-VII Virus Lineage, 2015–2016
- Novel *Salmonella enterica* Serovar Typhimurium Genotype Levels as Herald of Seasonal Salmonellosis Epidemics
- Urban Wild Boars and Risk for Zoonotic *Streptococcus suis*, Spain
- Human Endophthalmitis Caused by Pseudorabies Virus Infection, China, 2017
- Pulmonary Infections with Nontuberculous Mycobacteria, Catalonia, Spain, 1994–2014
- Westward Spread of Highly Pathogenic Avian Influenza A(H7N9) Virus among Humans, China
- Importation of Human Seoul Virus Infection to Germany from Indonesia

To revisit the June 2018 issue, go to:
https://wwwnc.cdc.gov/eid/articles/issue/24/6/table-of-contents

Patterns of Abundance, Host Use, and Everglades Virus Infection in *Culex* (*Melanoconion*) *cedecei* Mosquitoes, Florida, USA

Isaiah J. Hoyer, Carolina Acevedo, Keenan Wiggins, Barry W. Alto, Nathan D. Burkett-Cadena

Everglades virus (EVEV), subtype II within the Venezuelan equine encephalitis (VEE) virus complex, is a mosquito-borne zoonotic pathogen endemic to south Florida, USA. EVEV infection in humans is considered rare, probably because of the sylvatic nature of the vector, the *Culex* (*Melanoconion*) *cedecei* mosquito. The introduction of *Cx. panocossa*, a tropical vector mosquito of VEE virus subtypes that inhabits urban areas, may increase human EVEV exposure. Field studies investigating spatial and temporal patterns of abundance, host use, and EVEV infection of *Cx. cedecei* mosquitoes in Everglades National Park found that vector abundance was dynamic across season and region. Rodents, particularly *Sigmodon hispidus* rats, were primary vertebrate hosts, constituting 77%–100% of *Cx. cedecei* blood meals. Humans were fed upon at several locations. We detected EVEV infection in *Cx. cedecei* mosquitoes in lower and upper regions of Everglades National Park only during the wet season, despite an abundance of *Cx. cedecei* mosquitoes at other sampling times.

Everglades virus (EVEV) is a mosquitoborne alphavirus endemic to the state of Florida, USA, and is subtype II within the Venezuelan equine encephalitis (VEE) complex (*1*). The mosquito *Culex* (*Melanoconion*) *cedecei* is the sole enzootic vector of EVEV (*2–4*); rodents, particularly *Peromyscus gossypinus* (cotton mouse) and *Sigmodon hispidus* (hispid cotton rat), are the primary reservoir hosts (*5–7*). Clinical cases of EVEV infection in humans are considered rare; symptoms consist of nonspecific influenza-like febrile illness that can culminate in serious neurologic damage (*1*). The recent introduction and establishment of *Cx. panocossa* mosquitoes into Florida (*8*) could increase human exposure to EVEV because this species is a vector of endemic VEEV strains in Central America (*9,10*) and is abundant in manmade waterways supporting water lettuce (*8,11*). Studies in Panama concluded that *Cx. panocossa* (as *Cx. aikenii*) mosquitoes were the most important VEE vector on the basis of high VEE experimental transmission rates (*9*), high experimental infection rates (*9*), high population density (*9*), and feeding upon VEE reservoir hosts (*10,11*). The establishment of *Cx. panocossa* mosquitoes in urban areas could link sylvatic transmission foci of EVEV with densely populated areas such as the greater Miami metropolitan area through vegetated canals (*8*).

Evidence of sporadic human infections with EVEV in south Florida in the 1960s (*12,13*) spurred numerous field and laboratory studies to investigate the natural transmission cycle of the virus, focusing on determining the natural vectors and reservoirs of EVEV. These studies concluded that *Cx. cedecei* mosquitoes transmit EVEV between the amplifying rodent hosts (cotton mouse and hispid cotton rat) (*2–6*) in hammocks of the Greater Everglades ecosystem. Although EVEV vector and reservoirs were firmly incriminated, researchers repeatedly encountered unexplained large heterogeneity in EVEV transmission, even at very small scales, in Florida. For example, Chamberlain et al. (*2*) found that EVEV infection rates in vectors ranged from 0.18% (n = 533) to 1.7% (n = 58) in *Culex* (*Melanoconion*) spp. mosquitoes at 3 of 4 Everglades research areas in 1963 and 1964, but the virus was not recovered from Pa-hay-okee Overlook, despite relatively high exposure rates (20%) in rodents at that site (*2*). At Mahogany Hammock, 12 EVEV isolations were made from *Culex* (*Melanoconion*) females (average infection rate 0.53%), even though exposure rates in rodents at Mahogany Hammock were lower than at Pa-hay-okee (*2*). In subsequent field studies north of Everglades National Park (ENP), Bigler et al. (*14*) demonstrated that EVEV appeared and circulated at different time periods during the year at 2 hammocks, despite their similarity and proximity (<3 km). Although the density of cotton mice varied between hammocks, the populations and seasonal fluctuations in age ratios and breeding

Author affiliation: University of Florida, Vero Beach, Florida, USA

DOI: https://doi.org/10.3201/eid2506.180338

activity were comparable (*14*). The moderate abundance and low levels of EVEV activity in vectors led the researchers to hypothesize that mechanisms other than host densities, populations, age structure, and mosquito infection all contributed to fluctuations of EVEV transmission between the 2 hammocks (*14*).

We conducted our study to quantify the spatial and seasonal patterns of abundance, host use, and EVEV infection of *Cx. cedecei* mosquitoes in ENP to explore potential explanations for heterogeneity in EVEV prevalence observed in prior studies. We aspirated resting adult mosquitoes from 15 locations along ≈50 km of Main Park Road of ENP, where endemic EVEV transmission has been demonstrated in past studies. We used PCR assays to quantify host associations and EVEV infection in the mosquitoes and used logistic regression to investigate associations between EVEV infection, vector abundance, and host use.

Methods

We sampled mosquitoes in a variety of habitats along Main Park Road from the Everglades Visitor Center to Flamingo (permit EVER-2015-SCI-0054). The sampling locations were divided into 3 regions, upper, middle, and lower, representing natural physiographic regions of south Florida (Table 1; Figure 1). The upper region, from Royal Palm North (25°24′08.3″N, 80°36′56.7″W) to Pa-hay-okee South (25°25′56.0″N, 80°46′38.9″W), was dominated by large expanses of upland pine or hardwood forest. The middle region, from just south of Pa-hay-okee South extending to Nine Mile Pond (25°15′14.1″N, 80°47′53.5″W), was dominated by wet sawgrass prairie (Everglades marsh) with smaller hardwood hammocks (tree islands). The lower region, from Snake Bight Trail to Bear Lake Trail (25°8′55.82″N, 80°55′23.69″W), was dominated by extensive mangrove swamp.

We aspirated all mosquitoes from resting shelters (*15*), except at Mahogany Hammock, where we targeted natural resting sites, such as fallen logs and deep recesses, to abide by permit restrictions. We performed aspirations using a modified handheld battery-powered vacuum (DustBuster BDH1800S; Black and Decker Corporation, https://www.blackanddecker.com) fitted with a funnel and stainless-steel mesh-bottom collection cup (BioQuip model 2846D; BioQuip Products, Inc., https://www.bioquip.com), as described previously (*16,17*). Resting shelters were equivalent in size

Table 1. Collection of female *Culex cedecei* mosquitoes by sampling site, Everglades National Park, Florida, USA, 2016

Region	Site name and coordinates	Habitat	Mos. sampled	No. resting shelter days*	Total no. females	No. females/ shelter-day
Upper	Royal Palm North, 25°24′7.43″N, 80°36′56.40″W	Extensive hardwood hammock	Feb, May, Jun, Aug	60	810	13.50
	Long Pine Key North, 25°25′3.00″N, 80°38′20.00″W	Small island hammock	Jun, Aug	8	147	18.38
	Long Pine Key Campground, 25°24′0.10″N, 80°39′35.40″W	Extensive pine rockland	Feb	4	5	1.25
	Pinelands, 25°25′24.80″N, 80°40′47.00″W	Extensive pine rockland	May, Jun, Aug	44	107	2.43
	Pa-hay-okee South, 25°25′56.00″N, 80°46′38.90″W	Small island hammock	Feb, May	18	1	0.06
	Pa-hay-okee Overlook, 25°26′27.20″N, 80°47′1.60″W	Large island hammock	Jun, Aug	24	24	1.00
Middle	Ficus Pond, 25°21′24.00″N, 80°49′20.00″W	Small island hammock	Jun, Aug	8	47	5.88
	Mahogany Hammock East, 25°20′20.00″N, 80°49′4.80″W	Small island hammock	Feb, May, Jun, Aug	50	287	5.74
	Mahogany Hammock,† 25°19′22.50″N, 80°49′59.40″W	Large island hammock	May, Jun	4	2	0.50
	Sweet Bay Pond, 25°19′55.00″N, 80°48′10.00″W	Small island hammock	Jun, Aug	8	16	2.00
	Paurotis Pond, 25°18′7.00″N, 80°47′56.00″W	Small island hammock	Jun, Aug	8	42	5.25
	Nine Mile Pond, 25°15′13.93″N, 80°47′53.64″W	Ecotone of prairie and mangrove	Feb, May, Jun, Aug	53	942	17.77
Lower	Snake Bight Trail, 25°11′59.87″N, 80°52′27.08″W	Mangrove swamp	Feb, May, Jun, Aug	53	702	13.25
	Coot Bay Pond, 25°10′56.90″N, 80°53′51.80″W	Mangrove swamp	Feb	6	28	4.67
	Bear Lake Trail, 25° 8′55.82″N, 80°5523.69″W	Extensive cottonwood hammock	Feb, May, Jun, Aug	58	253	4.36
Totals				406	3,413	6.40

*Resting shelter days is no. of resting shelters deployed × total no. days sampled.
†Natural aspirations were performed to abide by permit restrictions.

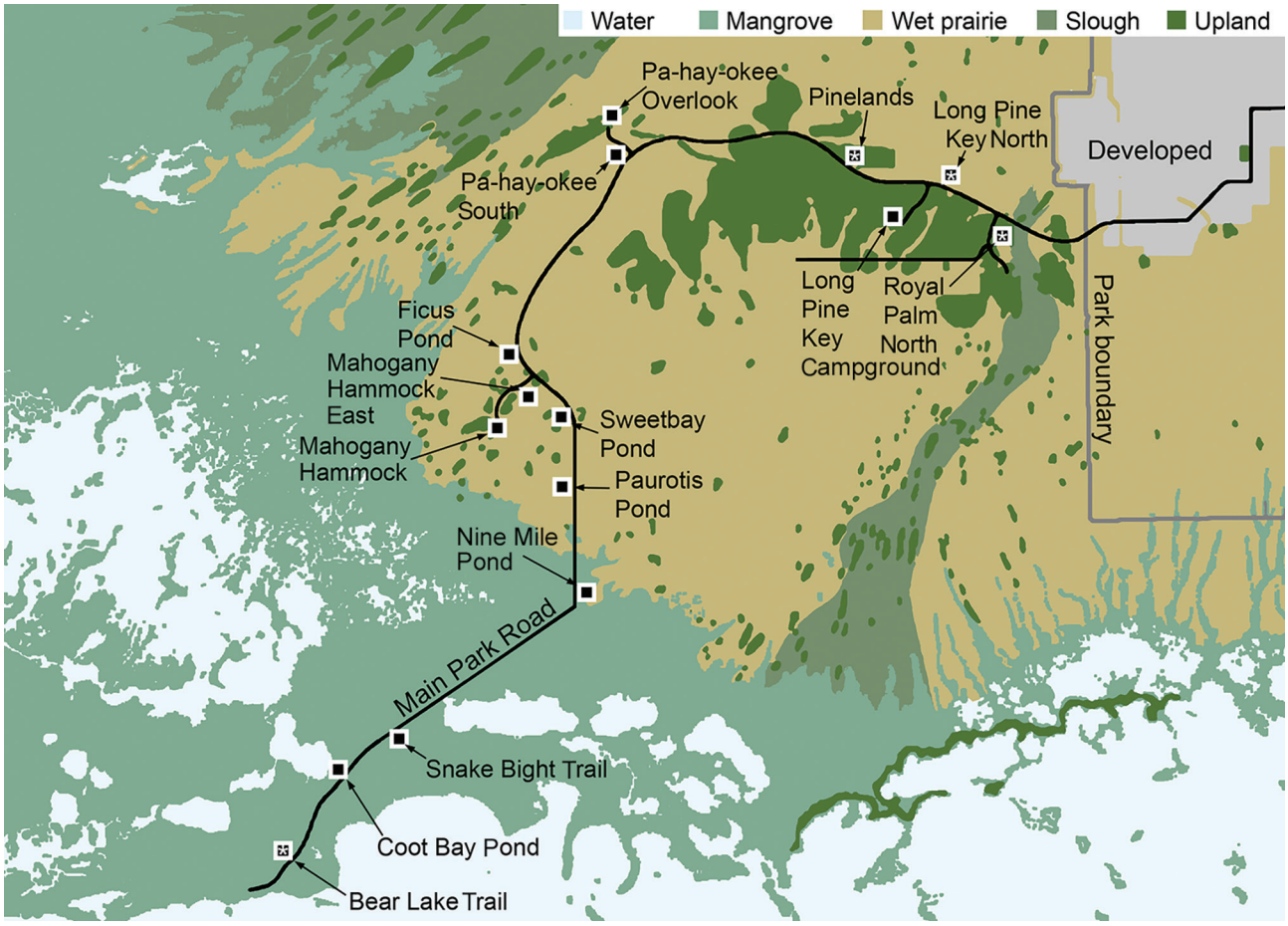

Figure 1. Everglades National Park, Florida, USA, showing dominant habitat types and sampling sites along Main Park Road. Black lines indicate paved roadways. Black squares indicate sampling sites; asterisks (*) within black squares denote detection of Everglades virus RNA in pooled *Culex cedecei* females by quantitative reverse transcription PCR.

and shape to previous models (*15*) but were constructed of PVC pipe and fittings so that they could be easily disassembled after each collecting trip, in accordance with permit requirements. We sampled a total of 406 resting shelter days in ENP, at a rate of 14–27 resting shelters per sampling period; we placed 1–5 shelters at each site and sampled them for 3–5 consecutive days between 7:00 AM and 1:00 PM. We placed resting shelters in areas with maximum shade within 90 m of Main Park Road or 45 m of trails. Sampling occurred within the Everglades dry season (in February and May) and wet season (in June and August) of 2016.

We identified mosquitoes to species using morphological features of the adult (*16*). Because of well-known difficulties of identifying *Culex* (*Melanoconion*) females (*17,18*), we initially confirmed identifications by morphology of the cibarial armature (*17*) and molecular assays targeting the 18s mitochondrial gene (*18*). Narrow decumbent scales of the vertex (*19*) served as a helpful diagnostic feature to separate *Cx. cedecei* from other *Culex* (*Melanoconion*) spp. in Florida.

We performed blood meal analysis on individual blood-engorged *Cx. cedecei* females using published PCR-based techniques (*20*). We amplified extracted DNA using PCR assays targeting cytochrome B and 16s rRNA genes of vertebrate hosts. We initially screened samples to identify blood meals from mammalian and amphibian hosts, using primers L2513/H2714 (*21*) that target 16S rRNA of the host animal (*20*). We then screened samples that produced no amplicon using primer pairs L0/H1 and/or L0/H0, both targeting the cytochrome b gene of birds (*22*), and primer pair 16L1/H3056 used in phylogenetic studies of reptiles (*23,24*). Primer sequences and cycling conditions are described in Blosser et al. (*20*). We sent PCR products to Eurofins Scientific (https://www.eurofins.com) for Sanger sequencing (forward direction only). We aligned sequences with published sequences in the National Center of Biotechnology Information sequence database using BLAST (https://blast.ncbi.nlm.nih.gov/Blast.cgi). We considered nucleotide similarity ≥95% a positive match. We maintained cold chain for

all samples from the time of capture until DNA/RNA extraction. To minimize host DNA cross-contamination during sorting and processing, we handled specimens by their legs (to avoid puncturing the abdomen) using clean forceps and gloved hands. In general, blood-engorged females from resting shelters were fully intact, with no evidence of ruptured abdomens. We discarded any specimen with ruptured abdomen.

We screened RNA extracts (QIAamp viral RNA mini kit; QIAGEN, https://www.qiagen.com) from pooled *Cx. cedecei* females for presence of EVEV RNA using quantitative reverse transcription PCR (qRT-PCR) assay with (5′→3′) primers (forward: CGAGGAGCTGTTTAAGGAGTATAA; reverse: CCTCTATGGCTATTGGGCTATG) and probe (6-FAM/CGTTAGGTGTGCCGTTGGGAGTT/3BHQ1/) targeting EVEV nucleocapsid structural protein (primers/probes design by Integrated DNA Technologies, https://www.idtdna.com). Cycling conditions were 50°C (30 min), 95°C (2 min), then 40 cycles of 95°C (15 s) and 61°C (1 min). For assay validation we used EVEV strain FE3-7C, obtained from the Centers for Disease Control and Prevention, propagated on Vero cells using standard techniques (*25,26*). Mosquito pools consisted of ≤32 unfed and gravid *Cx. cedecei* females aggregated by month and site. We determined samples with C_t values <33 to be positive for EVEV RNA.

Statistical Analysis

We used Poisson regression modeling (*27,28*) to test for statistically significant differences in mosquito abundance between wet and dry seasons for each of the most commonly collected mosquito species in each region, using Akaike information criterion (AIC) and the ratio of the Poisson regression coefficients to the SE (z) as test statistics. We calculated mosquito abundance as the number of females per shelter per sampling day. Only sites that were sampled during all sampling months were included in the analysis: Royal Palm North and Pinelands (upper), Mahogany Hammock East and Nine Mile Pond (middle), and Snake Bight Trail and Bear Lake Trail (lower). We performed χ^2 test of independence to determine whether *Cx. cedecei* blood meals were distributed differently among host species between season and region. Using multiple logistic regression, we determined whether vector abundance or reservoir host use better predicted detection of EVEV RNA from pooled mosquitoes. We quantified reservoir host use as the number of hispid cotton rat or cotton mouse blood meals per resting shelter per day. We performed statistical tests using R Studio version 3.4.3 (https://www.rstudio.com) and SAS version 9.4 (https://www.sas.com). For all statistical tests, $\alpha = 0.05$.

Results

Cx. cedecei mosquito abundance varied across season and region (Figure 2, panel A). Females were significantly more abundant in the wet season in upper (AIC = 228.22, z = 6.488; p<0.001) and middle (AIC = 295.24, z = 3.811; p<0.001) regions of the Everglades but significantly

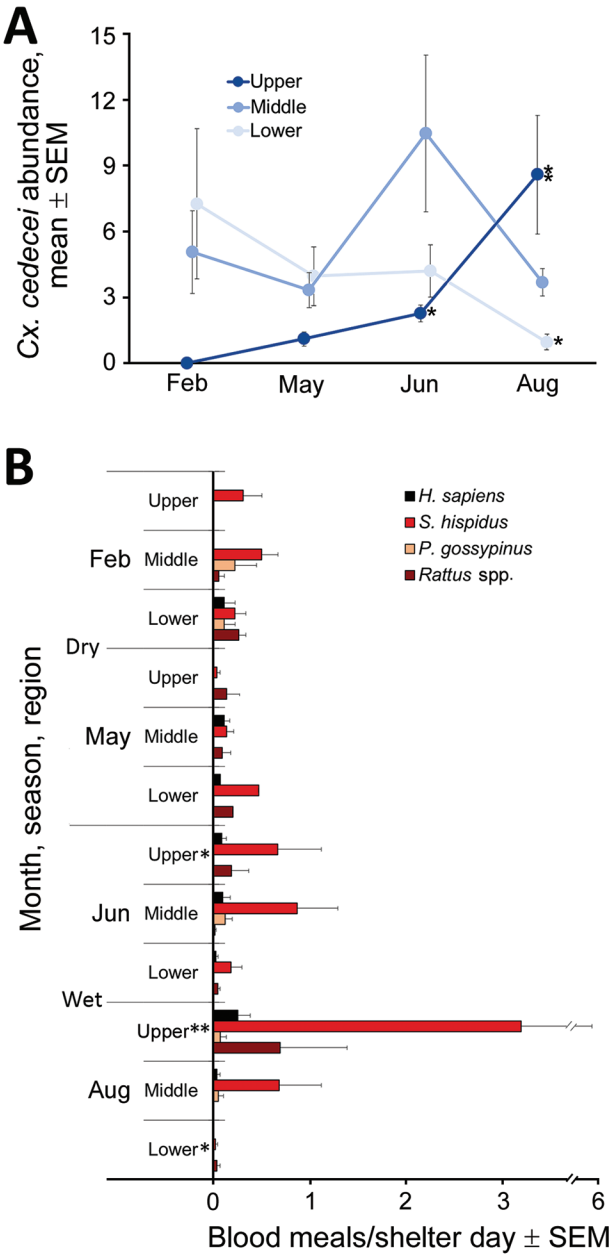

Figure 2. Regional and seasonal abundance and host use of *Culex cedecei* mosquitoes in Everglades National Park, Florida, USA. Wet season is April–October, and dry season is November–March. Each asterisk (*) denotes a pool of *Cx. cedecei* females that tested positive for Everglades virus RNA by quantitative reverse transcription PCR. A) Average number of females aspirated from resting shelters by month. B) Host use by *Cx. cedecei* mosquitoes, represented as blood meals per resting shelter day by region and season.

more abundant during the dry season in the lower region (AIC = 251.2, z = -3.897; p<0.001). No other mosquito species exhibited a pattern of greater abundance during the dry season in any region (Appendix Table 1, https://wwwnc.cdc.gov/EID/article/25/6/18-0338-App1.xlsx). For all other commonly collected mosquito species, abundance was greater during the wet season than dry season in all areas, although differences were not always significant (Appendix Table 1). Even within a single region and sampling period, *Cx. cedecei* mosquito abundance varied considerably. For example, we collected 13.50 females per resting shelter at Royal Palm North (60 shelter days), whereas we collected 2.43 females per resting shelter at Pinelands (44 shelter days); the distance between the sites was only ≈6.7 km.

The distribution of host species blood meals was significantly different spatially (χ^2 = 90.90, df = 20; p<0.001) between the lower, middle, and upper regions of ENP (Figure 2, panel B) but not seasonally (χ^2 = 14.49, df = 10; p = 0.152) (Figure 2, panel B). Rodents accounted for 77%–100% of the 347 total identifiable blood meals (77.0% of 451 samples returning ≥95% match), depending on season and region (Table 2). Blood meals from EVEV reservoirs (hispid cotton rat and cotton mouse combined) were a large percentage of total blood meals from all regions, constituting 48% of total blood meals from the lower, 84% from the middle, and 50% from the upper ENP region (Table 2). Reservoir host blood meals originated overwhelmingly from hispid cotton rat (Table 2; Figure 2, panel B), regardless of region or season. However, cotton mouse blood meals were relatively more common in the dry season in the lower and middle ENP (Figure 2, panel B). Blood meals from invasive *Rattus* spp. rodents contributed to the significant difference in distribution of host blood meals by region, such that much higher numbers of *Rattus* spp. blood meals were encountered in upper (40%) and lower (30%) than middle (2%) regions of ENP (Figure 2, panel B). Blood meals obtained from humans constituted 7.53% of total blood meals and were detected in all 3 regions and seasons. All other hosts constituted <1% of *Cx. cedecei* host blood meals (Table 2; Appendix Table 2).

Although the distribution of blood meals from different host species did not vary substantially between seasons, the number of blood meals from reservoir hosts by season and region did (Figure 2, panel B). The number of hispid cotton rat–fed females per resting shelter day was greatest in the wet season in the upper region, peaking at 3.20 hispid cotton rat blood meals per shelter-day in August in the upper region. By contrast, we encountered 0.02 hispid cotton rat blood meals per shelter-day in lower ENP that same month (Figure 2, panel B).

In total, we screened 3,673 females (1,326 in dry season, and 2,347 in wet season) for EVEV RNA by RT-PCR (average pool size ± SD of 22 ± 6 females) (Table 1), including 3,413 females from resting shelters and 260 females aspirated from natural resting sites. We found 4 pools of *Cx. cedecei* females, all of which were from the wet season (June or August), to be positive for EVEV by RT-PCR. These EVEV-positive pools included 1 pool of 25 females from Pinelands (upper region) in June (C_t = 21.3), 1 pool of 8 females from Bear Lake Trail (lower region) in August (C_t = 21.8), 1 pool of 25 females from Royal Palm North (upper region) in August (C_t = 24.8), and 1 pool of 25 females from Long Pine Key North (upper region) in August (C_t = 24.5). Multiple logistic regression showed no association between EVEV RNA detected in pooled *Cx. cedecei* and *Cx. cedecei* abundance, reservoir (hispid cotton rat plus cotton mouse) host use, or proportion of blood meals from reservoir hosts (χ^2 = 4.08, df = 3; p = 0.252).

Discussion

The dynamic nature of *Cx. cedecei* mosquito abundance is probably shaped by seasonal fluctuations in water levels through the seasonal filling and depletion of limestone solution holes (pits in karst that formed when sea level was lower than present levels), which constitute the primary habitat of *Cx. cedecei* larvae (*29*). The contrasting patterns of *Cx. cedecei* abundance in lower and upper regions of

Table 2. *Culex cedecei* mosquito blood meal host species, by park region and season, Everglades National Park, Florida, USA, 2016

	Lower		Middle		Upper		
Vertebrate host species	Dry	Wet	Dry	Wet	Dry	Wet	Total
Anolis sagrei	0	0	0	3	0	0	3
Homo sapiens sapiens	6	1	2	9	0	16	34
Lontra canadensis	0	0	0	0	0	1	1
Neotoma floridana	0	0	0	0	0	1	1
Odocoileus virginianus	1	0	0	1	0	1	3
Oryzomys palustris	0	1	0	1	0	0	2
Peromyscus gossypinus	3	0	4	6	0	1	14
Procyon lotor	1	1	0	0	0	0	2
Rattus spp.	12	3	1	1	5	52	85
Sigmodon hispidus	12	9	21	73	5	81	201
Sylvilagus floridanus	0	0	1	0	0	0	1
Undetermined	6	5	9	53	2	29	104
Total	41	20	38	147	12	193	451

ENP suggest that Everglades hydrology has a strong influence on the seasonal reproductive biology of *Cx. cedecei* mosquitoes, which may have consequences for EVEV transmission. In addition, the finding that *Cx. cedecei* was the only mosquito species more abundant in dry season in the lower region of ENP suggests that the positive association between precipitation and abundance of other mosquito species may not apply consistently for this species. Our study did not quantify precipitation nor the availability of larval habitat, so explanations of the links between season, region, and *Cx. cedecei* abundance are speculative. One possible explanation for the higher abundance of *Cx. cedecei* mosquitoes during the dry season in the lower region is seasonal drying in the low-elevation lower Everglades: during times of higher water, aquatic predators, particularly fish, disperse rapidly throughout ENP (*30,31*), whereas isolated pockets of water without fish may be more abundant during the dry season. Detailed field and laboratory studies focusing on the ecology of immature stages are needed to understand the mechanisms driving these contrasting patterns of *Cx. cedecei* abundance throughout the Everglades.

Variation in *Cx. cedecei* host use between regions has important implications for understanding the transmission of EVEV in Florida. Our data demonstrate that *Cx. cedecei* mosquitoes feed heavily on mammals; rodents make up a substantial portion of hosts, regardless of season or region. The finding that hispid cotton rat and cotton mouse together constituted a large portion (43.0%–86.2%) of *Cx. cedecei* blood meals confirms a strong association between *Cx. cedecei* mosquitoes and these EVEV reservoir host species (*3,14*). Both hispid cotton rat and cotton mouse are common throughout Florida, so their role in EVEV transmission is probably limited by the distribution and abundance of *Cx. cedecei* mosquitoes. However, the introduction and establishment of *Cx. panocossa* mosquitoes in Florida may change this dynamic, resulting in more areas at risk for EVEV transmission (*8*).

The importance of *Rattus* spp. rodents as hosts of EVEV in lower and upper regions of ENP bears additional investigation, because these rats were relatively common hosts of *Cx. cedecei* mosquitoes in these regions (20.0%–55.5% of total). We expect the lower and upper regions of the park, because of their proximity to park boundaries, campgrounds, parking lots, and human activity, to host larger populations of invasive rats than the middle region of ENP, which is comparatively undisturbed. Little information is available on the importance of *Rattus* spp. rodents as hosts of EVEV. Sanmartin et al. (*32*) made 4 isolations of VEEV from 41 *Rattus* spp. rodents sampled during an epizootic of VEEV in El Carmelo, Colombia, where subtypes IAB and IC circulate. In Florida, Bigler (*33*) detected EVEV antibodies in 12.5% (n = 40) *R. rattus* rats sampled east of ENP. These findings suggest that these widespread, invasive rats might also support the transmission of EVEV in Florida, although laboratory host competence studies are needed to address this hypothesis.

The regions of the park in which human footprint is greatest also had the greatest relative numbers of human blood meals (11.48% lower; 7.80% upper), compared with findings from the middle region (5.95%). These relatively high levels of feeding suggest that *Cx. cedecei* mosquitoes could serve not only as an enzootic and epizootic vector but also as a potential epidemic vector of EVEV where it comes into contact with humans.

The lack of a clear association between EVEV in pooled *Cx. cedecei* females and vector abundance or metrics of host use is perplexing. Three of 4 EVEV-positive pools were from upper ENP during the wet season (1 in June, 2 in August), when *Cx. cedecei* mosquitoes were more abundant (Figure 2, panel A) and obtained a large number of blood meals from cotton rats (Figure 2, panel B). Conversely, the EVEV-positive pool from lower ENP was also from the wet season (August), but *Cx. cedecei* mosquito numbers were relatively low (Figure 2, panel A), and we observed very few blood meals from rodents (Figure 2, panel B). It is possible that wet-season transmission of EVEV is driven largely by the ecology and reproductive biology of cotton mouse and hispid cotton rat; however, a complex picture of rodent breeding and population dynamics emerges from past studies on this topic. Bigler et al. (*14*) concluded that the preponderance of EVEV amplification occurred between July and October, when dense populations of both cotton mice and cotton rats inhabited hammocks in the Pinecrest area on the ecotone between the Big Cypress Swamp and the Everglades ecosystem, ≈38 km northwest of the nearest sampling sites in our study. Lord et al. (*34*) screened mammals for EVEV antibodies in both Big Cypress Swamp and the Everglades, including the upper (Royal Palm Hammock) and middle (Mahogany Hammock) regions sampled in our study. Those results indicated that rodent breeding in these Everglades regions peaked in the dry season (January–February), a reversal of breeding patterns found farther north (*14*). Smith and Vrieze (*35*), working on hammocks of Taylor Slough (southeast Everglades), stated that all rodent reproduction occurred in the wet season. These contrasting results indicate that *S. hispidus* rats and *P. gossypinus* mice are likely to time their breeding to coincide with local conditions, which may be substantially different across locales. Our results are evidence of spatial variation in seasonality of EVEV transmission as observed in our work and that of others.

It was surprising that we did not detect EVEV in *Cx. cedecei* mosquito samples from the middle region of ENP, despite relatively high *Cx. cedecei* abundance (Figure 2, panel A), a relatively high biting rate on hispid cotton rats

(Figure 2, panel B), and past evidence of EVEV circulation in mosquitoes in that region (*2*). Most *Cx. cedecei* females sampled from the middle region (70.5%; 942/1,336; Table 1) were captured at Nine Mile Pond on the ecotone between sawgrass marsh and mangrove swamps (Figure 1), a location for which historical data on EVEV prevalence is not available.

Although results of our work do not provide a complete understanding of EVEV transmission in ENP, they may help to clarify the perplexing heterogeneity observed in previous studies of EVEV in south Florida. The absence of EVEV in mosquitoes at Pa-hay-okee Overlook (*2*), for example, could be due to a near absence of *Cx. cedecei* mosquitoes at that site (Table 1). Differences in EVEV transmission at 2 adjacent hammocks observed by Bigler et al. (*14*) could be a result of differences in vector abundance, contact rates, or both between vectors and reservoir versus nonreservoir hosts, as observed in our study. We did not quantify the actual abundance of reservoir hosts in the field, so it is possible that a given set of mosquitoes all could have fed on a small number (in low population settings) or a large number (greater populations) of rodents. Our measure of host usage could not account for those differences, nor could it account for how many of those rodents were actually susceptible hosts. The number of available susceptible reservoir hosts is an important factor in maintaining enzootic cycling of viruses. Our data do support conclusions of past studies that EVEV transmission occurs seasonally and is heterogeneous across ENP. Relative number of feedings on reservoir hosts differs across regions of the park, indicating the vector infection ratio may be higher in specific habitats where *Cx. cedecei* mosquitoes have ample access to reservoir hosts, particularly young, virus-susceptible rodents.

Quantifying the spatial and temporal variation in abundance, host use, and virus infection of *Cx. cedecei* mosquitoes is a step toward understanding the ecology of EVEV transmission in the United States. Findings that *Cx. cedecei* mosquitoes feed on both reservoir hosts and humans in nature suggests that this insect could serve as both enzootic and epizootic vector. The establishment of the *Cx. panocossa* mosquito in Florida, and its putative spread, may change the spatial risk for EVEV transmission, if found to be a competent vector. Future work should evaluate the host competence of *Rattus* spp. rodents for EVEV and other VEEV subtypes, evaluate vector competence of *Cx. panocossa* mosquitoes for these viruses, and perform longitudinal studies of the focality of transmission in Florida.

Acknowledgments

We thank E. Blosser and L. Reeves for assistance in sampling and P. Walker for facilitating Everglades National Park permits. A. Carels Thompson performed molecular assays that contributed substantially to the results. We thank B. Russell for providing Everglades virus strain FE3-7C used to produce standard growth curves and validate RT-PCR assays. Two anonymous referees provided helpful comments to improve the manuscript.

This work was supported by IFAS Early Career Scientist Seed Grant and NIFA FLA-VME-005446.

About the Author

Mr. Hoyer is an entomologist for Project Premonition, a Microsoft Research endeavor to detect and track emerging infectious disease. His research interests include the ecology of vectorborne disease and its applications in public health for prevention of disease.

References

1. Weaver SC, Ferro C, Barrera R, Boshell J, Navarro JC. Venezuelan equine encephalitis. Annu Rev Entomol. 2004;49:141–74. http://dx.doi.org/10.1146/annurev.ento.49.061802.123422
2. Chamberlain RW, Sudia WD, Work TH, Coleman PH, Newhouse VF, Johnston JG Jr. Arbovirus studies in south Florida, with emphasis on Venezuelan equine encephalomyelitis virus. Am J Epidemiol. 1969;89:197–210. http://dx.doi.org/10.1093/oxfordjournals.aje.a120929
3. Edman JD. Host-feeding patterns of Florida mosquitoes (Diptera: Culicidae) VI. *Culex* (*Melanoconion*). J Med Entomol. 1979;15:521–5. http://dx.doi.org/10.1093/jmedent/15.5-6.521
4. Weaver SC, Scherer WF, Taylor CA, Castello DA, Cupp EW. Laboratory vector competence of *Culex* (*Melanoconion*) *cedecei* for sympatric and allopatric Venezuelan equine encephalomyelitis viruses. Am J Trop Med Hyg. 1986;35:619–23. http://dx.doi.org/10.4269/ajtmh.1986.35.619
5. Bigler WJ, Lewis AL, Wellings FM. Experimental infection of the cotton mouse (*Peromyscus gossypinus*) with Venezuelan equine encephalomyelitis virus. Am J Trop Med Hyg. 1974a;23:1185–8. http://dx.doi.org/10.4269/ajtmh.1974.23.1185
6. Coffey LL, Carrara AS, Paessler S, Haynie ML, Bradley RD, Tesh RB, et al. Experimental Everglades virus infection of cotton rats (*Sigmodon hispidus*). Emerg Infect Dis. 2004;10:2182–8. http://dx.doi.org/10.3201/eid1012.040442
7. Carrara AS, Coffey LL, Aguilar PV, Moncayo AC, Da Rosa AP, Nunes MR, et al. Venezuelan equine encephalitis virus infection of cotton rats. Emerg Infect Dis. 2007;13:1158–65. http://dx.doi.org/10.3201/eid1308.061157
8. Blosser EM, Burkett-Cadena ND. *Culex* (*Melanoconion*) *panocossa* from peninsular Florida, USA. Acta Trop. 2017;167:59–63. http://dx.doi.org/10.1016/j.actatropica.2016.12.024
9. Galindo P, Grayson MA. *Culex* (*Melanoconion*) *aikenii*: natural vector in Panama of endemic Venezuelan encephalitis. Science. 1971;172:594–5. http://dx.doi.org/10.1126/science.172.3983.594
10. Tempelis CH, Galindo P. Host-feeding patterns of *Culex* (*Melanoconion*) and *Culex* (*Aedinus*) mosquitoes collected in Panama. J Med Entomol. 1975;12:205–9. http://dx.doi.org/10.1093/jmedent/12.2.205
11. Galindo P, Adames AJ. Ecological profile of *Culex* (*Melanoconion*) *aikenii* (Diptera: Culicidae), vector of endemic Venezuelan encephalitis in Panama. Environ Entomol. 1973;2:81–6. http://dx.doi.org/10.1093/ee/2.1.81
12. Work TH. Serological evidence of arbovirus infection in the Seminole Indians of southern Florida. Science. 1964;145:270–2. http://dx.doi.org/10.1126/science.145.3629.270

13. Ehrenkranz NJ, Sinclair MC, Buff E, Lyman DO. The natural occurrence of Venezuelan equine encephalitis in the United States. N Engl J Med. 1970;282:298–302. http://dx.doi.org/10.1056/NEJM197002052820603
14. Bigler WJ, Ventura AK, Lewis AL, Wellings FM, Ehrenkranz NJ. Venezuelan equine encephalomyelitis in Florida: endemic virus circulation in native rodent populations of Everglades hammocks. Am J Trop Med Hyg. 1974b;23:513–21. http://dx.doi.org/10.4269/ajtmh.1974.23.513
15. Burkett-Cadena ND. A wire-frame shelter for collecting resting mosquitoes. J Am Mosq Control Assoc. 2011;27:153–5. http://dx.doi.org/10.2987/10-6076.1
16. Darsie RF Jr, Morris CD. Keys to the adult females and fourth instar larvae of the mosquitoes of Florida (Diptera, Culicidae). Technical Bulletin of the Florida Mosquito Control Association. Vero Beach (FL): Florida Mosquito Control Association; 2003.
17. Williams MR, Savage HM. Identification of *Culex (Melanoconion)* species of the United States using female cibarial armature (Diptera: Culicidae). J Med Entomol. 2009;46:745–52. http://dx.doi.org/10.1603/033.046.0404
18. Williams MR, Savage HM. Development of multiplexed species specific polymerase chain reaction assays for identification of the *Culex* (*Melanoconion*) species (Diptera: Culicidae) of the southeastern United States based on rDNA. J Med Entomol. 2011;48:961–6. http://dx.doi.org/10.1603/ME11081
19. Sallum MA, Forattini OP. Revision of the Spissipes section of *Culex* (*Melanoconion*) (Diptera:Culicidae). J Am Mosq Control Assoc. 1996;12:517–600.
20. Blosser EM, Stenn T, Acevedo C, Burkett-Cadena ND. Host use and seasonality of *Culex* (*Melanoconion*) *iolambdis* (Diptera: Culicidae) from eastern Florida, USA. Acta Trop. 2016;164:352–9. http://dx.doi.org/10.1016/j.actatropica.2016.10.001
21. Kitano T, Umetsu K, Tian W, Osawa M. Two universal primer sets for species identification among vertebrates. Int J Legal Med. 2007;121:423–7. http://dx.doi.org/10.1007/s00414-006-0113-y
22. Lee JC, Tsai LC, Huang MT, Jhuang JA, Yao CT, Chin SC, et al. A novel strategy for avian species identification by cytochrome *b* gene. Electrophoresis. 2008;29:2413–8. http://dx.doi.org/10.1002/elps.200700711
23. Hass CA, Hedges SB, Maxson LR. Molecular insights into the relationships and biogeography of West Indian anoline lizards. Biochem Syst Ecol. 1993;21:97–114. http://dx.doi.org/10.1016/0305-1978(93)90015-J
24. Vidal N, Kindl SG, Wong A, Hedges SB. Phylogenetic relationships of xenodontine snakes inferred from 12S and 16S ribosomal RNA sequences. Mol Phylogenet Evol. 2000;14:389–402. http://dx.doi.org/10.1006/mpev.1999.0717
25. Alto BW, Lord CC. Transstadial effects of *Bti* on traits of *Aedes aegypti* and infection with dengue virus. PLoS Negl Trop Dis. 2016;10:e0004370. http://dx.doi.org/10.1371/journal.pntd.0004370
26. Alto BW, Wiggins K, Eastmond B, Velez D, Lounibos LP, Lord CC. Transmission risk of two chikungunya lineages by invasive mosquito vectors from Florida and the Dominican Republic. PLoS Negl Trop Dis. 2017;11:e0005724. http://dx.doi.org/10.1371/journal.pntd.0005724
27. Coxe S, West SG, Aiken LS. The analysis of count data: a gentle introduction to Poisson regression and its alternatives. J Pers Assess. 2009; 91:121–36. http://dx.doi.org/10.1080/00223890802634175
28. McElduff F, Cortina-Borja M, Chan SK, Wade A. When t-tests or Wilcoxon-Mann-Whitney tests won't do. Adv Physiol Ed. 2010:34:128–33. https://doi.org/10.1152/advan.00017.2010
29. Hair JA. Observations on two species of *Culex* of the subgenus *Melanoconion.* Mosq News. 1968;28:425–29.
30. DeAngelis DL, Trexler JC, Loftus WF. Life history trade-offs and community dynamics of small fishes in a seasonally pulsed wetland. Can J Fish Aquat Sci. 2005;62:781–90. http://dx.doi.org/10.1139/f05-050
31. DeAngelis DL, Trexler JC, Cosner C, Obaza A, Jopp F. Fish population dynamics in a seasonally varying wetland. Ecol Modell. 2010;221:1131–7. http://dx.doi.org/10.1016/j.ecolmodel.2009.12.021
32. Sanmartín C, Mackenzie RB, Trapido H, Barreto P, Mullenax CH, Gutiérrez E, et al. Venezuelan equine encephalitis in Colombia, 1967 [in Spanish]. Bol Oficina Sanit Panam. 1973;74:108–37.
33. Bigler WJ. Venezuelan encephalitis antibody studies in certain Florida wildlife. Wildl Dis. 1969;5:267–70.
34. Lord RD, Calisher CH, Sudia WD, Work TH. Ecological investigation of vertebrate hosts of Venezuelan equine encephalomyelitis virus in south Florida. Am J Trop Med Hyg. 1973;22:116–23. http://dx.doi.org/10.4269/ajtmh.1973.22.116
35. Smith AT, Vrieze JM. Population structure of Everglades rodents: responses to a patchy environment. Journal of Mammalogy. 1979;60:778–94.

Address for correspondence: Nathan D. Burkett-Cadena, University of Florida–Florida Medical Entomology Laboratory, Institute of Food and Agricultural Science, Vero Beach, FL 32962, USA; email: nburkettcadena@ufl.edu

Assessment of Economic Burden of Concurrent Measles and Rubella Outbreaks, Romania, 2011–2012

Joseph Njau,[1] Denisa Janta, Aurora Stanescu, Sarah L. Pallas, Adriana Pistol, Nino Khetsuriani,[2] Susan Reef, Daniel Ciurea, Cassandra Butu, Aaron S. Wallace, Laura Zimmerman

We estimated the economic impact of concurrent measles and rubella outbreaks in Romania during 2011–2012. We collected costs from surveys of 428 case-patients and caretakers, government records, and health staff interviews. We then estimated financial and opportunity costs. During the study period, 12,427 measles cases and 24,627 rubella cases were recorded; 27 infants had congenital rubella syndrome (CRS). The cost of the outbreaks was US $9.9 million. Cost per case was US $439 for measles, US $132 for rubella, and US $44,051 for CRS. Up to 36% of households needed to borrow money to pay for illness treatment. Approximately 17% of patients continued to work while ill to pay their treatment expenses. Our key study findings were that households incurred a high economic burden compared with their incomes, the health sector bore most costs, and CRS costs were substantial and relevant to include in rubella outbreak cost studies.

Outbreaks of measles and rubella constitute serious public health events and entail a vigorous response from public health agencies. A typical response could include a range of complex activities, including isolation of case-patients, case–contact tracing, assessment of disease or vaccination history of each case-patient, identification of potentially susceptible persons, and, if required, vaccination or quarantine (*1*). Economic impact studies of measles and rubella outbreaks in high-income countries illustrate a high cost of outbreaks and response activities (*1*–*5*). However, little information is available on the economic impact of measles and rubella outbreaks in a middle-income country, and in 2011, this impact was identified as a global research priority (*6*). Concurrent measles and rubella outbreaks in Romania provided an opportunity to estimate this economic impact.

In coordination with other World Health Organization European Region countries, Romania has a goal of measles and rubella elimination by 2020. During 2000–2003, coverage with a first dose of measles-containing vaccine in Romania was reported to be ≥95%; for 2004–2010, combined measles and rubella vaccine first dose coverage was ≥95% and second dose coverage was ≥88%. In spite of these high national coverage rates among recent birth cohorts, unvaccinated subpopulations exist among older age cohorts and subnationally, which create conditions for continued measles or rubella outbreaks.

During 2011–2012, Romania experienced concurrent outbreaks of measles and rubella. Measles cases were primarily reported among children from the northwest part of the country, and rubella cases were reported primarily among adolescents and adults throughout Romania. The outbreaks resulted in 12,427 measles cases and 24,627 rubella cases during 2011–2012 (the number of measles cases officially associated with the outbreak was subsequently revised to 12,234 after our analysis was conducted) (*7*). We estimated the economic cost of these outbreaks and response activities incurred by the health sector and households of persons with measles or rubella infection.

Methods

Definitions and Costs

We assessed the cost of the measles and rubella outbreaks by collecting data on direct and indirect costs from households and the health sector. We defined economic cost as the sum of financial costs (i.e., the monetary value of goods and services provided to treat

Author affiliations: Centers for Disease Control and Prevention, Atlanta, Georgia, USA (J. Njau, S.L. Pallas, S. Reef, A.S. Wallace, L. Zimmerman); National Public Health Institute, Bucharest, Romania (D. Janta, A. Stanescu, A. Pistol); Centers for Disease Control and Prevention, Tbilisi, Georgia (N. Khetsuriani); Center for Health Policies and Services, Bucharest (D. Ciurea); World Health Organization Country Office, Bucharest (C. Butu)

DOI: https://doi.org/10.3201/eid2506.180339

[1]Current affiliation: JoDon Consulting Group LLC, Atlanta, Georgia, USA.

[2]Current affiliation: Centers for Disease Control and Prevention, Atlanta, Georgia, USA.

case-patients and to contain the outbreak) and opportunity costs (i.e., the value of the best alternative forgone by the health sector or households caused by measles or rubella illness or treatment) by using the societal costing perspective. The health sector included government entities from primary to tertiary level (i.e., health facilities, agencies, or departments) involved in providing treatment to measles or rubella case-patients and in designing and implementing the public health response to the outbreaks.

Data Sources and Collection Process

Household Direct and Indirect Costs

To collect household costs, we conducted a survey among a purposely selected sample of households that had recent cases (within the previous 18 months to minimize recall bias) drawn from the national measles and rubella surveillance database (Table 1; Appendix Figure, https://wwwnc.cdc.gov/EID/article/25/6/18-0339-App1.pdf). An initial sample of 1,217 persons met the inclusion criteria; of these, 789 case-patients or their representatives could not be reached or declined to participate and 428 were interviewed (response rate 35%).

Healthcare Provider Costs

Reimbursement data were obtained from the National Health Insurance House (Casa Nationala de Asigurari de Sanatate), which covered all registered government healthcare providers in Romania (Table 1). There were ≈10,000 primary care physicians or family doctors and >500 secondary or tertiary hospitals in the 42 health districts in Romania (*8*). Reimbursement fees are typically paid when doctors and hospitals submit claims to national health insurance funds for the service provided.

Table 1. Definitions and data sources used for cost components during assessment of economic burden of concurrent measles and rubella outbreaks, Romania, 2011–2012*

Cost component	Definition	Data sources
Healthcare provider	All reimbursements for diagnostic testing for measles and rubella, inpatient and outpatient care, emergency treatment, case management	Reimbursement data from National Health Insurance House (CNAS) covering all registered government healthcare providers using the Romanian national clinical diagnosis codes associated with measles and rubella diagnoses, outpatient and inpatient care, and vaccinations (Appendix Table, https://wwwnc.cdc.gov/EID/article/25/6/18-0339-App1.pdf) as submitted by healthcare providers
National outbreak response	Enhanced surveillance, laboratory diagnosis and confirmation, field activities such as case investigations, and outbreak response immunization, including actual expenses incurred for personnel, laboratory supplies, and vaccine doses provided to contacts of cases and to high-risk communities	Interviews with key personnel, including the Director of the National Institute for Public Health, Romanian MOH; the Team Leads for Measles and Rubella, National Center for Surveillance and Control of Communicable Diseases, MOH; a measles and rubella epidemiologist from the District Public Health Authorities, MOH; the Director of the reimbursement department and an analyst at the National Health Insurance House (CNAS); and the Head of Country Office and a public health officer at the World Health Organization country office in Romania
Direct medical and nonmedical household	Medical costs (e.g., consultation fees, laboratory tests and medications) and nonmedical costs (e.g., transport, food and lodging) paid out-of-pocket by cases and caregivers	Household survey of 428 recent case-patients (within last 18 months) by using structured telephone interviews
Indirect household	Workdays lost by cases and caregivers because of measles or rubella infections	Household survey of 428 recent case-patients (within last 18 months) by using structured telephone interviews; 2012 Romanian national minimum wage of 700 Lei/month was used as proxy to quantify the value of lost workdays by patients and caretakers ≥18 y of age (*8*).
CRS cases healthcare provider	All diagnostic services, inpatient and outpatient care reimbursements related to CRS diagnostic codes for identified CRS cases during timeframe	Reimbursement data from National Health Insurance House (CNAS) covering all registered government healthcare providers for the 27 CRS cases identified from the time of the outbreak up to the date of data collection; reimbursement data were obtained for 18 (11 surviving and 7 who had died) of the 27 case-patients
CRS cases lifetime discounted indirect	Workdays lost by CRS cases over assumed lifetime productive working years (18–63 y)	2012 Romanian national minimum wage of 700 Lei/month was used as a proxy to quantify the value of lost workdays by patients ≥18 y of age (*8*)

*CNAS, Casa Nationala de Asigurari de Sanatate; CRS, congenital rubella syndrome; MOH, Ministry of Health.

National Outbreak Response Costs

To assess national outbreak response costs, personnel involved in outbreak response activities were interviewed on the basis of referral from the National Institute for Public Health, Romanian Ministry of Health, which was charged with coordinating the national outbreak response. These open-ended interviews were conducted by members of the research team in Romanian at the offices of respondents and focused on collecting information about actual expenses incurred in measles and rubella outbreak response activities, including costs of enhanced surveillance, outbreak investigation, and outbreak response vaccination and vaccine stockpiling (Table 1).

Congenital Rubella Syndrome Costs

We requested reimbursement data for health services received by the 27 identified congenital rubella syndrome (CRS) cases from birth up to the date of data collection (at which point the surviving 15 CRS case-patients were 3–4 years old) from the National Health Insurance House; we obtained records for 18 (11 surviving and 7 who had died) of the 27 case-patients. The projection of their lifetime productivity losses used the same data sources and definitions as the main analysis of costs during the outbreak (Table 1). These 27 CRS case-patients were the only CRS cases included in the calculation of CRS costs during the outbreak.

All data collection activities occurred from mid-January through the end of May 2014. A post-hoc analysis of the costs of CRS cases was conducted in March–May 2016.

Data Analysis

We analyzed data by using Access and Excel (Microsoft, https://www.microsoft.com), and Stata version 13 (StataCorp LLC, https://www.stata.com). We calculated district-level weights on the basis of the number of measles and rubella cases as a proportion of the total population in each of the 42 districts of Romania. We then applied these weights to the household survey data, with the costs reported by a respondent multiplied by the weight of the district in which that respondent resided, to estimate the mean, median, and interquartile range of treatment expenditures per household for measles and rubella infections and the proportion of cases receiving treatment by admission status.

We calculated the indirect costs of measles or rubella infections by first calculating the number of measles and rubella case-patients and caregivers ≥18 years of age who were employed (based on employment rates reported in the patient survey). We then assumed that each of these employed case-patients and caregivers ≥18 years of age lost the average number of workdays missed on the basis of the household survey. We valued each day of work missed at the minimum wage of Romania.

We used a human capital approach to estimate the lifetime productivity losses for CRS case-patients (*9*). We assumed that had these children not been born with CRS, their working years would have been 18–63 years of age (until median retirement age in Romania) with the same labor force participation, employment rates, minimum wage, and exchange rate during these years as those used in the main analysis (i.e., constant 2012–2013 rates). We discounted lifetime productivity losses to 2013 US dollars by using a 3% discount rate.

All costs were adjusted for inflation by using the Romanian Consumer Price Index to 2013 prices and converted from Romanian local currency (Lei) into US dollars by using 2013 exchange rates (3.32 Lei/1 US dollar). Costs are presented in 2013 US dollars (*10*,*11*).

Sensitivity Analysis

We conducted univariate sensitivity analysis to characterize how total costs would change with different input values to reflect uncertainty. Reported number of outbreak cases, healthcare provider costs, and national outbreak response costs varied by ± 10%. Out-of-pocket treatment costs, number of days of work missed by cases and caregivers, and CRS case direct medical costs varied from the 25th to 75th percentiles, and proportion of cases receiving care varied from the 5th to 95th percentiles of the sample distribution. CRS case indirect costs were also calculated from birth to an average life expectancy of 74 years.

Ethics Approval and Informed Consent

The assessment protocol was approved by the Romanian National Health Research Ethics Review Board and determined not to be human subjects research by the US Centers for Disease Control and Prevention. Informed consent was obtained from participants after the objectives of the assessment were described to them. Participants were informed that the information would be confidential, there were no unique identifiers, and that participation was voluntary. The authors certify that this study has been conducted in an ethical way according to the international standards for authors.

Results

A retrospective review of the Romanian national measles and rubella surveillance database showed that 12,427 laboratory-confirmed and epidemiologically linked cases of measles and 24,627 laboratory-confirmed and epidemiologically linked cases of rubella were reported during the 2011–2012 outbreaks (Figure). In addition, 27 confirmed cases of CRS were reported.

Household Survey Results

The number of households with measles or rubella cases that were included in the survey was evenly split between urban and rural areas, and 46% of case-patients were employed (Table 2). Although approximately one third of responding measles or rubella case-patients were <18 years

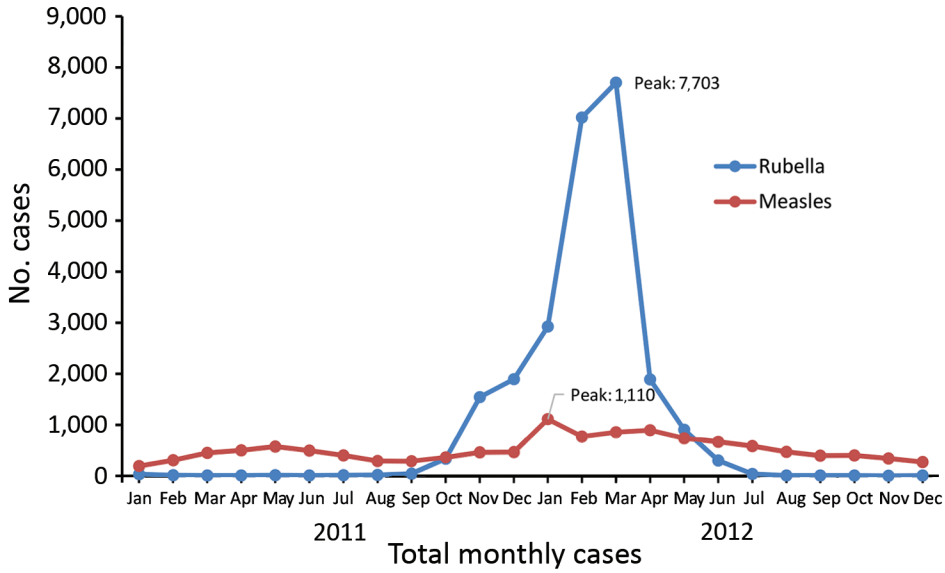

Figure. Reported cases of measles and rubella during concurrent outbreaks, Romania, 2011–2012. Values reflect revision of official case counts after analysis was completed.

of age, more case-patients in this age range were infants and preschoolers for measles (85%) than for rubella (44%). A slightly higher proportion of rubella case-patients (10%) sought care on multiple occasions compared with measles case-patients (4%). However, measles case-patients were 3.5 times more likely to have been admitted to a hospital than rubella case-patients (Table 2). Few measles or rubella case-patients (<2%) sought care at a private health facility. The distribution of sampled case-patients by sex was similar to those for the outbreaks overall, whereas in terms of age the sampled case-patients included a higher share of adults >18 years of age than the outbreaks overall.

Household Direct Medical and Nonmedical Costs

More than 90% of responding households with either measles or rubella cases incurred some type of treatment expense (Table 2). Case-patients with measles (36%) and rubella (7%) reported having to borrow money to pay for costs related to an episode of measles or rubella (Table 2). The largest share of household spending was on medications, followed by transportation. We found no notable differences in transportation or overall spending for households residing in rural areas compared with those in urban settings, which might reflect the history of widespread geographic availability of healthcare by state-owned polyclinics throughout Romania. Average household spending for measles and rubella patients <18 years old was more than that for patients ≥18 years old (US $112.51 vs. US $45.85). Weighted median inpatient costs for measles were 2.2 times higher than for rubella, and outpatient costs for measles were 1.5 times higher than for rubella (Table 3). Total estimated direct medical and nonmedical household costs for treatment were US $888,338 for the 12,427 measles cases and US $477,261 for the 24,627 rubella cases (Table 4).

Table 2. Descriptive characteristics of case-patients responding to household survey for assessment of economic burden of concurrent measles and rubella outbreaks, Romania, 2011–2012

	No. (%) case-patients		
Characteristic	Measles	Rubella	Total
Total sample	219	209	428
Age <18 y	74 (34)	63 (30)	137 (32)
Male sex	109 (50)	107 (51)	216 (50)
Urban domicile	98 (55)	115 (45)	213 (50)
Multiple care visits	8 (4)	21 (10)	29 (7)
Admission to hospital	185 (84)	38 18)	223 (52)
Care at private clinics	3 (1)	4 (2)	7 (2)
Age ≥18 y	145	146	291
Formal or informal employment	72 (50)	63 (43)	135 (46)
Students	13 (9)	66 (45)	79 (27)
Retired, unemployed, or housewives	60 (41)	17 (12)	77 (26)
Age <18 y	74	63	137
Infants and preschoolers	63 (85)	28 (44)	91 (66)
Schoolchildren	11 (15)	35 (56)	46 (34)
Treatment expenses	219	209	428
Incurred some treatment expenses	206 (94)	194 (93)	400 (93)
Borrowed money for treatment expenses	79 (36)	14 (7)	93 (22)

Household Indirect Costs

Among responding patients participating in the labor market, a median of 11.45 days were lost for measles and 9.62 days for rubella (Table 3). The maximum number of workdays lost were 68 days for a single episode of measles and 21 days for an episode of rubella. Of those ≥18 years of age, 27% reported working while ill. Among those who continued to work, the average number of days worked while ill with measles or rubella was 4 days. Students and schoolchildren reported an average of 10 days that they were unable to attend school because of measles or rubella infection. Total estimated indirect household costs were US $779,917 for the 12,427 measles cases and US $1,043,281 for the 24,627 rubella cases (Table 4).

Total Estimated Household Costs

We determined total estimated direct and indirect household costs. These values were US $1.7 million for 12,427 measles cases (US $133.84/case) and US $1.5 million for 24,627 rubella cases (US $61.74/case) (Tables 4, 5).

Healthcare Provider Costs

Healthcare providers received direct reimbursement fees from health insurance. These totals were US $3,275,757 for services provided to treat measles and US $674,633 for services provided to treat rubella infections during the outbreak (Table 4).

National Outbreak Response Costs

National response activities included enhanced surveillance, laboratory diagnostic testing, and immunization of at-risk populations at a total cost of US $1,559,975, of which ≈60% were for activities related to diagnosis and containment of rubella (Table 4). Virtually equal amounts of national resources were spent on measles and rubella containment efforts per case (US $41.55/case for measles and US $42.38/case for rubella) (Table 5). Most (87%) costs were incurred for laboratory reagents, laboratory tests, and overtime salaries for laboratory technicians (Table 3).

CRS Case Costs

Estimated health service reimbursement costs for the 27 CRS cases up to May 2016 were US $130,143 (Table 4). Estimated discounted lifetime productivity losses for the 12 CRS case-patients who had died by May 2016 were US $470,774. Under the assumption that the 15 surviving CRS case-patients would also be unable to work during their lifetimes, their estimated discounted lifetime productivity losses would be US $588,467 (US $1,059,241 for all 27 case-patients) (Table 4).

Societal Costs

Total societal costs of the measles and rubella outbreaks were US $9.9 million, of which US $5.5 million was for measles-related activities and US $4.4 million for rubella-related activities (the rubella-related activities included US $1.2 million in CRS-related costs) (Table 4). These costs translated to a total cost per case of US $439 for measles, US $132 for rubella (not including CRS), and US $44,051 for CRS (Table 5). Sensitivity analysis showed that total costs varied between US $9,266,779 (when the lower bound of measles treatment costs was used) and US $10,989,560 (when the upper bound of lifetime CRS case indirect costs was used) (Table 4).

Discussion

The large concurrent outbreaks of measles and rubella in Romania provided a major opportunity for an economic assessment of both diseases, as well as for CRS, in a middle-income country setting. Our key study findings were that households incurred a high economic burden of measles or rubella infection compared with income, the health sector bore most of the economic cost of the measles and rubella outbreaks, and CRS case costs were substantial and relevant to include in rubella outbreak cost studies. Our study contributes to the limited literature on measles and rubella outbreak costs in middle-income countries and to the evidence gap in this global research priority.

The economic burden of the measles and rubella outbreaks on the outbreak-affected households was substantial. Almost every household incurred costs relating to measles or rubella treatment. The direct household cost per case of measles or rubella was high compared with the average income in Romania in 2012: 30% of monthly income and 3% of annual income for measles, 9% of monthly income and 1% of annual income for rubella. Previous studies indicated that, when illness-related economic costs are >10% of annual household income, it is considered catastrophic because it potentially forces households to cut consumption of necessities, such as food and water, and leads to increased debt or greater poverty (*12–14*). Although direct household costs per case in our study in general did not exceed this threshold in Romania (≈US $263 in 2013), the highest cost households did; moreover, these costs were for only 1 medical event, and the financial burden would increase if other illnesses were considered.

For households, the unexpected measles and rubella treatment costs had to be met in the short term. High medical costs incurred in a short period are considered more detrimental than high costs incurred over a long period (*12*). Approximately 36% of households with measles and 7% with rubella reported borrowing money to pay for these expenses. Similar medical bill coping strategies, including informal payments, have also been confirmed in other studies in Romania (*15*,*16*). As a consequence of these expenses, studies in Romania and other countries in eastern Europe have reported that up to 60% of patients are forced to postpone or completely forgo treatments because of lack of money to pay

Table 3. Main analysis input and sensitivity analysis values used for cost analysis of economic burden of concurrent measles and rubella outbreaks, Romania, 2011–2012*

Cost component	Disease	Input	Input value	Median (25th–75th percentiles)	Proportion (95% CI)	Sensitivity analysis LB	Sensitivity analysis UB
Case distribution	Measles	No. cases	12,427	NA	NA	11,184	13,670
	Rubella	No. cases	24,627	NA	NA	22,164	27,090
	Rubella	No. CRS cases	27	NA	NA	NA	NA
	Rubella	Patients who died as of May 2016	12	NA	NA	NA	NA
	Rubella	Patients who survived as of May 2016	15	NA	NA	NA	NA
	Measles	Cases in 2011, %	39	NA	NA	NA	NA
	Measles	Cases in 2012, %	61	NA	NA	NA	NA
	Rubella	Cases in 2011, %	16	NA	NA	NA	NA
	Rubella	Cases in 2012, %	85	NA	NA	NA	NA
Healthcare provider	Measles	Reimbursement to healthcare providers for diagnostic codes, 2011	$1,313,049	NA	NA	$1,181,744	$1,444,353
	Measles	Reimbursement to healthcare providers for diagnostic codes, 2012	$1,962,708	NA	NA	$1,766,437	$2,158,979
	Rubella	Reimbursement to healthcare providers for diagnostic codes, 2011	$107,494	NA	NA	$96,745	$118,244
	Rubella	Reimbursement to healthcare providers for diagnostic codes, 2012	$567,138	NA	NA	$510,425	$623,852
National outbreak response	Measles	Personnel time for outbreak response	$5,164	NA	NA	$4,648	$5,680
	Measles	Reagent/test for outbreak response	$449,225	NA	NA	$404,303	$494,148
	Measles	Emergency vaccine purchases	$61,962	NA	NA	$55,766	$68,158
	Rubella	Personnel time for outbreak response	$10,437	NA	NA	$9,393	$11,481
	Rubella	Reagent/test for outbreak response	$907,951	NA	NA	$817,156	$998,746
	Rubella	Emergency vaccine purchases	$125,235	NA	NA	$112,712	$137,759
Direct medical and nonmedical household	Measles	Out-of-pocket cost for inpatient care	NA	$66.87 ($21.27–$110.94)	NA	$21.27	$110.94
	Rubella	Out-of-pocket cost for inpatient care	NA	$30.70 ($15.20–$82.06)	NA	$15.20	$82.06
	Measles	Out-of-pocket cost for outpatient care	NA	$18.23 ($4.55–$39.51)	NA	$4.55	$39.51
	Rubella	Out-of-pocket cost for outpatient care	NA	$12.50 ($6.07–$24.32)	NA	$6.07	$24.32
	Measles	Patients receiving outpatient care, %	NA	NA	19 (24–60)	24	60
	Measles	Patients receiving inpatient care, %	NA	NA	81 (80–109)	80	100
	Rubella	Patients receiving outpatient care, %	NA	NA	62 (17–27)	17	27
	Rubella	Patients receiving inpatient care, %	NA	NA	38 (24–91)	34	91
Indirect household	Measles	Employment rate for case-patients and caregivers, %	34	NA	NA	NA	NA
	Rubella	Employment rate for case-patients and caregivers, %	32	NA	NA	NA	NA
	Measles	No. work days missed by case-patients	NA	11.45 (7–18)	NA	7	18
	Rubella	No. work days missed by case-patients	NA	9.62 (7–14)	NA	7	14
	Measles	Case caregivers who missed work, %	89	NA	NA	NA	NA
	Rubella	Case caregivers who missed work, %	68	NA	NA	NA	NA
	Measles	No. work days missed by caregivers	NA	7 (3–10)	NA	3	10
	Rubella	No. work days missed by caregivers	NA	4.5 (3–7)	NA	3	7
	Both	Minimum daily wage	$10.44	NA	NA	NA	NA
CRS, direct medical	Rubella	Reimbursement to healthcare providers for patients who survived	NA	$6,455 ($1,749–$10,296)	NA	$1,749	$10,296
	Rubella	Reimbursement to healthcare providers for patients who died	NA	$2,777 ($1,734–$3,309)	NA	$1,734	$3,309
CRS, lifetime discounted indirect	Rubella	Minimum daily wage	$10.44	NA	NA	NA	NA
	Rubella	Years (range) of productivity loss	46 (18–63)	NA	NA	NA	74 (LE)
	Rubella	Labor force participation rate, %	65	NA	NA	NA	100
	Rubella	Unemployment rate, %	11	NA	NA	NA	0
	Rubella	Discount rate, %	3	NA	NA	NA	NA

*Monetary values are in US 2013 dollars. CRS is an outcome of rubella. CRS, congenital rubella syndrome; LB, lower bound; LE, life expectancy; NA, not applicable; UB, upper bound.

their medical bills (*15*,*17*). Because per capita health spending in Romania was less than that in the United States (US $580) during 2013 (*18*), the estimated direct household and health sector costs per case of measles (US $376) and rubella (US $89, not including CRS costs) were high.

The health sector bore 70% of the economic cost of the outbreak for measles and 39% for the outbreak of rubella. For measles, 86% of the health sector costs were for provider reimbursement. For rubella, 61% was for national outbreak response activities. More than 85% of the national outbreak response activities were for laboratory reagents and test kits for measles and rubella, but only 12% was for emergency vaccine purchase because large-scale supplemental immunization activities were not conducted. Assuming a cost per

Table 4. Estimated total costs by component for base case and sensitivity analyses for assessment of economic burden of concurrent measles and rubella outbreaks, Romania, 2011–2012*

Cost component	Disease or outcome	Main analysis base case	Sensitivity analysis variable	Sensitivity analysis LB	Sensitivity analysis UB	Total measles and rubella costs with LB	Total measles and rubella costs with UB
Healthcare provider	Measles	$3,275,757	Healthcare provider costs	$2,948,181	$3,603,332	$9,555,968	$10,211,120
	Rubella	$674,633	Healthcare provider costs	$607,169	$742,096	$9,816,081	$9,951,007
National outbreak response	Measles	$516,351	National outbreak response costs	$464,716	$567,986	$9,831,909	$9,935,179
	Rubella	$1,043,623	National outbreak response costs	$939,261	$1,147,985	$9,779,182	$9,987,906
Direct medical and nonmedical household	Measles	$883,338	Out-of-pocket inpatient and outpatient treatment costs	$266,573	$1,572,347	$9,266,779	$10,572,553
			Proportion of patients receiving inpatient or outpatient treatment	$716,509	$915,498	$9,716,715	$9,915,704
			No. cases	$795,004	$971,672	$9,795,210	$9,971,878
	Rubella	$477,261	Out-of-pocket inpatient and outpatient treatment costs	$141,497	$1,136,431	$9,547,779	$10,542,713
			Proportion of patients receiving inpatient or outpatient treatment	$310,302	$768,764	$9,716,584	$10,175,046
			No. cases	$429,535	$524,988	$9,835,818	$9,931,270
Indirect household	Measles	$779,917	No. work days missed by case-patients	$583,614	$1,068,856	$9,687,241	$10,172,484
			No. work days missed by caregivers	$622,875	$897,698	$9,726,502	$10,001,325
	Rubella	$1,043,281	No. work days missed by case-patients	$827,714	$1,403,658	$9,667,976	$10,243,920
			No. work days missed by caregivers	$959,358	$1,183,153	$9,799,621	$10,023,416
CRS cases direct medical	Rubella	$130,143	Reimbursement to healthcare providers for CRS cases	$47,038	$194,145	$9,800,438	$9,947,546
CRS cases lifetime discounted indirect	Rubella	$1,059,241	Productive years (labor force participation, unemployment rate)	NA	$2,165,257	NA	$10,989,560
Total	Measles	$5,455,363	NA	NA	NA	NA	NA
	Rubella	$4,428,182	NA	NA	NA	NA	NA
	Both	$9,883,545	NA	NA	NA	NA	NA

*CRS, congenital rubella syndrome; LB, lower bound; NA, not applicable; UB, upper bound.

Table 5. Estimated overall cost per case of measles, rubella, or congenital rubella syndrome during concurrent outbreaks, Romania, 2011–2012*

Cost type	Cost per case (sensitivity analysis lower bound–upper bound; 2013 US $)		
	Measles	Rubella, not CRS	CRS
Household direct medical and nonmedical	$71 ($21–$127)	$19 ($6–$46)	NA
Household indirect	$63 ($47–$86)	$42 ($34–$57)	NA
Healthcare provider	$264 ($237–290)	$27 ($25–30)	NA
National outbreak response	$42 ($37–46)	$42 ($38–47)	NA
CRS cases direct medical	NA	NA	$4,820 ($1,742–$7,191)
CRS cases lifetime discounted indirect	NA	NA	$39,231 (UB: $80,195)
Estimated total societal/case	$439 ($389–494)	$132 ($118–$158)	$44,051 ($40,973–$85,015)

*CRS, congenital rubella syndrome; NA, not applicable; UB, upper bound of sensitivity analysis.

dose administered of US $5, the cost of vaccinating all 36,861 confirmed case-patients with measles or rubella with 2 doses of the measles and rubella vaccine before the outbreak would have cost the health sector 10% of the amount paid for health sector costs for the measles outbreak and 21% of the amount paid for health sector costs for the rubella outbreak. Any pre-outbreak vaccination campaign would have had to vaccinate more than just the 36,861 persons who were infected during the outbreak to prevent the outbreak, and the costs of strategies to reach persistently unvaccinated subpopulations in Romania might be higher than typical campaign or routine immunization costs. Even so, such preemptive campaigns to reduce immunity gaps, coupled with continued robust routine immunization delivery, would have provided protection and reduced costs to the health sector, not only during the 2011–2012 outbreaks but also for future outbreaks. This finding is critical because Romania continues to have measles outbreaks.

Our study contributes to the ongoing efforts to document evidence of the economic burden of vaccine-preventable diseases in middle-income countries, with particular focus on measles and rubella. A study from Ethiopia reported an estimated household cost of US $29.18/case of measles treated during a measles outbreak in 2011 (*2*). As in Romania, the Ethiopian health sector bore most (80%) of the outbreak cost. A study in Latin America found the costs of measles treatment to range from US $43 in Nicaragua to US $210 in Argentina; the average cost was US $190 for the entire Latin America region (*19*). As an upper-middle-income country, economic costs for Romania are more comparable to those reported for countries such as the Netherlands, the United Kingdom, and Canada; a study from these countries in 2002 reported the societal costs of measles treatment as US $254 in Canada, US $276 in the Netherlands, and US $307 in the United Kingdom (*20*).

Our post-hoc analysis of CRS direct medical costs and estimated productivity losses adds to the limited literature on CRS costs in different economic settings (*21*). Studies from Brazil, Oman, and Uzbekistan reported that estimated CRS costs ranged from US $18,644 to >US $1.18 million/case (*22–24*). More than 90% of these costs constitute indirect CRS costs. Future studies of CRS economic burden in low- and middle-income countries are needed. In this assessment, we did not quantify the value of life lost because of measles or rubella infections occurring during the outbreak, aside from the CRS cost estimates.

Our cost estimates are subject to several limitations. The household cost estimates were retrospective, and some persons might have been susceptible to recall bias. The purposive sampling of recent cases and district-level weighting procedures used for the household survey do not necessarily provide a nationally representative estimate of household costs, and no adjustment was made to account for survey nonresponse (response rate 35%), which might introduce selection bias; household costs might be underestimated because of the smaller proportion of case-patients <18 years of age in our sample compared with the outbreaks overall. We only recorded the provider reimbursement claims that were actually paid by the national insurance companies. However, anecdotal information suggested that claims were sometimes reimbursed at lower standard amounts based on limited availability of funds at the national level. National outbreak response costs were based on interviews with key informants from the agencies responsible for response implementation and are believed to be exhaustive of the costs incurred. However, other agencies might have also provided outbreak response and might not have been known to the national health authorities we used as key informants for the agencies involved in outbreak response.

For the CRS cost analysis, we did not obtain information on 9 of the reported cases (response rate 67%), which might introduce selection bias in our results, although no systematic differences in clinical profiles between included and excluded cases were observed. Information on some types of future CRS care costs (e.g., special schooling, government disability payments) were not available and are therefore not included in the analysis. The CRS productivity losses assume that all surviving case-patients are fully unable to work; this assumption might overestimate the indirect costs of CRS if some of these case-patients are ultimately able to work for income. Because of the nonrepresentative sampling techniques used and nonresponse, no uncertainty bounds were calculated for these cost estimates. Finally, the estimation of economic costs was not fully comprehensive. The opportunity costs of healthcare workers devoting their time to doing other public health activities was not estimated because of incomplete data.

In conclusion, the costs of the 2011–2012 measles and rubella outbreaks in Romania were high, especially when compared with total average household incomes and national health expenditures per capita. In addition to the health consequences of these outbreaks, households faced major threats of financial insecurities during these outbreaks and the long-term economic impacts of productivity losses. Preventing outbreaks through routine vaccination also reduces the economic burden on the health sector. This study makes a major contribution to identifying the overall societal economic burden of measles and rubella outbreaks in Romania and improves our understanding of the magnitude of the costs of measles and rubella outbreaks in middle-income economies.

About the Author

At the time of study, Dr. Njau was an economist with the Global Immunization Program, Center for Global Health, Centers for Disease Control and Prevention, Atlanta, GA. He is currently a consultant at JoDon Consulting Group LLC, Atlanta, GA. His research interests are the economics of infectious diseases, including malaria, Ebola, and vaccine-preventable diseases, such as measles, rubella, rotavirus infection, and hepatitis B.

References

1. Ortega-Sanchez IR, Vijayaraghavan M, Barskey AE, Wallace GS. The economic burden of sixteen measles outbreaks on United States public health departments in 2011. Vaccine. 2014;32:1311–7. http://dx.doi.org/10.1016/j.vaccine.2013.10.012
2. Wallace AS, Masresha BG, Grant G, Goodson JL, Birhane H, Abraham M, et al. Evaluation of economic costs of a measles outbreak and outbreak response activities in Keffa Zone, Ethiopia. Vaccine. 2014;32:4505–14. http://dx.doi.org/10.1016/j.vaccine.2014.06.035
3. Lanzieri TM, Segatto TC, Siqueira MM, de Oliviera Santos EC, Jin L, Prevots DR. Burden of congenital rubella syndrome after a community-wide rubella outbreak, Rio Branco, Acre, Brazil, 2000 to 2001. Pediatr Infect Dis J. 2003;22:323–9. http://dx.doi.org/10.1097/01.inf.0000059401.07698.95
4. Njeru I, Onyango D, Ajack Y, Kiptoo E. Rubella outbreak in a Rural Kenyan District, 2014: documenting the need for routine rubella immunization in Kenya. BMC Infect Dis. 2015;15:245. http://dx.doi.org/10.1186/s12879-015-0989-6
5. Hahné S, Macey J, van Binnendijk R, Kohl R, Dolman S, van der Veen Y, et al. Rubella outbreak in the Netherlands, 2004–2005: high burden of congenital infection and spread to Canada. Pediatr Infect Dis J. 2009;28:795–800. http://dx.doi.org/10.1097/INF.0b013e3181a3e2d5
6. Curtale F, Perrelli F, Mantovani J, Ciofi degli Atti M, Filia A, Nicoletti L, et al. Description of two measles outbreaks in the Lazio Region, Italy (2006–2007). Importance of pockets of low vaccine coverage in sustaining the infection. BMC Infect Dis. 2010;10:62. http://dx.doi.org/10.1186/1471-2334-10-62
7. National Public Health Institute. National Center for Surveillance and Control of Communicable Diseases. The 2011/2012 measles outbreak in Romania. Bucharest (Romania): the Institute; 2013.
8. Vladescu C, Scintee G, Olsavszky V. Romania health system review. In: Mladovsky SA, editor. Health systems in transition. London: The European Observatory on Health Systems and Policies; 2008 [cited 2019 Mar 17]. http://www.euro.who.int/__data/assets/pdf_file/0017/317240/Hit-Romania.pdf?ua=1
9. Johannesson M. The willingness to pay for health changes, the human-capital approach and the external costs. Health Policy. 1996;36:231–44. http://dx.doi.org/10.1016/0168-8510(96)00815-9
10. National Bank of Romania (NBR). Exchange rates: monthly, quarterly and annual averages. Bucharest (Romania): NBR; 2013.
11. Institut National de Statistica. Consumer price index. December 2013 edition. Bucharest (Romania); The Institut; 2016.
12. Xu K, Evans DB, Kawabata K, Zeramdini R, Klavus J, Murray CJ. Household catastrophic health expenditure: a multicountry analysis. Lancet. 2003;362:111–7. http://dx.doi.org/10.1016/S0140-6736(03)13861-5
13. Xu K, Evans DB, Carrin G, Aguilar-Rivera AM, Musgrove P, Evans T. Protecting households from catastrophic health spending. Health Aff (Millwood). 2007;26:972–83. http://dx.doi.org/10.1377/hlthaff.26.4.972
14. Raban MZ, Dandona R, Dandona L. Variations in catastrophic health expenditure estimates from household surveys in India. Bull World Health Organ. 2013;91:726–35. http://dx.doi.org/10.2471/BLT.12.113100
15. Tambor M, Pavlova M, Rechel B, Golinowska S, Sowada C, Groot W. The inability to pay for health services in central and eastern Europe: evidence from six countries. Eur J Public Health. 2014;24:378–85. http://dx.doi.org/10.1093/eurpub/ckt118
16. Stepurko T, Pavlova M, Gryga I, Groot W. To pay or not to pay? A multicountry study on informal payments for health-care services and consumers' perceptions. Health Expect. 2014.
17. Atanasova E, Pavlova M, Moutafova E, Rechel B, Groot W. Out-of-pocket payments for health care services in Bulgaria: financial burden and barrier to access. Eur J Public Health. 2013;23:916–22. http://dx.doi.org/10.1093/eurpub/cks169
18. The World Bank. Health expenditure per capita (current US$). World development indicators. Washington: World Bank and World Health Organization; 2013.
19. Acharya A, Diaz-Ortega JL, Tambini G, de Quadros C, Arita I. Cost-effectiveness of measles elimination in Latin America and the Caribbean: a prospective analysis. Vaccine. 2002;20:3332–41. http://dx.doi.org/10.1016/S0264-410X(02)00296-7
20. Carabin H, Edmunds WJ, Kou U, van den Hof S, Nguyen VH. The average cost of measles cases and adverse events following vaccination in industrialised countries. BMC Public Health. 2002;2:22. http://dx.doi.org/10.1186/1471-2458-2-22
21. Hinman AR, Irons B, Lewis M, Kandola K. Economic analyses of rubella and rubella vaccines: a global review. Bull World Health Organ. 2002;80:264–70.
22. Lanzieri TM, Parise MS, Siqueira MM, Fortaleza BM, Segatto TC, Prevots DR. Incidence, clinical features and estimated costs of congenital rubella syndrome after a large rubella outbreak in Recife, Brazil, 1999–2000. Pediatr Infect Dis J. 2004;23:1116–22.
23. Al-Awaidy S, Griffiths UK, Nwar HM, Bawikar S, Al-Aisiri MS, Khandekar R, et al. Costs of congenital rubella syndrome (CRS) in Oman: evidence based on long-term follow-up of 43 children. Vaccine. 2006;24:6437–45. http://dx.doi.org/10.1016/j.vaccine.2006.05.089
24. Kurbanov B, Musabaev E, Latipov R. The economic burden of congenital rubella syndrome and vaccination in Tashkent City, Uzbekistan. EpiNorth. 2012;13:18–24.

Address for correspondence: Laura Zimmerman, Centers for Disease Control and Prevention, 1600 Clifton Rd NE, Mailstop H24-3, Atlanta, GA 30329-4017, USA; email: laz5@cdc.gov

Novel Orthobunyavirus Causing Severe Kidney Disease in Broiler Chickens, Malaysia, 2014–2017

Vilmos Palya, Edit Walkóné Kovács, Szilvia Marton, Tímea Tatár-Kis, Balázs Felföldi, Barbara Forró, Marianna Domán, Krisztián Bányai

During 2014–2017, we isolated a novel orthobunyavirus from broiler chickens with severe kidney lesions in the state of Kedah, Malaysia; we named the virus Kedah fatal kidney syndrome virus (KFKSV). Affected chickens became listless and diarrheic before dying suddenly. Necropsies detected pale and swollen kidneys with signs of gout, enlarged and fragile livers, and pale hearts. Experimental infection of broiler chickens with KFKSV reproduced the disease and pathologic conditions observed in the field, fulfilling the Koch's postulates. Gene sequencing indicated high nucleotide identities between KFKSV isolates (99%) and moderate nucleotide identities with the orthobunyavirus Umbre virus in the large (78%), medium (77%), and small (86%) genomic segments. KFKSV may be pathogenic for other host species, including humans.

In recent years, numerous arboviruses have reportedly caused major outbreaks among domestic or wild birds (*1,2*). Most arboviruses associated with widespread epizootics are members of the *Flaviviridae* family, although the poultry industry has been affected by other arboviruses (*3–5*). The order *Bunyavirales* comprises at least 9 families and 13 genera. Of the major genera, only viruses of the *Orthobunyavirus*, *Orthohantavirus*, *Orthonairovirus*, and *Phlebovirus* genera infect vertebrates (*6–8*). *Orthobunyavirus* is the most diverse genus within the *Bunyavirales* order, comprising ≈170 viruses classified into ≥18 serogroups on the basis of antigenic relationships; this serology correlates well with the phylogenetic analyses (*9*). For birds, particularly domestic poultry, descriptions of natural infections with orthobunyaviruses are scarce (*10,11*). Hubálek et al., in a recent comprehensive review on arboviruses, listed only a few orthobunyaviruses pathogenic to domestic poultry, most likely reflecting a minor role of orthobunyaviruses in poultry diseases (*5*).

Since 2014, sporadic cases of a new disease in broiler chickens, manifested as clinical signs of lethargy accompanied by some gastrointestinal symptoms and sudden death from severe kidney damage, have been reported in northwestern Malaysia. We identified and characterized the etiologic agent of this disease.

Materials and Methods

Detection and Identification of the Etiologic Agent

We collected samples of kidney and cecal tonsils from affected chickens in the field that died and submitted them to the Scientific Support and Investigation Laboratory of Ceva-Phylaxia (Budapest, Hungary) for detection of possible viral agents. The tissue samples were homogenized to give ≈10% (wt/vol) suspension in phosphate-buffered saline pH 7.2. The homogenized samples were centrifuged at 1,000 × *g* for 15 min at 4°C and then filtered through a 0.45-µm membrane. We inoculated 0.2 mL of the filtered supernatant via the chorioallantoic cavity into specific pathogen free (SPF) eggs, 9–11 days old, divided into groups of 5. After inoculation, we checked eggs daily for 7 days and discarded those that died within 24 h. The chorioallantoic fluid was harvested aseptically from embryos that died after 24 h, and these embryos were examined for the presence of gross pathologic lesions. If at the end of the 7-day observation period no embryos had died, we removed the eggs with live embryos and kept them at 4°C for 24 h and then collected the chorioallantoic fluid for the next passage. We conducted 3 blind passages before considering a sample negative for pathogens.

The chorioallantoic fluid of the embryos showing pathologic lesions was inoculated onto LMH (chicken hepatocellular carcinoma) and Vero (African green monkey kidney) cell cultures and checked for cytopathogenic agents. LMH cells were also used for propagation and titration of the isolated virus and for reisolation of

Author affiliations: Ceva-Phylaxia Veterinary Biologicals Co. Ltd., Budapest, Hungary (V. Palya, E.W. Kovács, T. Tatár-Kis, B. Felföldi); Hungarian Academy of Sciences, Budapest (S. Marton, B. Forró, M. Domán, K. Bányai)

DOI: https://doi.org/10.3201/eid2506.181661

the virus from kidney samples from experimentally infected chickens.

Supernatants of tissue cultures showing cytopathologic changes were centrifuged at 10,000 × *g* for 5 min, and 200 μL of the supernatant was used for nucleic acid extraction by use of the ZiXpress32 Viral Nucleic Acid Extraction Kit and ZiXpress32 robot (Zinexts Life Science, http://www.Zinexts.com). Random primed reverse-transcription PCR (RT-PCR) was performed as described elsewhere (*12,13*). We subjected 100 ng of cDNA to enzymatic fragmentation and adaptor ligation, following the manufacturer's recommendations (NEBNext Fast DNA Fragmentation & Library Prep Set for Ion Torrent; New England Biolabs, https://www.neb.com). The resulting cDNA libraries were measured on Qubit 2.0 equipment by using the Qubit dsDNA BR Assay kit (Invitrogen, https://www.thermofisher.com). The isothermal emulsion PCR that produced clonally amplified libraries was conducted according to the manufacturer's protocol by using the IA 500 kit (Life Technologies, https://www.thermofisher.com). Enrichment of the templated beads (on an Ion OneTouch ES machine; Life Technologies) and further steps of presequencing setup were performed according to the manufacturer's 200-bp protocol. We strictly followed the sequencing protocol recommended for the Ion PGM Hi-Q View Sequencing Kit on a 316 v2 chip (Life Technologies).

Sanger sequencing was used to validate results obtained by the viral metagenomics approach. Primer pairs were designed to amplify 0.8–1.2-kb fragments (not shown). The BrightDye Terminator Cycle Sequencing Kit (NimaGen, https://www.nimagen.com) was used in the amplification reaction, and dye-labeled products were run on an ABI 3500 sequencer (Life Technologies).

Sequence reads obtained by next-generation sequencing were trimmed by using CLC Genomics Workbench version 7 (http://www.clcbio.com). The minimal read length parameter was set to 40. The same software was used to assemble the genome sequence. After visually inspecting the sequence mappings, we created 1 consensus sequence for all 3 genome segments (small [S], medium [M], and large [L]). Sanger sequencing outputs were analyzed by using BioEdit software (*14*). Sequence contigs from the 2 sequencing platforms were assembled and further edited by using GeneDoc (*15*) and BioEdit software and then analyzed by similarity search with BLAST (*14–16*). We deposited newly generated nucleotide sequences into GenBank (accession nos. MK047401–MK047415). Multiple alignments were prepared by using the TranslatorX online program (*17*) and manually adjusted in GeneDoc, whereas phylogenetic analysis by the maximum-likelihood and the neighbor-joining methods was performed by using MEGA6 software (*18*). The coding potential was predicted by using ORF Finder (http://www.ncbi.nlm.nih.gov/gorf/gorf.html).

Development of Diagnostic RT-PCR

For assay development and quantification of the novel orthobunyavirus genomic RNA in organ samples of the experimental animals, we extracted viral RNA as previously described and designed primers and probes for the S genomic segment of the novel orthobunyavirus. The reaction mixture of quantitative RT-PCR (qRT-PCR) that we used was composed of 10 μL 2× qPCRBIO Probe 1-Step Mix (PCR Biosystems, http://www.pcrbio.com), 1.6 μL S gene specific forward (5′ GGGTAGCACTAGCATTTATCCA 3′) and reverse (5′ TGTAGACACCCACAAACGTATC 3′) primers (each from 10 μM stock solutions), 0.5 μL S gene specific probe (5′ [FAM] AGCTCACATACGAGGATACACAGGA [BHQ] 3′) from a 10 μmol/L stock solution, 1 μL 20× RTase with RNase inhibitor, 0.3 μL nuclease-free water, and 5 μL RNA. The thermal profile of the qRT-PCR was as follows: reverse transcription at 50°C for 10 min terminated by heating to 95 °C for 2 min, followed by amplification performed in 40 cycles consisting of denaturation at 95°C for 5 s and hybridization and elongation at 60°C for 20 s. Throughout the study, we used a Mic qPCR cycler (Bio Molecular Systems, https://biomolecularsystems.com), kindly provided for the project by Péter Kisfali, Amplicon Ltd.).

To test the assay specificity, we used a number of viruses from our strain collection, including avian nephritis virus (*Astroviridae*); QX-like, 4/91-like, and Massachusetts-like infectious bronchitis virus strains (*Coronaviridae*); representative isolates of avian metapneumovirus A, B, and C and Newcastle disease virus (*Paramyxoviridae*); isolates of influenza (H9N2) and (H5N8) viruses (*Orthomyxoviridae*); and Tembusu virus (*Flaviviridae*).

Experimental Reproduction of the Disease

We tested the pathogenicity of 1 of the isolates (D2756/1/2014/MY) in 5-day-old broiler chickens purchased from a commercial hatchery in Hungary. We inoculated 10 chickens with 0.2 mL of 5.1 $\log_{10}$ 50% tissue culture infective dose ($TCID_{50}$) of the isolate by either the subcutaneous or oral route; for negative controls, we inoculated 5 chickens of the same age with phosphate-buffered saline pH 7.2. We kept all birds in isolators with negative pressure and monitored them daily for overt clinical signs and death for 26 days after inoculation.

We recorded gross lesions of birds that died during the 26-day postinoculation period and collected samples from the spleen, liver, kidney, heart, pancreas, small intestine, bursa, and thymus and placed them in 10% buffered formalin for histologic analysis. We also collected tissue samples (spleen, liver, kidney, heart, intestine, and bursa) from 5 chickens in the subcutaneously infected group and 4 chickens from the orally infected group that died and processed them for viral RNA detection by

using qRT-PCR. We euthanized all remaining birds and inspected them for gross pathologic lesions, collecting samples for histologic analysis (spleens, livers, kidneys, hearts, and bursa Fabricii) and qRT-PCR (spleens and kidneys from all; hearts, livers, bursa Fabricii, and cecal tonsils from a few).

Histologic Analyses

Tissue samples were processed according to standard histologic procedures. Samples were embedded in paraffin, cut in 5-µm sections, stained with hematoxylin and eosin or trichrome, and examined under light microscopy.

Results

Epidemiologic and Clinical Observations

The first outbreaks of the disease occurred during July–September 2014 and recurred during the same months each subsequent year. All cases were from broiler farms with open-sided houses in Kedah (Figure 1).

Several chickens in the affected flocks became listless and exhibited signs of diarrhea. Affected birds died soon after the appearance of the first clinical signs. The disease sometimes occurred in birds ≈1 week of age but more routinely in those 2–4 weeks of age. Mortality rates varied within a wide range, from a low percentage to 30%–40% (Figure 2).

The most striking lesions in dead chickens were pale, swollen kidneys with uric acid deposits, frequently localized in the tubules and ureters (Figure 3) and also found on the surface of serosa covering the visceral organs. The livers were moderately enlarged and fragile. The heart muscle was pale. No obvious gross lesions were seen in any other organs.

Etiologic Agent

From the kidney and cecal tonsil samples submitted from 1 affected chicken in 2014 and 3 affected chickens in 2017, we obtained 5 virus isolates after 1 blind passage in SPF embryos. Embryo deaths occurred 3–5 days after inoculation with the organ homogenates. The dead embryos exhibited severe subcutaneous edema, congestion, and hemorrhages on the skin. No hemagglutinating agents were observed when chicken red blood cells were used in analysis of allantoic fluid from dead embryos.

Cytopathic effect was evident at 48–72 hours after inoculation of LMH and Vero cell cultures with the allantoic fluid from dead embryos. Elongated or rounded dark cells were seen in irregular clusters, expanding very fast to affect the whole cell sheet within 24–36 hours. The virus grown on LMH cell cultures reached a titer of 6.3–6.5 $\log_{10}$ $TCID_{50}$/mL.

Viral metagenomics performed from 2 cell culture supernatants (D2756/1/2014/MY and D2756/2/2014/MY)

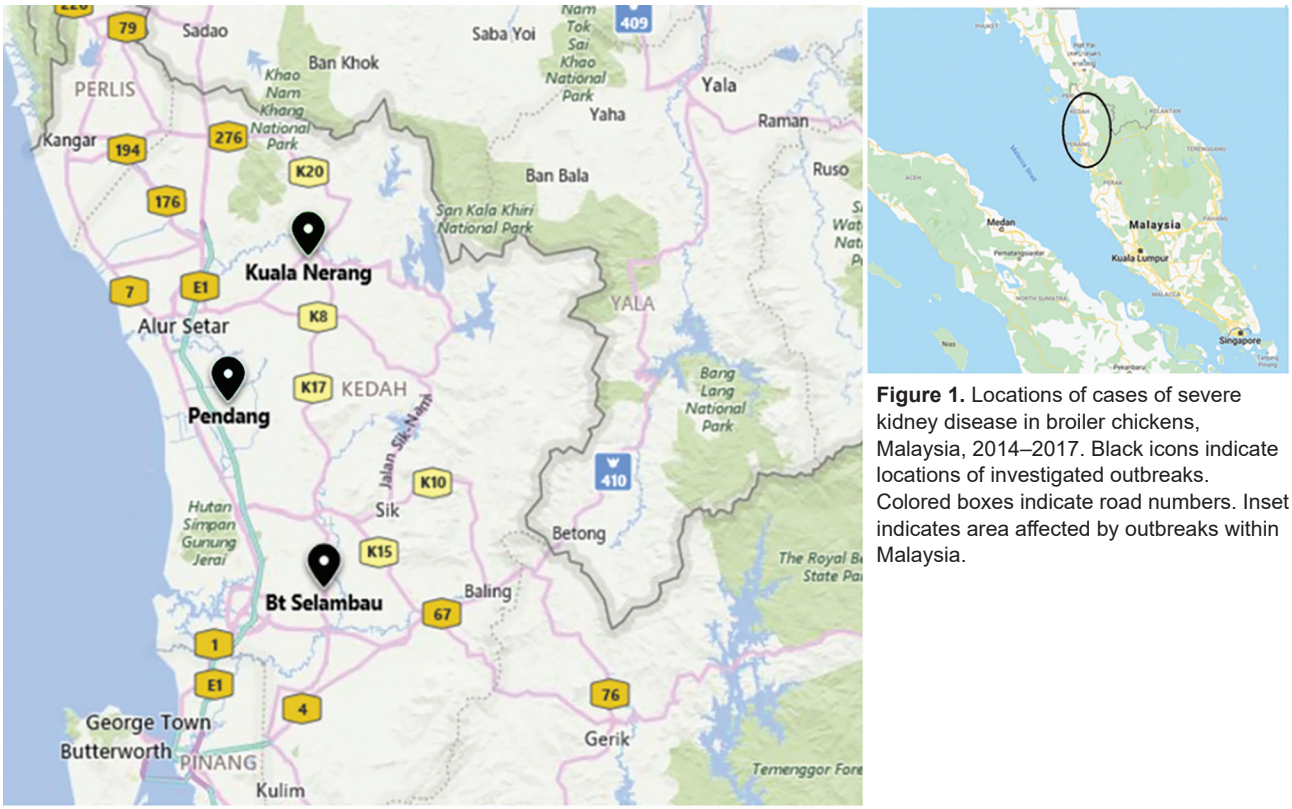

Figure 1. Locations of cases of severe kidney disease in broiler chickens, Malaysia, 2014–2017. Black icons indicate locations of investigated outbreaks. Colored boxes indicate road numbers. Inset indicates area affected by outbreaks within Malaysia.

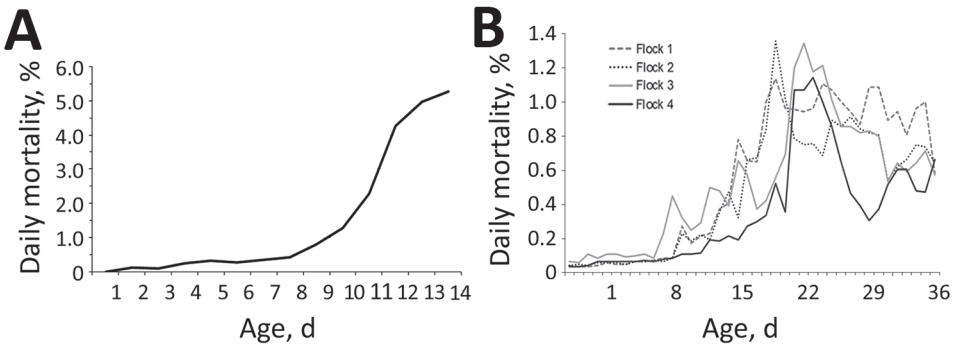

Figure 2. Daily mortality rates among broiler chickens with severe kidney disease, Malaysia, 2014–2017. A) Flock affected by the 2014 outbreak. B) Four flocks affected by the 2017 outbreaks.

identified sequence scaffolds with greatest BLAST hits to the orthobunyavirus Umbre virus (Turlock serogroup). The most 3′ and 5′ ends of the genomic RNA could not be determined with this method. To confirm the sequencing results obtained by next-generation sequencing, we also performed Sanger sequencing. The obtained nearly full-length genome sequences (L segment ≈6.9 kbp, M segment ≈4.3 kbp, S segment ≈0.8 kbp) showed >99% nt sequence identities between isolates D2756/1/2014/MY and D2756/2/2014/MY. When we compared sequences with Umbre virus, we identified 78% nt sequence identities along L, 77% along M, and 86% along S genomic segments.

Diagnostic qRT-PCR

The S genomic segment contained an ≈200-bp fragment that shared high sequence homology with Umbre virus. Primers and probes had been designed to detect Malaysia orthobunyavirus isolates and Umbre virus, although the assay was not tested against Umbre virus or other closely related strains within the Turlock serogroup. The assay exhibited high specificity when tested against a variety of viruses characterized by kidney tropism and was able to reproducibly detect the viral RNA from tissues that corresponded to as few as 3 $TCID_{50}$/mL virus culture supernatant (or 0.03 $TCID_{50}$ virus/5 μL RNA). The kidney samples submitted from the sick poultry in the field during 2014 and 2017 contained RNA copies corresponding to a viral titer of 9.00×10^4 to 4.81×10^5 $TCID_{50}$ of infectious virus per gram of organ specimen. Phylogenetic analysis based on the partial amino acid sequences of proteins encoded by the L, M, and S segments showed that all 5 isolates detected from 4 different outbreak cases over a 3-year period were highly similar in the regions analyzed (Figure 4).

Figure 3. Gross pathologic appearance of kidney from a chicken with severe kidney disease naturally infected with a novel orthobunyavirus (Kedah fatal kidney syndrome virus), Malaysia, 2014–2017.

Experimental Reproduction of the Disease

The pathologic condition of chickens in the field could be reproduced by experimental infection of chickens with 1 of the selected isolates (D2756/1/2014/MY). From postinoculation day 3, chickens became listless and showed loss of appetite. Deaths occurred during postinoculation days 3–5 in the subcutaneously infected group and started 2 days later (postinoculation day 5) in the orally infected group. The mortality rate was higher for the group infected by the subcutaneous route (Figure 5).

After clinical signs appeared, the chickens died within 12–24 hours. In those that died, gross lesions were mainly confined to the kidneys, which were pale and swollen with distended ureters filled with uric acid (Figure 6, panel A). In some chickens, visceral gout also developed (Figure 6, panel B). Other gross lesions that could be observed in most dead chickens were accumulation of serous exudate in the abdominal cavity and pericardium, signs of liver degeneration, and discoloration of the heart muscle. The chickens in the control group remained healthy throughout the observation period.

Histopathologic Findings

In the organs collected from the experimentally infected chickens that died, the predominant histologic lesions were in the kidney, liver, heart, and lymphoid organs. The most consistent lesions were tubulonephrosis with occasional tubular epithelium necrosis; intraglomerular urolithiasis and multifocal interstitial lympho-histiocytic infiltration (Figure 7, panel A); vacuolic degeneration and disintegration of liver cells with signs of hepatitis (Figure 7, panel B); acute serous myocarditis; and depletion of lymphocytes with scattered

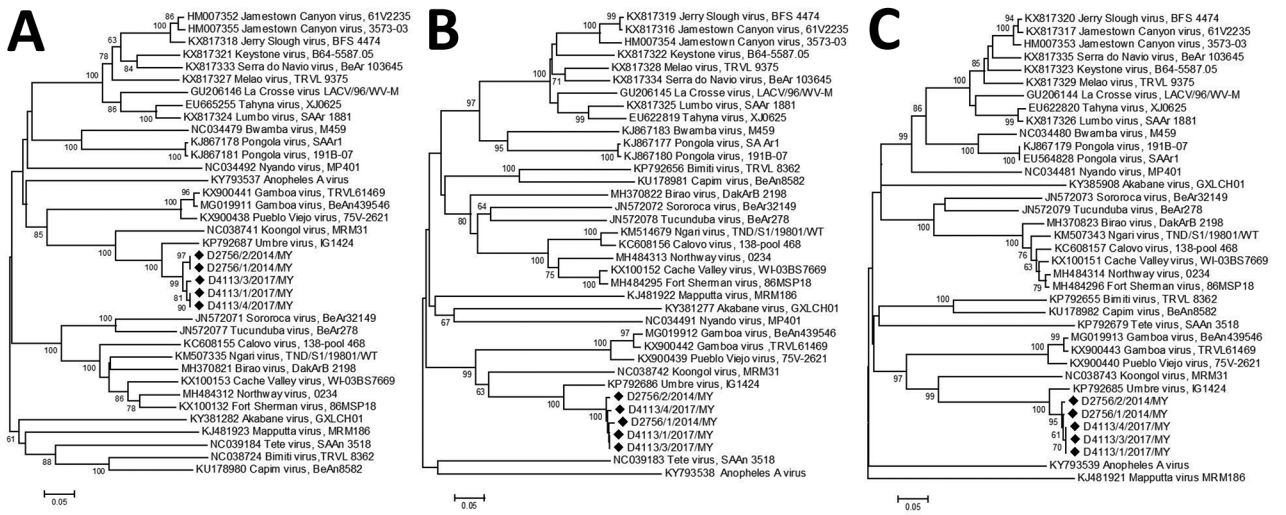

Figure 4. Phylogenetic trees of novel orthobunyavirus (Kedah fatal kidney syndrome virus) identified as the cause of severe kidney disease, Malaysia, 2014–2017 (black diamonds) and reference orthobunyaviruses. A) Large geneome segment–derived tree; B) medium geneome segment–derived tree; C) small geneome segment–derived tree. Scale bars indicate nucleotide substitutions per site.

lymphocyte necrosis in the lymphoid organs (spleen, bursa Fabricii, and thymus) (Figure 7, panels C and D).

Histopathologic changes were nearly completely missing in the birds sampled at the end of the experiment. Only some focal interstitial nephritis, hepatitis, and myocarditis could be found in a few birds.

Viral RNA in Tissue Samples from Infected Chickens

High viral loads in the different organ samples of dead chickens were similar, irrespective of the route of infection and time of death (Table). These results suggest that the virus could cause a high level of viremia and could replicate at a significant level in different organs (different cell types). The virus-specific nucleic acid was still present in the spleen of healthy chickens at the end of the observation period, but no viral RNA could be detected in kidney, cecal tonsil, and bursa tissues from these chickens.

Discussion

We found the causative agent of the disease outbreak of severe kidney damage among broiler chickens in Malaysia in 2014 to be a newly emerging orthobunyavirus. On the basis of the main pathologic features of the disease seen in the field and after experimental infection, we propose that the virus be designated Kedah fatal kidney syndrome virus (KFKSV) of broilers.

Analysis of the near full-genome sequence of 2 isolates, D2756/1/2014/MY and D2756/2/2014/MY, demonstrated that the virus is similar to Umbre virus, which belongs to the Turlock serogroup of the *Orthobunyavirus* genus (*19*). This serogroup is represented by 2 species and several virus isolates detected in Africa, Asia, Europe, and the Americas (*20*). So far, little information has been collected about the pathogenic potential of viruses belonging to the Turlock serogroup. Antibody response and transient viremia have been observed in chickens experimentally infected with Turlock virus (*21*).

Umbre virus was isolated during the 1950s from *Culex* mosquitoes and birds (*22*,*23*) from India and Malaysia, and antibodies have been measured in serum of wild birds and sentinel chickens from Malaysia (*24*). Although D2756/1/2014/MY, which we isolated, is genetically related to Umbre virus, we propose the name Kedah fatal kidney syndrome virus of broilers on the basis of its unique pathologic characteristics in meat-type chickens.

Several viruses within the *Orthobunyavirus* genus are of major veterinary and public health concern (*5*). Because KFKSV is a newly emerging virus, no experimental data are available regarding its pathogenicity and

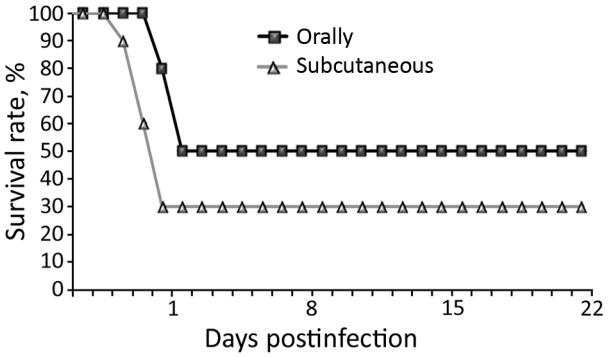

Figure 5. Daily survival rates among chickens experimentally infected with a novel orthobunyavirus (Kedah fatal kidney syndrome virus), isolated from broiler chickens with severe kidney disease, Malaysia, 2014–2017.

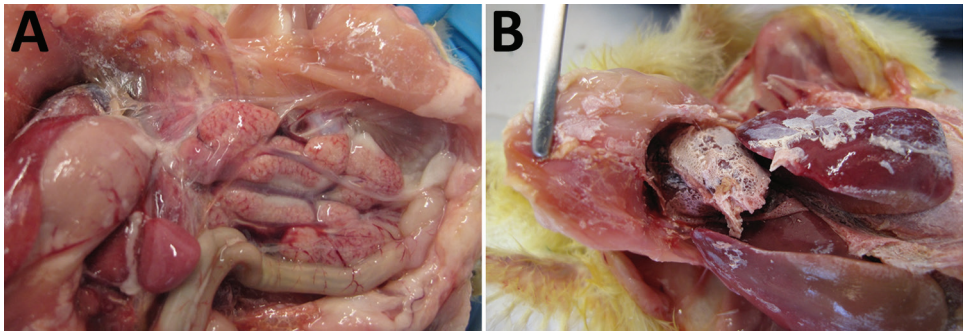

Figure 6. Gross pathologic appearance of chickens experimentally infected with a novel orthobunyavirus (Kedah fatal kidney syndrome virus) isolated from chickens with severe kidney disease, Malaysia, 2014–2017. A) Swollen and pale kidney; B) uric acid crystals on viscera (gout).

transmissibility. Disease in chickens could be reproduced by oral infection even though most orthobunyaviruses are vectorborne and the field cases in Malaysia occurred during mosquito season. Our results show that, after oral infection, high levels of virus could be detected in internal organs (including intestines) of infected chickens, which suggests that direct bird-to-bird transmission may contribute to the spread of this virus within an infected flock. The disease characteristics (e.g., sudden outbreaks, fast spread, and high morbidity rates) further support the existence of direct bird-to-bird transmission within a flock; however, the role of arthropods in introducing infection into a flock cannot be ruled out because of the seasonal occurrence of the disease. The fast spread of the disease in a flock and our experimental infection results, which proved that infection by the oral route is efficient, strongly suggest that mosquitoes may not be the exclusive vehicle for transmission of this virus within a flock.

The D2756/1/2014/MY isolate of KFKSV was highly pathogenic in young broiler chickens, causing mortality rates of 50%–70% and severe gross and histopathologic lesions in the kidneys and liver after experimental infection. The gross and histopathologic changes caused by the isolate were similar to those found in field-infected chickens. The virus could be detected from all tested internal organs of dead chickens, including intestines, but the spleen samples collected from asymptomatic chickens after recovery were also positive for KFKSV 3 weeks after infection. Therefore, investigation of virus persistence and transmission is needed.

There are no commercially available or standardized tests for diagnosing bunyavirus infections in poultry. Establishing

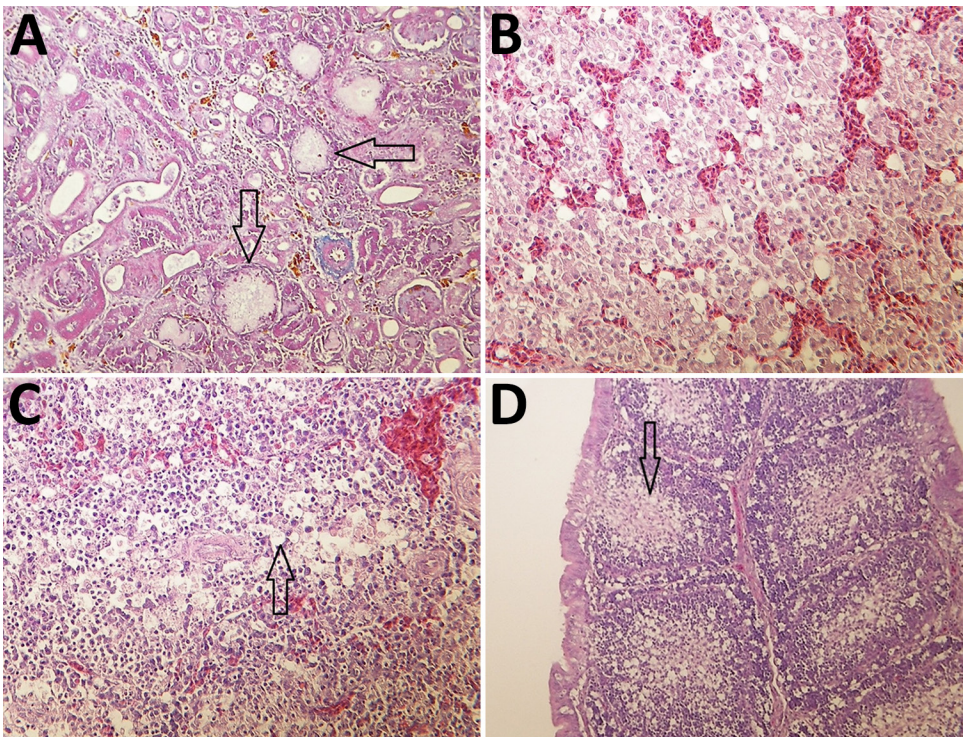

Figure 7. Histologic appearance of lesions in tissues from chickens experimentally infected with a novel orthobunyavirus (Kedah fatal kidney syndrome virus) isolated from broiler chickens with severe kidney disease, Malaysia, 2014–2017. A) Kidney, showing urate deposits in the dilated Bowman's capsule (arrows) and degeneration and dilatation of proximal convoluted tubules. Trichrome stain; original magnification ×200. B) Liver, showing vacuolar degeneration of hepatocytes and disorganization of lobular structure. Hematoxylin and eosin (H&E) stain; original magnification ×400. C) Spleen, showing marked lymphoid depletion and lymphocyte necrosis in the Malpighian body and vacuolation of reticulocytes in the red pulp (arrow). H&E stain; original magnification ×400. D) Bursa Fabricii, showing atrophy of bursal follicles with marked lymphoid depletion in the medullary region (arrow). H&E stain; original magnification ×200.

Table. Viral load in organs of chickens inoculated with orthobunyavirus isolated from broiler chickens with severe kidney disease, Malaysia, 2014*

Inoculation type and date of death, dpi	Viral load, log_{10} $TCID_{50}$/g					
	Spleen	Kidney	Heart	Liver	Cecal tonsil/intestine	Bursa
Subcutaneous						
4	5.8	5.1	NS	NS	NS	NS
5	4.7	5.9	NS	NS	NS	NS
5	4.1	5.7	NS	NS	NS	NS
5	5.3	5.4	NS	NS	NS	NS
6	5.1	5.4	NS	NS	NS	NS
Oral						
5	5.6	6.5	NS	NS	NS	NS
5	5.9	5.8	5.7	4.3	6.3	4.7
6	5.6	6.2	NS	NS	NS	NS
6	5.4	6.8	5.5	4.2	5.6	4.4
26	4.2	Neg	NS	NS	Neg	Neg
26	4.7	Neg	NS	NS	Neg	Neg
26	4.4	Neg	NS	NS	Neg	Neg

*dpi, days postinfection; neg, negative; NS, not sampled; $TCID_{50}$, 50% tissue culture infective dose.

a diagnosis requires submitting samples to specialized reference laboratories. KFKSV can be isolated and grown in chicken embryos and can be propagated in LMH and Vero cells. When reported disease and clinical history of a flock includes kidney lesions, diagnostic laboratories can use the molecular diagnostic method we describe in this article to check submitted materials for this newly discovered emerging species of orthobunyavirus. Similar kidney lesions could be observed after infection with avian infectious bronchitis virus, astrovirus, and leucocytozoonosis. Diagnosis of these infections is generally based on detection by RT-PCR and sequencing, virus isolation, and demonstration of an immune response by virus neutralization or enzyme immunoassay.

For determining a possible viral origin of an idiopathic disease, the viral metagenomics technique is useful, as is demonstrated by our investigation of this novel orthobunyavirus. The potential of this virus to spread to other animal species or humans cannot be excluded. Therefore, studies in which additional data are collected to elucidate the pathogenic potential of this virus in avian and other animal species should be initiated. Studies to scrutinize its potential as a public health hazard should also be considered. Because of the zoonotic nature of some orthobunyaviruses closely related to KFKSV (*5*,*25*–*27*), we highlight the need for wider surveillance of KFKSV in birds and mammals of other species in a more extended geographic area. Research in the surveillance of putative disease vectors and the possible prevalence of this virus in livestock and wildlife should be encouraged. The molecular diagnostic assay that we developed could help these research and disease surveillance efforts in the affected area, although the extent of its applicability against a broader diversity of orthobunyaviruses needs to be validated.

Acknowledgments

We are grateful to Edit Fodor for her technical assistance and to Ping Yin Kuan for her diligence and commitment to collecting samples and outbreak history.

Members of the research group at the Institute for Veterinary Medical Research (Hungarian Academy of Sciences) were supported by the Momentum Program (LP2011-10) and the Hungarian Scientific Research Fund (NKFI-OTKA, K120201).

About the Author

Dr. Palya is head of the Scientific Support and Investigation Unit at Ceva-Phylaxia, Budapest, Hungary. His research is focused on diagnosis, pathogenesis, epidemiology, and characterization of viruses that affect poultry.

References

1. Pello SJ, Olsen GH. Emerging and reemerging diseases of avian wildlife. Vet Clin North Am Exot Anim Pract. 2013;16:357–81. http://dx.doi.org/10.1016/j.cvex.2013.02.001
2. Chan JF-W, To KK-W, Chen H, Yuen K-Y. Cross-species transmission and emergence of novel viruses from birds. Curr Opin Virol. 2015;10:63–9. http://dx.doi.org/10.1016/j.coviro.2015.01.006
3. Liu P, Lu H, Li S, Wu Y, Gao GF, Su J. Duck egg drop syndrome virus: an emerging Tembusu-related flavivirus in China. Sci China Life Sci. 2013;56:701–10. http://dx.doi.org/10.1007/s11427-013-4515-z
4 Cadar D, Lühken R, van der Jeugd H, Garigliany M, Ziegler U, Keller M, et al. Widespread activity of multiple lineages of Usutu virus, western Europe, 2016. Euro Surveill. 2017;22:30452. http://dx.doi.org/10.2807/1560-7917.ES.2017.22.4.30452
5. Hubálek Z, Rudolf I, Nowotny N. Arboviruses pathogenic for domestic and wild animals. Adv Virus Res. 2014;89:201–75. http://dx.doi.org/10.1016/B978-0-12-800172-1.00005-7
6. Horne KM, Vanlandingham DL. Bunyavirus-vector interactions. Viruses. 2014;6:4373–97. http://dx.doi.org/10.3390/v6114373
7. Elliott RM. Bunyaviridae. In: Knipe DM, Howley PM, editors. Fields virology, 6th ed, vol. 1. Philadelphia: Wolters Kluwer Health; 2013. p. 1244–82.
8. International Committee on Taxonomy of Viruses. Master species list 2017 v1.0 [cited 2018 Mar 12]. https://talk.ictvonline.org/files/master-species-lists
9. Wilson WC, Gaudreault NN, Hossain MM, McVey DS. Lesser-known bunyavirus infections. Rev Sci Tech. 2015;34:419–29. http://dx.doi.org/10.20506/rst.34.2.2368

10. Whitmer SLM, Yadav PD, Sarkale P, Chaubal GY, Francis A, Klena J, et al. Characterization of unknown orthobunya-like viruses from India. Viruses. 2018;10:E451. http://dx.doi.org/10.3390/v10090451
11. Al'kovskhovskiĭ SV, Shchetinin AM, L'vov DK, Shchelkanov MI, Deriabin PG, L'vov DN, et al. [The Khurdun virus (KHURV): a new representative of the orthobunyavirus (Bunyaviridae)] [in Russian.]. Vopr Virusol. 2013;58:10–3.
12. Djikeng A, Halpin R, Kuzmickas R, Depasse J, Feldblyum J, Sengamalay N, et al. Viral genome sequencing by random priming methods. BMC Genomics. 2008;9:5. http://dx.doi.org/10.1186/1471-2164-9-5
13. Bányai K, Kemenesi G, Budinski I, Földes F, Zana B, Marton S, et al. Candidate new rotavirus species in Schreiber's bats, Serbia. Infect Genet Evol. 2017;48:19–26. http://dx.doi.org/10.1016/j.meegid.2016.12.002
14. Hall TA. BioEdit: a user-friendly biological sequence alignment editor and analysis program for windows 95/98/NT [cited 2018 Oct 4]. http://jwbrown.mbio.ncsu.edu/JWB/papers/1999Hall1.pdf.
15. Nicholas KB, Nicholas HB Jr, Deerfield DWII. GeneDoc: analysis and visualization of genetic variation. Embnew News. 1997;4:14.
16. Altschul SF, Gish W, Miller W, Myers EW, Lipman DJ. Basic local alignment search tool. J Mol Biol. 1990;215:403–10. http://dx.doi.org/10.1016/S0022-2836(05)80360-2
17. Abascal F, Zardoya R, Telford MJ. TranslatorX: multiple alignment of nucleotide sequences guided by amino acid translations. Nucleic Acids Res. 2010;38(suppl_2):W7–13. http://dx.doi.org/10.1093/nar/gkq291
18. Tamura K, Stecher G, Peterson D, Filipski A, Kumar S. MEGA6: molecular evolutionary genetics analysis version 6.0. Mol Biol Evol. 2013;30:2725–9. http://dx.doi.org/10.1093/molbev/mst197
19. Calisher CH, Lazuick JS, Wolff KL, Muth DJ. Antigenic relationships among Turlock serogroup Bunyaviruses as determined by neutralization tests. Acta Virol. 1984;28:148–51.
20. Shchetinin AM, Lvov DK, Deriabin PG, Botikov AG, Gitelman AK, Kuhn JH, et al. Genetic and phylogenetic characterization of Tataguine and Witwatersrand viruses and other orthobunyaviruses of the Anopheles A, Capim, Guamá, Koongol, Mapputta, Tete, and Turlock Serogroups. Viruses. 2015;7:5987–6008. http://dx.doi.org/10.3390/v7112918
21. Scott TW, McLean RG, Francy DB, Mitchell CJ, Card CS. Experimental infections of birds with Turlock virus. J Wildl Dis. 1983;19:82–5. http://dx.doi.org/10.7589/0090-3558-19.2.82
22. Yadav PD, Mishra AC, Mourya DT. Molecular characterization of Umbre virus (*Bunyaviridae*). Virol J. 2008;5:115. http://dx.doi.org/10.1186/1743-422X-5-115
23. Dandawate CN, Rajagopalan PK, Pavri KM, Work TH. Virus isolations from mosquitoes collected in North Arcot district, Madras state, and Chittoor district, Andhra Pradesh between November 1955 and October 1957. Indian J Med Res. 1969; 57:1420–6.
24. Wallace HG, Rudnick A, Rajagopal V. Activity of Tembusu and Umbre viruses in a Malaysian community: mosquito studies. Mosquito News 1977;37: 35–42.
25. Sakkas H, Bozidis P, Franks A, Papadopoulou C. Oropouche fever: a review. Viruses. 2018;10:E175. http://dx.doi.org/10.3390/v10040175
26. Noronha LE, Wilson WC. Comparison of two zoonotic viruses from the order Bunyavirales. Curr Opin Virol. 2017;27:36–41. http://dx.doi.org/10.1016/j.coviro.2017.10.007
27. Lundström JO. Mosquito-borne viruses in western Europe: a review. J Vector Ecol. 1999;24:1–39.

Address for correspondence: Vilmos Palya, Ceva-Phylaxia Veterinary Biologicals Co. Ltd., Scientific Support and Investigation Unit,Szállás u. 5, Budapest 1107, Hungary; email: vilmos.palya@ceva.com

WORLD HEALTH DAYS

Visit the World Health Days section on our website for the latest articles and information on emerging infectious diseases in our global community.

http://wwwnc.cdc.gov/eid/page/world-health-days

Joint Estimation of Relative Risk for Dengue and Zika Infections, Colombia, 2015–2016

Daniel Adyro Martínez-Bello,[1] Antonio López-Quílez, Alexander Torres Prieto

We jointly estimated relative risk for dengue and Zika virus disease (Zika) in Colombia, establishing the spatial association between them at the department and city levels for October 2015–December 2016. Cases of dengue and Zika were allocated to the 87 municipalities of 1 department and the 293 census sections of 1 city in Colombia. We fitted 8 hierarchical Bayesian Poisson joint models of relative risk for dengue and Zika, including area- and disease-specific random effects accounting for several spatial patterns of disease risk (clustered or uncorrelated heterogeneity) within and between both diseases. Most of the dengue and Zika high-risk municipalities varied in their risk distribution; those for Zika were in the northern part of the department and dengue in the southern to northeastern parts. At city level, spatially clustered patterns of dengue high-risk census sections indicated Zika high-risk areas. This information can be used to inform public health decision making.

Dengue and Zika virus disease (hereafter referred to as Zika) are infectious diseases caused by arboviruses in the family *Flaviviridae*. Dengue virus has 4 serotypes (1–4); serotypes 2 and 3 are associated with severe disease in persons with second dengue infections. Zika virus infection is associated with congenital malformations in babies born from women infected during pregnancy and with Guillain-Barré syndrome in infected adults (*1*).

Colombia is highly affected by vectorborne diseases. Villar et al. (*2*) reviewed the dengue epidemic in this country for 2000–2010 and reported an increasing epidemic trend for the period; outbreaks occurred in 2001, 2003, and 2010. In 2016, health authorities in Colombia reported >101,016 dengue cases that resulted in 289 deaths (*3*) and 9,799 Zika cases that were laboratory confirmed and 96,860 suspected Zika cases diagnosed by clinical signs (*4*).

For this study, we concentrated on the spatial patterns assessment of risk for dengue and Zika; in particular, we focused on the relative risk (RR) estimation for areal data by using hierarchical Bayesian models for these infections. RR represents the excess (or lack) of risk in a small area compared with the background risk. RR is mostly based on models and supported by Bayesian estimation methods (5). We used the following as study regions: the municipalities in the department of Santander, Colombia (1 of the departments where incidence of dengue and Zika for 2015–2016 was highest), and the city census sections belonging to the capital city of Santander (1 of the cities most affected by dengue and Zika for the same period).

Racloz et al. (*6*) and Louis et al. (*7*) reviewed the spatial patterns assessment of dengue risk; specifically for RR estimation of dengue, Ferreira and Schmidt (*8*) and Martínez-Bello et al. (*9*) estimated RR for dengue on a local spatial scale; and Restrepo et al. (*10*) and Martínez-Bello et al. (*11*) applied methods for the spatiotemporal assessment of dengue risk. Examples for the spatial patterns assessment of Zika risk run from merely descriptive methods to model-based approaches. For instance, in Colombia, descriptive risk maps associating Zika incidence rates with environmental and sociodemographic factors have been produced in the departments of Sucre (*12*), Tolima (*13*), Guajira (*14*), Santander, and Norte de Santander (*15*) and in the city of Pereira in the department of Risaralda (*16*). Model-based spatial patterns assessment of Zika risk have been developed for the 33 departments in Colombia by using Poisson models for the RR for Zika (*17*). The distribution of risk for Zika transmission among counties/districts in Guangdong Province, China, was assessed by using analytic hierarchy process models (*18*).

Zika, dengue, and chikungunya are also jointly studied by using the spatial patterns assessment of risk because the viruses share similar transmission routes (*Aedes* mosquitoes). On a large scale in Brazil, ecological studies have explored the risk factors for unusual spatial patterns of microcephaly, including dengue, Zika, and chikungunya data (*19*). Also estimated is the potential spatial risk for Zika and chikungunya according to socioenvironmental factors,

Author affiliations: University of Valencia, Valencia, Spain (D.A. Martínez-Bello, A. López-Quílez); Secretary of Health of the Department of Santander, Bucaramanga, Colombia (A. Torres Prieto)

DOI: https://doi.org/10.3201/eid2506.180392

[1]Current affiliation: Health and Environment Secretary, Bucaramanga, Colombia.

estimating the size of the populations at risk for both diseases (*20*). On a small geographic scale, the risk factors for cocirculating arboviruses (dengue, Zika, chikungunya) at the community level have been evaluated (*21*).

In Colombia, Krystosik et al. (*22*) generated city-level risk maps of chikungunya, Zika, and dengue supporting vector-control strategies; Martínez-Bello et al. (*23*) estimated the RR for dengue and Zika by using spatiotemporal interaction effects models for 1 department and 1 city in Colombia. Riou et al. (*24*) assessed the spatial patterns of risk for the 2013 Zika and chikungunya outbreaks in the French Polynesia islands, and Funk et al. (*25*) jointly modeled Zika and dengue time series data from the Zika outbreak in Yap Island in the Pacific Ocean.

Our aim with this study was to jointly estimate the disease- and area-specific RRs for dengue and Zika by using hierarchical Bayesian joint models accounting for the spatial association between both diseases. We used data from the 2015–2016 Zika outbreak in Colombia and analyzed 2 levels of spatial data aggregation: the department level (disease counts aggregated per municipality) in the department of Santander and the city level (disease counts aggregated per census section) in the city of Bucaramanga (Santander).

Materials and Methods

Colombia (Figure 1, panel A), population 48.7 million, comprises ≈1.14 million km^2 divided into 33 administrative regions called departments, each 49.6–110,029.4 km^2 (Table 1). The department of Santander (Figure 1, panel B) covers 30,642 km^2, is divided into 87 municipalities, and has >2 million inhabitants. Santander is in the northeastern region of Colombia, and its administrative center, Bucaramanga (Figure 1, panel C), is in the northeastern region of the department. Bucaramanga covers 162 km^2 (urban area 49.6 km^2), is divided into 293 urban census sections, and according to the 2016 census has a population of 528,575.

The Zika epidemic started on August 9, 2015 (*26*). Up to the first epidemiologic week of 2017, Colombia reported 106,659 Zika cases (219 cases/100,000 population) that were suspected by clinical signs and confirmed by laboratory. For the epidemiologic year 2016, the country reported 101,016 dengue cases (207.6 cases/100,000 population; Table 2). Since 2001, one of the departments with the highest dengue incidence in Colombia has been Santander (*2*); in 2016, its dengue incidence was the sixth highest among the 33 departments (331.63 cases/100,000 population) (*3*); in 2015–2016, its Zika incidence was the seventh highest (493.09 cases/100,000 population) (*4*). The incidence rate for Zika in Santander was higher than the national average, accounting for 9.76% of the total cases in Colombia (*3*). With regard to dengue, in 2016 Santander reported 6.67% of the total cases for Colombia (Table 2). Within the department, 35.52% of Zika cases (692.81/100,000) and 35.62% of dengue cases (467.3/100,000) were reported in Bucaramanga (Table 2).

Department-Level Data

We aggregated cases of dengue and Zika for the study period (from epidemiologic week 42 in 2015 through epidemiologic week 52 in 2016) obtained from SIVIGILA (the public health surveillance system of Colombia) in the 87 municipalities of Santander by using cartography from the National Geostatistical Framework (*27*). The case definitions for dengue and Zika correspond to codes 210 (dengue), 220 (severe dengue), 580 (dengue mortality), and 895 (Zika), obtained from the SIVIGILA protocols

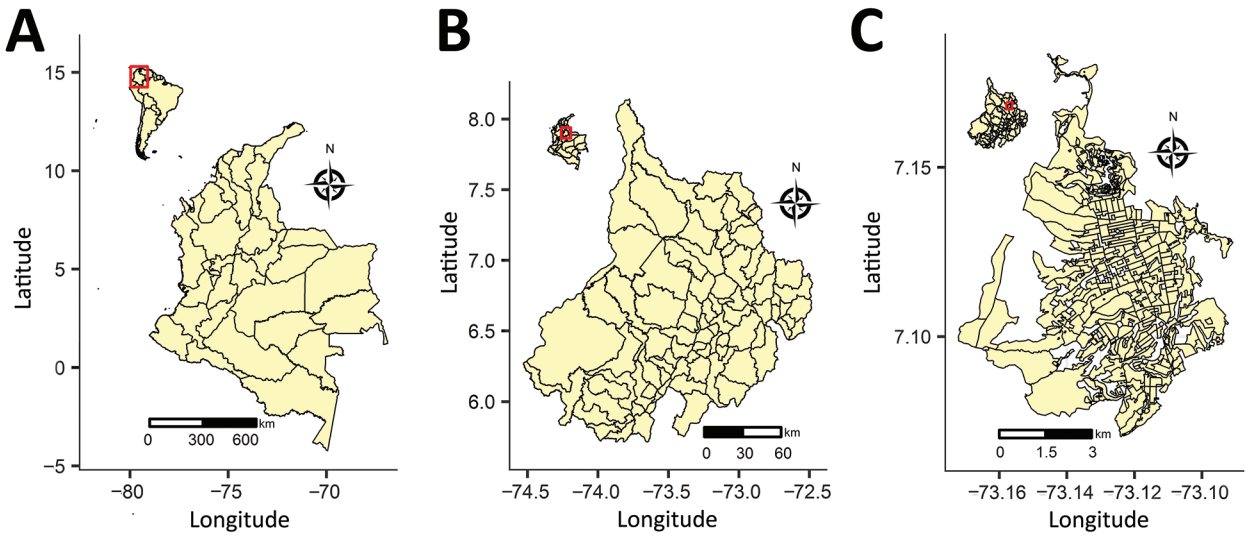

Figure 1. Location of the areas included in joint estimation of relative risk for dengue and Zika virus infections, Colombia, 2015–2016. A) Country of Colombia; inset shows location of Colombia in South America. B) Department of Santander; inset shows location of Santander in Colombia. C) City of Bucaramanga; inset shows location of Bucaramanga in Santander.

Table 1. Geographic divisions at national, department, and city levels, Colombia

Level	Division	Area, km^2			
		Minimum	Mean	Maximum	Total
Colombia	33 departments	49.6	34,678.30	110,029.40	1,144,385
Santander	87 municipalities	18.8	352.20	3173.80	30,642
Bucaramanga	293 census sections	0.01	0.17	2.64	49.6

for dengue (*28*) and Zika (*29*). We calculated expected values of dengue and Zika by municipality by using 2016 population projections provided by the Colombia Administrative Department of National Statistics. We first calculated incidence rates for dengue and Zika for 5-year patient age groups and for sex on the basis of observed cases recorded during the study period. We then multiplied these age- and sex-specific incidence rates to the population structure of each municipality, generating disease-specific expected values for both diseases. Last, we aggregated the age- and sex-specific expected values per municipality of dengue and Zika to obtain standardized expected counts per municipality for dengue and Zika.

City-Level Data

Cases of dengue and Zika, notified in Bucaramanga and obtained from SIVIGILA for the study period, were geocoded and allocated to 293 census sections in the city (*27*). A census section is a cartographic unit comprising 1–9 census blocks, consisting of built or unbuilt lots bounded by public roads or pedestrian walkways (*27*). We calculated expected values of dengue and Zika by census sections by using a similar method to the one applied at the department level. Using the 2016 population projections provided by the Colombia statistical office, we calculated incidence rates for dengue and Zika by 5-year patient age groups and sex for the study period. Next, we multiplied the incidence rates for the population structure (by sex and age group) of each census section obtained from the Colombia Census and aggregated the age- and sex-specific expected counts per census section to obtain the standardized expected values of dengue and Zika per census section.

Joint Models for Estimating Relative Risk

We assumed that the observed counts of dengue or Zika aggregated by area (87 municipalities at the department level or 293 census sections at the city level) follow a Poisson distribution, with mean parameter equal to the product of the disease- and area-specific expected values and RR. The logarithm of the RR is the additive result of disease- and area-specific random effects accounting for the uncorrelated and clustered spatial patterns of risk and possibly covariates (*30*). Random effects for spatially clustered patterns of risk are unobserved variables recovering risk autocorrelation between adjacent areas, indicating that risk in one area is highly associated with risk in neighboring areas. The lack of spatial risk autocorrelation is accounted for by spatial uncorrelated random effects (*5,31*).

A joint model of RR for dengue and Zika defines a structure for the nature of the spatial association between the diseases (*5*). To that end, we fitted 8 Bayesian Poisson models (*5,31*) of joint estimation of RR to the dengue and Zika data at the department and city levels. Formulation of the statistical model is available in the Appendix (https://wwwnc.cdc.gov/EID/article/25/6/18-0392-App1.pdf). Here we describe the spatial patterns of risk for every joint model.

Model 1 contains area- and disease-specific random effects capturing uncorrelated spatial patterns of dengue and Zika risk. Choosing this model implies that dengue and Zika high-risk areas are not associated with each other and show no clustering (Figure 2, panel A).

Model 2 incorporates area- and disease-specific random effects capturing uncorrelated spatial patterns of dengue and Zika risk, where the random effects of both diseases are spatially associated. Model 2 assumes that the

Table 2. Zika and dengue suspected and confirmed cases reported in Colombia, department of Santander, and city of Bucaramanga, 2015–2016

Disease, level	Suspected*	Confirmed†	Total‡	Incidence rate§	Population × 1,000
Zika					
Colombia¶	96,860	9,799	106,659	219.0	48,654
Santander#	9,420	547	9,967	493.1	2,090
Bucaramanga**	No data	No data	3,662	692.8	529
Dengue					
Colombia††	100,117	899	101,016	207.6	48,654
Santander††	No data	No data	6934	331.6	2,090
Bucaramanga**	No data	No data	2470	467.3	529

*Based on clinical signs.
†Laboratory confirmed.
‡Suspected cases with laboratory confirmation.
§(Total no. cases/population × 1,000) × 100,000.
¶August 9, 2015–January 5, 2017 (*3*).
#Epidemiologic week 45 of 2015 to epidemiologic week 52 of 2016 (*3*).
**Epidemiologic week 45 of 2015 to epidemiologic week 52 of 2016 (this study).
††Epidemiologic weeks 1–52, 2016 (*2*).

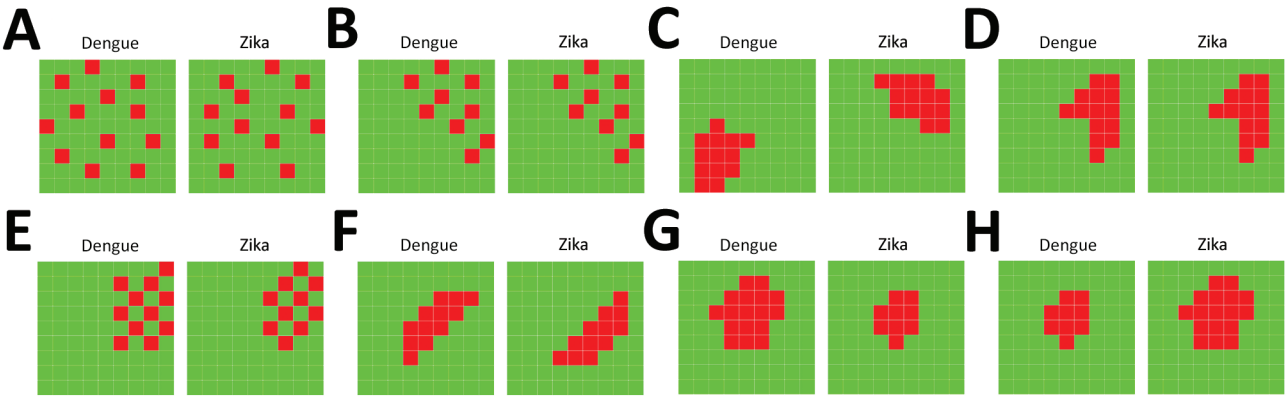

Figure 2. Schematic representation of the spatial patterns of dengue and Zika risk revealed by the joint models of relative risk models, Colombia, 2015–2016. A) Model 1; B) model 2; C) model 3; D) model 4; E) model 5; F) model 6; G) model 7; H) model 8. For a set of small areas, high-risk areas are represented in red and low-risk areas are represented in green, depicting several patterns that could or could not be shared for both diseases in the same geographic area.

random effects for uncorrelated spatial patterns are linearly associated for both diseases; thus, dengue and Zika high-risk areas occur at the same position (Figure 2, panel B).

Model 3 contains area- and disease-specific random effects representing spatially clustered patterns of dengue and Zika risk, where the random effects are not associated between diseases. In this model, dengue high-risk areas are clustered and Zika high-risk areas are clustered, but dengue and Zika high-risk clustered areas are not spatially associated (Figure 2, panel C).

Model 4 contains area- and disease-specific random effects revealing spatially clustered patterns of dengue and Zika risk, where the random effects are linearly associated between diseases. In this model, dengue and Zika high-risk areas are spatially associated; thus, there are spatially clustered patterns of dengue and Zika high-risk areas at the same spatial locations (Figure 2, panel D).

Model 5 incorporates area- and disease-specific random effects revealing uncorrelated spatial patterns of dengue and Zika risk, and the spatial association between both diseases is modeled by using shared components of clustered spatial patterns of dengue and Zika risk. In this model, dengue high-risk areas are next to Zika high-risk areas, but dengue high-risk areas are not clustered and Zika high-risk areas are not clustered (Figure 2, panel E).

Model 6 incorporates area- and disease-specific random effects revealing spatially clustered patterns of dengue and Zika high risk, and the spatial association between both diseases is accounted for by using shared random effects of spatially clustered patterns of dengue and Zika high risk. In this model, spatially clustered patterns of dengue high-risk areas are adjacent to spatially clustered patterns of Zika high-risk areas (Figure 2, panel F).

Model 7 contains area- and disease-specific random effects accounting for spatially clustered patterns of Zika high risk conditioned on random effects for spatially clustered patterns of dengue high risk. Thus, dengue high-risk areas are determinants of the presence of Zika high-risk areas (Figure 2, panel G).

Model 8 contains area- and disease-specific random effects accounting for spatially clustered patterns of dengue high risk conditioned on random effects for spatially clustered patterns of Zika high risk. Thus, Zika high-risk areas are determinants of the presence of dengue high-risk areas (Figure 2, panel H).

We summarized the association structure of the joint models of RR (Table 3); every model captures the nature of the spatial association between dengue and Zika risk. We fitted the Bayesian Poisson models by applying Markov chain Monte Carlo simulations and using WinBUGS 1.4 software

Table 3. Association structure assumed by relative risk models fitted to department-and city-level dengue and Zika data for the 2015–2016 Zika virus disease outbreak, Colombia

Model no.	Spatially structured association between dengue and Zika high-risk areas	Joint association between dengue and Zika high-risk areas
1	No	No
2	No	Yes, linear
3	Yes	No
4	Yes	Yes, linear
5	No	Spatially structured shared component
6	Yes	Spatially structured shared component
7	Yes	Zika risk conditioned by dengue risk
8	Yes	Dengue risk conditioned by Zika risk

(*32*) for Bayesian analysis. We selected noninformative prior distributions for the parameters and hyperparameters; model specifications are presented in the Appendix. Every model was fitted by using 100,000 burn-in iterations, 10,000 iterations for inferences, a thinning of 10, three chains, and 1,000 iterations per chain for final inferences. For model selection, we used the deviance information criterion (DIC) (*33*), for which the lowest DIC estimates the model with the best predictions subject to the DIC difference between the model with minimum DIC and the next model being >5, as substantial evidence in favor of the first model with respect to the second (*34*).

Results

For the Santander department, the analysis included 10,051 Zika patients (63.1% female, 36.9% male) and 7,891 dengue patients (48.6% female, 51.4% male). The analysis of Bucaramanga city included 3,662 Zika patients (61.2% female, 38.8% male) and 2,470 dengue patients (49.3% female, 50.7% male). Figure 3 (https://wwwnc.cdc.gov/EID/article/25/6/18-0392-F1.htm) shows the age- and sex-specific incidence rates for dengue and Zika in Santander (Figure 3, panel A) and Bucaramanga (Figure 3, panel B). At the department and city levels, reported Zika cases were consistently higher among female patients in the 10–14 and 55–59 year age groups, and reported dengue cases were highest among patients of both sexes in the 5–9 and 20–24 year age groups. The age- and sex-specific incidence rates were slightly higher at the city level than the department level.

We mapped the incidence rates (cases/100,000 population) and the standardized incidence ratios (observed values/expected values) for dengue and Zika (Figure 4). At the department level, the incidence rate for Zika was 0–3,688 cases/100,000 population; for dengue, 0–4,285 cases/100,000 population (Figure 4, panel A). At the department level, the incidence rate for dengue was highest in the southeastern municipalities; for Zika, in the northeastern municipalities. The standardized incidence ratios for dengue and Zika at the department level follow the findings of the incidence rate map; however, the standardized incidence ratio accounts for the expected number of cases, so some areas with a high observed incidence rate do not show a high standardized incidence ratio (Figure 4, panel

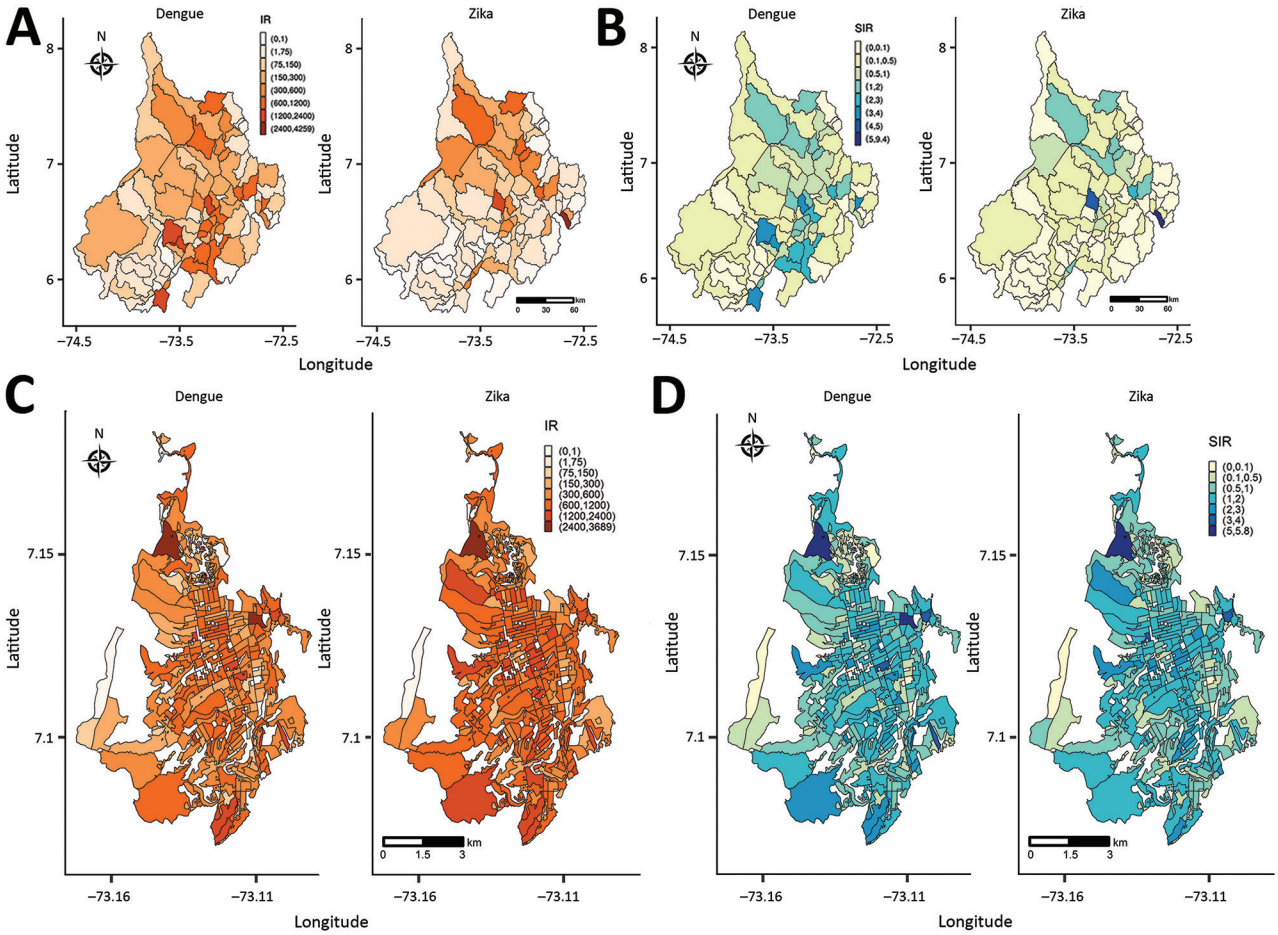

Figure 4. IRs and SIRs for dengue and Zika virus disease, Colombia, 2015–2016. A) Santander IR; B) Santander SIR; C) Bucaramanga IR; D) Bucaramanga SIR. IR, incidence rate; SIR, standardized incidence rate.

Table 4. Selection statistics from the joint models of relative risk for dengue and Zika, department of Santander, Colombia, 2015–2016*

				Δ-DIC						
Model no.	Deviance	Parameter	DIC	M2	M3	M4	M5	M6	M7	M8
1	810.9	144.6	955.5	1.3	359.9	321.6	12.6	330.7	5.5	4.1
2	814.2	140.0	954.2		361.2	322.9	11.3	332	4.2	2.8
3	991.4	324.0	1315.4			38.3	372.5	29.2	365.4	364
4	976.8	300.4	1277.1				334.2	9.1	327.1	325.7
5	808.3	134.6	942.9					343.3	7.1	8.5
6	987.3	299.0	1286.2						336.2	334.8
7	810.4	139.6	950.0							1.4
8	811.7	139.7	951.4							

*Blank cells indicate no data available. DIC, deviance information criterion; M, model; Δ-DIC, DIC difference.

B). We determined heterogeneous incidence rates for dengue and Zika at the city level (Figure 4, panel C); some high incidence rate census sections are in the northern and central areas of the city. We also determined the standardized incidence ratio per census section (Figure 4, panel D); as before, the standardized incidence ratio map shows the findings of the incidence rate, smoothing the geographic incidence estimates by census sections in Bucaramanga.

We compiled the results of the selection statistics for the joint models of RR at the department level (Table 4). Based on the lowest DIC, model 5 (disease-specific random effects for uncorrelated spatial patterns of risk and shared random effects of spatially clustered patterns for both diseases) is the selected model (deviance 808.3, DIC 942.9) for Santander; at the city level (Table 5), model 7 (Zika risk distribution conditioned by dengue risk) is the selected final model (deviance 2,869.7, DIC 3,119.3) for Bucaramanga. We included the DIC differences between models, showing that after the final selected model, models 7 and 8 were the closest models at the department level; models 8 and 4, at the city level (Tables 4, 5).

Figure 5 displays the posterior mean RR and the lower bound of the 95% credible interval (CrI) of RR >1 (95% CrI RR >1) of dengue and Zika obtained from the selected final models in Tables 4 and 5. In Santander, the posterior mean RR (Figure 5, panel A) shows the standardized incidence ratio pattern displayed in Figure 4, panel A; as a byproduct of the modeling process, Figure 5, panel B, shows the municipalities with 95% probability of RR higher than that for the other municipalities. Most of the dengue and Zika high-risk municipalities differ in risk distribution: Zika high-risk municipalities are in the northern part of the department, and dengue high-risk municipalities are in the southern to northeastern parts. For Bucaramanga, the dengue and Zika posterior mean RR maps revealed the nonclustered risk pattern of the diseases (Figure 5, panel C), also displayed by the standardized incidence ratio map in Figure 4, panel C. However, the model shrinks the posterior mean RR, capturing the close association between Zika and dengue high-risk distribution per census sections. We identified the census sections with 95% probability of RR being higher than in the other areas (Figure 5, panel D), showing dengue high-risk census sections associated with Zika high-risk census sections at the city level.

Discussion

Our study illustrates the joint estimation of RR for dengue and Zika at the department and city levels in Colombia. A battery of joint models of RR captured the spatial association between the diseases during the 2015–2016 Zika outbreak. The model selection process was based on DIC statistics; and we assessed the model's goodness-of-fit by using residual analysis, fitted-observed scatter plots, and the posterior predictive checks of overdispersion recovery (Appendix).

At the department level, the selected model 5 reveals spatially clustered patterns of high-risk municipalities for both diseases, while keeping disease- and area-specific uncorrelated spatial patterns of high-risk municipalities, precluding selection of other feasible but not optimal models, such as models 7 and 8, containing area- and disease-specific spatially clustered patterns of high risk. The selected

Table 5. Selection statistics from the joint models of relative risk for dengue and Zika, city of Bucaramanga, Colombia, 2015–2016*

				Δ-DIC						
Model no.	Deviance	Parameter	DIC	M2	M3	M4	M5	M6	M7	M8
1	2870.1	364.9	3232.1	99.8	22.3	101.3	97.9	100	112.8	102.9
2	2853.3	279.0	3132.3		122.1	1.5	1.9	0.2	13	3.1
3	2922.4	331.9	3254.4			123.6	120.2	122.3	135.1	125.2
4	2884.2	246.6	3130.8				3.4	1.3	11.5	1.6
5	2856.8	277.4	3134.2					2.1	14.9	5
6	2888.9	243.3	3132.1						12.8	2.9
7	2869.7	249.6	3119.3							9.9
8	2874.2	255.0	3129.2							

*Blank cells indicate no data available. DIC, deviance information criterion; M, model; Δ-DIC, DIC difference.

model shows that dengue- and Zika-specific high-risk municipalities are not clustered but that dengue high-risk municipalities are next to Zika high-risk municipalities.

At the city level, the selected model 7 contains conditional random effects for spatially clustered patterns of high-risk census sections, where Zika high-risk census sections are conditioned on dengue high-risk census sections; thus, Zika high-risk census sections are highly associated with dengue high-risk census sections. Models 8 and 4 were other feasible but not optimal options; although both models reveal the spatially clustered distribution of risk, the spatial data distributions do not support strong spatial association of dengue high-risk areas at the same locations as Zika high-risk areas. Model 7 shows that dengue or Zika high-risk areas are spatially clustered; dengue and Zika high-risk census sections are near other high-risk census sections. Thus, at the city level, clustered census sections display favorable conditions for transmission of both diseases, justifying a deeper study of environmental, infrastructural, and socioeconomic conditions associated with dengue and Zika high risk in those areas.

Model-based estimates of posterior means and lower bounds of CrIs of RR were represented in risk maps. These maps identified areas with a given risk probability and highlighted municipalities or census sections with high probable risk for dengue or Zika.

The area- and disease-specific risk estimates from the joint models accounting for the spatial association of both diseases (models 5 [department level] and model 7 [city level]) were more accurate than the estimates recovered ignoring the association of both diseases. It would be useful to compare risk estimates from joint models, with estimates ignoring the association structure of cocirculating arboviral diseases. For instance, Krystosik et al. (*22*) estimated the combined risk for dengue, Zika, and chikungunya but did not provide disease-specific risk estimates; Costa et al. (*35*) found associations in the spatial distribution of dengue, Zika, and chikungunya but did not use the information on the diseases' association to improve the accuracy of the risk estimates. The special characteristics of the joint modeling of cocirculating arboviruses provide an epidemiologic tool for transmission control and disease mitigation (*36*).

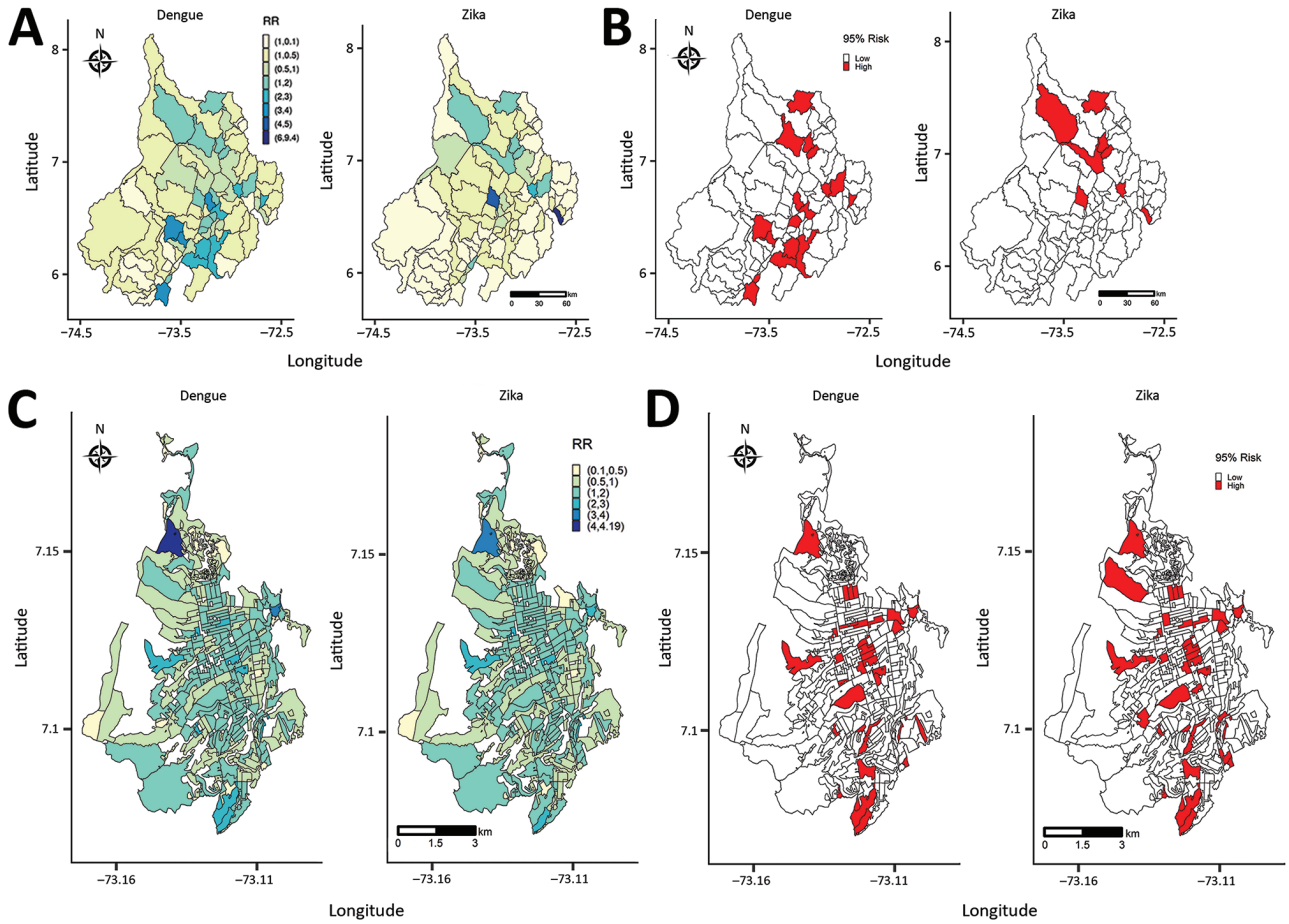

Figure 5. Posterior mean RR and 95% credible interval (CrI) of RR >1 (95% CrI RR >1), from model 5 for the department of Santander and from model 7 for the city of Bucaramanga, Colombia, 2015–2016. A) Posterior mean RR for Santander; B) 95% CrI RR >1 for Santander; C) posterior mean RR for Bucaramanga; D) 95% CrI RR >1 for Bucaramanga. RR, relative risk.

Our study has some limitations. Although notification of dengue and Zika is compulsory in Colombia, a large proportion of reported cases are diagnosed by clinical signs and not laboratory confirmed. Because we used suspected and confirmed dengue and Zika cases, some cases included in the study may have been misdiagnosed. Another potential source of study bias is underreporting, as shown by Romero-Vega et al. (*37*) for dengue in Colombia; the National Health Institute of Colombia calculated an underreporting rate of 49% for Zika in a high-incidence town in Colombia (*38*). However, we used the same data that the Colombia authorities use to generate public health information for making decisions about controlling and preventing activities of public and private health institutions, extending the current information produced by the public health surveillance system, supporting surveillance activities for Zika and dengue, providing information for monitoring the geographic distribution of both diseases, and characterizing spatially the disease distribution in the population (*39*).

Determinants of dengue and Zika risk as covariates within the joint models (e.g., using datasets such as the ecological and environmental spatial dataset developed by Siraj et al. [*40*] for Colombia) remain to be elucidated. Other joint models available in the spatial analysis literature should be tested, jointly modeling other arboviral diseases such as chikungunya together with dengue and Zika and including joint models of RR of dengue and Zika within real-time surveillance platforms (*41*).

In summary, our method for mapping cocirculating dengue and Zika provides a tool for describing disease distribution, based on the epidemiologic complexities of both diseases. Information on the association between diseases is of value, especially in areas where multiple arboviruses cocirculate, and can be used to improve inferences and interpretations and thus contribute to informed public health decision making.

A.L.-Q. was supported by the Ministerio de Economía y Competitividad (research grant MTM2016-77501-P, jointly financed with the European Regional Development Fund). D.A.M.-B. was supported by the Colombian Administrative Department of Science and Technology (grant 646-2014) for doctoral studies abroad.

About the Author

Mr. Martínez-Bello is a PhD student in statistics and optimization. His research interests are spatial analysis of arboviral diseases, health and economics geography, and Bayesian statistics.

References

1. Plourde AR, Bloch EM. A literature review of Zika virus. Emerg Infect Dis. 2016;22:1185–92. http://dx.doi.org/10.3201/eid2207.151990
2. Villar LA, Rojas DP, Besada-Lombana S, Sarti E. Epidemiological trends of dengue disease in Colombia (2000-2011): a systematic review. PLoS Negl Trop Dis. 2015;9:e0003499. http://dx.doi.org/10.1371/journal.pntd.0003499
3. National Health Institute. Event report: dengue, 2016 [in Spanish] [cited 2019 Apr 1]. http://www.ins.gov.co/buscador-http://www.ins.gov.co/buscador-eventos/Informesdeevento/Dengue%202016.pdf
4. National Health Institute of Colombia. Weekly epidemiological bulletin number 52 of 2016, 25 December–31 December [in Spanish] [cited 2019 Apr 1]. http://www.ins.gov.co/buscador-eventos/ BoletinEpidemiologico/2016%20Bolet%C3%ADn%20epidemiol%C3%B3gico%20semana%2052%20-.pdf
5. Banerjee S, Carlin BP, Gelfand AE. Hierarchical modeling and analysis for spatial data. In: Bunea F, Isham V, Keiding N, Louis T, Smith RL, Tong H, editors. Chapman & Hall/CRC Monographs on Statistics & Applied Probability. 2nd ed. Boca Raton (FL): Taylor & Francis Group; 2014. p. 305–24.
6. Racloz V, Ramsey R, Tong S, Hu W. Surveillance of dengue f ever virus: a review of epidemiological models and early warning systems. PLoS Negl Trop Dis. 2012;6:e1648. http://dx.doi.org/10.1371/journal.pntd.0001648
7. Louis VR, Phalkey R, Horstick O, Ratanawong P, Wilder-Smith A, Tozan Y, et al. Modeling tools for dengue risk mapping—a systematic review. Int J Health Geogr. 2014;13:50. http://dx.doi.org/10.1186/1476-072X-13-50
8. Ferreira GS, Schmidt AM. Spatial modelling of the relative risk of dengue fever in Rio de Janeiro for the epidemic period between 2001 and 2002. Braz J Probab Stat. 2006;20:29–47.
9. Martínez-Bello DA, López-Quílez A, Torres Prieto A. Relative risk estimation of dengue disease at small spatial scale. Int J Health Geogr. 2017;16:31. http://dx.doi.org/10.1186/s12942-017-0104-x
10. Restrepo AC, Baker P, Clements ACA. National spatial and temporal patterns of notified dengue cases, Colombia 2007-2010. Trop Med Int Health. 2014;19:863–71. http://dx.doi.org/10.1111/tmi.12325
11. Martínez-Bello D, López-Quílez A, Torres Prieto A. Spatiotemporal modeling of relative risk of dengue disease in Colombia. Stochastic Environ Res Risk Assess. 2018;32:1587–601. http://dx.doi.org/10.1007/s00477-017-1461-5
12. Rodriguez-Morales AJ, Patiño-Cadavid LJ, Lozada-Riascos CO, Villamil-Gómez WE. Mapping Zika in municipalities of one coastal department of Colombia (Sucre) using geographic information systems during the 2015–2016 outbreak: implications for public health and travel advice. Int J Infect Dis. 2016;48:70–2. http://dx.doi.org/10.1016/j.ijid.2016.05.012
13. Rodriguez-Morales AJ, Galindo-Marquez ML, García-Loaiza CJ, Sabogal-Roman JA, Marin-Loaiza S, Ayala AF, et al. Mapping Zika virus infection using geographical information systems in Tolima, Colombia, 2015–2016. F1000 Res. 2016;5:568. http://dx.doi.org/10.12688/f1000research.8436.1
14. Rodriguez-Morales AJ, García-Loaiza CJ, Galindo-Marquez ML, Sabogal-Roman JA, Marin-Loaiza S, Lozada-Riascos CO, et al. Zika infection GIS-based mapping suggest high transmission activity in the border area of La Guajira, Colombia, a northeastern coast Caribbean department, 2015-2016: implications for public health, migration and travel. Travel Med Infect Dis. 2016;14:286–8. http://dx.doi.org/10.1016/j.tmaid.2016.03.018
15. Rodriguez-Morales AJ, Haque U, Ball J, García-Loaiza CJ, Galindo-Marquez ML, Sabogal-Roman JA, et al. Spatial distribution of Zika virus infection in northeastern Colombia. Infez Med. 2017;25:241–6.
16. Rodriguez-Morales AJ, Ruiz P, Tabares J, Ossa CA, Yepes-Echeverry MC, Ramirez-Jaramillo V, et al. Mapping the ecoepidemiology of Zika virus infection in urban and rural areas of Pereira, Risaralda, Colombia, 2015-2016: implications for public health and travel medicine. Travel Med Infect Dis. 2017;18:57–66. http://dx.doi.org/10.1016/j.tmaid.2017.05.004
17. Chien L-C, Lin R-T, Liao Y, Sy FS, Pérez A. Surveillance on the endemic of Zika virus infection by meteorological factors in Colombia: a population-based spatial and temporal study. BMC Infect Dis. 2018;18:180. http://dx.doi.org/10.1186/s12879-018-3085-x

18. Li X, Liu T, Lin L, Song T, Du X, Lin H, et al. Application of the analytic hierarchy approach to the risk assessment of Zika transmission in Guangdong Province, China. BMC Infect Dis. 2017;17:65. http://dx.doi.org/10.1186/s12879-016-2170-2
19. Campos MC, Dombrowski JG, Phelan J, Marinho CRF, Hibberd M, Clark TG, et al. Zika might not be acting alone: using an ecological study approach to investigate potential co-acting risk factors for an unusual pattern of microcephaly in Brazil. PLoS One. 2018;13:e0201452. http://dx.doi.org/10.1371/journal.pone.0201452
20. Aguiar BS, Lorenz C, Virginio F, Suesdek L, Chiaravalloti-Neto F. Potential risks of Zika and chikungunya outbreaks in Brazil: a modeling study. Int J Infect Dis. 2018;70:20–9. http://dx.doi.org/10.1016/j.ijid.2018.02.007
21. Rodrigues NCP, Daumas RP, de Almeida AS, Dos Santos RS, Koster I, Rodrigues PP, et al. Risk factors for arbovirus infections in a low-income community of Rio de Janeiro, Brazil, 2015–2016. PLoS One. 2018;13:e0198357. http://dx.doi.org/10.1371/journal.pone.0198357
22. Krystosik AR, Curtis A, Buritica P, Ajayakumar J, Squires R, Dávalos D, et al. Community context and sub-neighborhood scale detail to explain dengue, chikungunya and Zika patterns in Cali, Colombia. PLoS One. 2017;12:e0181208. http://dx.doi.org/10.1371/journal.pone.0181208
23. Martínez-Bello DA, López-Quílez A, Torres Prieto A. Spatio-temporal modeling of Zika and dengue infections within Colombia. Int J Environ Res Public Health. 2018;15:1376. http://dx.doi.org/ 10.3390/ijerph15071376
24. Riou J, Poletto C, Boëlle PY. A comparative analysis of chikungunya and Zika transmission. Epidemics. 2017;19:43–52. http://dx.doi.org/10.1016/j.epidem.2017.01.001
25. Funk S, Kucharski AJ, Camacho A, Eggo RM, Yakob L, Murray LM, et al. Comparative analysis of dengue and Zika outbreaks reveals differences by setting and virus. PLoS Negl Trop Dis. 2016;10:e0005173. http://dx.doi.org/10.1371/journal.pntd.0005173
26. Pacheco O, Beltrán M, Nelson CA, Valencia D, Tolosa N, Farr SL, et al. Zika virus disease in Colombia—preliminary report. [cited 2019 Apr 15] https://www.nejm.org/doi/full/10.1056/NEJMoa1604037
27. Administrative Department of National Statistics, Colombia. Direction of geostatistics, urban section level layer, National Geostatistical Framework, 2005 [in Spanish] [cited 2018 Nov 10]. http://www.dane.gov.co
28. National Health Institute of Colombia. Protocol of public health surveillance, dengue, code: 210, 220, 580 [in Spanish] [cited 2018 Nov 10]. https://www.ins.gov.co/buscador-eventos/ZIKA%20Lineamientos/Dengue%20PROTOCOLO.pdf
29. National Health Institute of Colombia. Protocol of public health surveillance, Zika, code 895 [in Spanish] [cited 2019 Apr 1]. http://www. ins.gov.co/buscador-eventos/Lineamientos/PRO%20Zika.pdf
30. Besag J, York J, Mollie A. Bayesian image restoration with two applications in spatial statistics. Ann Inst Stat Math. 1991;43:1–59. http://dx.doi.org/10.1007/BF00116466
31. Ma H, Carlin BP. Bayesian multivariate areal Wombling for multiple disease boundary analysis [cited 2017 Oct 10]. http://www.biostat.umn.edu/~brad/software/mc.pdf
32. Lunn D, Spiegelhalter D, Thomas A, Best N. The BUGS project: evolution, critique and future directions. Stat Med. 2009; 28:3049–67. http://dx.doi.org/10.1002/sim.3680
33. Spiegelhalter DJ, Best NG, Carlin BP, van der Linde A. Bayesian measures of model complexity and fit. Stat Methodol. 2002;64:583–639. http://dx.doi.org/10.1111/1467-9868.00353
34. Spiegelhalter D, Thomas A, Best N, Lunn D. OpenBUGS user manual: advanced use of the BUGS language [cited 2017 Nov 12]. http://www.ins.gov.co/buscador-eventos/Informesdeevento/Dengue%202016.pdf
35. Costa SDSB, Branco MDRFC, Aquino Junior J, Rodrigues ZMR, Queiroz RCS, Araujo AS, et al. Spatial analysis of probable cases of dengue fever, chikungunya fever and Zika virus infections in Maranhao State, Brazil. Rev Inst Med Trop Sao Paulo. 2018;60:e62. http://dx.doi.org/10.1590/s1678-9946201860062
36. Christofferson RC. Zika virus emergence and expansion: lessons learned from dengue and chikungunya may not provide all the answers. Am J Trop Med Hyg. 2016;95:15–8. http://dx.doi.org/10.4269/ajtmh.15-0866
37. Romero-Vega L, Pacheco O, de la Hoz-Restrepo F, Díaz-Quijano FA. Evaluation of dengue fever reports during an epidemic, Colombia. Rev Saude Publica. 2014;48:899–905. http://dx.doi.org/10.1590/S0034-8910.2014048005321
38. National Health Institute of Colombia. Subregister of Zika in Girardot, Cundinamarca, 2015–2016 [in Spanish] [cited 2018 Nov 15]. http://www.ins.gov.co/buscador-eventos/IQEN/Forms/AllItems.aspx
39. Saiz J-C, Martín-Acebes MA, Bueno-Marí R, Salomón OD, Villamil-Jiménez LC, Heukelbach J, et al. Zika virus: what have we learnt since the start of the recent epidemic? Front Microbiol. 2017;8:1554. http://dx.doi.org/10.3389/fmicb.2017.01554
40. Siraj AS, Rodriguez-Barraquer I, Barker CM, Tejedor-Garavito N, Harding D, Lorton C, et al. Spatiotemporal incidence of Zika and associated environmental drivers for the 2015–2016 epidemic in Colombia. Sci Data. 2018;5:180073. http://dx.doi.org/10.1038/sdata.2018.73
41. Jaramillo-Martínez GA, Vasquez-Serna H, Chavarro-Ordoñez R, Rojas-Gomez OF, Jimenez-Canizales CE, Rodriguez-Morales AJ. Ibagué Saludable: a novel tool of information and communication technologies for surveillance, prevention and control of dengue, chikungunya, Zika and other vector-borne diseases in Colombia. J Infect Public Health. 2018;11:145–6. http://dx.doi.org/10.1016/j.jiph.2017.03.001

Address for correspondence: Daniel A. Martínez-Bello, Department of Statistics and Operations Research, Faculty of Mathematics, University of Valencia, C/Dr. Moliner, 50 46100 Burjassot, Valencia, Spain; email: danieladyro@gmail.com

Respiratory Syncytial Virus Seasonality, Beijing, China, 2007–2015

Jianxing Yu,[1] Chunyan Liu,[1] Yan Xiao,[1] Zichun Xiang, Hongli Zhou, Lan Chen, Kunling Shen, Zhengde Xie,[2] Lili Ren,[2] Jianwei Wang[2]

During July 2007–June 2015, we enrolled 4,225 hospitalized children with pneumonia in a study to determine the seasonality of respiratory syncytial virus (RSV) infection in Beijing, China. We defined season as the period during which ≥10% of total PCRs performed each week were RSV positive. We identified 8 distinctive RSV seasons. On average, the season onset occurred at week 41 (mid-October) and lasted 33 weeks, through week 20 of the next year (mid-May); 97% of all RSV-positive cases occurred during the season. RSV seasons occurred 3–5 weeks earlier and lasted ≈6 weeks longer in RSV subgroup A–dominant years than in RSV subgroup B–dominant years. Our analysis indicates that monitoring such RSV subgroup shifts might provide better estimates for the onset of RSV transmission. PCR-based tests could be a flexible or complementary way of determining RSV seasonality in locations where RSV surveillance is less well-established, such as local hospitals throughout China.

Respiratory syncytial virus (RSV) is a major cause of lower respiratory tract infection in young children worldwide (*1–3*); 2.7–3.8 million hospitalizations and 94,600–149,400 deaths occur each year among children <5 years of age as a result of RSV infection (*4*). Studies have also demonstrated the contribution of RSV to respiratory tract infections in adults (*5*,*6*). However, no licensed RSV vaccine is available (*7*), and the only approved specific therapy, palivizumab (anti-RSV antibody), has limited uses among infants at high risk for severe respiratory illness in high-resource settings (*8*).

RSV causes epidemics in the winter in regions with temperate climates (*8*,*9*). However, spatiotemporal variations have been observed in the timing of RSV activity (*10*,*11*), and knowledge of the exact timing is helpful for guiding healthcare providers and health officials on the timing of diagnostic testing and immunoprophylaxis for infants at high risk for infection (*12*). RSV circulation is monitored in the United States year-round through the National Respiratory and Enteric Virus Surveillance System (*10*) and in 15 countries of Europe through the European Influenza Surveillance Network (*13*). Since 2017, the World Health Organization has also conducted RSV surveillance to guide its global RSV prevention strategy (*9*) using the Global Influenza Surveillance and Response System (*14*). However, most of the real-time data on RSV seasonality comes from RSV surveillance, and data are lacking in many places of the world. Because disease surveillance is labor- and resource-intensive, information on seasonality from other sources is needed.

China has a high burden of RSV infection (*4*), but RSV surveillance in this country is less established, and implementation of diagnostic tests is limited. Several previous studies reported an RSV prevalence of 17%–33% among children with severe acute respiratory illness (*15*,*16*), but few have assessed the seasonality or trends of RSV infections in China. Not having data available on RSV seasonality in China could encumber implementation of therapy and prophylactic interventions for RSV.

Since July 2007, we have been monitoring for RSV infection among hospitalized children with pneumonia in Beijing, China. In this study, we evaluated the PCR results collected in 8 consecutive years (2007–2015) to characterize the seasonality of RSV by year. Also, because disease and death attributable to RSV varies from year to year (*4*,*11*,*17*), we explored the factors that might affect RSV activity.

Materials and Methods

Study Design

During July 1, 2007–June 30, 2015, we enrolled children with pneumonia who were admitted into wards of the Departments of Respiratory Medicine, Infectious Diseases,

Author affiliations: National Health Commission Key Laboratory of Systems Biology of Pathogens, Beijing, China (J. Yu, Y. Xiao, Z. Xiang, H. Zhou, L. Chen, L. Ren, J. Wang); Institute of Pathogen Biology of Chinese Academy of Medical Sciences and Peking Union Medical College, Beijing (J. Yu, Y. Xiao, Z. Xiang, H. Zhou, L. Chen, L. Ren, J. Wang); Capital Medical University Beijing Children's Hospital, Beijing (C. Liu, K. Shen, Z. Xie)

DOI: https://doi.org/10.3201/eid2506.180532

[1]These authors contributed equally to this article.

[2]These senior authors contributed equally to this article.

and Emergency Medicine and the pediatric intensive care unit (PICU) of Beijing Children's Hospital (Beijing, China). We recruited children 28 days–13 years of age who had symptoms of acute infection, defined as fever (body temperature ≥38.0°C) or hypothermia (body temperature <35.5°C), leukocytosis (leukocyte count >15,000 cells/mL for children <5 years of age or >11,000 cells/mL for children ≥5 years of age), or leukopenia (leukocyte count <5,000 cells/mL for children <5 years of age or <4,000 cells/mL for children ≥5 years of age); had ≥1 respiratory sign or symptom (i.e., cough, sputum production, shortness of breath, tachypnea [≥60 breaths/min for patients <2 months of age, ≥50 breaths/min for patients 2–11 months of age, ≥40 breaths/min for patients 12–59 months of age, and ≥30 breaths/min for patients >5 years of age], wheezing or crackles, dyspnea, or chest pain); and had radiographic evidence suggestive of pneumonia (e.g., chest radiograph showing consolidation, infiltrates, or pleural effusion). We excluded children known to be immunosuppressed (defined as having received a solid organ or hematopoietic stem cell transplant, undergoing chemotherapy, having a history of HIV or AIDS, or using steroids for >30 days).

We obtained informed consent from each child's parents or guardians before enrollment. The study protocol was approved by the ethics review committee at the Institute of Pathogen Biology, Chinese Academy of Medical Sciences, Beijing, China.

Specimen Collection and Laboratory Testing

We transferred the nasopharyngeal aspirates of each enrolled patient into Universal Transport Medium (Copan Group, https://www.copangroup.com), distributed them into aliquots, and stored them at –80°C. We screened for RSV subgroups A (RSV-A) and B (RSV-B) and other common respiratory viruses, including influenza virus (A and B), human rhinovirus, human parainfluenza viruses 1–4, human adenovirus, human enterovirus, human bocavirus, human metapneumovirus, and human coronavirus (229E, OC43, NL63, and HKU1), using multiplex reverse transcription PCR and PCR assays as described (*18*).

Data Collection

At enrollment, using a standardized reporting form, we collected demographic data (sex and age), epidemiologic data (date of illness onset and history of prematurity [defined as birth at gestational age <37 weeks]), and clinical data (signs, symptoms, and concurrent medical conditions). Concurrent medical conditions included congenital heart disease (CHD; i.e., children with an International Classification of Diseases, Ninth Revision [ICD-9], diagnostic code 745.xx, 746.xx, or 747.xx), chronic lung disease (e.g., bronchopulmonary dysplasia), chromosomal anomalies (e.g., Down syndrome), moderate to severe anemia (hemoglobin <90 g/L), and malnutrition. We also collected data on clinical outcomes, including PICU admission, noninvasive ventilation (e.g., continuous positive airway pressure), invasive ventilation (i.e., mechanical ventilation involving tracheostomy or endotracheal tube), acute respiratory failure (ICD-9 code 518.81), shock (ICD-9 code 785.5x), sepsis (ICD-9 code 038.xx), and death, by abstracting data from medical charts.

Statistical Analysis

We fitted a logistic regression model (with sine and cosine functions of the illness onset week) to individual patient data and retained a seasonal curve as described previously (*19*). To profile the seasonality of RSV with a smooth seasonal curve, we adopted an approach described previously by the US Centers for Disease Control and Prevention: we defined the RSV season as consecutive weeks during which the percentage of tests positive for RSV per week exceeded a threshold of 10% (*20*,*21*). The peak was expected to occur between the dates of onset and offset, unless an outbreak took place outside of the season.

We used a multivariable logistic regression model to explore the factors that could affect RSV transmission over a period of years. We introduced a pair of sine and cosine functions of illness onset week into the model as described in the previous paragraph. We modeled age and year using a restricted cubic spline with 5 knots (*22*). We also introduced into the model other factors that differed significantly ($p \leq 0.10$ in bivariate analysis), such as sex, dominant RSV subgroup in each season, concurrent medical conditions, and PICU admission during hospitalization. We conducted all analyses in R version 2.15.3 (https://cran.r-project.org) using mgcv package version 1.8–15 (*23*).

Results

Characteristics of Patients

During the study period, 9,950 children with a primary diagnosis of pneumonia (ICD-9 codes 480–488) were admitted to Beijing Children's Hospital (Figure 1, panel A). Of these, 4,225 patients (2,604 [62%] boys, 1,621 [38%] girls) were recruited into the study (Table 1). Median age was 1.4 (interquartile range 0.4–6.1) years. Of the recruited patients, 493 (12%) had a concurrent medical condition at the time of hospital admission. The most frequent condition was CHD (7%, 278/4,225), followed by history of prematurity (4%, 182/4,225), chronic lung disease (1%, 28/4,225), anemia (<1%, 21/4,225), malnutrition (<1%, 13/4,225), and chromosomal anomalies (<1%, 3/4,225). During the 8-year study, the number enrolled decreased from 718 in the 2007–08 RSV year to 282 in the 2014–15 RSV year, a 61% decrease. The age of children also differed each year ($p<0.001$); the last 2 years included more children ≥5 years of age.

Overall, RSV was identified in 1,270 (30%) children among the enrolled cohort. We observed a holiday effect for the Chinese Spring Festival (occurring in late January or early February) each year. A sharp decrease in sample number and samples positive for RSV were observed each year during this event, resulting in a bimodal distribution curve (Figure 1, panel B). Overall, 785 (62%) RSV-positive samples were RSV-A and 485 (38%) were RSV-B. Although almost equal numbers of RSV-A and RSV-B were identified in 2013–14, we assigned 2013–14 as an RSV-B–dominant season for modeling purposes. This assignment does not subvert our findings that subgroups A and B alternate biennially. Each RSV subgroup dominated for 2 consecutive years during our study period, for a total of 4 years each (RSV-A during 2007–08, 2010–11, 2011–12, and 2014–15; RSV-B during 2008–09, 2009–10, 2012–13, and 2013–14) (Figure 1, panel B). Of 1,270 RSV-positive children, 726 (57%) were ill during the winter (i.e., December–February), 669 (53%) were young infants 28 days–5 months of age (Figure 2, panel A), 113 (9%) had CHD, and 61 (5%) had a history of prematurity. Among infants 28 days–5 months of age with pneumonia, the average proportion positive for RSV was 54% (669/1,235); the proportion increased to 61%–67% in RSV-A–dominant years (2007–08, 2010–11, and 2011–12) but was <50% in RSV-B–dominant years (Figure 2, panel B).

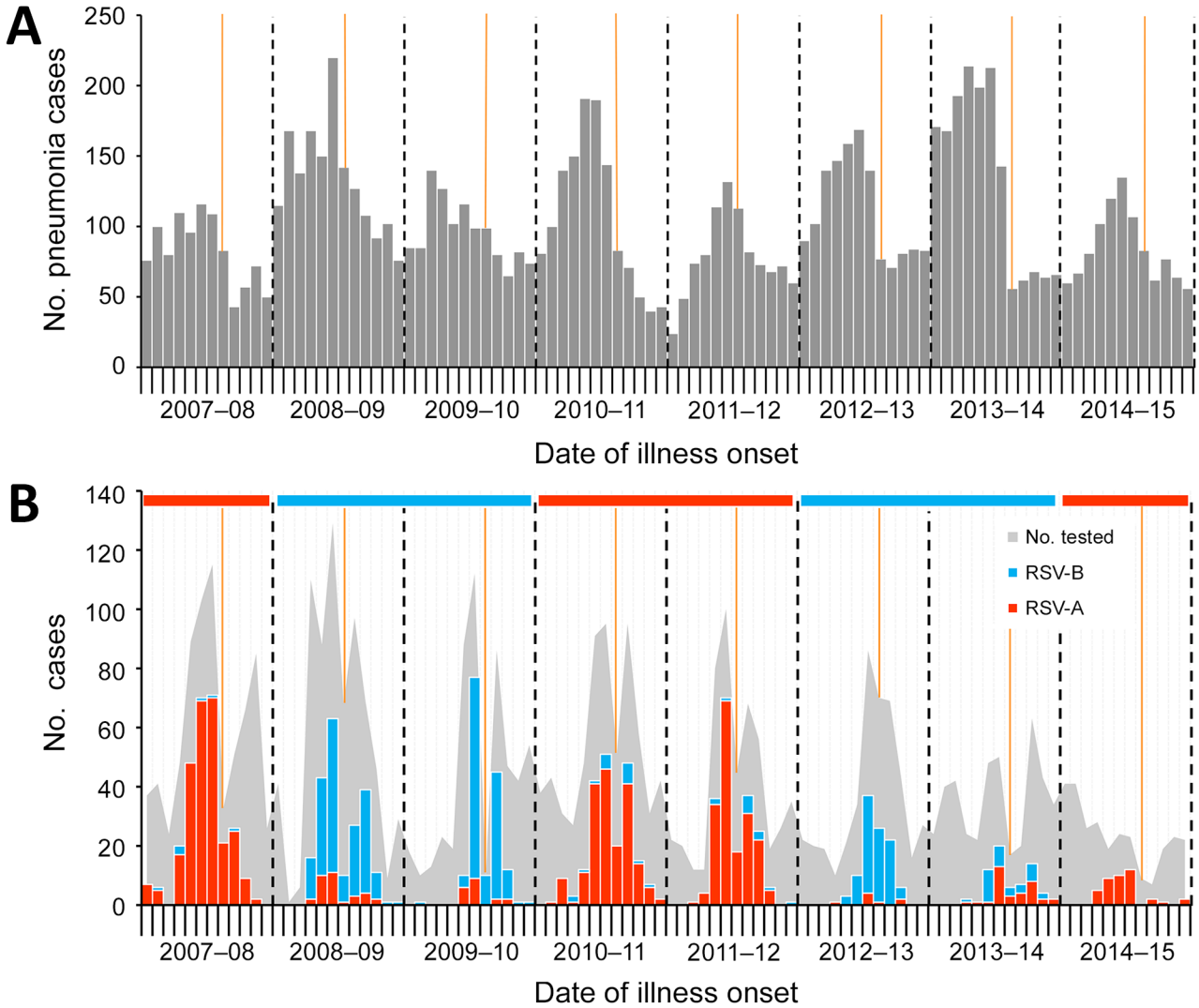

Figure 1. Cases of pneumonia and RSV infection in hospitalized children 28 days–13 years of age, by month, Beijing, China, July 1, 2007–June 30, 2015. A) Cases of pneumonia (defined as International Classification of Diseases, 9th Revision, codes 480–488), including children not enrolled in the study (n = 9,950). B) RSV-positive cases (n = 1,270), by subgroup. The shaded area represents the total number of children enrolled in study (n = 4,225). The horizontal ribbon on top of the chart denotes the dominant RSV subgroup for that year. We assigned 2013–14 as an RSV-B–dominant season for the purposes of modeling, although the numbers of RSV-A and RSV-B cases were almost equal. Orange vertical lines denote the Chinese Spring Festival; dashed vertical lines indicate divisions between seasons. RSV, respiratory syncytial virus; RSV-A, RSV subgroup A; RSV-B, RSV subgroup B.

Table 1. Demographic characteristics of hospitalized children with pneumonia, Beijing, China, July 1, 2007–June 30, 2015, by respiratory syncytial virus year*

Characteristics	2007–08	2008–09	2009–10	2010–11	2011–12	2012–13	2013–14	2014–15	p value
No. patients	718	693	522	650	495	438	427	282	
Sex									
M	455 (63)	418 (60)	363 (70)	387 (60)	309 (62)	260 (59)	251 (59)	161 (57)	0.003
F	263 (37)	275 (40)	159 (30)	263 (40)	186 (38)	178 (41)	176 (41)	121 (43)	
Age, y, median (IQR)	0.7 (0.2–3.8)	0.9 (0.3–3.3)	0.8 (0.2–2.7)	2 (0.6–6.1)	1.4 (0.4–6.1)	2.2 (0.5–7.3)	5 (2.1–8.6)	3.8 (0.6–7.5)	<0.001
Age group, mo†									<0.001
1–5	304 (42)	228 (33)	210 (40)	140 (22)	147 (30)	108 (25)	38 (9)	60 (21)	
6–11	127 (18)	154 (22)	89 (17)	84 (13)	68 (14)	60 (14)	28 (7)	28 (10)	
12–23	54 (8)	94 (14)	71 (14)	104 (16)	69 (14)	48 (11)	39 (9)	19 (7)	
24–59	78 (11)	82 (12)	61 (12)	118 (18)	60 (12)	63 (14)	110 (26)	55 (20)	
≥60	155 (22)	135 (19)	91 (17)	204 (31)	151 (31)	159 (36)	212 (50)	120 (43)	
Underlying medical condition	68 (9)	103 (15)	65 (12)	88 (14)	71 (14)	44 (10)	32 (7)	22 (8)	<0.001
History of prematurity‡	8 (1)	23 (3)	24 (5)	36 (6)	29 (6)	27 (6)	22 (5)	13 (5)	<0.001
Congenital heart disease§	49 (7)	76 (11)	38 (7)	47 (7)	38 (8)	13 (3)	10 (2)	7 (2)	<0.001
Chronic lung diseases¶	6 (1)	5 (1)	2 (0)	6 (1)	4 (1)	3 (1)	0	2 (1)	0.700
Anemia#	5 (1)	2 (0)	5 (1)	4 (1)	1 (0)	3 (1)	0	1 (0)	0.424
Malnutrition	5 (1)	2 (0)	2 (0)	3 (0)	0	1 (0)	0	0	0.337
Chromosomal anomalies**	2 (0)	1 (0)	0	0	0	0	0	0	0.441

*Values are no. (%) except where indicated. IQR, interquartile range.
†Some columns do not add up to 100% because of rounding.
‡Prematurity was defined as birth at gestational age <37 weeks.
§Congenital heart disease (defined as International Classification of Diseases, Ninth Revision, codes 745.xx, 746.xx, or 747.xx) was diagnosed at hospital admission.
¶For example, bronchopulmonary dysplasia.
#Moderate to severe anemia, defined as hemoglobin <90 g/L at hospital admission.
**For example, Down syndrome.

During the study, 335 (8%) hospitalized children with pneumonia were admitted into the PICU, and 8 died (median age 1.4 years, range 4 months–13 years). RSV-positive children were more likely than RSV-negative children to be admitted into the PICU (positive 10% vs. negative 7%; p = 0.001), receive noninvasive ventilation (positive 20% vs. negative 10%; p<0.001), and have respiratory failure (positive 16% vs. negative 9%; p<0.001) (Table 2). Of the 8 deceased children, 2 were positive for adenovirus, 1 for enterovirus, and 1 for both human parainfluenza virus 1 and human bocavirus; none of the deceased children tested positive for RSV. All 8 deceased children were born at term, and only 2 had concurrent medical conditions at hospital admission (1 CHD, 1 IgA nephropathy).

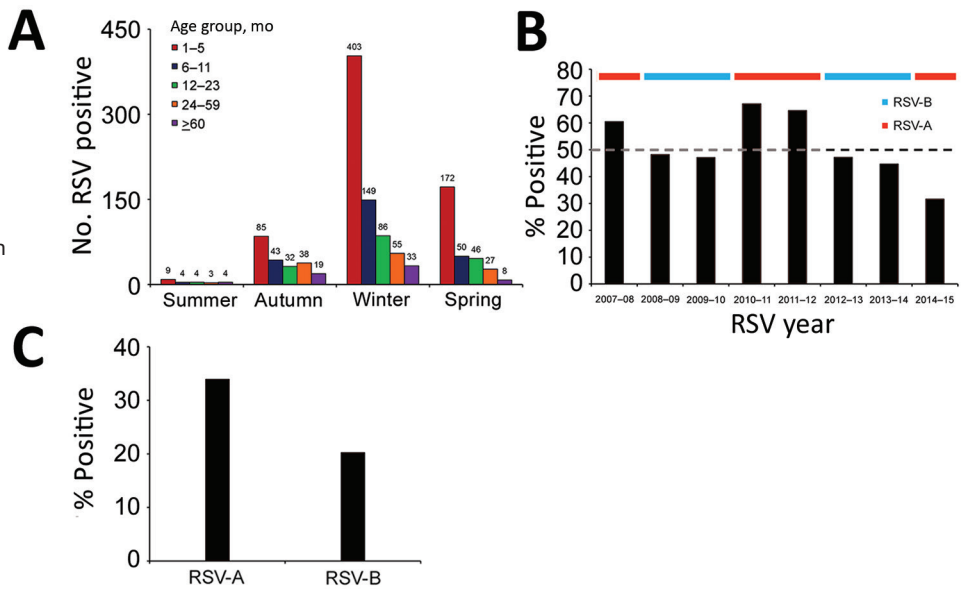

Figure 2. Hospitalized children with pneumonia testing positive for RSV, by age group, calendar season, and RSV subgroup, Beijing, China, July 1, 2007–June 30, 2015. A) Number of RSV-positive children (indicated by numbers above bars) by age group and season. Summer is defined as June–August, autumn as September–November, winter as December–February, and spring as March–May. B) Percentage of infants aged 28 days–5 months positive for RSV, by RSV season. The horizontal ribbon on top of the chart denotes the dominant RSV subgroup for that season. We assigned 2013–14 as an RSV-B–dominant season for the purposes of modeling, although the numbers of RSV-A and RSV-B cases were almost equal. Dashed line indicates 50% positivity. C) Percentage of infants 28 days–5 months of age positive for RSV, by RSV subgroup. RSV, respiratory syncytial virus; RSV-A, RSV subgroup A; RSV-B, RSV subgroup B.

Table 2. Clinical outcomes of children with pneumonia, by RSV positivity, Beijing, China, July 1, 2007–June 30, 2015*

Characteristic	All children, n = 4,225	RSV-positive children, n = 1,270	RSV-negative children, n = 2,955	p value
Admission into PICU	335 (7.9)	127 (10.0)	208 (7.0)	0.001
Mechanical ventilation	606 (14.3)	264 (20.8)	342 (11.6)	<0.001
Invasive	108 (2.6)	29 (2.3)	79 (2.7)	0.524
Tracheostomy	37 (0.9)	6 (0.5)	31 (1.0)	0.072
Endotracheal tube	99 (2.3)	25 (2.0)	74 (2.5)	0.319
Noninvasive†	553 (13.1)	258 (20.3)	295 (10.0)	<0.001
Respiratory failure	466 (11.0)	208 (16.4)	258 (8.7)	<0.001
Shock	21 (0.5)	2 (0.2)	19 (0.6)	0.053
Sepsis	94 (2.2)	21 (1.7)	73 (2.5)	0.112
Death	8 (0.2)	0	8 (0.3)	0.115

*All values are no. (%). PICU, pediatric intensive care unit; RSV, respiratory syncytial virus.
†Includes continuous positive airway pressure.

Trends of RSV Infection

We identified 8 distinctive RSV seasons during the study period (July 1, 2007–June 30, 2015) using our model (p<0.001 for all), even though the number of RSV-positive children varied (from 41 to 280) by study year. The percentage of PCR tests positive for RSV each week throughout the summer months typically exceeded 3% but was <10%; once the 10% positivity threshold was exceeded, the percentage of tests positive for RSV increased rapidly. Overall, 97% of RSV-positive PCRs occurred within the period defined by the 10% threshold (Table 3; Figure 3). Using the 10% cutoff point and a fitted seasonal curve, we determined the following RSV season parameters for each of the 8 years of our study: season onset (first of 2 consecutive weeks during which RSV positivity in seasonal curve exceeded 10%), duration, peak (week with highest RSV positivity in seasonal curve), offset (last week that RSV positivity in seasonal curve exceeded 10%), and percentage of RSV-positive samples captured within the season. Data show that the average season onset occurred at calendar week 41 (mid-October) and lasted 33 weeks, through week 20 (mid-May) of the next year (Table 3). The peak of RSV activity occurred at calendar week 3 (mid-January). RSV circulated at low levels during off-seasons. Overall, 24 (3.3%) of 724 children tested were positive for RSV in summer, a finding consistent with Broberg et al. (*13*). Variations in RSV activity were observed from year to year (Figure 4). RSV activity in 2007–08, 2011–12, and 2014–15 (RSV-A–dominant years) peaked early (during calendar week 1) and in 2009–10 and 2013–14 (RSV-B–dominant years) peaked late (calendar week 7, in February). In general, the RSV season started earlier (RSV-A week 40 vs. RSV-B week 45), lasted longer (RSV-A 34 weeks vs. RSV-B 28 weeks), and peaked earlier (RSV-A week 2 vs. RSV-B week 5) in RSV-A–dominant seasons than in RSV-B–dominant seasons (Table 3).

Factors Associated with RSV Infection

We explored factors that significantly affected RSV activity by using multivariable modeling. After adjusting for week of illness onset, year, PICU admission, and CHD, age had a strong decreasing monotonic effect on RSV infection

Table 3. RSV positivity, by subgroup, and RSV season characteristics defined by the 10% positivity threshold, Beijing, China, July 1, 2007–June 30, 2015*

RSV year	No. RSV positive: Total	No. RSV positive: RSV-A:RSV-B ratio	Calendar week no. of season (date of last day of week): Onset	Peak	Offset	Season duration, wk	% RSV-positive PCRs captured
2007–08	280	273:7	38 (2007 Sep 15)	1 (2008 Jan 5)	19 (2008 May 10)	35	95
2008–09	211	33:178	43 (2008 Nov 25)	3 (2009 Jan 17)	17 (2009 Apr 25)	28	92
2009–10	157	19:138	52 (2009 Dec 26)	7 (2010 Feb 13)	18 (2010 May 1)	20	93
2010–11	210	192:18	40 (2010 Oct 02)	3 (2011 Jan 15)	22 (2011 May 28)	36	94
2011–12	198	184:14	40 (2011 Oct 01)	1 (2012 Jan 7)	17 (2012 Apr 21)	31	98
2012–13	105	8:97	49 (2012 Dec 01)	5 (2013 Feb 2)	16 (2013 Apr 20)	21	94
2013–14†	68	35:33	48 (2013 Nov 30)	7 (2014 Feb 15)	19 (2014 May 10)	25	90
2014–15	41	41:0	43 (2014 Oct 25)	1 (2015 Jan 3)	13 (2015 Mar 28)	24	90
2007–15 combined‡	1,270	785:485	41 (mid-Oct)	3 (mid-Jan)	20 (mid-May)	33	97
RSV-A dominant§	729	690:39	40 (early Oct)	2 (early Jan)	20 (mid-May)	34	96
RSV-B dominant¶	541	95:446	45 (early Nov)	5 (early Feb)	19 (early May)	28	95

*RSV season was defined as consecutive weeks during which the percentage of RSV-specific PCRs testing positive per week exceeded a 10% threshold. RSV, respiratory syncytial virus; RSV-A, RSV subgroup A; RSV-B, RSV subgroup B.
†We classified 2013–14 as an RSV-B–dominant season for the purpose of modeling, even though an almost equal number of RSV-A and RSV-B cases were identified in that season.
‡All children (n = 4,225) in the 8 years of the study (2007–2015) were included in a model to give an average estimate of RSV seasonal characteristics for 2007–15 combined.
§Children who were ill during the 2007–08, 2010–11, 2011–12, and 2014–15 seasons (n = 2,145) were included in a model to give an average estimate of RSV seasonal characteristics for RSV-A–dominant seasons.
¶Children who were ill during the 2008–09, 2009–10, 2012–13, and 2013–14 seasons (n = 2,080) were included in a model to give an average estimate of RSV seasonal characteristics for RSV-B–dominant seasons.

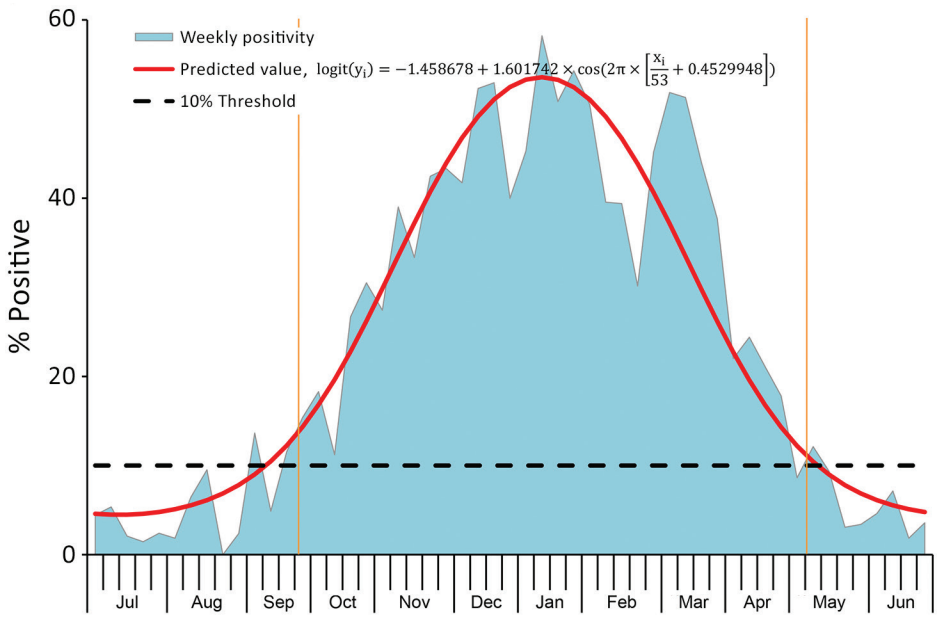

Figure 3. Average percentage of PCR tests positive for respiratory syncytial virus (RSV) per week among hospitalized children 28 days–13 years of age with pneumonia, Beijing, China, July 1, 2007–June 30, 2015. Graph begins at calendar week 27. A seasonal curve is superimposed onto the graph. RSV season was defined as consecutive weeks during which the percentage of RSV-specific PCRs testing positive per week exceeded a 10% threshold. Season onset and offset are indicated by the 2 orange vertical lines.

($p<0.001$; Figure 5, panel A). We also observed a yearly cyclic pattern with a distinct periodicity of 4 years for RSV year in the response plot ($p<0.001$; Figure 5, panel B). However, when we introduced RSV-A–dominant year into the model as a factor to be adjusted for, the cyclic trends and the year's association with RSV activity diminished ($p = 0.11$).

Discussion

We performed a PCR-based RSV screening in a cohort of children with pneumonia in Beijing to assess RSV seasonality. Our findings show that on average the RSV season starts at calendar week 41 (mid-October) and lasts 33 weeks through week 20 of the next year (mid-May); 97% of total RSV-positive PCRs occur during this period. This seasonal pattern is highly consistent with that reported in the United States (*10*), a country at the same latitude as China in the Northern Hemisphere. The World Health Organization is expecting an RSV vaccine on the market within 5–10 years (*24*); ≈62 RSV vaccine candidates are under development, and 19 of them are undergoing clinical trials. Our study of RSV seasonality and trends in Beijing could inform vaccine development and the optimization of future vaccination strategies, such as the timing of administration (year-round or seasonal), target population (mothers or infants), and ingredients, for China, the country with the largest population in the world.

We used RSV percent positivity to determine RSV seasonality because this method is highly sensitive and can be used to define RSV season not only retrospectively at the end of the season but also during the year in real-world

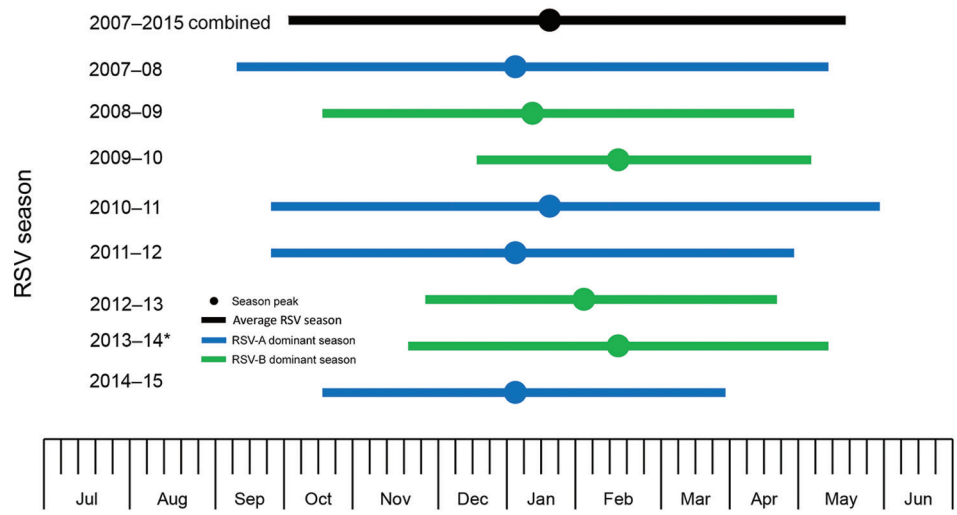

Figure 4. RSV season duration and peak, by year, Beijing, China, July 1, 2007–June 30, 2015. RSV season was defined as consecutive weeks during which the percentage of RSV-specific PCRs testing positive per week exceeded a 10% threshold. Graph begins at calendar week 27. *We assigned 2013–14 as an RSV-B–dominant season for modeling purposes, although almost equal numbers of RSV-A and RSV-B were identified that season. RSV, respiratory syncytial virus; RSV-A, RSV subgroup A; RSV-B, RSV subgroup B.

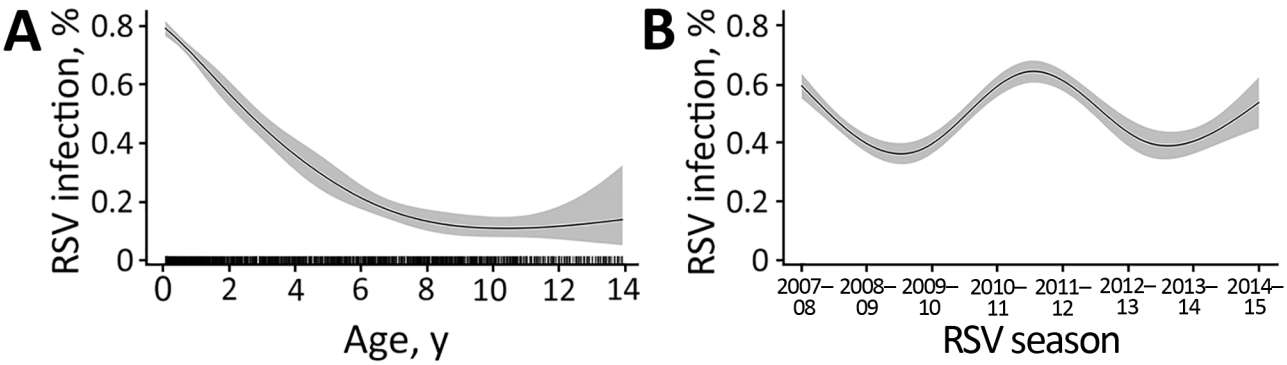

Figure 5. Analysis of nonlinear influence of age and RSV year on RSV activity among children 28 days–13 years of age hospitalized with RSV infection, Beijing, China, July 1, 2007–June 30, 2015. Graphs show effect of age (A) and RSV season (B) on probability of infection ($p<0.001$ for both). The rug plot along the *x* axis shows the observed values; gray shading indicates 95% CIs. RSV, respiratory syncytial virus.

practice. The main disadvantage of this strategy is that results can be driven in large part by the denominator; the presence of other cocirculating pathogens that cause pneumonia, especially influenza viruses, can influence the parameters of the RSV season.

Although the number of PCRs performed each year varied considerably and a shift toward older age was evident among affected children in the last 2–3 years of the study, the seasonal pattern each year remained consistent and reproducible when classifying the study year by the prevailing RSV subgroup. During the 8 consecutive years of the study, the number of children admitted with pneumonia dropped from 718 in the first year to 282 in the last; RSV positivity also decreased remarkably, from 280 in the first year to 41 in the last. The reasons for this decrease might be attributable to a decrease in the occurrence of RSV-associated pneumonia in the pediatric population or, more likely, a fall in pediatrician interest for enrolling patients into the study over time, given we did not observe a simultaneously drastic drop of pneumonia cases in the hospital (Figure 1, panel A). Moreover, the demographic characteristics of patients also differed throughout the study years. In the first study year, more children 28 days–5 months of age (42%) were enrolled, and in the last, more children ≥5 years of age (43%) were enrolled. Despite this change, the observed seasonal characteristics in each year changed little if any, indicating that viral factors rather than demographic factors had more of an influence over RSV seasonality. When study years were classified by the prevailing RSV subgroup, the observed season onset, peak, and offset showed good reproducibility. We found that >90% of RSV-positive PCRs could be captured during the RSV season for all 8 study years, and the average capture was 97% for 2007–2015 combined. The method we used in our study (PCR-based testing) can be used by local hospitals in China where surveillance data are lacking to compile the extensive amount of data needed to assess RSV seasonality.

The shifting in dominance from RSV-A to RSV-B every 2 years was repeatedly observed in our study and others (*25*). These shifts have been shown to be strongly associated with changes in the dominant RSV strain circulating (*11*,*25*); however, this phenomenon has not been investigated in detail. Similar to previous studies (*8*,*26*,*27*), the positivity for RSV-A (19%, 785/4,225) was significantly higher than that for RSV-B (11%, 485/4,225; $p<0.001$) in our study. The season onset and peak in RSV-A–prevailing years occurred ≈3–5 weeks earlier and duration was ≈6 weeks longer than those observed in RSV-B–prevailing years. The response plot showing the effect of year on RSV activity also indicated patterns of regular peaks in the years RSV-A prevailed (i.e., 2007–08, 2010–11, 2011–12, and 2014–15), but the effect of the year diminished when RSV-A–prevailing year was adjusted for as a factor in the model, suggesting that repeated shifting between RSV-A and RSV-B might play a substantial role in driving RSV transmission dynamics in populations. This observation is also supported by a model proposed by White et al., who found that the transmission rate of RSV-A (8%) was slightly higher than that of RSV-B (*25*). Just like the influencing factors explored in other studies (e.g., geographic latitude and longitude, social and demographic factors, population density, and climate) (*11*,*13*,*22*), RSV subgroup replacement might play a key role in the activity of RSV. The alternating nature of RSV subgroups could explain the alternating early-big or late-small pattern and year-to-year variation in epidemic size and timing of RSV transmission observed previously (*11*,*25*). Our finding that RSV subgroup shifting was associated with RSV activity suggests that when using RSV seasonal data or conducting RSV surveillance, one should pay attention to the prevailing subgroups in the season to optimize the timing of immunoprophylaxis. This finding indicates the significance of genotyping in RSV surveillance.

Although RSV-A cases outnumbered RSV-B in our study, we did not determine the reason for this finding,

whether RSV-A caused more symptomatic illness or transmitted more quickly than RSV-B among children. The relationship between RSV subgroup infection and disease severity is still controversial (*8*,*26*,*28*,*29*), and this issue warrants further study.

In our study, more than half of the RSV hospitalizations occurred in infants 28 days–5 months of age. A monotonic decreasing effect on the activity of RSV with age was observed in the response plot (Figure 5, panel A), indicating that younger age is a risk factor for RSV infection. Children who were in their first months of life had the highest risk for RSV infection (*3*,*30*). Administration of 1 dose of palivizumab (15 mg per kg body weight) each month for 5 months has been recommended to protect children at high risk for severe respiratory infection (e.g., preterm infants and infants with CHD in their first year of life) (*12*). As of March 2019, palivizumab is not licensed for use in China, and no immunoprophylaxis is available to prevent severe RSV infection. One third (30%) of children in our study with pneumonia requiring hospitalization had RSV infection; this finding is similar to previous estimates of 28%–34% in other countries (*1*,*2*). Considering the high positivity rate of RSV in children with pneumonia, RSV-associated illness should be considered a high priority for public health authorities in China. Our study of the relationship between age and RSV infection gives urgency to developing RSV diagnostics and indicates the need to study long-lasting and high-affinity new therapeutics and vaccines in the future (*9*,*31*).

Our study has some limitations. First, our study was conducted at 1 local hospital. Because no national RSV seasonality data were available for comparison, whether our results could represent other regions in China with an RSV burden is unknown. However, overall, our data are comparable with those observed in the United States. In addition, a previous study conducted in 15 countries of Europe showed that RSV seasons peaked later and lasted longer with increasing latitude (*13*). Because China is a large country that spans several geographic zones and climates, further studies are needed at other locations to fully characterize RSV seasonality in China. Second, our study was conducted in children with pneumonia, a population that usually has a high RSV positivity rate. Seasonality should also be evaluated in children with mild symptoms and in adults. Third, we did not evaluate the size of the local hospital or the minimum number of tests needed each year to conduct a more reliable analysis of RSV seasonality. Fourth, we excluded children without fever from our study. Because illness caused by RSV can manifest without fever, particularly among infants (*32*), the case definition used in our study was suboptimal, and we might have missed some children infected with RSV. Considering no international RSV case definition exists (*13*), we encourage researchers in future studies to determine a working case definition that can balance the many attributes (e.g., accuracy, feasibility, flexibility, and usefulness) of the various definitions that have been used to conduct RSV surveillance or study disease burden.

In conclusion, RSV infection showed distinctive seasonal patterns in Beijing, China. The prevailing RSV subgroup in a given season appears to affect the timing of RSV activity. Monitoring alterations of RSV subgroups might provide a better and more comprehensive description of RSV transmission and trends. A PCR-based diagnostic test at local hospitals could be a useful tool to determine RSV seasonality in circumstances where RSV season is unknown or surveillance is less established.

Acknowledgments

We are thankful to all the patients participating in the study. We are also thankful to the clinicians and other medical staff who helped collect the samples and clinical data.

This work was supported by the National Major Science and Technology Project for Control and Prevention of Major Infectious Diseases in China (2017ZX10103004), the Chinese Academy of Medical Sciences Innovation Fund for Medical Sciences (2016-I2M-1-014), the Peking Union Medical College Postdoctoral Fund, and Foundation Merieux.

About the Author

Dr. Yu is an epidemiologist at the Institute of Pathogen Biology, Chinese Academy of Medical Sciences and Peking Union Medical College in Beijing, China. Dr. Yu's research interests focus on the epidemiology of enteric and respiratory viral infections, including norovirus, rotavirus, and RSV.

References

1. Berkley JA, Munywoki P, Ngama M, Kazungu S, Abwao J, Bett A, et al. Viral etiology of severe pneumonia among Kenyan infants and children. JAMA. 2010;303:2051–7. http://dx.doi.org/10.1001/jama.2010.675
2. Jain S, Williams DJ, Arnold SR, Ampofo K, Bramley AM, Reed C, et al.; Centers for Disease Control and Prevention EPIC Study Team. Community-acquired pneumonia requiring hospitalization among U.S. children. N Engl J Med. 2015;372:835–45. http://dx.doi.org/10.1056/NEJMoa1405870
3. Stockman LJ, Curns AT, Anderson LJ, Fischer-Langley G. Respiratory syncytial virus-associated hospitalizations among infants and young children in the United States, 1997–2006. Pediatr Infect Dis J. 2012;31:5–9. http://dx.doi.org/10.1097/INF.0b013e31822e68e6
4. Shi T, McAllister DA, O'Brien KL, Simoes EAF, Madhi SA, Gessner BD, et al.; Respiratory Syncytial Virus Global Epidemiology Network. Global, regional, and national disease burden estimates of acute lower respiratory infections due to respiratory syncytial virus in young children in 2015: a systematic review and modelling study. Lancet. 2017;390:946–58. http://dx.doi.org/10.1016/S0140-6736(17)30938-8

5. Falsey AR, Hennessey PA, Formica MA, Cox C, Walsh EE. Respiratory syncytial virus infection in elderly and high-risk adults. N Engl J Med. 2005;352:1749–59. http://dx.doi.org/10.1056/NEJMoa043951
6. Thompson WW, Shay DK, Weintraub E, Brammer L, Cox N, Anderson LJ, et al. Mortality associated with influenza and respiratory syncytial virus in the United States. JAMA. 2003;289:179–86. http://dx.doi.org/10.1001/jama.289.2.179
7. Mazur NI, Martinón-Torres F, Baraldi E, Fauroux B, Greenough A, Heikkinen T, et al.; Respiratory Syncytial Virus Network. Lower respiratory tract infection caused by respiratory syncytial virus: current management and new therapeutics. Lancet Respir Med. 2015;3:888–900. http://dx.doi.org/10.1016/S2213-2600(15)00255-6
8. Griffiths C, Drews SJ, Marchant DJ. Respiratory syncytial virus: infection, detection, and new options for prevention and treatment. Clin Microbiol Rev. 2017;30:277–319. http://dx.doi.org/10.1128/CMR.00010-16
9. Higgins D, Trujillo C, Keech C. Advances in RSV vaccine research and development–a global agenda. Vaccine. 2016;34:2870–5. http://dx.doi.org/10.1016/j.vaccine.2016.03.109
10. Rose EB, Wheatley A, Langley G, Gerber S, Haynes A. Respiratory syncytial virus seasonality—United States, 2014–2017. MMWR Morb Mortal Wkly Rep. 2018;67:71–6. http://dx.doi.org/10.15585/mmwr.mm6702a4
11. Pitzer VE, Viboud C, Alonso WJ, Wilcox T, Metcalf CJ, Steiner CA, et al. Environmental drivers of the spatiotemporal dynamics of respiratory syncytial virus in the United States. PLoS Pathog. 2015;11:e1004591. http://dx.doi.org/10.1371/journal.ppat.1004591
12. American Academy of Pediatrics Committee on Infectious Diseases; American Academy of Pediatrics Bronchiolitis Guidelines Committee. Updated guidance for palivizumab prophylaxis among infants and young children at increased risk of hospitalization for respiratory syncytial virus infection. Pediatrics. 2014;134:415–20. http://dx.doi.org/10.1542/peds.2014-1665
13. Broberg EK, Waris M, Johansen K, Snacken R, Penttinen P. European Influenza Surveillance Network. Seasonality and geographical spread of respiratory syncytial virus epidemics in 15 European countries, 2010 to 2016. Euro Surveill. 2018;23:1–11. http://dx.doi.org/10.2807/1560-7917.ES.2018.23.5.17-00284
14. World Health Organization. WHO global respiratory syncytial virus surveillance. 2017 May 15 [cited 2017 May 24]. http://www.who.int/influenza/rsv
15. Feng L, Li Z, Zhao S, Nair H, Lai S, Xu W, et al. Viral etiologies of hospitalized acute lower respiratory infection patients in China, 2009-2013. PLoS One. 2014;9:e99419. http://dx.doi.org/10.1371/journal.pone.0099419
16. Huo X, Fang B, Liu L, Yu H, Chen H, Zheng J, et al. Clinical and epidemiologic characteristics of respiratory syncytial virus infection among children aged <5 years, Jingzhou City, China, 2011. J Infect Dis. 2013;208(Suppl 3):S184–8. http://dx.doi.org/10.1093/infdis/jit518
17. Centers for Disease Control and Prevention. Respiratory syncytial virus activity—United States, July 2011–January 2013. MMWR Morb Mortal Wkly Rep. 2013;62:141–4.
18. Ren L, Gonzalez R, Wang Z, Xiang Z, Wang Y, Zhou H, et al. Prevalence of human respiratory viruses in adults with acute respiratory tract infections in Beijing, 2005–2007. Clin Microbiol Infect. 2009;15:1146–53. http://dx.doi.org/10.1111/j.1469-0691.2009.02746.x
19. Stolwijk AM, Straatman H, Zielhuis GA. Studying seasonality by using sine and cosine functions in regression analysis. J Epidemiol Community Health. 1999;53:235–8. http://dx.doi.org/10.1136/jech.53.4.235
20. Haynes AK, Prill MM, Iwane MK, Gerber SI; Centers for Disease Control and Prevention. Respiratory syncytial virus—United States, July 2012–June 2014. MMWR Morb Mortal Wkly Rep. 2014;63:1133–6.
21. Midgley CM, Haynes AK, Baumgardner JL, Chommanard C, Demas SW, Prill MM, et al. Determining the seasonality of respiratory syncytial virus in the United States: the impact of increased molecular testing. J Infect Dis. 2017;216:345–55. http://dx.doi.org/10.1093/infdis/jix275
22. Gupta P, Beam BW, Rettiganti M. Temporal trends of respiratory syncytial virus–associated hospital and ICU admissions across the United States. Pediatr Crit Care Med. 2016;17:e343–51. http://dx.doi.org/10.1097/PCC.0000000000000850
23. Wood SN. Generalized additive models: an introduction with R. Boca Raton (FL): CRC Press; 2006.
24. Giersing BK, Karron RA, Vekemans J, Kaslow DC, Moorthy VS. Meeting report: WHO consultation on respiratory syncytial virus (RSV) vaccine development, Geneva, 25–26 April 2016. Vaccine. 2017;S0264-410X(17)30293-1.
25. White LJ, Waris M, Cane PA, Nokes DJ, Medley GF. The transmission dynamics of groups A and B human respiratory syncytial virus (hRSV) in England & Wales and Finland: seasonality and cross-protection. Epidemiol Infect. 2005;133:279–89. http://dx.doi.org/10.1017/S0950268804003450
26. Jafri HS, Wu X, Makari D, Henrickson KJ. Distribution of respiratory syncytial virus subtypes A and B among infants presenting to the emergency department with lower respiratory tract infection or apnea. Pediatr Infect Dis J. 2013;32:335–40. http://dx.doi.org/10.1097/INF.0b013e318282603a
27. Esposito S, Piralla A, Zampiero A, Bianchini S, Di Pietro G, Scala A, et al. Characteristics and their clinical relevance of respiratory syncytial virus types and genotypes circulating in northern Italy in five consecutive winter seasons. PLoS One. 2015;10:e0129369. http://dx.doi.org/10.1371/journal.pone.0129369
28. Gilca R, De Serres G, Tremblay M, Vachon ML, Leblanc E, Bergeron MG, et al. Distribution and clinical impact of human respiratory syncytial virus genotypes in hospitalized children over 2 winter seasons. J Infect Dis. 2006;193:54–8. http://dx.doi.org/10.1086/498526
29. Do LA, Bryant JE, Tran AT, Nguyen BH, Tran TT, Tran QH, et al. Respiratory syncytial virus and other viral infections among children under two years old in southern Vietnam 2009-2010: clinical characteristics and disease severity. PLoS One. 2016;11:e0160606. http://dx.doi.org/10.1371/journal.pone.0160606
30. Hall CB, Weinberg GA, Iwane MK, Blumkin AK, Edwards KM, Staat MA, et al. The burden of respiratory syncytial virus infection in young children. N Engl J Med. 2009;360:588–98. http://dx.doi.org/10.1056/NEJMoa0804877
31. Heath PT, Culley FJ, Jones CE, Kampmann B, Le Doare K, Nunes MC, et al. Group B streptococcus and respiratory syncytial virus immunisation during pregnancy: a landscape analysis. Lancet Infect Dis. 2017;17:e223–34. http://dx.doi.org/10.1016/S1473-3099(17)30232-3
32. Saha S, Pandey BG, Choudekar A, Krishnan A, Gerber SI, Rai SK, et al. Evaluation of case definitions for estimation of respiratory syncytial virus associated hospitalizations among children in a rural community of northern India. J Glob Health. 2015;5:010419. http://dx.doi.org/10.7189/jogh.05.020419

Address for correspondence: Jianwei Wang, Institute of Pathogen Biology of Chinese Academy of Medical Sciences and Peking Union Medical College, No. 9 Dong Dan San Tiao, Dongcheng District, Beijing 100730, China; email: wangjw28@163.com

Enhancement of Risk for Lyme Disease by Landscape Connectivity, New York, New York, USA

Meredith C. VanAcker, Eliza A.H. Little, Goudarz Molaei, Waheed I. Bajwa, Maria A. Diuk-Wasser

Most tickborne disease studies in the United States are conducted in low-intensity residential development and forested areas, leaving much unknown about urban infection risks. To understand Lyme disease risk in New York, New York, USA, we conducted tick surveys in 24 parks throughout all 5 boroughs and assessed how park connectivity and landscape composition contribute to *Ixodes scapularis* tick nymphal densities and *Borrelia burgdorferi* infection. We used circuit theory models to determine how parks differentially maintain landscape connectivity for white-tailed deer, the reproductive host for *I. scapularis* ticks. We found forested parks with vegetated buffers and increased connectivity had higher nymph densities, and the degree of park connectivity strongly determined *B. burgdorferi* nymphal infection prevalence. Our study challenges the perspective that tickborne disease risk is restricted to suburban and natural settings and emphasizes the need to understand how green space design affects vector and host communities in areas of emerging urban tickborne disease.

Lyme disease, or Lyme borreliosis, is the most commonly reported arthropodborne disease in the United States and Europe (*1*). In the eastern United States, this disease is caused by *Borrelia burgdorferi* sensu stricto (hereafter *B. burgdorferi*), a spirochete transmitted by the blacklegged tick, *Ixodes scapularis,* and maintained in a horizontal transmission cycle between larval and nymphal *I. scapularis* ticks and a vertebrate reservoir host community (*2*). *I. scapularis* ticks vector 6 other tickborne pathogens, including *Babesia microti* (the cause of human babesiosis) and *Anaplasma phagocytophilum* (the cause of human granulocytic anaplasmosis). The geographic expansion of these pathogens has followed the spread of their shared vector across the northeastern and midwestern United States over the past 50 years (*3*). The range expansion of *I. scapularis* ticks is attributed to reforestation (*4*), the increase in deer populations (*4*), and climate-facilitated expansion (*5*). Although historically associated with the incursion of suburban and exurban development into rural areas (*4*), tickborne diseases are an emerging urban threat, indicated by an unprecedented increase in locally acquired cases in New York City (NYC), NY, USA (*6*), and *B. burgdorferi*–infected *I. scapularis* in Chicago, IL, USA (*7*). In contrast with several European studies on urban Lyme borreliosis (*8*), the risk for acquiring *B. burgdorferi* infection in US cities is unknown.

As tickborne diseases spread into urban areas, key issues are what ecologic and sociobehavioral conditions enable establishment of the enzootic cycle and pathogen spillover to humans. Landscape modification, such as forest fragmentation (breaking up of large continuous forests into smaller patches), has been linked to increased transmission risk for Lyme disease (*9*,*10*). Forest fragmentation increases edge habitat and might reduce host biodiversity by increasing densities of white-footed mice (*Peromyscus leucopus*), a major host for immature *I. scapularis* ticks and *B. burgdorferi*, relative to less competent hosts. Fragmentation might also favor white-tailed deer (*Odocoileus virginianus*) (hereafter deer), the reproductive host for adult *I. scapularis* ticks, through increased forage quality and predator release (*9*,*10*), and might bring humans in closer contact with forests and tick vectors, increasing human–tick contact rates (*10*). However, extreme fragmentation of suitable habitat patches within an impermeable urban matrix might decrease disease risk if connectivity is reduced to the point of limiting host and tick movement (*11*). This connectivity might be partially restored by establishing green spaces and habitat corridors within cities, which can lead to an introduction of tick populations and pathogens into new areas (*7*,*12*,*13*).

With high human densities in cities, emerging tickborne infections can cause a major public health burden (*12*). Human risk for acquiring Lyme disease is dependent on the density and infection prevalence of nymphal *I. scapularis* ticks, the hazard, or potential source of harm (*14*). Thus, understanding the drivers of vector and pathogen

Author affiliations: Columbia University, New York, New York, USA (M.C. VanAcker, M.A. Diuk-Wasser); Connecticut Agricultural Experiment Station, New Haven, Connecticut, USA (E.A.H. Little, G. Molaei); Yale University, New Haven (G. Molaei); New York City Department of Health and Mental Hygiene, New York, New York, USA (W.I. Bajwa)

DOI: https://doi.org/10.3201/eid2506.181741

distribution is critical for designing effective intervention strategies. Because of increasing incidence of locally acquired Lyme disease cases on Staten Island (*6*), a borough of NYC, and the potential for expansion to other boroughs, we sought to determine the hazard posed by *I. scapularis* ticks in public parks in NYC, and characterize the effect of landscape composition and connectivity in and around parks on nymphal *I. scapularis* tick densities and *B. burgdorferi* infection prevalence.

Materials and Methods

Site Selection

We surveyed 24 public parks in NYC (Figure 1; Table 1): 13 on Staten Island, 2 in Manhattan, 2 in Brooklyn, 3 in the Bronx, and 4 in Queens. Fifteen of these parks are included in ongoing tick surveillance by the NYC Department of Health and Mental Hygiene. The inclusion criteria we used to select the parks were location (representing all 5 boroughs), size (26–794 ha), and forest area (7–433 ha) gradients.

Nymphal Tick Collection

We performed tick collections under a City of New York Parks and Recreation research permit and a New York State Department of Environmental Conservation license to collect. We surveyed parks twice, with a minimum of 2 weeks separation, during the nymphal activity peak (*15*) of May 30–June 30, 2017 (Table 1). All tick collections were conducted by the same 2 persons. We scaled transect coverage by the park area and restricted transects to continuous forest patches that were large enough to complete 100-m transects (Appendix Table 1, https://wwwnc.cdc.gov/EID/article/25/6/18-1741-App1.pdf). Within each park, we divided the effort by 50% along trail/forest edge and 50% perpendicular to the trail into interior forest. We collected ticks every 20 m along the transects by dragging a 1 m^2 white corduroy cloth (*16*), then removed ticks with forceps, placed them in vials containing 100% ethanol, and identified them to species and life stage by using a standard key (*17*). We recorded global positioning system waypoints at the beginning of each transect and every 20 m. Surveys were not conducted on days with rain.

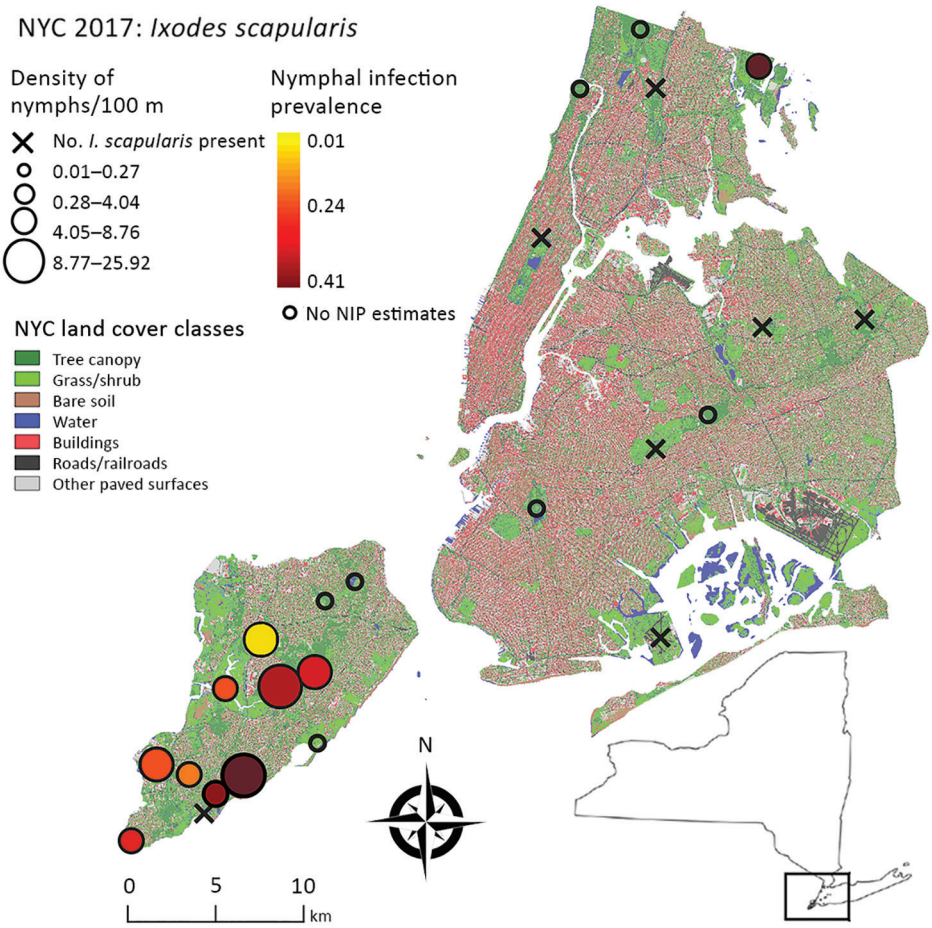

Figure 1. Study area for analysis of *Ixodes scapularis* nymphal tick densities and *Borrelia burgdorferi* infection prevalence, New York, New York, USA, 2017. Open circles indicate parks where tick sample size was too low to estimate nymphal infection prevalence. Inset shows location of study area in New York state. NIP, nymphal infection prevalence; NYC, New York City.

Table 1. Sampling effort for study of enhancement of Lyme disease risk by landscape connectivity, New York, New York, USA*

Park	Borough	Geographic coordinates, °N, °W	No. *Ixodes scapularis* ticks tested for *Borrelia burgdorferi*/no. collected	No. sampling efforts
Alley Pond Park	Queens	40.7476, –73.7425	0/0	2
Bloomingdale Park	Staten Island	40.5334, –74.2105	39/39	2
Blue Heron Park	Staten Island	40.5314, –74.1746	54/422	2
Bronx Park	Bronx	40.8716, –73.8740	0/0	2
Central Park	Manhattan	40.7982, –73.9561	0/0	3
Clay Pit Ponds State Park Preserve	Staten Island	40.5393, –74.2321	52/156	2
Clove Lakes Park	Staten Island	40.6185, –74.1139	0/1	2
Conference House Park	Staten Island	40.5010, –74.2516	51/83	2
Floyd Bennett Field	Brooklyn	40.5983, –73.8967	0/0	2
Forest Park	Queens	40.7033, –73.8508	0/1	2
Freshkills Park	Staten Island	40.5763, –74.1835	57/82	2
Great Kills Park	Staten Island	40.5463, –74.1252	0/5	2
High Rock Park	Staten Island	40.5825, –74.1232	51/122	2
Highland Park	Queens	40.6873, –73.8871	0/0	2
Inwood Hill Park	Manhattan	40.8732, –73.9250	0/1	2
Kissena Park	Queens	40.7435, –73.8057	0/0	2
Latourette Park	Staten Island	40.5880, –74.1395	105/622	3
Lemon Creek Park	Staten Island	40.5115, –74.1977	0/0	2
Pelham Bay Park	Bronx	40.8673, –73.8106	52/85	4
Prospect Park	Brooklyn	40.6606, –73.9712	0/1	2
Silver Lake Park	Staten Island	40.6276, –74.0932	0/2	2
Van Cortlandt Park	Bronx	40.9020, –73.8823	0/1	2
Willowbrook Park	Staten Island	40.6005, –74.1581	49/72	2
Wolfe's Pond Park	Staten Island	40.5242, –74.1952	50/60	2

*Sampling effort describes how many visits were made to the park during the sampling period. All ticks were collected from the environment while questing.

Screening of *I. scapularis* Ticks for Infection with *B. burgdorferi*

We screened ≈50 nymphal ticks for *B. burgdorferi* infection in each park (with 1 exception, Bloomingdale Park [n = 39]). We considered this screening conservative because we estimated that ≥10 ticks should be screened to be 95% confident the site is negative for *B. burgdorferi* if the expected infection prevalence is 26.6%. We homogenized ticks and extracted genomic DNA by using the DNeasy Blood and Tissue Kit (QIAGEN, https://www.qiagen.com) or DNA-zol BD (Molecular Research Center, https://www.mrcgene.com) according to the manufacturers' recommendations with modifications (*18*). We used PCRs to screen for infection with *B. burgdorferi* by using primer sets for flagellin (*19*), 16S rRNA (*20*), and outer surface protein A (*21*) genes (thermocycling conditions provided in the Appendix). DNA isolated from *B. burgdorferi* strain 2591 culture and from uninfected laboratory-reared ticks were used as positive and negative controls in all PCRs. We identified positive samples by their band size and sequenced amplicon subsamples to confirm the genetic product identity.

Landscape Analyses

Land Cover Layers

We used a high-resolution (1 m × 1 m) land cover dataset for NYC derived from 2010 Light Detection and Ranging (https://catalog.data.gov/dataset?tags=lidar) data and 2008 4-band orthoimagery. Data were classified by using a rule-based expert system into 7 land cover classes: tree canopy, grass/shrub, bare soil, water, buildings, roads, and other paved surfaces (*22*). We combined buildings, roads, and paved surfaces into 1 impervious surface land cover class. We extracted the 24 park polygons from the NYC Open Spaces file (*23*) and quantified the park area and forest area within each park.

Land Cover Composition Surrounding Parks

We used buffering, a geographic information system procedure, to extract the proportion of each land cover class within a fixed width area surrounding the park boundaries, excluding coastal waterways. To assess the most predictive buffer size, we calculated the percentage of each land cover class (tree canopy, grass, soil, water, and impervious surfaces) for 5 buffer widths spaced every 100 m from 100 through 500 m. We used the buffer surrounding the park edge as a predictor of *I. scapularis* tick density within the park to indicate the accessibility of the park to hosts carrying feeding ticks or the pathogen.

Landscape Connectivity Metrics

For parks in all boroughs, we calculated the Euclidean distance between each pair of park centroids. We set all values in the distance matrix >4.8 km to 0 (distance threshold; i.e., all parks that were >4.8 km were considered unconnected); all park pairs ≤4.8 km were set to 1. This threshold is based on the average deer movement on Staten Island of 4.0–4.8

km (*24*) and the assumption that new tick populations are established from female adult ticks dropping off of deer. We used the total number of connections between park pairs according to the distance threshold as a model covariate.

We conducted connectivity analyses based on circuit theory only for Staten Island because this borough had a large number of established tick populations with variable densities among parks. We calculated a metric called flow centrality by using the programs Circuitscape (*25*), Linkage Mapper, and Centrality Mapper to assess the importance of each sampled park in maintaining connectivity across the island for deer, ticks, and pathogens (Appendix). We considered the outline of the parks as nodes, or the population sources, and the remaining raster pixels as the matrix. We assigned resistance values to each land cover class in the matrix according to its resistance to deer movement (*26–28*) and gene flow (*29*). Although focusing on deer, the resistance values broadly represented connectivity for other known host species of *I. scapularis* ticks and *B. burgdorferi* (Appendix Table 2). We applied Linkage Mapper (*30*), which uses parameters from Circuitscape to identify the least cost paths (LCPs), the single best path of lowest resistance that an animal may use to move through the matrix. We used the LCP network in Centrality Mapper, which assigns each link between nodes a resistance equivalent to the cost-weighted distance of the corresponding LCP. Centrality Mapper applies 1 amp of current into a pair of nodes, iterating through each possible pair of nodes, to calculate the flow centrality score or the current sum across all nodes and connections. Flow centrality is a measure of the contribution of a park to maintaining network connectivity on Staten Island and was used as a covariate in tick density and infection prevalence models.

Model Development

Covariate Standardization and Buffer Size Selection

We developed 1 model to examine the presence of *I. scapularis* ticks in parks across all NYC boroughs and 2 models with only Staten Island data to determine the best predictors of *I. scapularis* tick density and nymphal infection prevalence. We standardized all landscape covariates used in the 3 models by subtracting the mean and dividing by 1 SD. To determine the most predictive buffer size of *I. scapularis* nymphs, we ran univariate negative binomial generalized linear models (GLMs; glm.nb in the MASS package [*31*] in R [*32*]) for all land cover buffer sizes. We included an offset term, the natural log of the total transect length in a given park, to account for sampling effort. We compared the univariate models of the 5 buffer sizes for each land cover class by using the Akaike Information Criterion (AIC) scores (*33*) and retained the buffer size with the lowest AIC for future analyses (Appendix Table 3).

Model Selection

We used GLMs (binomial and negative binomial families) without interactions or random effects to examine the NYC-wide and Staten Island data. For all global models, we assessed multicolinearity between the covariates by using the variance inflation factor (VIF) (*34*) and retained covariates for each final analysis that had a VIF score <4 (*34*). We used an information theoretic approach (*33*) and AIC for small sample sizes (AICc) to identify the best-fitting models describing presence, density, and infection prevalence of *I. scapularis* ticks. We used multimodel inference, which uses model averaging (MuMIn package [*35*] in R [*32*]) to include information from competing models that significantly explain the data. The averaged model is based on a subset of models within 95% of the cumulative AIC weights. The relative importance (RI) of each covariate ranges from 0 through 1 and describes the sum of the Akaike weights in each model in which the covariate is present. If there were no closely competing models (within ΔAIC <2 from the lowest AICc score), we did not use model averaging and selected the final candidate model with the lowest AICc score. We evaluated model fit with McFadden R^2 (*36*) for logistic regression models and assessed the root mean squared error (RMSE) for the negative binomial model. We included the same offset term as above in all models.

I. scapularis Nymphs in NYC

We used a binomial GLM to examine drivers of presence of *I. scapularis* ticks at parks throughout the 5 boroughs. We considered established parks those where ≥6 ticks were collected during 2 surveys. This threshold was used by Dennis et al. (*37*) and Eisen et al. (*38*) to classify US counties and was meant to distinguish reproductive tick populations from individual immature ticks that might have detached from a bird. Covariates used to model tick presence were tree canopy area within the park (square meters); the number of connections to other parks within 4.8 km (range 0–5 connections); and the land cover composition of the park buffers, including tree canopy, impervious surfaces, water, grass/shrub (percentage within 100 m of park edge), and soil (percentage within 300 m of park edge).

Density of *I. scapularis* Nymphs on Staten Island, NY

We used a negative binomial GLM to examine relationships between landscape metrics and tick density (nymphal count/transect length). The negative binomial error structure was selected by using a likelihood ratio test that compared the fit with a poisson error structure. The covariates included in the models were the same as the presence/absence model for NYC, with the addition of the flow centrality scores (range 14.9–41.3) (Figure 2). We examined the global spatial autocorrelation of residuals from the tick density regression model by using a Moran's I test (*39*).

Prevalence of *I. scapularis* Nymphs Infected with *B. burgdorferi* on Staten Island

We used a binomial GLM model to assess the best covariates to predict the nymphal infection prevalence (NIP) at 9 parks on Staten Island. The covariates included in the models were the same as those used in the nymphal density model for Staten Island in addition to the density of nymphs.

Results

Buffer Size Selection

The coefficient signs stayed constant for all buffer sizes within the same land cover class in the univariate GLMs (Appendix Table 3). All models examining percentage of tree canopy in the buffer showed a positive effect on tick density; all models that included percentage of grass, soil, water, and impervious surfaces in the buffer had negative effects on tick density. A buffer size of 100 m was the best fit for all land cover classes except bare soil, for which a 300 m buffer had the lowest AIC (Appendix Table 3).

I. scapularis Ticks in NYC

At least 1 *I. scapularis* nymph was found at 17 of 24 parks surveyed throughout NYC. Of these parks, 10 had >6 nymphs and were categorized as established for *I. scapularis* populations; all of these sites were on Staten Island, except for Pelham Bay Park in the Bronx (Table 1). The model with the lowest AIC included the number of connections a park had to surrounding parks within 4.8 km (p = 0.005) (Appendix Figure 1). This model explained moderate levels of variation with a McFadden R^2 of 0.38.

Density of *I. scapularis* Ticks on Staten Island

Because 9 of 10 parks with established tick populations were on Staten Island, we limited the analysis of *I. scapularis* density to this borough. Blacklegged ticks were most abundant in the central and southern regions of the island (Figure 1). We removed 1 covariate that had a VIF >4, percentage of grass in the buffer. We identified 4 multivariate models with considerable support (ΔAIC <2), these were within 95% of the cumulative AIC weights that composed the averaged model. Flow centrality, percentage tree canopy, soil, and water within the buffer were the major covariates (RI = 1.00) and were present in all 4 models comprising the averaged model (Table 2; Appendix Table 4). The percentage impervious surfaces within a 100-m buffer (RI = 0.36) and the tree canopy area within the park (RI = 0.65) showed no major effect on *I. scapularis* tick density (CIs include 0) in the averaged model, although tree canopy area showed major positive effects in a subset of models that comprised the averaged model. The RMSE of the model residuals was 1.04; a total of 64.8% of the values fell within 1 RMSE and 98.9% of the values fell within 2 RMSE. Residuals from the regression model were not spatially autocorrelated

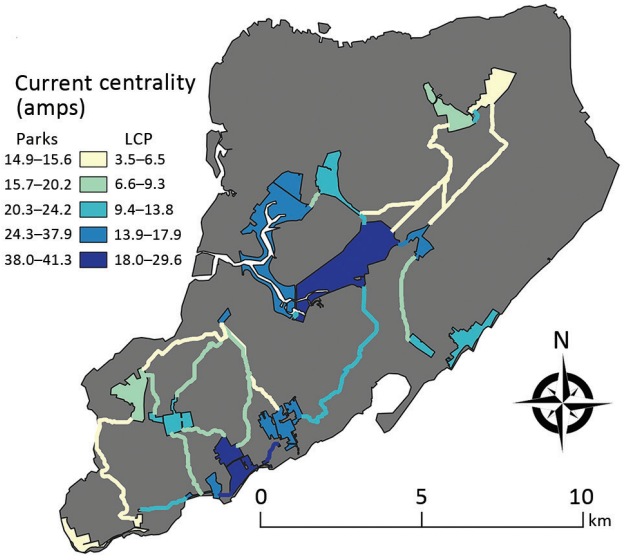

Figure 2. Current centrality for parks and linkages on Staten Island, New York, USA, 2017. In connectivity analysis, the park outlines were used as nodes, and gray indicates the matrix used for the resistance layer. The parks and linkages are color-graded according to their centrality values. Lighter colors indicate lower centrality, and darker colors indicate higher centrality for the network. Amps is the unit used to describe the flow of charge through the nodes. LCP, least cost path.

Table 2. Averaged model for *Ixodes scapularis* tick density in study of enhancement of Lyme disease risk by landscape connectivity, New York, New York, USA*

Variable	Coefficient estimate	95% CI	RI
Intercept	–3.0262	–3.20 to –2.84	NC
Flow centrality, amps	0.4058	0.13 to 0.67	1.00
Tree canopy area in park, m^2	0.1821	–0.001 to 0.55	0.65
% Trees†	0.5068	0.27 to 0.73	1.00
% Impervious†‡	0.0454	–0.13 to 0.38	0.36
% Water†	–0.4285	–0.64 to –0.20	1.00
% Soil§	–0.5684	–0.88 to –0.25	1.00

*Values are for 13 parks on Staten Island. If the CI includes 0, there was no significant effect of the covariate on tick density. NC, not considered; RI, relative importance.
†Within 100-m buffer.
‡Buildings, roads, and paved surfaces.
§Within 300-m buffer.

according to the Moran's I test results (p = 0.09), indicating the tick surveys can be considered independent.

Prevalence of *I. scapularis* Nymphs Infected with *B. burgdorferi* on Staten Island

We estimated NIP for 9 parks on Staten Island and 1 park in the Bronx (Table 3). A total of 8%–40% of ticks tested at each site were positive for *B. burgdorferi* (Table 3; Figure 1), and the average NIP across all sites was 26.6% (149/560) positive for *B. burgdorferi*.

We assessed the VIF of the global model limited to the NIP for Staten Island and removed 2 covariates with VIF scores >4, percentage of tree canopy within a 100-m buffer, and density of nymphs. The univariate model with flow centrality had a model weight of 0.45, and no other model combinations were within ≤2 ΔAIC from the lowest AIC. Therefore, we did not apply model averaging and determined that flow centrality was the significant factor (p = 0.009) in predicting NIP at parks on Staten Island (Figure 3). The McFadden R^2 for this model showed low explained variation (R^2 = 0.13), likely caused by small sample size.

Discussion

We examined how urban landscape composition and configuration reflects the environmental and ecologic conditions driving the distribution of ticks and their pathogens. We found the distance between urban parks best explained whether *I. scapularis* ticks were present and that flow centrality of parks, an indicator of the connectivity of parks for deer and other hosts, had the largest positive effect on the density and infection prevalence of *I. scapularis* nymphs. Covariates that describe the composition of the landscape surrounding each park also had a major positive (percentage tree canopy) or negative (percentage water and soil) effect on the densities of *I. scapularis* nymphs.

Table 3. *Ixodes scapularis* tick nymphal infection prevalence for *Borrelia burgdorferi* in study of enhancement of Lyme disease risk by landscape connectivity, New York, New York, USA*

Park	No. nymphs positive/no. tested	Site NIP
Bloomingdale Park	5/39	0.128
Blue Heron Park	22/54	0.407
Clay Pit Ponds State Park Preserve	11/52	0.211
Conference House Park	12/51	0.235
Freshkills Park	12/57	0.210
High Rock Park	13/51	0.254
Latourette Park	30/105	0.285
Pelham Bay Park	21/52	0.403
Willowbrook Park	4/49	0.081
Wolfe's Pond Park	19/50	0.380
Total	149/560	0.266

*Screening results for *B. burgdorferi* infection in nymphal *I. scapularis* ticks from 1 park in the Bronx and 9 parks on Staten Island. Ticks were screened from parks with ≥39 collected ticks. NIP, nymphal infection prevalence.

Environmental conditions can limit *I. scapularis* tick population establishment and persistence. The negative effect of bare soil surrounding parks might reflect deer aversion to open habitats and tick physiology. To prevent desiccation, ticks seek microclimates that have higher ambient humidity (*40*). Ticks achieve water replenishment when they descend to lower vegetation layers (*40*), often leaf litter. Without vegetation, ticks might quickly desiccate when dropped in bare soil. Furthermore, the amount of water surrounding the park negatively affected *I. scapularis* tick density, suggesting that water might also serve as a barrier for deer movement into particular parks and could limit tick population persistence. Our findings are consistent with studies that have found agricultural fields, large urbanized areas (*27*), and a combination of landscape features with low permeability, such as waterways and roads, to impede deer movement (*29*), potentially slowing tick expansion.

The introduction of *I. scapularis* ticks into new habitats can occur through multiple pathways. Because these ticks move only a few meters during each life stage, host movement and habitat use during tick feeding determine dispersal patterns (*41*). Landscape structure and connectivity might differentially affect reservoir (rodents, medium-size mammals, and birds) and reproductive host (deer) movement. Adult *I. scapularis* ticks are mainly distributed by deer (*41*); they serve as the primary host for adult ticks, and >90% of female *I. scapularis* ticks feed on deer (*42*). Although locally dispersing or migrating passerine birds play a role in moving immature ticks longer distances (*43*), deer are key hosts for establishing new populations locally because 1 female adult tick will lay ≈2,000 eggs after a successful blood meal from a deer (*44*). We were unable

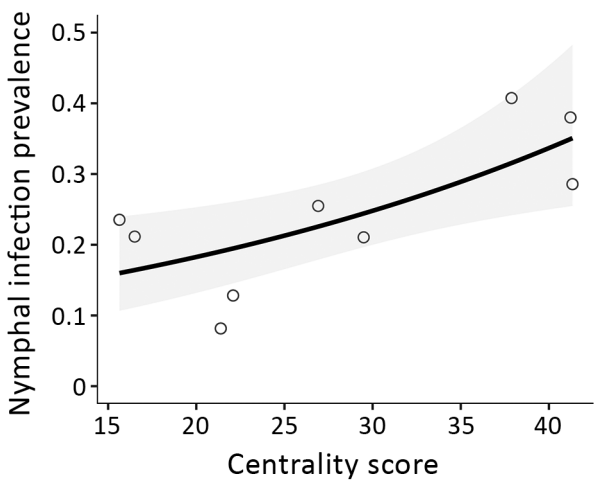

Figure 3. *Ixodes scapularis* tick nymphal infection prevalence and flow centrality model for Staten Island, New York, USA, 2017. The centrality score of 9 parks was the best predictor for nymphal infection prevalence. Shown are results of the binomial generalized linear model (p = 0.009). SE (± 0.1040) is indicated in gray. The coefficient estimate is 0.2714.

to sample larvae and adults; however, a previous study has shown a positive linear relationship between the density of larvae and nymphs (*9*). Without sufficient deer available, tick populations cannot be sustained or are sustained at much lower levels (*42*). The lack of deer reported in parks where we did not find established *I. scapularis* tick populations (*45*) indicates a strong link between deer and presence of *I. scapularis* ticks in NYC parks.

Landscape structure and connectivity also impacts the distribution and movement of small and medium-size mammals that are hosts for immature ticks and *B. burgdorferi*. Rodent hosts can contribute to a slower range expansion of *B. burgdorferi* and infected immature ticks (*46*). Rodent movement is determined by their ability to penetrate habitats, and sources of landscape resistance imposed on movement of white-footed mice, Eastern chipmunks, and red squirrels are similar between these host species (*47*).

Our results show that landscape composition and configuration have direct implications on urban Lyme disease risk. This finding is especially useful because >80% of persons in North America now reside in urban centers (*48*), the distribution of *I. scapularis* ticks continues to expand (*38*), and interest is increasing in urban green space serving as a key moderator of poverty, health, health equity, and environmental justice (*49*). Initiatives that increase urban green space have clear benefits for human well-being, climate change mitigation, and wildlife conservation. However, our study calls attention to the need to understand the drivers of tick distribution and densities within urban green spaces in the United States. Our findings on the role of flow centrality in maintaining tick and pathogen populations indicate a potential nonlinear effect of forest fragmentation on tickborne disease risk by emphasizing that fragment connectivity is a neglected key factor (however, see reports by Mechai et al. [*47*] and McClure and Diuk-Wasser [*50*]). A better understanding of how landscape shapes host communities, their movement, and tick habitat in urban and suburban regions is critical to ameliorate the risk for tickborne diseases.

Acknowledgments

We thank our field assistant, Robert Carson, for providing research support and Alex Diaz, Mallery Breban, and Dasha Pokutnaya for providing technical assistance. We also thank the NYC Department of Parks and Recreation and the NYC Department of Health and Mental Hygiene for their contribution.

This study was supported by Cooperative Agreement No. U01CK000509-01 from the Centers for Disease Control and Prevention. M.A.D.-W. was supported by the National Institutes of Health, Ecology and Evolution of Infectious Disease Program (R01 GM105246). Robert Carson was funded by the Earth Institute.

About the Author

Ms. VanAcker is a doctoral student in the Department of Ecology, Evolution, and Environmental Biology at Columbia University, New York, NY. Her primary research interests include zoonotic infectious diseases, landscape ecology, wildlife conservation, and the use of next-generation sequencing for vectorborne diseases.

References

1. Steere AC, Coburn J, Glickstein L. The emergence of Lyme disease. J Clin Invest. 2004;113:1093–101. http://dx.doi.org/10.1172/JCI21681
2. Diuk-Wasser MA, Hoen AG, Cislo P, Brinkerhoff R, Hamer SA, Rowland M, et al. Human risk of infection with *Borrelia burgdorferi*, the Lyme disease agent, in eastern United States. Am J Trop Med Hyg. 2012;86:320–7. http://dx.doi.org/10.4269/ajtmh.2012.11-0395
3. Telford SR III, Goethert HK. Emerging tick-borne infections: rediscovered and better characterized, or truly 'new'? Parasitology. 2004;129(Suppl):S301–27. http://dx.doi.org/10.1017/S0031182003004669
4. Barbour AG, Fish D. The biological and social phenomenon of Lyme disease. Science. 1993;260:1610–6. http://dx.doi.org/10.1126/science.8503006
5. Ogden NH, Bigras-Poulin M, Hanincová K, Maarouf A, O'Callaghan CJ, Kurtenbach K. Projected effects of climate change on tick phenology and fitness of pathogens transmitted by the North American tick *Ixodes scapularis.* J Theor Biol. 2008;254:621–32. http://dx.doi.org/10.1016/j.jtbi.2008.06.020
6. Daskalakis DC. Department of Health and Mental Health. Advisory #14: tick-borne disease advisory. New York City, NY, 2017 [cited 2019 Jan 15]. https://www1.nyc.gov/assets/doh/downloads/pdf/han/advisory/tick-borne-disease-advisory14.pdf
7. Hamer SA, Goldberg TL, Kitron UD, Brawn JD, Anderson TK, Loss SR, et al. Wild birds and urban ecology of ticks and tick-borne pathogens, Chicago, Illinois, USA, 2005–2010. Emerg Infect Dis. 2012;18:1589–95. http://dx.doi.org/10.3201/eid1810.120511
8. Rizzoli A, Silaghi C, Obiegala A, Rudolf I, Hubálek Z, Földvári G, et al. *Ixodes ricinus* and its transmitted pathogens in urban and peri-urban areas in Europe: new hazards and relevance for public health. Front Public Health. 2014;2:251. http://dx.doi.org/10.3389/fpubh.2014.00251
9. Allan BF, Keesing F, Ostfeld RS. Effect of forest fragmentation on Lyme disease risk. Conserv Biol. 2003;17:267–72. http://dx.doi.org/10.1046/j.1523-1739.2003.01260.x
10. Brownstein JS, Skelly DK, Holford TR, Fish D. Forest fragmentation predicts local scale heterogeneity of Lyme disease risk. Oecologia. 2005;146:469–75. http://dx.doi.org/10.1007/s00442-005-0251-9
11. Estrada-Peña A. Understanding the relationships between landscape connectivity and abundance of *Ixodes ricinus* ticks. Exp Appl Acarol. 2002;28:239–48. http://dx.doi.org/10.1023/A:1025362903620
12. LaDeau SL, Allan BF, Leisnham PT, Levy MZ. The ecological foundations of transmission potential and vector-borne disease in urban landscapes. Funct Ecol. 2015;29:889–901. http://dx.doi.org/10.1111/1365-2435.12487
13. Uspensky I. Tick pests and vectors (Acari: Ixodoidea) in European towns: introduction, persistence and management. Ticks Tick Borne Dis. 2014;5:41–7. http://dx.doi.org/10.1016/j.ttbdis.2013.07.011
14. Pepin KM, Eisen RJ, Mead PS, Piesman J, Fish D, Hoen AG, et al. Geographic variation in the relationship between human Lyme disease incidence and density of infected host-seeking *Ixodes scapularis* nymphs in the Eastern United States. Am J Trop Med Hyg. 2012;86:1062–71. http://dx.doi.org/10.4269/ajtmh.2012.11-0630

15. Diuk-Wasser MA, Gatewood AG, Cortinas MR, Yaremych-Hamer S, Tsao J, Kitron U, et al. Spatiotemporal patterns of host-seeking *Ixodes scapularis* nymphs (Acari: Ixodidae) in the United States. J Med Entomol. 2006;43:166–76. http://dx.doi.org/10.1093/jmedent/43.2.166
16. Falco RC, Fish D. A comparison of methods for sampling the deer tick, *Ixodes dammini*, in a Lyme disease endemic area. Exp Appl Acarol. 1992;14:165–73. http://dx.doi.org/10.1007/BF01219108
17. Clifford CM, Anastos G, Elbl A. The larval ixodid ticks of the eastern United States (Acarina-Ixodidae). Miscellaneous Publications of the Entomological Society of America. 1961;2:213–37.
18. Molaei G, Andreadis TG, Armstrong PM, Anderson JF, Vossbrinck CR. Host feeding patterns of *Culex* mosquitoes and West Nile virus transmission, northeastern United States. Emerg Infect Dis. 2006;12:468–74. http://dx.doi.org/10.3201/eid1203.051004
19. Barbour AG, Maupin GO, Teltow GJ, Carter CJ, Piesman J. Identification of an uncultivable *Borrelia* species in the hard tick *Amblyomma americanum*: possible agent of a Lyme disease-like illness. J Infect Dis. 1996;173:403–9. http://dx.doi.org/10.1093/infdis/173.2.403
20. Gazumyan A, Schwartz JJ, Liveris D, Schwartz I. Sequence analysis of the ribosomal RNA operon of the Lyme disease spirochete, *Borrelia burgdorferi.* Gene. 1994;146:57–65. http://dx.doi.org/10.1016/0378-1119(94)90833-8
21. Persing DH, Telford SR III, Spielman A, Barthold SW. Detection of *Borrelia burgdorferi* infection in *Ixodes dammini* ticks with the polymerase chain reaction. J Clin Microbiol. 1990;28:566–72.
22. University of Vermont Spatial Analysis Laboratory, NYC Urban Field Station. New York City Landcover 2010, 2012 [cited 2019 Jan 16]. https://www.nrs.fs.fed.us/nyc/local-resources/downloads/NYC_Urban_Field_Station_2014_Science_Plan.pdf
23. NYC Department of Information Technology and Telecommunications. NYC planimetric database, 2015 [cited 2019 Jan 15]. https://www1.nyc.gov/site/doitt/index.page
24. DeNicola AJ. Staten Island deer research program final summary report. New York City, NY; 2017 [cited 2019 Jan 16]. https://www.nrs.fs.fed.us/nyc/local-resources/downloads/2017_NYC_UFS_Progress_Report.pdf
25. McRae BH, Dickson BG, Keitt TH, Shah VB. Using circuit theory to model connectivity in ecology, evolution, and conservation. Ecology. 2008;89:2712–24. http://dx.doi.org/10.1890/07-1861.1
26. Girardet X, Conruyt-Rogeon G, Foltête JC. Does regional landscape connectivity influence the location of roe deer roadkill hotspots? Eur J Wildl Res. 2015;61:731–42. http://dx.doi.org/10.1007/s10344-015-0950-4
27. Kelly AC, Mateus-Pinilla NE, Brown W, Ruiz MO, Douglas MR, Douglas ME, et al. Genetic assessment of environmental features that influence deer dispersal: implications for prion-infected populations. Popul Ecol. 2014;56:327–40. http://dx.doi.org/10.1007/s10144-013-0427-9
28. Long ES, Difenbach DR, Rosenberry CS, Wallingford BD, Grund MD. Forest cover influences dispersal distance of white-tailed deer. J Mammal. 2005;86:623–9. http://dx.doi.org/10.1644/1545-1542(2005)86[623:FCIDDO]2.0.CO;2
29. Coulon A, Guillot G, Cosson J-F, Angibault JM, Aulagnier S, Cargnelutti B, et al. Genetic structure is influenced by landscape features: empirical evidence from a roe deer population. Mol Ecol. 2006; 15:1669–79. http://dx.doi.org/10.1111/j.1365-294X. 2006.02861.x
30. McRae B, Kavanagh D. Linkage mapper connectivity analysis software. Fort Collins (CO): The Nature Conservancy; 2011.
31. Venables WN, Ripley BD. Modern applied statistics with S, 4th ed. New York: Springer; 2002.
32. R Core Team. R: A language and environment for statistical computing. Vienna: R Foundation for Statistical Computing; 2017.
33. Burnham KP, Anderson DR. Model selection and multimodel inference: a practical information-theoretic approach. New York: Springer; 2002.
34. Fox J. Applied regression analysis and generalized linear models. Thousand Oaks (CA): Sage Publications; 2015.
35. Bartoń K. MuMIn: multi-model inference, 2018 [cited 2019 Jan 15]. https://rdrr.io/cran/MuMIn/man/MuMIn-package.html
36. McFadden D. Conditional logit analysis of qualitative choice behavior, 1973 [cited 2019 Jan 15]. https://eml.berkeley.edu/reprints/mcfadden/zarembka.pdf
37. Dennis DT, Nekomoto TS, Victor JC, Paul WS, Piesman J. Reported distribution of *Ixodes scapularis* and *Ixodes pacificus* (Acari: Ixodidae) in the United States. J Med Entomol. 1998;35:629–38. http://dx.doi.org/10.1093/jmedent/35.5.629
38. Eisen RJ, Eisen L, Beard CB. County-scale distribution of *Ixodes scapularis* and *Ixodes pacificus* (Acari: Ixodidae) in the continental United States. J Med Entomol. 2016;53:349–86. http://dx.doi.org/10.1093/jme/tjv237
39. Gittleman JL, Kot M. Adaptation: statistics and a null model for estimating phylogenetic effects. Syst Zool. 1990;39:227–41. http://dx.doi.org/10.2307/2992183
40. Knulle W, Rudolph D. Humidity relationships and water balance of ticks. In: Obenchain FD, Galun R, editors. Physiology of ticks. Oxford (UK): Pergamon Press Ltd.; 1982. p. 43–70.
41. Spielman A, Wilson ML, Levine JF, Piesman J. Ecology of *Ixodes dammini*–borne human babesiosis and Lyme disease. Annu Rev Entomol. 1985;30:439–60. http://dx.doi.org/10.1146/annurev.en.30.010185.002255
42. Kilpatrick HJ, LaBonte AM, Stafford KC III. The relationship between deer density, tick abundance, and human cases of Lyme disease in a residential community. J Med Entomol. 2014; 51:777–84. http://dx.doi.org/10.1603/ME13232
43. Ogden NH, Barker IK, Francis CM, Heagy A, Lindsay LR, Hobson KA. How far north are migrant birds transporting the tick *Ixodes scapularis* in Canada? Insights from stable hydrogen isotope analyses of feathers. Ticks Tick Borne Dis. 2015;6:715–20. http://dx.doi.org/10.1016/j.ttbdis.2015.06.004
44. Sonenshine DE, Roe MR, editors. Biology of ticks. New York: Oxford University Press; 2014.
45. New York City Wildlife. White-tailed deer (*Odocoileus virginianus*), 2018 [cited 2018 Oct 14]. https://www1.nyc.gov/site/wildlifenyc/animals/deer.page
46. Madhav NK, Brownstein JS, Tsao JI, Fish D. A dispersal model for the range expansion of blacklegged tick (Acari: Ixodidae). J Med Entomol. 2004;41:842–52. http://dx.doi.org/10.1603/0022-2585-41.5.842
47. Mechai S, Margos G, Feil EJ, Lindsay LR, Michel P, Kotchi SO, et al. Evidence for an effect of landscape connectivity on *Borrelia burgdorferi* sensu stricto dispersion in a zone of range expansion. Ticks Tick Borne Dis. 2018;9:1407–15. http://dx.doi.org/10.1016/j.ttbdis.2018.07.001
48. United Nations. Department of Economic and Social Affairs PD, 2014. World urbanization prospects: the 2014 revision, highlights (ST/ESA/SER.A/352), 2014 [cited 2019 Jan 15]. https://www.compassion.com/multimedia/world-urbanization-prospects.pdf
49. Jennings V, Baptiste AK, Osborne Jelks N, Skeete R. Urban green space and the pursuit of health equity in parts of the United States. Int J Environ Res Public Health. 2017;14:E1432. http://dx.doi.org/10.3390/ijerph14111432
50. McClure M, Diuk-Wasser M. Reconciling the entomological hazard and disease risk in the Lyme disease system. Int J Environ Res Public Health. 2018;15:1048. http://dx.doi.org/10.3390/ijerph15051048

Address for correspondence: Meredith C. VanAcker, Department of Ecology, Evolution, and Environmental Biology, Columbia University, 1102 Schermerhorn Extension Bldg, 1200 Amsterdam Ave, New York, NY 10027, USA; email: mv2640@columbia.edu

Use of Single-Injection Recombinant Vesicular Stomatitis Virus Vaccine to Protect Nonhuman Primates Against Lethal Nipah Virus Disease

Chad E. Mire, Joan B. Geisbert, Krystle N. Agans, Krista M. Versteeg, Daniel J. Deer, Benjamin A. Satterfield,[1] Karla A. Fenton, Thomas W. Geisbert

Nipah virus (NiV) is a zoonotic pathogen that causes high case-fatality rates (CFRs) in humans. Two NiV strains have caused outbreaks: the Malaysia strain (NiV_M), discovered in 1998–1999 in Malaysia and Singapore (≈40% CFR); and the Bangladesh strain (NiV_B), discovered in Bangladesh and India in 2001 (≈80% CFR). Recently, NiV_B in African green monkeys resulted in a more severe and lethal disease than NiV_M. No NiV vaccines or treatments are licensed for human use. We assessed replication-restricted single-injection recombinant vesicular stomatitis vaccine NiV vaccine vectors expressing the NiV glycoproteins against NiV_B challenge in African green monkeys. All vaccinated animals survived to the study endpoint without signs of NiV disease; all showed development of NiV F Ig, NiV G IgG, or both, as well as neutralizing antibody titers. These data show protective efficacy against a stringent and relevant NiV_B model of human infection.

Nipah virus (NiV) and Hendra virus (HeV) are highly pathogenic zoonotic agents in the paramyxovirus genus *Henipavirus*. Human case-fatality rates (CFRs) for these viruses historically have ranged from 40% to >90% (*1*). NiV is categorized as a Biosafety Level 4 (BSL-4) pathogen because of the substantial illness and death it causes and the lack of approved vaccines and therapeutic drugs for human use. In 2015, the World Health Organization listed NiV as a priority pathogen because it is likely to cause severe outbreaks and, in early 2018, placed NiV on the Blueprint list of priority diseases (https://www.who.int/blueprint/priority-diseases). This WHO designation was bolstered because of a deadly NiV outbreak (CFR 89%) during spring 2018 in southwestern India, where NiV had not previously been reported (*2*).

Author affiliations: Galveston National Laboratory, Galveston, Texas, USA; University of Texas Medical Branch, Galveston

DOI: https://doi.org/10.3201/eid2506.181620

Bats of the genus *Pteropus* are the primary reservoir in nature for NiV (*3*), but several other mammal species can be infected by NiV (*4–7*). Analysis of NiV genomes has identified 2 NiV strains responsible for outbreaks: Malaysia strain NiV_M and Bangladesh strain (NiV_B). NiV_M caused the first identified outbreak of NiV during 1998–1999 in Malaysia and Singapore (≈270 persons infected; CFR ≈40%) (*8*,*9*) and perhaps was responsible for a 2014 outbreak in the Philippines (CFR ≈52%); however, this speculation is based on short genomic reads, so the NiV strain that caused this outbreak is not known (*10*). NiV_B has caused repeated outbreaks in Bangladesh and northeastern India; outbreaks occurred almost every year during 2001–2015 (*11–15*). These NiV_B outbreaks had higher CFRs, averaging ≈80% (*14*), and showed documented human-to-human transmission (*11*,*16*).

Eight experimental preventive candidate vaccines against henipaviruses have been evaluated in NiV_M animal models: 1) canarypox and 2) vaccinia viruses encoding the NiV_M fusion protein (F) or the NiV_M attachment protein (G) that have shown protection against NiV_M in hamsters and pigs (*17*,*18*); 3) a recombinant adeno-associated vaccine expressing the NiV_M G protein that completely protected hamsters against homologous NiV_M challenge (*19*); 4) recombinant vesicular stomatitis viruses (rVSVs) expressing the NiV_M F protein or the NiV_M G protein that had 100% efficacy in hamsters against NiV_M (*20*); 5) rVSVs expressing the NiV_B F protein or the NiV_B G protein that completely protected ferrets from NiV_M disease (*21*); 6) an rVSV expressing the Zaire ebolavirus (EBOV) glycoprotein (GP) and the NiV_M G protein (rVSV-EBOV-GP-NiVG) that demonstrated efficacy in NiV_M hamster (*22*) and African green monkey (*Chlorocebus aethiops*) (*23*) models; 7) a recombinant measles virus vector expressing the NiV_M G

[1]Current affiliation: Mayo Clinic, Rochester, Minnesota, USA.

protein that had efficacy in the NiV_M African green monkey model (*24*); and 8) a recombinant subunit vaccine based on the HeV G protein (sG_{HeV}) that completely protected small animals against lethal HeV and NiV_M infections (*25–27*) and was efficacious in the robust African green monkey model of HeV (*28*) and NiV_M infection (*29*). Of 8 vaccines, the sG_{HeV} vaccine is furthest along in evaluation; it has received licensure as a veterinary vaccine for HeV in horses (Equivac HeV, Zoetis, https://www.zoetis.com) in Australia and is being considered as a human vaccine against NiV. When tested against NiV, these 8 vaccine vectors have been tested only against NiV_M infection in animal models, and although the antigenicity of these vaccines should not be a concern given that HeV G is an immunogen against NiV_M infection, there are new data on the NiV_B African green monkey model to consider as far as dose/regimen of vaccines.

NiV_B infection in African green monkeys is more pathogenic than NiV_M infection (*30*). This difference resulted in significantly reduced efficacy of antibody therapy because of temporal differences in viral load. Specifically, the human monoclonal antibody m102.4 that had been shown to completely protect African green monkeys against lethal NiV_M disease when treatment was delayed until day 5 after virus exposure provided no protection when African green monkeys were challenged with NiV_B and treated beginning at day 5 after virus challenge (*30*,*31*). Considering these new data, the current vaccines against NiV need to be evaluated for possible differences in dose/regimen against the more pathogenic NiV_B infection in the robust African green monkey model. To assess single-dose vaccine efficacy, we evaluated the rVSV vaccine vectors expressing either the NiV_B F or NiV_B G proteins 28 days after a single-dose vaccination in the NiV_B African green monkey model, which most faithfully recapitulates human disease (*5*,*30*).

Methods

rVSV Vaccine Vectors and NiV_B Challenge Stock

We recovered the rVSV NiV_B vaccines (rVSV-ΔG-NiV_B/F-GFP and rVSV-ΔG-NiV_B/G-GFP) and rVSV-ΔG-GFP using methods as previously described (*21*,*32*). The isolate of NiV_B used in this vaccine study was obtained from a fatal human case (200401066) described previously (*30*).

Statistical Analyses

Animal studies in BSL-4 and nonhuman primate work generally restrict the number of animals used, the volume of biological samples that can be obtained, and the ability to repeat assays independently and thus limit statistical analysis. Consequently, we present these data as the mean calculated from replicate samples, not replicate assays, and error bars represent SD across replicates (Figure 1, panels B, C, and D).

Animal Ethics Considerations and Experiments

Healthy adult African green monkeys were handled in the animal BSL-4 containment space at the Galveston National Laboratory (Galveston, TX, USA). Research was approved under animal protocol 1310040 by the University of Texas Medical Branch Institutional Animal Care and Use Committee (Appendix, https://wwwnc.cdc.gov/EID/article/25/6/18-1620-App1.pdf).

We used 10 adult African green monkeys weighing 3.5–6.0 kg in this study. One animal served as control (received G_{In}* rVSV-ΔG-GFP), and 3 animals per vaccine group received G* rVSV-ΔG-NiV_B/F-GFP, G* rVSV-ΔG-NiV_B/G-GFP, or rVSVΔG-NiV_B/F/G. For vaccination, animals were anesthetized with ketamine and vaccinated with $\approx 10^7$ PFU by intramuscular injection (day –28). Twenty-eight days after vaccination, the animals were exposed to $\approx 5 \times 10^5$ PFU of NiV_B; the dose was equally divided between the intratracheal and the intranasal routes for each animal. Animals were monitored for clinical signs of illness (i.e., temperature, respiration quality, blood count, and clinical pathologic findings) at 0, 3, 6, 8, 10, 15, 21, and 28 days postchallenge (dpc).

NiV_B Serum Neutralization Assays

We determined neutralization titers against NiV_B using a conventional serum neutralization assay. In brief, we serially diluted serum 5-fold or 2-fold depending on magnitude of neutralization titers and incubated with ≈100 PFU of NiV_B for 1 h at 37°C, as previously described (*30*).

RNA Isolation from NiV_B-Infected African Green Monkeys

We isolated RNA from NiV_B-infected animals as described previously (*30*). For viremia, we added 100 µL of blood to 600 µL of AVL viral lysis buffer (QIAGEN, https://www.qiagen.com) for RNA extraction. For virus load in tissue, we stored ≈100 mg in 1 mL RNAlater (QIAGEN) for 7 d to stabilize RNA, removed the RNA later completely, and homogenized tissues in 600 µL RLT buffer (QIAGEN) in a 2-mL cryovial using a tissue lyser (QIAGEN) and ceramic beads.

Detection of NiV_B Load

We isolated RNA from blood or tissues and assessed it using primers and probe targeting the N gene and the intergenic region between N and P genes of NiV_B for quantitative reverse transcription PCR (qRT-PCR). The probe used was 6FAM-5′CGT CAC ACA TCA GCT CTG ACA A 3′-6TAMRA (Life Technologies, https://www.thermofisher.com), as described previously (*30*).

Hematology and Serum Biochemistry

We assessed clinical pathology of NiV_B-infected African green monkeys by hematology and serum biochemistry

analysis as described previously (*30*). We performed the hematology assays using a laser-based hematologic analyzer (Beckman Coulter, https://www.beckmancoulter.com) and serum biochemistry analysis using a Piccolo point-of-care analyzer and Biochemistry Panel Plus analyzer discs (Abaxis, https://www.abaxis.com).

Histopathology and Immunohistochemistry

We performed necropsies on all animals and collected tissue samples of all major organs. We performed histopathologic and immunohistochemical examination and analyses as described previously (*30*).

Results

Immunization of African Green Monkeys and Measuring the Humoral Immune Response

Previously, single-injection, single-round replication rVSV vaccine vectors expressing the NiV_B F or NiV_B G proteins were described, characterized, and shown to be efficacious against NiV_B challenge in ferrets (*21*). To assess the efficacy of these vectors in the NiV_B African green monkey model, 4 groups of African green monkeys received a single intramuscular vaccination of rVSV vectors on day –28 (Figure 2). To analyze the antibody response to rVSV-ΔG-NiV_B vaccinations, we assessed circulating antibodies for neutralization activity against NiV_B before and after vaccination by using a 50% plaque-reduction neutralization titer ($PRNT_{50}$) assay. All 4 groups had no detectable neutralizing antibody titers before vaccination (Table 1, day –28). On the day of challenge, the control animal (C-1) did not have detectable neutralizing antibody titers against NiV_B, whereas all animals from the specific NiV protein vaccination groups (F, G, and F/G) had detectable neutralizing antibodies against NiV_B (Table 1, day 0). Overall, the detectable neutralizing antibody response against NiV_B reached a 1:640 dilution titer in the G and F/G groups and from 1:160 to 1:640 in the F group.

NiV_B Challenge and Viral Load of Vaccinated African Green Monkeys

To determine the efficacy of the rVSV-ΔG-NiV_B vectors against NiV_B disease in African green monkeys, we challenged these animals by combined intratracheal and intranasal routes with a lethal challenge dose of NiV_B on day 0 (Figure 1). All African green monkeys were closely monitored for up to 28 dpc for clinical signs of illness. The NiV_B antigen vaccinated animals in the F (F-1–3), G (G-1–3), and F/G (F/G-1–3) groups showed no signs of clinical illness (Table 2) and were 100% protected against NiV_B challenge (Figure 1, panel A), whereas the animal in the nonspecific vaccinated control group (C-1) exhibited clinical signs of disease (Table 2) and died of infection on day 8 (Figure 1, panel A). In addition, the control animal was the only NiV_B-infected animal to have lymphopenia and serosanguinous nasal discharge during the course of disease (Table 2).

To determine the level of NiV_B replication in animals after challenge, we assessed viral load by qRT-PCR on

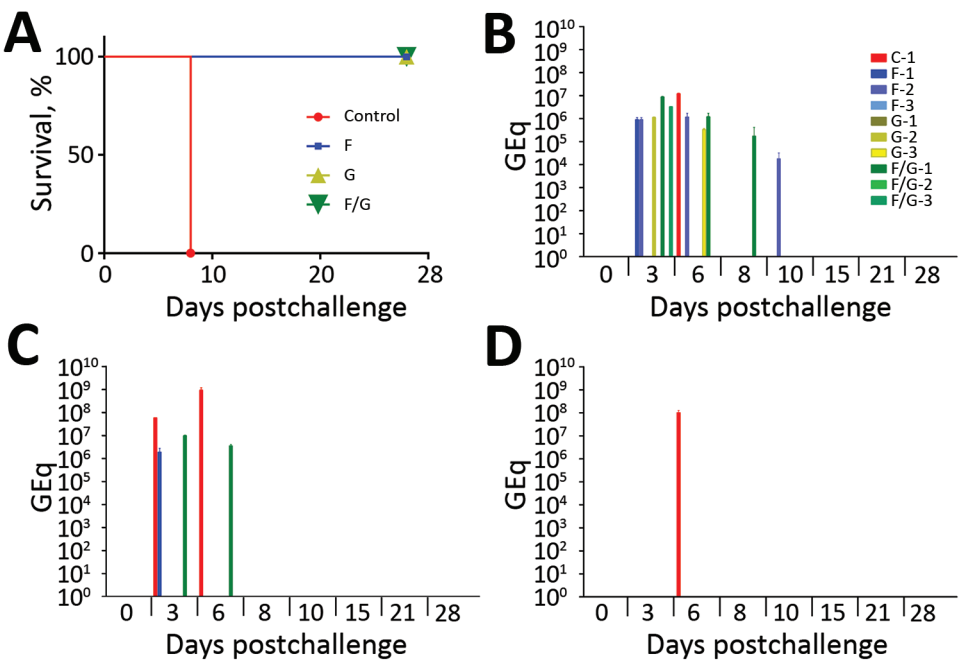

Figure 1. Protection of African green monkeys (*Chlorocebus aethiops*) from Nipah virus Bangladesh strain (NiV_B)–mediated disease and viral load. A) Kaplan-Meier survival curve for each vaccine group and historical controls after NiV_B challenge: controls (vaccine, n = 1; historical, n = 14), F group (n = 3), G group (n = 3), and F/G group (n = 3). C–D) Viral load in the animals as detected by NiV_B GEq by reverse transcription quantitative PCR from nasal swab samples: as GEq per swab (B), oral swab samples as GEq per swab (C), and blood as GEq/mL (D). Red, control group (G_{Ind}*rVSV-ΔG-GFP expressing no glycoprotein); blue, F group (G_{Ind}* rVSV-NiV_B /F-GFP expressing the NiV_B F protein); yellow, G group (G_{Ind}*rVSV-NiV_B/G-GFP expressing the NiV_B G protein); green, F/G group (single-cycle infectious virions with NiV_B F and G proteins on the cell surface). Error bars indicate SD. C, control; F, fusion; G, attachment; GEq, genome equivalent.

Table 1. NiV_B serum neutralization titers in vaccinated African green monkeys (*Chlorocebus aethiops*)*

Vaccine	Animal no.	Day −28†	Day 0†	Day 28†
None	C-1	<20	<20	40‡
F only vaccine	F-1	<20	640	1,280
	F-2	<20	160	2,560
	F-3	<20	320	5,120
G only vaccine	G-1	<20	640	5,120
	G-2	<20	640	5,120
	G-3	<20	640	5,120
F+G vaccine	F/G-1	<20	640	2,560
	F/G-2	<20	640	5,120
	F/G-3	<20	640	2,560

*Titers are reciprocal serum dilution at which 50% of virus was neutralized. NiV, Nipah virus; NiV_B, NiV Bangladesh strain.
†Day postchallenge.
‡Terminal day 8 postchallenge.

nasal and oral swab samples and whole blood samples (Figure 1, panels B–D). We detected NiV_B genome equivalents (GEq) from nasal swab samples (Figure 1, panel B) in the control, F, G, and F/G groups. The following animals were positive for viral RNA: C-1 at 6 dpc; F-1 at 3 dpc; F-2 at 3, 6, and 10 dpc; G-1 at 3 dpc; G-3 at 6 dpc; F/G-1 at 3, 6, and 8 dpc; and F/G-3 at 3 dpc. At 6 dpc, when C-1 was positive for NiV RNA in nasal swab samples, the levels were >1 log higher than they were for the NiV-antigen vaccinated groups F, G, and F/G. Oral swab samples were negative for NiV RNA in all animals in the G-vaccinated group (Figure 1, panel C), and NiV_B GEq were detected from oral swab samples in the control, F, and F/G groups. The following animals were positive for viral RNA: C-1 at 3 and 6 dpc, F-1 at 3 dpc, and F/G-1 at 3 and 6 dpc. Within these oral swab sample results, C-1 had NiV RNA levels up to 100-fold higher than the F and F/G animals that had positive oral swab samples (Figure 1, panel C). Unlike the results for swab samples, which represent tissues initially exposed to NiV, systemic and circulating NiV_B GEq were not detected in whole blood from animals in the F, G, and F/G groups, whereas the control animal was positive in the blood sample from 6 dpc (Figure 1, panel D). The lack of systemic and circulating detection of NiV_B RNA correlated with survival (Table 2; Figure 1, panel A).

Gross Pathologic, Histopathologic, and Immunohistochemical Analyses of NiV_b-Infected African Green Monkeys

In the F, G, and F/G groups, we observed no gross pathologic findings at study endpoint. However, in the control animal that died of NiV_B infection, gross pathologic findings included serosanguinous pleural effusion, failure of all lung lobes to collapse with severe pulmonary hemorrhage and congestion, and multifocal to coalescing hemorrhage of the mucosal surface of the urinary bladder.

Lung sections examined from the control animal had moderate lymphoplasmacytic interstitial pneumonia characterized by a diffuse thickening of alveolar septae by moderate numbers of lymphocytes, plasma cells, polymerized fibrin, and edema fluid. The alveolar spaces were flooded by edema fluid, polymerized fibrin, foamy alveolar macrophages, and cellular debris. Endothelial syncytial cells were most apparent in medium- to small- caliber vessels (Figure 3, panel A). The animals in the F, G, and F/G groups had no major histologic findings in the lung sections (Figure 3, panels C, E, G). Immunohistochemical analysis revealed strong NiV antigen immunoreactivity within scattered alveolar macrophages and the endothelium of the alveolar septae and syncytial cells within medium- to small- caliber vessels in up to ≈75% of the examined pulmonary tissues (Figure 3, panel B). The lung sections of the F, G, and F/G groups were devoid of detectable NiV antigen (Figure 3, panels D, F, H).

Spleen sections from the control animal were depleted of lymphocytes in the multifocal follicular germinal centers within the splenic white pulp and were effaced by hemorrhage, fibrin, syncytial cell formation (Figure 4, panel A). Spleens from the F, G, and F/G groups had no major histologic findings (Figure 4, panels C, E, G). Immunohistochemical analysis of the spleen from the

Table 2. Clinical findings and outcome of Nipah virus Bangladesh strain–challenged African green monkeys*

Animal no.	Sex	Group	Clinical illness	Clinical and gross pathology findings†
C-1	F	Control ΔG vaccine	Loss of appetite (d 6–8); labored breathing (d 6–8). Died on d 8.	Lymphopenia (d 6); serosanguinous nasal and oral discharge (d 8), serosanguinous pleural fluid, severely inflated, enlarged lungs with severe congestion and hemorrhage of all lobes, multifocal to coalescing hemorrhage of the mucosal surface of the urinary bladder.
F-1	F	F vaccine	None	Thrombocytopenia (d 15); >3 fold increase in ALT (d 6), >3 fold increase in AST
F-2	M	F vaccine	None	None
F-3	M	F vaccine	None	Increase in CRP (d 6)
G-1	F	G vaccine	None	None
G-2	M	G vaccine	None	None
G-3	M	G vaccine	None	None
F/G-1	F	F + G vaccine	None	Increase in CRP (d 8)
F/G-2	M	F + G vaccine	None	Thrombocytopenia (d 21, d 28); increase in CRP (d 8, d 10, d 15)
F/G-3	M	F + G vaccine	None	Thrombocytopenia (d 8)

*ALT, alanine aminotransferase; AST, aspartate aminotransferase; CRP, C-reactive protein.
†Lymphopenia is defined as a ≥30% decrease in number of lymphocytes; thrombocytopenia is defined as a ≥30% decrease in number of platelets.

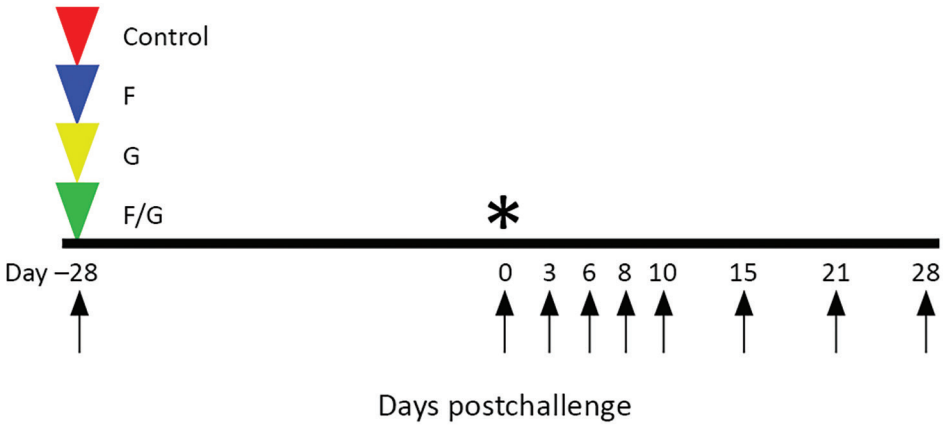

Figure 2. Groups of African green monkeys (*Chlorocebus aethiops*) receiving recombinant vesicular stomatitis virus (rVSV) vaccine against Nipah virus Bangladesh strain (NiV_B). Triangles indicate days of vaccination; arrows indicate days of sampling; and asterisk (*) indicates day of challenge. Red indicates control group (G_{Ind}*rVSV-ΔG-GFP expressing no glycoprotein); blue indicates F group (G_{Ind}* rVSV-NiV_B/F-GFP expressing the NiV_B F protein); yellow indicates G group (G_{Ind}*rVSV-NiV_B /G-GFP expressing the NiV_B G protein); F/G group (single-cycle infectious virions with NiV_B F and G proteins on the cell surface). F, fusion; G, attachment

control animal revealed strong immunoreactivity for NiV antigen within the endothelium, syncytial cells, and scattered mononuclear cells in up to ≈50% of the examined splenic tissue (Figure 4, panel B), whereas the spleen sections of groups F, G, and F/G were devoid of detectable NiV antigen (Figure 4, panels D, F, H).

Discussion

An important step in the preclinical development of a vaccine is efficacy testing in standards of animal models of disease. For NiV, the standard is the African green monkey model. Although the initial studies on the NiV_M model in African green monkeys were reported as near uniformly lethal, data from several groups have revealed the model is not 100% lethal, depending on dose and route of infection (*5*,*24*,*29–31*,*33*,*34*). Combining the control animals from these studies, in which African green monkeys were challenged with various combinations of routes (e.g., intratracheal, intranasal, intraperitoneal, oral, small particle aerosol) at various doses, revealed that 18 (72%) of 25 animals died; however, most of the control animals were positive for circulating NiV RNA and had signs of clinical disease to varying degrees. Historically, our previous studies with the NiV_B model has resulted in the deaths of all 14 control African green monkeys; the mean time to death was 7.14 days (Figure 1, panel A). We recently compared the pathogenesis of NiV_M and NiV_B strains in African green monkeys and observed that NiV_B caused more pulmonary and splenic pathologic findings (*30*). We also observed the efficacy of time to treatment post-NiV challenge with a human monoclonal antibody m102.4 was shorter for NiV_B-infected animals than for NiV_M-infected animals (*30*). With these animal data in mind and the fact that NiV_B has been responsible for most NiV outbreaks since 2002, we wanted to test our rVSV NiV vaccine vectors expressing NiV_B F and G proteins as immunogens, which had 100% efficacy against NiV_M challenge in ferrets (*21*), against NiV_B challenge in African green monkeys.

In this study, we vaccinated 1 control African green monkey with a nonglycoprotein rVSV vector control, G_{Ind}* rVSV-ΔG-GFP, and 3 groups of 3 African green monkeys with NiV antigen vectors: G_{Ind}* rVSV-ΔG-NiV_B/F-GFP, G_{Ind}* rVSV-ΔG-NiV_B/G-GFP, or G_{Ind}* rVSV-ΔG-NiV_B/F/G-GFP. The control animal, C-1, did not develop NiV_B neutralizing antibodies by the day of challenge; had detectable circulating NiV RNA at 6 dpc; had clinical signs of NiV-mediated disease; and ultimately died of infection, showing typical NiV gross pathology and histopathologic findings. Conversely, the 3 rVSV NiV vaccine groups had animals in which detectable circulating NiV F, G, or F and G IgG developed, and circulating neutralizing antibody titers developed in all 3 groups by 28 days postvaccination. Each vaccine cohort had detectable NiV_B RNA in nasal swab samples and only the F and F/G groups in oral swab samples, but none of the cohorts had any detectable circulating NiV_B RNA throughout the course of the study. Consistent with the vaccine response from each cohort and the control of systemic spread of NiV_B infection and control of NiV-mediated disease, all of the specifically vaccinated African green monkeys survived NiV_B challenge.

The results of this study are similar to what we observed with these rVSV NiV constructs in the ferret model, which showed 100% protection regardless of the vaccine construct (*21*). Differences were that we found higher $PRNT_{50}$ results for neutralizing antibody titers on day of challenge in this study and detected no circulating NiV RNA in the African green monkeys but did have detectable viral RNA at 6 dpc in the ferret study. Although we

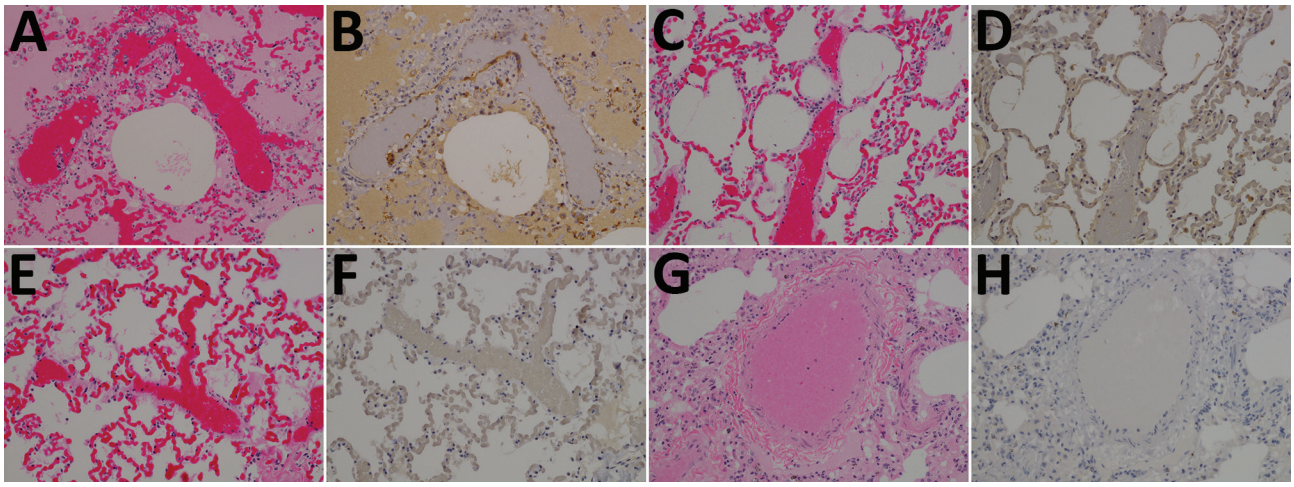

Figure 3. Results of testing for Nipah virus (NiV) in lung tissue from representative vaccinated African green monkeys (*Chlorocebus aethiops*). A, C, E, G) Hematoxylin and eosin staining; B, D, F, H) immunohistochemistry of tissues labeled with NiV N protein–specific polyclonal rabbit antibody. In stained tissue from the control animal (A), diffuse thickening of alveolar septae by moderate numbers of lymphocytes, plasma cells, polymerized fibrin, and edema fluid within the alveolar spaces were found; stained sections examined from the NiV F (C), NiV G (E), and NiV F/G (G) groups were unremarkable in comparison with sections from the control animal. In antibody-labeled tissue from the control animal (B), strong immunolabeling for NiV antigen with alveolar septae, scattered alveolar macrophages, and the endothelium of small caliber vessels were found, including syncytial cells with strong cytoplasmic immunolabeling for NiV antigen; no immunolabeling for NiV antigen was identified from the NiV F (D), NiV G (F), and NiV F/G (H) groups. Original magnification ×20.

did not detect circulating viral RNA in the African green monkeys, the increase of neutralizing antibody titers at the study endpoint suggests sterilizing immunity was not achieved, and dosing or regimen will require further testing to reach sterilizing immunity with this single-round replication vaccine vector.

The single-round replication rVSV NiV vectors in this study and the replication-competent rVSV-EBOV-GP-NiVG (*23*) are the only vaccine vectors to show 100% single-dose vaccine efficacy against NiV in the African green monkey model. Although both studies used this model, they differed in several ways. Our study used NiV_B and challenged through the intratracheal and intranasal routes, whereas the other study used NiV_M by the intratracheal route only (intratracheal challenge route used in initial model [*5*]). Here, we report detectable levels of NiV RNA in nasal swab samples at early times postchallenge, whereas the rVSV-EBOV-GP-NiVG study did not report any detectable NiV RNA in nasal swab samples. Whether these differences resulted from use of the intranasal route as part of the challenge cannot be determined here; however, neither study reported circulating levels of NiV RNA, indicating the prevention of systemic spread of NiV infection. Both studies reported the detection of circulating neutralizing antibodies on the day of challenge (28 [this study] and 29 days postvaccination). However, we reported on PFU reduction, and the rVSV-EBOV-GP-NiVG study reported on reduction of 200 50% tissue culture infectious dose in a tissue culture infectious dose assay, so the peak neutralizing titers at NiV challenge cannot be directly compared.

The $PRNT_{50}$ titers we reported can be directly compared with the recombinant subunit sG_{HeV} vaccine NiV study in African green monkeys that also was 100% efficacious (*29*), whereas we detected higher $PRNT_{50}$ titers against NiV from the single injection of single-round replication vectors (from 160 to 640; Table 1) versus the $PRNT_{50}$ titers 2 weeks after boost vaccination (from 28 to 379) for the recombinant subunit sG_{HeV} vaccine. However, these lower titers most likely are due to the sG_{HeV} vaccine being heterotypic because the $PRNT_{50}$ titers against HeV in a similar African green monkey study were 640–1,280 on day of challenge (*28*). The development of neutralizing antibodies to the NiV glycoproteins after vaccination are important for protection, as highlighted by a single monoclonal antibody against the henipavirus G protein, m102.4, that is 100% protective against HeV, NiV_M, and NiV_B when administered at least 3 dpc (*30*,*31*,*35*).

In our study, the F cohort did not produce as consistent a neutralizing antibody titer response as did the G and F/G cohorts. Further analysis also revealed that, although no major changes occurred in hematologic and blood chemistry results for any of the vaccine cohorts, minor changes occurred in the F and F/G cohorts (Table 1). These data, taken together with the lack of detectable NiV_B RNA in the oral swab samples of the G group, suggest the rVSV NiV G vector might be the better option among the 3 vaccine vectors.

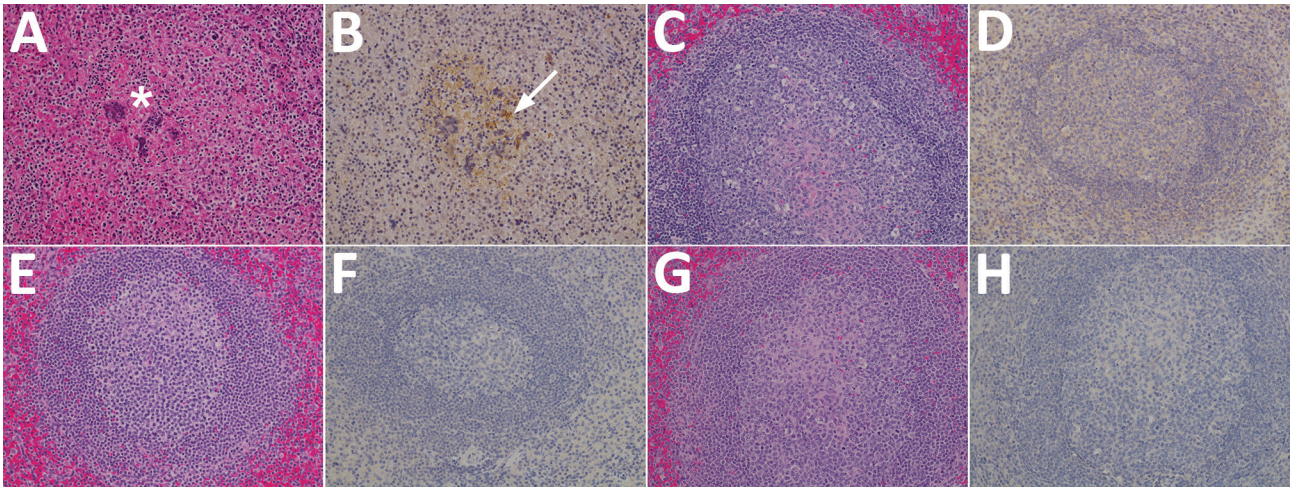

Figure 4. Results of testing for Nipah virus (NiV) in spleen tissue from representative vaccinated African green monkeys (*Chlorocebus aethiops*). A, C, E, G) Hematoxylin and eosin staining; B, D, F, H) immunohistochemistry of tissues labeled with NiV N protein–specific polyclonal rabbit antibody. In stained tissue from the control animal (A), moderate necrosis and drop out of the white pulp (*), with hemorrhage, and fibrin within germinal centers are seen; stained sections examined from the NiV F (C), NiV G (E), and NiV F/G (G) groups were devoid of any significant lesions compared with sections from the control animal. In antibody-labeled tissues from the control animal (B), strong immunolabeling for NiV antigen with scattered mononuclear cells (white arrow) and syncytial cells within germinal centers were found, and the endothelium of small caliber vessels had strong cytoplasmic immunolabeling for NiV antigen; no immunolabeling for NiV antigen was identified from the NiV F (D), NiV G (F), and NiV F/G (H) groups. Original magnification ×20.

In summary, we found that single-round replication rVSV vectors against NiV_B provided 100% efficacy against NiV_B challenge using a single-dose regimen. The rVSV vaccine platform has received attention recently because the replication-competent rVSV-ZEBOV GP vaccine vector against EBOV has now been given to >16,000 humans in clinical trials ranging from phase 1 to phase 3 and has been safe and efficacious (*36*); however, data for pregnant women and immunocompromised persons are not yet available. A single-round replication rVSV vaccine vector that is immunogenic and efficacious would have an attractive safety profile. Whether these single-round replication rVSV NiV vaccine vectors are as safe as the recombinant subunit sG_{HeV} vaccine has yet to be determined, and the subunit vaccine has yet to be tested with a single-dose vaccine regimen. Although multidose vaccine regimens would be a potential strategy for laboratory and healthcare workers and for first responders in stable settings with defined risk for an NiV outbreak, an outbreak setting or a case of deliberate release of NiV would require rapid protection with a single administration of vaccine. The single-dose strategy was successfully enacted using a close-contact ring vaccination strategy with the rVSV-ZEBOV-GP vaccine at the end of the 2013–2016 EBOV epidemic (*37–39*). The strategy was so successful that it became the World Health Organization recommendation for future EBOV outbreaks and has recently been set into motion in the ongoing outbreak in the Democratic Republic of the Congo (*40*). Recent studies also suggest that the ring vaccination strategy for viruses such as EBOV (depending on transmissibility) that are endemic to countries that might not be able to afford a mass herd-immunity vaccination strategy might be more effective than mass vaccinations at controlling outbreaks (*41*). Further studies should examine the time to immunity of the G_{Ind}* rVSV-ΔG-NiV_B/G in the NiV_B African green monkey model because these data will be instrumental in providing information about whether this vaccine vector could be implemented in a ring vaccination strategy during future NiV outbreaks, such as the current one in India (*2*).

Acknowledgments

We thank the staff of the University of Texas Medical Branch Animal Resources Center for animal husbandry, Robert W. Cross for assistance with the animal study, and Natalie Dobias for assistance with histologic processing. We thank Thomas G. Ksiazek for kindly providing the NiV_B isolate used in this study.

This study was supported in part by National Institutes of Health (U01 AI082121 for research and UC7AI094660 for BSL-4 operations) and by funds provided to T.W.G. by the UTMB Department of Microbiology and Immunology.

About the Author

Dr. Mire is an associate professor in the Department of Microbiology and Immunology at the University of Texas Medical Branch–Galveston and the Galveston National Laboratory. His research focuses on understanding host–pathogen interactions of highly pathogenic RNA viruses.

References

1. Wang L, Harcourt BH, Yu M, Tamin A, Rota PA, Bellini WJ, et al. Molecular biology of Hendra and Nipah viruses. Microbes Infect. 2001;3:279–87. http://dx.doi.org/10.1016/S1286-4579(01)01381-8
2. Chatterjee P. Nipah virus outbreak in India. Lancet. 2018;391:2200. http://dx.doi.org/10.1016/S0140-6736(18)31252-2
3. Halpin K, Hyatt AD, Fogarty R, Middleton D, Bingham J, Epstein JH, et al.; Henipavirus Ecology Research Group. Pteropid bats are confirmed as the reservoir hosts of henipaviruses: a comprehensive experimental study of virus transmission. Am J Trop Med Hyg. 2011;85:946–51. http://dx.doi.org/10.4269/ajtmh.2011.10-0567
4. Bossart KN, Zhu Z, Middleton D, Klippel J, Crameri G, Bingham J, et al. A neutralizing human monoclonal antibody protects against lethal disease in a new ferret model of acute Nipah virus infection. PLoS Pathog. 2009;5:e1000642. http://dx.doi.org/10.1371/journal.ppat.1000642
5. Geisbert TW, Daddario-DiCaprio KM, Hickey AC, Smith MA, Chan YP, Wang LF, et al. Development of an acute and highly pathogenic nonhuman primate model of Nipah virus infection. PLoS One. 2010;5:e10690. http://dx.doi.org/10.1371/journal.pone.0010690
6. Hooper P, Zaki S, Daniels P, Middleton D. Comparative pathology of the diseases caused by Hendra and Nipah viruses. Microbes Infect. 2001;3:315–22. http://dx.doi.org/10.1016/S1286-4579(01)01385-5
7. Wong KT, Grosjean I, Brisson C, Blanquier B, Fevre-Montange M, Bernard A, et al. A golden hamster model for human acute Nipah virus infection. Am J Pathol. 2003;163:2127–37. http://dx.doi.org/10.1016/S0002-9440(10)63569-9
8. Chua KB, Bellini WJ, Rota PA, Harcourt BH, Tamin A, Lam SK, et al. Nipah virus: a recently emergent deadly paramyxovirus. Science. 2000;288:1432–5. http://dx.doi.org/10.1126/science.288.5470.1432
9. Uppal PK. Emergence of Nipah virus in Malaysia. Ann N Y Acad Sci. 2000;916:354–7. http://dx.doi.org/10.1111/j.1749-6632.2000.tb05312.x
10. Ching PKG, de los Reyes VC, Sucaldito MN, Tayag E, Columna-Vingno AB, Malbas FF Jr, et al. Outbreak of henipavirus infection, Philippines, 2014. Emerg Infect Dis. 2015;21:328–31. http://dx.doi.org/10.3201/eid2102.141433
11. Gurley ES, Montgomery JM, Hossain MJ, Bell M, Azad AK, Islam MR, et al. Person-to-person transmission of Nipah virus in a Bangladeshi community. Emerg Infect Dis. 2007;13:1031–7. http://dx.doi.org/10.3201/eid1307.061128
12. Harcourt BH, Lowe L, Tamin A, Liu X, Bankamp B, Bowden N, et al. Genetic characterization of Nipah virus, Bangladesh, 2004. Emerg Infect Dis. 2005;11:1594–7. http://dx.doi.org/10.3201/eid1110.050513
13. Hsu VP, Hossain MJ, Parashar UD, Ali MM, Ksiazek TG, Kuzmin I, et al. Nipah virus encephalitis reemergence, Bangladesh. Emerg Infect Dis. 2004;10:2082–7. http://dx.doi.org/10.3201/eid1012.040701
14. Lo MK, Lowe L, Hummel KB, Sazzad HM, Gurley ES, Hossain MJ, et al. Characterization of Nipah virus from outbreaks in Bangladesh, 2008–2010. Emerg Infect Dis. 2012;18:248–55. http://dx.doi.org/10.3201/eid1802.111492
15. Luby SP, Hossain MJ, Gurley ES, Ahmed BN, Banu S, Khan SU, et al. Recurrent zoonotic transmission of Nipah virus into humans, Bangladesh, 2001–2007. Emerg Infect Dis. 2009;15:1229–35. http://dx.doi.org/10.3201/eid1508.081237
16. Homaira N, Rahman M, Hossain MJ, Epstein JH, Sultana R, Khan MS, et al. Nipah virus outbreak with person-to-person transmission in a district of Bangladesh, 2007. Epidemiol Infect. 2010;138:1630–6. http://dx.doi.org/10.1017/S0950268810000695
17. Guillaume V, Contamin H, Loth P, Georges-Courbot MC, Lefeuvre A, Marianneau P, et al. Nipah virus: vaccination and passive protection studies in a hamster model. J Virol. 2004;78:834–40. http://dx.doi.org/10.1128/JVI.78.2.834-840.2004
18. Weingartl HM, Berhane Y, Caswell JL, Loosmore S, Audonnet J-C, Roth JA, et al. Recombinant Nipah virus vaccines protect pigs against challenge. J Virol. 2006;80:7929–38. http://dx.doi.org/10.1128/JVI.00263-06
19. Ploquin A, Szécsi J, Mathieu C, Guillaume V, Barateau V, Ong KC, et al. Protection against henipavirus infection by use of recombinant adeno-associated virus-vector vaccines. J Infect Dis. 2013;207:469–78. http://dx.doi.org/10.1093/infdis/jis699
20. Lo MK, Bird BH, Chattopadhyay A, Drew CP, Martin BE, Coleman JD, et al. Single-dose replication-defective VSV-based Nipah virus vaccines provide protection from lethal challenge in Syrian hamsters. Antiviral Res. 2014;101:26–9. http://dx.doi.org/10.1016/j.antiviral.2013.10.012
21. Mire CE, Versteeg KM, Cross RW, Agans KN, Fenton KA, Whitt MA, et al. Single injection recombinant vesicular stomatitis virus vaccines protect ferrets against lethal Nipah virus disease. Virol J. 2013;10:353. http://dx.doi.org/10.1186/1743-422X-10-353
22. DeBuysscher BL, Scott D, Marzi A, Prescott J, Feldmann H. Single-dose live-attenuated Nipah virus vaccines confer complete protection by eliciting antibodies directed against surface glycoproteins. Vaccine. 2014;32:2637–44. http://dx.doi.org/10.1016/j.vaccine.2014.02.087
23. Prescott J, DeBuysscher BL, Feldmann F, Gardner DJ, Haddock E, Martellaro C, et al. Single-dose live-attenuated vesicular stomatitis virus-based vaccine protects African green monkeys from Nipah virus disease. Vaccine. 2015;33:2823–9. http://dx.doi.org/10.1016/j.vaccine.2015.03.089
24. Yoneda M, Georges-Courbot M-C, Ikeda F, Ishii M, Nagata N, Jacquot F, et al. Recombinant measles virus vaccine expressing the Nipah virus glycoprotein protects against lethal Nipah virus challenge. PLoS One. 2013;8:e58414. http://dx.doi.org/10.1371/journal.pone.0058414
25. Mungall BA, Middleton D, Crameri G, Bingham J, Halpin K, Russell G, et al. Feline model of acute nipah virus infection and protection with a soluble glycoprotein-based subunit vaccine. J Virol. 2006;80:12293–302. http://dx.doi.org/10.1128/JVI.01619-06
26. Pallister J, Middleton D, Wang LF, Klein R, Haining J, Robinson R, et al. A recombinant Hendra virus G glycoprotein-based subunit vaccine protects ferrets from lethal Hendra virus challenge. Vaccine. 2011;29:5623–30. http://dx.doi.org/10.1016/j.vaccine.2011.06.015
27. Pallister JA, Klein R, Arkinstall R, Haining J, Long F, White JR, et al. Vaccination of ferrets with a recombinant G glycoprotein subunit vaccine provides protection against Nipah virus disease for over 12 months. Virol J. 2013;10:237. http://dx.doi.org/10.1186/1743-422X-10-237
28. Mire CE, Geisbert JB, Agans KN, Feng YR, Fenton KA, Bossart KN, et al. A recombinant Hendra virus G glycoprotein subunit vaccine protects nonhuman primates against Hendra virus challenge. J Virol. 2014;88:4624–31. http://dx.doi.org/10.1128/JVI.00005-14
29. Bossart KN, Rockx B, Feldmann F, Brining D, Scott D, LaCasse R, et al. A Hendra virus G glycoprotein subunit vaccine protects African green monkeys from Nipah virus challenge. Sci Transl Med. 2012;4:146ra107. http://dx.doi.org/10.1126/scitranslmed.3004241
30. Mire CE, Satterfield BA, Geisbert JB, Agans KN, Borisevich V, Yan L, et al. Pathogenic differences between Nipah virus Bangladesh and Malaysia strains in primates: implications for

antibody therapy. Sci Rep. 2016;6:30916. http://dx.doi.org/10.1038/srep30916
31. Geisbert TW, Mire CE, Geisbert JB, Chan YP, Agans KN, Feldmann F, et al. Therapeutic treatment of Nipah virus infection in nonhuman primates with a neutralizing human monoclonal antibody. Sci Transl Med. 2014;6:242ra82. http://dx.doi.org/10.1126/scitranslmed.3008929
32. Whitt MA, Geisbert TW, Mire CE. Single-vector, single-injection recombinant vesicular stomatitis virus vaccines against high-containment viruses. Methods Mol Biol. 2016;1403:295–311. http://dx.doi.org/10.1007/978-1-4939-3387-7_16
33. Cong Y, Lentz MR, Lara A, Alexander I, Bartos C, Bohannon JK, et al. Loss in lung volume and changes in the immune response demonstrate disease progression in African green monkeys infected by small-particle aerosol and intratracheal exposure to Nipah virus. PLoS Negl Trop Dis. 2017;11:e0005532. http://dx.doi.org/10.1371/journal.pntd.0005532
34. Johnston SC, Briese T, Bell TM, Pratt WD, Shamblin JD, Esham HL, et al. Detailed analysis of the African green monkey model of Nipah virus disease. PLoS One. 2015;10:e0117817. http://dx.doi.org/10.1371/journal.pone.0117817
35. Bossart KN, Geisbert TW, Feldmann H, Zhu Z, Feldmann F, Geisbert JB, et al. A neutralizing human monoclonal antibody protects African green monkeys from hendra virus challenge. Sci Transl Med. 2011;3:105ra103. http://dx.doi.org/10.1126/scitranslmed.3002901
36. Suder E, Furuyama W, Feldmann H, Marzi A, de Wit E. The vesicular stomatitis virus-based Ebola virus vaccine: from concept to clinical trials. Hum Vaccin Immunother. 2018;14:2107–13. http://dx.doi.org/10.1080/21645515.2018.1473698
37. Gsell PS, Camacho A, Kucharski AJ, Watson CH, Bagayoko A, Nadlaou SD, et al. Ring vaccination with rVSV-ZEBOV under expanded access in response to an outbreak of Ebola virus disease in Guinea, 2016: an operational and vaccine safety report. Lancet Infect Dis. 2017;17:1276–84. http://dx.doi.org/10.1016/S1473-3099(17)30541-8
38. Henao-Restrepo AM, Camacho A, Longini IM, Watson CH, Edmunds WJ, Egger M, et al. Efficacy and effectiveness of an rVSV-vectored vaccine in preventing Ebola virus disease: final results from the Guinea ring vaccination, open-label, cluster-randomised trial (Ebola Ça Suffit!). Lancet. 2017;389:505–18. http://dx.doi.org/10.1016/S0140-6736(16)32621-6
39. Henao-Restrepo AM, Longini IM, Egger M, Dean NE, Edmunds WJ, Camacho A, et al. Efficacy and effectiveness of an rVSV-vectored vaccine expressing Ebola surface glycoprotein: interim results from the Guinea ring vaccination cluster-randomised trial. Lancet. 2015;386:857–66. http://dx.doi.org/10.1016/S0140-6736(15)61117-5
40. Wise J. WHO is “cautiously optimistic” about Ebola ring vaccination programme in DRC. BMJ. 2018;361:k2388. http://dx.doi.org/10.1136/bmj.k2388
41. Masterson SG, Lobel L, Carroll MW, Wass MN, Michaelis M. Herd immunity to Ebolaviruses is not a realistic target for current vaccination strategies. Front Immunol. 2018;9:1025. http://dx.doi.org/10.3389/fimmu.2018.01025

Address for correspondence: Thomas W. Geisbert, University of Texas Medical Branch, Microbiology and Immunology, 301 University Blvd, Galveston, TX 77550-0610, USA; email: twgeisbe@utmb.edu

Performance of 2 Commercial Serologic Tests for Diagnosing Zika Virus Infection

Séverine Matheus, Cheikh Talla, Bhety Labeau, Franck de Laval, Sébastien Briolant, Lena Berthelot, Muriel Vray, Dominique Rousset

Reliable serologic tests are needed for diagnosis and surveillance of Zika virus infection. We evaluated the Euroimmun and Dia.Pro serologic tests for detection of Zika virus IgM and IgG by using a panel of 199 samples from a region endemic for flaviviruses. Kinetics of Zika virus antibodies were monitored from 300 sequential specimens sampled over a period of 10 months after infection. We observed suboptimal performance; sensitivity for Zika virus IgM was low, especially in the Euroimmun assay (49%), whereas IgM could be detected for months with the Dia.pro assay. The specificity of the Zika virus IgG assays was also low, especially that of Dia.Pro (62%); findings were strongly influenced by the epidemiologic context. These results highlight the complexity of serologic diagnosis of Zika virus infection in regions endemic for flaviviruses. Accurate analysis of the performance of assays is required to adapt and interpret algorithms.

Zika virus belongs to the Flaviviridae family, genus *Flavivirus*, and is an arbovirus transmitted mainly by mosquitoes of the genus *Aedes* (*Stegomyia*). Initially isolated in 1947 from a sentinel monkey during yellow fever surveillance in Uganda, Zika virus was reported as causing only sporadic human infections, associated with asymptomatic or mild, self-limiting illness, until 2007 (*1,2*). In 2007, Zika virus spread first to Pacific islands and then throughout the Americas, resulting in large outbreaks in several regions of the world. Zika virus infection is estimated to be symptomatic in 18%–73% of cases (*3–5*); severe complications have been reported, including neurologic disorders, such as Guillain-Barré syndrome, and congenital Zika virus syndrome, which is characterized by severe microcephaly, brain and ocular anomalies, congenital contractures, and neurologic impairment in the fetuses and newborns of mothers infected during pregnancy (*3,4,6*).

The mild signs and symptoms of Zika virus infection include fever, rash, joint pain, conjunctivitis, headache, and myalgia (*7*). These manifestations are difficult to distinguish clinically from those caused by other arboviral infections, such as dengue or chikungunya, which are often observed in the same geographic areas. Therefore, specific, reliable diagnostic tools are needed.

Several commercial kits are available for direct viral detection by nucleic acid–based testing, which enable diagnosis during the acute phase of the disease (*8,9*): up to 7 days after symptom onset in serum samples, up to 20 days in urine, and even longer in semen (*10–13*). This virologic window, combined with the high proportion of asymptomatic forms, makes the monitoring of Zika virus infection difficult, especially in pregnant women. Therefore, serologic tools for diagnosis of Zika virus infection are urgently needed. This challenge remains because of cross-reactivity among flaviviruses, especially in a context of secondary flavivirus infection or previous immunization.

The first objective of this study was to evaluate the performance of two commercial serologic kits for the detection of Zika virus–specific IgM and IgG in serum samples from patients with an arboviral-like syndrome in a region where other arboviruses are known to circulate, including dengue and chikungunya viruses. The 2 commercial kits (4 assays) studied were the Euroimmun Zika virus IgM and IgG ELISAs (https://www.euroimmun.com) and Dia.Pro Zika virus IgM and IgG ELISAs (Diagnostic Bioprobes Srl, https://www.diapro.it). The second objective was to determine the kinetics of Zika virus IgM and IgG induced after infection, as defined by these kits.

Material and Methods

Clinical Samples and Study Design

The clinical samples used in this study were selected according to the standards for reporting diagnostic accuracy

Author affiliations: Institut Pasteur de la Guyane, Cayenne, French Guiana (S. Matheus, B. Labeau, L. Berthelot, D. Rousset); Institut Pasteur de Dakar, Dakar, Senegal (C. Talla, M. Vray); French Armed Forces Health Service in French Guiana, Cayenne (F. de Laval); French Military Centre for Epidemiology and Public Health, Marseille, France (F. de Laval); Institut de Recherche Biomédicale des Armées, Marseille (S. Briolant); Aix Marseille Université, Marseille (S. Briolant)

DOI: https://doi.org/10.3201/eid2506.180361

requirements. Two thirds came from the serum collection of the National Reference Centre (NRC) for Arboviruses in French Guiana and one third from samples collected for a descriptive prospective study of Zika virus disease in the French military community in French Guiana (ZIFAG) (*14*). The NRC collection comprises clinical specimens received during 2002–2017 for routine diagnosis and expertise. The protocol of the ZIFAG study received ethics approval from the Comité de Protection des Personnes Sud-Méditerranée I (ID RCB: 2016-A00394–47); all participants provided written informed consent. All the selected specimens were obtained from patients with an arboviral-like syndrome and an etiologic diagnosis confirmed by real-time reverse transcription PCR (RT-PCR) on acute-phase serum or urine samples. A commercial qualitative RT-PCR kit (Altona Diagnostics, https://www.altona-diagnostics.com) was used for Zika virus detection and NRC in-house real-time RT-PCR for dengue and chikungunya viruses.

We first evaluated the performance of the 2 commercial immunoassays against a panel of 199 serum samples collected from days 3 through 20 after the onset of symptoms (onset defined as day 0—that is, within the first 24 hours) (Table 1). We evaluated the sensitivity of the assays in a subgroup of 90 serum samples from 90 patients with confirmed Zika virus infection diagnosed from the end of 2015 through 2016, during the outbreak in French Guiana (Zika subgroup). We evaluated the specificity of the assays in a subgroup of 109 serum samples with a strong potential for causing flavivirus cross-reactions (non-Zika subgroup). This subgroup comprised serum samples obtained from 35 patients with confirmed dengue virus infection sampled during 2002–2013 dengue epidemics; 29 patients with confirmed chikungunya virus infection sampled during the chikungunya outbreak in French Guiana in 2014–2015, just after the dengue outbreak in 2012–2013; and 45 patients with neither dengue virus, chikungunya virus, nor Zika virus infection sampled just before the Zika virus outbreak. We peformed Zika microneutralization tests on the Zika virus, dengue virus, and chikungunya virus–negative subgroup of serum samples, enabling confirmation of the absence of Zika neutralizing antibodies.

To determine the kinetics of Zika virus antibodies, we used a panel of 300 serum samples collected from 124 patients with confirmed Zika virus infection from day 0 through day 300 after the onset of symptoms (Table 1). We collected 1–8 samples from each Zika virus–infected patient. The distribution of samples according to time since onset was as follows: 76 samples collected during days 0–4, 50 during days 5–14, 55 during days 15–30, 19 during days 31–60, 32 during days 61–90, 44 during days 91–180, and 24 during days 181–300.

Euroimmun and Dia.Pro Zika Virus IgM and IgG ELISAs

We tested all samples with the Euroimmun ELISAs according to the manufacturer's recommendations and calculated signal-to-cutoff (S/CO) ratios; values <0.8 were regarded as negative, ≥0.8 to <1.1 as equivocal, and ≥1.1 as positive. We tested all serum specimens with the respective Dia.Pro ELISAs for qualitative determination of IgM and IgG, according to the manufacturer's instructions; we interpreted results as positive if the S/CO ratio was ≥1.1, negative if <0.9, and equivocal if 0.9–1.1. Recombinant Zika virus nonstructural protein 1 was the antigen in both the Euroimmun and Dia.Pro assays.

Statistical Analysis

Continuous variables were expressed as mean (± SD) or median with interquartile range (IQR) and discrete variables as percentages and 95% CIs. We calculated the sensitivity and specificity of the assays with 95% CIs. The differences in the S/CO ratios of the IgM and IgG assays at each time were compared with the Student *t* test. We performed all statistical analyses using R 3.4 statistical software (https://www.r-project.org).

Table 1. Characteristics of panels evaluated in study of Zika virus diagnostic tests

Panel	Sample characterization	No. samples	Mean time to collection after onset of fever, d (± SD)
Panel performance evaluation 3–20 days after onset			
Zika virus subgroup	Positive Zika virus	90	10 ± 6
Non–Zika virus subgroup	Negative Zika virus with confirmed dengue virus infection	35	10 ± 3
	Negative Zika virus with confirmed chikungunya virus infection	29	13 ± 3
	Negative Zika virus, dengue virus, chikungunya virus	45	11 ± 5
Total panel performance		199	10 ± 5
Panel IgM–IgG kinetics 0–300 days after onset			
Positive Zika virus		300*	Minimum 0, maximum 300, median 20, interquartile range 4–81

*300 samples from 124 patients, including the 90 positive Zika virus samples in the first panel.

Results

Patient Characteristics

The 199 samples used to evaluate the performance of the serologic kits came from patients with a mean ± SD age of 36 ± 16 years (range 1–74 years; IQR 27–46 years). This panel was composed of the Zika virus–positive subgroup (n = 90), 51 (57%) female and 39 (43%) male, with a mean age ± SD of 39 ± 12 years; and the Zika virus–negative subgroup (n = 109), 62 (57%) female and 45 (43%) male, with a mean ± SD age of 34 ± 18 years (Table 1).

The 300 samples used to determine the kinetics of Zika virus IgM and IgG came from 124 patients, 82 (66%) female and 42 (34%) male. The age range of these patients was 8–74 years (mean ± SD 37 ± 11 years).

Performance of Zika Virus IgM ELISAs

We evaluated the sensitivity and specificity of the 2 Zika virus IgM tests against 90 Zika virus subgroup samples and 109 non-Zika subgroup samples (Table 2). Each test gave inconclusive results for 6 of the 199 samples: with the Euroimmun test, we obtained 6 inconclusive results from the 90 samples from the Zika virus subgroup, and with the Dia.Pro test, we obtained 4 inconclusive results of the 90 samples from the Zika virus subgroup and 2 for samples collected on day 9 after onset of disease from patients with confirmed dengue virus infection.

The sensitivity of the Euroimmun Zika virus IgM test was 49% (41/84; 95% CI 38%–60%); sensitivity of the Dia.Pro test was 69% (59/86; 95% CI 59%–79%). Only 1 of the 109 non-Zika subgroup serum samples was positive in the Euroimmun test, indicating 99% specificity (95% CI 97%–100%). Four non-Zika subgroup samples were detected as positive by the Dia.Pro IgM test, including 3 samples from patients with acute dengue virus infection, indicating a specificity of 96% (103/107; 95% CI 92%–100%).

Performance of Zika Virus IgG ELISAs

We used the same panel to evaluate the performance of Euroimmun and Dia.Pro Zika virus IgG kits (Table 2). With the Euroimmun test, 16 (8%) of the 199 samples gave inconclusive results, 8 among positive Zika virus samples collected on days 5 (1 sample) and 9 (7 samples) of disease onset; 8 negative Zika virus samples also gave inconclusive results (5 chikungunya virus–positive samples and 3 from the group negative for dengue virus, chikungunya virus, and Zika virus). The sensitivity of this assay was 71% (58/82; 95% CI 92%–100%) and the specificity 70% (71/101; 95% CI 61%–79%). With the Dia.Pro IgG test, 8 samples gave inconclusive results: 5 samples from the Zika virus–positive group (2 collected before day 5 and the others on day 9 or later after the onset of illness) and 3 samples from the Zika virus–negative group (collected on days 4 to 6 after onset) (Table 2). The sensitivity of this assay was 79% (67/85; 95% CI 70%–88%) and the specificity 62% (66/106; 95% CI 53%–71%).

The false positivity rate of the 2 Zika virus IgG assays varied according to the subpanel used. These rates were 40%–58.6% for positive dengue virus or chikungunya virus sample subgroups and 11.9%–21.4% for the negative dengue virus, negative chikungunya virus, and negative Zika virus sample subgroup (Table 3).

Table 2. Performance of Zika virus IgM and IgG assays in panels of characterized samples obtained during days 3–20 after onset of symptoms*

Results	Zika subgroup	Non–Zika subgroup				Total	Sensitivity (95% CI), specificity (95% CI)
		All	Zika–/DENV+	Zika–/CHIKV+	Zika–/DENV–/CHIKV–		
Euroimmun IgM test							
Positive	41	1	0	0	1	42	49% (38–60), 99% (97–100)
Negative	43	108	35	29	44	151	
Inconclusive	6	0	0	0	0	6	
Total	90	109	35	29	45	199	
Dia.Pro IgM test							
Positive	59	4	3	1	0	63	69% (59–79), 96% (92–100)
Negative	27	103	30	28	45	130	
Inconclusive	4	2	2	0	0	6	
Total	90	109	35	29	45	199	
Euroimmun IgG test							
Positive	58	30	14	11	5	88	71% (61–81), 70% (61–79)
Negative	24	71	21	13	37	95	
Inconclusive	8	8	0	5	3	16	
Total	90	109	35	29	45	199	
Dia.Pro IgG test							
Positive	67	40	14	17	9	107	79% (70–88), 62% (53–71)
Negative	18	66	21	12	33	84	
Inconclusive	5	3	0	0	3	8	
Total	90	109	35	29	45	199	

*CHIKV, chikungunya virus; DENV, dengue virus; +, positive; –, negative.

Table 3. Rate and ratio of false Zika virus IgG–positive samples obtained with Euroimmun and Dia.Pro Zika virus IgG assays according to the non–Zika virus sample subgroup

Test	Positive for dengue virus, collected before 2013	Positive for chikungunya virus, collected in 2014	Negative for Zika, dengue, and chikungunya viruses, collected at end of 2015
Euroimmun IgG test			
False positivity rate, % (pos/pos + neg)	40% (14/35)	45.8% (11/24)	11.9% (5/42)
IgG S/C ratio of false-positive IgG, mean (range)	3.9 (1.1–6.7)	2.0 (1.2–2.9)	2.0 (1.3–3.7)
Dia.Pro IgG test			
False positivity rate, % (pos/pos + neg)	40% (14/35)	58.6% (17/29)	21.4% (9/42)
IgG S/C ratio of false-positive IgG, mean (range)	9.2 (2.5–14.4)	3.1 (1.1–7.7)	4.3 (1.1–10.1)

*Neg, negative; pos, positive.

Performance of Combined IgM/IgG Assays

The sensitivity of the combined Euroimmun Zika virus IgM and IgG assays was 82% (71/87; 95% CI 74%–90%) and the specificity was 69% (70/101; 95% CI 60%–78%). The sensitivity of the combined Dia.Pro Zika virus IgM and IgG assays was 87% (75/86; 95% CI 80%–94%) and specificity was 62% (66/106; 95% CI 53%–71%).

Time-Course Analysis of Zika Virus IgM and IgG, Days 0–300 after Onset of Symptoms

We used the panel of sequential samples from patients with confirmed Zika virus infection to determine the kinetics of Zika virus IgM and IgG over 10 months after clinical onset (Figure 1). For the Euroimmun Zika virus IgM test, maximum percentage detection (71%) was 15–30 days after the onset of disease. After this time, the percentage of detectable IgM decreased rapidly, to only 21% of samples collected in days 31–60 and <9% for those collected >60 days after infection (Figure 1, panel A). The Dia.Pro Zika virus IgM test was more sensitive, with higher rates of positive samples observed over a longer time: 29% positive samples on days 0–4 after clinical onset, increasing to a maximum of 93% positivity during days 15–30. The positivity rate decreased more slowly than with the Euroimmun test, and 29% of samples were still positive for IgM during days 181–300 after infection. For Zika virus IgG, both assays detected the antibody in >40% of samples collected during the acute phase of disease (days 0–4) and in 100% of samples collected during days 31–180 after onset of disease (Figure 1, panel B). A slight decrease in the positivity rate for IgG observed with the Euroimmun assay before day 300 suggests a possible lack of sensitivity over time.

We also evaluated the evolution of the overall mean S/CO ratios by time and the test used (Figure 1, panels C and D). We observed similar kinetics for the mean S/CO ratios

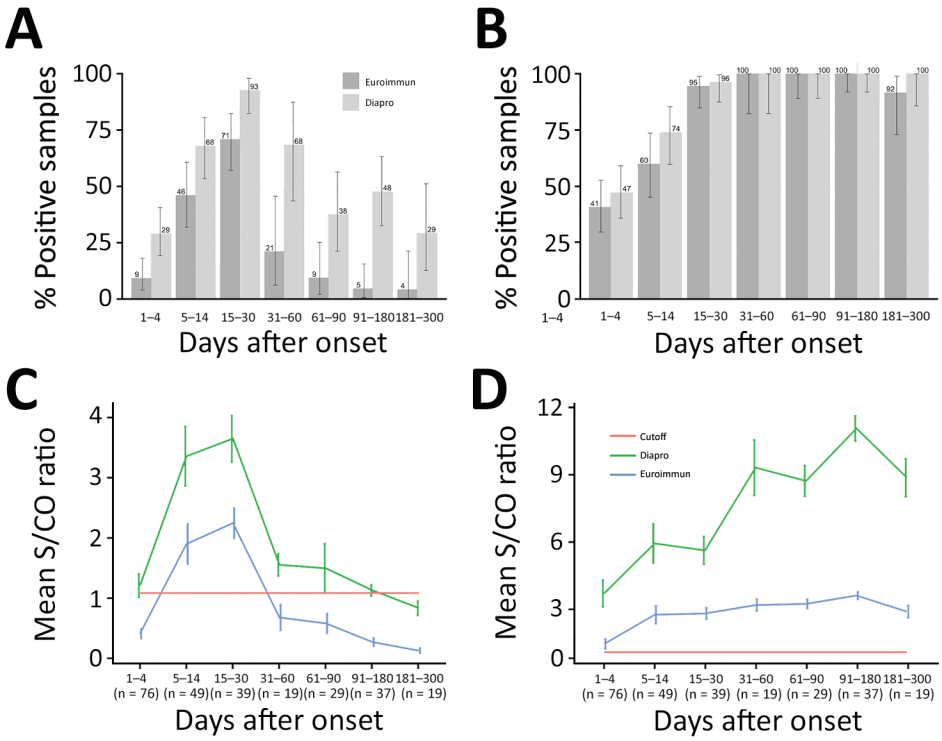

Figure 1. Kinetics of Zika virus IgM and IgG as determined with Euroimmun and Dia.Pro kits for patient samples collected in the first 10 months after infection, by time interval. A, B) Percent positive for Zika virus IgM (A) and IgG (B). Values are given with binomial proportion CI). C, D) Overall time course of mean signal-to-cutoff ratios of Zika virus IgM (C) and IgG (D). Values are shown with SEs. The number of patients sampled is provided for each time interval.

for the 2 assays: the maximum mean S/CO ratio peaked during days 15–31 for the IgM assays and during days 91–180 for the IgG assays. Nevertheless, the differences between the mean S/CO ratios for both the IgM and the IgG assays at each time after infection class were significant (all $p<0.05$) (Figure 1, panels C and D). The Dia.Pro assays gave higher S/CO ratios for the same threshold values, explaining the greater sensitivity of these tests. We obtained the kinetics of Zika virus IgM and IgG with both assays for patients for whom we had ≥5 sequential samples (Figure 2).

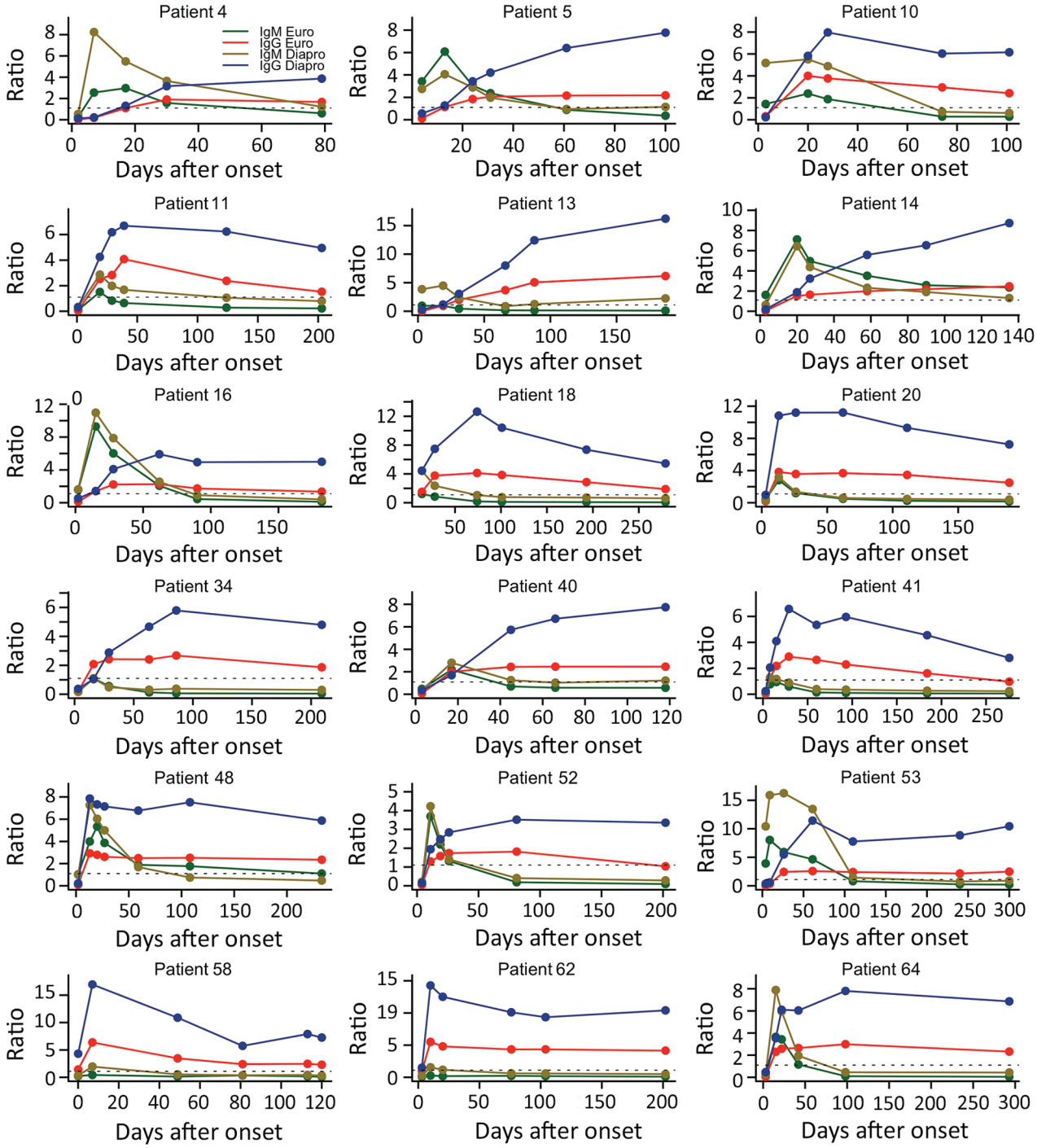

Figure 2. Individual time-course analyses of Zika virus IgM and IgG signal-to-cutoff ratios obtained by using Euroimmun and Dia.Pro kits for 18 patients for whom 5 or more sequential samples were available.

Discussion

In this assessment of the performance of Euroimmun and Dia.Pro Zika virus IgM and IgG ELISAs for diagnosis of Zika virus infection, we had a large panel of well-characterized samples from areas endemic for arboviruses, the dates of symptom onset, and infection confirmed by real-time RT-PCR. Although the Dia.Pro IgM assay was more sensitive (69%) than the Euroimmun IgM test (49%), the performance of both IgM assays was suboptimal. The sensitivity of a screening test is a major factor in determining its usefulness, because poor sensitivity of the first test used in a diagnostic algorithm could lead to false-negative results that would not be further evaluated.

The sensitivity of the Euroimmun Zika virus IgM test was significantly lower than that reported previously (*15–18*). The differences might be caused by differences in study design, selection criteria, and the few positive samples in the previous studies (*17–18*). The lower sensitivity we found for this assay might also be the result of the larger proportion of secondary flavivirus infections in the panel used, as the samples were taken in an area endemic–epidemic for dengue and with mandatory vaccination against yellow fever. A significant lower sensitivity of the Euroimmun Zika virus IgM assay has also been reported in travelers from Israel compared with travelers from Europe and Chile, possibly related to the West Nile virus background immunity of the population of Israel (*19*). More recent evaluations have also reported low sensitivity (39.5% and 37%) of the Euroimmun assays (*20,21*).

Sensitivity is essential for a frontline diagnostic test, and specificity should also be carefully evaluated. In our study, we assessed the specificity of all the tests with various non–Zika virus samples to evaluate potential cross-reactivity. A first subpanel of samples from patients with confirmed acute dengue virus infection was formed because of the high potential for flavivirus cross-reactivity; a second subpanel consisted of samples from patients with confirmed chikungunya virus infection; and a third subpanel consisted of samples from patients with no dengue virus, chikungunya virus, or Zika virus infection. The specificity of the Euroimmun Zika virus IgM assay was 99% and that of the Dia.Pro test was 96%, with cross-reactivity varying according to the subpanel. Most cross-reactions were observed in the subpanel of acute dengue samples, in which 3 of 33 samples were false positive for Zika virus IgM, whereas 1 of 74 samples collected >1 year after the dengue epidemic (chikungunya virus subpanel and dengue virus, chikungunya virus, and Zika virus negative subpanel) was false positive. Maximum cross-reactivity of IgG tests was seen in the subpanel collected in the post–dengue epidemic period in 2014–2015. The false-positivity rate was 40% (14/35) in the acute dengue subpanel for both commercial tests; the rate grew to 45.8% (11/24) for the Euroimmun Zika virus IgG test and 58.6% (17/29) for the Dia.Pro Zika virus IgG test in the subpanel of acute chikungunya virus samples collected right after the dengue epidemic period in 2014–2015. The IgG cross-reactions tended to decrease with time: 2 years after the end of the latest dengue epidemic in French Guiana, 5/42 (11.9%) samples were falsely positive by the Euroimmun IgG test and 9/42 (21.4%) samples were falsely positive with the Dia.Pro test. All samples except 2 with a false-positive result for Zika virus IgG were positive for dengue virus IgG by our in-house IgG antibody capture ELISA technique. The predictive positive value of both Zika virus IgG assays therefore largely depends on the epidemiologic situation of other flaviviruses, like dengue virus.

A study performed in Martinique during March–June 2016 during the Zika virus epidemic showed a good correlation between a high Euroimmun Zika virus IgG ratio and a positive Zika virus seroneutralization result. Ratios >4 were associated with positive seroneutralization in >95% of cases, whereas ratios >5 were associated with seroneutralization in 100% of cases (*22*). At the time of the study, only sporadic dengue cases were reported in Martinique, as the previous epidemic occurred in 2013–2014, >2 years earlier. In our assessment, the IgG S/C ratio value of false Zika virus IgG–positive samples varied from 1.1 to 6.7 (mean 3.9) for acute dengue samples to 1.2 to 3.7 (mean 2.0) for other non–Zika virus samples. These results underline the importance and potential efficacy of using selected panels to evaluate performance and, especially, the specificity of serologic assays. These results also indicate that when there is major cocirculation of dengue virus and Zika virus, the interpretation of serologic assays could be increasingly complex.

The overall specificity of the Euroimmun Zika virus IgG assay was 79% and that of the Dia.Pro assay was 62%. These results indicate suboptimal specificity, which is lower than that reported previously (*20,21*), and is a concern for serologic diagnosis of Zika virus infection. Seroneutralization is the classical reference test for confirming contact with Zika virus in cases of positive results with ELISA assays in regions where flaviviruses cocirculate; however, even seroneutralization tests could be difficult to interpret, leading the US Centers for Disease Control and Prevention to change its guidance for interpretation of Zika virus antibody test results in May 2016 (*23,24*). In cases of secondary flavivirus infection, a microneutralization test might not discriminate between the past and recent infecting viruses, leading to an assumption of just a recent flavivirus exposure.

As reported previously by others, when IgM and IgG results were combined, sensitivity increased to 82% for Euroimmun and 87% for Dia.Pro assays, whereas specificity decreased to 69% for Euroimmun and 62% for Dia.Pro

(*20,21*). However, according to this combined analysis, 42% (30/71) of samples positive by the Euroimmun assays and 21% (16/75) for the Dia.Pro assays correspond to IgM negative/IgG positive samples, for which distinction between recent and past infections is not possible. Thus, a combined interpretation is not suitable for Zika infection diagnosis in the context of endemic–epidemic circulation.

We not only assessed the performance of Euroimmun and Dia.Pro Zika virus IgM and IgG tests but also evaluated the kinetics of the antibodies through 300 days after the onset of symptoms. A major concern in serologic diagnosis of Zika virus infection is determining the date of infection, due to the high proportion of asymptomatic forms. Data on the duration of IgM persistence after Zika virus infection are still limited, but our results indicate that this antibody could persist for at least several months, as described for other arboviruses (*25*). Such persistence could preclude determination of the recent nature of an infection, and other assays should be evaluated. The analysis of individual Zika virus antibody kinetics revealed distinct patterns. In some patients (such as patients 4, 5, 10, 16, 53), high IgM ratios during the acute phase were associated with delayed and moderate increases in Zika virus IgG ratios, possibly reflecting a primary flavivirus or Zika virus infection; for other patients (such as patients 20, 34, 41, 58, 62), an early increase in the IgG ratio was combined with a low or even negative Zika virus IgM ratio throughout follow-up, indicating secondary flavivirus infections. These 2 types of kinetics showed contrasted signal intensities, which are not observed with our in-house ELISA assays, in which whole Zika virus is used as an antigen (data not shown).

A limitation of our study is that the Zika virus–positive samples were confirmed by RT-PCR and thus were all from symptomatic cases. If antibody levels are different in symptomatic and asymptomatic infections, as described for dengue, the performance and antibody kinetics observed in this study might be considerably different in samples from asymptomatic infections (*26,27*).

This study highlights the complexity of interpreting serologic assays in areas where various arboviruses cocirculate and demonstrates the importance of evaluating serologic assays with serum specimens from persons living in endemic–epidemic areas and use of parallel testing antibodies to maximize the reliability of diagnosis. Further studies are also needed to identify specific biomarkers of each flavivirus infection for diagnosis after the acute phase of disease.

This study was supported by Institut Pasteur de la Guyane and Santé Publique France (Saint-Maurice, France) and received assistance from Investissement d'Avenir grants managed by the French Agence Nationale de la Recherche (CEBA ANR-10-LABEX-25-01).

About the Author

Dr. Matheus is a research assistant at the Institut Pasteur de la Guyane, Cayenne, French Guiana. Her primary research interest is the diagnosis and pathophysiology of arboviruses.

References

1. Dick GW, Kitchen SF, Haddow AJ. Zika virus. I. Isolations and serological specificity. Trans R Soc Trop Med Hyg. 1952;46: 509–20. http://dx.doi.org/10.1016/0035-9203(52)90042-4
2. Faye O, Freire CC, Iamarino A, Faye O, de Oliveira JV, Diallo M, et al. Molecular evolution of Zika virus during its emergence in the 20th century. PLoS Negl Trop Dis. 2014;8:e2636. http://dx.doi.org/10.1371/journal.pntd.0002636
3. Duffy MR, Chen TH, Hancock WT, Powers AM, Kool JL, Lanciotti RS, et al. Zika virus outbreak on Yap Island, Federated States of Micronesia. N Engl J Med. 2009;360:2536–43. http://dx.doi.org/10.1056/NEJMoa0805715
4. Saiz JC, Martín-Acebes MA, Bueno-Marí R, Salomón OD, Villamil-Jiménez LC, Heukelbach J, et al. Zika virus: What have we learnt since the start of the recent epidemic? Front Microbiol. 2017;8:1554. http://dx.doi.org/10.3389/fmicb.2017.01554
5. de Laval F, Matheus S, Maquart M, Yvrard E, Barthes N, Combes C, et al. Prospective Zika virus disease cohort: systematic screening. Lancet. 2016;388:868. http://dx.doi.org/10.1016/S0140-6736(16)31429-5
6. Cao-Lormeau VM, Blake A, Mons S, Lastere S, Roche C, Vanhomwegen J, et al. Guillain-Barré syndrome outbreak associated with Zika virus infection in French Polynesia: a case-control study. Lancet. 2016;387:1531–9. http://dx.doi.org/10.1016/S0140-6736(16)00562-6
7. Ahmad SS, Amin TN, Ustianowski A. Zika virus: management of infection and risk. BMJ. 2016;352:i1062. http://dx.doi.org/10.1136/bmj.i1062
8. L'Huillier AG, Lombos E, Tang E, Perusini S, Eshaghi A, Nagra S, et al. Evaluation of Altona Diagnostics RealStar Zika virus reverse transcription-PCR test kit for Zika virus PCR testing. J Clin Microbiol. 2017;55:1576–84. http://dx.doi.org/10.1128/JCM.02153-16
9. Ölschläger S, Enfissi A, Zaruba M, Kazanji M, Rousset D. Diagnostic validation of the RealStar® Zika virus reverse transcription polymerase chain reaction kit for detection of Zika virus RNA in urine and serum specimens. Am J Trop Med Hyg. 2017;97:1070–1. http://dx.doi.org/10.4269/ajtmh.17-0268
10. Lanciotti RS, Kosoy OL, Laven JJ, Velez JO, Lambert AJ, Johnson AJ, et al. Genetic and serologic properties of Zika virus associated with an epidemic, Yap State, Micronesia, 2007. Emerg Infect Dis. 2008;14:1232–9. http://dx.doi.org/10.3201/eid1408.080287
11. Gourinat AC, O'Connor O, Calvez E, Goarant C, Dupont-Rouzeyrol M. Detection of Zika virus in urine. Emerg Infect Dis. 2015;21:84–6. http://dx.doi.org/10.3201/eid2101.140894
12. Bingham AM, Cone M, Mock V, Heberlein-Larson L, Stanek D, Blackmore C, et al. Comparison of test results for Zika virus RNA in urine, serum, and saliva specimens from persons with travel-associated Zika virus disease—Florida, 2016. MMWR Morb Mortal Wkly Rep. 2016;65:475–8. http://dx.doi.org/10.15585/mmwr.mm6518e2
13. de Laval F, Matheus S, Labrousse T, Enfissi A, Rousset D, Briolant S. Kinetics of Zika viral load in semen. N Engl J Med. 2017;377:697–9. http://dx.doi.org/10.1056/NEJMc1612600
14. Bossuyt PM, Reitsma JB, Bruns DE, Gatsonis CA, Glasziou PP, Irwig L, et al.; STARD Group. STARD 2015: an updated list of essential items for reporting diagnostic accuracy studies. BMJ. 2015;351:h5527. http://dx.doi.org/10.1136/bmj.h5527

15. Steinhagen K, Probst C, Radzimski C, Schmidt-Chanasit J, Emmerich P, van Esbroeck M, et al. Serodiagnosis of Zika virus (ZIKV) infections by a novel NS1-based ELISA devoid of cross-reactivity with dengue virus antibodies: a multicohort study of assay performance, 2015 to 2016. Euro Surveill. 2016;21:30426. http://dx.doi.org/10.2807/1560-7917.ES.2016.21.50.30426
16. Pasquier C, Joguet G, Mengelle C, Chapuy-Regaud S, Pavili L, Prisant N, et al. Kinetics of anti-ZIKV antibodies after Zika infection using two commercial enzyme-linked immunoassays. Diagn Microbiol Infect Dis. 2018;90:26–30. http://dx.doi.org/10.1016/j.diagmicrobio.2017.09.001
17. Granger D, Hilgart H, Misner L, Christensen J, Bistodeau S, Palm J, et al. Serologic testing for Zika virus: comparison of three Zika virus IgM-screening enzyme-linked immunosorbent assays and initial laboratory experiences. J Clin Microbiol. 2017; 55:2127–36. http://dx.doi.org/10.1128/JCM.00580-17
18. Huzly D, Hanselmann I, Schmidt-Chanasit J, Panning M. High specificity of a novel Zika virus ELISA in European patients after exposure to different flaviviruses. Euro Surveill. 2016;21:30203. 10.2807/1560-7917.ES.2016.21.16.30203 http://dx.doi.org/10.2807/1560-7917.ES.2016.21.16.30203
19. Lustig Y, Zelena H, Venturi G, Van Esbroeck M, Rothe C, Perret C, et al. Sensitivity and kinetics of an NS1-based Zika virus enzyme-linked immunosorbent assay in Zika virus-infected travelers from Israel, the Czech Republic, Italy, Belgium, Germany, and Chile. J Clin Microbiol. 2017;55:1894–901. 10.1128/JCM.00346-17 http://dx.doi.org/10.1128/JCM.00346-17
20. L'Huillier AG, Hamid-Allie A, Kristjanson E, Papageorgiou L, Hung S, Wong CF, et al. Evaluation of Euroimmun Anti-Zika virus IgM and IgG enzyme-linked immunosorbent assays for Zika virus serologic testing. J Clin Microbiol. 2017;55:2462–71. http://dx.doi.org/10.1128/JCM.00442-17
21. Safronetz D, Sloan A, Stein DR, Mendoza E, Barairo N, Ranadheera C, et al. Evaluation of 5 commercially available Zika virus immunoassays. Emerg Infect Dis. 2017;23:1577–80. http://dx.doi.org/10.3201/eid2309.162043
22. Gallian P, Cabié A, Richard P, Paturel L, Charrel RN, Pastorino B, et al. Zika virus in asymptomatic blood donors in Martinique. Blood. 2017;129:263–6. http://dx.doi.org/10.1182/blood-2016-09-737981
23. Rabe IB, Staples JE, Villanueva J, Hummel KB, Johnson JA, Rose L, et al.; MTS. Interim guidance for interpretation of Zika virus antibody test results. MMWR Morb Mortal Wkly Rep. 2016;65:543–6. http://dx.doi.org/10.15585/mmwr.mm6521e1
24. Keasey SL, Pugh CL, Jensen SM, Smith JL, Hontz RD, Durbin AP, et al. Antibody responses to Zika virus infections in environments of flavivirus endemicity. Clin Vaccine Immunol. 2017;24: e00036-17. http://dx.doi.org/10.1128/CVI.00036-17
25. Talarmin A, Labeau B, Lelarge J, Sarthou JL. Immunoglobulin A-specific capture enzyme-linked immunosorbent assay for diagnosis of dengue fever. J Clin Microbiol. 1998;36:1189–92.
26. Yeo AS, Rathakrishnan A, Wang SM, Ponnampalavanar S, Manikam R, Sathar J, et al. Dengue patients exhibit higher levels of PrM and E antibodies than their asymptomatic counterparts. Biomed Res Int. 2015;2015:420867. http://dx.doi.org/10.1155/2015/420867
27. Simon-Lorière E, Duong V, Tawfik A, Ung S, Ly S, Casadémont I, et al. Increased adaptive immune responses and proper feedback regulation protect against clinical dengue. Sci Transl Med. 2017;9:eaal5088. http://dx.doi.org/10.1126/scitranslmed.aal5088

Address for correspondence: Dominique Rousset, Institut Pasteur de la Guyane, Laboratoire de Virologie, 23 avenue Pasteur, BP 6010, 97306 Cayenne CEDEX, French Guiana; email: drousset@pasteur-cayenne.fr

EID Podcast:
Probable Unusual Transmission of Zika Virus

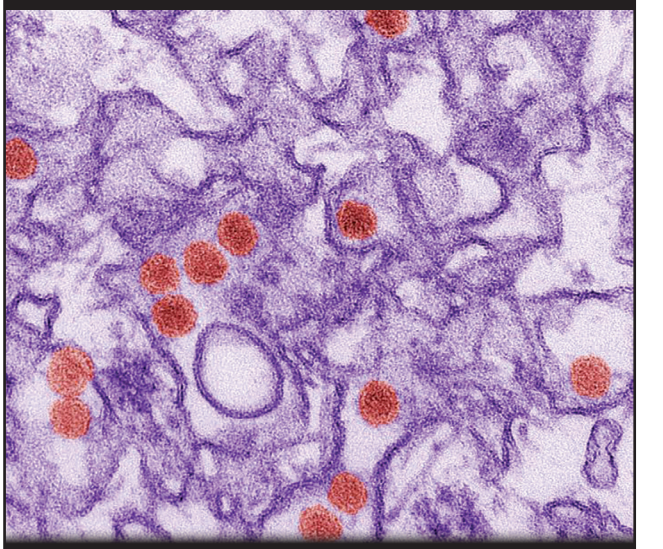

Zika virus, a mosquito-transmitted flavivirus, has been isolated from sentinel monkeys, mosquitoes, and sick persons in Africa and Southeast Asia. Serologic surveys indicate that Zika virus infections can be relatively common among persons in southeastern Senegal and other areas of Africa, but that Zika virus-associated disease may be underreported or misdiagnosed. In 2007, a large outbreak of Zika virus infection occurred on Yap Island in the southwestern Pacific that infected ≈70% of the island's inhabitants, which highlighted this virus as an emerging pathogen. The purpose of this study was to investigate and report 3 unusual cases of arboviral disease that occurred in Colorado in 2008.

Clinical and serologic evidence indicate that two American scientists contracted Zika virus infections while working in Senegal in 2008. One of the scientists transmitted this arbovirus to his wife after his return home. Direct contact is implicated as the transmission route, most likely as a sexually transmitted infection.

Visit our website to listen:
https://www2c.cdc.gov/podcasts/player.asp?f=7106489

EMERGING INFECTIOUS DISEASES®

Sequential Emergence and Wide Spread of Neutralization Escape Middle East Respiratory Syndrome Coronavirus Mutants, South Korea, 2015

Yeon-Sook Kim,[1] Abdimadiyeva Aigerim,[1] Uni Park,[1] Yuri Kim, Ji-Young Rhee, Jae-Phil Choi, Wan Beom Park, Sang Won Park, Yeonjae Kim, Dong-Gyun Lim, Kyung-Soo Inn, Eung-Soo Hwang, Myung-Sik Choi, Hyoung-Shik Shin,[2] Nam-Hyuk Cho[2]

The unexpectedly large outbreak of Middle East respiratory syndrome in South Korea in 2015 was initiated by an infected traveler and amplified by several "superspreading" events. Previously, we reported the emergence and spread of mutant Middle East respiratory syndrome coronavirus bearing spike mutations (I529T or D510G) with reduced affinity to human receptor CD26 during the outbreak. To assess the potential association of spike mutations with superspreading events, we collected virus genetic information reported during the outbreak and systemically analyzed the relationship of spike sequences and epidemiology. We found sequential emergence of the spike mutations in 2 superspreaders. In vivo virulence of the mutant viruses seems to decline in human patients, as assessed by fever duration in affected persons. In addition, neutralizing activity against these 2 mutant viruses in serum samples from mice immunized with wild-type spike antigen were gradually reduced, suggesting emergence and wide spread of neutralization escapers during the outbreak.

Middle East respiratory syndrome coronavirus (MERS-CoV) is a newly emerging zoonotic pathogen that causes an acute and fatal respiratory disease (*1*). The viral pathogen was first identified in September 2012 in an acute pneumonia patient in Saudi Arabia and has since been associated with 2,279 confirmed cases (with a death rate of ≈35.4%) in 27 countries as of March 2019 (https://www.who.int/emergencies/mers-cov). Although primary transmission of MERS-CoV to humans is linked to contact with dromedary camels, up to 50% of outbreak cases have been associated with human-to-human transmission, especially in healthcare settings (*1*). During May–July 2015, an unexpectedly large outbreak of MERS swept South Korea, resulting in 186 confirmed cases and 38 deaths (death rate 20.4%). This outbreak was initiated by an infected traveler from the Middle East region and amplified by several "superspreading" events (defined as ≥4 human-to-human transmissions) in healthcare settings (*2*). Three superspreaders (P001, P014, and P016) were epidemiologically linked to 73.1% of the human transmissions and infected 28, 85, and 23 subjects, respectively. Even though nosocomial superspreading might be facilitated by delayed diagnosis and poor infection control in healthcare facilities (*1*), the contribution of biologic factors, including host responses and virologic changes, has been poorly characterized. In addition, superspreading events continue to sporadically arise and lead to unexpectedly large outbreaks of MERS (*2–4*). Therefore, host–pathogen interactions driving virus evolution and human adaptation, which are potentially associated with rare superspreading events during host changes of the enzoonotic virus (*5*), need to be further investigated.

In previous studies, we reported the emergence and spread of mutant MERS-CoV bearing spike mutations (I529T or D510G) in receptor binding domain (RBD) with reduced affinity to human CD26 receptor during the South

Author affiliations: Chungnam National University School of Medicine, Daejeon, South Korea (Y.-S. Kim); Seoul National University College of Medicine, Seoul, South Korea (A. Aigerim, U. Park, Y. Kim, W.B. Park, S.W. Park, E.-S. Hwang, M.-S. Choi, N.-H. Cho); Dankook University College of Medicine, Cheonan, South Korea (J.-Y. Rhee); Seoul Medical Center, Seoul (J.-P. Choi); National Medical Center, Seoul (Y. Kim, D.-G. Lim, H.S. Shin); Kyung Hee University, Seoul (K.-S. Inn); Seoul National University Medical Research Center and Bundang Hospital, Seoul (N.-H. Cho)

DOI: https://doi.org/10.3201/eid2506.181722

[1]These first authors contributed equally to this article.

[2]These authors were co-principal investigators.

Korea outbreak (*6*). These unexpected findings suggest that MERS-CoV adaptation during human-to-human spread might be driven by host immunologic pressure, such as neutralizing antibodies (*7–9*), that result in impaired virus fitness and virulence, rather than positive selection for a better affinity to CD26. A recent report also showed that changes in D510G and I529T reduced spike protein binding to CD26 and diminished virus entry (*10*).

To assess the potential contribution of new emerging mutations to superspreading events, we collected virus genetic information reported during the South Korea outbreak and systemically analyzed its variations, especially spike sequences, in relationship to individual disease severity and epidemiology. We also attempted to confirm whether the spike mutations affect virus dynamics in an in vitro infection model and virus escape from neutralizing antibody responses by using serum samples from mice immunized with wild-type spike antigen and from MERS patients in South Korea who had been infected with wild-type virus. Systemic overview of clinical and virologic data obtained during the transient but large outbreak driven by unexpected superspreading events among humans might provide novel insight into understanding the evolutionary pathways of the emerging coronavirus during animal-to-human transmission.

Materials and Methods

Study Design and Ethics

We collected genetic information on spike genes of MERS-CoV analyzed in the patients' specimens from the National Center for Biotechnology Information (http://www.ncbi.nlm.nih.gov/) and a previous analysis by Park et al. (*11*). As of January 31, 2018, a total of 75 spike gene sequences from 48 patients in South Korea were available for analysis (Appendix Tables 1, 2, https://wwwnc.cdc.gov/EID/article/25/6/18-1722-App1.pdf). Baseline characteristics of the patients are summarized (Table; Appendix Table 1). Clinical data and serum samples (from P002, P009, and P010) obtained from the MERS patients were used in this study. Experimental methods are described more fully in the Appendix.

Ethics approval was granted by the institutional review boards of Chungnam National University Hospital (approval no. CNUH2017–12–004), National Medical Center (approval no. H-1510–059–007), Seoul National University Hospital (approval nos. 1509–103–705 and 1511–117–723), Seoul National University Boramae Medical Center (approval no. 26–2016–8), Seoul Medical Center (approval no. Seoul 2015–12–102), and Dankook University Hospital (approval no. DKUH2016–02–014).

This study was conducted in accordance with the ethical standards laid down in the 1964 Declaration of Helsinki and all subsequent revisions. Animal experiments were approved by the Seoul National University Institutional Animal Care and Use Committee (permit no. SNU-170828–1-2) and performed in strict accordance with the recommendations in South Korea's National Guideline for the Care and Use of Laboratory Animals.

Results

We collected and analyzed genetic information of spike genes reported during the South Korea outbreak. All the information on the spike mutations in 48 patients and their sampling dates are summarized in Appendix Tables 1 and 2. The timelines of the detection of spike mutations are depicted in Figure 1. We focused on 2 mutations (D510G and I529T) in the RBD region because these 2 novel mutations substantially reduced MERS-CoV affinity to human receptor CD26 and were observed in multiple patients during the outbreak (*6*). In addition, no nonsynonymous spike mutation was consistently associated with the 2 spike mutations (Appendix Table 2). Wild-type MERS-CoV was detected in the index patient (P001) on May 19, 2015; however, the I529T mutation was observed 3 days later (May 22, 2015), suggesting that the I529T mutation emerged within 11 days after symptom onset. The potential change in spike gene is consistent with the fact that early contactors (P002, P009, and P010) with P001 also carried the wild-type virus, but most of the subsequent patients, including 2 superspreaders (P014 and P016), were infected with I529T mutant viruses. Moreover, the second mutation (D510G) was first detected in P014. The respiratory sample collected from P014 on June 1, 2015, included mixed spike sequences (wild-type, I529T, or D510G) and a rare double mutation (D510G–I529T) (*11*). Even though most of the patients infected by P014 carried MERS-CoV with the I529T mutation, the second mutant D510G was transiently or consistently observed in some of the tertiary and quaternary cases (P050, P066,

Table. Baseline characteristics of MERS patients and associated MERS coronavirus spike genotypes identified from the 2015 MERS outbreak in South Korea*

	No. (%) patients		Patient age, y,	No. associated spike genotypes				
Severity group	Men	Women	mean ± SD	WT	I529T	D510G	WT–I529T	WT–I529T–D510G
I	3 (50.0)	3 (50.0)	54 ± 13	1	2	1	1	1
II	9 (47.4)	10 (52.6)	46 ± 11	0	10	2	6	1
III	8 (75.0)	4 (25.0)	48 ± 12	3	4	0	4	1
IV	7 (63.6)	4 (36.4)	68 ± 13	1	6	0	3	1

*MERS, Middle East respiratory syndrome; WT, wild-type.

P080, P122, P155, and P168) (*11*). These results indicate that P014 initially harbored mixed wild-type and I529T mutant viruses and generated the D510G mutation, but the I529T mutant virus dominated the exposure period. In addition, this patient spread both mutants simultaneously during subsequent human-to-human transmission. The D510G mutant was detected only in the patient group infected by P014 but not in those infected by P001 or P016, further indicating that P014 is the probable origin of the D510G mutation. The I529T mutant was initially dominant in 2 patients (P077 and P080), but wild-type MERS-CoV later overtook as the major population, suggesting a fluctuation of wild-type and mutant viruses in the hosts.

Whether spike mutations of MERS-CoV are associated with disease morbidity has not yet been determined. We reviewed the clinical data of 48 patients for whom virus spike sequence information was available and classified them into 4 groups on the basis of disease severity and death rates during the MERS outbreak (Table; Appendix Table 1) (*12*). Group I includes 6 persons who

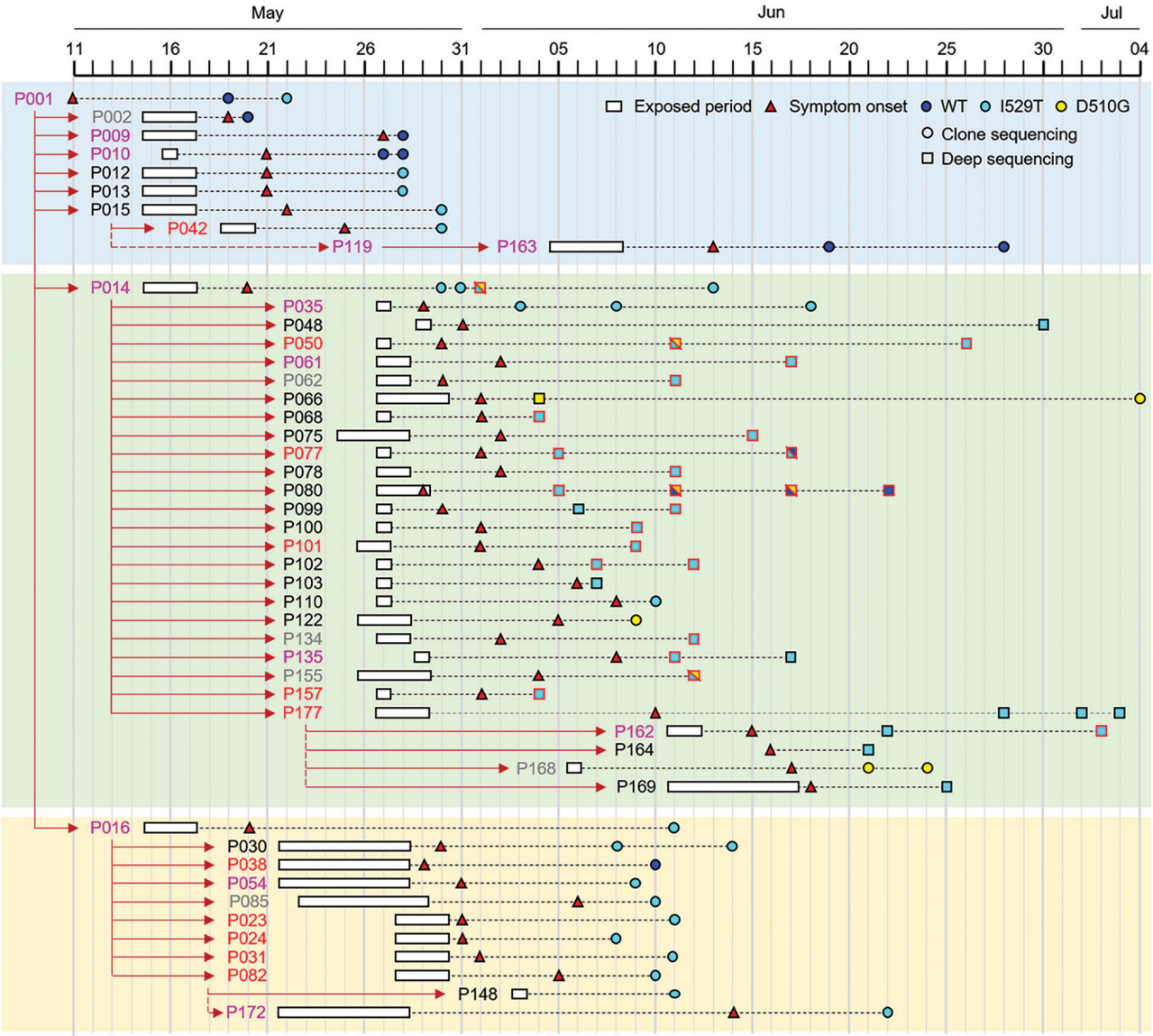

Figure 1. Emergence and spread of Middle East respiratory syndrome coronavirus (MERS-CoV) bearing the I529T or D510G mutation in the spike protein during the 2015 outbreak in South Korea. Transmission chain of infection and the timeline of potential virus exposure, symptom onset, date of specimen collection from patients, and identified mutation in the spike protein of MERS-CoV analyzed in this study. Case-patients' IDs are colored on the basis of disease severity (gray, group I; black, group II; pink, group III; red, group IV). Spike sequences analyzed by targeted deep sequencing (*10*) are denoted as a square with black (single genotype) or red (mixed genotypes with wild-type) borderline. Others are marked as circles (direct sequencing). Detailed information on patients' characteristics and their associated spike sequences of MERS-CoV are available in Appendix Tables 1 and 2 (https://wwwnc.cdc.gov/EID/article/25/6/18-1722-App1.pdf). WT, wild-type.

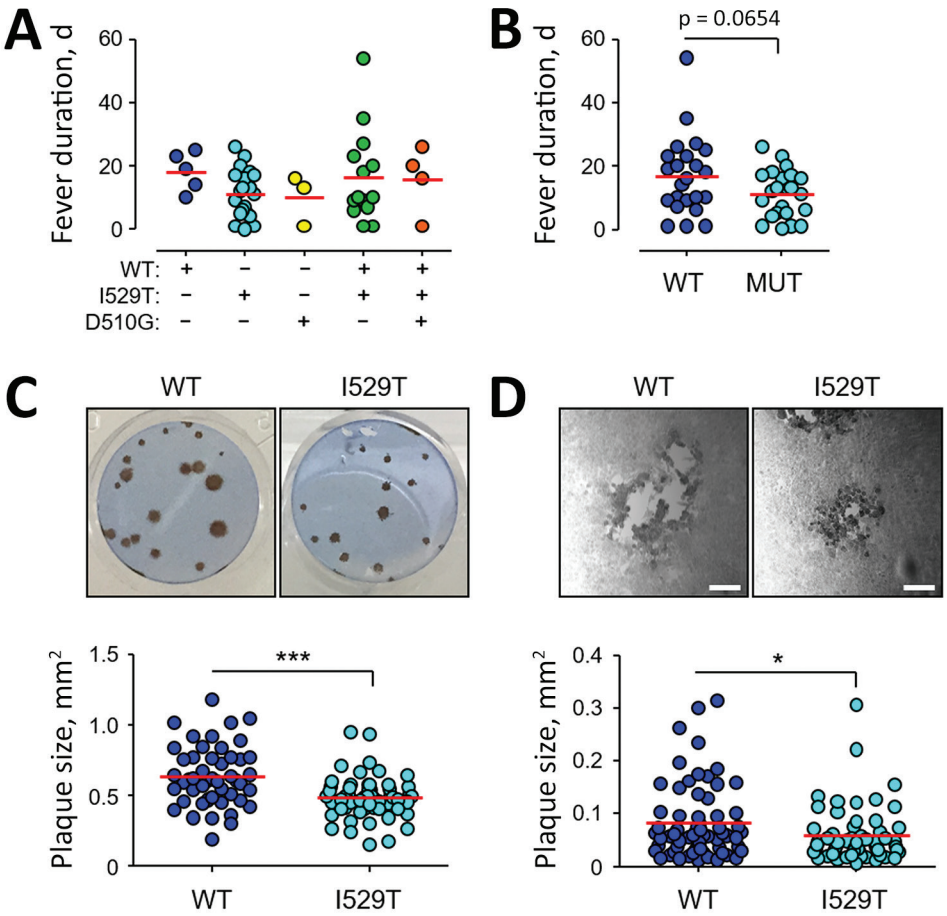

Figure 2. Effect of spike mutations in Middle East respiratory syndrome coronavirus (MERS-CoV) on fever duration and virus growth in vitro during the 2015 outbreak in South Korea. A) Fever duration of 48 patients for whom virus spike sequence information is available is presented depending on the associated spike genotypes. B) Fever duration of patient group associated with WT virus, including mixed infection (n = 23) and those infected only with either of the mutant viruses (n = 25). Mean value of each group is indicated by red lines. Baseline information of the patients and their associated MERS-CoV spike sequences are summarized in online Appendix Table 1 (https://wwwnc.cdc.gov/EID/article/25/6/18-1722-App1.pdf). C, D) Distribution of viral plaque sizes in Vero cells (panel C: WT, n = 48; I529T, n = 58) or 293T–CD26 cells (panel D: WT, n = 65; I529T, n = 55) infected with MERS-CoV bearing WT or I529T mutant spike at 3 days after infection. Representative results of plaque assay are presented in the upper panels, and size distribution of viral plaques are plotted in the lower panel. Mean values are indicated by red lines. Significance was calculated by using a 2-tailed student's *t*-test. WT, wild-type. ***p<0.001, *p<0.05. Scale bar indicates 100 μm.

were asymptomatic or had fever without pneumonia. Group II includes 19 patients who had mild pneumonia without hypoxemia. Twelve persons who recovered from more prolonged and severe pneumonia are classified as group III. Group III subjects experienced hypoxemia and were treated with oxygen during hospitalization. Eleven

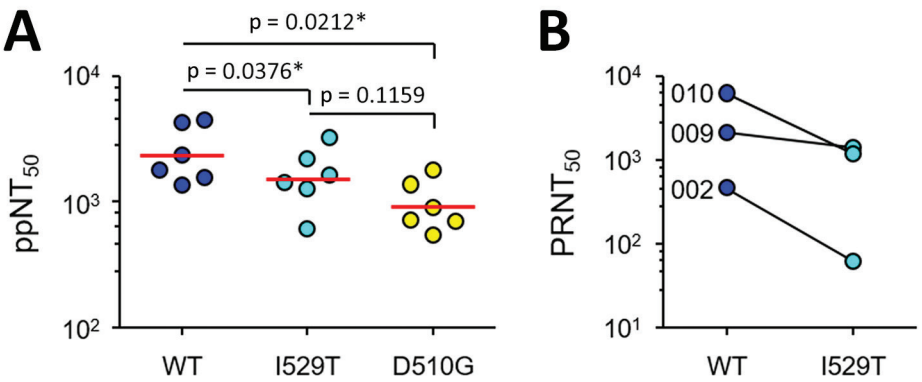

Figure 3. Increased resistance of Middle East respiratory syndrome coronavirus (MERS-CoV) against antibody-mediated neutralization by spike mutations during the 2015 outbreak in South Korea. A) Neutralizing activity of serum samples against lentiviruses bearing WT and mutant spikes. 50% pseudoparticle neutralization test titers against lentiviruses bearing WT or mutant spikes (I529T or D510G) in serum samples from mice (n = 6) immunized with WT spike antigen are plotted. Mean values are indicated by red lines. Statistical significance was calculated by using analysis of variance with Newman–Keuls post *t*-test correction. *p<0.05. B) Neutralization activity against MERS-CoV bearing WT or I529T mutant spike mutation in serum samples from 3 recovered patients (P002, P009, and P010) who carried only WT MERS-CoV. $ppNT_{50}$, 50% pseudoparticle neutralization test; $PRNT_{50}$, 50% plaque reduction neutralization test; WT, wild-type.

patients who died from acute respiratory distress syndrome are classified as group IV. Baseline characteristics of the patients, including exposure period, date of symptom onset, and fever duration, are summarized (Figure 1; Appendix Table 1). Initially, we assessed the potential association of spike mutations with disease severity (Table), but could not observe any statistically significant association of MERS severity with spike mutations or mixed spike genotype infection. However, the average days of fever duration in MERS patients was generally longer in cases associated with wild-type virus (mean ± SD, 18 ± 6 days) or mixed infection including wild-type (mean ± SD, 16 ± 14 days) compared with fevers in patients infected only with I520T (mean ± SD, 11 ± 8 days) or D510G (mean ± SD, 10 ± 8) mutant (Figure 2, panel A). Even though differences in fever duration between the patient group associated with wild-type virus, including mixed infection (17 ± 12 days), and those infected only with either of the mutant viruses (mean ± SD, 11 ± 7 days) are statistically marginal ($p = 0.0654$) (Figure 2, panel B), potentially because of limited data, the reduction of fever duration in patients associated only with the primary and secondary mutations seems to be consistent.

Because the disease severity and case-fatality rate of MERS is associated with viral load (*12*), we next examined whether mutant viruses with reduced affinity to human CD26 receptor had also reduced cell-to-cell spread, virus growth, or both. We performed plaque-forming assay in vitro and compared viral plaques between wild-type and I529T MERS-CoV. The average size of viral plaques formed by I529T mutant MERS-CoV (mean ± SD, 0.49 ± 0.15 mm^2) was significantly smaller (≈23%) than that of wild-type virus (mean ± SD, 0.64 ± 0.21 mm^2) in Vero E6 cells (Figure 2, panel C). It was consistently observed in a human embryonic kidney cell line, 293T cells overexpressing human CD26 (293T–CD26) (Figure 2, panel D). The average size of plaques induced by I529T mutant (mean ± SD, 0.08 ± 0.07 mm^2) was also smaller (≈25%) than that of wild-type MERS-CoV (mean ± SD, 0.06 ± 0.05 mm^2) in 293T–CD26 cells. These results clearly indicate that spike mutation generated during the South Korea outbreak have reduced transmissibility, reduced growth rate, or both in an in vitro infection model.

To examine whether the spike mutations affect sensitivity to the neutralizing activity of antibodies against wild-type spike, we investigated whether the antibodies generated in mice immunized with wild-type spike antigen are able to neutralize the spike mutant viruses as efficiently as wild-type virus. We performed a 50% pseudoparticle neutralization test assay on wild-type and mutant spike-pseudotyped lentiviruses and then compared their neutralizing efficacy. Average titers of serum samples from the immunized mice showed gradually decreased neutralization of I529T (mean ± SD, 1,727 ± 897) or D510G mutant viruses (1,009 ± 482) than wild-type virus (mean ± SD, 2,629 ± 1,384) (Figure 3, panel A), demonstrating that the mutant viruses are neutralization escapers. Finally, we measured the neutralizing antibody titers (using a 50% plaque reduction neutralization test [$PRNT_{50}$]) against MERS-CoV bearing wild-type and I529T mutant in serum samples from the 3 recovered patients (P002, P009, and P010) who carried only wild-type MERS-CoV. Neutralizing efficacy ($PRNT_{50}$ titers) of the serum samples against wild-type MERS-CoV were consistently higher than those against I529T mutant MERS-CoV (Figure 3, panel B). Average $PRNT_{50}$ titers of the 3 serum samples against wild-type (mean ± SD, 2,943 ± 2,994) were 3.3-fold higher than those against I529T mutant MERS-CoV (mean ± SD, 888 ± 723), indicating that I529T mutant MERS-CoV escapes better from neutralizing antibodies generated by infection with wild-type virus. $PRNT_{50}$ titers of serum samples from P009 and P010, who had more severe disease, were higher than those of P002, who had only mild symptoms.

Discussion

Even though multiple environmental and behavioral factors might be associated with the zoonotic coronavirus outbreaks in human populations, the advent of "superspreaders" that cause a large number of new infections during the early stage of an outbreak might play a critical amplifying role (*13*). Such superspreading persons have been well documented in a previous severe acute respiratory syndrome (SARS) epidemic and recent ongoing MERS outbreaks (*13*). Although the underlying biologic causes and determinants of superspreading are still poorly understood, superspreading events of zoonotic coronaviruses might be related to higher levels of virus shedding for prolonged periods of uncontrolled exposure to susceptible contacts early in the outbreak, before the need for infection control is appreciated (*5*). Our study systemically assesses MERS-CoV genetic changes during the 2015 MERS outbreak in Korea and highlights potential biologic factors associated with the short-term evolutionary pathway of zoonotic coronavirus adapting to the human population in the context of superspreading events.

Microevolution toward reduced host affinity of MERS-CoV might be associated with host antibody responses. In this study, we showed that antibodies generated in immunized mice with wild-type spike antigen or in human patients who had recovered from wild-type MERS-CoV infection were generally less efficient at neutralizing the mutant virus bearing I529T or D510G spike mutations than wild-type virus (Figure 3). In addition, in vitro virus growth of I529T mutant MERS-CoV, its cell-to-cell spread, or both are significantly reduced compared with that of

wild-type virus (Figure 2, panel C and D). Given that there are only 2 amino acid differences in spike RBD (I529T and V534L) and 5 nonsynonymous nucleotide changes throughout the whole virus genome (GenBank accession no. KT029139.1 for wild-type and KT868873.1 for I529T mutant) between the wild-type and I529T mutant isolates from Korea used in this study, the difference in plaque sizes is primarily attributable to the spike mutation (Appendix Table 3). A recent study demonstrated that changes D510G or I529T increased resistance of spike protein–driven entry to neutralization by monoclonal antibodies and serum from MERS patients (*10*). The study also confirmed that changes D510G or I529T reduced spike protein binding to CD26 but showed that this reduction only translates into diminished virus entry when expression of CD26 on target cells is low (*10*). Neither mutation modulated spike protein binding to sialic acids, spike protein activation by host cell proteases, or inhibition of spike protein–driven entry by interferon-induced transmembrane proteins (*10*). In this study, however, we consistently observed that the average size of viral plaques formed by the mutant MERS-CoV bearing I529T mutation was significantly reduced in 2 types of permissive cells, Vero E6 and HEK293T-CD26 cells expressing high levels of CD26 (*14*,*15*), compared with that of wild-type MERS-CoV (Figure 2C and 2D).

Because a previous study employed a pseudotyped vesicular stomatitis virus system bearing wild-type or mutant MERS-CoV spike proteins (*10*), our current result using MERS-CoV isolated from human patients might reflect more intrinsic characteristics of spike protein in the context of the natural form of MERS-CoV. Further studies are needed to characterize the effect of the spike mutations on virus growth or spread in in vitro and in vivo infection systems.

The emergence of spike mutations that affect affinity to host receptors might be a critical cause of superspreading events. A similar observation was made regarding the 2002–2003 SARS epidemic (*13*). However, those mutations generally enhanced the affinity of spike to human receptor ACE2 and was detected from the beginning of human-to-human transmission (*16*–*19*). Both the 2002–2003 SARS epidemic and the 2015 MERS outbreak in South Korea were associated virus mutations that change affinity to human receptors, but in opposing ways: SARS-CoV acquires mutations to replicate more efficiently and become more pathogenic (*13*), whereas MERS-CoV mutants, which have less affinity to receptors on human cells and potentially less pathogenicity, emerged in superspreaders during the outbreak in South Korea.

A recent study reported that both MERS-CoV and SARS-CoV spike trimers have inherently flexible RBD structure with 2 states (buried flat or exposed in a standing position) as observed by cryoelectron microscopic analysis (*20*). That study proposed that 1 CD26 molecule might cross-link 2 MERS-CoV spike trimers by binding to standing RBDs, 1 from each trimer, whereas the monomeric ACE2 receptor will bind to the SARS-CoV spike trimer with 1 receptor to 1 spike trimer, enabling MERS-CoV to have higher avidity to receptor binding than SARS-CoV (*20*). Inherent differences in avidity to the cellular receptors of spike trimers might partially explain why these 2 animal coronaviruses evolved in opposing directions in terms of receptor affinity when they switch hosts to the human population; spike mutations with higher affinity might be the only way to ensure successful human-to-human transmission in SARS-CoV with intrinsic lower avidity, whereas the higher spike avidity of MERS-CoV might afford the virus to have spike mutations with lower affinity to human receptors for increased antibody escape. Therefore, a vaccine immunogen designed to broadly raise neutralizing antibodies would preferably target the conserved and surface exposed stem region rather than RBD (*20*). Recently, a study showed that single mutations can make influenza virus completely resistant to both narrow strain-specific antibodies and a broad antibody that targets residues in hemagglutinin RBD, whereas broad antibodies to hemagglutinin's stalk are more resistant to virus escape through single mutations (*21*).

The microevolution of spike genes in MERS-CoV toward reduced human affinity but enhanced escape from neutralizing antibodies in a single patient might increase the probability of a spreading event by extending the virus replication period in the host. The 3 superspreaders in South Korea (P001, P014, and P016) belong to group III and had severe and prolonged viral pneumonia (*2*). The group III patients produced a significantly higher number of viruses in their respiratory secretions for longer periods than patients with milder cases (*12*,*22*). The superspreaders in South Korea were suspected to produce MERS-CoV with high copy numbers (10^8–10^9 copies/mL) in their respiratory secretions during the early phase of MERS symptom development (*12*,*22*,*23*) and exposure to susceptible contacts for 9–11 days (*2*). They were also positive for virus in their respiratory secretions for prolonged periods (44, 30, and 27 days, respectively, after symptom onset) even after isolation (*12*,*22*,*24*). In addition, a new spike mutant emerged in the index patient (P001) and P014, who combined infected >80 patients, within 2 weeks after symptom onset, such that they harbored mixed infection with wild-type and spike mutant viruses. Consequently, P001 and P014 spread mixed viruses during the early phase of the outbreak (Figure 1) (*11*).

Mixed infection with wild-type and spike mutant viruses was confirmed in the majority of the tertiary case-patients infected by P014 by targeted deep sequencing, and the

intrapatient heterogeneity of MERS-CoVs was the highest in superspreader specimens (*11*). Although the frequency of D510G and I529T varied greatly among specimens analyzed using targeted deep sequencing, the combined frequency of the single mutants was consistently high (≈88% on average), whereas the frequency of the wild-type was low (≈7% on average), supporting the hypothesis that selective pressure exerted by host neutralizing antibody responses played a critical role in shaping genetic variants (*11*).

Fluctuations of wild-type population with higher affinity to host and mutant viruses that can escape neutralizing antibodies in a single person might facilitate sustained virus replication with higher loads. Wild-type virus was dominant in several tertiary patients (e.g., P077 and P080) at the later stage of infection, although mutant virus was the major population in the earlier stage (Figure 1). P077 had hypotension, chronic respiratory disease, and pancreatitis. P080 had lymphoma and respiratory illness before infection by P014. P077 died 13 days after symptom onset, and P080 died of lymphoma 174 days after symptom onset. In both cases, wild-type and mutant viruses were detected initially (*11*), suggesting a mixed infection from P014, and the patient might have suffered from immunosuppression upon virus infection either by initial high viral load (in the case of P077), as observed in other fatal cases (*12*), or by previous cancer treatment (in the case of P080). Failing adaptive immunity in these patients might provide a specific environment that allowed wild-type virus with higher affinity to host to resurge among the mixed population in the later stage of infection. Indeed, serial samples from P077 and P080 show a substantial decrease in normalized leukocyte count and a simultaneous increase in the frequency of the wild-type allele (*11*). Again, these results suggest that the selection pressure exerted by the host immune response might favor variants with reduced affinity to the host receptor, but wild-type virus with high affinity is dominant when immune pressure is reduced.

Taken together, the emergence of antibody escaping mutants under mounting immunologic pressure in a host might ensure sustained virus replication, higher virus shedding into respiratory secretions for longer periods, and delay in antigen-specific immunity, thereby increasing the probability of a patient becoming a superspreader. Nevertheless, this evolutionary pathway of coronaviruses during human-to-human spread might result in serial decrease of host affinity and pathogenicity, as well as milder respiratory symptoms, if their transmission in the human population is not properly restricted at the initial outbreak stage.

Acknowledgments

This study was supported by the Korea Health Technology R&D Project through the Korea Health Industry Development Institute (grant no. HI15C3227), funded by the Ministry of Health and Welfare and by the National Research Foundation of Korea (grant no. 2017M3A9E4061998), which are funded by the government of South Korea. A.A., U.P., and Y.K. received a scholarship from the BK21-plus education program provided by the National Research Foundation of South Korea. The authors declare no competing financial interests.

About the Author

Dr. Yeon-Sook Kim is a physician at the Chungnam National University Hospital, Daejeon, South Korea. Her primary research interests are epidemiology and pathogenesis of various emerging infectious diseases.

1. Hui DS, Azhar EI, Kim YJ, Memish ZA, Oh MD, Zumla A. Middle East respiratory syndrome coronavirus: risk factors and determinants of primary, household, and nosocomial transmission. Lancet Infect Dis. 2018;18:e217–27. http://dx.doi.org/10.1016/S1473-3099(18)30127-0
2. Korea Centers for Disease Control and Prevention. Middle East respiratory syndrome coronavirus outbreak in the Republic of Korea, 2015. Osong Public Health Res Perspect. 2015;6:269–78. http://dx.doi.org/10.1016/j.phrp.2015.08.006
3. Assiri A, McGeer A, Perl TM, Price CS, Al Rabeeah AA, Cummings DA, et al.; KSA MERS-CoV Investigation Team. Hospital outbreak of Middle East respiratory syndrome coronavirus. N Engl J Med. 2013;369:407–16. http://dx.doi.org/10.1056/NEJMoa1306742
4. Amer H, Alqahtani AS, Alzoman H, Aljerian N, Memish ZA. Unusual presentation of Middle East respiratory syndrome coronavirus leading to a large outbreak in Riyadh during 2017. Am J Infect Control. 2018;46:1022–5. http://dx.doi.org/10.1016/j.ajic.2018.02.023
5. Parrish CR, Holmes EC, Morens DM, Park EC, Burke DS, Calisher CH, et al. Cross-species virus transmission and the emergence of new epidemic diseases. Microbiol Mol Biol Rev. 2008;72:457–70. http://dx.doi.org/10.1128/MMBR.00004-08
6. Kim Y, Cheon S, Min CK, Sohn KM, Kang YJ, Cha YJ, et al. Spread of mutant Middle East respiratory syndrome coronavirus with reduced affinity to human CD26 during the South Korean outbreak. MBio. 2016;7:e00019. http://dx.doi.org/10.1128/mBio.00019-16
7. Rockx B, Donaldson E, Frieman M, Sheahan T, Corti D, Lanzavecchia A, et al. Escape from human monoclonal antibody neutralization affects in vitro and in vivo fitness of severe acute respiratory syndrome coronavirus. J Infect Dis. 2010;201:946–55. http://dx.doi.org/10.1086/651022
8. Li W, Wong SK, Li F, Kuhn JH, Huang IC, Choe H, et al. Animal origins of the severe acute respiratory syndrome coronavirus: insight from ACE2-S-protein interactions. J Virol. 2006;80:4211–9. http://dx.doi.org/10.1128/JVI.80.9.4211-4219.2006
9. Tang XC, Agnihothram SS, Jiao Y, Stanhope J, Graham RL, Peterson EC, et al. Identification of human neutralizing antibodies against MERS-CoV and their role in virus adaptive evolution. Proc Natl Acad Sci U S A. 2014;111:E2018–26. http://dx.doi.org/10.1073/pnas.1402074111
10. Kleine-Weber H, Elzayat MT, Wang L, Graham BS, Müller MA, Drosten C, et al. Mutations in the spike protein of Middle East respiratory syndrome coronavirus transmitted in Korea increase resistance to antibody-mediated neutralization. J Virol. 2019;93:E01381–18.

11. Park D, Huh HJ, Kim YJ, Son DS, Jeon HJ, Im EH, et al. Analysis of intrapatient heterogeneity uncovers the microevolution of Middle East respiratory syndrome coronavirus. Cold Spring Harb Mol Case Stud. 2016;2:a001214. http://dx.doi.org/10.1101/mcs.a001214
12. Min CK, Cheon S, Ha NY, Sohn KM, Kim Y, Aigerim A, et al. Comparative and kinetic analysis of viral shedding and immunological responses in MERS patients representing a broad spectrum of disease severity. Sci Rep. 2016;6:25359. http://dx.doi.org/10.1038/srep25359
13. Wong G, Liu W, Liu Y, Zhou B, Bi Y, Gao GF. MERS, SARS, and Ebola: the role of super-spreaders in infectious disease. Cell Host Microbe. 2015;18:398–401. http://dx.doi.org/10.1016/j.chom.2015.09.013
14. Raj VS, Mou H, Smits SL, Dekkers DHW, Müller MA, Dijkman R, et al. Dipeptidyl peptidase 4 is a functional receptor for the emerging human coronavirus-EMC. Nature. 2013;495:251–4. http://dx.doi.org/10.1038/nature12005
15. Cockrell AS, Peck KM, Yount BL, Agnihothram SS, Scobey T, Curnes NR, et al. Mouse dipeptidyl peptidase 4 is not a functional receptor for Middle East respiratory syndrome coronavirus infection. J Virol. 2014;88:5195–9. http://dx.doi.org/10.1128/JVI.03764-13
16. Wu K, Peng G, Wilken M, Geraghty RJ, Li F. Mechanisms of host receptor adaptation by severe acute respiratory syndrome coronavirus. J Biol Chem. 2012;287:8904–11. http://dx.doi.org/10.1074/jbc.M111.325803
17. Kan B, Wang M, Jing H, Xu H, Jiang X, Yan M, et al. Molecular evolution analysis and geographic investigation of severe acute respiratory syndrome coronavirus-like virus in palm civets at an animal market and on farms. J Virol. 2005;79:11892–900. http://dx.doi.org/10.1128/JVI.79.18.11892-11900.2005
18. Li W, Zhang C, Sui J, Kuhn JH, Moore MJ, Luo S, et al. Receptor and viral determinants of SARS-coronavirus adaptation to human ACE2. EMBO J. 2005;24:1634–43. http://dx.doi.org/10.1038/sj.emboj.7600640
19. Lu G, Wang Q, Gao GF. Bat-to-human: spike features determining 'host jump' of coronaviruses SARS-CoV, MERS-CoV, and beyond. Trends Microbiol. 2015;23:468–78. http://dx.doi.org/10.1016/j.tim.2015.06.003
20. Yuan Y, Cao D, Zhang Y, Ma J, Qi J, Wang Q, et al. Cryo-EM structures of MERS-CoV and SARS-CoV spike glycoproteins reveal the dynamic receptor binding domains. Nat Commun. 2017;8:15092. http://dx.doi.org/10.1038/ncomms15092
21. Doud MB, Lee JM, Bloom JD. How single mutations affect viral escape from broad and narrow antibodies to H1 influenza hemagglutinin. Nat Commun. 2018;9:1386. http://dx.doi.org/10.1038/s41467-018-03665-3
22. Oh MD, Park WB, Choe PG, Choi SJ, Kim JI, Chae J, et al. Viral load kinetics of MERS coronavirus infection. N Engl J Med. 2016;375:1303–5. http://dx.doi.org/10.1056/NEJMc1511695
23. Yang JS, Park S, Kim YJ, Kang HJ, Kim H, Han YW, et al. Middle East respiratory syndrome in 3 persons, South Korea, 2015. Emerg Infect Dis. 2015;21:2084–7. http://dx.doi.org/10.3201/eid2111.151016
24. Lee JY, Kim YJ, Chung EH, Kim DW, Jeong I, Kim Y, et al. The clinical and virological features of the first imported case causing MERS-CoV outbreak in South Korea, 2015. BMC Infect Dis. 2017;17:498. http://dx.doi.org/10.1186/s12879-017-2576-5

Address for correspondence: Nam-Hyuk Cho, Seoul National University, College of Medicine, 103 Daehak-ro, Jongno-gu, Seoul 03080, South Korea; email: chonh@snu.ac.kr; Hyoung-Shik Shin, National Medical Center, 245 Eulji-ro, Jung-gu, Seoul 04564, South Korea; email: hyoungsshin@nmc.or.kr

EID Podcast:
Unraveling the Mysteries of Middle East Respiratory Syndrome Coronavirus

Middle East respiratory syndrome coronavirus (MERS-CoV) is a novel CoV known to cause severe acute respiratory illness in humans; approximately 40% of confirmed cases have been fatal. Human-to-human transmission and multiple outbreaks of respiratory illness have been attributed to MERS-CoV, and severe respiratory illness caused by this virus continues to be identified. As of February 23, 2014, the World Health Organization has reported 182 laboratory-confirmed cases of MERS-CoV infection, including 79 deaths, indicating an ongoing risk for transmission to humans in the Arabian Peninsula.

Visit our website to listen:
http://www2c.cdc.gov/podcasts/player.asp?f=8631627

EMERGING INFECTIOUS DISEASES®

Mass Die-Off of Saiga Antelopes, Kazakhstan, 2015

Sasan Fereidouni, Graham L. Freimanis, Mukhit Orynbayev, Paolo Ribeca, John Flannery, Donald P. King, Steffen Zuther, Martin Beer, Dirk Höper, Aidyn Kydyrmanov, Kobey Karamendin, Richard Kock

In 2015, a mass die-off of ≈200,000 saiga antelopes in central Kazakhstan was caused by hemorrhagic septicemia attributable to the bacterium *Pasteurella multocida* serotype B. Previous analyses have indicated that environmental triggers associated with weather conditions, specifically air moisture and temperature in the region of the saiga antelope calving during the 10-day period running up to the event, were critical to the proliferation of latent bacteria and were comparable to conditions accompanying historically similar die-offs in the same areas. We investigated whether additional viral or bacterial pathogens could be detected in samples from affected animals using 3 different high-throughput sequencing approaches. We did not identify pathogens associated with commensal bacterial opportunisms in blood, kidney, or lung samples and thus concluded that *P. multocida* serotype B was the primary cause of the disease.

The saiga antelope (*Saiga tatarica tatarica* and *S.t. mongolica*) is a critically endangered species (*1*) with populations located in Kazakhstan in addition to small remnants in Russia and Uzbekistan and a subspecies in Mongolia. Each year during the month of May, Saiga antelopes gather in Kazakhstan for calving. Mass die-offs in their populations have been reported previously and were attributed to viral and bacterial etiologies, including pasteurellosis (*2*). However, the diagnosis in most of these events has been unreliable because of insufficient fresh sampling and diagnostic work (*2*).

During a large outbreak in 2015, extensive diagnostics and environmental studies were undertaken, subject to restricting factors such as remoteness and limited cold chain resources. Annual disease monitoring in saiga antelopes had been established after die-offs occurred in western Kazakhstan in 2010, and an international multidisciplinary research team was on the ground at the time of the die-off, performing routine surveillance (*3,4*).

The mass die-off of saiga antelopes in Kazakhstan started around May 10, 2015, and caused ≈200,000 deaths across several calving groups within 3 weeks. These subgroups of saiga antelopes were spread discretely across a landscape of several hundreds of thousands of square kilometers. The number of dead animals constituted more than two thirds of the global population of saiga antelope at the time. The outbreak wiped out 88% of the Betpak-Dala population in central Kazakhstan (*5*) and appeared to have a 100% case-fatality rate.

Laboratory results on the microbiologic, pathologic, and environmental conditions at the time of the 2015 outbreak suggested hemorrhagic septicemia caused by *Pasteurella multocida* serotype B and triggered by environmental conditions (*3*,*6*). However, whether a second unknown infectious agent had predisposed the animals to infection with *P. multocida* was unclear from the laboratory results. Given the opportunistic nature of *Pasteurella*, the objective of our study was to attempt to identify whether any additional unknown potential causative pathogens were present in samples (taken from 10 animals) that might may have contributed to the die-off.

Materials and Methods

Field Assessment

The first dead animals were detected in the Amangeldy District (Kostanay region) of Kazakhstan on May 10, 2015, and additional die-offs were recorded in unconnected discrete locations in the Aktobe and Akmola regions (*3*). A primary diagnosis of hemorrhagic septicemia as the cause of death was proposed at the sites on the basis of clinical signs and gross pathology. We took FTA papers of whole blood spots from 8 freshly dead, female animals (Table 1) in a 2-km radius on the last 2 days of the operation and sent them to international reference laboratories for high-throughput sequencing (HTS) protocols. FTA cards were

Author affiliations: University of Veterinary Medicine Vienna, Vienna, Austria (S. Fereidouni); The Pirbright Institute, Pirbright, UK (G.L. Freimanis, P. Ribeca, J. Flannery, D.P. King); Research Institute for Biological Safety Problems, Otar, Kazakhstan (M. Orynbayev); Association for the Conservation of Biodiversity of Kazakhstan, Astana, Kazakhstan (S. Zuther); Frankfurt Zoological Society, Frankfurt, Germany (S. Zuther); Friedrich-Loeffler-Institut, Greifswald-Insel Riems, Germany (M. Beer, D. Höper); Institute of Microbiology and Virology, Almaty, Kazakhstan (A. Kydrymanov, K. Karamendin); Royal Veterinary College, London, UK (R. Kock)

DOI: https://doi.org/10.3201/eid2506.180990

Table 1. Details outlining the origins of the 8 FTA samples, including animals and GPS data, used in an investigation of a mass die-off of saiga antelopes, Kazakhstan, 2015*

Sample no.	Species	Age, y/sex	Comment	Sample type	GPS no.	Date
1	*Saiga tatarica*	3–4/F	Postmortem	FTA x2	427	2015 May 26
2	*Saiga tatarica*	3/F	Postmortem	FTA x2	426	2015 May 26
3	*Saiga tatarica*	1–2/F	Postmortem	FTA x2	456	2015 May 26
4	*Saiga tatarica*	1–2/F	Postmortem	FTA x2	452	2015 May 26
5	*Saiga tatarica*	5–6/F	Postmortem	FTA x2	457	2015 May 26
6	*Saiga tatarica*	>5/F	Postmortem	FTA x2	458	2015 May 26
7	*Saiga tatarica*	2/F	Postmortem	FTA x2	455	2015 May 26
8	*Saiga tatarica*	13/F	Postmortem	FTA x2	NA	2015 Jun 25

*GPS, global positioning system; NA, no information available.

used as backup given the limited resources available and difficulties in maintaining cold chain and in transportation of fresh samples to local laboratories. Lung and kidney tissue from 2 dead saiga antelopes (lung tissue from animal X and kidney tissue from animal Y) from the Turgai River region were also processed for 16S metagenomics sequencing in the city of Almaty, Kazakhstan. Although these samples were from a region 175 km from the site where the FTA card samples were taken, they were considered part of the same saiga antelope population. Given the uniformity of the clinical syndrome and consistency of the pathogenesis, the sample of cases selected was small relative to the scale of the die-off, but each case was evaluated in considerable depth and considered representative of the affected population on the basis of the consistent pathology and disease characteristics observed in all the affected animals (*3*).

Laboratory Assessment

We submitted samples of dried blood spots (2 cm in diameter) on FTA papers taken from 8 animals to 2 different research institutions (the Pirbright Institute in the United Kingdom and the Friedrich-Loeffler-Institut [FLI] in Germany) for HTS analyses (Figure 1) under 2 different HTS protocols (random amplification–based sequencing at Pirbright and RNA sequencing at FLI). Six of the 8 FTA blood spot samples were processed for further testing by using HTS at Pirbright, and 4 of the 8 samples were processed for further testing at FLI. Two of the 8 samples were processed by both laboratories. Lung and kidney tissue from 2 dead saiga antelopes (Table 2) were tested for 16S bacterial diversity by using a 16S metagenomic sequencing protocol developed by the Institute of Microbiology and Virology in Almaty (Figure 2).

Results

We analyzed reads from each of the parallel investigations by using established bioinformatics pipelines to identify microbial agents present within each sample. All raw datasets, de novo assemblies, and 16S sequencing metagenome data sets have been submitted to the European Nucleotide Archive

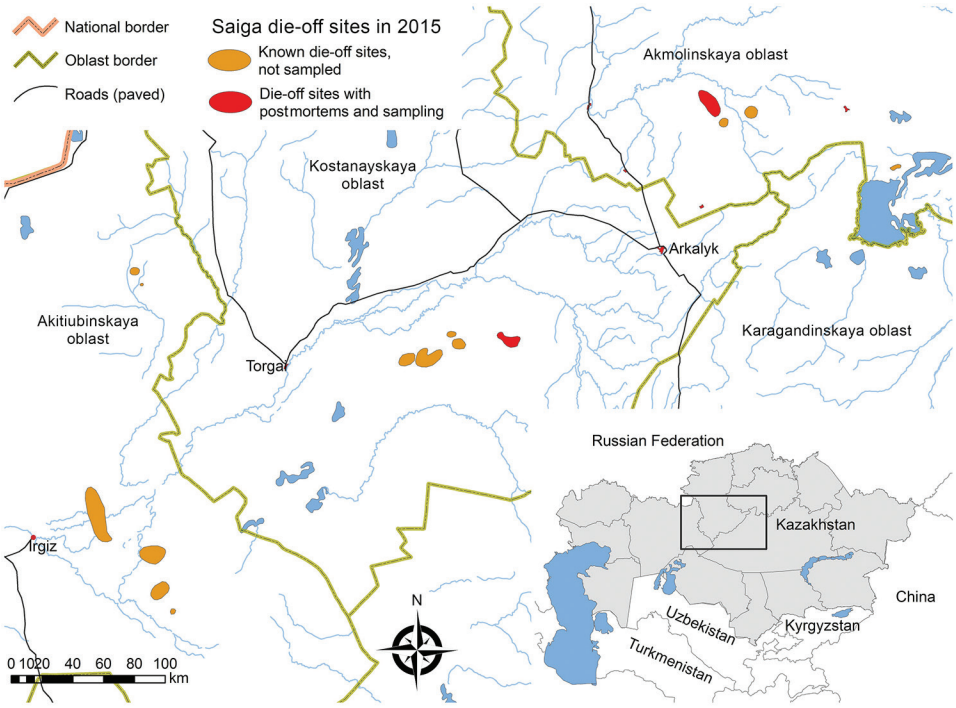

Figure 1. Geographic distribution of saiga antelope die-off events, Kazakhstan, 2015. Red and orange areas indicate known outbreak locations of the 3 saiga populations. Inset shows area in relation to the rest of Kazakhstan and neighboring countries of central Asia.

Table 2. Characteristics of fresh tissue samples transferred to Almaty for 16S ribosomal profiling used in an investigation of a mass die-off of saiga antelopes, Kazakhstan, 2015*

Animal	Date	GPS	Species	Age y/sex	Sample used for HTS
Animal X	2015 May 16	49°46.586N/ 65°26.369E	*Saiga tatarica*	2/F	Lung
Animal Y	2015 May 19	49°45.001N/065°27.536E	*S. tatarica*	3/F	Kidney

*HTS, high-throughput sequencing.

and GenBank (accession nos. PRJEB28164, PRJEB28184, and PRJNA486600).

Random Amplification–Based Sequencing Protocol

The Pirbright protocol consisted of a random amplification workflow, with libraries sequenced using the MiSeq System (Illumnia, https://www.illumina.com) to identify microbial nucleic acids present in dried peripheral blood spots. The classification of sequenced reads into different taxonomic groups was conducted by using 2 approaches; the first was a k-mer–based approach that assigned each read independently (Table 3; Appendix Table 1, https://wwwnc.cdc.gov/EID/article/25/6/18-0990-App1.pdf), and the second was a de novo approach that first assembled reads into contigs and then assigned contigs (Table 4; Appendix Tables 2–4). Approximately 72% of the original reads mapped to the assembly produced by the de novo approach. Neither of these 2 approaches conclusively identified a single virus as a causative agent in all samples. In all 6 samples tested, 46.4% (geometric mean [GM]) of reads were unclassified against the Mini-Kraken Database (https://ccb.jhu.edu/software/kraken) and were possibly host-derived; these reads were labeled as unclassified (Table 3). This determination was further supported by the de novo analysis, which identified the largest contigs as being host-derived, having 35% of reads accounting for host material. In terms of microbial organisms, in 6 of 6 samples, the largest numbers of hits (GM 39%) were identified as *Pasteurella* spp. The specificity of this finding was increased for the *P. multocida* genome, which exhibited the greatest number of matches (GM 69,760 hits/sample [35.4%]). The microbial organism with the second highest number of hits in all samples was *Alteromonas macleodii* (GM 215 hits/sample [0.11%]). K-mers present in all 6 samples also aligned with the *Achromobacter xylosoxidans* (GM 102 hits/sample), *Haemophilus* spp. (GM 40 hits/sample), *Mannheimia haemolytica* (GM 13 hits/sample), *Klebsiella* spp. (GM 23 hits/sample), and *Aggregatibacter* spp. (GM 16 hits/sample),

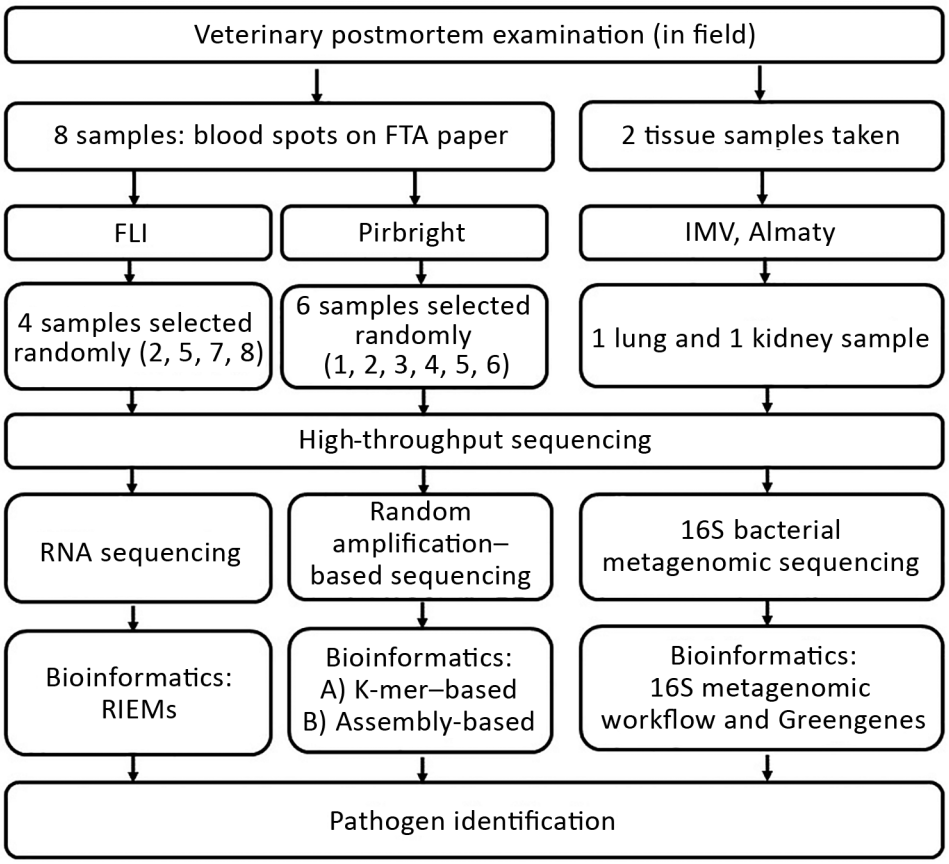

Figure 2. Outline of the process of sampling and high-throughput sequencing protocols performed at 3 research institutes in an investigation of a mass die-off of saiga antelopes, Kazakhstan, 2015. FLI, Friedrich-Loeffler-Institut; IMV, Institute of Microbiology and Virology.

Table 3. Main results of the k-mer–based approach on the random amplification metatranscriptomic dataset used in an investigation of a mass die-off of saiga antelopes, Kazakhstan, 2015*

Organism	No. reads (% total reads)					
	Sample 1	Sample 2	Sample 3	Sample 4	Sample 5	Sample 6
Total no. reads	231,907	773,835	272,102	300,807	235,255	187,049
Total no. reads passing QC	109,302 (47.1)	553,163 (71.48)	174,613 (64.17)	233,888 (77.8)	171,409 (72.86)	138,292 (73.93)
Unclassified/nonmicrobial	50,478 (46.18)	343,404 (62.08)	86,165 (49.35)	133,456 (57.06)	57,812 (33.73)	50,731 (36.68)
Virus	47 (0.03)	141 (0.03)	33 (0.03)	174 (0.05)	73 (0.04)	51 (0.04)
Pasteurellaceae	53,097 (48.58)	129,337 (23.38)	69,251 (39.66)	63,817 (27.29)	93,378 (54.48)	72,799 (52.64)
Pasteurella multocida	49,844 (45.6)	115,231 (20.83)	60,504 (34.65)	56,775 (24.27)	86,664 (50.56)	67,406 (48.74)
Alteromondales	1303 (1.19)	2690 (0.49)	35 (0.02)	499 (0.21)	32 (0.02)	51 (0.04)
Enterobacteriaceae	52 (0.05)	208 (0.04)	153 (0.09)	112 (0.05)	77 (0.04)	48 (0.03)
Haemophilus	23 (0.02)	77 (0.01)	31 (0.02)	36 (0.02)	63 (0.04)	37 (0.03)
Betaproteobacteria	86 (0.08)	13160 (2.38)	30 (0.02)	86 (0.04)	18 (0.01)	22 (0.02)
Mannheimia	10 (0.0)	18 (0.0)	12 (0.01)	18 (0.01)	19 (0.01)	9 (0.01)
Aggregatibacter	8 (0.0)	37 (0.0)	13 (0.0)	18 (0.0)	16 (0.0)	18 (0.01)
Klebsiella	11 (0.0)	58 (0.01)	16 (0.0)	54 (0.01)	16 (0.0)	14 (0.0)

*Only organisms that were identified in all samples and with >10 reads are listed. Samples 2 and 5 were also tested at Friedrich-Loeffler-Institut by using an RNA sequencing protocol. QC, quality control.

albeit to a lower level than the top 2 results. All the other organisms tested had matches of <10 hits and were not considered statistically significant.

The de novo analysis approach also did not identify any homologies with unexpected viral genomes. Several bacteria were identified by both k-mer and de novo analysis protocols, including *P. multocida* and *M. haemolytica*, although these bacteria had smaller contigs (182 bp and 85 bp, respectively) and were thus not included in the results (Table 4). We were unable to identify 195 contigs produced by the de novo assembly despite using several BLAST databases (https://blast.ncbi.nlm.nih.gov/Blast.cgi). We subjected these contigs to an extended analysis in which they were first aligned to BLAST databases with tblastx to find similarities at the protein level. That analysis generated matches for 35 contigs; the distribution of the matches in terms of species mirrors quite closely the one found by nucleotide BLAST (Appendix Tables 2–4). Separately, we also translated and subjected the unknown contigs to a search using SUPERFAMILY (http://supfam.org). This approach returned hits for 87 contigs (Appendix Tables 2–4), of which most appeared to be homologs of bacterial proteins. No further pathogens could be conclusively identified using this analysis. Further analysis of the assembled sequences attributed to *P. multocida* did not permit accurate conclusions to be drawn because of the fragmented nature of the contigs.

RNA Sequencing Protocol

By using the RIEMS analysis pipeline, we performed taxonomic analysis of the sequencing reads obtained from libraries generated from RNA extracted from 4 blood spots from FTA cards that had been transcribed into cDNA using random hexamer priming followed by shotgun library preparation. Of the samples tested at FLI, samples 2 and 5 were also tested at Pirbright. Overall, these analyses classified 77.9%–93.5% of the reads as *P. multocida* (Table 5). The remainder mainly represented host sequences (0.9%–16.2%). With a few exceptions for phage reads, no reads were classified as being of viral origin, which was concordant with findings of the Pirbright dataset. In all samples, the proportion of reads remaining unclassified after analysis of the nucleic acid sequences was low (0.42%–0.45%); these unclassified reads had median lengths of

Table 4. Main results obtained using a de novo approach on the random amplification meta-transcriptomic dataset used in an investigation of a mass die-off of saiga antelopes, Kazakhstan, 2015*

Read area	No. contigs†	Total length, bp	Attribution‡	Comment
796	2	271	*Pasteurella bettyae* CCUG 2042	
1,758,115	162	27,999	*Ovis canadensis canadensis*	Host
1,676,355	23	5,780	*Capra hircus* (goat)	
36,795	7	1,287	*Bubalus bubalis* (water buffalo)	
30,763	14	1,959	*Bos taurus* (cattle)	
3,252	6	1,366	*Saiga tatarica*	
2,625	8	1,283	*Ovis aries* (sheep)	
2,414	5	969	*Bos indicus*	
1,650	2	317	*Eudorcas thomsonii* (Thomson's gazelle)	
14,221,307	6,641	2,103,430	*Pasteurella multocida*	Other
69,009	195	27036	Unknown sequence	
35,246	1	401	Uncultured eukaryote	
796	2	271	*Pasteurella bettyae* CCUG 2042	

*Equivalent to the contig length × the average read coverage.
†Number of contigs with the same attribution.
‡As determined by the best blastn hit.

Table 5. Summary of the most relevant results obtained by RIEMS analyses of the datasets (sequenced from shotgun libraries generated from random primed cDNA) used in an investigation of a mass die-off of saiga antelopes, Kazakhstan, 2015

	No. (%) reads			
Organism	Sample 2* (lib01416)	Sample 5* (lib01417)	Sample 7 (lib01418)	Sample 8 (lib01419)
Input reads	411,640 (100)	376,210 (100)	372,387 (100)	354,958 (100)
Quality filtered reads†	12,786 (3.1)	10,793 (2.9)	11,559 (3.1)	10,895 (3.1)
Unclassified reads†	1,776 (0.43)	1,520 (0.40)	1,626 (0.44)	1,494 (0.42)
Classified reads†	397,078 (96.5)	363,897 (96.7)	359,202 (96.5)	342,569 (96.5)
Host‡	64,618 (16.3)	4,770 (1.3)	3,414 (1.0)	4,784 (1.4)
Pasteurellaceae‡	317,009 (79.8)	345,893 (95.1)	339,484 (94.5)	324,770 (94.8)

*Samples 2 and 5 were also tested by using high-throughput sequencing at the Pirbright Institute.
†Percentage is of the number of input reads.
‡Percentage is of the number of classified reads.

35 bp (interquartile range 25–45 bp) and accounted for 0.068%–0.082% of the total bases. Therefore, the information content of the unclassified portion of the datasets was too low to provide additional information even by additional analyses on the basis of the amino acid sequences deduced from these reads.

To conduct a detailed analysis of the numerous *P. multocida* organisms detected, we mapped the complete datasets along the *P. multocida* genome sequence (GenBank accession no. NC_002663.1). We then performed blastx (*7*) analyses of the resulting contigs for a basic function prediction of the expressed genes. Besides detecting genes encoding proteins of gene expression, general metabolism, and cell division, these analyses detected several proteins associated with pathogenicity. For example, proteins facilitating active iron uptake (iron ABC transporter permease [GenBank accession no. WP_010906625], iron ABC transporter substrate binding protein [accession no. WP_005715971.1], iron binding protein [accession no. WP_005726096.1], and iron permease [accession no. WP_010906655.1]) or proteins of the oxidative stress response (catalase [accession no. WP_010906440], superoxide dismutase [accession no. WP_005750998], peroxiredoxin [accession no. WP_005716614.1]). These analyses also revealed expression of genes encoding stress- and starvation-induced proteins (stringent starvation protein A homologue [accession no. WP_005726291.1]) and the virulence factor SrfB (accession no. WP_005755436.1).

16S Metagenomic Sequencing Protocol

We applied a metagenomics workflow for classifying organisms from the V3 and V4 regions of the 16S rRNA gene by using a Greengenes database (http://greengenes.lbl.gov) to test tissue taken from 2 animals (lung tissue from animal X and kidney tissue from animal Y) (Table 6). Among the variable regions of 16S gene, V3 is a highly variable region that can distinguish bacteria to the genus level. V4 is also efficient but less so than V3 (*8*). The output of the workflow classified the reads at the primary taxonomic levels (kingdom, phylum, class, order, family, genus, and species).

Sequencing statistics revealed the number of total reads to be 63,508 for lung tissue and 15,422 for kidney tissue. The number of reads passing quality filtering was 58,161 for lung tissue and 14,291 for kidney tissue. The percentage of reads passing quality filtering was 91.6% for lung tissue and 92.7% for kidney tissue.

Of all reads generated, 86.80%–89.05% of all short reads were from bacteria of the genus *Pasteurella*, of which 44.06%–48.32% were identified as *P. multocida*. Other species were *Pasteurellaceae* (10.75%–12.21%), *P. pneumotropica* (4.06%–5.67%), and those unclassified at species level (34.91%–36.53%) (Table 5). More than 80% of unclassified reads at the species level belonged to the *Pasteurella* genus.

Discussion

Saiga antelopes are a critically endangered species (*1*), and the population is increasingly fragmented and vulnerable to stochastic events such as disease epidemics. The mass die-off in Kazakhstan and the small population of ≈10,000 in Mongolia recently devastated by peste des petits ruminants (PPR) virus in 2017 illustrates this point (*3*). The saiga antelopes undertake large-scale seasonal migrations between their summer and winter ranges because of the extreme variation in climate conditions and the need for pastures offering sufficient forage. The calving sites are highly variable from year to year and depend on plant phenology, environmental factors, and anthropogenic effects (*9*). The analysis of available data showed that the number of saiga antelopes in Kazakhstan over the past 60 years has fluctuated widely, from ≈2 million in the 1970s to ≈50,000 animals in the early 21st century because of poaching and other factors, including a series of mass die-offs (*10*,*11*). A few incidences of infectious disease, including foot-and-mouth disease, have been confirmed (*12*), but most events were attributable to pasteurellosis; *M. haemolytica* and *P. multocida* were isolated on occasion (*13*). However, diagnoses are lacking comprehensive clinical, pathological, epidemiologic, and environmental investigation and remain tentative in all cases outside the 2015 event. Diagnosis of wildlife deaths is constrained by the fact these populations are not managed nor always monitored regularly, meaning die-offs occur frequently and investigators often do not have access to fresh carcasses. In the 2015

Table 6. Top 8 of 94 species classification results after 16S bacterial metagenome sequencing in an investigation of a mass die-off of saiga antelopes, Kazakhstan, 2015*

	No. reads		% Total reads	
Classification	Lung (animal X)	Kidney (animal Y)	Lung (animal X)	Kidney (animal Y)
Pasteurella multocida	25,625	6,907	44.06	48.32
Unclassified at species level	21,246	4,990	36.53	34.91
Pasteurellaceae	7,101	1,536	12.21	10.75
Pasteurella pneumotropica	3,298	580	5.67	4.06
Mannheimia caviae	462	78	0.79	0.55
Serratia entomophila	50	17	0.09	0.12
Bacillus horneckiae	49	16	0.08	0.11
Vagococcus teuberi	39	13	0.07	0.09
Sporolactobacillus putidus	50	0	0.09	0
Acinetobacter gerneri	49	0	0.08	0
Gallibacterium melopsittaci	39	0	0.07	0

*Total species-level taxonomic categories identified: 94 for lung sample (animal X) and 68 for kidney sample (animal Y).

saiga antelope event, a monitoring team was in place in 2 of the 15 die-off locations and were equipped for general diagnostic work. This situation was unusual and provided a unique opportunity, but the unpredictability of such an event happening limited the extent of the outbreak investigation. Sampling was necessarily strategic, and because all of the animals in the population were affected by the same syndrome and died, the sample size did not need to be large or statistically representative. Each case would have an equal chance of providing the result, and failure to diagnose would be more likely a product of insufficient material per case or loss of viability of organisms because of cold chain and storage issues.

Nevertheless, the findings obtained from this work are representative of the population for a few reasons. First, the clinical syndrome was uniform in both the adult and calf populations. We observed no statistically significant variation in the temporal progression once symptoms were noted, and clinical signs and gross pathology were highly consistent. Second, the 100% mortality rate among the herds indicates a universal effect, and no samples taken were likely to be nonrepresentative or attributable to an alternate etiology. In addition, the rapidity of the syndrome precluded large numbers of cases being investigated by our relatively small team because necropsy and sampling for each case took several hours to complete.

Microbiologic and virologic diagnostic methods showed that in samples from >90% of saiga antelopes that died in 2015, the cause was pasteurellosis (*3*,*6*). Previous studies had demonstrated the absence of other potential causative agents by diagnostic PCR, including bacteria (e.g., anthrax bacillus, *Coxiella burnetti*, *Erysipelothrix rhusiopathiae*, and *Listeria* spp.), mycoplasma (e.g., *Mycoplasma ovipneumoniae*), and virus diseases (e.g., foot-and-mouth disease, bluetongue, PPR, epizootic hemorrhagic disease, sheep pox, Akabane, Aujesky's disease, bovine viral diarrhea, visna-maedi, and malignant catarrhal fever) (*3*,*6*). Furthermore, these studies used capsular typing with specific primers to show that strains of *P. multocida* from saiga antelopes belonged to serogroup B (*3*,*6*). Our 16S analysis also showed that the *P. multocida* isolated from saiga antelopes in 2015 in Akmola and Kostanay oblasts were genetically identical to the bacteria isolated from saiga antelopes in 1988, 2010, 2011, and 2012, as well as *P. multocida* subsp.*multocida*_PM30 strain (GenBank accession no. AY299312) isolated from ill cattle with hemorrhagic septicemia in 2004 (*6*).

Three different HTS protocols were used in parallel to identify unknown microbial pathogens that played a potential role in disease pathogenesis: a protocol based on random amplification using Illumina sequencing; an RNA-based analysis without amplification combined with sequencing on an Ion Torrent (ThermoFisher, https://www.thermofisher.com); and a bacterial 16S sequencing pipeline using Illumina technology. Each of these workflows demonstrated the potential for different experimental challenges in obtaining metagenomic datasets (e.g., biases in amplification-based protocols and the use of low-input starting material in no-amplification protocols) (*14*). The high sensitivity of such methods to detect small amounts of nucleic acids also poses challenges in terms of prevention of contamination and false-positive results. Caution should be exercised in drawing conclusions from such datasets without appropriate validation. In addition to blood spots, other tests, including bacteriologic and virologic tests on various tissues and samples taken, were conducted locally in Kazakhstan at government laboratories and reported elsewhere (*3*).

Despite the high sensitivity of the methodologies we used, our study is somewhat limited by the sample type (FTA cards), which precludes the detection of pathogens in lymphoid tissues and other organs. The use of FTA cards might also introduce biases in the testing protocols, which can favor or hinder the detection of certain types of viruses (*15*).

Both metagenomic protocols conclusively identified *Pasteurella* spp. in large numbers of reads compared with other pathogens; these findings were then confirmed in a third pipeline using 16S bacterial ribosomal RNA sequencing. Further analysis of *P. multocida* bacterial sequences

suggested that the expression of metabolic- and stress-related proteins might suggest that the bacteria were actively growing and in active competition with the host organism for essential nutrients, especially iron, as shown by the expression of the genes coding for iron uptake systems.

Our de novo assembly approach also identified 195 short contigs that could not be attributed to any sequence present in several BLAST databases; of those, only 47 were identified using tblastx. The subsequent analysis based on SUPERFAMILY was only able to find protein homologies for 6 contigs, with most of them having homologies to bacterial genes. Whether this result is important is unclear; our unknown contigs might belong to ≥1 uncultured bacteria that have not been sequenced before. Previously published metagenomic studies have resulted in as many as 50% unidentifiable reads (*16*,*17*); the figures for our work are reduced in comparison, in particular when considering the results of our de novo approach (≈72% of our reads map to our assembly and <1% of the reads map to the contigs that we are unable to identify) (Appendix Table 2). Overall, the amount of unexplained sequence seems relatively small, in particular when considering the substantial number of species of bacterial, viral, and eukaryotic genome that remain either to be discovered or characterized. The simple fact that not all organisms have been sequenced or are available on central sequence repositories will always contribute to a percentage of unidentifiable reads.

P. multocida is a ubiquitous organism, most probably widely present in the saiga antelope population in its latent form. The potential pathogenicity is inherent in the organism and can be triggered opportunistically at any time in response to environmental triggers. The epidemiology of and observations on the spatiotemporal distribution of ill animals and carcasses in this study suggests that transmission of bacteria from animal to animal did not occur in most cases (except from mothers to calves, which occurred through infected milk). The near synchronous events in discrete subpopulations, with large distances between aggregations of many hundreds of kilometers, further precluded an infective process spreading across the population.

Research to date suggests that environmental conditions in the 10 days leading up to a die-off are critical and significantly associated with increased heat and humidity (*3*). The trends in climate in the region are for warmer and wetter conditions, which might have been an important factor in these recent events that have occurred irregularly over the last few decades. Immunocompetence was not thought to be a factor in the pathogenesis because the population was behaving normally, was unstressed, and was in apparent good health and body condition with large fat reserves observed postmortem. In addition, genetic analysis of the saiga antelope population shows them to be the most heterogeneous of any mammal species on record (S. Zuther, unpub. data), thus excluding inbreeding as a factor, despite the potential bottlenecking of the population in recent times.

The mechanism behind the mass die-off might be an environmentally triggered bacterial proliferation that overwhelmed the mucosal immunity of the upper respiratory and gastrointestinal tracts. This hypothesis is further supported by the observation that calves, which are unlikely to be infected with the commensal bacteria in the first couple days of life, died some hours or longer after their mothers, most likely from suckling infected milk from ill or dead mothers, activity that was observed by investigators (*3*).

In this study, HTS was used to identify pathogens that might have predisposed or contributed to the severity of the saiga antelope die-off in 2015. In previous studies, *P. multocida* type B was identified by culture, and viruses of veterinary importance (foot-and-mouth, PPR, and bluetongue viruses) were ruled out by using pathogen-specific diagnostic tests. In our study, 3 laboratories using 3 distinct HTS analytic approaches failed to identify additional pathogens. These findings, combined with clinical, necroscopic, microbiologic, and histopathologic investigations, indicate hemorrhagic septicemia caused by *P. multocida* serotype B is the proximate cause, and possibly the only cause, of this die-off. Environmental factors might have triggered nearly simultaneous bacterial proliferation and subsequent virulence in affected aggregations.

Comprehensive field monitoring and additional experimental studies of *P. multocida* infection in saiga antelopes are necessary to evaluate the potential co-factors triggering the virulence of bacteria. These recurrent mass die-offs could cause extinction of saiga antelope populations in just 1 event, especially if, in future outbreaks, additional pathogens in combination with *P. multocida* affect the population.

This study was undertaken with the approval of the Royal Veterinary College Ethical Review Board (unique reference no. 2015 1435), the Biosafety Institute of the Ministry of Science and Education, the Committee for Forestry and Wildlife, and the Veterinary Reference Laboratory Astana, Ministry of Agriculture, Republic of Kazakhstan.

This study was funded by the National Environment Research Council of the United Kingdom urgency research grant (no. NE/N007646/1), the Association for the Conservation of Biodiversity of Kazakhstan, the Flora and Fauna International, the People's Trust for Endangered Species, the Saiga Conservation Alliance, the Royal Society for the Protection of Birds, and the Frankfurt Zoological Society. G.L.F. was funded through a research project (EpiSeq) by the European and Major Infectious Disease of Livestock–European Research Area. S.F., D.H., and M.B. received funding from the European Union Horizon 2020 Research and Innovation Program COMPARE

(grant no. 643476). J.F. and D.P.K. were funded through grants from the Department of the Environment, Fisheries, and Rural Agriculture. P.R. received support from the Biotechnology and Biological Sciences Research Council of the United Kingdom (project nos. BB/E/I/00007035, BB/E/I/00007036, and BBS/E/I/00007039).

About the Author

Dr. Fereidouni is a senior scientist at the Research Institute of Wildlife Ecology at the University of Veterinary Medicine of Vienna. His primary research interests include wildlife conservation and health, wildlife diseases and emerging pathogens, One Health, and eco-immunology.

References

1. Mallon DP. *Saiga tatarica* ssp. In: IUCN red list of threatened species. Version 2011.2. Cambridge: International Union for Conservation of Nature Global Species Programme Red List Unit; 2011.
2. Kock R, Grachev Y, Zhakypbayev A, Usenbayev A, Zuther S, Klimanova O, et al. G. A retrospective assessment of saiga antelope *Saiga tatarica* die-off in Western Kazakhstan 2010–2011. Saiga News. 2011;14:1–4.
3. Kock R, Orynbayev M, Robinson S, Zuther S, Singh N, Beauvais W, et al. Saigas on the brink: multi-disciplinary analysis of the factors influencing mass mortality events. Sci Adv. 2018;4:eaao2314.
4. Zuther S. The saiga antelope mass die-off in the Betpak-Dala population in May 2015. Saiga News. 2016;20:6–8.
5. Abdrakhmanov A. Overview of the 2015 saiga mass mortality event in Kazakhstan. Presented at: Technical Workshop of the Third Meeting of Signatories of the Memorandum of Understanding Concerning Conservation, Restoration, and Sustainable Use of the Saiga Antelope (*Saiga* spp.), October 2015, Tashkent, Uzbekistan [in Russian] [cited 2018 Jan 7]. https://www.cms.int/en/document/technical-workshop-2610-overview-2015-saiga-mass-mortality-event-kazakhstan
6. Orynbayev M, Sultankulova K, Sansyzbay A, Rystayeva R, Shorayeva K, Namet A, et al. Biological characterization of *Pasteurella multocida* present in the Saiga population. BMC Microbiol. 2019;19:37. http://dx.doi.org/10.1186/s12866-019-1407-9
7. Altschul SF, Madden TL, Schäffer AA, Zhang J, Zhang Z, Miller W, et al. Gapped BLAST and PSI-BLAST: a new generation of protein database search programs. Nucleic Acids Res. 1997;25:3389–402. http://dx.doi.org/10.1093/nar/25.17.3389
8. Chakravorty S, Helb D, Burday M, Connell N, Alland D. A detailed analysis of 16S ribosomal RNA gene segments for the diagnosis of pathogenic bacteria. J Microbiol Methods. 2007;69:330–9. http://dx.doi.org/10.1016/j.mimet.2007.02.005
9. Singh NJ, Grachev IA, Bekenov AB, Milner-Gulland EJ. Saiga antelope calving site selection is increasingly driven by human disturbance. Biol Conserv. 2010;143:1770–9. http://dx.doi.org/10.1016/j.biocon.2010.04.026
10. Milner-Gulland E, Kholodova M, Bekenov A, Bukreeva O, Grachev I, Amgalan L, et al. Dramatic declines in saiga antelope populations. Oryx. 2001;35:340–5. http://dx.doi.org/10.1017/S0030605300032105
11. Grachev Y. Results of the 2013 aerial survey in Kazakhstan. Saiga News. 2013;17:5.
12. Orynbayev MB, Beauvais W, Sansyzbay AR, Rystaeva RA, Sultankulova KT, Kerimbaev AA, et al. Seroprevalence of infectious diseases in saiga antelope (*Saiga tatarica tatarica*) in Kazakhstan 2012-2014. Prev Vet Med. 2016;127:100–4. http://dx.doi.org/10.1016/j.prevetmed.2016.03.016
13. Bekenov AB, Pole SB, Khakhin GV, Grachev YA. Mortality from diseases and parasitic invasions. In: Sokolov VE and Zhirnov LV, editors. The saiga antelope. Moscow: Russian Academy of Sciences; 1998. p 247–52.
14. Höper D, Mettenleiter TC, Beer M. Metagenomic approaches to identifying infectious agents. Rev Sci Tech. 2016;35:83–93. http://dx.doi.org/10.20506/rst.35.1.2419
15. Conceição-Neto N, Zeller M, Lefrère H, De Bruyn P, Beller L, Deboutte W, et al. Modular approach to customise sample preparation procedures for viral metagenomics: a reproducible protocol for virome analysis. Sci Rep. 2015;5:16532. http://dx.doi.org/10.1038/srep16532
16. Yooseph S, Andrews-Pfannkoch C, Tenney A, McQuaid J, Williamson S, Thiagarajan M, et al. A metagenomic framework for the study of airborne microbial communities. PLoS One. 2013;8:e81862. http://dx.doi.org/10.1371/journal.pone.0081862
17. Afshinnekoo E, Meydan C, Chowdhury S, Jaroudi D, Boyer C, Bernstein N, et al. Geospatial resolution of human and bacterial diversity with city-scale metagenomics. Cell Syst. 2015;1:72–87. http://dx.doi.org/10.1016/j.cels.2015.01.001

Address for correspondence: Richard Kock, The Royal Veterinary College, Hawkshead Lane, North Mymms, Hatfield, Hertfordshire AL9 7TA, UK; email: rkock@rvc.ac.uk

Survey of Crimean-Congo Hemorrhagic Fever Enzootic Focus, Spain, 2011–2015

Ana Negredo, Miguel Ángel Habela, Eva Ramírez de Arellano, Francisco Diez, Fátima Lasala, Pablo López, Ana Sarriá, Nuria Labiod, Rafael Calero-Bernal, Miguel Arenas, Antonio Tenorio, Agustín Estrada-Peña, Maria Paz Sánchez-Seco

During 2011–2015, we conducted a Crimean-Congo hemorrhagic fever virus (CCHFV) survey in captured ticks that were feeding mainly on wild and domestic ungulates in Spain, where presence of this virus had been reported previously. We detected CCHFV RNA in *Hyalomma lusitanicum* and *H. marginatum* ticks for 3 of the 5 years. The rate of infected ticks was 2.78% (44/1,579), which was similar to those for other countries in Europe with endemic foci for CCHFV (Kosovo, Bulgaria, and Albania). These data confirm the established spread of CCHFV into western Europe. Phylogenetic study of the small RNA segment showed Africa-3 clade as the only genotype identified, although we observed cocirculation of genetic variants during 2011 and 2015. We could not rule out genetic reassortments because of lack of sequence data for the medium and large RNA segments of the virus genome.

Crimean-Congo hemorrhagic fever virus (CCHFV), an RNA virus of the family *Nairoviridae*, is the most widespread tickborne virus affecting humans. It causes Crimean-Congo hemorrhagic fever (CCHF), which has a high mortality rate in humans (*1*) in many countries in Asia, the Middle East, eastern Asia, Africa, and Europe (*2,3*). Recently, CCHF has been detected in Spain, indicating its spread into western Europe (*4,5*).

CCHF is a zoonosis maintained between ticks and vertebrate animals. Ticks are both the vector and the natural reservoir of CCHFV. Ticks transmit CCHFV to large and small mammals, which act as amplifier hosts without signs of illness. Birds are predominantly refractory to CCHFV infection (*6–8*). The virus has been isolated from several genera and species of ixodid ticks (*9*). However, most data are for ticks collected while feeding, a method that provides an unrealistic view of the actual species vectors (*10*).

The main vectors involved in CCHFV transmission are ticks of the genus *Hyalomma* (*11–14*). Immature ticks acquire the virus by feeding on infected small vertebrates or by the transovarial route. Once infected, they remain infected throughout their development and, when they are mature, transmit the infection to large animals, such as livestock. Transovarian and venereal transmission pathways have also been demonstrated (*2*). Another transmission mechanism is co-feeding, which results from spreading of the virus in tick saliva directly to other ticks feeding nearby (*13*).

In disease-endemic areas, CCHF is sporadic and is transmitted to humans by tick bites or contact with viremic animals or humans and occurs mainly in remote or agricultural regions (*15–21*). CCHF is seasonal in association with the life cycle and activity levels of local tick populations. CCHF outbreaks and nosocomial transmission has also been reported most often when an infectious case is not suspected early enough to permit use of proper containment protocols (*22*). Persons at risk are most frequently found among farmers and their families, as well as slaughterhouse and healthcare workers, veterinarians, and military personnel (*23*).

Only 2 autochthonous human cases of CCHF have been reported in Spain in an episode with tick and nosocomial transmission. The cases occurred in 2016, and the viruses isolated from these patients were included in the Africa-3 clade (genotype III) (*5,24*), the same clade that was found in local ticks (*4,25*) and 1 of the 6/7 genetic clades in which CCHFV strains are grouped on the basis of small (S) RNA segment sequence homology (*26,27*). Previously, the CCHFV genome was detected in ticks collected in 2010 from red deer in Cáceres, Spain (*4*), which is 300 km from the area (Ávila Province) where the index case-patient acquired the disease through tick bite transmission. After autochthonous human cases were detected,

Author affiliations: National Center of Microbiology, Madrid, Spain (A. Negredo, E. Ramírez de Arellano, F. Diez, F. Lasala, P. López, N. Labiod, A. Tenorio, M.P. Sánchez-Seco); University of Extremadura, Cáceres, Spain (M.Á. Habela, R. Calero-Bernal); La Paz Hospital, Madrid (A. Sarriá); University of Vigo, Pontevedra, Spain (M. Arenas); University of Zaragoza, Zaragoza, Spain (A. Estrada-Peña)

DOI: https://doi.org/10.3201/eid2506.180877

a surveillance study on ticks was conducted to investigate the spread of CCHFV in Spain. Results showed 4 geographic regions with CCHFV-positive results (Figure 1) and the presence of CCHFV in 128 (3.2%) of 3,959 pools of ticks collected from wild and domestic animals (*28*). All CCHFV-positive ticks were collected while they were feeding on wild animals.

These data highlighted the emerging threat for CCHF in Spain and potentially all of western Europe. A new case of CCHF also linked to tick bite transmission occurred in August 2018 in Spain. A study of the presence of CCHFV in Spain was initiated in 2011 to analyze principally its circulation in the region of original detection. We report the results of a survey covering 5 years of collection.

Materials and Methods

Study Area and Tick Collections

Tick collection in Cáceres Province (southwestern Spain, 37°N–41°N, 3°W–7°W) (Figure 1) was focused on adult ticks infesting red deer (*Cervus elaphus*) and, to a lesser extent, other mammals, such as fallow deer (*Dama dama*), red foxes (*Vulpes vulpes*), and wild boars (*Sus scrofa ferus*), legally hunted in privately owned estates during October–February. Sampling areas are located within typical Mediterranean *Quercus* forest in several protected areas and reserves (Tajo International Natural Park and Sierra de San Pedro Mountain Range), which constitute an optimum ecosystem for wild ungulates. Collection of ticks from cattle was also conducted in Cáceres Province. We directly shipped ticks collected at room temperature to the Parasitology Laboratory of the Faculty of Veterinary Medicine at the University of Extremadura (Cáceres). Ticks were identified to species within 1–2 days upon arrival, and frozen at –65°C while alive until isolation of RNA. Tick collection in Segovia Province (41.21°N, 3.59°W) was conducted during the sheep shearing process, and adult ticks captured were identified in the Spanish National Center of Microbiology. Tick collections on the ground were also performed in Huesca (42.21°N, 0.13°W) and Toledo (39.23°N, 4.29°W) Provinces. We captured mainly adult ticks and identified them in the Animal Pathology Department of the Faculty of Veterinary Medicine at the University of Zaragoza. All ticks were sent in dry ice to the Spanish National Center of Microbiology (Madrid, Spain) for processing.

Extraction of RNA from Tick Species

Ticks were washed twice with water and once with ethanol and then individually crushed by using a plastic homogenizer in 500 µL AVL buffer (QIAGEN, https://www.qiagen.com). We conducted homogenization in a Biosafety Level-3 laboratory. After homogenization, we stored 250

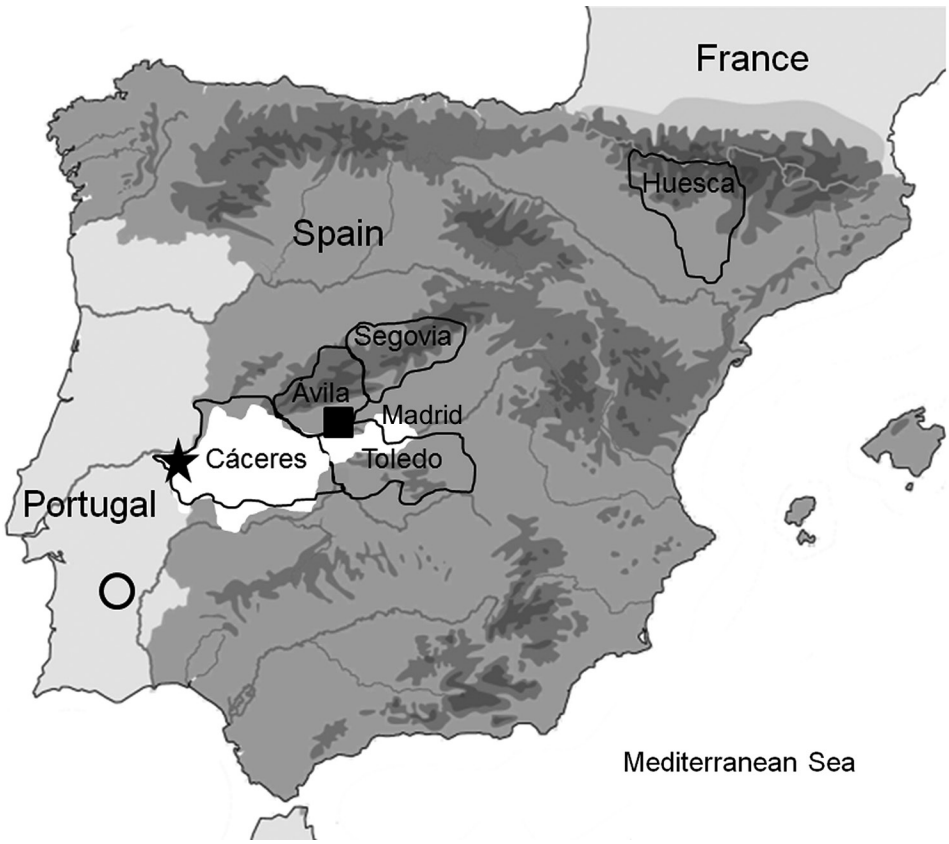

Figure 1. Study site locations in the Iberian Peninsula in which Crimean-Congo hemorrhagic fever virus was detected: Cáceres, Toledo, Segovia, and Huesca Provinces. Square shows presence of CCHFV in humans bitten by a tick, star shows presence of CCHFV in ticks with positive results by PCR, circle indicates region where serum samples positive for CCHFV were detected in Portugal, and white area shows regions in 4 localities (Cáceres, Ávila, and Toledo Provinces and Madrid) in Spain where CCHFV-positive ticks had been previously identified.

µL of the sample in AVL buffer at -80°C and used 250 µL for total extraction of RNA with the QIAamp Viral RNA Mini Kit (QIAGEN), according to the recommendations of the manufacturer. RNA was eluted in 60 µL of RNAase-free water and stored at –80°C until needed.

Reverse Transcription PCR

We used an in-house nested reverse transcription PCR specific for the S genome segment (*5*). We individually analyzed ticks.

DNA Sequencing

We purified amplified DNA by using an Illustra ExoProStar Kit (GE Healthcare Life Sciences, https://www.gelifesciences.com). We sequenced double-stranded DNA directly by using the Sanger chain-termination method and the BigDye Terminator v3.1 Cycle Sequencing Kit Protocol and the ABI PRISM 3700 DNA Analyzer (Applied Biosystems, https://www.thermofisher.com). We used sequencing primers CrCon2+ and CrCon2–, the same used in the nested PCR (*5*). We assembled consensus sequences of each segment and analyzed them by using the SeqMan Program in the Lasergene Package (https://www.dnastar.com).

Phylogenetic Analysis

We aligned nucleotide sequences by using Muscle in MEGA version 7 (https://www.megasoftware.net). Because recombination can bias phylogenetic tree reconstruction, we analyzed recombination in the alignment with the Recombination Detection Program (http://web.cbio.uct.ac.za/~darren/rdp.html) and the Hypothesis Testing Using Phylogenies Program (http://hyphy.org). We did not detect genetic signatures of recombination.

We generated a maximum clade credibility (MCC) genealogy by using BEAUTi and BEAST (*29*). We ran the Markov chain Monte Carlo method for 100 million generations, sampling every 1,000 steps, and analyzed convergence with Tracer (http://www.beast2.org) to ensure that effective sample sizes were >200. We applied the uncorrelated lognormal clock model, the general time-reversible matrix with gamma distribution and proportion of invariable sites substitution model, and the exponential tree prior. We summarized reconstructed trees by applying the MCC approach implemented in TreeAnnotator version 1.8.4 (http://beast.community/treeannotator), used the mean value as the node height, and discarded the first 10% of the generated trees as burn-in. We visualized the MCC tree by using FigTree version 1.4.3 (http://tree.bio.ed.ac.uk). We deposited nucleotide sequences with lengths >200 nt obtained with primers CrCon1+ and CrCon 1– (*5*) in the European Molecular Biology Laboratory/GenBank databases (accession nos. MH337845 and MH337846).

Results

We collected 1,579 ticks in 4 geographic regions in Spain (Figure 1), 206 from vegetation and 1,373 from animals. Of ticks collected from animals, 1,329 (96.79%) were from wild animals and 44 (3.35%) were from domestic animals.

Collected ticks that we could identify belonged to 1 of 4 genera: *Rhipicephalus* (46, 2.91%), *Hyalomma* (1,317, 83.40%), *Dermacentor* (1, 0.06%), or *Ixodes* (3, 0.18%); 212 ticks could not be identified. Most ticks were *H. lusitanicum* (1,079, 68.33%) and *H. marginatum* (238, 15.07%) (Table). *H. lusitanicum* ticks were obtained mainly from wild animals (1,063/1,329), and *H. marginatum* ticks (206/238) were collected principally from vegetation.

We detected CCHFV RNA in 44 (2.78%) of 1,579 ticks collected (Table). All CCHFV-positive ticks were detected in Cáceres (3.25%; 44/1,352). We collected ticks in 31 localities within Cáceres; 5 (16.12%) localities (1, 2, 23, 27, and 28) had virus-positive ticks. Rates for CCHV-positive ticks were 8.79% in locality 1, 9.03% in locality 2, 7.14% in locality 23, 2.77% in locality 27, and 2.22% in locality 28. CCHFV-positive ticks were collected during 2011, 2013, and 2015. In Cáceres, the rate of CCHFV in ticks was 4.1% in 2011, 6.4% in 2013, and 3.42% in 2015.

A total of 43 *H. lusitanicum* ticks and 1 *H. marginatum* tick were positive for CCHFV (Table); 41 of 43 CCHFV-positive *H. lusitanicum* ticks were collected while feeding on red deer, and CCHFV-positive *H. marginatum* ticks were collected from 1/6 bovine animals analyzed in locality 23 (Table). Six *H. lusitanicum* ticks and 1 *H. marginatum* tick were found on this animal. Of these ticks, 1 *H. lusitanicum* male and 1 *H. marginatum* female were positive for CCHFV. This animal might not have been viremic, which would explain why only 2 of 6 ticks were infected by the co-feeding transmission mechanism, in which virus present in tick saliva can spread directly to other ticks feeding nearby. In locality number 23, CCHFV-positive *H. lusitanicum* ticks were detected on a second cow and 1 red deer.

We obtained sequences from 43 of 44 CCHFV-positive ticks. CCHFV sequences from Spain had the highest identities (90.6%–99.6%) with the Sudan AB-1–2009 strain in the analyzed fragment of the S RNA segment.

Phylogenetic analyses based on a 175-bp fragment of the S RNA segment separated CCHFV into 7 well-supported groups in association with the geographic distribution Asia 1, Asia 2, Africa 1–3, and Europe 1 and 2. All sequences grouped with clade Africa-3 (genotype III) viruses from South Africa and West Africa (Figure 2) and showed 4 groups with identities of 100%. One group (A) was formed by 4 sequences, the second group (B) by 12, the third group (C) by 24, and the fourth group (D) by 4.

For each group, the percentage of diversity was 0.07%–0.09%. Bayesian analysis showed that the estimated time to the most recent common ancestor (tMRCA) of lineage A was ≈1979 (95% highest posterior density [HPD] 1968–1984), which diverged before lineages B (1999; 95% HPD, 1986–2009), C (2004; 95% HPD, 1992–2014), and D (1996; HPD 1973–2013). Use of the 175-nt fragment to calculate the tMRCA of lineage A was supported by results reported by Cajimat et al. (*25*), who used the complete S segment (1965; 95% HPD 1948–1980).

Table. Characteristics of ticks positive for Crimean-Congo hemorrhagic fever virus, Spain, 2011–2015*

Year (no. ticks)	Province (no. ticks)	Sampling site	Collection site or host	Tick species	No. positive ticks/ wno. tested (%)
2011 (474)	Toledo (78)	31	Ground	*Hyalomma marginatum*	0/78
	Huesca (128)	32	Ground	*H. marginatum*	0/128
	Cáceres (268)				
		1	Deer	*H. lusitanicum*	**8/139 (5.75)**
		2	Deer	*H. lusitanicum*	**3/35 (8.57)**
		3	Deer	*H. marginatum*	0/4
		4	Deer	Unknown	0/20
		5	Red fox	Unknown	0/3
		6	Cattle	Unknown	0/2
		7	Deer	*H. lusitanicum*	0/24
		8	Deer	Unknown	0/3
		9	Deer	Unknown	0/7
		10	Deer	Unknown	0/20
		11	Deer	*Rhipicephalus bursa* nymphs	0/11
2012 (48)	Cáceres (27)	1	Deer	*H. lusitanicum*	0/27
	Segovia (21)	33	Cattle/sheep	*Rhipicephalus* sp.	0/21
2013 (201)	Cáceres (201)				
		1	Deer	*H. lusitanicum*	**13/68 (19.11)**
		2	Deer	Unknown	0/5
		10	Deer	*H. lusitanicum*	0/53
		12	Deer	*H. lusitanicum*	0/24
		13	Deer	*R. bursa*	0/5
		14	Deer	*H. marginatum*	0/23
		15	Deer	Unknown	0/6
		16	Deer	Unknown	0/17
2014 (272)	Cáceres (272)				
		1	Deer	*H. lusitanicum*	0/57
		4	Deer	Unknown	0/41
		15	Deer	Unknown	0/17
		17	Deer and wild boar	Unknown	0/18
		18	Deer and wild boar	*H. lusitanicum*	0/20
		19	Deer	Unknown	0/31
		20	Deer	*H. lusitanicum*	0/35
		21	Deer and wild boar	Unknown	0/19
		22	Deer	*H. lusitanicum*	0/18
		23	Deer	*H. lusitanicum*	0/16
2015 (584)	Cáceres (584)				
		1	Deer	*H. lusitanicum*	**3/66 (4.54)**
		2	Deer	*H. lusitanicum*	**11/120 (9.16)**
		4	Deer	*H. lusitanicum*	0/25
		18	Deer	*H. lusitanicum*	0/40
		19	Deer	30 *H. lusitanicum*, 1 *R. bursa*	0/31
		23	Deer	34 *H. lusitanicum*, 1 *Ixodes ricinus*	**1/35 (2.85)**
			Cattle	16 *H. lusitanicum*, 5 *H. marginatum*	**3/21 (14.28)**
		24	Deer	14 *H. lusitanicum*, 8 *R.bursa*, 1 *Dermacentor* sp.	0/23
		25	Fallow deer	6 *H. lusitanicum*, 2 *I. ricinus*. 3 unknown	0/11
		26	Deer	*H lusitanicum*	0/32
		27	Deer	*H. lusitanicum*	1/36 (2.77)
		28	Deer	*H. lusitanicum*	1/45 (2.22)
		29	Deer	*H. lusitanicum*	0/72
		30	Deer	*H. lusitanicum*	0/27
Total					**44/1579 (2.78)**

*Ticks positive for Crimean-Congo hemorrhagic fever virus are indicated in bold. Animals tested were red fox (*Vulpes vulpes*), red deer (*Cervus elaphus*), fallow deer (*Dama dama*), and wild boar (*Sus scrofa ferus*).

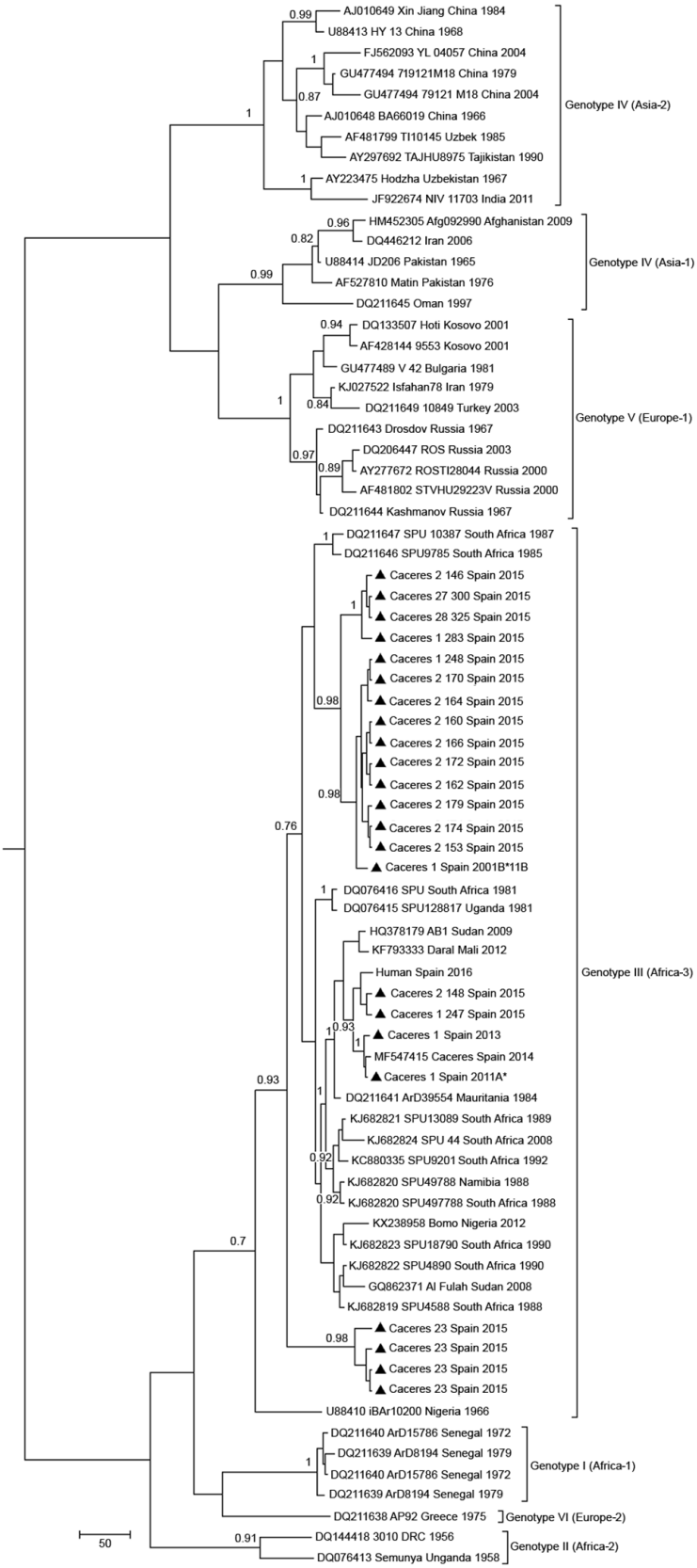

Figure 2. Maximum clade credibility genealogy based on partial (175-nt) sequences of the Crimean-Congo hemorrhagic fever virus small RNA segment of viruses from Spain and reference sequences. Numbers along branches indicate posterior probability values for the groups (values <0.70 are not shown). Triangles indicate newly sequenced strains from Spain reported in this study, which are identified by geographic origin, sampling site, and sampling year. Other sequences are indicated by GenBank accession number, strain, geographic origin, and sampling year. Sequences from this study indicated with an asterisk are included in European Molecular Biology Laboratory/GenBank databases. Genotypes are indicated in roman numerals and named according to Carroll et al. (*30*). Equivalent clade nomenclature is listed according to Chamberlain et al. (*31*) and indicated at right. Scale bar indicates nucleotide substitutions per site.

Discussion

An ongoing surveillance study of CCHFV in ticks was conducted because this virus was detected in Spain in 2010 (*4*). Thus, ticks were collected during 2011–2015, mainly in wild animals in the region where CCHFV was detected (Cáceres) and also in other regions (Huesca and Toledo) that are colonized by *Hyalomma* spp., or that have an abundance of domestic ungulates (Segovia). We detected CCHFV in Cáceres in 3 of the 5 years, indicating the resilience of a CCHFV focus in Spain and confirming the established spread of CCHFV into western Europe.

The rate of CCHFV-infected ticks determined in this study (2.78%, 44/1,579) was similar to those for other countries in Europe that have enzoonotic foci, such as Kosovo (3.6%, 40/1,102) (*12*), Bulgaria (2%–4.83%) (*32*), and Albania (3%) (*23*). Despite these data, no human cases were documented in Spain during the years of the study. This situation shows that human cases probably occur rarely, even though the virus is quite active in host-seeking ticks in the area. We detected CCHFV in *Hyalomma* ticks collected on cattle and deer in Cáceres in 5 of 31 hunting areas, 2 of which have repeatedly been found to be positive for CCHFV. In the maintenance of active CCHFV foci, habitat fragmentation, such as in the Cáceres region studied, might lead to isolated populations of ticks and hosts producing an amplification cycle in which ticks feed on infected hosts (*33*). However, birds carrying infected ticks on their surface or infected small mammals, such as brown hares and rabbits, can spread the virus to new areas. In August 2016, in a rural area of Ávila, Spain (Figure 1), where no evidence of CCHFV circulation was previously described and that is 300 km from the CCHFV enzoonotic focus in Cáceres, a human infection occurred after a tick bite (*5*).

Our study spanned 5 years; virus was detected during 2011, 2013, and 2015. In 2012, the number of samples collected was low. During 2014, our laboratory obtained 2 CCHFV-positive ticks that had low viral loads that could not be confirmed, although virus circulation during that year in Cáceres was demonstrated by Cajimat et al. (*25*). This finding reflects intermittent activity of the CCHFV foci in Cáceres, which becomes periodically apparent as described in other countries (*13,34*). In southern Portugal, which is close to this region (Figure 1), antibodies against this virus were detected in 2 human serum samples during 1980 (*35*), suggesting silent circulation of the virus in the Iberian Peninsula. Introduction of the virus into Spain has been calculated to have occurred ≈50 years ago (*25*), which was corroborated by our study.

In our study, of the 4 genera of ticks collected, only *Hyalomma* ticks were found to harbor CCHFV (Table). All CCHFV-positive ticks were collected while feeding on ruminants, red deer, and cattle. All except 2 CCHFV-positive ticks, 1 *H. lusitanicum* and 1 *H. marginatum,* were collected on red deer. This finding confirmed that this tick–host relationship had a primary role in maintenance of CCHFV enzootic cycles in Spain and the role of red deer as a prominent host. The CCHFV-positive *H. marginatum* tick was collected from a cow along with an *H. lusitanicum* tick. Presumably, these ticks were infected by a co-feeding transmission mechanism in nonviremic animals because only 2 of 6 ticks feeding on the same animal were positive for CCHFV. Until now, CCHFV-positive *H. marginatum* ticks have not been detected in Spain, although this species is considered to be the main reservoir of CCHFV in Europe. This tick species can increase the risk for human cases of infection in Spain because of its proximity to human populations when compared with *H. lusitanucum* ticks. In addition, CCHFV-positive *H. marginatum* ticks have been captured in domestic animals that have close contact with humans. Previous studies in Spain that analyzed 2,500 ticks (*28*) and 1,408 ticks (*36*) collected from domestic ungulates did not report any CCHFV-infected ticks. Our results clearly show that the virus is active in the Cáceres region and that cattle might play a major role in transmission of the virus to new generations of ticks that could act as bridge vectors.

CCHFV sequences from Spain isolated during this study grouped with clade Africa-3. This clade contains strains separated by large spatial distances, mainly from Mauritania to Senegal, Nigeria, Sudan, and South Africa, suggesting that virus is most likely spread by migratory birds that transmit infected ticks or by secondary introductions after importation of commercial livestock. The presence of the Africa-3 clade in Europe must be considered because of the increased risk for its spread to other countries in Europe where *Hyalomma* ticks are present. In Greece, the Africa-3 clade was detected in ticks from migratory birds in the Greek archipelago (*37*), although this clade has not been detected in continental Greece. Virus sequences found in ticks in Spain are more closely related to CCHFV strains from central-northern Africa, a finding that supports the theory that the virus was spread northward by migrating birds. Moreover, the Africa-3 clade was detected recently in ticks from migratory birds in Morocco (*38*).

Although it is recognized that 175 nt is a small genetic fragment for robust comparisons between closely related viruses, phylogenetic analyses of CCHFVs showed 4 well-supported clusters (with bootstrap values >0.7 and p distances among clusters of 0.07%–0.09%). We detected cocirculation of different clusters: 2 clusters during 2011 and 4 during 2015. Phylogenetic analysis showed that the tMRCA of the 4 CCHFV variants diverged to produce 2 lineages, 1 containing variants A, B, and C and the other containing variant D. Whether this divergence occurred in Africa or in Spain cannot be determined with the limited

sequence data currently available. The estimated tMRCA of lineage A was ≈1979 and it diverged before lineages B (1999), C (2004), and D (1996). Use of the 175-nt fragment to estimate the tMRCA of lineage A is supported by results from another study (*25*), in which the complete S RNA segment was used (1965; 95% HPD 1948–1980). Circulation of genetic variants of the same genotype could indicate multiple introductions of the virus or genetic evolution of a variant that has acted as an ancestor in autochthonous *H. lusitanicum* ticks in the Iberian Peninsula. Thus, adaptation of CCHFV to region-specific vectors and hosts leads to emergence of local virus variants as described recently in Kosovo (*12*). Genetic variability of these variants should be considered in molecular diagnostic methods (*39*).

The data obtained in this study, together with the CCHFV survey of ticks collected from animals conducted recently in Spain (*28*), as well as identification of 2 clinical cases caused by tick bites during 2016 and 2018 (*5*), show how the epidemiologic scenario of CCHF should include western Europe as an enzoonotic area and that surveillance studies on CCHFV in Spain and Portugal are necessary. Determining seroprevalence in animals and humans, as well as virus detection in ticks, would better define the risk for infection with CCHF in the Iberian Peninsula. These studies will help to determine the epidemiologic processes behind the known distribution of CCHFV in western Europe and establish adequate prevention and control measures to minimize the risk for cases of disease in Spain.

Acknowledgments

We thank Frank Hodgkins for reviewing the manuscript.

This study was supported by Instituto de Salud Carlos III (Projects RD12/0018/0006 and RD16CIII/0003/0003), Red de Enfermedades Tropicales Subprogram Redes Temáticas de Investigación Cooperativa en Salud Plan Estatal de I+D+I 2013–2016, Federación Española de Enfermedades Rares (Una Manera de Hacer Europa), and European Project EMERGE.

About the Author

Dr. Negredo is a senior researcher at the Arbovirus and Imported Viral Diseases Laboratory, National Center of Microbiology, Madrid, Spain. Her primary research interests are virus hemorrhagic fever and detection of emerging viruses that circulate in Spain.

References

1. World Health Organization. Crimean-Congo hemorrhagic fever. Fact sheet no. 208; 2013 [cited 2019 Mar 6]. http://www.who.int/mediacentre/factsheets/fs208/en
2. Whitehouse CA. Crimean-Congo hemorrhagic fever. Antiviral Res. 2004;64:145–60. http://dx.doi.org/10.1016/j.antiviral.2004.08.001
3. Ergonul O. Crimean-Congo hemorrhagic fever virus: new outbreaks, new discoveries. Curr Opin Virol. 2012;2:215–20. http://dx.doi.org/10.1016/j.coviro.2012.03.001
4. Estrada-Peña A, Palomar AM, Santibáñez P, Sánchez N, Habela MA, Portillo A, et al. Crimean-Congo hemorrhagic fever virus in ticks, southwestern Europe, 2010. Emerg Infect Dis. 2012;18:179–80. http://dx.doi.org/10.3201/eid1801.111040
5. Negredo A, de la Calle-Prieto F, Palencia-Herrejón E, Mora-Rillo M, Astray-Mochales J, Sánchez-Seco MP, et al.; Crimean Congo Hemorrhagic Fever@Madrid Working Group. Autochthonous Crimean-Congo hemorrhagic fever in Spain. N Engl J Med. 2017;377:154–61. http://dx.doi.org/10.1056/NEJMoa1615162
6. Hoogstraal H. The epidemiology of tick-borne Crimean-Congo hemorrhagic fever in Asia, Europe, and Africa. J Med Entomol. 1979;15:307–417. http://dx.doi.org/10.1093/jmedent/15.4.307
7. Gonzalez JP, Camicas JL, Cornet JP, Wilson ML. Biological and clinical responses of west African sheep to Crimean-Congo hemorrhagic fever virus experimental infection. Res Virol. 1998; 149:445–55. http://dx.doi.org/10.1016/S0923-2516(99)80013-2
8. Spengler JR, Estrada-Peña A, Garrison AR, Schmaljohn C, Spiropoulou CF, Bergeron É, et al. A chronological review of experimental infection studies of the role of wild animals and livestock in the maintenance and transmission of Crimean-Congo hemorrhagic fever virus. Antiviral Res. 2016;135:31–47. http://dx.doi.org/10.1016/j.antiviral.2016.09.013
9. Wasfi F, Dowall S, Ghabbari T, Bosworth A, Chakroun M, Varghese A, et al. Sero-epidemiological survey of Crimean-Congo hemorrhagic fever virus in Tunisia. Parasite. 2016;23:10. http://dx.doi.org/10.1051/parasite/2016010
10. Gargili A, Estrada-Peña A, Spengler JR, Lukashev A, Nuttall PA, Bente DA. The role of ticks in the maintenance and transmission of Crimean-Congo hemorrhagic fever virus: a review of published field and laboratory studies. Antiviral Res. 2017;144:93–119. http://dx.doi.org/10.1016/j.antiviral.2017.05.010
11. Gunes T, Poyraz O, Vatansever Z. Crimean-Congo hemorrhagic fever virus in ticks collected from humans, livestock, and picnic sites in the hyperendemic region of Turkey. Vector Borne Zoonotic Dis. 2011;11:1411–6. http://dx.doi.org/10.1089/vbz.2011.0651
12. Sherifi K, Cadar D, Muji S, Robaj A, Ahmeti S, Jakupi X, et al. Crimean-Congo hemorrhagic fever virus clades V and VI (Europe 1 and 2) in ticks in Kosovo, 2012. PLoS Negl Trop Dis. 2014;8:e3168. http://dx.doi.org/10.1371/journal.pntd.0003168
13. Bente DA, Forrester NL, Watts DM, McAuley AJ, Whitehouse CA, Bray M. Crimean-Congo hemorrhagic fever: history, epidemiology, pathogenesis, clinical syndrome and genetic diversity. Antiviral Res. 2013;100:159–89. http://dx.doi.org/10.1016/j.antiviral.2013.07.006
14. Spengler JR, Estrada-Peña A. Host preferences support the prominent role of *Hyalomma* ticks in the ecology of Crimean-Congo hemorrhagic fever. PLoS Negl Trop Dis. 2018;12:e0006248. http://dx.doi.org/10.1371/journal.pntd.0006248
15. Papa A, Ma B, Kouidou S, Tang Q, Hang C, Antoniadis A. Genetic characterization of the M RNA segment of Crimean Congo hemorrhagic fever virus strains, China. Emerg Infect Dis. 2002;8:50–3. http://dx.doi.org/10.3201/eid0801.010087
16. Burt FJ, Swanepoel R. Molecular epidemiology of African and Asian Crimean-Congo hemorrhagic fever isolates. Epidemiol Infect. 2005;133:659–66. http://dx.doi.org/10.1017/S0950268805003730
17. Christova I, Di Caro A, Papa A, Castilletti C, Andonova L, Kalvatchev N, et al. Crimean-Congo hemorrhagic fever, southwestern Bulgaria. Emerg Infect Dis. 2009;15:983–5. http://dx.doi.org/10.3201/eid1506.081567
18. Maltezou HC, Maltezos E, Papa A. Contact tracing and serosurvey among healthcare workers exposed to Crimean-Congo hemorrhagic fever in Greece. Scand J Infect Dis. 2009;41:877–80. http://dx.doi.org/10.3109/00365540903173619

19. Mishra AC, Mehta M, Mourya DT, Gandhi S. Crimean-Congo hemorrhagic fever in India. Lancet. 2011;378:372. http://dx.doi.org/10.1016/S0140-6736(11)60680-6
20. Aradaib IE, Erickson BR, Karsany MS, Khristova ML, Elageb RM, Mohamed ME, et al. Multiple Crimean-Congo hemorrhagic fever virus strains are associated with disease outbreaks in Sudan, 2008–2009. PLoS Negl Trop Dis. 2011;5:e1159. http://dx.doi.org/10.1371/journal.pntd.0001159
21. Mustafa ML, Ayazi E, Mohareb E, Yingst S, Zayed A, Rossi CA, et al. Crimean-Congo hemorrhagic fever, Afghanistan, 2009. Emerg Infect Dis. 2011;17:1940–1. http://dx.doi.org/10.3201/eid1710.110061
22. Nabeth P, Cheikh DO, Lo B, Faye O, Vall IO, Niang M, et al. Crimean-Congo hemorrhagic fever, Mauritania. Emerg Infect Dis. 2004;10:2143–9. http://dx.doi.org/10.3201/eid1012.040535
23. Papa A, Velo E, Papadimitriou E, Cahani G, Kota M, Bino S. Ecology of the Crimean-Congo hemorrhagic fever endemic area in Albania. Vector Borne Zoonotic Dis. 2009;9:713–6. http://dx.doi.org/10.1089/vbz.2008.0141
24. Ramírez de Arellano E, Hernández L, Goyanes MJ, Arsuaga M, Cruz AF, Negredo A, et al. Phylogenetic Characterization of Crimean-Congo Hemorrhagic fever virus, Spain. Emerg Infect Dis. 2017;23:2078–80. http://dx.doi.org/10.3201/eid2312.171002
25. Cajimat MN, Rodriguez SE, Schuster IU, Swetnam DM, Ksiazek TG, Habela MA, et al. Genomic characterization of Crimean-Congo hemorrhagic fever virus in *Hyalomma* tick from Spain, 2014. Vector Borne Zoonotic Dis. 2017;17:714–9. http://dx.doi.org/10.1089/vbz.2017.2190
26. Deyde VM, Khristova ML, Rollin PE, Ksiazek TG, Nichol ST. Crimean-Congo hemorrhagic fever virus genomics and global diversity. J Virol. 2006;80:8834–42. http://dx.doi.org/10.1128/JVI.00752-06
27. Zehender G, Ebranati E, Shkjezi R, Papa A, Luzzago C, Gabanelli E, et al. Bayesian phylogeography of Crimean-Congo hemorrhagic fever virus in Europe. PLoS One. 2013;8:e79663. http://dx.doi.org/10.1371/journal.pone.0079663
28. de Sanidad M, Sociales e Igualdad S. Status report and assessment of the risk of transmission of Crimean-Congo hemorrhagic fever (FHCC) in Spain, April 2017 [in Spanish] [cited 2017 May 1]. http://www.msssi.gob.es/profesionales/saludPublica/enfermedadesEmergentes/Crimea_Congo/docs/ACTUALIZACION_ER_FHCC_20.04.2017.pdf
29. Drummond AJ, Suchard MA, Xie D, Rambaut A. Bayesian phylogenetics with BEAUti and the BEAST 1.7. Mol Biol Evol. 2012;29:1969–73. http://dx.doi.org/10.1093/molbev/mss075
30. Carroll SA, Bird BH, Rollin PE, Nichol ST. Ancient common ancestry of Crimean-Congo hemorrhagic fever virus. Mol Phylogenet Evol. 2010;55:1103–10. http://dx.doi.org/10.1016/j.ympev.2010.01.006
31. Chamberlain J, Cook N, Lloyd G, Mioulet V, Tolley H, Hewson R. Co-evolutionary patterns of variation in small and large RNA segments of Crimean-Congo hemorrhagic fever virus. J Gen Virol. 2005;86:3337–41. http://dx.doi.org/10.1099/vir.0.81213-0
32. Gergova I, Kunchev M, Kamarinchev B. Crimean-Congo hemorrhagic fever virus tick survey in endemic areas in Bulgaria. J Med Virol. 2012;84:608–14. http://dx.doi.org/10.1002/jmv.23214
33. Estrada-Peña A, Vatansever Z, Gargili A, Ergönul O. The trend towards habitat fragmentation is the key factor driving the spread of Crimean-Congo hemorrhagic fever. Epidemiol Infect. 2010;138:1194–203. http://dx.doi.org/10.1017/S0950268809991026
34. Spengler JR, Bente DA. Crimean-Congo hemorrhagic fever in Spain: new arrival or silent resident? N Engl J Med. 2017;377:106–8. http://dx.doi.org/10.1056/NEJMp1707436
35. Filipe AR, Calisher CH, Lazuick J. Antibodies to Congo-Crimean hemorrhagic fever, Dhori, Thogoto and Bhanja viruses in southern Portugal. Acta Virol. 1985;29:324–8.
36. Palomar AM, Portillo A, Santibáñez S, García-Álvarez L, Muñoz-Sanz A, Márquez FJ, et al. Molecular (ticks) and serological (humans) study of Crimean-Congo hemorrhagic fever virus in the Iberian Peninsula, 2013–2015. Enferm Infecc Microbiol Clin. 2017;35:344–7. http://dx.doi.org/10.1016/j.eimc.2017.01.009
37. Lindeborg M, Barboutis C, Ehrenborg C, Fransson T, Jaenson TG, Lindgren PE, et al. Migratory birds, ticks, and Crimean-Congo hemorrhagic fever virus. Emerg Infect Dis. 2012;18:2095–7. http://dx.doi.org/10.3201/eid1812.120718
38. Palomar AM, Portillo A, Santibáñez P, Mazuelas D, Arizaga J, Crespo A, et al. Crimean-Congo hemorrhagic fever virus in ticks from migratory birds, Morocco. Emerg Infect Dis. 2013;19:260–3. http://dx.doi.org/10.3201/eid1902.121193
39. Vanhomwegen J, Alves MJ, Zupanc TA, Bino S, Chinikar S, Karlberg H, et al. Diagnostic assays for Crimean-Congo hemorrhagic fever. Emerg Infect Dis. 2012;18:1958–65. http://dx.doi.org/10.3201/eid1812.120710

Address for correspondence: Ana Negredo, National Center of Microbiology, Arbovirus and Imported Viral Diseases Laboratory, Crta. Majadahonda-Pozuelo Km 2, 28220 Majadahonda, Madrid, Spain; email: anabelnegredo@isciii.es

Equine Influenza Virus—A Neglected, Reemergent Disease Threat

Alexandra Sack, Ann Cullinane, Ulziimaa Daramragchaa, Maitsetseg Chuluunbaatar, Battsetseg Gonchigoo, Gregory C. Gray

Equine influenza virus (EIV) is a common, highly contagious equid respiratory disease. Historically, EIV outbreaks have caused high levels of equine illness and economic damage. Outbreaks have occurred worldwide in the past decade. The risk for EIV infection is not limited to equids; dogs, cats, and humans are susceptible. In addition, equids are at risk from infection with avian influenza viruses, which can increase mortality rates. EIV is spread by direct and indirect contact, and recent epizootics also suggest wind-aided aerosol transmission. Increased international transport and commerce in horses, along with difficulties in controlling EIV with vaccination, could lead to emergent EIV strains and potential global spread. We review the history and epidemiology of EIV infections, describe neglected aspects of EIV surveillance, and discuss the potential for novel EIV strains to cause substantial disease burden and subsequent economic distress.

Equine influenza is a common, highly contagious respiratory disease of equids with a near-global distribution. Central Asia, Australia, and Japan experienced large equine influenza virus (EIV) outbreaks in 2007 (*1*,*2*). Serious outbreaks of EIV have occurred throughout history, causing substantial economic distress worldwide in the 19th and 20th centuries (*3*).

The most common clinical signs of EIV infection in equids are fever, lethargy, anorexia, nasal discharge, and a nonproductive dry cough (*4*). Mortality rates are generally low during EIV outbreaks; death is most common among foals or equids with preexisting poor health (*5*). Horses usually recover in 2 weeks with rest, but clinical signs, especially cough, can persist. EIV can result in a secondary bacterial bronchopneumonia, which can be fatal, particularly in young horses (*6*). Along with loss of life, the rest period required for equine recovery can cause economic hardship in areas where people rely on equids for income, such as for transportation or milk. EIV outbreaks also can disrupt economic drivers, such as the horse racing and show industries. EIV often is overlooked as a disease threat outside of equine communities, despite its known historical commercial importance and current zoonotic potential.

Author affiliations: Institute of Veterinary Medicine, Ulaanbaatar, Mongolia (A. Sack, U. Daramragchaa, M. Chuluunbaatar, B. Gonchigoo); Duke University, Durham, North Carolina, USA (A. Sack, G.C. Gray); Irish Equine Centre, Johnstown, Ireland (A. Cullinane); Duke-NUS Medical School, Singapore, Singapore (G.C. Gray); Duke-Kunshan University, Kunshan, China (G.C. Gray)

DOI: https://doi.org/10.3201/eid2506.161846

Overview of Equine Influenza Viruses

EIVs are believed to have originated from avian influenza strains (*7*,*8*). Two subtypes, H7N7 and H3N8, historically have infected horses. EIV H7N7 was first recovered from horses in Europe during 1956 (*9*); it has not been isolated in horses since the 1970s, but serologic evidence suggests subclinical circulation through the 1990s (*7*,*8*). EIV H3N8 has 2 lineages, Eurasian and American. The American lineage includes Florida, Kentucky, and South America sublineages (*10*). The Florida sublineage is further divided into 2 antigenically distinct clades; both have been detected in Asia and Europe, but only clade 1 has been detected in North America. No Eurasian lineage viruses have been isolated since 2007, when it was detected in Switzerland (*11*). In 2016, all isolated EIV viruses were from the Florida lineage, clade 2 in Europe and clade 1 in the United States (*8*,*10*).

Historical Impact

EIV-like equine respiratory diseases have been recorded since the 13th century (*9*). Although historical records predate human understanding of viral pathogens, they show EIV-like outbreaks preceded or, less commonly, followed several human influenza outbreaks. Despite the possibility that these illnesses were caused by pathogens other than EIVs (*3*), a review of records for 1688–1888 identified 56 years with documented outbreaks of influenza-like human or equine diseases in the Western Hemisphere (*3*). Records included 21 years in which both horses and humans were involved, 25 years with human-only involvement, and 10 years in which only horses were involved (*3*). Some of the

largest assumed EIV outbreaks with smaller accompanying human influenza outbreaks occurred in 1727, 1750, 1760, and 1872 (*3*). EIV outbreaks generally occurred in spring or fall and were followed by similar human outbreaks 3 weeks later (*12*). Human influenza epidemics without equine infections were more common during winter months (*12*). Historical records provide a glimpse into a likely association between human and equine respiratory disease, but their reliability is limited by the lack of diagnostic testing. Others have provided more comprehensive reviews of these historical records (*3*,*12*,*13*).

A massive 1872 outbreak is considered the largest recorded EIV epizootic (*12*). Starting in Toronto in late September 1872, EIV spread along shipping routes across the United States and eventually into Central America and the Caribbean, stopping in Panama, which had no equine population to support EIV spread (*12*). Illness rates approached 100%, and the mortality rates were 2%–4% (*12*). Newspaper and veterinary reports from the time indicate travel, mail, and delivery of goods were severely hampered in the United States for weeks after the outbreak (*12*,*14*). This presumed outbreak of EIV also was blamed in part for a costly fire in Boston because fire wagons, pulled by young men instead of horses, could not reach the fire promptly (*12*,*14*). A mild human influenza was reported in people working with horses during the 1872 outbreak, but it is not known whether this was an EIV infection or human virus infection (*3*).

Major EIV outbreaks continued through the 1900s (Appendix Table, https://wwwnc.cdc.gov/EID/article/25/6/16-1846-App1.pdf). Many were associated with importation of horses, including outbreaks in South Africa in 1986, India in 1987, Hong Kong in 1992, and Dubai in 1995 (*15*). Earlier outbreaks in the 1990s might have gone unrecorded due to poor diagnostics or reporting mechanisms.

Selected Outbreaks in the Past Decade

Influenza is endemic in horses in the United States and much of the world, with the exception of New Zealand and Iceland (*16*). Outbreaks of EIV infections in horses occurred globally throughout the 2000s. All inhabited continents had >1 country with an EIV outbreak during 2006–2017 (Figure) (*8*,*17*), and in 2015, China, France, Germany, Ireland, Malaysia, Sweden, the United Kingdom, and the United States experienced EIV outbreaks. Ireland, the United Kingdom, and the United States also had cases or outbreaks in 2016–2017 (*17*), as did China and Japan in 2017 (*8*,*17*). The United States recently experienced considerable EIV activity where the virus was detected in 23 states in 2015, 16 states in 2016, and 22 states in 2017 (*8*,*17*).

Australia experienced a large outbreak in 2007, involving 70,000 horses living on >9,000 properties, that resulted in a 5% mortality rate (*18*,*19*). The virus was introduced by thoroughbred horses imported from Japan (*18*). Authorities believe EIV escaped a quarantine station due to lax biosecurity protocols. In addition, many horses certified as vaccinated against EIV had no protective antibodies, suggesting poor immune response, lack of vaccination

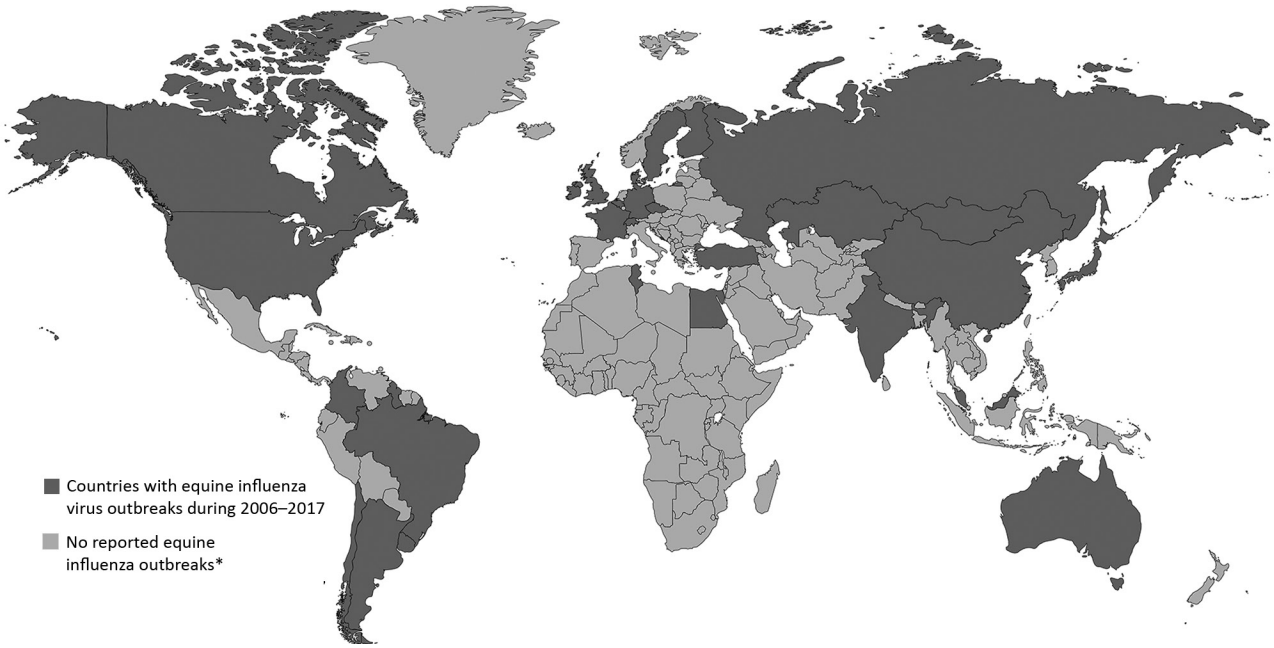

Figure. Equine influenza distribution map 2006–2015, compiled from Expert Surveillance Panel on Equine Influenza Vaccine Composition reports, 2006–2017 (*17*). Created with mapchart.net (http://www.mapchart.net).*No outbreaks occurred or no data reported

compliance, or ineffective vaccines (*20*). Australia implemented an awareness and information campaign to supplement its interventions, which included quarantining, restricting horse movement, decontaminating properties, establishing disease control zones, and increasing surveillance and vaccination. The country was declared EIV-free in 2008 (*20*), but estimates of the economic cost to the equine industry are ≥$1 billion Aus (*18*).

During 2011–2012, an outbreak of EIV Florida clade 1 began in Chile and spread to multiple countries in South America (*4*) through the movement of horses in the rodeo and thoroughbred racing industries. EIV-positive horses were exported from Uruguay to Dubai (*4*), demonstrating the ease with which international transport could contribute to the spread of EIV. This importation was identified and stopped in the Dubai quarantine facility. Also during 2011–2012, a Florida clade 2 virus circulated in central Asia, Kazakhstan, western Mongolia, India, and western China (*1*).

In Mongolia, government records show 4 large EIV outbreaks with some of the highest known mortalities during 1974–1975, 1983–1984, 1993–1994, and 2007–2008 (*21*). Mortality rates of 20%–30% were reported for all but the 2007–2008 outbreak, during which the country implemented vaccination and the mortality rate decreased to ≈5% (*21*). Whereas some of these mortality rates are confounded partially by extreme weather and differences in reporting, diagnostics, and nutrition among horses, the reduced mortality rate seen with vaccination appears to be real. A 2012 EIV outbreak in Mongolia was linked to an outbreak in Kazakhstan that year and an outbreak in China in 2013 (*1*,*2*). Additional EIV outbreaks have occurred in Malaysia in 2015, the United States and Ireland in 2016, and Chile in 2018 (*8*,*17*).

The primary focus of EIV prevention has been on domestic horses, but EIV is transmissible to all equids, including feral and wild herds, such as Przewalski's horses. A 2007 outbreak in China affected ≈13,600 donkeys, resulting in 77 deaths. The donkeys had the typical clinical signs of EIV, and the most severe cases occurred in animals 6 months to 3 years of age (*22*). The Takhi herd of wild horses in China also experienced an illness rate near 100% and a 5% mortality rate (*23*) during that outbreak. Feral horses also were considered as a route of transmission during the 2007 outbreak in Australia, and the country set up a vaccination buffer zone. Although authorities considered the risk for infection low for feral horses, they considered risk to domestic horses from infected feral horses high (*24*).

Potential for Cross-Species Spread

EIV infection is not limited to equids. Sporadic spillover of EIV to dogs has been detected in the United Kingdom and Australia (*25*–*27*). In the early 2000s, a canine H3N8 influenza of equine origin was discovered in the United States, where it continues to circulate with high transmission rates in dog shelters (*25*). Canine influenza in Australia occurred simultaneously with the 2007 EIV outbreak in horses (*26*). During 2004–2006, surveillance for influenza viruses in pigs in China discovered 2 H3N8 strains of equine origin (*28*).

Cats experimentally infected with EIV demonstrated respiratory signs and virus shedding with transmission to other cats (*29*). A strain of influenza discovered in a camel in Mongolia was directly related to a circulating equine H3N8 strain, but horizontal spread in camels could not be determined (*30*). Although cross-species infections appear to be rare, horses potentially could play a role in the generation or amplification of a novel virus.

One of the most severe outbreaks of EIV occurred in China and involved an EIV related to an avian H3N8 strain. The outbreak had a mortality rate of ≈20% (*31*), but the virus was not sustained in the equine population (*32*). However, the close relationship between this EIV and avian H3N8 strains of the time (*31*,*32*) raises concerns that novel, highly virulent avian influenza viruses might adapt to horses and cause severe future mortality rates.

In another instance in 2009, donkeys with moderate respiratory infection in a village in Egypt were found to have H5N1 during a simultaneous outbreak of highly pathogenic H5N1 in poultry (*33*). Historical reports in newspapers from the United States in 1872 describe a highly pathogenic disease in poultry that seems clinically similar to modern avian influenza viruses (*12*). Although the connection of this avian disease to the 1872 EIV epizootic is unknown, local newspaper reports linked it with the movement of infected horses (*12*), suggesting equids could be a potential reservoir or amplifying host for future avian influenza infections.

Humans are also a potential host for EIV. Experimental infection of antibody-negative human volunteers in the 1960s saw >60% of them seroconvert and have positive virus cultures from throat swabs collected 2–6 days after nasal inoculation. Most of the human volunteers also shed virus from day 2 through day 5 but rarely shed past day 6 (*34*,*35*). In the same study, horses became infected by strains of EIV passed through humans (*34*). During 1958–1963, human serum samples were tested in the Netherlands for EIV antibodies. Less than 0.5% of people <60 years of age had elevated antibody titers, but 11.5% of people >60 years of age had elevated EIV antibodies, with >40% EIV antibody elevation among people >70 years of age. The authors surmised that a virus resembling the 1963 EIV strain infected humans during 1896–1900 (*36*). The study was performed before the human H3 influenza virus was recorded and determined

to have crossed from ducks to humans in 1965, although the equine H3 strain is older (*37*). The evidence suggests past equine-to-human interspecies transmission.

Studies of humans exposed to horses during the 2007 EIV outbreak in Australia found only 10% of people had serologic reaction against EIV, all at a low level, suggesting cross-reactivity with human influenza strains (*38*). A similar study in Mongolia found only 4.8% of people tested had elevated EIV antibodies, all at low titer levels that could be explained by cross-reactivity with seasonal human influenza virus infection or vaccine (*39*). However, a study in Iowa using new serologic assays found that people regularly exposed to horses were more likely to have elevated antibodies against EIV than people not exposed to horses in the previous 10 years (*40*). Smoking was an added risk factor for elevated antibodies against EIV, possibly because of oral contamination from touching horses before smoking or because of a compromised immune system from smoking (*40*). A single probable horse-to-human EIV transmission case was observed in Chile during 1973, but the human's influenza virus was not typed (*41*). Although experimental infection of humans has been demonstrated, evidence for natural infection is more equivocal.

Environmental Transmission

EIV has multiple potential direct and indirect routes of transmission and is especially communicable when it enters a large, previously unexposed population of equids. Research is clarifying the role of the environment and weather on EIV transmission. During the 2007 outbreak in Australia, wind speeds >30 kph from the direction of infected horses correlated with an increased risk for infection for horses downwind (*19*). Humidity and temperature also might have contributed to EIV transmission (*19*). These findings match results from a laboratory study that found enhanced aerosolizing of influenza virus with colder and drier conditions (*42*). Further analysis in Queensland, Australia, found east to west spread of EIV with distances of 1–2 km consistent with wind patterns (*43*). In addition, some avian influenza virus strains persist in water and remain infectious for >2 months (*44*), implying water also is a potential source of transmission for EIV.

Vaccination and Prevention Strategies

The World Organisation for Animal Health (OIE) recommends current EIV vaccines include both Florida clade 1 and clade 2 H3N8 strains (*8*). Because EIV H7N7 has not been isolated since the late 1970s and the Eurasian strain of H3N8 has not been seen since 2007 (*8*,*11*), OIE suggests omitting these from equine influenza vaccines. The American Association of Equine Practitioners recommends EIV vaccination unless a horse is in a closed and isolated facility and that high-risk populations, including young show and race horses, be vaccinated every 6 months (*16*). Horse shows and races have been recognized mechanisms of increased dispersal and spread of EIV since a 1963 EIV outbreak across the continental United States linked to infected horses imported by air from Argentina into Florida (*45*). Most EIV infections in the United States in 2017 were in show and race horses with an unknown vaccination history (*2*,*8*,*20*). As the number of horses transported by air for breeding or racing increases, so does the probability of future EIV outbreaks among horses (*15*).

Because previously vaccinated horses shed virus without clinical signs, EIV vaccine is useful for reducing clinical signs and reducing virus shed but does not eliminate potential transmission (*20*,*46*). In 2003, an outbreak of EIV closely related to the Kentucky sublineage occurred in regularly vaccinated thoroughbred horses in England (*47*). Before this outbreak, the American strain included in the vaccine was considered sufficient to protect horses. This outbreak helped redefine how antigenic drift reduces the efficacy of EIV vaccinations (*47*). A study of vaccine containing H3N8 A/eq/Kentucky/98 found >40% of vaccinated ponies shed EIV after experimental challenge with aerosolized EIV, although for fewer days than animals in an unvaccinated control group (*46*).

More effective vaccines are needed, especially considering the role failed vaccination potentially played in the 2007 outbreak in Australia (*20*). Even while the OIE recommends all vaccines contain Florida clade 1 and clade 2 virus, many vaccines contain outdated strains (*8*). A review of current vaccinations found that many commercial vaccines are not updated until a major outbreak, such as the one in Australia (*48*).

Because vaccination does not prevent viral shedding, good management practices are imperative for preventing EIV outbreaks (*46*). Before reaching its goal of 80%–90% EIV vaccination rates in high-risk areas, Australia saw a decline in new cases likely related to adoption of movement restrictions and biosecurity protocols (*49*). Ring vaccination, however, is credited for stopping the spread and reducing risk for EIV infection so normal equine activities could be resumed (*49*).

Preventive measures should include international surveillance and investigation of vaccine failure (*8*). Veterinarians can further help educate owners in order to help improve surveillance, diagnostics, and increase EIV vaccination (*15*).

Surveillance Efforts

After major EIV outbreaks in 1989 related to outdated vaccine strains, the OIE Biological Standards Commission initiated the formal global Equine Influenza

Surveillance Programme in 1995 (*50*). OIE currently has reference laboratories in Ireland, the United Kingdom, and the United States. Additional laboratories in Asia, Europe, and South America collect data on outbreaks of EIV and strain characterization, which the Expert Surveillance Panel on Equine Influenza Vaccine Composition reviews annually. The panel, composed of OIE and World Health Organization representatives, makes recommendations on vaccine updates, which it publishes in an annual bulletin (*8*).

The level of active or passive EIV surveillance in each country depends on the nature of the horse industry, status of the disease, laboratory capability, and financial resources available for veterinary intervention. Many laboratories involved in EIV surveillance experience difficulty obtaining sufficient samples because horse owners seldom request a confirmatory diagnosis for influenza (*15*). Surveillance is compounded by the failure of some diagnostic laboratories to characterize virus or to submit positive real-time PCR samples to an OIE reference laboratory for virus isolation and antigenic characterization.

OIE continues to develop global EIV surveillance through its Laboratory Twinning Programme (http://www.oie.int/support-to-oie-members/laboratory-twinning), which transfers skills and reagents from OIE reference laboratories to other institutes to increase their capacity to implement effective surveillance programs and contribute data. Recently, the OIE reference laboratory at the Animal Health Trust (Suffolk, UK) completed a 3-year twinning project with the National Research Centre on Equines in Hisar, India. In 2016, the OIE reference laboratory at the Irish Equine Centre (Johnstown, Ireland) completed a twinning project with Harbin Veterinary Institute in Harbin, China. Currently, no OIE reference laboratory for equine influenza exists outside of Europe or North America, but OIE anticipates that twinning will help a laboratory in Asia meet the necessary requirements, develop a regional network, and provide diagnostic support to neighboring countries. At the time of our report, the surveillance program reports that Australia and New Zealand are EIV free and that a large EIV outbreak with fatalities in donkeys has been reported in Africa, but there is a lack of sufficient information from many countries in the Middle East and elsewhere EIV may be circulating (http://www.oie.int/wahis_2/public/wahid.php/Reviewreport/Review/viewsummary?reportid=29135).

Future Challenges

Equine influenza is a highly contagious virus with the potential to cause global harm. The 2007 EIV outbreak in Australia demonstrated the economic impact the virus can have when introduced into a previously unexposed equine population (*18*). Furthermore, potential novel and virulent avian influenza virus strains could cross into horses and rapidly spread despite previous equid vaccinations (*31*,*33*). Risk from avian strains is compounded by EIV's potential for infecting humans (*13*). Although the role of humans in EIV evolution is unknown, historical and serologic evidence suggests EIV has zoonotic potential and is known to infect other nonhuman species (*26*,*28*,*30*). Historical review suggests the 1889 human influenza pandemic might have been of equine origin, with equids playing the role that swine play in modern outbreaks (*12*). With all this in mind, we posit that EIV should be recognized as a potential epidemic, if not pandemic, threat.

This research was made possible by the Fogarty International Center of the US National Institutes of Health (grant no. 5D43TW009373, G.C.G., principal investigator).

About the Author

At the time of this research, Dr. Sack was a postdoctoral associate with the School of Medicine and the Global Health Institute at Duke University. She is now a postdoctoral fellow at Tufts Clinical and Translational Science Institute, Boston, Massachusetts, USA. Her primary research interests include zoonoses, specifically involving human, livestock, and wildlife interactions.

References

1. Karamendin K, Kydyrmanov A, Kasymbekov Y, Khan E, Daulbayeva K, Asanova S, et al. Continuing evolution of equine influenza virus in Central Asia, 2007–2012. Arch Virol. 2014;159:2321–7. http://dx.doi.org/10.1007/s00705-014-2078-3
2. Motoshima M, Okamatsu M, Asakura S, Kuribayashi S, Sengee S, Batchuluun D, et al. Antigenic and genetic analysis of H3N8 influenza viruses isolated from horses in Japan and Mongolia, and imported from Canada and Belgium during 2007–2010. Arch Virol. 2011;156:1379–85. http://dx.doi.org/10.1007/s00705-011-1000-5
3. Morens DM, Taubenberger JK. Pandemic influenza: certain uncertainties. Rev Med Virol. 2011;21:262–84.
4. Perglione CO, Gildea S, Rimondi A, Miño S, Vissani A, Carossino M, et al. Epidemiological and virological findings during multiple outbreaks of equine influenza in South America in 2012. Influenza Other Respi Viruses. 2016;10:37–46. http://dx.doi.org/10.1111/irv.12349
5. Powell DG, Watkins KL, Li PH, Shortridge KF. Outbreak of equine influenza among horses in Hong Kong during 1992. Vet Rec. 1995;136:531–6. http://dx.doi.org/10.1136/vr.136.21.531
6. Patterson-Kane JC, Carrick JB, Axon JE, Wilkie I, Begg AP. The pathology of bronchointerstitial pneumonia in young foals associated with the first outbreak of equine influenza in Australia. Equine Vet J. 2008;40:199–203. http://dx.doi.org/10.2746/042516408X292214
7. Madić J, Martinović S, Naglić T, Hajsig D, Cvetnić S. Serological evidence for the presence of A/equine-1 influenza virus in unvaccinated horses in Croatia. Vet Rec. 1996;138:68. http://dx.doi.org/10.1136/vr.138.3.68
8. World Organisation for Animal Health. OIE Expert Surveillance Panel on Equine Influenza Vaccine Composition. 2018 March 22. Conclusions and recommendations. 2018 [cited 2018 Dec 22].

http://www.oie.int/our-scientific-expertise/specific-information-and-recommendations/equine-influenza
9. Sovinova O, Tumova B, Pouska F, Nemec J. Isolation of a virus causing respiratory disease in horses. Acta Virol. 1958;2:52–61.
10. Bryant NA, Rash AS, Woodward AL, Medcalf E, Helwegen M, Wohlfender F, et al. Isolation and characterisation of equine influenza viruses (H3N8) from Europe and North America from 2008 to 2009. Vet Microbiol. 2011;147:19–27. http://dx.doi.org/10.1016/j.vetmic.2010.05.040
11. Bryant NA, Rash AS, Russell CA, Ross J, Cooke A, Bowman S, et al. Antigenic and genetic variations in European and North American equine influenza virus strains (H3N8) isolated from 2006 to 2007. Vet Microbiol. 2009;138:41–52. http://dx.doi.org/10.1016/j.vetmic.2009.03.004
12. Morens DM, Taubenberger JK. Historical thoughts on influenza viral ecosystems, or behold a pale horse, dead dogs, failing fowl, and sick swine. Influenza Other Respi Viruses. 2010;4:327–37. http://dx.doi.org/10.1111/j.1750-2659.2010.00148.x
13. Xie T, Anderson BD, Daramragchaa U, Chuluunbaatar M, Gray GC. A review of evidence that equine influenza viruses are zoonotic. Pathogens. 2016;5:50. http://dx.doi.org/10.3390/pathogens5030050
14. Judson AB. History and course of the epizoötic among horses upon the North American continent in 1872–73. Public Health Pap Rep. 1873;1:88–109.
15. Cullinane A, Elton D, Mumford J. Equine influenza—surveillance and control. Influenza Other Respi Viruses. 2010;4:339–44. http://dx.doi.org/10.1111/j.1750-2659.2010.00176.x
16. American Association of Equine Practitioners. Risk-based vaccination guidelines: equine influenza. 2017 [cited 2018 Aug 27]. https://aaep.org/guidelines/vaccination-guidelines/risk-based-vaccination-guidelines/equine-influenza.
17. World Organisation for Animal Health. OIE Expert Surveillance Panel on Equine Influenza Vaccine Composition. 2006–2016. Conclusions and recommendations. 2016 [cited 2018 April 8]. https://doc.oie.int/dyn/portal/index.seam?fonds=0&req=5&page=listalo&va_0=%22surveillance+panel%22
18. Smyth GB, Dagley K, Tainsh J. Insights into the economic consequences of the 2007 equine influenza outbreak in Australia. Aust Vet J. 2011;89(Suppl 1):151–8. http://dx.doi.org/10.1111/j.1751-0813.2011.00777.x
19. Firestone SM, Cogger N, Ward MP, Toribio J-ALML, Moloney BJ, Dhand NK. The influence of meteorology on the spread of influenza: survival analysis of an equine influenza (A/H3N8) outbreak. PLoS One. 2012;7:e35284. http://dx.doi.org/10.1371/journal.pone.0035284
20. Watson J, Daniels P, Kirkland P, Carroll A, Jeggo M. The 2007 outbreak of equine influenza in Australia: lessons learned for international trade in horses. Rev Sci Tech. 2011;30:87–93. http://dx.doi.org/10.20506/rst.30.1.2021
21. Yondon M, Heil GL, Burks JP, Zayat B, Waltzek TB, Jamiyan BO, et al. Isolation and characterization of H3N8 equine influenza A virus associated with the 2011 epizootic in Mongolia. Influenza Oth er Respi Viruses. 2013;7:659–65. http://dx.doi.org/10.1111/irv.12069
22. Qi T, Guo W, Huang W, Dai L, Zhao L, Li H, et al. Isolation and genetic characterization of H3N8 equine influenza virus from donkeys in China. Vet Microbiol. 2010;144:455–60. http://dx.doi.org/10.1016/j.vetmic.2010.01.006
23. Yin X, Lu G, Guo W, Qi T, Ma J, Zhu C, et al. Identification of equine influenza virus infection in Asian wild horses (Equus przewalskii). Arch Virol. 2014;159:1159–62. http://dx.doi.org/10.1007/s00705-013-1908-z
24. Gilchrist P, Sergeant ESG. Risk of an equine influenza virus reservoir establishing in wild horses in New South Wales during the Australian epidemic. Aust Vet J. 2011;89 Suppl 1(1):75. https://doi.org/10.1111/j.1751-0813.2011.00752.x|
25. Crawford PC, Dubovi EJ, Castleman WL, Stephenson I, Gibbs EPJ, Chen L, et al. Transmission of equine influenza virus to dogs. Science. 2005;310:482–5. http://dx.doi.org/10.1126/science.1117950
26. Crispe E, Finlaison DS, Hurt AC, Kirkland PD. Infection of dogs with equine influenza virus: evidence for transmission from horses during the Australian outbreak. Aust Vet J. 2011;89 Suppl 1(s1):27–8. http://dx.doi.org/10.1111/j.1751-0813.2011.00734.x
27. Daly JM, Blunden AS, Macrae S, Miller J, Bowman SJ, Kolodziejek J, et al. Transmission of equine influenza virus to English foxhounds. Emerg Infect Dis. 2008;14:461–4. http://dx.doi.org/10.3201/eid1403.070643
28. Tu J, Zhou H, Jiang T, Li C, Zhang A, Guo X, et al. Isolation and molecular characterization of equine H3N8 influenza viruses from pigs in China. Arch Virol. 2009;154:887–90. http://dx.doi.org/10.1007/s00705-009-0381-1
29. Su S, Wang L, Fu X, He S, Hong M, Zhou P, et al. Equine influenza A(H3N8) virus infection in cats. Emerg Infect Dis. 2014;20:2096–9. http://dx.doi.org/10.3201/eid2012.140867
30. Yondon M, Zayat B, Nelson MI, Heil GL, Anderson BD, Lin X, et al. Equine influenza A(H3N8) virus isolated from Bactrian camel, Mongolia. Emerg Infect Dis. 2014;20:2144–7. http://dx.doi.org/10.3201/eid2012.140435
31. Guo Y, Wang M, Kawaoka Y, Gorman O, Ito T, Saito T, et al. Characterization of a new avian-like influenza A virus from horses in China. Virology. 1992;188:245–55. http://dx.doi.org/10.1016/0042-6822(92)90754-D
32. Guo Y, Wang M, Zheng GS, Li WK, Kawaoka Y, Webster RG. Seroepidemiological and molecular evidence for the presence of two H3N8 equine influenza viruses in China in 1993–94. J Gen Virol. 1995;76:2009–14. http://dx.doi.org/10.1099/0022-1317-76-8-2009
33. Abdel-Moneim AS, Abdel-Ghany AE, Shany SA. Isolation and characterization of highly pathogenic avian influenza virus subtype H5N1 from donkeys. J Biomed Sci. 2010;17:25. http://dx.doi.org/10.1186/1423-0127-17-25
34. Kasel JA, Couch RB. Experimental infection in man and horses with influenza A viruses. Bull World Health Organ. 1969;41:447–52.
35. Alford RH, Kasel JA, Lehrich JR, Knight V. Human responses to experimental infection with influenza A/Equi 2 virus. Am J Epidemiol. 1967;86:185–92. http://dx.doi.org/10.1093/oxfordjournals.aje.a120723
36. Masurel N, Mulder J. Studies on the content of antibodies for equine influenza viruses in human sera. Bull World Health Organ. 1966;34:885–93.
37. Bean WJ, Schell M, Katz J, Kawaoka Y, Naeve C, Gorman O, et al. Evolution of the H3 influenza virus hemagglutinin from human and nonhuman hosts. J Virol. 1992;66:1129–38.
38. Burnell FJ, Holmes MA, Roiko AH, Lowe JB, Heil GL, White SK, et al. Little evidence of human infection with equine influenza during the 2007 epizootic, Queensland, Australia. J Clin Virol. 2014;59:100–3. http://dx.doi.org/10.1016/j.jcv.2013.11.011
39. Khurelbaatar N, Krueger WS, Heil GL, Darmaa B, Ulziimaa D, Tserennorov D, et al. Little evidence of avian or equine influenza virus infection among a cohort of Mongolian adults with animal exposures, 2010–2011. PLoS One. 2014;9:e85616. http://dx.doi.org/10.1371/journal.pone.0085616
40. Larson KRL, Heil GL, Chambers TM, Capuano A, White SK, Gray GC. Serological evidence of equine influenza infections among persons with horse exposure, Iowa. J Clin Virol. 2015;67:78–83. http://dx.doi.org/10.1016/j.jcv.2015.04.009
41. Berríos E P. Equine influenza in Chile (1963–1992): a possible human case [in Spanish]. Rev Chilena Infectol. 2005;22:47–50. http://dx.doi.org/10.4067/S0716-10182005000100006

42. Lowen AC, Mubareka S, Steel J, Palese P. Influenza virus transmission is dependent on relative humidity and temperature. PLoS Pathog. 2007;3:e151. PubMed http://dx.doi.org/10.1371/journal.ppat.0030151
43. Davis J, Garner MG, East IJ. Analysis of local spread of equine influenza in the Park Ridge region of Queensland. Transbound Emerg Dis. 2009;56:31–8. http://dx.doi.org/10.1111/j.1865-1682.2008.01060.x
44. Brown JD, Swayne DE, Cooper RJ, Burns RE, Stallknecht DE. Persistence of H5 and H7 avian influenza viruses in water. Avian Dis. 2007;51(Suppl):285–9. http://dx.doi.org/10.1637/7636-042806R.1
45. Scholtens RG, Steele JH, Dowdle WR, Yarbrough WB, Robinson RQ. U.S. Epizootic of equine influenza, 1963. Public Health Rep. 1964;79:393–402. http://dx.doi.org/10.2307/4592142
46. Crouch CF, Daly J, Hannant D, Wilkins J, Francis MJ. Immune responses and protective efficacy in ponies immunised with an equine influenza ISCOM vaccine containing an "American lineage" H3N8 virus. Vaccine. 2004;23:418–25. http://dx.doi.org/10.1016/j.vaccine.2004.01.074
47. Barquero N, Daly JM, Newton JR. Risk factors for influenza infection in vaccinated racehorses: lessons from an outbreak in Newmarket, UK in 2003. Vaccine. 2007;25:7520–9. http://dx.doi.org/10.1016/j.vaccine.2007.08.038
48. Elton D, Bryant N. Facing the threat of equine influenza. Equin Vet J. 2011:43:250–8. https://doi.org/10.1111/j.2042-3306.2010.00357.x
49. Perkins NR, Webster WR, Wright T, Denney I, Links I. Vaccination program in the response to the 2007 equine influenza outbreak in Australia. Aust Vet J. 2011;89 Suppl 1(1):126. https://doi.org/10.1111/j.1751-0813.2011.00766.x
50. Binns MM. Genetic and antigenic analysis of an equine influenza H3 isolate from the 1989 epidemic. Arch Virol. 1993;130:33–43. Erratum in: Arch Vriol. 1993;133:235–7.

Address for correspondence: Gregory C. Gray, Duke Infectious Diseases and Duke Global Health Institute, DUMC Box 102359, Durham, NC 27710, USA; email: gregory.gray@duke.edu

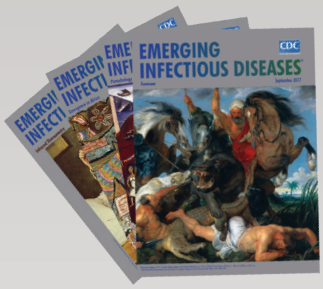

EMERGING INFECTIOUS DISEASES®

September 2017

Zoonoses

- Bioinformatic Analyses of Whole-Genome Sequence Data in a Public Health Laboratory
- Convergence of Humans, Bats, Trees, and Culture in Nipah Virus Transmission, Bangladesh
- Processes Underlying Rabies Virus Incursions across US–Canada Border as Revealed by Whole-Genome Phylogeography
- Real-Time Whole-Genome Sequencing for Surveillance of *Listeria monocytogenes*, France
- Role of Food Insecurity in Outbreak of Anthrax Infections among Humans and Hippopotamuses Living in a Game Reserve Area, Rural Zambia
- Molecular Antimicrobial Resistance Surveillance for *Neisseria gonorrhoeae*, Northern Territory, Australia
- Estimated Annual Numbers of Foodborne Pathogen–Associated Illnesses, Hospitalizations, and Deaths, France, 2008–2013
- Epidemiology of *Salmonella enterica* Serotype Dublin Infections among Humans, United States, 1968–2013
- Prevalence of *Yersinia enterocolitica* Bioserotype 3/O:3 among Children with Diarrhea, China, 2010–2015
- Risk for Low Pathogenicity Avian Influenza Virus on Poultry Farms, the Netherlands, 2007–2013
- Patterns of Human Plague in Uganda, 2008–2016
- Serologic Evidence for Influenza C and D Virus among Ruminants and Camelids, Africa, 1991–2015
- Norovirus in Bottled Water Associated with Gastroenteritis Outbreak, Spain, 2016
- Group A Rotavirus Associated with Encephalitis in Red Fox
- Protective Effect of Val_{129}-PrP against Bovine Spongiform Encephalopathy but not Variant Creutzfeldt-Jakob Disease
- Genetic Diversity of Highly Pathogenic Avian Influenza A(H5N8/H5N5) Viruses in Italy, 2016–17
- Microcephaly Caused by Lymphocytic Choriomeningitis Virus
- Influenza A(H3N2) Virus in Swine at Agricultural Fairs and Transmission to Humans, Michigan and Ohio, USA, 2016
- Use of Blood Donor Screening to Monitor Prevalence of HIV and Hepatitis B and C Viruses, South Africa
- Emergence of Plasmid-Mediated Fosfomycin-Resistance Genes among *Escherichia coli* Isolates, France
- Determination of the Ferret Enteric Coronavirus Genome in Laboratory Ferrets

To revisit the September 2017 issue, go to:

https://wwwnc.cdc.gov/eid/articles/issue/23/9/table-of-contents

Outbreak of Vaccinia Virus Infection from Occupational Exposure, China, 2017

Bing Lu,[1] Lun-Biao Cui,[1] Min-Hua Gu, Chao Shi, Chuan-Wu Sun, Kang-Chen Zhao, Jun Bi, Zhong-Ming Tan, Xi-Ling Guo, Xiang Huo, Chang-Jun Bao

Human infections with vaccinia virus (VACV), mostly from laboratory accidents or contact with infected animals, have occurred since smallpox was eradicated in 1980. No recent cases have been reported in China. We report on an outbreak of VACV from occupational exposure to rabbit skins inoculated with VACV.

Vaccinia virus (VACV; genus *Orthopoxvirus* [OPV]) is used as a lyophilized live virus vaccine against smallpox, variola virus (*1*). VACV, cowpox virus, and monkeypox virus are OPVs of concern because of pathogenicity in humans, possible adverse effects in vulnerable populations, potential spread and introduction in other areas, and public health burden (*2*). After smallpox was declared eradicated in 1980, mandatory routine vaccination was suspended worldwide, including in China (*3*). Immunological cross-reaction herd immunity to OPVs also subsided. Those who might have contact with OPVs often receive VACV vaccination, including those collecting OPV samples, responding to outbreaks, treating patients, or handling OPVs in the laboratory, as well as military personnel, especially in the United States.

Human infections with OPVs frequently emerge or reemerge, including cowpox virus in Europe (*4*), monkeypox virus in Africa and North America (*5*), buffalopox in India (*6*), and VACV in South America (*7*), especially in Brazil (*8*). Most human cases have occurred from occupational exposure to infected animals or laboratory accidents, such as needle sticks or eye splashes (*9*). No human cases of VACV infection have been reported in China in recent decades.

Author affiliations: Wuxi Municipal Center for Disease Control and Prevention, Wuxi, China (B. Lu, C. Shi); Jiangsu Provincial Center for Disease Control and Prevention, Nanjing, China (L.-B. Cui, K.-C. Zhao, Z.-M. Tan, X.-L. Guo, X. Huo, C.-J. Bao); Jiangyin Center for Disease Control and Prevention, Wuxi (M.-H. Gu); Xuzhou Municipal Center for Disease Control and Prevention, Xuzhou, China (C.-W. Sun, J. Bi)

DOI: https://doi.org/10.3201/eid2506.171306

The Study

On March 9, 2017, case-patient 1, an industrial worker, was admitted to a local hospital with high fever and a pustular eruption on his left thumb that appeared 3 days earlier (Figure 1, panel A). Case-patients 2–5 began having fever and skin lesions almost simultaneously and were seen as outpatients at community clinics during March 7–9. Case-patient 1 became ill with severe pneumonia and was transferred to a tertiary hospital for treatment on March 13.

All 5 case-patients worked in a powder processing company. On March 2, they pulverized a batch of frozen skins (Figure 1, panel D) from rabbits inoculated with VACV (Figure 1, panel E) in a biopharmaceutical laboratory 5 days before. Three biopharmaceutical company employees brought the skins to the powder processing company and used the pulverized skins to study the analgesic function of its extracts. The 5 case-patients pulverized the skins in an enclosed workspace (Figure 1, panel G) and did not wear personal protective equipment at any time during the process, which took ≈1 hour. Case-patients 2, 4, and 5 touched the skins with ungloved hands before and after pulverizing. After the pulverizing process, case-patients 3 and 4 disassembled the pulverizer (Figure 1, panel F), and case-patients 1 and 3 washed it with a water cannon. The 3 biopharmaceutical company employees were in the workspace but wore masks and did not participate in the pulverizing process; none became ill or exhibited symptoms.

On March 14, the municipal Center for Disease Control and Prevention initiated an investigation of the 5 febrile case-patients (Appendix Figure, http://wwwnc.cdc.gov/EID/article/25/6/17-1306-App1.pdf). All 5 case-patients were male, 21–53 years of age (Table). Case-patients 1–4 were otherwise healthy and not taking any long-term medications. Case-patient 5 had a history of hypertension; he had fever but no exanthema. Case-patients 3, 4, and 5 reported having a smallpox vaccination in the 1970s; each had a vaccination scar on his left arm. All case-patients had fevers that began 2–5 days after exposure, with high temperatures of 39.0°C–42.0°C. Case-patients 1, 2, and 4 had painful vesicular-pustular lesions on their hands. Case-patient 2 had ≥7 pustules with a diameter of ≈0.6 cm on each hand (Figure 1, panels B and C). All 5 case-patients

[1]These authors contributed equally to this article.

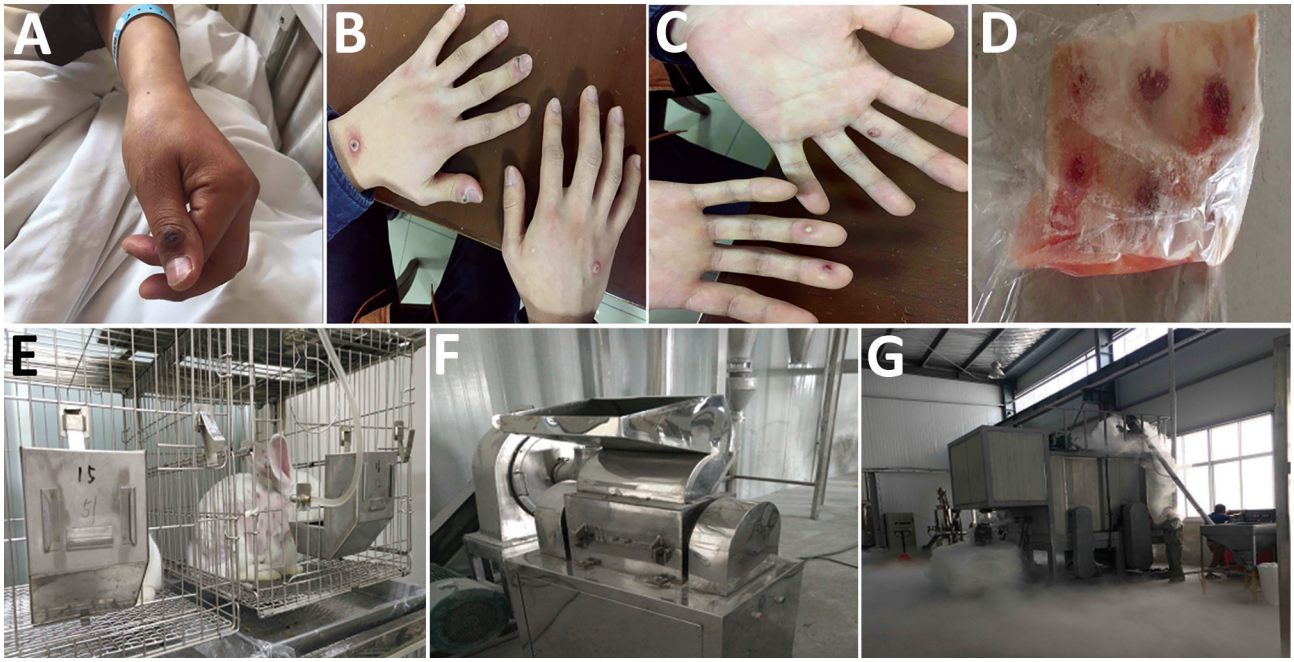

Figure 1. Images from outbreak of vaccinia virus (VACV) from occupational exposure, China, March 2017. A) Lesion on thumb of case-patient 1; B, C) lesions on hands of case-patient 2; D) batch of frozen rabbit skin inoculated with VACV by a biopharmaceutical laboratory; E) live rabbit after VACV inoculation in the biopharmaceutical laboratory; F) machine used to pulverize rabbit skin; G) closed workspace where 5 case-patients pulverized rabbit skin.

had pulmonary infections seen on computed tomography scans on March 20.

Case-patients 2–5 were prescribed antipyretic and antiinflammatory medications, which they took for 9–16 days, and were afebrile 5–9 days after illness onset. They were advised to avoid contact with family members and friends until they were afebrile and escharosis exfoliation was complete. Case 1 was the only patient hospitalized. He was kept in isolation in the tertiary hospital until being discharged on March 24. No transmission occurred from the case-patients to other contacts, and none had scar formation.

Epidemiologic investigation and clinical manifestations raised concerns that cowpox or tularemia were likely etiologies. Nasopharyngeal swab, whole blood, and serum samples were collected from all 5 case-patients on March 14. Clinicians also collected samples of content from scabs from case-patient 1 and liquid from blisters from case-patient 2.

We extracted viral DNA using the QIAamp MinElute Virus Spin Kit (QIAGEN, https://www.qiagen.com). We conducted real-time PCR to screen for OPV (*10*) and suspected bacteria, including *Francisella tularensis* and *Bacillus anthracis*. Case-patients 1–4 tested positive for VACV. All 5 case-patients were negative for cowpox virus, monkeypox virus, *F. tularensis*, and *B. anthracis*. We used Hep2 cells (SGST accession no. TCHu 21) to isolate the virus in positive samples, which showed characteristic cytopathic effects, including cell rounding, loss of adherence, and cellular debris 48 hours postinfection.

To establish the relationship between the illness and exposure, we collected residue from the pulverizer blade and outlet and from the surrounding floor. We used real-time PCR to detect VACV-specific nucleic acids in these specimens. We amplified the hemagglutinin gene A56R and sequenced it using an Applied Biosystems 3130 Genetic Analyzer (ThermoFisher Scientific, https://www.thermofisher.com) (*11*). We aligned nucleotide sequences using ClustalW (http://www.clustal.org/clustal2) and constructed a phylogenetic tree with MEGA5 (https://www.megasoftware.net).

We obtained A56R gene sequences from 5 positive specimens, 1 each from case-patients 1, 2, and 4; 1 from the pulverizer; and 1 from the rabbit skin (GenBank accession nos. MF598168–72). All sequences showed 100% identity match with each other and had 99.6% identity match with isolate VACV-MNR-76 (GenBank accession no. DQ792504) (Figure 2). Unfortunately, we could not trace the vaccine strain used to inoculate the rabbits.

Conclusions

Epidemiologic and molecular data implicated VACV as the etiology of this outbreak, the source of which was rabbit skins inoculated with smallpox vaccine. The

Table. Epidemiologic characteristics in 5 case-patients infected with vaccinia virus from occupational exposure, China, 2017*

Characteristics	Case-patients				
	1 (index)	2	3	4	5
General information					
Age, y	37	21	50	52	53
Sex	M	M	M	M	M
Occupation	Worker	Worker	Worker	Worker	Intermediary
Underlying conditions	N	N	N	N	Y†
Current medications	N	N	N	N	N
Immunosuppressant drugs	N	N	N	N	N
Smallpox vaccination, y	N	N	Y, 1974	Y, 1976	Y, 1977
Vaccination scar	N	N	Y	Y	Y
Date of exposure, March 2017	2	2	2	2	2
Exposure type and duration, min					
Inside enclosed work area	60	60	60	60	30
Contact with rabbit skins, ungloved hand	0	5	0	20	5
Contact with pulverized rabbit skins	0	2–3	0	10	10
Disassembling pulverizer	0	0	30	30	0
Washing pulverizer	5	0	5	0	0
Wearing PPE	N	N	N	N	N
Clinical manifestations					
Date of symptom onset, March 2017	6	6	7	4	6
Date of first doctor visit, March 2017	9	7	8	8	9
Highest temperature, °C; duration, d	42.0; 9	39.2; 7	39.0; 5	42.0; 9	39.2; 8
No. painful vesicular-pustular lesions	1	7	0	3	0
Site of painful vesicular-pustular lesions	Left hand	Both hands	NA	Right hand, torso, upper leg	NA
Other symptoms or laboratory findings	N	N	Headache, muscular pain	Headache, vomiting	Elevated leukocyte count
Complication	Pneumonia	Pulmonary infection	Pulmonary infection	Pulmonary infection	Pulmonary infection
Admitted to hospital	Y	N	N	N	N
Treatment duration, d	16	9	16	10	13
Sequelae of scar formation	N	N	N	N	N
Laboratory results with real-time PCR					
Vaccinia virus (source)	+ (BL, SE, NPS, CS)	+ (BL, SE, NPS, LB)	+ (BL, SE, NPS)	+ (BL, SE, NPS)	–
Cowpox virus	–	–	–	–	–
Monkeypox virus	–	–	–	–	–
Francisella tularensis	–	–	–	–	–
Bacillus anthracis	–	–	–	–	–

*BL, blood; CS, content of scabs; LB, liquid form blisters; NA, not available; NPS, nasopharyngeal swabs; SE, serum; +, positive; –, negative.
†Hypertension and hyperthyroidism.

phylogenetic tree revealed a close relationship between the isolated strains and the TianTan strain (Figure 2), a highly attenuated VACV strain used in smallpox vaccine in China. The likely transmission route was contact with infected rabbit skins. However, we cannot exclude transmission through aerosolized or suspended infectious particles, considering all 5 case-patients had pulmonary infection and only 3 case-patients had characteristic VACV skin lesions. The transmission mode in this outbreak differs from outbreaks in Brazil and Europe, where human cases were related to contact with infected dairy cattle or to laboratory accidents (*12–14*).

Case-patients 3, 4, and 5 received prior smallpox vaccination and had less severe clinical manifestations than the other 2 case-patients, indicating that vaccination might have reduced illness severity but failed to protect them from infection (*13*). Decreased immunity over time and increased virulence of the VACV strain involved might account for the infections.

VACV is commonly used in research settings and the biopharmaceutical industry. Functional studies on extracts from rabbit skins inoculated with VACV are common in China (*15*). The inadvertent introduction of virulent VACV to local domestic and wild animals could cause a severe outbreak, such as occurred in Brazil (*14*). Besides using standard contact protections, those who handle animals vaccinated with VACV, or their products, should use proper respiratory protection. In addition, we recommend increased supervision of biopharmaceutical uses of VACV and smallpox vaccination for laboratory and other workers at risk for occupational exposure to OPVs, as recommended in the United States (*3*).

Acknowledgments

We are grateful to those who assisted in collecting data and specimens from the local Municipal Center for Disease Control and Prevention (CDC) in Jiangyin and Peizhou counties; to Keith Dear, who helped review and edit the manuscript; and to Yayun Tan, who assisted in drawing the appendix figure.

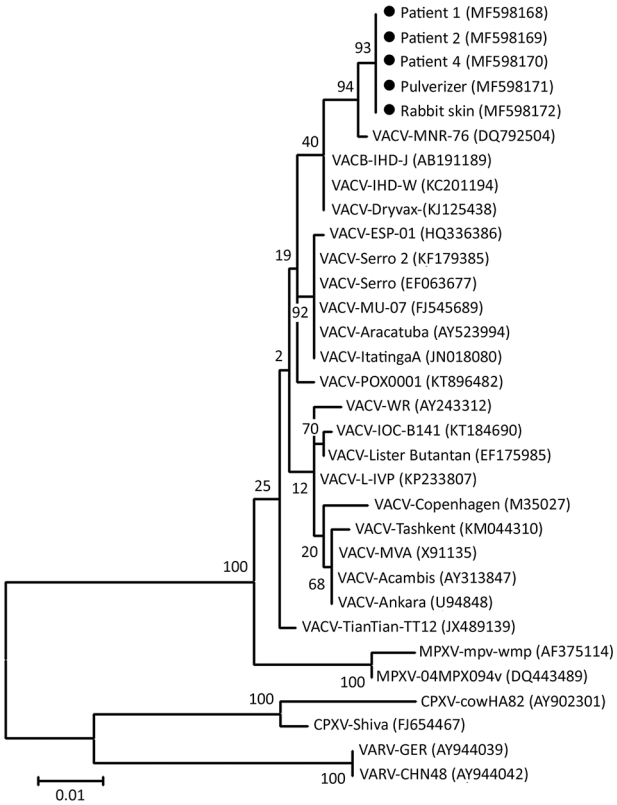

Figure 2. Phylogenetic tree of isolates from outbreak of vaccinia virus from occupational exposure, China, 2017, compared with reference isolates. The tree was constructed by using nucleotide sequences of *Orthopoxvirus* A56R hemagglutinin genes and the maximum-likelihood method with 1,000 bootstrap replicates in MEGA5 (https://www.megasoftware.net). Black dots indicate isolates from this study. Numbers along branches indicate bootstrap values. Scale bar indicates nucleotide substitutions per site. CPXV, cowpox virus; MPXV, monkeypox virus; VACV, vaccinia virus; VARV, variola virus.

This work was supported partly by grants from Science & Technology Demonstration Project for Major Emerging Infectious Diseases Control and Prevention (nos. BE2015714, BE2017749), National Nature Science Foundation of China (no. 81373055), National Major Science & Technology Projects for Infectious Disease Control and Prevention (no. 2017ZX10103008), and Key Medical Discipline of Epidemiology (no. ZDXK A2016008), Medical Talent (no. ZDRC A2016032), and the 333 Project of Jiangsu Province.

About the Author

Dr. Lu is a senior field epidemiologist who works for Wuxi Municipal Center for Disease Control and Prevention, Jiangsu. His research interests include emerging viral infectious diseases and outbreak preparedness and rapid response.

References

1. Essbauer S, Pfeffer M, Meyer H. Zoonotic poxviruses. Vet Microbiol. 2010;140:229–36. http://dx.doi.org/10.1016/j.vetmic.2009.08.026
2. Shchelkunov SN. An increasing danger of zoonotic orthopoxvirus infections. PLoS Pathog. 2013;9:e1003756. http://dx.doi.org/10.1371/journal.ppat.1003756
3. Petersen BW, Harms TJ, Reynolds MG, Harrison LH. Use of vaccinia virus smallpox vaccine in laboratory and health care personnel at risk for occupational exposure to *Orthopoxviruses*–recommendations of the Advisory Committee on Immunization Practices (ACIP), 2015. MMWR Morb Mortal Wkly Rep. 2016;65:257–62. http://dx.doi.org/10.15585/mmwr.mm6510a2
4. Maksyutov RA, Gavrilova EV, Meyer H, Shchelkunov SN. Real-time PCR assay for specific detection of cowpox virus. J Virol Methods. 2015;211:8–11. http://dx.doi.org/10.1016/j.jviromet.2014.10.004
5. McCollum AM, Damon IK. Human monkeypox. Clin Infect Dis. 2014;58:260–7. http://dx.doi.org/10.1093/cid/cit703
6. Gurav YK, Raut CG, Yadav PD, Tandale BV, Sivaram A, Pore MD, et al. Buffalopox outbreak in humans and animals in Western Maharashtra, India. Prev Vet Med. 2011;100:242–7. http://dx.doi.org/10.1016/j.prevetmed.2011.03.008
7. de Assis FL, Vinhote WM, Barbosa JD, de Oliveira CH, de Oliveira CM, Campos KF, et al.; Jônatas. Reemergence of vaccinia virus during zoonotic outbreak, Pará State, Brazil. Emerg Infect Dis. 2013;19:2017–20. http://dx.doi.org/10.3201/eid1912.130589
8. Kroon EG, Mota BE, Abrahão JS, da Fonseca FG, de Souza Trindade G. Zoonotic Brazilian vaccinia virus: from field to therapy. Antiviral Res. 2011;92:150–63. http://dx.doi.org/10.1016/j.antiviral.2011.08.018
9. MacNeil A, Reynolds MG, Damon IK. Risks associated with vaccinia virus in the laboratory. Virology. 2009;385:1–4. http://dx.doi.org/10.1016/j.virol.2008.11.045
10. Shchelkunov SN, Shcherbakov DN, Maksyutov RA, Gavrilova EV. Species-specific identification of variola, monkeypox, cowpox, and vaccinia viruses by multiplex real-time PCR assay. J Virol Methods. 2011;175:163–9. http://dx.doi.org/10.1016/j.jviromet.2011.05.002
11. Ropp SL, Jin Q, Knight JC, Massung RF, Esposito JJ. PCR strategy for identification and differentiation of small pox and other orthopoxviruses. J Clin Microbiol. 1995;33:2069–76.
12. Costa GB, Moreno EC, de Souza Trindade G; Studies Group in Bovine Vaccinia. Neutralizing antibodies associated with exposure factors to *Orthopoxvirus* in laboratory workers. Vaccine. 2013;31:4706–9. http://dx.doi.org/10.1016/j.vaccine.2013.08.023
13. Hsu CH, Farland J, Winters T, Gunn J, Caron D, Evans J, et al.; Centers for Disease Control and Prevention (CDC). Laboratory-acquired vaccinia virus infection in a recently immunized person—Massachusetts, 2013. MMWR Morb Mortal Wkly Rep. 2015;64:435–8.
14. Abrahão JS, Campos RK, de Souza Trindade G, Fonseca FG, Ferreira PC, Kroon EG. Outbreak of severe zoonotic vaccinia virus infection, southeastern Brazil. Emerg Infect Dis. 2015;21:695–8. http://dx.doi.org/10.3201/eid2104.140351
15. Zhang J, Zhang X, Cui J. Therapeutic evaluation of intradermal injection of inflamed rabbit skin inoculated with vaccinia virus in herpes zoster patients and incidence of post herpetic neuralgia [in Chinese]. Chinese Journal of Experimental and Clinical Virology. 2016;30:566–9.

Address for correspondence: Chang-Jun Bao, Jiangsu Provincial Center for Disease Control and Prevention, Department of Acute Infectious Disease Control and Prevention, 172 Jiangsu Rd, Nanjing, Jiangsu 210009, China; e-mail: bao2000_cn@163.com

Pertactin-Negative and Filamentous Hemagglutinin-Negative *Bordetella pertussis*, Australia, 2013–2017

Zheng Xu, Sophie Octavia, Laurence Don Wai Luu, Michael Payne, Verlaine Timms, Chin Yen Tay, Anthony D. Keil, Vitali Sintchenko, Nicole Guiso, Ruiting Lan

During the 2008–2012 pertussis epidemic in Australia, pertactin (Prn)–negative *Bordetella pertussis* emerged. We analyzed 78 isolates from the 2013–2017 epidemic and documented continued expansion of Prn-negative *ptxP3 B. pertussis* strains. We also detected a filamentous hemagglutinin-negative and Prn-negative *B. pertussis* isolate.

Despite high vaccination coverage, pertussis remains a major public health concern. In many industrialized countries, including Australia, whole-cell vaccine was replaced by the less reactogenic acellular vaccine (ACV). In Australia, the 3-component ACV (containing pertactin [Prn], pertussis toxin [Ptx], and filamentous hemagglutinin [Fha]) has been more widely used than the 5-component ACV (which also contains fimbrial antigen: Fim2 and Fim3).

Since 1991, when notifications began, pertussis has reemerged in Australia, and epidemics occur every 3–5 years. The largest epidemic occurred in 2008–2012; 39,000 cases were recorded at its peak in 2011 (*1*,*2*). Most *Bordetella pertussis* isolates from that epidemic belonged to 1 genetic group, referred to as single-nucleotide polymorphism (SNP) cluster I (*1*–*3*). SNP cluster I had *prn2* allele of the *prn* gene and *ptxP3* allele of the Ptx promoter (*3*).

In a study of the 2008–2012 epidemic, Lam et al. (*1*) reported a rapid increase in the number of isolates not expressing the ACV antigen Prn (Prn-negative), from 5.13% in 2008 to 77.78% in 2012. Sequencing of 22 isolates revealed 5 epidemic lineages (ELs) (EL1–EL5) and independent origins of Prn-negative strains in different ELs (*4*). A smaller epidemic occurred during 2013–2017, peaking at 22,000 cases in 2015 (Figure 1, panel A). We investigated the genotypic and phenotypic characteristics of 78 *B. pertussis* isolates from 2013–2017 to determine the epidemic trends of pertussis in Australia.

University of New South Wales, Sydney, New South Wales, Australia (Z. Xu, S. Octavia, L.D.W. Luu, M. Payne, R. Lan); New South Wales Health Pathology and Westmead Hospital, Sydney (V. Timms, V. Sintchenko); The University of Sydney, Sydney (V. Timms, V. Sintchenko); University of Western Australia, Perth, Western Australia, Australia (C.Y. Tay); Perth Children's Hospital, Perth (A.D. Keil); Institut Pasteur, Paris, France (N. Guiso)

DOI: https://doi.org/10.3201/eid2505.180240

The Study

We sequenced 78 *B. pertussis* isolates (Appendix 1 Table 1) from New South Wales (NSW) (17/78 [21.8%]) and Western Australia (WA) (61/78 [78.2%]) that were collected during the 2013–2017 epidemic. We conducted SNP detection (Appendix 1 Table 2) and examined variation in ACV antigen genes (*prn*, *ptxA*, *ptxP*, and the 2 fimbrial genes *fim2* and *fim3*). Using the SNP-based classification scheme by Octavia et al. (*3*), we typed the 78 isolates into 2 SNP profiles (SPs): SP13 (SNP cluster I, *ptxP3*, 75/78 [96.2%]) and SP18 (noncluster I, *ptxP1*, 3/78 [3.8%]). All isolates harbored the *ptxA1* allele. Most (75/78 [96.2%]) of the SP13 isolates had the *prn2* and *fim3A* alleles. The 3 noncluster I SP18 isolates had a *fim3A** allele that differs from *fim3A* by a synonymous mutation (*3*) with genotype *ptxP1-fim3A*-prn1*. The frequency of *ptxP3* and *fim3A* alleles was higher than during the 2008–2012 epidemic (Figure 1, panels B, C). All but 1 isolate carried the *fim2–1* allele. One isolate (L2263 [SP18]) contained a *fim2* allele with a new 3-nucleotide insertion (AGA) at position 506, resulting in the insertion of a lysine in the epitope (F2.9) region of Fim2 (*5*). PROVEAN analysis (*6*) suggests that the insertion does not affect protein structure and thus might or might not affect immune recognition. We designated this allele as *fim2–3* (GenBank accession no. MG824989). Western immunoblotting showed that all isolates expressed Ptx, and all but 1 (L2228) expressed Fha. For Prn, 89.7% (70/78) isolates were Prn-negative (Figure 1, panel D), suggesting continued expansion of Prn-negative strains.

We found multiple mechanisms of *prn* inactivation in the isolates, all but 1 of which were reported previously (*1*,*7*–*9*). For most (66/70) isolates, inactivation was caused by insertion sequences (IS), including 45 IS*481*F insertions (F/R denotes insertion orientation relative to *prn*), 17 IS*481*R insertions, and 4 IS*1002*R insertions (Table). We found an IS*481*F insertion, which has been reported in *prn1*

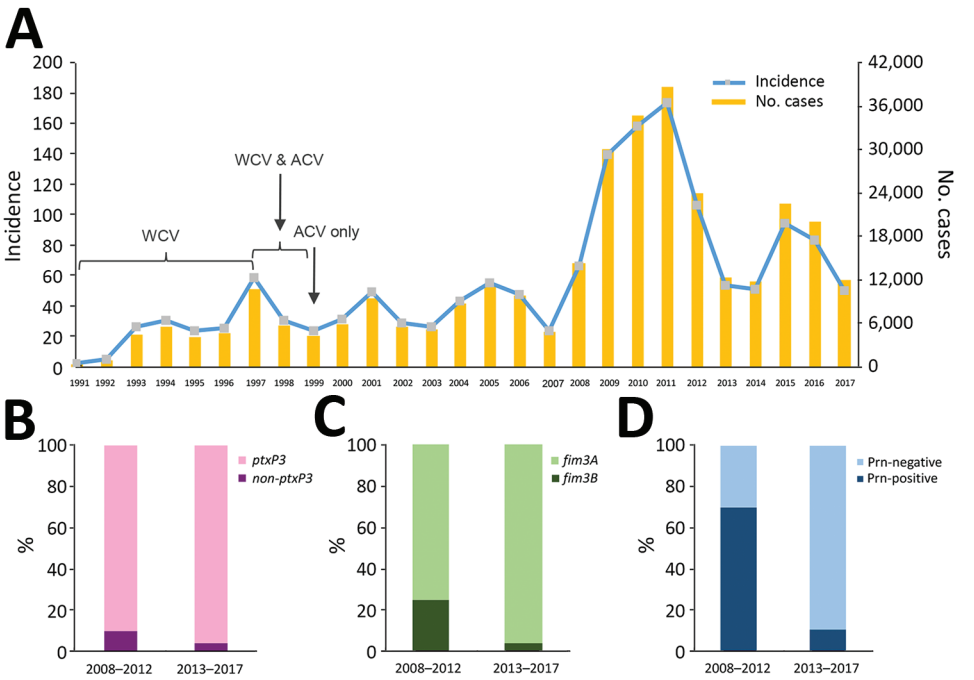

Figure 1. Pertussis trends and temporal changes of allele frequencies of vaccine antigens genes, Australia. A) Pertussis notifications in Australia, 1991–2017. Source: National Notifiable Diseases Surveillance System (http://www9.health.gov.au/cda/source/cda-index.cfm). Incidence is number of cases per 100,000 population. Reporting system was established in 1991. ACV was first introduced in Australia in 1997, and WCV was replaced with ACV in 1999. A large pertussis epidemic occurred during 2008–2012, and another epidemic occurred during 2013–2017. B) Percentage of *Bordetella pertussis* isolates carrying *ptxP3* allele in the 2 epidemic periods. C) Percentage of *B. pertussis* isolates carrying *fim3A* and *fim3B* allele in the 2 epidemic periods. D) Percentage of pertactin-expressing (Prn-positive) and pertactin-deficient (Prn-negative) *B. pertussis* isolates in the 2 epidemic periods. ACV, acellular vaccine; Prn, pertactin; WCV, whole-cell vaccine.

and *prn2* isolates only (*1*,*8*), in 3 of the *prn3* isolates. One Prn-negative isolate contained a SNP (C→T) in position 223, resulting in a stop codon, a mutation found previously in US isolates only (*10*). Two isolates had a deletion (position –297, 1325 [relative to the initiation codon ATG]) between the promoter and 5′ end of *prn* that was replaced with a fragment of IS*1663*, which might have mediated the deletion (Table). A similar but slightly different deletion (position –292, 1340) was reported in US isolates (*7*). We identified a new inactivation by a 4-bp deletion, from position 2020 to 2023 in *prn*, in 1 isolate (L2210) (Appendix 1 Table 1).

Table. Mechanisms of pertactin deficiency and characteristics of *Bordetella pertussis* isolates from pertussis epidemics, Australia, 2013–2017*

Prn deficiency mechanism	Position in *prn*†	*prn* allele type	State (no. of isolates)	Year (no. isolates)	References
IS*481*F	1613	*prn2*	Western Australia (32) New South Wales (10)	2013 (13) 2014 (5) 2015 (11) 2016 (9) 2017 (4)	(*1*)
IS*481*R	1613	*prn2*	Western Australia (12) New South Wales (5)	2013 (6) 2014 (5) 2015 (4)	(*1*)
IS*481*F	1598	*prn3*	Western Australia (3)	2013 (1) 2014 (2)	This study
IS*1002*R	1613	*prn2*	Western Australia (4)	2013 (2) 2016 (1) 2017 (1)	(*1*)
Deletion	–297 to 1325	Not determined‡	Western Australia (2)	2014 (1) 2015 (1)	(*8*), newly found in Australia
Stop codon	223	*prn2*	Western Australia (1)	2014 (1)	(*10*), newly found in Australia
Deletion	2020–2023	*prn2*	Western Australia (1)	2013 (1)	This study

*F/R denotes IS insertion orientation relative to prn. F, forward; IS, insertion sequence; Prn, pertactin; R, reverse.
†The nucleotide positions are relative to the initiation codon (ATG) of the *prn* in Tohama I.
‡*prn* allele type was not determinable because the repeat regions that define *prn* allele type were deleted in this mechanism.

One Prn-negative isolate (L2228) was also Fha-negative (i.e., Prn–, Fha–) by Western immunoblotting. The Fha inactivation probably resulted from changes within the homopolymeric G tract (site: 1078–1087) from 10 Gs to 11 Gs in *fhaB*, resulting in a downstream stop codon that produces a truncated FhaB protein (*11*). Both Illumina and Sanger sequencing (Appendix 2) showed a mixture of 10 Gs and 11 Gs. The bacterial population most likely contained predominantly 11 Gs with a lower proportion of 10 Gs. Proteomic analysis using liquid chromatography tandem mass spectrometry (*12*) found that, in the whole cell of L2228, only 2.3% of the FhaB protein was detected as peptides and derived mainly from the first 350 aa of the FhaB protein. In contrast, in the Fha-positive isolate (L2248), 30.7% of the FhaB protein was detected as peptides and derived from the entire protein. However, in the supernatant of L2228, we detected peptides across the entire FhaB protein and at a higher coverage of 22.7% than for whole-cell FhaB. For the Fha-positive isolate, we detected 52.0% of the FhaB across the entire protein. Western immunoblotting could not detect any FhaB in supernatant or whole-cell proteins of the Fha-negative isolate.

Together with the 27 *B. pertussis* isolates from Australia previously sequenced, we analyzed a total of 105 *B. pertussis* isolates to determine their genomic relationships (Figure 2). Five preepidemic SP13 isolates from 1997–2002 were ancestral to the SP13 epidemic clade as expected; 3 noncluster I (*ptxP1*) isolates grouped together as a separate clade outside SNP cluster I. Most (68/75) isolates grouped into 4 previously defined ELs (EL1–EL4) (*4*). However, no isolates from the new epidemic fell into the 2008–2012 EL5. Four isolates (L2233, L2234, L2261, and L2262) did not cluster with any of the ELs.

Prn-positive isolates from the 2008–2012 and 2013–2017 epidemics were distributed among different lineages. Prn-negative isolates were largely grouped by mechanism of inactivation in different ELs. Prn-negative isolates in EL1 and EL4 were caused by IS*481*R insertion. All but 1 Prn-negative isolate in EL2 was caused by IS*1002* insertion; the exception was an IS*481*R insertion. Prn-negative isolates in EL3 were caused by IS*481*F insertion. Three Prn-negative isolates with new inactivation mechanisms found in Australia were distributed in EL4 (*prn*::del [-297, 1325]; note that the *prn* allele was indeterminate) and non-ELs (*prn2*::stop [C233T]).

EL1 contained isolates from NSW (6/20) and WA (14/20). EL2 was a small lineage (8 isolates), but these isolates were from both periods and both states. EL3 was predominantly a WA lineage; 30/33 isolates from WA and nearly half of the WA isolates (30/61) from 2013–2017 were EL3. EL4 was largely an NSW lineage (14/23 isolates).

Conclusions

The 2013–2017 pertussis epidemic in Australia was predominantly caused by Prn-negative strains, with local and

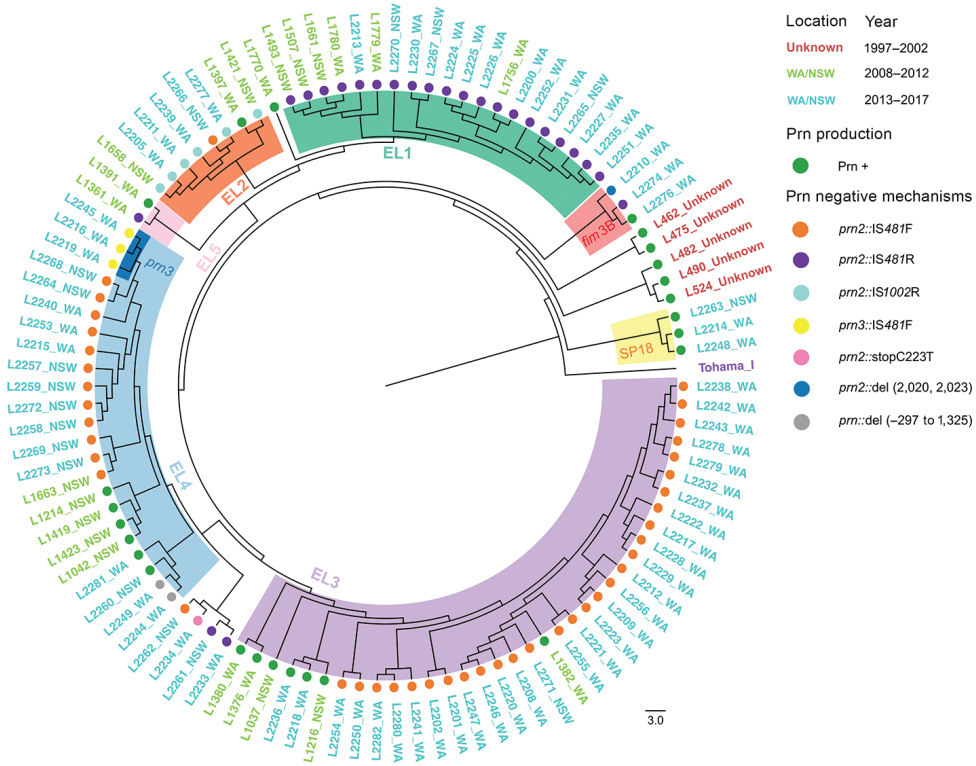

Figure 2. Phylogenomic relationship of 105 *Bordetella pertussis* epidemic isolates from Australia. The minimum-evolution tree was constructed using 705 SNPs. The isolates are labeled by name (L numbers), followed by states with color to indicate years of isolates. Shaded areas inside circle indicate ELs (EL1–EL5) and branches with isolates belonging to SP18 and those carrying *fim*3B and *prn*3 alleles. Prn-positive isolates and different mechanisms of Prn-negative isolates are marked by circles with different colors. Scale bar represents 3 SNPs. EL, epidemic lineage; NSW, New South Wales; Prn, pertactin; SNP, single-nucleotide polymorphism; SP, SNP profile; WA, Western Australia.

interstate expansion of 4 epidemic lineages. The ongoing expansion of Prn-negative strains is most likely due to continued vaccine selection pressure because Australia has been using ACVs that contain Prn since their introduction. This observation contrasts with the declining circulation of Prn-negative strains in Japan, where changes in the vaccine probably caused the decrease because 2 of the 3 vaccines used after 2012 did not contain Prn (*13*). The emergence of an Fha-negative and Prn-negative *B. pertussis* in Australia may offer higher potential to escape ACV-induced immunity.

Our results provide further evidence of *B. pertussis* evolution under vaccine selection. Continued surveillance of *B. pertussis* will provide a better understanding of the effect of vaccination on the evolution of the pathogen and optimize strategies to reduce the occurrence of pertussis.

Acknowledgments

We thank Narelle Raven for technical assistance.

This study was supported by a grant from the National Health and Medical Research Council of Australia (grant no.1146938). Z.X. is supported by a University of New South Wales scholarship.

About the Author

Ms. Xu is a PhD candidate in the School of Biotechnology and Biomolecular Sciences, University of New South Wales, Sydney, NSW, Australia. Her research interests include the epidemiology and evolution of human pathogens.

References

1. Lam C, Octavia S, Ricafort L, Sintchenko V, Gilbert GL, Wood N, et al. Rapid increase in pertactin-deficient *Bordetella pertussis* isolates, Australia. Emerg Infect Dis. 2014;20:626–33. https://doi.org/10.3201/eid2004.131478
2. Octavia S, Sintchenko V, Gilbert GL, Lawrence A, Keil AD, Hogg G, et al. Newly emerging clones of *Bordetella pertussis* carrying *prn2* and *ptxP3* alleles implicated in Australian pertussis epidemic in 2008-2010. J Infect Dis. 2012;205:1220–4. https://doi.org/10.1093/infdis/jis178
3. Octavia S, Maharjan RP, Sintchenko V, Stevenson G, Reeves PR, Gilbert GL, et al. Insight into evolution of *Bordetella pertussis* from comparative genomic analysis: evidence of vaccine-driven selection. Mol Biol Evol. 2011;28:707–15. https://doi.org/10.1093/molbev/msq245
4. Safarchi A, Octavia S, Wu SZ, Kaur S, Sintchenko V, Gilbert GL, et al. Genomic dissection of Australian *Bordetella pertussis* isolates from the 2008-2012 epidemic. J Infect. 2016;72:468–77. https://doi.org/10.1016/j.jinf.2016.01.005
5. Williamson P, Matthews R. Epitope mapping the Fim2 and Fim3 proteins of *Bordetella pertussis* with sera from patients infected with or vaccinated against whooping cough. FEMS Immunol Med Microbiol. 1996;13:169–78.
6. Choi Y, Sims GE, Murphy S, Miller JR, Chan AP. Predicting the functional effect of amino acid substitutions and indels. PLoS One. 2012;7:e46688. https://doi.org/10.1371/journal.pone.0046688
7. Weigand MR, Peng Y, Cassiday PK, Loparev VN, Johnson T, Juieng P, et al. Complete genome sequences of *Bordetella pertussis* isolates with novel pertactin-deficient deletions. Genome Announc. 2017;5:e00973–17. https://doi.org/10.1128/genomeA.00973-17
8. Pawloski LC, Queenan AM, Cassiday PK, Lynch AS, Harrison MJ, Shang W, et al. Prevalence and molecular characterization of pertactin-deficient *Bordetella pertussis* in the United States. Clin Vaccine Immunol. 2014;21:119–25. https://doi.org/10.1128/CVI.00717-13
9. Otsuka N, Han HJ, Toyoizumi-Ajisaka H, Nakamura Y, Arakawa Y, Shibayama K, et al. Prevalence and genetic characterization of pertactin-deficient *Bordetella pertussis* in Japan. PLoS One. 2012;7:e31985. https://doi.org/10.1371/journal.pone.0031985
10. Weigand MR, Peng Y, Loparev V, Batra D, Bowden KE, Burroughs M, et al. The history of *Bordetella pertussis* genome evolution includes structural rearrangement. J Bacteriol. 2017;199:e00806–16. https://doi.org/10.1128/JB.00806-16
11. Bart MJ, Harris SR, Advani A, Arakawa Y, Bottero D, Bouchez V, et al. Global population structure and evolution of *Bordetella pertussis* and their relationship with vaccination. MBio. 2014;5:e01074. https://doi.org/10.1128/mBio.01074-14
12. Luu LDW, Octavia S, Zhong L, Raftery M, Sintchenko V, Lan R. Characterisation of the *Bordetella pertussis* secretome under different media. J Proteomics. 2017;158:43–51. https://doi.org/10.1016/j.jprot.2017.02.010
13. Hiramatsu Y, Miyaji Y, Otsuka N, Arakawa Y, Shibayama K, Kamachi K. Significant decrease in pertactin-deficient *Bordetella pertussis* isolates, Japan. Emerg Infect Dis. 2017;23:699–701. https://doi.org/10.3201/eid2304.161575

Address for correspondence: Ruiting Lan, School of Biotechnology and Biomolecular Sciences, University of New South Wales, Sydney, NSW 2052, Australia; email: r.lan@unsw.edu.au

Increase in Enterovirus D68 Infections in Young Children, United Kingdom, 2006–2016

Everlyn Kamau, Heli Harvala, Soile Blomqvist, Dung Nguyen, Peter Horby, Richard Pebody, Peter Simmonds

We determined the change in seroprevalence of enterovirus D68 (EV-D68) in the United Kingdom in age-stratified cohorts from 2006 to 2016, the period during which EV-D68 emerged as a cause of severe respiratory disease occasionally leading to paralysis. Infections were acquired primarily in infants and young children, and incidence was markedly higher in 2016.

Enterovirus D68 (EV-D68) is a member of the *Enterovirus D* species (genus *Enterovirus;* family *Picornaviridae*). EV-D68 is distributed worldwide and is typically associated with upper respiratory tract infections. Although EV-D68 infections were infrequently reported in the United States and elsewhere before 2010 (*1*,*2*), multiple novel clades of EV-D68 have emerged worldwide (*3*) and have been associated with occasional outbreaks of more severe respiratory infections (*4*). However, it was not until 2014 that a series of large-scale EV-D68 outbreaks resulting in severe illness and death were reported from the United States and Canada and subsequently, in 2016, from Europe (Netherlands, Spain, Germany, Italy, Ireland, Austria, France, Luxembourg), Japan, China, and elsewhere in Asia (*4*–*6*).

While primarily regarded as a respiratory pathogen, EV-D68 has been occasionally associated with acute flaccid myelitis (AFM) (*7*). This apparent change in tropism for cells in the central nervous system (*8*) may be linked to the emergence of novel genetically distinct EV-D68 lineages (*3*). An alternative possibility is that the increased number of reports of severe, AFM-associated infections with EV-D68 reflects larger-scale changes in population immunity that have enabled outbreaks to occur in potentially vulnerable age groups. Severe infections typically target infants >6 months of age, when maternal antibody protection wanes (*4*). The World Health Organization recently identified EV-D68 as a potential major public health risk and recommends enhanced surveillance and more effective diagnostics (*9*). We investigated potential changes in exposure to EV-D68 in the general population of the United Kingdom over the period in which the worldwide outbreaks of EV-D68 occurred.

Author affiliations: University of Oxford, Oxford, UK (E. Kamau, D. Nguyen, P. Horby, P. Simmonds); National Health Service Blood and Transplant, London, UK (H. Harvala); National Institute for Health and Welfare, Helsinki, Finland (S. Blomqvist); Public Health England, London (R. Pebody)

DOI: https://doi.org/10.3201/eid2506.181759

The Study

For this study, we obtained serum samples collected as an approximately representative age-stratified cross section of the UK population (*10*). These samples were collected in 2006, before the reports of increased number of EV-D68 cases (n = 516), and in 2016, after the 2014 EV-D68 outbreak (n = 566) (Figure 1, panel A). We used a standard microneutralization assay for serum samples (Appendix, https://wwwnc.cdc.gov/EID/article/25/6/18-1759-App1.pdf).

To determine the optimal strain to measure neutralizing antibody titer (Nab) assays, we compared titers of selected serum samples to the prototype Fermon (1962) strain and those of more recent EV-D68 isolates isolated in 2005 (FI_2005) and 2016 (FI_2016) (Appendix Figure 1). We identified genotypes of D for FI_2005 and B3 for FI_2016 by phylogenetic comparison of the viral protein 1 sequences. We selected samples for comparing titers to narrow down times of EV-D68 exposure: patients >40 years of age in 2006, representing serologic responses to infections acquired substantially before 2006; patients 6 months–5 years of age in 2006, representing responses to infections acquired during 2001–2006; and patients 6 months–5 years of age in 2016, representing responses to infections acquired during 2011–2016. Geometric mean titers (GMTs) of NAbs to Fermon and FI_2016 were comparable between exposure groups (Appendix Figure 2), whereas samples collected from children infected during 2001–2006 showed some evidence for proportionately higher seroreactivity to the 2005 strain. Overall, differences in GMTs were minor, and we selected the FI_2016 strain for NAb screening.

We determined seroreactivity to EV-D68 by GMT calculations for each age and year category and proportions of samples with different neutralizing antibody titers (Figure 1, panel A). We determined seroprevalence and inferred frequencies of past infection using a conservative 1:16 titer threshold (Figure 1, panel B). Frequencies and titers of

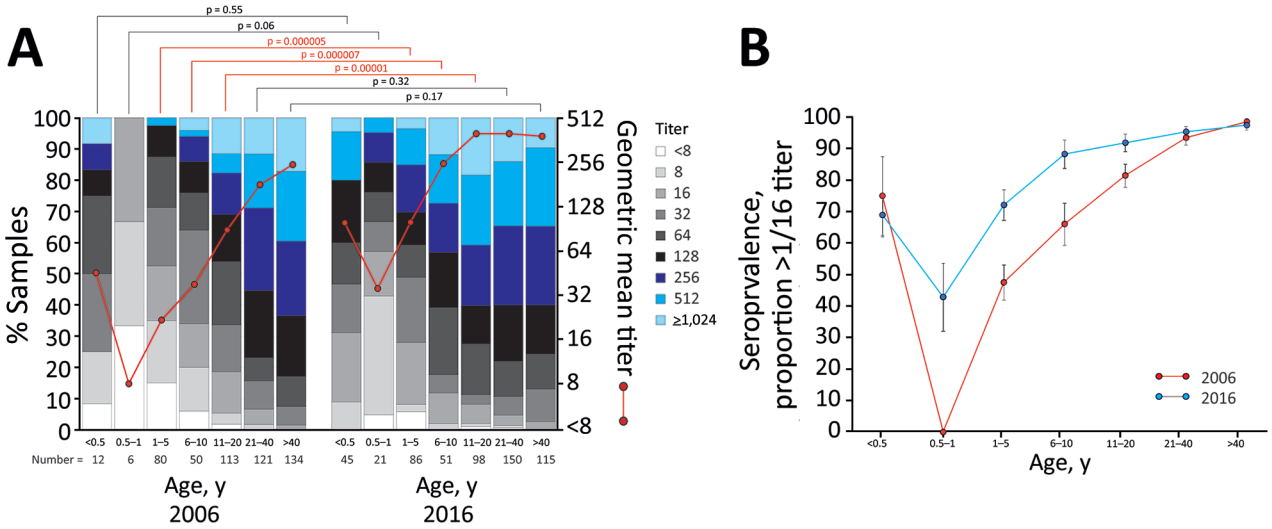

Figure 1. Comparison of enterovirus D68 (EV-D68) seroprevalence in the United Kingdom in 2006 and 2016. A) Seroreactivity to EV-D68 of samples collected in 2006 and 2016 from different age categories. Results are expressed as percentage of samples displaying neutralizing antibody titers <8 or ≥1,024 (histogram) and geometric mean titers (red line). We performed the Kruskal-Wallace nonparametric test to evaluate differences in titer distributions between samples collected at the 2 points in each band (red text indicates p<0.05). B) Seroprevalence of neutralizing antibodies to EV-D68 in different age categories in 2006 (red) and 2016 (blue). Error bars show SEs of the proportions.

EV-D68 NAbs differed substantially between the 2 collection years in young children (in the categories 0.5–1 year, 1–5 years, and 6–10 years of age). The difference narrowed in older age groups, and seroprevalence approached 100% in those >40 years of age. Seroprevalence and titer distributions were elevated in the <0.5-year age group, likely reflecting the presence of maternal antibody in these infants.

The differences in seroprevalence in the young children between 2006 and 2016 demonstrate greater infection rates in 2016. To identify the age at which this greater exposure occurred, we divided sample sets into narrower age bands and determined seroprevalence (Figure 2, panel A). For both groups, infections were acquired at a very early age, with extremely high incidences in the 0.5–2-year and 3–4-year age ranges in both sample years but a marked reduction for children ≥5 years of age. Annualized incidence of EV-D68 infection in the 0.5–5-year age band increased from 36 infections/1,000 population during 2001–2005 to 53 infections/1,000 population during 2012–2016, an increase of 50% (Figure 2, panel B). The increased incidence in the <5-year age group in our study would equate to >35,000 additional EV-D68 infections/year, primarily in young children 0.5–2 years of age. Incidence in older age groups was comparable or reduced, as we expected with greater rates of EV-D68 exposure and seroconversion in the younger age ranges.

Conclusions

The seroprevalence of EV-D68 approached 100% in adult UK populations in this study, consistent with previous seroepidemiology studies conducted in Finland and China (*11*,*12*). Our findings provide further evidence for the wide circulation of EV-D68 infections before reported outbreaks in 2014 and 2016. We demonstrated high incidences of EV-D68 infection in young children; around one half are already infected by 2 years of age in both sampling periods. However, the seroprevalence of EV-D68 infection was consistently higher throughout childhood in 2016 samples than in 2006 samples (Figure 1).

Changes in population immunity, virus antigenicity, transmissibility, cellular tropism, and pathogenicity may contribute to the recent upsurge of severe EV-D68 infections worldwide. Concerning the first potential explanation, seroprevalences in age groups <40 years were consistently lower in 2006 than 2016 (Figure 1, panel B), although EV-D68 circulated extensively, and adults were almost always seropositive and immune before and after periods of greater disease severity in the United Kingdom and elsewhere (*4*,*13*). Changes in NAb susceptibility and escape from population immunity appear unlikely to be a cause of changes in incidence; we found no evidence for major differences in antigenicity between Fermon, genotype D, or B3 isolates (Appendix; Appendix Figure 1). Another possible cause is increased transmissibility of subgenotypes B2 and B3 in younger age groups (Figure 2, panel A), reflecting a possible change in tropism or persistence of virus shedding and longer periods of infectivity after changes in receptor use, cellular tropisms, or both. The Fermon prototype strain of EV-D68 isolated in 1962 has a stronger affinity to α2,6-sialic acid primarily in the airways than to α2,3-linked sialic acid present in the

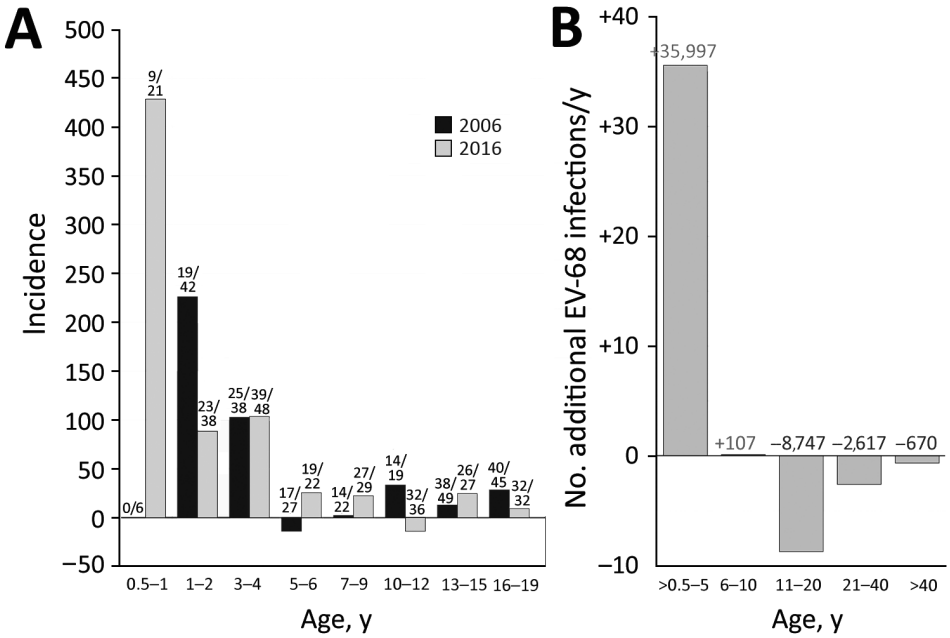

Figure 2. Comparison of incidence of enterovirus D68 (EV-D68) in the United Kingdom in 2006 and 2016. A) Estimated annual incidence of EV-D68 infection for each age group. Incidence was inferred from the difference in seroprevalence from that of the previous age band and converted into infections/year/1,000 population (by dividing the difference in prevalence by the number of years in the age band and multiplying by 1,000). Frequencies of samples with neutralizing antibody titer >16 are shown above bars. B) Change in incidence of EV-D68 infections from 2006 to 2016, expressed as additional EV-68 infections/year (y-axis scale). Figures above bars indicate the predicted positive and negative change in number infections if these incidences were applied to the whole UK population, based on age-stratified population totals for 2016 obtained from Statista (https://www.statista.com/statistics/281174/uk-population-by-age).

lower respiratory tract (*14*). Whether the newer EV-D68 strains causing an outbreak of severe respiratory infections in 2008–2010 were evolved to use primarily α2,3-linked sialic acid or have switched to a sialic acid-independent mechanism of virus entry (*14*), such as ICAM5 (*15*), needs further investigation. Of note, only contemporary EV-D68 strains were able to infect neuroblastoma-derived neuronal cell line SH-SY5Y and cause paralysis in a mouse model, indicating that additional changes in virus strains might have occurred around or after 2012 (*8*), although the relationship of this finding to increased transmissibility of EV-D68 has not been studied.

In summary, we document the greater circulation and force of EV-D68 infection in infants and young children in the United Kingdom over the period in which EV-D68 has emerged as an important respiratory pathogen and potential cause of paralytic disease, reflecting its changed transmissibility and pathogenic potential. Such rapid changes in virus behavior emphasize the importance of ongoing surveillance and appropriate diagnostics for emerging enteroviruses in the future.

Acknowledgments

We thank Lieke Brouwer for technical assistance in performing the neutralization assays and the personnel in the National Polio Laboratory, THL, Helsinki, for culturing the virus strains. We thank Simon Tonge and colleagues at the Vaccine Evaluation Unit, PHE, Manchester, for provision of archive samples. The project was supported by a Wellcome Trust Institutional Strategic Support Fund 2016 (ISSF 204826/Z/16/Z) grant to P.H. and P.S. E.K. was supported in part by a Wellcome Trust investigator grant (WTA102975).

About the Author

Ms. Kamau is a virologist at the University of Oxford. Her research interests are immunoepidemiology and molecular evolution.

References

1. Khetsuriani N, Lamonte-Fowlkes A, Oberst S, Pallansch MA; Centers for Disease Control and Prevention. Enterovirus surveillance—United States, 1970–2005. MMWR Surveill Summ. 2006;55:1–20.
2. Centers for Disease Control and Prevention (CDC). Clusters of acute respiratory illness associated with human enterovirus 68—Asia, Europe, and United States, 2008–2010. MMWR Morb Mortal Wkly Rep. 2011;60:1301–4.
3. Tokarz R, Firth C, Madhi SA, Howie SR, Wu W, Sall AA, et al. Worldwide emergence of multiple clades of enterovirus 68. J Gen Virol. 2012;93:1952–8. http://dx.doi.org/10.1099/vir.0.043935-0
4. Holm-Hansen CC, Midgley SE, Fischer TK. Global emergence of enterovirus D68: a systematic review. Lancet Infect Dis. 2016;16:e64–75. http://dx.doi.org/10.1016/S1473-3099(15)00543-5
5. Knoester M, Schölvinck EH, Poelman R, Smit S, Vermont CL, Niesters HG, et al. Upsurge of enterovirus D68, the Netherlands, 2016. Emerg Infect Dis. 2017;23:140–3. http://dx.doi.org/10.3201/eid2301.161313
6. Messacar K, Robinson CC, Pretty K, Yuan J, Dominguez SR. Surveillance for enterovirus D68 in Colorado children reveals

continued circulation. J Clin Virol. 2017;92:39–41. http://dx.doi.org/10.1016/j.jcv.2017.05.009
7. Sejvar JJ, Lopez AS, Cortese MM, Leshem E, Pastula DM, Miller L, et al. Acute flaccid myelitis in the United States, August–December 2014: results of nationwide surveillance. Clin Infect Dis. 2016;63:737–45. http://dx.doi.org/10.1093/cid/ciw372
8. Brown DM, Hixon AM, Oldfield LM, Zhang Y, Novotny M, Wang W, et al. Contemporary circulating enterovirus D68 strains have acquired the capacity for viral entry and replication in human neuronal cells. MBio. 2018;9:e01954-18. http://dx.doi.org/10.1128/mBio.01954-18
9. World Health Organization. R&D Blueprint: list of Blueprint priority diseases. 2018 [cited 2018 Dec 11]. https://www.who.int/blueprint/priority-diseases
10. Osborne K, Gay N, Hesketh L, Morgan-Capner P, Miller E. Ten years of serological surveillance in England and Wales: methods, results, implications, and action. Int J Epidemiol. 2000;29:362–8. http://dx.doi.org/10.1093/ije/29.2.362
11. Smura T, Ylipaasto P, Klemola P, Kaijalainen S, Kyllönen L, Sordi V, et al. Cellular tropism of human enterovirus D species serotypes EV-94, EV-70, and EV-68 in vitro: implications for pathogenesis. J Med Virol. 2010;82:1940–9. http://dx.doi.org/10.1002/jmv.21894
12. Sun SY, Gao F, Hu YL, Bian LL, Mao QY, Wu X, et al. Seroepidemiology of enterovirus D68 infection in infants and children in Jiangsu, China. J Infect. 2018;76:563–9. http://dx.doi.org/10.1016/j.jinf.2018.02.003
13. Carrion Martin AI, Pebody RG, Danis K, Ellis J, Niazi S, DE Lusignan S, et al. The emergence of enterovirus D68 in England in autumn 2014 and the necessity for reinforcing enterovirus respiratory screening. Epidemiol Infect. 2017;145:1855–64. http://dx.doi.org/10.1017/S0950268817000590
14. Baggen J, Thibaut HJ, Staring J, Jae LT, Liu Y, Guo H, et al. Enterovirus D68 receptor requirements unveiled by haploid genetics. Proc Natl Acad Sci U S A. 2016;113:1399–404. http://dx.doi.org/10.1073/pnas.1524498113
15. Wei W, Guo H, Chang J, Yu Y, Liu G, Zhang N, et al. ICAM-5/telencephalin is a functional entry receptor for enterovirus D68. Cell Host Microbe. 2016;20:631–41. http://dx.doi.org/10.1016/j.chom.2016.09.013

Address for correspondence: Heli Harvala, NHS Blood and Transplant, Microbiology Services, Colindale, London NW9 5BG, UK; email: heli.simmonds@hotmail.com; Peter Simmonds, University of Oxford, Nuffield Department of Medicine, Peter Medawar Building, South Parks Rd, Oxford OX1 3SY, UK; email: peter.simmonds@ndm.ox.ac.uk

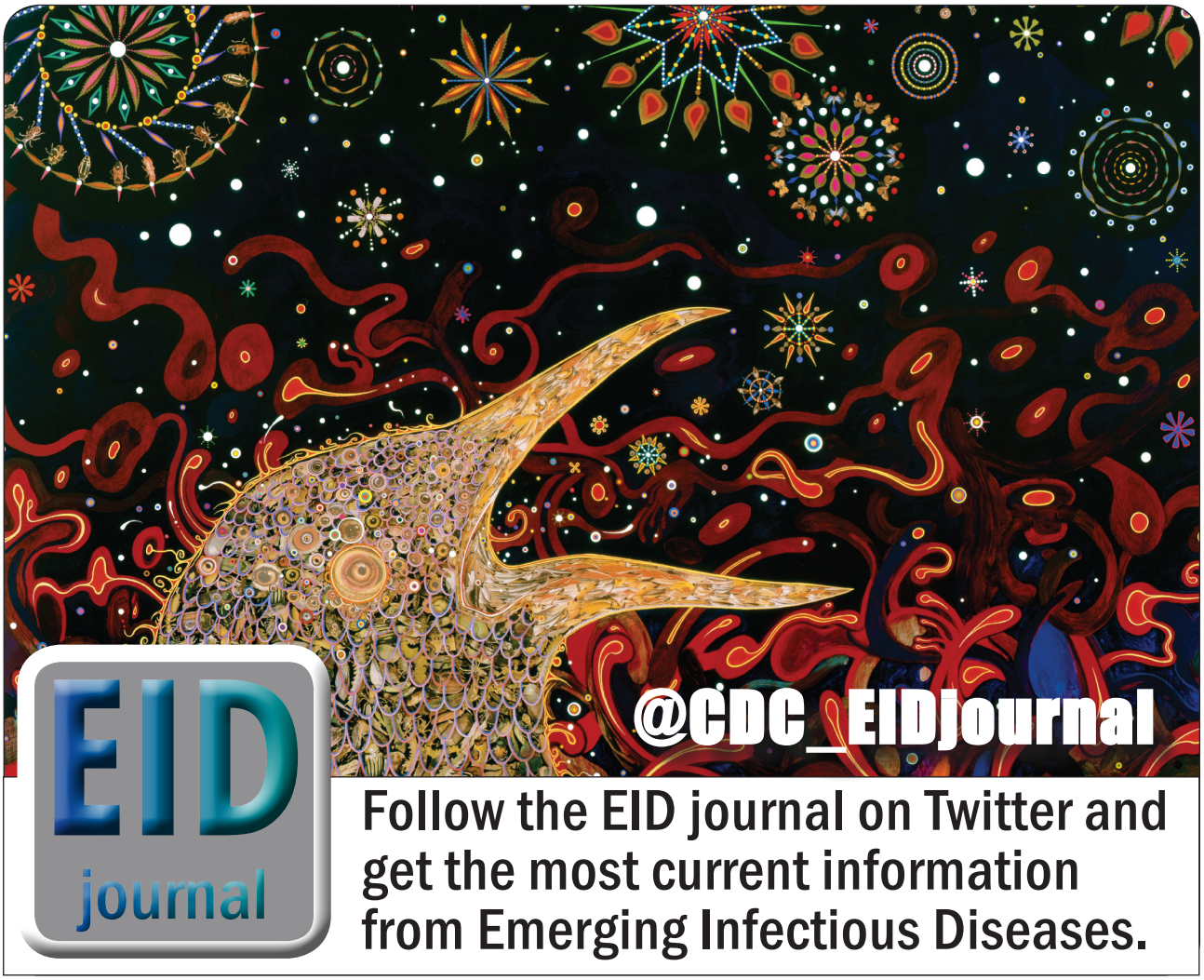

Multirecombinant Enterovirus A71 Subgenogroup C1 Isolates Associated with Neurologic Disease, France, 2016–2017

Stéphanie Tomba Ngangas, Alexander Lukashev, Gwendoline Jugie, Olga Ivanova, Jean-Michel Mansuy, Catherine Mengelle, Jacques Izopet, Anne-Sophie L'honneur, Flore Rozenberg, David Leyssene, Denise Hecquet, Stéphanie Marque-Juillet, David Boutolleau, Sonia Burrel, Hélène Peigue-Lafeuille, Christine Archimbaud, Kimberley Benschop, Cécile Henquell, Audrey Mirand, Jean-Luc Bailly

In 2016, an upsurge of neurologic disease associated with infection with multirecombinant enterovirus A71 subgenogroup C1 lineage viruses was reported in France. These viruses emerged in the 2000s; 1 recombinant is widespread. This virus lineage has the potential to be associated with a long-term risk for severe disease among children.

Enterovirus A71 (EV-A71) comprises 7 genogroups (A–G) and various subgenogroups (e.g., B0–B5, C1–C5) (*1*). B4, B5, and C4 viruses circulate mainly in Asia, and C1 and C2 viruses have been detected in Europe (*2*). In 2016, an upsurge in neurologic manifestations of enterovirus infection was reported in France (*3*). These cases were associated with an emerging lineage of subgenogroup C1 enteroviruses first reported in 2015 in Germany and later in Spain and 4 other countries (Figure 1, panel A) (*4–8*). Our aim was to obtain the full genomes of the viruses from the specimens collected in France and track down the origin of this emerging lineage, hereafter referred to as C1v2015.

Author affiliations: Université Clermont Auvergne, Clermont-Ferrand, France (S. Tomba Ngangas, G. Jugie, H. Peigue-Lafeuille, C. Archimbaud, C. Henquell, A. Mirand, J.-L. Bailly); Sechenov University, Moscow, Russia (A. Lukashev); Chumakov Federal Scientific Center for Research and Development of Immune-and-Biological Products, Moscow (O. Ivanova); Centre Hospitalier Universitaire de Toulouse, Toulouse, France (J.-M. Mansuy, C. Mengelle, J. Izopet); Assistance Publique-Hôspitaux de Paris Cochin, Paris, France (A.-S. L'honneur, F. Rozenberg); Centre Hospitalier de la Côte Basque, Bayonne, France (D. Leyssene); Centre Hospitalier Universitaire Amiens, Amiens, France (D. Hecquet); Centre Hospitalier de Versailles, Le Chesnay, France (S. Marque-Juillet); Assistance Publique-Hôspitaux de Paris Pitié-Salpêtrière-Charles Foix, Paris (D. Boutolleau, S. Burrel); CHU Clermont-Ferrand, Clermont-Ferrand (H. Peigue-Lafeuille, C. Archimbaud, C. Henquell, A. Mirand, J.-L. Bailly); National Institute for Public Health and the Environment, Bilthoven, the Netherlands (K. Benschop)

DOI: https://doi.org/10.3201/eid2506.181460

The Study

According to consolidated data recorded from the French Enterovirus Surveillance Network, 77 laboratory-confirmed cases of C1v2015 infection occurred during March–October 2016; in comparison, 136 EV-A71 infections of all genogroups combined were recorded during 2010–2015. The C1v2015 cases were widespread throughout France and associated with various clinical manifestations, including meningitis, cerebellitis, encephalitis, and myelitis, as well as hand, foot and mouth disease (HFMD) (Figure 1, panels B, C). One fatal case resulted from HFMD and cardiorespiratory failure. We analyzed 32 clinical specimens available from 25 patients reported as having a C1v2015 infection in 2016 and 2017 (Table 1; Appendix Table 1, https://wwwnc.cdc.gov/EID/article/25/6/18-1460-App1.pdf). Specimens and clinical data were collected during routine clinical work-up and epidemiologic surveillance, and patient data were deidentified before this study was conducted. The study was approved by the review board Comité de Protection des Personnes Sud-Est VI (no. 2018/CE44) in Clermont-Ferrand, France. The study population comprised 16 hospitalized children (median age 0.1 years), 4 children seen via ambulatory care (median age 1.8 years), and 5 children with asymptomatic infection (median age 1.4 years) in a childcare facility placed under community surveillance. We obtained the complete genomes, including the full 5′ and 3′ untranslated regions (UTRs), of 18 of 20 specimens and partial genomes of 2 of 20 specimens (2,893-nt and 4,380-nt long) acquired from 18 children (Appendix) (*2*). We also determined the genomes of 12 isolates recovered during routine enterovirus surveillance to investigate their genetic relationships with C1v2015 (Appendix Table 2); we selected these viruses on the basis of previous exploratory investigations of their partial sequences (*2*,*9*,*10*).

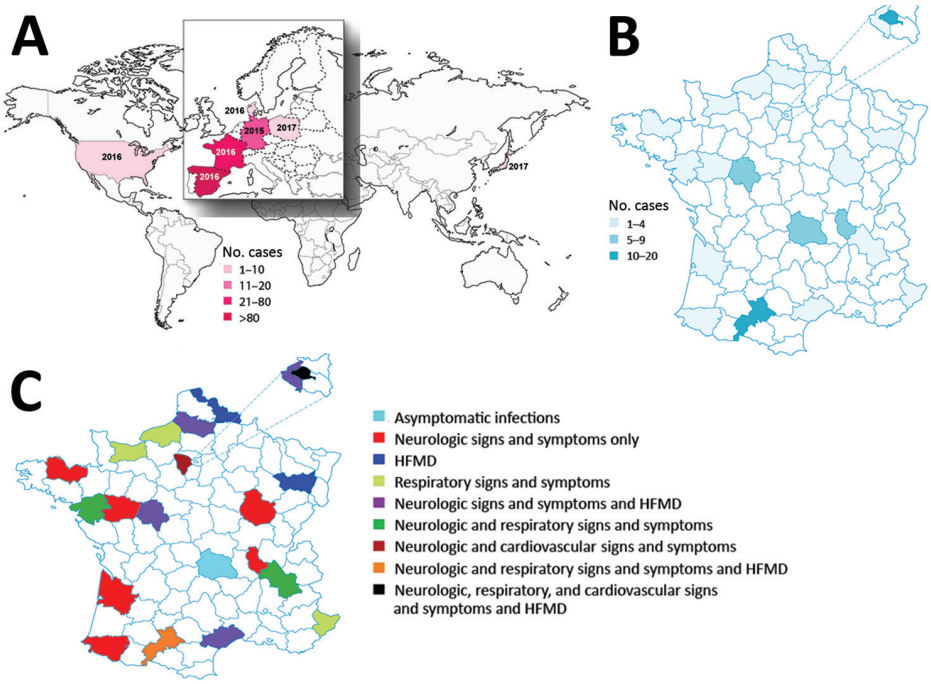

Figure 1. Geographic locations and numbers of enterovirus A71 (EV-A71) subgenogroup C1v2015 infections reported during 2015–2017. A) Countries in which EV-A71 C1v2015 was reported. The year the virus was first reported is indicated. The size of Europe is increased for easier visualization. B) Geographic distribution and number of cases of EV-A71 C1v2015 infection reported in hospitals, by department, France, 2016–2017. C) Geographic distribution of clinical manifestations associated with EV-A71 C1v2015 infection reported in hospitals, by department, France, 2016–2017. The size of a select set of departments is enlarged for easier visualization. HFMD, hand, foot and mouth disease.

Table 1. Characteristics of patients with EV-A71 subgenogroup C1v2015 infection, France, 2016–2017*

Patient no.	Specimen no.	Care setting (City)	Clinical diagnosis	Specimen material	Collection date	C_t
01	01†	Hospital (Toulouse)	Acute meningitis	Throat swab	2016 May 3	25
02	02	Hospital (Toulouse)	Fever	Nasopharyngeal aspirate	2016 May 19	30
02	03	Hospital (Toulouse)	Fever	Feces	2016 May 19	31
03	04	Hospital (Paris)‡	Fever	Plasma	2016 Jun 7	37
04	05	Hospital (Paris)‡	Fever	Plasma	2016 Jun 10	32
05	06	Hospital (Bayonne)	Encephalitis	Cerebrospinal fluid	2016 Jun 12	35
05	07†	Hospital (Bayonne)	Encephalitis	Throat swab	2016 Jun 24	35
05	08	Hospital (Bayonne)	Encephalitis	Rectal swab	2016 Jun 24	35
06	09	Hospital (Toulouse)	Infant fever	Feces	2016 Jul 10	31
07	10†	Hospital (Toulouse)	Sepsis-like disease	Throat swab	2016 Aug 10	24
07	11†	Hospital (Toulouse)	Sepsis-like disease	Nasopharyngeal aspirate	2016 Aug 10	NR
08	12†	Hospital (Paris)‡	Convulsions	Nasopharyngeal aspirate	2016 Aug 11	28
09	13§	Ambulatory (Mirecourt)	HFMD	Mouth swab	2016 Aug 30	32
10	14†	Ambulatory (Mirecourt)	HFMD	Throat swab	2016 Aug 30	29
11	15†	Hospital (Paris)‡	Fever, hypotonia	Blood	2016 Sep 5	30
12	16§	Hospital (Toulouse)	Acute meningitis, HFMD	Throat swab	2016 Sep 7	33
13	17†	Ambulatory (Toulouse)	HFMD	Mouth swab	2016 Sep 14	29
14	18†	Hospital (Paris)‡	Fever	Feces	2016 Sep 27	20
15¶	19†	Daycare (Volvic)	NR	Feces	2016 Oct 4	29
16¶	20†	Daycare (Volvic)	NR	Feces	2016 Oct 4	31
17¶	21†	Daycare (Volvic)	NR	Feces	2016 Oct 4	31
18¶	22†	Daycare (Volvic)	NR	Feces	2016 Oct 4	29
19¶	23†	Daycare (Volvic)	NR	Feces	2016 Oct 4	31
20	24	Hospital (Toulouse)	Sepsis-like disease	Throat swab	2016 Oct 5	33
21	25	Hospital (Versailles)	Diarrhea	Cerebrospinal fluid	2016 Oct 9	35
22	26	Hospital (Toulouse)	Acute meningitis, cerebellitis	Throat swab	2016 Oct 10	36
22	27	Hospital (Toulouse)	Acute meningitis, cerebellitis	Feces	2016 Oct 10	30
23	28†	Hospital (Toulouse)	Fever	Throat swab	2016 Oct 11	27
23	29	Hospital (Toulouse)	Fever	Feces	2016 Oct 12	29
24	30†	Hospital (Amiens)	Myelitis	Nasopharyngeal swab	2016 Oct 18	30
24	31†	Hospital (Amiens)	Myelitis	Feces	2016 Oct 20	33
25	32†	Ambulatory (Montesson)	Atypical HFMD, herpangina	Throat swab	2017 Jul 3	22

*See Appendix Table 1 (https://wwwnc.cdc.gov/EID/article/25/6/18-1460-App1.pdf) for extended data, including GenBank accession nos. C_t, cycle threshold; EV-A71, enterovirus A71; HFMD, hand, foot and mouth disease; NR, not reported.
†Specimens for which the complete viral genomes (including the full 5′ and 3′ untranslated regions) were obtained.
‡Assistance Publique-Hôpitaux de Paris Cochin, Paris, France.
§Specimens for which partial genomes were obtained.
¶Patients 15–19 were children in the same daycare facility who had no evidence of clinical disease.

We performed whole-genome sequence analyses as previously described (*11*) to identify which viruses were the closest relatives of C1v2015. The C1v2015 genome appears to be a mosaic comprising 4 modules defined by distinct patterns of similarity possibly arising through recombination (Figure 2, panel A). The nucleotide similarity patterns for module 2 (genomic region P1 comprising 4 capsid protein genes) suggest this region was inherited en bloc from an earlier subgenogroup C1 lineage. We used genomic region P1 to determine the evolutionary

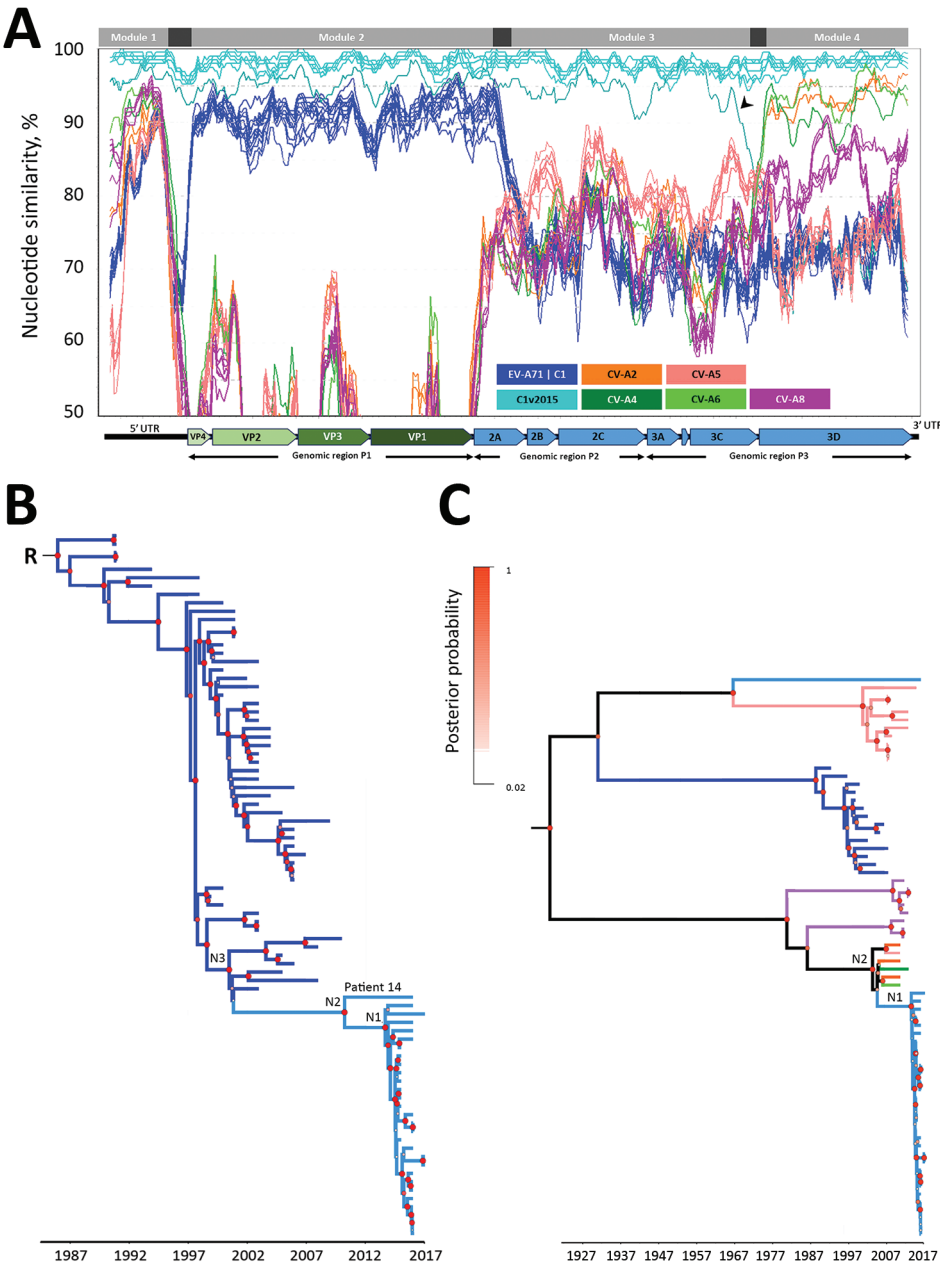

Figure 2. Nucleotide similarity and phylogenetic analyses of EV-A71 subgenogroup C1v2015 isolates, France, 2016–2017, constructed to determine temporal origin of C1v2015 lineage. A) Nucleotide similarity patterns between EV-A71 C1v2015 and other EV-A lineages indicate the C1v2015 genome has a mosaic structure. A schematic diagram of the enterovirus genome is shown at the bottom of the panel. Four genomic modules (labeled at top of panel) with different genetic origins are identified; genomic modules are indicated in dark gray. The arrowhead indicates a previously undescribed recombinant lineage of C1v2015 (Appendix Figure 2, https://wwwnc.cdc.gov/EID/article/25/6/18-1460-App1.pdf). B) Phylogenetic tree constructed by using genomic region P1, encoding capsid proteins VP1–VP4, and methods described earlier (*11*). We performed this analysis with 85 sequences assigned to the EV-A71 C1 and C1v2015 lineages. Tree shows the temporal distribution of lineages, including the emergence of lineage C1v2015. C) Phylogenetic tree constructed by using 3Dpol, encoding the viral RNA polymerase common to C1v2015 and several CV-A strains. The dataset comprised 70 sequences: 24 CV-A (including 5 from this study), 14 EV-A71 C1 (including 6 from this study), 12 publicly available C1v2015, and 20 C1v2015 from this study. Recombination analyses provided no evidence of internal breakpoints within the sequences. N1 represents the time to most recent common ancestor (MRCA) of all included EV-A71 C1v2015 isolates except the virus from patient 14; N2 in panel B represents the MRCA of all EV-A71 C1v2015 isolates, including the virus from patient 14; N2 in panel C represents the MRCA of EV-A71 C1v2015 and its parent C1 lineage; and N3 represents the MRCA of EV-A71 C1v2015 and its parent C1 lineage (see Table 2). Diameters of circles at nodes reflect posterior probability. Branches of trees are color coded according to virus lineage as indicated in panel A. C1v2015, enterovirus subgenogroup C1 strain discovered in 2015; CV-A, coxsackievirus genogroup A; EV-A71C1, enterovirus A71 subgenogroup C1; N, node; UTR, untranslated region; VP, viral protein. An expanded version of this figure and legend describing complete methods and providing details of the trees in panels B and C is available online (https://wwwnc.cdc.gov/EID/article/25/6/18-1460-F2.htm).

relatedness between C1v2015 and earlier C1 viruses and to date when the upsurge of C1v2015 infections began in Europe (Figure 2, panel B). All C1v2015 viruses clustered in a lineage distinct from that comprising the C1 viruses reported during 1991–2010. The nucleotide substitution rate of C1v2015 (5.2238 [95% highest probability density HPD interval 4.124–6.3737] × 10^{-3} nt substitutions/y) and earlier C1 lineages (4.6302 [95% HPD interval 4.1769–5.1353] × 10^{-3} nt substitutions/y) was similar. All of the P1 sequences from these viruses, except that of the virus from patient 14, had a maximum nucleotide sequence difference from each other of 2%; the P1 sequence of the virus from patient 14 differed from that of other C1v2015 viruses by 4.8%. The close genetic relatedness between the C1v2015 sequences reported during 2015–2017 in France, Germany, Japan, and the United States was indicative of rapid widespread transmission. We estimated that interpersonal transmission of this lineage began during 2009–2011 (Table 2; Figure 2, panel B) and that its spread was sustained during 2013–2014, just 1–2 years before C1v2015 was first reported. The most recent common ancestor between C1v2015 and earlier C1 viruses was dated to 2000–2002. Seven EV-A71 subgenogroup C1 viruses from Africa and Europe were located at the base of the C1v2015 lineage (Figure 2, panel B), suggesting that the C1 strain involved in the emergence of C1v2015 was circulating in this region during the 2000s.

The C1v2015 genomic module 4 comprises the entire 3Dpol gene and has a 90%–95% nucleotide similarity with 4 distinct EV-A genomes: coxsackievirus A2 (CV-A2) and CV-A5 from Russia, CV-A4 from China, and CV-A6 from Turkmenistan (Figure 2, panel A). We performed another phylogenetic analysis to assess the temporal origin of C1v2015 using this module. With the 3Dpol phylogenetic analysis, we estimated that C1v2015 began spreading in 2010–2014 (Table 2; Figure 2, panel C), an estimate similar to that calculated with the P1 phylogeny. The nucleotide substitution rates with this analysis were also similar (C1v2015 3.7689 [95% HPD interval 1.3003–6.5838] × 10^{-3} nt substitutions/y and C1 3.6318 [95% HPD interval 1.6064–6.2072] × 10^{-3} nt substitutions/y). Whole-genome sequencing analysis showed that the isolate from patient 14 (14|COC286037|FRA|2016) shared distinct 3Dpol genes with other C1v2015 viruses (Appendix Figure 1). Overall, data indicate that the virus from patient 14 was an early recombinant of the C1v2015 lineage (Appendix Figure 2).

Within genomic module 1 (5′ UTR, first 600 nt), we found areas of moderate nucleotide similarity (90%–95%) between the C1v2015 genome and the CV-A6 and CV-A8 genomes and lower similarity (<88%) with the EV-A71 subgenogroup C1 genomes (Figure 2, panel A). The C1v2015 5′ UTR was therefore inherited from an EV-A lineage virus but not from the C1 ancestors that provided the capsid region. The pattern of sequence variation in the 5′ UTR precludes the possibility of analysis with a molecular clock.

Table 2. Estimation of year of MRCA of EV-A71 subgenogroup C1v2015 lineage by using different enteroviruses*

	Year of MRCA (95% HPD interval)	
Node†	Genomic region P1	3Dpol gene
1‡	2013.6 (2013.2–2014.1)	2013.6 (2012.9–2014.3)
2§	2010.2 (2009–2011.3)	2004.1 (2001.7–2006.2)
3¶	2000.5 (2000.1–2001.6)	ND
Root	1986 (1984.7–1987.3)	ND

*EV-A71, enterovirus A71; HPD, highest probability density; MRCA, most recent common ancestor; ND, not done.
†MRCAs were determined for nodes and root in Figure 2.
‡Node 1 represents the MRCA of all included EV-A71 C1v2015 isolates except the virus from patient 14.
§For genomic region P1, node 2 represents the MRCA of all EV-A71 C1v2015 isolates, including the virus from patient 14. For 3Dpol gene, node 2 represents the MRCA of EV-A71 C1v2015 and its parent C1 lineage.
¶Node 3 represents the MRCA of EV-A71 C1v2015 and its parent C1 lineage.

The genomic module 3 of C1v2015 had low similarity with all the publicly available EV-A genomes; thus, the precise origin remains unknown (Figure 2, panel A). The highest nucleotide similarity scores (<90% with CV-A5 genomes) indicate only a distant genetic relationship. We conclude that genes 2A (except the 5′ terminus), 2B, 2C, and 3A–3C were transferred into the C1v2015 genome from a previously unreported lineage.

Conclusions

Thirty years after the outbreaks in central Europe (*12*,*13*), the 2016 upsurge of infections is a reminder that EV-A71 is of growing public health concern. After the B5 and C4 subgenogroup upsurges, C1v2015 is the latest example of an emerging recombinant EV-A71 associated with neurologic manifestations. Recombination, which frequently occurs in enteroviruses, is considered a factor driving this viral emergence (*14*,*15*). Compared with earlier circulating lineages of EV-A71, C1v2015 is a multirecombinant that arose through complete shuffling of all nonstructural genomic regions, although the capsid genes are phylogenetically typical of C1 viruses. Shuffling involved ≥2 recombination events with EV-A genomes before the emergence of C1v2015 as a life-threatening pathogen (Appendix Figure 2). From a public health perspective, the spread of C1v2015 could have resulted from acquired genomic features, notably a unique combination of the 5′ UTR and 3Dpol gene, because recombination events clearly preceded the extensive circulation of C1v2015. The mosaic structure of the genome indicates that C1v2015 is an integral part of a large recombination network including multiple EV-A viruses transmitted in Eurasia. Given the propensity of enteroviruses to recombine their genomes and spread rapidly across distant countries (*2*,*11*) and that C1v2015 circulation continued throughout

2017 and 2018 in France, we need to determine if this virus is associated with a long-term recurrent risk for severe disease in the pediatric population through sharing data from global surveillance.

Acknowledgments

The authors are indebted to Patrice Bouissou, Annick Givois, and Martine Wagner-Vaucard, who obtained samples in children with hand, foot and mouth disease. We acknowledge the technical contribution of Jeroen Cremer, Adeline Duard, Nathalie Rodde, and Isabelle Simon for helpful assistance with molecular typing and sequencing. We thank Jeffrey Watts for help in preparing the manuscript in English.

Financial support was provided by the University Clermont Auvergne, France.

About the Author

Ms. Tomba Ngangas is a doctoral candidate at the Université Clermont Auvergne in Clermont-Ferrand, France. Her research interests are in characterizing viruses that cause neurologic disease and hand, foot and mouth disease.

References

1. Bessaud M, Razafindratsimandresy R, Nougairède A, Joffret ML, Deshpande JM, Dubot-Pérès A, et al. Molecular comparison and evolutionary analyses of VP1 nucleotide sequences of new African human enterovirus 71 isolates reveal a wide genetic diversity. PLoS One. 2014;9:e90624. http://dx.doi.org/10.1371/journal.pone.0090624
2. Hassel C, Mirand A, Lukashev A, TerletskaiaLadwig E, Farkas A, Schuffenecker I, et al. Transmission patterns of human enterovirus 71 to, from, and among European countries, 2003 to 2013. Euro Surveill. 2015;20:30005. http://dx.doi.org/10.2807/1560-7917.ES.2015.20.34.30005
3. Antona D, Kossorotoff M, Schuffenecker I, Mirand A, Leruez-Ville M, Bassi C, et al. Severe paediatric conditions linked with EV-A71 and EV-D68, France, May to October 2016. Euro Surveill. 2016;21:30402. http://dx.doi.org/10.2807/1560-7917.ES.2016.21.46.30402
4. Böttcher S, Obermeier PE, Neubauer K, Diedrich S; Laboratory Network for Enterovirus Diagnostics. Recombinant enterovirus A71 subgenogroup C1 strains, Germany, 2015. Emerg Infect Dis. 2016;22:1843–6. http://dx.doi.org/10.3201/eid2210.160357
5. Karrasch M, Fischer E, Scholten M, Sauerbrei A, Henke A, Renz DM, et al. A severe pediatric infection with a novel enterovirus A71 strain, Thuringia, Germany. J Clin Virol. 2016;84:90–5. http://dx.doi.org/10.1016/j.jcv.2016.09.007
6. Casas-Alba D, de Sevilla MF, Valero-Rello A, Fortuny C, García-García JJ, Ortez C, et al. Outbreak of brainstem encephalitis associated with enterovirus-A71 in Catalonia, Spain (2016): a clinical observational study in a children's reference centre in Catalonia. Clin Microbiol Infect. 2017;23:874–81. http://dx.doi.org/10.1016/j.cmi.2017.03.016
7. Wieczorek M, Purzyńska M, Krzysztoszek A, Ciąćka A, Figas A, Szenborn L. Genetic characterization of enterovirus A71 isolates from severe neurological cases in Poland. J Med Virol. 2018;90:372–6. http://dx.doi.org/10.1002/jmv.24958
8. Midgley SE, Nielsen AG, Trebbien R, Poulsen MW, Andersen PH, Fischer TK. Co-circulation of multiple subtypes of enterovirus A71 (EV-A71) genotype C, including novel recombinants characterised by use of whole genome sequencing (WGS), Denmark 2016. Euro Surveill. 2017;22:30565. http://dx.doi.org/10.2807/1560-7917.ES.2017.22.26.30565
9. Lukashev AN, Shumilina EY, Belalov IS, Ivanova OE, Eremeeva TP, Reznik VI, et al. Recombination strategies and evolutionary dynamics of the human enterovirus A global gene pool. J Gen Virol. 2014;95:868–73. http://dx.doi.org/10.1099/vir.0.060004-0
10. van der Sanden S, van der Avoort H, Lemey P, Uslu G, Koopmans M. Evolutionary trajectory of the VP1 gene of human enterovirus 71 genogroup B and C viruses. J Gen Virol. 2010;91:1949–58. http://dx.doi.org/10.1099/vir.0.019695-0
11. Hassel C, Mirand A, Farkas A, Diedrich S, Huemer HP, Peigue-Lafeuille H, et al.; HFMD French Study Network. Phylogeography of coxsackievirus A16 reveals global transmission pathways and recent emergence and spread of a recombinant genogroup. J Virol. 2017;91:e00630-17. http://dx.doi.org/10.1128/JVI.00630-17
12. Chumakov M, Voroshilova M, Shindarov L, Lavrova I, Gracheva L, Koroleva G, et al. Enterovirus 71 isolated from cases of epidemic poliomyelitis-like disease in Bulgaria. Arch Virol. 1979;60:329–40. http://dx.doi.org/10.1007/BF01317504
13. Nagy G, Takátsy S, Kukán E, Mihály I, Dömök I. Virological diagnosis of enterovirus type 71 infections: experiences gained during an epidemic of acute CNS diseases in Hungary in 1978. Arch Virol. 1982;71:217–27. http://dx.doi.org/10.1007/BF01314873
14. McWilliam Leitch EC, Cabrerizo M, Cardosa J, Harvala H, Ivanova OE, Koike S, et al. The association of recombination events in the founding and emergence of subgenogroup evolutionary lineages of human enterovirus 71. J Virol. 2012;86:2676–85. http://dx.doi.org/10.1128/JVI.06065-11
15. Kyriakopoulou Z, Pliaka V, Amoutzias GD, Markoulatos P. Recombination among human non-polio enteroviruses: implications for epidemiology and evolution. Virus Genes. 2015;50:177–88. http://dx.doi.org/10.1007/s11262-014-1152-y

Address for correspondence: Jean-Luc Bailly, Université Clermont Auvergne, LMGE UMR 6023, Clermont-Ferrand, France; email: j-luc.bailly@uca.fr

New Delhi Metallo-β-Lactamase 5–Producing *Klebsiella pneumoniae* Sequence Type 258, Southwest China, 2017

Xin Zhang,[1] Weimin Wan,[1] Hua Yu,[1] Min Wang, Haifang Zhang, Jingnan Lv, Yi-Wei Tang, Barry N. Kreiswirth, Hong Du, Liang Chen

We isolated a New Delhi metallo-β-lactamase 5 (NDM-5)–producing *Klebsiella pneumoniae* sequence type (ST) 258 strain in southwest China during 2017. The bla_{NDM-5} gene was acquired by horizontal plasmid transfer from NDM-5–producing *Escherichia coli*. We identified genomic characteristics in ST258 strains that differed from those of global *K. pneumoniae* carbapenemase–producing strains.

Carbapenem-resistant *Klebsiella pneumoniae* has emerged as one of the major multidrug-resistant bacterial pathogens worldwide. The international spread of this pathogen has been linked to a few high-risk clone group (CG) strains, including CG258, CG14/15, CG17/20, CG43, CG147, and CG307 (*1*), of which CG258 is the most widely spread. Within CG258, sequence type (ST) 258 predominates in North America and Europe, but ST11 is the primary carbapenem-resistant *K. pneumoniae* clone in eastern Asia, especially in China (*2–4*).

In recent years, *K. pneumoniae* ST11 strains have been increasingly identified in North America. In contrast, ST258 strains are still rarely reported in China (*5*). Unlike other high-risk clones, such as ST11, that harbor different types of carbapenemases, carbapenem-resistant *K. pneumoniae* ST258 are almost exclusively associated with *K. pneumoniae* carbapenemase (KPC) (*6*). We report identification of a New Delhi metallo-β-lactamase 5 (NDM-5)–producing *K. pneumoniae* ST258 strain from Chengdu in southwest China.

The Study

In June 2017, a *K. pneumoniae* strain (Kp2588) that has an extended-spectrum β-lactamase phenotype was isolated from a blood culture of a male patient in a large tertiary-care hospital in Chengdu in southwest China. Two days later, a carbapenem-resistant *Escherichia coli* strain (Ec2551) was isolated from a urine culture, and 1 week later, a carbapenem-resistant *K. pneumoniae* strain (Kp2573) was isolated from another urine culture, both from the same patient (Appendix, https://wwwnc.cdc.gov/EID/article/25/6/18-1939-App1.pdf).

PCR testing and Sanger sequencing showed that Ec2551 and Kp2573 both harbored the New Delhi metallo-β-lactamase gene bla_{NDM-5}. Multilocus sequence typing further showed that Ec2551 is an ST48 strain, and Kp2588 and Kp2573 belong to the high-risk clone ST258.

Susceptibility testing showed that the initial Kp2588 blood isolate was resistant to most cephalosporins and aztreonam but susceptible to cefepime, carbapenems, amoxicillin/clavulanic acid, piperacillin/tazobactam, amikacin, and tigecycline (Table). In contrast, the urinary isolates Ec2551 and Kp2573 were resistant to all β-lactams and β-lactam/β-lactamase inhibitors, including the 4 carbapenems tested in this study (Table).

We conducted next-generation sequencing (NGS; Illumina Hiseq, https://www.illumina.com) for all 3 isolates and deposited data in the National Center for Biotechnology (NCBI) Bioproject PRJNA354234 (https://www.ncbi.nlm.nih.gov/bioproject) GenBank database (accession nos. RXHE00000000, RXHG00000000 and RXHF00000000, respectively). Analysis of resistance genes and plasmid sequences showed that the 2 ST258 *K. pneumoniae* isolates carried similar resistance and plasmid replicon genes, except that Kp2573 harbored bla_{NDM-5} and an IncX3 plasmid replicon (Figure 1). *E. coli* strain Ec2551 had the same bla_{NDM-5} and IncX3 replicon genes as Kp2573, but also had a diverse array of other resistance and plasmid replicon genes in comparison with the 2 *K. pneumoniae* isolates (Figure 2).

We then transferred bla_{NDM-5}–harboring plasmids from Ec2551 and Kp2573 to recipient strain *E. coli* J53^{AZR} by conjugation, followed by plasmid NGS as described. Plasmid sequence analysis showed that Ec2551 and Kp2573 carry an identical bla_{NDM-5}–harboring IncX3 plasmid. The plasmid is 46,161 bp and is identical to several bla_{NDM-5}–harboring plasmids identified in China and other countries

Author affiliations: Sichuan Academy of Medical Science, and Sichuan Provincial People's Hospital, Sichuan, China (X. Zhang, H. Yu); Memorial Sloan Kettering Cancer Center, New York, New York, USA (X. Zhang, Y.-W. Tang); The Second Affiliated Hospital of Soochow University, Suzhou, China (W. Wan, M. Wang, H. Zhang, J. Lv, H. Du); Rutgers University, Newark, New Jersey, USA (B.N. Kreiswirth, L. Chen)

DOI: https://doi.org/10.3201/eid2506.181939

[1]These authors contributed equally to this article.

Table. Antimicrobial drug susceptibility of 3 bacterial isolates producing New Delhi metallo-β-lactamase 5, southwest China, 2017*

Characteristic	Species, strain, and MIC, mg/L		
	Klebsiella pneumoniae, Kp2588	*Escherichia coli*, Ec2551	*K. pneumoniae*, Kp2573
Source	Blood	Urine	Urine
Sequence type	258	48	258
Drug			
Meropenem	≤0.25	**≥16**	**≥16**
Imipenem	≤0.25	**≥16**	**≥16**
Doripenem	≤0.12	**≥8**	**≥8**
Ertapenem	≤0.5	**≥8**	**≥8**
Ampicillin	**≥32**	**≥32**	**≥32**
Ticarcillin	**≥128**	**≥128**	**≥128**
Cephalothin	**≥64**	**≥64**	**≥64**
Cefazolin	**≥64**	**≥64**	**≥64**
Cefuroxime	**≥64**	**≥64**	**≥64**
Ceftazidime	16	**≥64**	**≥64**
Cefotaxime	**≥64**	**≥64**	**≥64**
Ceftriaxone	**≥64**	**≥64**	**≥64**
Cefpodoxime	**≥8**	**≥8**	**≥8**
Ceftizoxime	≤1	**≥64**	**≥64**
Cefepime	2	**≥64**	**≥64**
Cefotetan	≤4	**≥64**	**≥64**
Aztreonam	**≥64**	**≥64**	**≥64**
Piperacillin	**≥128**	**≥128**	**≥128**
Ampicillin/sulbactam	**≥32/16**	**≥32/16**	**≥32/16**
Amoxicillin/clavulanic acid	16/8	**≥32/16**	**≥32/16**
Piperacillin/tazobactam	64/4	**≥128/4**	**≥128/4**
Nitrofurantoin	**256**	≤16	**256**
Gentamicin	**≥16**	**≥16**	**≥16**
Tobramycin	**≥16**	**≥16**	**≥16**
Amikacin	4	≤2	4
Ciprofloxacin	**≥4**	**≥4**	**≥4**
Levofloxacin	**≥8**	**≥8**	**≥8**
Moxifloxacin	**≥8**	**≥8**	**≥8**
Trimethoprim/sulfamethoxazole	**≥16/304**	**≥16/304**	**≥16/304**
Nalidixic acid	**≥32**	**≥32**	**≥32**
Tetracycline	**≥16**	**≥16**	**≥16**
Tigecycline	2	≤0.5	2

*Drug-resistant MICs are indicated in bold. Antimicrobial susceptibility testing was conducted by using the VITEK 2 system (bioMérieux, https://www.biomerieux.com).

(e.g., GenBank accession nos. CP032424, MF679143, MG591703, CP028705, and CP024820). Core single-nucleotide polymorphism (SNP) analysis showed that Kp2588 differed from Kp2573 by 1 SNP. These results strongly suggest that carbapenem-resistant Kp2573 might have evolved from the carbapenem-susceptible blood isolate Kp2588 by acquisition of a $bla_{\text{NDM-5}}$–harboring IncX3 plasmid from the same patient.

To date, carbapenemases other than KPC have rarely been described in clinical *K. pneumoniae* ST258 strains (*7*,*8*). In this study, we had the opportunity to investigate the phylogenetic relationship between NDM-5–producing ST258 (designated as the China ST258 clone) and other global KPC-producing ST258 strains (Figure 2, panel A). Phylogenetic analysis of core SNPs from the 2 China ST258 genomes and 76 completely closed ST258 (n = 39) and ST11 (n = 36) genomes from NCBI showed that Kp2573/Kp2588 belongs to a separate clade distinct from global ST258 and ST11 strains (Figure 2, panel A). Kp2573/Kp2588 differs from global ST258 genomes by an average of 88 core SNPs (range 54–135) and from ST11 strains by an average of 109 core SNPs (range 79–132).

Results indicated that Kp2573/Kp2588 and the global ST258 strains both evolved from a common ancestor. A different core SNP phylogenetic analysis of Kp2573/Kp2588 with 824 ST258 genomes (including both draft assemblies and completely closed genomes) from NCBI showed similar results, suggesting that Kp2573/Kp2588 has unique genetic characteristics in comparison with other global ST258 strains.

Recent phylogenetic analysis showed that global ST258 strains have unique genetic characteristics that might contribute to their epidemic spread. For example, global ST258 strains carry a unique integrative and conjugative element (ICE) known as ICEKp258.2 (*3*). This chromosomal element is conserved among nearly all ST258 strains, harboring a type IV pilus gene cluster and a type III restriction-modification system, which might contribute to plasmid acquisition or plasmid–host specificity (*9*). However, ICEKp258.2 is absent from genomes of Kp2573/Kp2588 (Figure 2, panel A). In addition, global

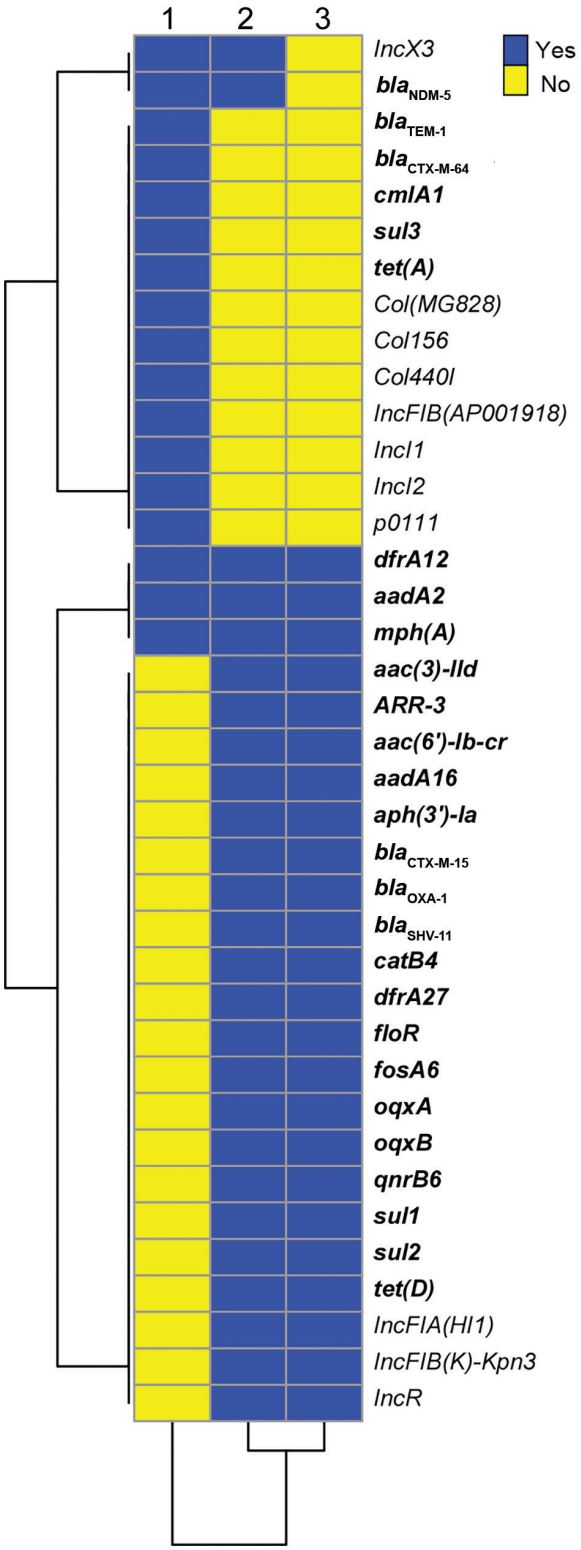

Figure 1. Comparison of resistance genes and plasmid replicons for 3 bacterial isolates producing New Delhi metallo-β-lactamase 5, southwest China, 2017. 1, *Escherichia coli* 2551; 2, *Klebsiella pneumoniae* 2573; 3, *K. pneumoniae* 2588. Resistance genes are shown in bold.

ST258 strains have a common Ser34Phe amino acid substitution in the homodimerization region of MarR, a transcriptional regulator protein of the multiple antimicrobial drug resistance repressor family (*10*). It is hypothesized that this substitution might affect the overall metabolic activity in ST258 (*10*). Kp2573/Kp2588 has the ancestral MarR Ser34 genotype, similar to ST11 strains, but all global ST258 strains have the Phe34 genotype. Furthermore, all global ST258 strains contain a frame-shift mutation that results in a premature stop codon at amino acid position 89 in outer membrane protein OmpK35 because of a guanine insertion at nt position 121. In contrast, Kp2573/Kp2588 do not have the nt121G insertion in the *ompK35* gene but have an IS*1* insertion at nt position 28. These genetic changes further suggest that the 2 China ST258 strains have distinct evolutionary paths compared with those of global ST258 strains.

These observations have also updated our previous hypothesis regarding the molecular evolution of ST258 (Figure 2, panel B) (*9*). Our initial study suggested that the prototypical ST258 strain arose as a consequence of recombination of large segments of the ST11 and ST442 genomes, such that it has the same *wzi154*/KL107 (previously named *cps-2*/clade II) capsular type as the parental ST442 strain (*9*). Additional genotypic changes, including acquisition of ICEKp258.2, the MarR Ser34Phe substitution, and the *ompK35* nt121G insertion, as well as the acquisition of KPC plasmids in ST258 clade II strains, define the global KPC-producing carbapenem-resistant *K. pneumoniae* ST258 clone.

A second molecular event, generated by replacement of the ST258 clade II *cps* region with the corresponding region from ST42, subsequently created the equally prevalent ST258 clade I clone (*9*). Both clades I and II ST258 strains have shown the ability to host diverse KPC plasmids, which might in part contribute to the spread of global ST258 strains. In contrast, the China ST258 strains appear to have evolved separately, recently acquiring the *bla*NDM5–harboring plasmid (Figure 2, panel B), highlighting the continuing evolution of *K. pneumoniae* ST258 strains.

Conclusions

We report the genotype of an NDM-5–producing *K. pneumoniae* ST258 strain isolated in southwest China. The $bla_{\text{NDM-5}}$ gene was likely acquired by a carbapenem-susceptible ST258 strain from an NDM-5–producing *E. coli* strain in vivo in the same patient as a result of horizontal transfer of a $bla_{\text{NDM-5}}$–harboring IncX3 plasmid. Genomic comparison of the ST258 strain from China with other carbapenem-resistant *Klebsiella pneumoniae* ST258 strains indicated that they both evolved from a common ancestral strain but with distinct genetic characteristics suggestive of separate evolutionary histories. Further genomic comparisons between ST258 strains from China and their global ST258

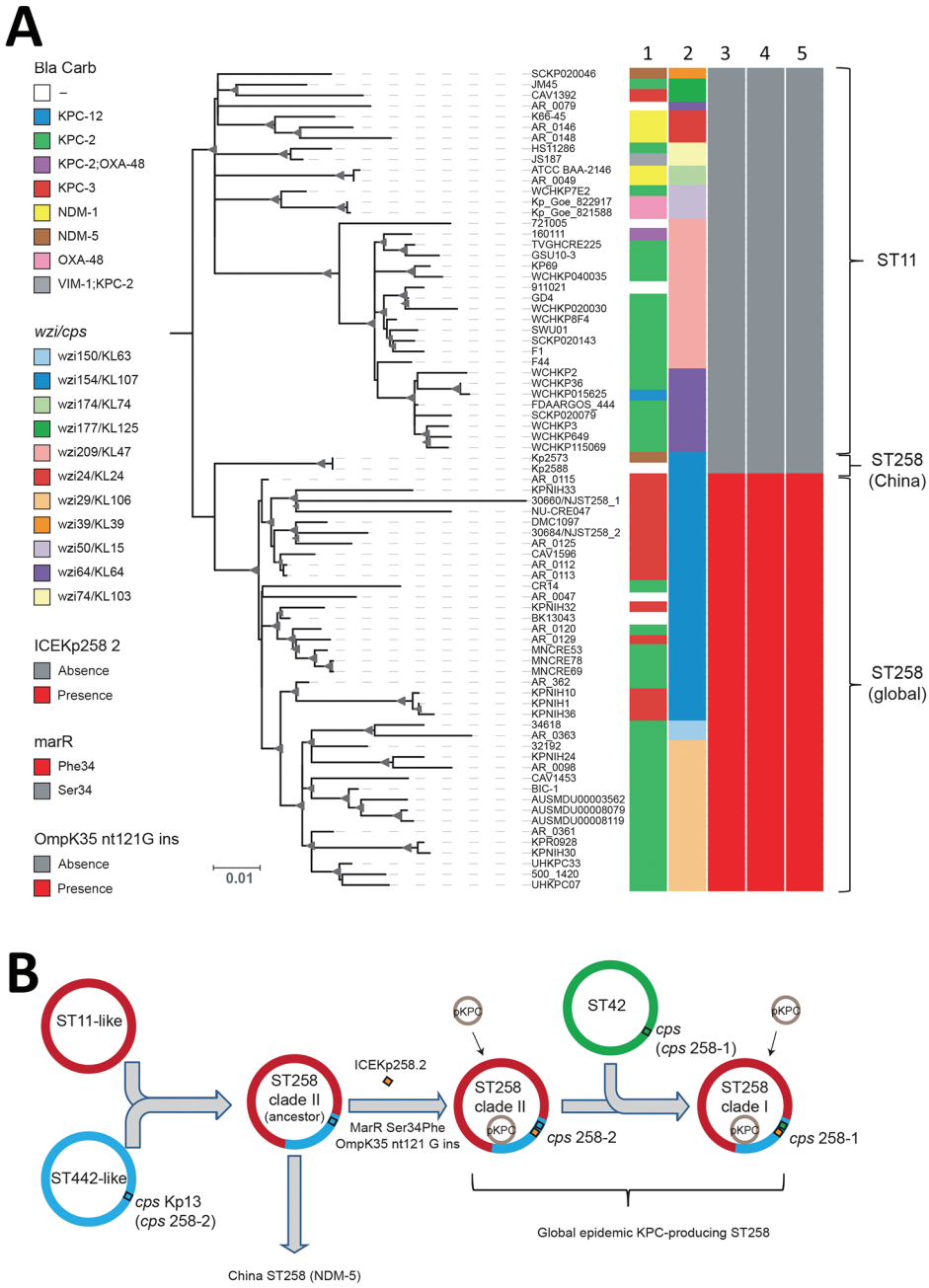

Figure 2. Phylogenetic analysis of KPC-producing and NDM-5–producing CG258 *Klebsiella pneumoniae* strains from China, 2017, and reference strains. A) Core SNP phylogenetic analysis of 76 global CG258 (ST258 and ST11) and 2 ST258 strains from China. Lane 1, Bla_carb; lane 2, *wzi* (cps); lane 3, integrative and conjugative element Kp258.2; lane 4, *marR*; lane 5, *omp*K35 gene (guanine insertion at nt position 121). The maximum-likelihood tree was rooted by using ST11 strains. Bootstrap values >90% are indicated as gray triangles at branch points. Sizes are proportion to values. Scale bar indicates nucleotide substitutions per site. B) Updated hypothesis of the molecular evolution of carbapenem-resistant *K. pneumoniae* ST258 (*9*). Bla, β-lactamase; Carb, carbapenemase; *cps*, capsular polysaccharide gene; ICE, integrative and conjugative element; ins, insertion; KPC, *Klebsiella pneumoniae* carbapenemase; MarR, transcriptional regulator protein of the multiple antimicrobial drug resistance repressor family; NDM, New Delhi metallo-β-lactamase; ompK35, outer membrane protein K35; OXA, oxacillinase; pKPC, plasmid carrying KPC; ST, sequence type; VIM-1, Verona integron–encoded metallo-β-lactamase 1; *wzi*, surface assembly of capsule gene.

counterparts will help elucidate the molecular mechanisms underscoring the spread of this high-risk clone.

This study was supported by the National Natural Science Foundation of China (81572032); the Six Talent Peaks Project in Jiangsu Province (2016-WSN-112); the Key Research and Development Project of Jiangsu Provincial Science and Technology Department (BE2017654); Gusu Key Health Talent of Suzhou; the Jiangsu Youth Medical Talents Program (QN-866, 867); the Science and Technology Program of Suzhou (SZS201715 and SYS201619); and the National Institutes of Health (R01AI090155, R21AI117338, and P30CA008748).

About the Author

Dr. Xin Zhang is a clinical microbiologist at the Sichuan Academy of Medical Science, Sichuan, China. Her research interests include the clinical epidemiology of antimicrobial drug resistance and infectious disease.

References

1. Wyres KL, Holt KE. *Klebsiella pneumoniae* population genomics and antimicrobial-resistant cones. Trends Microbiol. 2016;24: 944–56. http://dx.doi.org/10.1016/j.tim.2016.09.007
2. Patel G, Bonomo RA. “Stormy waters ahead”: global emergence of carbapenemases. Front Microbiol. 2013;4:48. http://dx.doi.org/10.3389/fmicb.2013.00048

3. Chen L, Mathema B, Chavda KD, DeLeo FR, Bonomo RA, Kreiswirth BN. Carbapenemase-producing *Klebsiella pneumoniae*: molecular and genetic decoding. Trends Microbiol. 2014; 22:686–96. http://dx.doi.org/10.1016/j.tim.2014.09.003
4. Zhang R, Liu L, Zhou H, Chan EW, Li J, Fang Y, et al. Nationwide surveillance of clinical carbapenem-resistant *Enterobacteriaceae* (CRE) strains in China. EBioMedicine. 2017;19:98–106. http://dx.doi.org/10.1016/j.ebiom.2017.04.032
5. Lascols C, Peirano G, Hackel M, Laupland KB, Pitout JD. Surveillance and molecular epidemiology of *Klebsiella pneumoniae* isolates that produce carbapenemases: first report of OXA-48-like enzymes in North America. Antimicrob Agents Chemother. 2013;57:130–6. http://dx.doi.org/10.1128/AAC.01686-12
6. Navon-Venezia S, Kondratyeva K, Carattoli A. *Klebsiella* | *pneumoniae*: a major worldwide source and shuttle for antibiotic resistance. FEMS Microbiol Rev. 2017;41:252–75. http://dx.doi.org/10.1093/femsre/fux013
7. Mathers AJ, Peirano G, Pitout JD. The role of epidemic resistance plasmids and international high-risk clones in the spread of multidrug-resistant *Enterobacteriaceae.* Clin Microbiol Rev. 2015;28:565–91. http://dx.doi.org/10.1128/CMR.00116-14
8. Pitout JD, Nordmann P, Poirel L. Carbapenemase-producing *Klebsiella pneumoniae*, a key pathogen set for global nosocomial dominance. Antimicrob Agents Chemother. 2015;59:5873–84. http://dx.doi.org/10.1128/AAC.01019-15
9. Chen L, Mathema B, Pitout JD, DeLeo FR, Kreiswirth BN. Epidemic *Klebsiella pneumoniae* ST258 is a hybrid strain. MBio. 2014;5:e01355–14. http://dx.doi.org/10.1128/mBio.01355-14
10. Bowers JR, Kitchel B, Driebe EM, MacCannell DR, Roe C, Lemmer D, et al. Genomic analysis of the emergence and rapid global dissemination of the clonal group 258 *Klebsiella pneumoniae* pandemic. PLoS One. 2015;10:e0133727. http://dx.doi.org/10.1371/journal.pone.0133727

Address for correspondence: Hong Du, Department of Clinical Laboratory, the Second Affiliated Hospital of Soochow University, 1055 Sanxiang Rd, Suzhou, Jiangsu, 215004, China; email: hong_du@126.com

The Public Health Image Library (PHIL)

The Public Health Image Library (PHIL), Centers for Disease Control and Prevention, contains thousands of public health–related images, including high-resolution (print quality) photographs, illustrations, and videos.

PHIL collections illustrate current events and articles, supply visual content for health promotion brochures, document the effects of disease, and enhance instructional media.

PHIL images, accessible to PC and Macintosh users, are in the public domain and available without charge.

Visit PHIL at: http://phil.cdc.gov/phil

Scrub Typhus in Continental Chile, 2016–2018[1]

Thomas Weitzel, Constanza Martínez-Valdebenito, Gerardo Acosta-Jamett, Ju Jiang, Allen L. Richards, Katia Abarca

Endemic scrub typhus was recently detected on Chiloé Island in southern Chile. We report a series of cases, acquired over a wide geographical range in continental Chile during 2016–2018, demonstrating that this emerging rickettsial infection is also found on the mainland of South America.

Scrub typhus is a vectorborne zoonosis caused by *Orientia* spp. bacteria; infection carries a potentially severe outcome (*1*). Although widely underrecognized, scrub typhus is considered one of the most important rickettsial infections worldwide in terms of prevalence and severity (*2*). Until recently, scrub typhus was associated with only a single species, *O. tsutsugamushi*, which is transmitted by larvae of trombiculid mites (chiggers) and threatens >1 billion human inhabitants within the so-called tsutsugamushi triangle in the Asia–Pacific region (*1*). Since 2006, the discoveries of scrub typhus in 4 patients on Chiloé Island in Chile (*3,4*) and in 1 patient from Dubai, United Arab Emirates (*5*), have suggested the emergence of the disease farther afield (*6*). This change of paradigm has been reinforced by recent studies mainly from Africa (*7*). The emergence of endemic scrub typhus on Chiloé Island has been confirmed by ongoing studies of our working group in Chile (*8,9*). Whether this disease is only endemic to Chiloé Island or has a wider distribution is unknown. We report 9 patients who had scrub typhus diagnosed after visiting different regions of continental Chile during 2016–2018.

The Study

After the confirmation of autochthonous scrub typhus cases in Chiloé in 2016 (*4*), the Chilean Ministry of Health issued a clinical alert advising healthcare providers in Chile to confirm possible cases in cooperation with our research group. Most of the patients described in this report were identified as a result of the clinical alert and are included in an ongoing clinical–epidemiologic scrub typhus project.

We tested serum samples obtained during acute and convalescent phases of infection for *Orientia*-specific antibodies by using a commercial IgG indirect immunofluorescence assay (Fuller Laboratories, http://www.fullerlabs.com), based on whole-cell *O. tsutsugamushi* Gilliam, Karp, Kato, and Boryong strains, and by using Scrub Typhus Detect IgG and IgM ELISA (InBios International Inc., http://www.inbios.com) with recombinant 56-kD type–specific antigens of *O. tsutsugamushi* Karp, Kato, Gilliam, and TA716 strains. We examined DNA extracted from eschar material by using 16S rRNA (*rrs*) and 47 kDa gene (*htrA*) seminested PCR and sequencing, as previously described (*10*), except that we changed the forward primer of the PCR step of *rrs* from 16SU17 to 16SOR155f. We also tested all samples by using a recently developed *Orientia* genus–specific quantitative real-time PCR assay targeting *rrs* (*11*).

Among the 37 patients with suspected scrub typhus who were tested during 2016–2018, 13 were from mainland Chile. Of those, 9 had scrub typhus diagnosed both serologically and molecularly. None of these 9 patients lived in or traveled to Chiloé Island or other regions with endemic scrub typhus, but all were exposed to natural habitats on mainland Chile (Table 1). Seven patients were male and 2 female; median age was 28 years.

All cases occurred after outdoor activities during the summer months of February and March. We defined probable exposure sites as those locations where patients reported outdoor activities with close contact to natural environments within the 7–20 days before symptom onset. Most infections were acquired in the Los Lagos Region, which includes Chiloé Island. However, 2 cases were acquired farther south, in the Aysén Region, and another case farther north, in the Bio Bío Region (Figure). The sites of exposure ranged over a total distance of >1,120 km (https://ec.europa.eu/programmes/erasmus-plus/resources/distance-calculator_en), from 38°03′S to 47°47′ S. Details of the activities leading to the exposure have been described elsewhere (*12*).

All patients had fever, generalized maculopapular rash, eschar, and headache; other frequent symptoms were

Author affiliations: Clinica Alemana, Universidad del Desarrollo, Santiago, Chile (T. Weitzel); Pontificia Universidad Católica de Chile, Santiago (C. Martínez-Valdebenito, K. Abarca); Universidad Austral de Chile, Valdivia, Chile (G. Acosta-Jamett); Naval Medical Research Center, Silver Spring, Maryland, USA (J. Jiang, A.L. Richards)

DOI: https://doi.org/10.3201/eid2506.181860

[1]Preliminary results from this study were presented at the 67th Annual Meeting of the American Society of Tropical Medicine and Hygiene, October 28–November 2, 2018, New Orleans, Louisiana, USA.

Table 1. Demographic and epidemiologic data of 9 scrub typhus cases in continental Chile, 2016–2018

Case no.	Age, y/sex	Month of probable exposure	Location of probable exposure	
			Region	Site
1	43/M	2016 Mar	Aysén	Caleta Tortel
2	56/M	2017 Feb	Los Lagos	Pumalín
3	25/M	2017 Mar	Los Lagos	Cochamó
4	69/M	2018 Feb	Aysén	Queulat
5	22/F	2018 Feb	Los Lagos	Puelo
6	25/M	2018 Feb	Los Lagos	Puelo
7	39/M	2018 Feb	Los Lagos	Tagua Tagua
8	28/M	2018 Mar	Bío Bío	Alto Bío Bío
9	21/F	2018 Mar	Los Lagos	Cochamó

myalgia (8 patients) and regional lymphadenopathy (5 patients). Laboratory abnormalities included elevated C-reactive protein (8 patients) and transaminases (6 patients), thrombocytopenia (4 patients), and leukopenia (4 patients). Eight patients required hospitalization. We noted a serologic response to *O. tsutsugamushi* antigens in all 9 patients. Eight patients were positive for IgG by indirect immunofluorescence assay, mostly with low titers, and 3 of the 6 patients for whom convalescent-phase samples were available showed seroconversion or a ≥4-fold rise in titer. IgG and IgM results by ELISA were positive in 6 of 9 patients on the basis of local cutoff values (Table 2). All cases were confirmed by detection of *Orientia*-specific DNA from eschar material using 3 different PCR assays (Table 2). After treatment with doxycycline (7 patients) or azithromycin (1 patient), patients recovered rapidly; 1 patient recuperated after 6 days of fever without receiving any scrub typhus–specific treatment.

Conclusions

Our understanding of the global epidemiology of *Orientia* spp. as human pathogens has undergone important changes. Most importantly, the paradigm of the geographic limitation of scrub typhus to the Asia–Pacific region, which had been unchallenged since the first scientific description of this disease at the beginning of the last century, has been superseded in light of the recent identification of scrub typhus cases on the Arabian Peninsula (Dubai) and South America (Chiloé Island in Chile) (*4,5*). The Dubai patient was infected by a distinct *Orientia* species, *Candidatus* O. chuto; the complete description of the isolates from Chile is pending.

Further studies in rodents and vectors have demonstrated molecular evidence of *Orientia* spp. or *Orientia*-like organisms in South Africa, Kenya, Senegal, and France (*6,13,14*). In addition, serologic reports point to possible human exposure to *Orientia* microorganisms in Djibouti, Kenya, Republic of the Congo, Cameroon, and Peru (*6,7,15*). Current data suggest that *Candidatus* O. chuto might be the *Orientia* species from Africa and the Arabian Peninsula (*5,14*). Clinical data from these regions are scarce, but 1 molecularly proven case and 2 cases diagnosed on the basis of serologic results occurred in patients with typical symptoms of scrub typhus (*5,6*).

The case series we report provides important epidemiologic information for South America, highlighting that scrub typhus is not limited to Chiloé Island but also occurs over a wide range of continental Chile. The actual incidence of the infection remains unknown; the observed increase from 1 case in 2016 to 6 cases in 2018 most probably reflects the growing awareness of scrub typhus among

Figure. Locations of probable exposures (red circles) of 9 scrub typhus patients in continental Chile, 2016–2018. Inset map shows the study area (red box) and the location of Chile (gray shading) within South America.

Table 2. Serologic and molecular diagnosis of scrub typhus cases in continental Chile, 2016–2018*

	Serologic testing results						Eschar molecular testing results		
	IFA IgG†		ELISA IgG‡		ELISA IgM‡				
Case no.	Acute	Conv	Acute	Conv	Acute	Conv	PCR *rrs*	PCR 47kDa	qPCR *rrs*
1	256	256	+	+	+	–	+	+	+
2	≤32	128	–	–	–	–	+	+	+
3	64	512	–	+	+	–	+	+	+
4	128	256	–	–	–	–	+	+	+
5	128	NA	+	NA	+	NA	+	+	+
6	128	NA	–	NA	–	NA	+	+	+
7	128	256	–	+	+	+	+	+	+
8	≤32	NA	+	NA	+	NA	+	+	+
9	64	256	–	+	–	+	+	+	+

*Acute, acute-phase; conv, convalescent-phase; NA, not available; qPCR, quantitative PCR; +, positive; –, negative.
†Highest titer among 4 antigens.
‡Cutoff values calculated as mean optical density of negative local population ± 3 SD.

infectious diseases physicians in Chile. Because all of the case-patients we describe were included through a surveillance based on passive case detection, we believe that they only represent the tip of the iceberg for scrub typhus in Chile and South America.

The clinical data of this series showed the classical scrub typhus manifestation: fever, generalized maculopapular rash, and eschar at the inoculation site. However, this finding has to be interpreted cautiously because our epidemiologic alert describes these manifestations as typical, which biases the physicians' attention toward these presentations. Less typical clinical signs and symptoms (e.g., without rash or with predominant respiratory symptoms), which are present in Asia in a relevant percentage of cases (*1*), might go undiagnosed in Chile.

All patients were serologically positive according to ≥1 of the applied commercial assays, which were based on *O. tsutsugamushi* antigens. The low seroreactivity against these antigens, however, suggests a distinct strain or species, which is supported by our preliminary molecular analyses (data not shown). Eschar material, which can be stored and transported under simple conditions (i.e., in a dry plastic tube at 4°C), proved to be the best and most practical specimen, permitting a rapid and reliable confirmation by molecular methods. Studies are ongoing to culture the *Orientia* species in Chile and to understand its life cycle, including vectors and possible zoonotic reservoirs.

Acknowledgments

We thank the following physicians, who clinically suspected scrub typhus and permitted the confirmation of the patients of this case series, for their important contribution: Teresa Bidart, Johanna Cabrera, Mario Calvo, María Pilar Gambra, Iván Jara, Miguel Lagos, Alejandra Marcotti, José Manuel Munita, and Luis Thompson.

This work was supported by the Fondo Nacional de Desarrollo Científico y Tecnológico (FONDECYT grant no. 1170810) and the Global Emerging Infectious Diseases Section (work unit no. A1402).

The views expressed in this article are those of the authors and do not necessarily reflect the official policy or position of the Department of the Navy, Department of Defense nor the U.S. Government. A.L.R. is an employee of the US Government. This work was prepared as a part of his official duties. Title 17 U.S.C. §105 provides that "copyright protection under this title is not available for any work of the United States Government." Title 17 U.S.C. §101 defines a US Government work as a work prepared by a military service member or employee of the US Government as part of that person's official duties. J.J. and A.L.R. provided training and consultation, but did not have contact with patients or participate in the data collection at Naval Medical Research Center, USA.

About the Author

Dr. Weitzel is a clinical microbiologist and infectious diseases physician specializing in tropical and travel medicine at Clínica Alemana and a professor at the Clínica Alemana Medical School of the Universidad del Desarrollo in Santiago, Chile. His main research interests include vectorborne zoonoses and imported tropical infections.

References

1. Kim IS, Walker DH. Scrub Typhus. In: Guerrant RL, Walker DH, Weller PF, editors. Tropical infectious diseases: principles, pathogens and practice. 3rd edition. New York: Elsevier Inc.; 2011. p. 334–8.
2. Paris DH, Shelite TR, Day NP, Walker DH. Unresolved problems related to scrub typhus: a seriously neglected life-threatening disease. Am J Trop Med Hyg. 2013;89:301–7. http://dx.doi.org/10.4269/ajtmh.13-0064
3. Balcells ME, Rabagliati R, García P, Poggi H, Oddó D, Concha M, et al. Endemic scrub typhus-like illness, Chile. Emerg Infect Dis. 2011;17:1659–63. http://dx.doi.org/10.3201/eid1709.100960
4. Weitzel T, Dittrich S, López J, Phuklia W, Martinez-Valdebenito C, Velásquez K, et al. Endemic scrub typhus in South America. N Engl J Med. 2016;375:954–61. http://dx.doi.org/10.1056/NEJMoa1603657
5. Izzard L, Fuller A, Blacksell SD, Paris DH, Richards AL, Aukkanit N, et al. Isolation of a novel *Orientia* species (*O. chuto* sp. nov.) from a patient infected in Dubai. J Clin Microbiol. 2010;48:4404–9. http://dx.doi.org/10.1128/JCM.01526-10

6. Luce-Fedrow A, Lehman ML, Kelly DJ, Mullins K, Maina AN, Stewart RL, et al. A review of scrub typhus (*Orientia tsutsugamushi* and related organisms): then, now, and tomorrow. Trop Med Infect Dis. 2018;3:8. http://dx.doi.org/10.3390/tropicalmed3010008
7. Xu G, Walker DH, Jupiter D, Melby PC, Arcari CM. A review of the global epidemiology of scrub typhus. PLoS Negl Trop Dis. 2017;11:e0006062. http://dx.doi.org/10.1371/journal.pntd.0006062
8. Weitzel T, Jiang J, Acosta-Jamett G, Martínez-Valdebenito C, López J, Richards AL, et al. Canine seroprevalence to *Orientia* species in southern Chile: a cross-sectional survey on the Chiloé Island. PLoS One. 2018;13:e0200362. http://dx.doi.org/10.1371/journal.pone.0200362
9. Abarca K, Weitzel T, Martínez-Valdebenito C, Acosta-Jamett G. Scrub typhus, an emerging infectious disease in Chile [in Spanish]. Rev Chilena Infectol. 2018;35:696–9.
10. Weitzel T, Aylwin M, Martínez-Valdebenito C, Jiang J, Munita JM, Thompson L, et al. Imported scrub typhus: first case in South America and review of the literature. Trop Dis Travel Med Vaccines. 2018;4:10. http://dx.doi.org/10.1186/s40794-018-0070-8
11. Jiang J, Martínez-Valdebenito C, Weitzel T, Abarca K, Richards AL. Development of an *Orientia* genus-specific quantitative real-time PCR assay and the detection of *Orientia* species in DNA preparations from *O. tsutsugamushi, Candidatus* Orientia chuto, and *Orientia* species from Chile. In: Abstracts of the 29th Meeting of the American Society for Rickettsiology; Milwaukee, USA; 2018 Jun 16–19, Abstract no. 46.
12. Weitzel T, Acosta-Jamett G, Martínez-Valdebenito C, Richards AL, Grobusch MP, Abarca K. Martínez-Valdebenito, Richards AL, Grobusch MP, Abarca K. Scrub typhus risk in travelers to southern Chile. Travel Med Infect Dis. 2019 Jan 9 [Epub ahead of print]. http://dx.doi.org/10.1016/j.tmaid.2019.01.004
13. Kolo AO, Sibeko-Matjila KP, Maina AN, Richards AL, Knobel DL, Matjila PT. Molecular detection of zoonotic rickettsiae and *Anaplasma* spp. in domestic dogs and their ectoparasites in Bushbuckridge, South Africa. Vector Borne Zoonotic Dis. 2016;16:245–52. http://dx.doi.org/10.1089/vbz.2015.1849
14. Masakhwe C, Linsuwanon P, Kimita G, Mutai B, Leepitakrat S, Yalwala S, et al. Identification and characterization of *Orientia chuto* in trombiculid chigger mites collected from wild rodents in Kenya. J Clin Microbiol. 2018;56:e01124–18. http://dx.doi.org/10.1128/JCM.01124-18
15. Kocher C, Jiang J, Morrison AC, Castillo R, Leguia M, Loyola S, et al. Serologic evidence of scrub typhus in the Peruvian Amazon. Emerg Infect Dis. 2017;23:1389–91. http://dx.doi.org/10.3201/eid2308.170050

Address for correspondence: Thomas Weitzel, Laboratorio Clínico, Clínica Alemana, Av Vitacura 5951, Santiago, Chile; email: thomas.weitzel@gmail.com; Katia Abarca, Departamento de Enfermedades Infecciosas e Inmunología Pediátricas, Pontificia Universidad Católica de Chile, Diagonal Paraguay 362, Santiago, Chile; email: katia@med.puc.cl

etymologia revisited

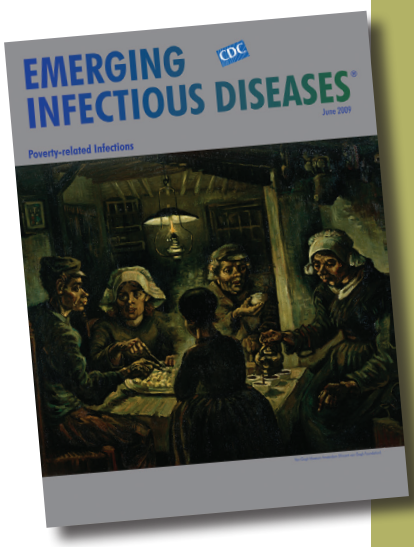

Originally published in June 2009

Typhus [ti′ fəs]

From Greek τῖφος [*typhos*], meaning heavy stupor; also related to Greek *typhein*, to smoke. A disease known since antiquity, typhus has been described as follows: "A kind of continued fever, attended with great prostration of the nervous and vascular systems, with a tendency to putrefaction in the fluids and vitiation in the secretions; putrid fever. A genus of the order *Febres*, class *Pyrexia*, of Cullen's nosology" (J. Thomas, 1885).

Today, typhus refers to any of a group of acute infections caused by rickettsiae and transmitted to persons by the bite of arthropods such as fleas and lice. Epidemic typhus, caused by *Rickettsia prowazekii*, is characterized by headache, high fever, chills, rash, and, in serious cases, by stupor or lack of awareness of reality. Outbreaks usually occur in crowded or unsanitary environments.

Source: Dorland's illustrated medical dictionary, 31st ed. Philadelphia: Saunders; 2007; http://www.merriam-webster.com; Thomas J. A complete pronouncing medical dictionary. Philadelphia: JB Lippincott; 1885.

https://wwwnc.cdc.gov/eid/article/15/6/et-2009_article

National Surveillance of Legionnaires' Disease, China, 2014–2016

Tian Qin, Hongyu Ren, Dongke Chen, Haijian Zhou, Luxi Jiang, Duorong Wu, Jilu Shen, Fengyan Pei

Author affiliations: Chinese Center for Disease Control and Prevention, Beijing, China (T. Qin, H. Ren, H. Zhou, L. Jiang); State Key Laboratory for Infectious Disease Prevention and Control, Beijing (T. Qin, H. Zhou); Collaborative Innovation Center for Diagnosis and Treatment of Infectious Diseases, Hangzhou, China (T. Qin, H. Zhou); Beijing Hospital, Beijing (D. Chen); Haikou People's Hospital, Haikou, China (D. Wu); The Fourth Affiliate Hospital of Anhui Medical University, Hefei, China (J. Shen); Jinan Central Hospital, Jinan, China (F. Pei)

DOI: https://doi.org/10.3201/eid2506.171431

We report national surveillance of Legionnaires' disease in China. Urine samples from 11 (3.85%) of 286 patients with severe pneumonia of unknown cause were positive for the *Legionella pneumophila* serogroup 1 antigen. We isolated *Legionella* strains from 7 patients. Improved diagnostic testing is needed for this underestimated disease in China.

Legionnaires' disease is a form of atypical pneumonia caused by bacteria of the genus *Legionella*. *L. pneumophila* serogroup 1 causes most Legionnaires' disease (*1*). Although Legionnaires' disease has been reported worldwide, only a few sporadic cases have been reported in China (*2*). Investigation of *Legionella* infection is urgently needed in China to describe its prevalence and epidemiology.

During 2014–2016, we conducted surveillance of Legionnaires' disease in 18 hospitals in China under the coordination of the Chinese Center for Disease Control and Prevention (China CDC). The Ethical Committee of the National Institute for Communicable Disease Control and Prevention, China CDC (ICDC-2014009), provided ethics approval for this study. The distribution of the 18 hospitals accounted for all regions of China (Appendix Figure 1, https://wwwnc.cdc.gov/EID/article/25/6/17-1431-App1.pdf). The hospital's clinical diagnostic level, pneumonia pathogen detection level, and degree of cooperation with this investigation were also considered. All 18 hospitals are level 3 first-class general hospitals, representing the highest level of healthcare in their cities.

The 3,132 severe pneumonia cases were defined and detected according to the Guidelines for the Diagnosis and Treatment of Community-Acquired Pneumonia in Adults in China (2016 edition) (*3*) (Appendix Figure 2). Among them, 1,885 cases were diagnosed as noninfectious or nonbacterial infections, and 771 cases were diagnosed as bacterial infections other than *Legionella* by daily testing, including bacterial culture, viral nucleic acid detection, and immunologic detection in hospital laboratories. Patients with the remaining 476 cases of pneumonia with unknown cause were enrolled and tested for *Legionella* infection. Among them, 190 left the hospital, died, or were unwilling to cooperate. Thus, urine samples were collected from 286 patients and sent for urine antigen detection for *L. pneumophila* serogroup 1 (BinaxNow, https://www.alere.com) (Appendix Figure 2). Sputum samples were obtained from 211 of the 286 patients and sent to the laboratory of China CDC (Beijing, China) for *Legionella* culture, which used both buffered charcoal yeast extract agar and buffered charcoal yeast extract agar supplemented with *Legionella* GVPC (glycine, vancomycin, polymyxin, cycloheximide) Selective Supplement (Oxoid, https://www.thermofisher.com). Eleven (3.85%) of the 286 urine samples yielded positive results, and we isolated *Legionella* strains from 7 of them. All 7 *L. pneumophila* cultures were obtained from the same patients who tested positive by urine antigen detection. The positive rate of *Legionella* culture was 3.32% (7/211). All isolated *Legionella* strains were *L. pneumophila* serogroup 1.

All 11 urine antigen–positive patients were male, 23–76 years of age (average 56 years) (Table). They

Table. Characteristics of 11 Legionnaires' disease patients, China*

Patient ID	Age, y	Date of diagnosis	Onset city	Underlying illness	Length of hospitalization, d	ICU admission	Outcome	SBT type of isolates
1	45	2014 Sep	Shenyang	None	15	Yes	Recovered	ST2344
2	70	2014 Aug	Beijing	None	93	Yes	Recovered	ST59
3	53	2015 Aug	Hefei	None	18	No	Recovered	ST2369
4	63	2016 Jan	Jinan	None	16	No	Recovered	ST42
5	67	2016 Aug	Haikou	Diabetes	21	No	Recovered	ST742
6	23	2016 Jul	Beijing	AIDS	7	Yes	Died	ST2366
7	53	2016 Sep	Shanghai	None	14	Yes	Recovered	ST2368
8	58	2016 May	Lishui	None	8	No	Recovered	NS
9	49	2014 Jul	Shenyang	Cirrhosis	14	Yes	Died	NS
10	76	2015 Jul	Beijing	None	17	Yes	Recovered	NS
11	59	2016 Sep	Jinan	None	22	No	Recovered	NS

*All patients were male. ICU, intensive care unit; ID, identification; NS, no strain isolated; SBT, sequence-based typing; ST, sequence type.

resided in 7 cities, and most (9/11) cases were observed in summer (in China, July–September). All were hospitalized; length of hospitalization ranged from 7 to 93 days. Six were admitted to an intensive care unit. The case-fatality rate was 18.2% (2/11) after antimicrobial and supportive therapies.

We performed antimicrobial susceptibility testing using E-test strips (bioMérieux, https://www.biomerieux.com). According to the epidemiologic cutoff values of the European Committee on Antimicrobial Susceptibility Testing (*4*) or as determined by a previous study (*5*), all 7 strains were susceptible to fluoroquinolones, macrolides, and rifampin but not to cefuroxime (Appendix Table 1).

We subtyped the 7 strains using pulsed-field gel electrophoresis (*6*) and sequence-based typing (SBT) (*7*). All 7 strains were identified as different pulsed-field gel electrophoresis and SBT types (Appendix Figure 3). Submission to the European Working Group on *Legionella* Infections *L. pneumophila* SBT database (http://www.ewgli.org) identified 4 profiles as new; these profiles were assigned new sequence types (STs) (ST2344, ST2366, ST2368, and ST2369). Querying the European Working Group on *Legionella* Infections database showed that 2 STs (ST42 and ST59) contained strains that are distributed worldwide (Appendix Table 2). We also tested the 7 strains for their intracellular growth ability using previously described methods (*8*), and all showed high intracellular growth in J774 cells, suggesting that these strains are pathogenic (Appendix Figure 4).

Many Legionnaires' disease cases are reported worldwide, including hundreds in the United States and Europe each year (*8,9*). However, no data are available on the prevalence of Legionnaires' disease in China. In China, no *Legionella* urine antigen test reagent has been approved for clinical diagnosis and few hospitals conduct *Legionella* culture, so in clinical laboratories, Legionnaires' disease is difficult to detect; therefore, diagnosis is based mainly on signs and symptoms. Legionnaires' disease is usually diagnosed as unexplained pneumonia.

The results of this study showed that *L. pneumophila* is an important pathogen for pneumonia patients in China, and current diagnostic methods in China may misdiagnose or overlook it. We suggest establishment of a routine monitoring reporting system to investigate the prevalence and epidemiology of Legionnaires' disease in China.

This study was supported by grants from the National Natural Science Foundation of China (grant no. 81671985) and the Science Foundation for the State Key Laboratory for Infectious Disease Prevention and Control from China (grant no. 2015SKLID508).

About the Author

Dr. Qin is a microbiologist at the National Institute for Communicable Disease Control and Prevention, Chinese CDC, Beijing. Her research interests are surveillance of Legionnaires' disease, and the molecular subtyping and genomic diversity of *Legionella*.

References

1. Diederen BMW. *Legionella* spp. and Legionnaires' disease. J Infect. 2008;56:1–12. http://dx.doi.org/10.1016/j.jinf.2007.09.010
2. Zhang Q, Zhou H, Chen R, Qin T, Ren H, Liu B, et al. Legionnaires' disease caused by *Legionella pneumophila* serogroups 5 and 10, China. Emerg Infect Dis. 2014;20:1242–3. http://dx.doi.org/10.3201/eid2007.131343
3. Chinese Society of Respiratory Diseases, Chinese Medical Association. Guidelines for the diagnosis and treatment of community-acquired pneumonia in adults in China (2016 edition). Chinese Journal of Tuberculosis and Respiratory Diseases. 2016;39:253–79.
4. The European Committee on Antimicrobial Susceptibility Testing. Antimicrobial susceptibility testing of *Legionella pneumophila*. [cited 2016 Sep 9]. http://www.eucast.org/fileadmin/src/media/PDFs/EUCAST_files/General_documents/Legionella_guidance_document_20160909.pdf
5. Bruin JP, Ijzerman EP, den Boer JW, Mouton JW, Diederen BM. Wild-type MIC distribution and epidemiological cut-off values in clinical *Legionella pneumophila* serogroup 1 isolates. Diagn Microbiol Infect Dis. 2012;72:103–8. http://dx.doi.org/10.1016/j.diagmicrobio.2011.09.016
6. Zhou H, Ren H, Zhu B, Kan B, Xu J, Shao Z. Optimization of pulsed-field gel electrophoresis for *Legionella pneumophila* subtyping. Appl Environ Microbiol. 2010;76:1334–40. http://dx.doi.org/10.1128/AEM.01455-09
7. Ratzow S, Gaia V, Helbig JH, Fry NK, Lück PC. Addition of *neuA*, the gene encoding N-acylneuraminate cytidylyl transferase, increases the discriminatory ability of the consensus sequence-based scheme for typing *Legionella pneumophila* serogroup 1 strains. J Clin Microbiol. 2007;45:1965–8. http://dx.doi.org/10.1128/JCM.00261-07
8. Qin T, Zhang W, Liu W, Zhou H, Ren H, Shao Z, et al.; Centers for Disease Control and Prevention (CDC). Legionellosis—United States, 2000–2009. MMWR Morb Mortal Wkly Rep. 2011;60:1083–6.
9. Joseph CA, Ricketts KD, Collective on behalf of the European Working Group for Legionella Infections. Legionnaires disease in Europe 2007–2008. Euro Surveill. 2010;15:19493. http://dx.doi.org/10.2807/ese.15.08.19493-en

Address for correspondence: Tian Qin, National Institute for Communicable Disease Control and Prevention, Chinese Center for Disease Control and Prevention. PO Box 5, Changping, Beijing 102206, China; email:qintian@icdc.cn

Molecular Evidence of Human Monkeypox Virus Infection, Sierra Leone

Fei Ye,[1] Jingdong Song,[1] Li Zhao,[1] Yi Zhang, Lianxu Xia, Lingwei Zhu, Idrissa Laybohr Kamara, Jiao Ren, Wenling Wang, Houwen Tian, Guizhen Wu, Wenjie Tan

Author affiliations: China Center for Disease Control and Prevention, Beijing, China (F. Ye, J. Song, L. Zhao, Y. Zhang, J. Ren, W. Wang, H. Tian, G. Wu, W. Tan); Sierra Leone–China Friendship Biological Safety Laboratory, Freetown, Sierra Leone (F. Ye, J. Song, Y. Zhang, L. Xia, L. Zhu, I.L. Kamara)

DOI: https://doi.org/10.3201/eid2506.180296

Monkeypox virus is a zoonotic disease endemic to Africa. In 2017, we confirmed a case of human monkeypox virus in Sierra Leone by molecular and serologic methods. Sequencing analysis indicated the virus belongs to the West African clade and data suggest it was likely transmitted by wild animals.

Monkeypox virus (MPXV), of the genus *Orthopoxvirus*, was identified in captive cynomolgus monkeys in Copenhagen in 1958 (*1*). The first documented case of human MPXV infection was reported in a patient from the Democratic Republic of the Congo in 1971 (*2*). Other outbreaks have occurred, including a large one in the United States in 2003, in which 47 confirmed and probable human cases of MPXV infection were identified after importation of wild rodents from Ghana (*3*). Phylogenetic analyses of MPXVs have revealed 2 distinct clades, West African and Congo Basin (*4*). In the past decade, human MPXV infections also have increased in Central and West Africa (*5*).

Ecologic niche modeling shows that Sierra Leone is in a geographic region suitable for transmission of MPXV (*6*). Several cases of human MPXV have been detected in West Africa, including a case in Sierra Leone in 1970 and another in March 2014 (*5*). We report confirmation of an MPXV infection in Sierra Leone in March 2017.

A 35-year-old man from Kpaku village, Galliness Perri chiefdom, Pujehun district, in southern Sierra Leone near the border with Liberia, sought treatment on March 16, 2017, for fever, body pain, malaise, dysphagia, and enlarged cervical lymph nodes. The patient reported hunting and eating squirrels ≈10 days before becoming ill, and traveling to Pelewahun gee bu in Bo district 3 days before his symptoms began. On March 17, he began having generalized vesicular skin eruptions. Clinicians sent vesicular swab specimens and blood samples collected on March 28 (12 days after the patient sought treatment) and on May 10 (day 55 after the patient sought treatment) to the Sierra Leone–China Friendship Biologic Safety Laboratory in Freetown, Sierra Leone.

We conducted MPXV-specific real-time PCR, as previously described (*7*), and detected MPXV DNA in the day 12 blood sample (cycle threshold = 35.88). In addition, we performed MPXV-specific IgG ELISA, as previously described (*8*). The day 12 sample was positive at 1:800 dilution and the day 55 sample was positive at 1:3,200 dilution, demonstrating a >4-fold increase in the MPXV-specific antibody response during the patient's recovery.

We amplified a 1,028-bp fragment of DNA for further Sanger sequencing (Figure, panel A) and submitted it to GenBank under Monkeypox virus Sierra Leone 2017 (accession no. MG906726). Phylogenetic analysis showed this strain is closer to MPXV isolates from the West African clade than from the Congo Basin clade (Figure, panel B). In addition, we found only a single nucleotide difference between the Sierra Leone 2017 fragment and MPXV Utrecht, UTC_1964 (Appendix Figure, panel A, https://wwwnc.cdc.gov/EID/article/25/6/18-0296-App1.pdf).

For further comparison, we selected previous MPXV sequences from NCBI (https://www.ncbi.nlm.nih.gov) and aligned these to Sierra Leone 2017 (Appendix Figure, panel B) using DNAMAN software (Lynnon Corporation, https://www.lynnon.com/dnaman.html). We found that Sierra Leone 2017 was closely related to UTC_1964. In addition, a 6-nucleotide deletion (GTATAC, a repeat unit) was more evident in the dUTPase region of Sierra Leone 2017 compared with other MPXVs from Africa. Also, a 25-nucleotide insertion (5× repeat of TCCAT unit) in the kelch-like protein-encoding region was more evident in the USA_2003_039 genome compared with most MPXV isolates from Africa. This insertion leads the N-terminal amino acids of the protein sequence that changed from EWNGMEWNGK in USA_2003_039 to VNNFEIK in Sierra Leone 2017.

Recent studies have shown that genome-region deletion in the Congo Basin MPXV clade can affect viral replication and pathogenicity (*9*). The deletion we noted in Sierra Leone 2017, which is absent in previously isolated MPXVs from Africa, might be a molecular signature and further evaluation is needed to determine whether it plays a role in viral replication and pathogenicity.

The case-patient lived in a region with large areas of tropical forest and many wild mammals. An ecologic niche model suggests this region is suitable for MPXV transmission (*6*). Considering the patient's history of hunting and eating squirrels, and the lack of new cases among 16 identified community contacts in Pujehun, we hypothesize

[1]These authors contributed equally to this article.

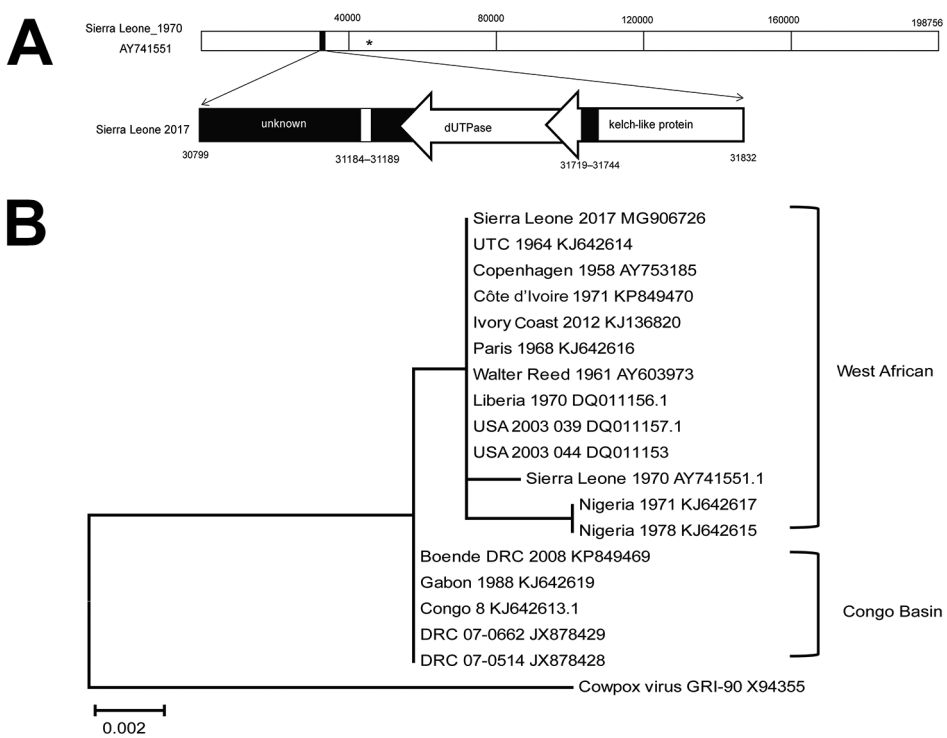

Figure. Phylogenetic analysis and molecular signatures of monkeypox virus (MPXV) Sierra Leone 2017 and other collected MPXV isolates. A) Schematic representation of the MPXV Sierra Leone 2017 genomic fragment by reference to genomic data on MPXV Sierra Leone 1970. MPXV Sierra Leone 2017 contains 3 parts: an unknown region, genes encoding dUTPase, and genes encoding partial kelch-like protein. *, binding position of primers used for real-time PCR detection. Bottom panel displays genes described. Arrows indicate direction of transcription. B) Phylogenetic relationships between genomic fragments of MPXV collected in Sierra Leone and other orthopoxviruses. Neighbor-joining phylograms constructed by using MEGA6 (https://www.megasoftware.net) and the maximum-likelihood method. Scale bar indicates nucleotide substitutions per site.

that the patient was likely infected by contact with wild animals. Of note, MPXV genetic evidence from this case-patient was closely related to UTC_1964, a strain that was isolated from an animal imported from Africa to the Rotterdam Zoo in 1966 (*10*). Because the reservoir species of MPXV remains unknown, we hypothesize that our case-patient was probably infected by exposure to wild animals and not from MPXV imported to Sierra Leone from Central Africa. However, further serologic surveys of animals in this region could provide useful evidence for the origin of MPXV strain Sierra Leone 2017.

In summary, we described a confirmed case of human MPXV in Sierra Leone in 2017 and molecular evidence hinting of its animal origin. We suggest MPXV circulation in wild animals and humans in West Africa requires more attention, and emphasize the value of local surveillance and molecular characterization of MPXV to help determine its origin.

Acknowledgment

We thank the staff of the Ministry of Health and Sanitation, Government of Sierra Leone, for providing information on this case.

This study was supported by the National Key Research and Development Program of China (grant nos. 2016YFD0500301, 2016YFC1200905, and 2016YFC1200200), and the Megaproject for Infectious Disease Research of China (grant no. 2016ZX10004222-002).

About the Author

Dr. Ye is a scientist in the National Institute for Viral Disease Control and Prevention, Chinese Center for Disease Control and Prevention. His primary research interest is the surveillance of viral diseases, especially poxvirus and coronavirus.

References

1. Magnus PV, Andersen EK, Petersen KB, Birch-Andersen A. A pox-like disease in cynomolgus monkeys. Acta Pathol Microbiol Scand. 1959;46:156–76. http://dx.doi.org/10.1111/j.1699-0463.1959.tb00328.x
2. Ladnyj IDZ, Ziegler P, Kima E. A human infection caused by monkeypox virus in Basankusu Territory, Democratic Republic of the Congo. Bull World Health Organ. 1972;46:593–7.
3. Reynolds MG, Davidson WB, Curns AT, Conover CS, Huhn G, Davis JP, et al. Spectrum of infection and risk factors for human monkeypox, United States, 2003. Emerg Infect Dis. 2007; 13:1332–9. http://dx.doi.org/10.3201/eid1309.070175
4. Esposito JJ, Knight JC. Orthopoxvirus DNA: a comparison of restriction profiles and maps. Virology 1985;143:230–51. https://doi.org/10.1016/0042-6822(85)90111-4
5. Durski KN, McCollum AM, Nakazawa Y, Petersen BW, Reynolds MG, Briand S, et al. Emergence of monkeypox– West and Central Africa, 1970–2017. MMWR Morb Mortal Wkly Rep. 2018;67:306–10. http://dx.doi.org/10.15585/mmwr.mm6710a5
6. Nakazawa Y, Emerson GL, Carroll DS, Zhao H, Li Y, Reynolds MG, et al. Phylogenetic and ecologic perspectives of a monkeypox outbreak, southern Sudan, 2005. Emerg Infect Dis. 2013; 19:237–45. http://dx.doi.org/10.3201/eid1902.121220
7. Kulesh DA, Loveless BM, Norwood D, Garrison J, Whitehouse CA, Hartmann C, et al. Monkeypox virus detection in rodents using real-time 3′–minor groove binder TaqMan

assays on the Roche LightCycler. Lab Invest. 2004;84:1200–8. http://dx.doi.org/10.1038/labinvest.3700143
8. Hammarlund E, Lewis MW, Carter SV, Amanna I, Hansen SG, Strelow LI, et al. Multiple diagnostic techniques identify previously vaccinated individuals with protective immunity against monkeypox. Nat Med. 2005;11:1005–11. http://dx.doi.org/10.1038/nm1273
9. Lopera JG, Falendysz EA, Rocke TE, Osorio JE. Attenuation of monkeypox virus by deletion of genomic regions. Virology. 2015;475:129–38. http://dx.doi.org/10.1016/j.virol.2014.11.009
10. Peters JC. An epizootic of monkey pox at Rotterdam Zoo. Int Zoo Yearb. 1966;6:274–5. http://dx.doi.org/10.1111/j.1748-1090.1966.tb01794.x

Address for correspondence: Wenjie Tan, Chinese Center for Disease Control and Prevention, 155 Changbai Rd, Changping District, Beijing 102206, China; email: tanwj28@163.com

Leishmaniasis in Norway Rats in Sewers, Barcelona, Spain

Maria Teresa Galán-Puchades, Mercedes Gómez-Samblás, Jose M. Suárez-Morán, Antonio Osuna, Joan Sanxis-Furió, Jordi Pascual, Rubén Bueno-Marí, Sandra Franco, Víctor Peracho, Tomás Montalvo, Màrius V. Fuentes

Author affiliations: Universitat de València, Burjassot-Valencia, Spain (M.T. Galán-Puchades, J. Sanxis-Furió, M.V. Fuentes); Universidad de Granada, Granada, Spain (M. Gómez-Samblás, J.M. Suárez-Morán, A. Osuna); Laboratorios Lokímica, Catarroja-Valencia, Spain (J. Sanxis-Furió, R. Bueno-Marí); Agència de Salut Pública de Barcelona, Barcelona, Spain (J. Pascual, S. Franco, V. Peracho, T. Montalvo); CIBER Epidemiology and Public Health, Barcelona (T. Montalvo)

DOI: https://doi.org/10.3201/eid2506.181027

We detected *Leishmania infantum* in 98 Norway rats (*Rattus norvegicus*) trapped in parks and sewers of Barcelona, Spain. The 84 rats from the sewers showed a prevalence of 33.3% and up to 2,272 estimated parasites. These results, in the most abundant potential reservoir in cities, is of public health concern.

Canine and human leishmaniasis caused by *Leishmania infantum* is considered an emerging disease in the Mediterranean basin (*1*). In addition to dogs, several wild mammals have been found infected by *L. infantum* in rural environments in Europe (*2*). With regard to the epidemiologic factors promoting infection with *Leishmania*, the appearance of new animal reservoirs besides dogs has been highlighted (*1*). In this context, only a few studies examine the possible reservoir role of synanthropic animals in cities, where the role of certain domestic mammals has been analyzed exclusively (*1*).

Because human leishmaniasis is endemic in Barcelona, Spain (*3*), we investigated and quantified the presence of *L. infantum* in an urban population of the Norway rat, *Rattus norvegicus,* using a highly sensitive quantitative PCR (qPCR) method for *Leishmania* DNA detection. Rat leishmaniasis could complicate the epidemiologic situation of human and canine leishmaniasis, considering that the Norway rat is the most widespread mammal in the world after humans and also the most abundant animal in cities.

We trapped 98 Norway rats, 84 in the sewage system and 14 in parks, during the winter of 2016–17 in a rodent surveillance and control program in Barcelona (permission no. SF/044 obtained from the regional government of Catalonia). We treated the rats according to Directive 2010/63/EU of the European Parliament and Council decision of September 22, 2010. We obtained DNA from 10 mg of spleen using the Purification of Total DNA Kit (QIAGEN, https://www.qiagen.com), following the manufacturer's instructions. We processed the samples whose DNA concentration was too low with the extraction kit by the phenol–chloroform–isoamyl (25:24:1) DNA extraction technique. We quantified the parasite DNA by qPCR using Taqman probe with Fam fluorochrome (*4*).

Only 1 rat (7.1%) captured in the parks tested positive for *L. infantum*. However, rats captured in the sewage system showed a 33.3% prevalence (28/84) of *L. infantum* infection. The estimated number of parasites in the positive samples from spleens varied considerably, ranging from 0.28 to >2,200 (Table). Histologic sections of positive spleens were stained by Giemsa and by the streptavidin–biotin peroxidase complex immunohistochemical method (*5*) (Appendix Figure, https://wwwnc.cdc.gov/EID/article/25/6/18-1027-App1.pdf).

The low number of infected Norway rats found in Mediterranean countries in Europe so far has led to the species being categorized as an incidental host, capable of becoming infected but considered irrelevant to the long-term persistence of the disease (*2*,*6*–*8*). However, our study demonstrates the importance of the trapping site for finding a large *Leishmania*-infected rat population.

According to the World Health Organization, the incrimination of a particular mammal as a *Leishmania* reservoir must depend on an accumulation of evidence (*9*). First, the reservoir must be sufficiently abundant

Table. Real-time PCR results for the 29 *Leishmania infantum*–positive Norway rats analyzed, Barcelona, Spain*

Rat no.	C_t†	Estimated no. parasites	SD
1	32.81	75.67	25.70
2	32.33	50.68	12.21
3	29.25	723.15	345.67
4	30.84	344.30	56.40
5	38.50	0.28	0.20
6	28.49	10.81	3.36
7	28.46	2,272.46	771.72
8	32.32	118.12	63.76
9	29.60	516.20	199.36
10	28.10	14.24	2.98
11	30.19	566.28	7.32
12	28.41	11.98	5.09
13	29.96	679.46	35.59
14	31.47	31.38	0.20
15	31.46	215.66	66.84
16	30.79	356.32	42.03
17	33.01	66.31	31.43
18	29.68	465.21	68.73
19	30.75	370.40	70.72
20	31.60	1.44	1.51
21	26.52	48.81	20.15
22	31.82	159.43	27.73
23	28.15	0.33	17.66
24	28.56	9.98	1.30
25	30.25	547.67	93.15
26	30.93	161.73	11.80
27	28.38	11.59	2.70
28	29.84	761.38	223.52
29	33.16	55.22	1.41

*C_t, cycle threshold.
†Mean values of the 3 replicates of each sample. Cutoff established: positive result, C_t <35; negative result, C_t ≥35.

and long-lived. In this sense, the Norway rat is the most abundant mammal in cities, with a lifespan of around 1–3 years. The lack of predators or interspecific competition in cities guarantees a longer lifetime than in wild environments. Second, intense host–sand fly contact is necessary. Sewers are a breeding site for *Phlebotomus* sand flies, which can reach abundant population levels (*10*). Third, the prevalence of *Leishmania* infection should be >20%. Our study revealed a 33.3% prevalence in Norway rats in the sewers. Fourth, the course of infection should be nonpathogenic and long enough to enable the parasites to survive any nontransmission season. Neither splenomegaly nor hepatomegaly were evident in the affected animals, although further studies should be addressed to assess the true pathogenic degree of rat leishmaniasis. Finally, parasites should be available in the skin or the blood in sufficient numbers to be taken up by a sand fly. The availability of the parasite to the sand fly cannot be proved by our findings. However, in naturally infected Norway rats in Spain, *L. infantum* was detected in the hair of the rats by molecular methods (*7*).

Only counting sewer rats, and not those living above ground, a 0.13 rat-per-person scenario is suspected for Barcelona (Agència de Salut Pública de Barcelona, pers. comm., June 2018). Therefore, the prevalence found in the sewers in this study means that there could be >70,000 underground rats with leishmaniasis in Barcelona (1,620,809 human inhabitants in 2017), a figure of public health concern for a potential reservoir.

If future xenodiagnostic studies determine that sand flies become infected successfully by the rats, as has already been demonstrated in the case of its congener, the black rat, (*R. rattus*) (*11*), the finding of a new reservoir, besides the dog, would be a major advance in the epidemiology of leishmaniasis. However, the complexity of rat control would represent a great hindrance to overcome.

About the Author

Dr. Galán-Puchades is director of the Parasites and Health Research Group of the University of Valencia, Burjassot-Valencia, Spain. Her research interests include neglected parasitic diseases.

References

1. Miró G, López-Vélez R. Clinical management of canine leishmaniosis versus human leishmaniasis due to *Leishmania infantum*: putting "One Health" principles into practice. Vet Parasitol. 2018;254:151–9. http://dx.doi.org/10.1016/j.vetpar.2018.03.002
2. Millán J, Ferroglio E, Solano-Gallego L. Role of wildlife in the epidemiology of *Leishmania infantum* infection in Europe. Parasitol Res. 2014;113:2005–14. http://dx.doi.org/10.1007/s00436-014-3929-2
3. Riera C, Napp S, Manzanares S. Epidemiology of human leishmaniasis in the city of Barcelona (1997–2014) [in Spanish]. Rev Enf Emerg. 2016;15:68–76.
4. Francino O, Altet L, Sánchez-Robert E, Rodriguez A, Solano-Gallego L, Alberola J, et al. Advantages of real-time PCR assay for diagnosis and monitoring of canine leishmaniosis. Vet Parasitol. 2006;137:214–21. http://dx.doi.org/10.1016/j.vetpar.2006.01.011
5. Tafuri WL, Santos RL, Arantes RM, Gonçalves R, de Melo MN, Michalick MS, et al. An alternative immunohistochemical method for detecting *Leishmania* amastigotes in paraffin-embedded canine tissues. J Immunol Methods. 2004;292:17–23. http://dx.doi.org/10.1016/j.jim.2004.05.009
6. Psaroulaki A, Antoniou M, Toumazos P, Mazeris A, Ioannou I, Chochlakis D, et al. Rats as indicators of the presence and dispersal of six zoonotic microbial agents in Cyprus, an island ecosystem: a seroepidemiological study. Trans R Soc Trop Med Hyg. 2010;104:733–9. http://dx.doi.org/10.1016/j.trstmh.2010.08.005
7. Muñoz-Madrid R, Belinchón-Lorenzo S, Iniesta V, Fernández-Cotrina J, Parejo JC, Serrano FJ, et al. First detection of *Leishmania infantum* kinetoplast DNA in hair of wild mammals: application of qPCR method to determine potential parasite reservoirs. Acta Trop. 2013;128:706–9. http://dx.doi.org/10.1016/j.actatropica.2013.08.009
8. Tsakmakidis I, Angelopoulou K, Dovas CI, Dokianakis E, Tamvakis A, Symeonidou I, et al. *Leishmania* infection in rodents in Greece. Trop Med Int Health. 2017;22:1523–32. http://dx.doi.org/10.1111/tmi.12982
9. World Health Organization. Control of the leishmaniases. WHO Technical Report Series no. 949. Geneva: The Organization; 2010.

10. Lucientes J, Castillo JA, Gracia MJ, Perbáñez A. *Phlebotomus*, from the biology to the control [in Spanish]. REDVET. 2005;6 [cited 2018 May 16]. http://www.veterinaria.org/revistas/redvet/n080805.html
11. Gradoni L, Pozio E, Gramiccia M, Maroli M, Bettini S. Leishmaniasis in Tuscany (Italy): VII. Studies on the role of the black rat, *Rattus rattus*, in the epidemiology of visceral leishmaniasis. Trans R Soc Trop Med Hyg. 1983;77:427–31. http://dx.doi.org/10.1016/0035-9203(83)90102-5

Address for correspondence: Maria Teresa Galán-Puchades, University of Valencia, Department of Parasitology, Faculty of Pharmacy, Av Vicent Andrés Estellés s/n, 46100 Burjassot-Valencia, Spain; email: mteresa.galan@uv.es

Influenza D Virus Infection in Dromedary Camels, Ethiopia

Shin Murakami, Tomoha Odagiri, Simenew Keskes Melaku, Boldbaatar Bazartseren, Hiroho Ishida, Akiko Takenaka-Uema, Yasushi Muraki, Hiroshi Sentsui, Taisuke Horimoto

Author affiliations: University of Tokyo, Tokyo, Japan (S. Murakami, T. Odagiri, H. Ishida, A. Takenaka-Uema, T. Horimoto); Addis Ababa Science and Technology University, Addis Ababa, Ethiopia (S.K. Melaku); Institute of Veterinary Medicine, Ulaanbaatar, Mongolia (B. Bazartseren); Iwate Medical University, Iwate, Japan (Y. Muraki); Nihon University, Kanagawa, Japan (H. Sentsui)

DOI: https://doi.org/10.3201/eid2506.181158

Influenza D virus has been found to cause respiratory diseases in livestock. We surveyed healthy dromedary camels in Ethiopia and found a high seroprevalence for this virus, in contrast to animals co-existing with the camels. Our observation implies that dromedary camels may play an important role in the circulation of influenza D virus.

Influenza D virus (IDV) was first isolated from pigs with respiratory symptoms in the United States in 2011 (*1*). Epidemiologic analyses revealed that the most likely main host of IDV is cattle, because the seropositivity rate in these animals is higher than that for other livestock (*2–4*). In a recent report, dromedary camels (*Camelus dromedaries*) exhibited substantially high seroprevalence (99%) for IDV in Kenya (*5*), suggesting that this animal is a potential reservoir of IDV. We examined seroprevalence of IDV in dromedary camels in Ethiopia and in Bactrian camels (*Camelus bactrianus*) in Mongolia.

We collected serum samples from dromedary camels (n = 38; average age 4.3 years, range 1–13 years), goats (n = 20; average age 3.9 years, range 1–8 years), sheep (n = 20; average age 2.7 years, range 1–4 years), cattle (n = 15; average age 6.7 years, range, 1–11 years), and donkeys (n = 2; ages 1 and 6) from 2 herds in Bati district, Amhara region, and 1 herd in Fafen district, Somali region, Ethiopia. All animals were apparently healthy, shared the same pasturage during the day, and stayed in barns specific for each animal species at night. To detect influenza D infection, we titrated the serum samples by hemagglutination inhibition (HI) assay using 3 antigenically distinct influenza D strains: D/swine/Oklahoma/1334/2011 (D-OK lineage; D/OK) (*1*), D/bovine/Nebraska/9–5/2013 (D/660-lineage; D/NE) (*6*), and D/bovine/Yamagata/10710/2016 (D/Japan-lineage; D/Yamagata) (*7*). For the HI test, we treated the samples with receptor-destroying enzyme (RDEII; Denka Seiken, http://www.keyscientific.com) at 37°C for 16 h, followed by heat inactivation at 56°C for 30 min. We then reacted serially diluted samples with each virus (4 HAU) at room temperature for 30 min and incubated them with a 0.6% suspension of turkey red blood cells at room temperature for 30 min. The HI titer of each sample was expressed as the reciprocal of the highest sample dilution that completely inhibited HA. We considered samples with HI titer ≥1:40 positive, to eliminate nonspecific reactions at low dilutions (*4,8,9*).

Of the 21 dromedary camel samples from Bati, 10 were positive for D/OK, 11 for D/NE, and 19 for D/Yamagata (Figure). Of other animal samples, only 1 goat sample was positive (titer 1:40), indicating that the prevalence rate of influenza D antibodies was higher in dromedary camels than in co-grazing ruminants in the tested herd. The data on the camels' age indicated that the HI antibodies were not detected due to maternal antibodies, which is only stable for 5–6 months in dromedary camels (*10*). Much closer face-to-face contact may be required for virus transmission among different animal species. The HI titers in camel samples were higher for D/Yamagata (range 1:40–1:160) than those for D/OK and D/NE (1:40–1:80). Meanwhile, we found several positives in dromedary camel samples from Fafen, albeit at lower positive rates and titers compared with those in Bati (Figure).

We confirmed the specificity of the HI reaction with a viral neutralizing test using HI-positive samples (data not shown). HI titers obtained were not high, suggesting that the infections may have occurred in these animals some time ago or that results might have been due to the variance of HI

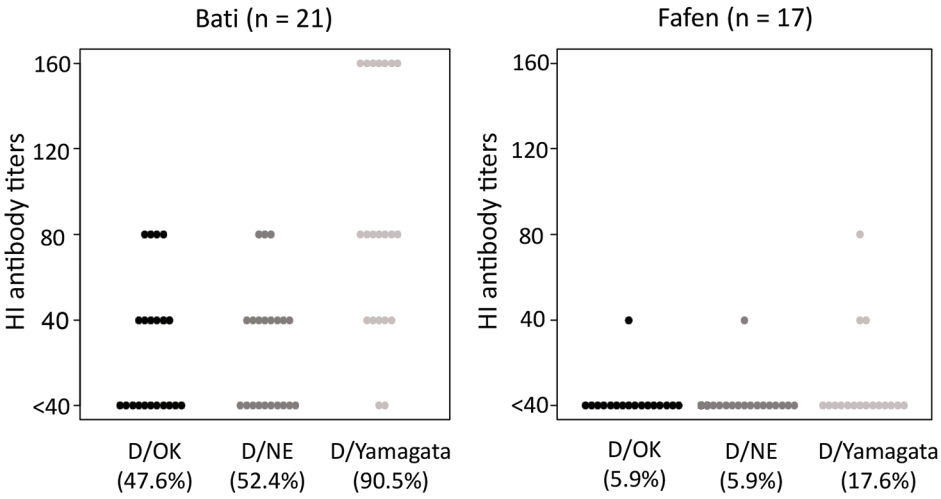

Figure. Hemagglutination inhibition (HI) antibody titers for influenza D viruses in serum samples from dromedary camels, Bati and Fafen Districts, Ethiopia. Each dot represents 1 camel. HI assay was performed with RDE(II)-treated serum samples and turkey red blood cells (0.6%) against D/swine/Oklahoma/1334/2011 (D/OK), D/bovine/Nebraska/9–5/2013 (D/NE), and D/bovine/Yamagata/10710/2016 (D/Yamagata). HI-positive rate for each virus is shown below the virus name.

methods used in each laboratory. For example, turkey red blood cell was used in this study, whereas horse red blood cell was used in a previous study (*5*). Nonetheless, these data suggest that the virus antigenically related to D/Yamagata was circulating in dromedary camels in this region.

In a previous report, a considerable number of dromedary camels in Kenya were seropositive not only for influenza D but also for influenza C virus (ICV) (*5*). Thus, we additionally used C/Ann Arbor/1/1950 virus as an antigen for HI assay. The results suggest a limited circulation of ICV in this area because 0 samples in Bati were positive and only 2 in Fafen, which were negative for IDV, were positive (titers 1:40). In addition, we performed the HI test using selected samples following preadsorption with ICV. We did not observe any significant decrease in HI titers to IDV, suggesting no cross-reactivity between IDV and ICV in our samples.

We also collected serum samples of apparently healthy Bactrian camels (n = 40) in Dundgovi, Zavkhan, and Umnugovi Provinces, Mongolia, and tested for HI antibody for IDV. These samples did not test positive for these IDV strains.

Despite the limited samples tested, this study suggests that dromedary camels in East Africa might play a substantial role in the circulation of IDV. Further studies using additional samples from multiple countries are expected to clarify the role of this animal on the ecology and epidemiology of this virus, including its reservoir potential in nature.

Acknowledgments

We thank Ben M. Hause for the viruses used in the study.

T.H. is supported by Livestock Promotion Funds from the Japan Racing Association. S.M. is supported by a Grant-in-Aid for the Encouragement of Young Scientists (A) (grant no. 17H05042).

About the Author

Dr. Murakami is an associate professor at the Graduate School of Agricultural and Life Sciences, University of Tokyo, Tokyo, Japan. His research interests include epidemiological and molecular biological studies of animal viruses, including influenza viruses.

References

1. Hause BM, Ducatez M, Collin EA, Ran Z, Liu R, Sheng Z, et al. Isolation of a novel swine influenza virus from Oklahoma in 2011 which is distantly related to human influenza C viruses. PLoS Pathog. 2013;9:e1003176. http://dx.doi.org/10.1371/journal.ppat.1003176
2. Hause BM, Collin EA, Liu R, Huang B, Sheng Z, Lu W, et al. Characterization of a novel influenza virus in cattle and swine: proposal for a new genus in the Orthomyxoviridae family. MBio. 2014;5:e00031–14. http://dx.doi.org/10.1128/mBio.00031-14
3. Ferguson L, Eckard L, Epperson WB, Long LP, Smith D, Huston C, et al. Influenza D virus infection in Mississippi beef cattle. Virology. 2015;486:28–34. http://dx.doi.org/10.1016/j.virol.2015.08.030
4. Luo J, Ferguson L, Smith DR, Woolums AR, Epperson WB, Wan XF. Serological evidence for high prevalence of influenza D viruses in cattle, Nebraska, United States, 2003–2004. Virology. 2017;501:88–91. http://dx.doi.org/10.1016/j.virol.2016.11.004
5. Salem E, Cook EAJ, Lbacha HA, Oliva J, Awoume F, Aplogan GL, et al. Serologic evidence for influenza C and D virus among ruminants and camelids, Africa, 1991–2015. Emerg Infect Dis. 2017;23:1556–9. http://dx.doi.org/10.3201/eid2309.170342
6. Collin EA, Sheng Z, Lang Y, Ma W, Hause BM, Li F. Cocirculation of two distinct genetic and antigenic lineages of proposed influenza D virus in cattle. J Virol. 2015;89:1036–42. http://dx.doi.org/10.1128/JVI.02718-14
7. Nakatsu S, Murakami S, Shindo K, Horimoto T, Sagara H, Noda T, et al. Influenza C and D viruses package eight organized ribonucleoprotein complexes. J Virol. 2018;92:e02084–17. http://dx.doi.org/10.1128/JVI.02084-17
8. Murakami S, Endoh M, Kobayashi T, Takenaka-Uema A, Chambers JK, Uchida K, et al. Influenza D virus infection in herd of cattle, Japan. Emerg Infect Dis. 2016;22:1517–9. http://dx.doi.org/10.3201/eid2208.160362

9. Quast M, Sreenivasan C, Sexton G, Nedland H, Singrey A, Fawcett L, et al. Serological evidence for the presence of influenza D virus in small ruminants. Vet Microbiol. 2015;180:281–5. http://dx.doi.org/10.1016/j.vetmic.2015.09.005
10. Meyer B, Juhasz J, Barua R, Das Gupta A, Hakimuddin F, Corman VM, et al. Time course of MERS-CoV infection and immunity in dromedary camels. Emerg Infect Dis. 2016;22: 2171–3. http://dx.doi.org/10.3201/eid2212.160382

Address for correspondence: Taisuke Horimoto, University of Tokyo, Department of Veterinary Microbiology, Graduate School of Agricultural and Life Sciences, 1-1-1 Yayoi, Bunkyo-ku, Tokyo 113-8657, Japan; email: ahorimo@mail.ecc.u-tokyo.ac.jp

Absence of *Neospora caninum* DNA in Human Clinical Samples, Spain

Rafael Calero-Bernal, Pilar Horcajo, Marta Hernández, Luis Miguel Ortega-Mora, Isabel Fuentes

Author affiliations: Complutense University of Madrid, Madrid, Spain (R. Calero-Bernal, P. Horcajo, L.M. Ortega-Mora); Carlos III Institute of Health, Madrid (M. Hernández, I. Fuentes)

DOI: https://doi.org/10.3201/eid2506.181431

Low antibody titers to *Neospora caninum* have been reported in humans, but infection has not been confirmed. We used *N. caninum*–specific PCR to test 600 clinical samples from patients with toxoplasmosis signs but *Toxoplasma gondii*–negative PCR results. We did not detect *N. caninum* DNA, demonstrating it is an unlikely opportunistic zoonotic agent.

The coccidian parasite *Neospora caninum* (Apicomplexa: Sarcocystidae) is a major abortifacient agent in ruminants, especially cattle. It is phylogenetically close to *Toxoplasma gondii* (*1*), a parasite of high prevalence in humans, but biologically different. *N. caninum* parasites have a restricted host range but can infect primates (*2,3*).

N. caninum infection causes neuromuscular disease in dogs and reproductive disorders in ruminants, causing fetal loss due to vertical transfer of parasites during acute infections or reactivation of chronic infections. Clinical neosporosis in animals resembles the disease outcome of toxoplasmosis (*1*).

Table. Types of samples analyzed and demographic and clinical data for 600 patients tested for *Neospora caninum* parasites, Spain*

Characteristics	No. (%)
Sample type	
Amniotic fluid	267 (44.5)
Cerebrospinal fluid	113 (18.8)
Blood	100 (16.7)
Placental tissue	51 (8.5)
Bronchoalveolar lavage	25 (4.2)
Urine	17 (2.8)
Brain biopsy	12 (2.0)
Aqueous humor	4 (0.7)
Fetal tissues and fluids	4 (0.7)
Lymph node aspirate	3 (0.5)
Vitreous humor	2 (0.3)
Bone marrow aspirate	1 (0.2)
Hepatic abscess aspirate	1 (0.2)
Patient demographic information	
Sex	
Unknown	6 (1.0)
M	135 (22.5)
F	459 (76.5)
Of childbearing age, 17–42 y	333 (55.5)
Age, y	
>1, average 36.1	481 (80.2)
<1	116 (19.3)
Native country	
Spain	382 (63.7)
Other†	36 (6.0)
Unknown	182 (30.3)
Patient clinical information	
Immune status	
Immunocompetent	458 (76.3)
Immunodepressed or immunosuppressed	83 (13.8)
HIV/AIDS	19 (22.9)
Chemotherapy	29 (34.9)
Organ transplant	35 (42.2)
Unknown	59 (9.8)
Pregnancy-related disorders	454 (75.7)
Seroconversion–infection suspicion and lymphadenopathy	418 (92.1)
Spontaneous abortion	27 (5.9)
Ophthalmic	4 (0.9)
Other fetal signs‡	5 (1.1)
Neurologic and ocular symptoms and conditions§	108 (18.0)
Neurologic condition with ocular signs	8 (7.4)
Ophthalmic only	3 (2.7)
General signs, n = 38	38 (6.3)
Pneumonia	24 (63.2)
Lymphadenopathy	2 (5.3)
Hematologic or oncologic	12 (31.6)

*Patients were from 12 regions: Andalusia, Aragon, Asturias, Balearic Islands, Cantabria, Castile-La Mancha, Castile and Leon, Extremadura, Galicia, Madrid, Navarre, Valencia.
†Africa, 8; Asia, 1; Europe, 8; Latin America, 19.
‡Anencephaly, malformations, and microcephaly.
§Neurologic symptoms and conditions include ataxia, disorientation, sudden blindness, encephalitis, calcifications, and intracranial space occupying lesions; ophthalmic symptoms and conditions include chorioretinitis, panuveitis, posterior uveitis, and vitritis.

N. caninum parasites have been successfully cultured in human cell lines, but low antibody titers of unconfirmed specificity against *N. caninum* have been reported in human serum samples (*1*,*4*,*5*). The significance

of these findings is uncertain because neither parasite DNA nor viable parasites have been demonstrated in human tissues. Unconfirmed reports of *N. caninum*–specific antibodies in the human population (*4,5*) prompted us to test specifically for *Neospora* DNA in human clinical specimens and assess its possible role in human illness.

We obtained 600 DNA samples from a collection of anonymized human clinical samples from the National Registry of Biobanks (no. C.0004715) in Spain that were deemed exempt from a second ethics approval. Our criteria for selection included any pregnancy-related disorder affecting women or fetuses, toxoplasmosis-like clinical signs or suspicion of toxoplasmosis, and negative results for *T. gondii*–specific real-time PCR (*6*) and nested PCR (*7*) (Table).

We isolated total DNA using a QIAamp DNA Mini Kit (QIAGEN, https://www.qiagen.com) and used a single-tube nested PCR to amplify the *N. caninum* internal transcribed spacer 1 region using external primers NN1–NN2 and internal primers NP1–NP2, as previously described (*8*,*9*). We expected a diagnostic 249-bp fragment. In each batch of amplifications, positive PCR controls included genomic DNA of 10, 1, and 0.1 *N. caninum* tachyzoites. Using these PCR methods, we found that the analytical sensitivity was <1 tachyzoite of *Neospora* spp. or *T. gondii*.

We did not detect *N. caninum*–specific DNA in the samples analyzed. Previously, transplacental neosporosis was experimentally demonstrated in rhesus macaques (*Macaca mulatta*) in the United States (*2*,*3*). A literature review summarized reports of unconfirmed presence of antibodies against *N. caninum* in patients with neurologic disorders, pregnant women, and healthy people, including blood donors (*1*). Findings of *N. caninum* IgG in HIV-infected patients from Brazil and France (*4*,*5*) are of special interest because of possible association with *T. gondii* infections.

We believe *N. caninum* parasites are an unlikely opportunistic zoonotic agent. Application of direct methods for parasite detection in a greater number of samples from HIV-positive patients should complement unclear serologic findings to fully dispel suspicion of human neosporosis.

This work was supported by National Health Research Funds Project P13/01106. Carlos III Health Institute Spanish Ministry of Science and Innovation. R.C-B. is funded by Complutense University of Madrid, Madrid, Spain (grant no. CT65/16).

About the Author

Dr. Calero-Bernal is a postdoctoral researcher at the Saluvet Research Group of the Complutense University, Madrid. His major research interests are Apicomplexan parasites of zoonotic interest, epidemiology of foodborne parasites, and molecular pathways in virulence and drug susceptibility in protozoans.

References

1. Dubey JP, Hemphill A, Calero-Bernal R, Schares G. Neosporosis in animals. Boca Raton (FL): CRC Press; 2017.
2. Barr BC, Conrad PA, Sverlow KW, Tarantal AF, Hendrickx AG. Experimental fetal and transplacental *Neospora* infection in the nonhuman primate. Lab Invest. 1994;71:236–42.
3. Ho MS, Barr BC, Tarantal AF, Lai LT, Hendrickx AG, Marsh AE, et al. Detection of *Neospora* from tissues of experimentally infected rhesus macaques by PCR and specific DNA probe hybridization. J Clin Microbiol. 1997;35:1740–5.
4. Lobato J, Silva DA, Mineo TW, Amaral JD, Segundo GR, Costa-Cruz JM, et al. Detection of immunoglobulin G antibodies to *Neospora caninum* in humans: high seropositivity rates in patients who are infected by human immunodeficiency virus or have neurological disorders. Clin Vaccine Immunol. 2006;13:84–9. http://dx.doi.org/10.1128/CVI.13.1.84-89.2006
5. Robert-Gangneux F, Klein F. Serologic screening for *Neospora caninum,* France. Emerg Infect Dis. 2009;15:987–8. http://dx.doi.org/10.3201/eid1506.081414
6. Reischl U, Bretagne S, Krüger D, Ernault P, Costa JM. Comparison of two DNA targets for the diagnosis of Toxoplasmosis by real-time PCR using fluorescence resonance energy transfer hybridization probes. BMC Infect Dis. 2003;3:7. http://dx.doi.org/10.1186/1471-2334-3-7
7. Fuentes I, Rodriguez M, Domingo CJ, del Castillo F, Juncosa T, Alvar J. Urine sample used for congenital toxoplasmosis diagnosis by PCR. J Clin Microbiol. 1996;34:2368–71.
8. Buxton D, Maley SW, Wright S, Thomson KM, Rae AG, Innes EA. The pathogenesis of experimental neosporosis in pregnant sheep. J Comp Pathol. 1998;118:267–79. http://dx.doi.org/10.1016/S0021-9975(07)80003-X
9. Hurtado A, Aduriz G, Moreno B, Barandika J, García-Pérez AL. Single tube nested PCR for the detection of *Toxoplasma gondii* in fetal tissues from naturally aborted ewes. Vet Parasitol. 2001;102:17–27. http://dx.doi.org/10.1016/S0304-4017(01)00526-X

Address for correspondence: Rafael Calero-Bernal, SALUVET Group, Animal Health Department, Complutense University of Madrid, Avda. Complutense s/n, 28040, Madrid, Spain; email: r.calero@ucm.es

etymologia

Neospora caninum [ne-os'pə-rə ca-nin'um]

Ronnie Henry

From the *neo*- (Latin, "new") + *spora* (Greek, "seed") and *canis* (Latin, "dog"), *Neospora caninum* is a sporozoan parasite that was first described in 1984. It is a major pathogen of cattle and dogs but can also infect horses, goats, sheep, and deer. Antibodies to *N. caninum* have been found in humans, predominantly in those with HIV infection, although the role of this parasite in causing or exacerbating illness is unclear.

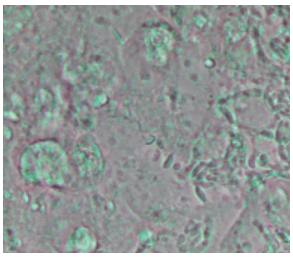

Neospora caninum, a coccidian parasite, which identified as a species in 1988. It is a major cause of spontaneous abortion in infected livestock. Image from WIkipedia (https://en.wikipedia.org/wiki/Neospora_caninum#/media/File:Neospora_caninum_(5256961091).jpg).

Sources

1. Bjerkås I, Mohn SF, Presthus J. Unidentified cyst-forming sporozoon causing encephalomyelitis and myositis in dogs. Z Parasitenkd. 1984;70:271–4. http://dx.doi.org/10.1007/BF00942230
2. Dubey JP. Review of *Neospora caninum* and neosporosis in animals. Korean J Parasitol. 2003; 41:1–16. http://dx.doi.org/10.3347/kjp.2003.41.1.1
3. Lobato J, Silva DA, Mineo TW, Amaral JD, Segundo GR, Costa-Cruz JM, et al. Detection of immunoglobulin G antibodies to *Neospora caninum* in humans: high seropositivity rates in patients who are infected by human immunodeficiency virus or have neurological disorders. Clin Vaccine Immunol. 2006;13:84–9. http://dx.doi.org/10.1128/CVI.13.1.84-89.2006

Address for correspondence: Ronnie Henry, Centers for Disease Control and Prevention, 1600 Clifton Rd NE, Mailstop E28, Atlanta, GA 30329-4027, USA; email: boq3@cdc.gov

DOI: https://doi.org/10.3201/eid2506.ET2506

Reemergence of Classical Swine Fever, Japan, 2018

Alexander Postel,[1] Tatsuya Nishi,[1] Ken-ichiro Kameyama, Denise Meyer, Oliver Suckstorff, Katsuhiko Fukai, Paul Becher

Author affiliations: University of Veterinary Medicine, Hannover, Germany (A. Postel, D. Meyer, O. Suckstorff, P. Becher); National Agriculture and Food Research Organization, Tokyo, Japan (T. Nishi, K. Kameyama, K. Fukai)

DOI: https://doi.org/10.3201/eid2506.181578

In September 2018, classical swine fever reemerged in Japan after 26 years, affecting domestic pigs and wild boars. The causative virus belongs to the 2.1 subgenotype, which caused repeated outbreaks in eastern and Southeast Asia. Intensive surveillance of swine and vaccination of wild boars will help control and eradicate this disease in Japan.

Classical swine fever (CSF) is one of the economically most devastating diseases worldwide and is notifiable to the World Organisation for Animal Health (OIE). The presence of CSF in a pig population results in severe restrictions on international trade of pigs and pork products. Many countries have implemented compulsory eradication programs and perform intensive surveillance. Most countries with industrialized pig production and high biosecurity standards have achieved the OIE status of being CSF free, including Japan in 2015 (*1*). Nevertheless, CSF is endemic to many countries that have a high number of backyard pigs. Because wild boars are as susceptible to CSF virus (CSFV) as domestic pigs, eradication of CSF in wild boars is of epidemiologic value (*2*).

CSFV, a positive-sense RNA virus (family *Flaviviridae*, genus *Pestivirus*) is divided into 3 major genotypes (*1*–*3*) and several subgenotypes (*3*,*4*). In Europe, the more recent outbreaks were caused by genotype 2.1 (Lithuania, 2009 and 2011) and genotype 2.3 (Latvia, 2013–2015) (*5*). In Asia, recent outbreaks were caused mainly by CSFV genotypes 1.1, 2.1, 2.2, and 2.3.

The spread of African swine fever (ASF) across China in 2018 has increased awareness of ASF and CSF in Southeast Asia. During August 16–September 3, 2018, at a pig farm in Gifu city, Gifu Prefecture, Japan, ≈20 fattening pigs died. A veterinarian recognized that the pigs were weakened and inappetent; no clinical signs were detected before

[1]These authors contributed equally to this article.

August 20. Staff from the Gifu prefectural animal hygiene service center collected and sent samples from the following animals to the National Institute of Animal Health (Tokyo, Japan) to test for ASF and CSF viruses: 6 live pigs on August 24, 1 dead pig on September 3, and 11 live pigs and 1 dead pig on September 8. The CSFV genome was detected by reverse transcription PCR and confirmed by nucleotide sequencing. Control measures comprised culling of ≈600 pigs from the infected farm, movement restrictions, disinfection, epidemiologic investigations, clinical and laboratory investigations of 13 farms with epidemiologic links, and intensified surveillance. On September 13, a dead wild boar was found in the restriction zone of the initial outbreak and was CSFV positive. By March 7, 2019,

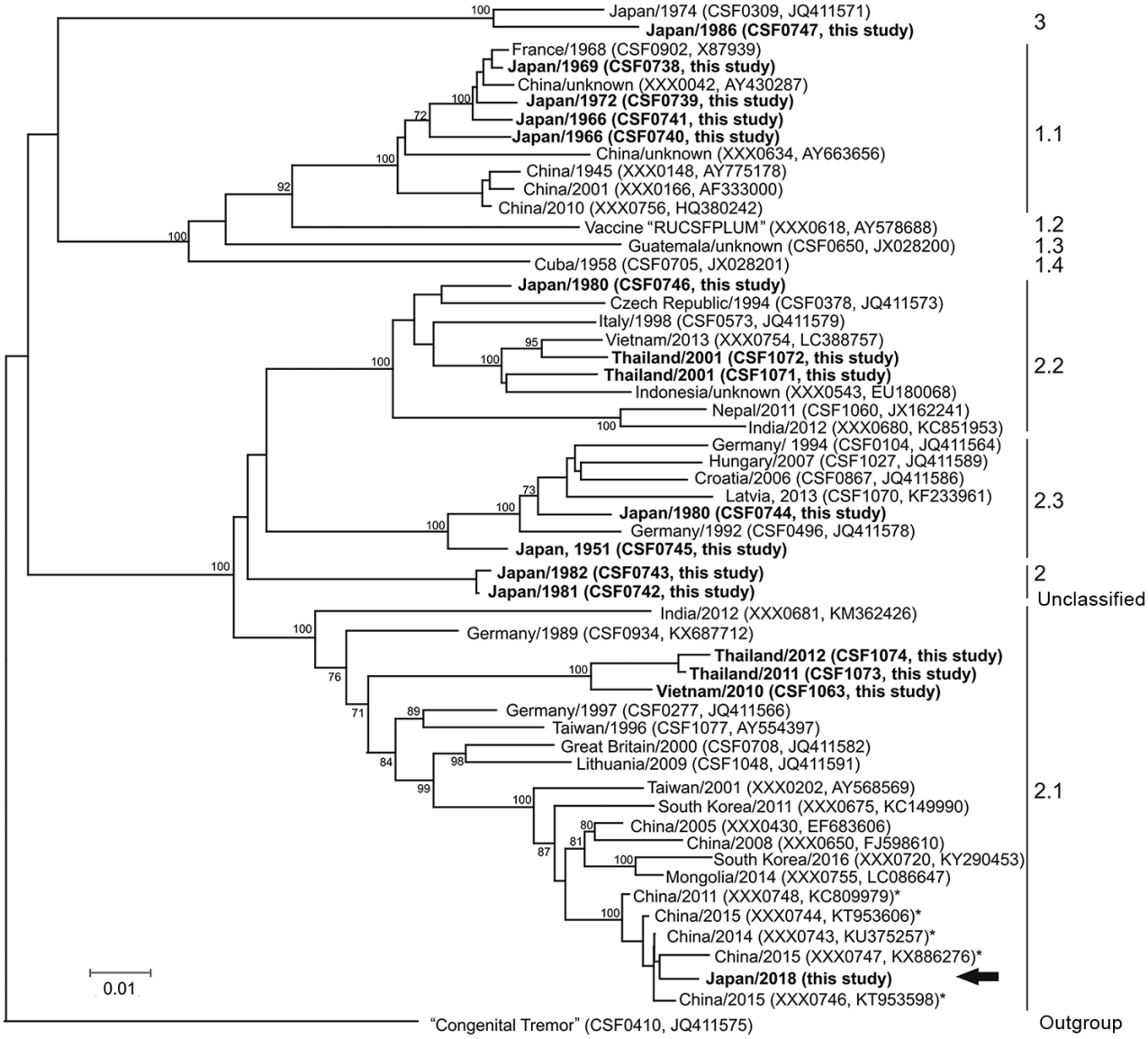

Figure. Phylogenetic tree displaying the genetic relatedness of the classical swine fever virus (CSFV) isolate obtained from the 2018 classical swine fever (CSF) outbreak in Japan to other CSFV isolates. Phylogenetic analyses were performed by using the neighbor-joining method with complete E2 (1,119 nt) sequences, including 1,000 iterations for bootstrap analysis, and were generated by the genetic typing module of the CSF database at the European Union and OIE Reference Laboratory for Classical Swine Fever (*6*). Only bootstrap values ≥70% are indicated. For each isolate, country and year are given, along with catalog number of the CSF database and the GenBank accession number in parentheses. The arrow indicates the sequence of the virus isolate obtained from a domestic pig during the 2018 CSF outbreak in Japan (Japan/2018) (GenBank accession no. LC425432). Boldface indicates additional newly generated sequences (GenBank accession nos. MK026451–65). Two ancient sequences from Japan (CSF0742, CSF0743) were identified as belonging to genotype 2 with no clear affiliation to any of the 3 established subgenotypes 2.1, 2.2, and 2.3 (indicated as genotype 2, unclassified). Asterisks indicate 5 E2 sequences belonging to a group of sequences that are most closely related to the E2 sequence of the CSFV isolate Japan/2018. Scale bar indicates nucleotide substitutions per site.

a total of 68 dead and 153 live wild boars in Gifu and Aichi Prefectures had been found to be CSFV positive.

The last CSF outbreak in Japan (Kumamoto Prefecture) occurred in 1992; since 2006, vaccination against CSF has been banned. The absence of CSF in Japan for 26 years strongly suggests reintroduction of the virus from outside Japan. To support epidemiologic investigations, we performed molecular typing based on the partial 5′ untranslated region (UTR) (150 nt) and on the complete E2 gene (1,119 nt) by using the CSF sequence database and the integrated tool for phylogenetic analysis (*3*,*6*). Most similar sequences identified by database search (GenBank, https://www.ncbi.nlm.nih.gov/nuccore; BLAST, https://blast.ncbi.nlm.nih.gov/Blast.cgi) were included in the analysis together with 15 complete E2 encoding sequences (GenBank accession nos. MK026451–65) newly generated from isolates originating from Japan (10 sequences in 1951–1986), Thailand (4 sequences in 2001, 2011, and 2012), and Vietnam (1 sequence in 2010) (Figure). Phylogenetic analyses revealed that the 2018 isolate from Japan belongs to genotype 2.1; the E2 (Figure) and 5′-UTR sequences (Appendix, https://wwwnc.cdc.gov/EID/article/25/6/18-1578-App1.pdf) were most closely related to CSFV detected in China during 2011–2015 (98%–99% identity in E2 sequences; Figure) and China and Mongolia during 2014–2015 (98%–99% identity in partial 5′-UTR; Appendix). Subsequently, a complete genome sequence of the index isolate was determined (GenBank accession no. LC425854); the closest genetic relationship (98.9% identity) was with 2 recent isolates (GenBank accession nos. MG387217–8) from Beijing, China (*7*). Members of this phylogenetic clade reportedly form an emerging group of moderately virulent CSFV that is becoming more prevalent in China (*8*,*9*). Despite good availability of sequence data from China, much less information is available from other countries in the region. Therefore, similar viruses may be in other countries in eastern and Southeast Asia. Additional CSFV sequences from previous outbreaks in Japan, Thailand, and Vietnam were only distantly related to the sequence of the isolate from Japan. Partial E2 and 5′UTR sequences (GenBank accession nos. LC425434–5) obtained from the first positive wild boar (index case) revealed 100% identity to the index isolate.

Japan is among the top 10 pork-producing countries worldwide; in 2017, an estimated 16.3 million pigs were slaughtered in Japan. Presence of CSFV in wild boars remains a serious threat for domestic pigs. By February 2019, the virus had further spread from Gifu Prefecture into other prefectures in Japan, emphasizing the need for defined strategies to control the outbreak, including vaccination of wild boar, in addition to the standard policy of culling. Moreover, intensive surveillance is needed to monitor the situation carefully and will contribute to the control and eradication of CSF in Japan.

Acknowledgments

We are grateful to the regional and national authorities in Japan. We thank all providers of sequence information, diagnostic materials, and virus isolates. In particular, we thank Regional Animal Health Office No. 6, Ho Chi Minh City, Vietnam, and the National Institute of Animal Health, Bangkok, Thailand. We are thankful to the team of the European Union and OIE Reference Laboratory for CSF and all colleagues who actively support the CSF sequence database and virus bank in Hannover as well as the work of the OIE Reference Laboratories for CSF. We thank Yoshihiro Sakoda for his valuable support and discussions.

This work in part was financially supported by the Directorate-General for Health and Consumers of the European Commission and the Ministry of Agriculture, Forestry and Fisheries of Japan. The funding sources had no influence on the study design or data presented.

About the Author

Dr. Postel is a veterinarian and head of the Laboratory for Molecular Biology of the European Union and OIE Reference Laboratory for Classical Swine Fever at the Institute of Virology of the University of Veterinary Medicine in Hannover, Germany. His research interests are molecular evolution and pathogenesis of pestiviruses, characterization of novel pestivirus isolates, and diagnosis and control of classical swine fever. Dr. Nishi is a veterinarian and a researcher at the National and OIE Reference Laboratory for Classical Swine Fever at the National Institute of Animal Health, Japan. His research interests are molecular characterization, diagnosis, and control of transboundary infectious disease viruses.

References

1. Postel A, Austermann-Busch S, Petrov A, Moennig V, Becher P. Epidemiology, diagnosis and control of classical swine fever: recent developments and future challenges. Transbound Emerg Dis. 2017; 2018;65(Suppl 1):248–61.
2. Moennig V. The control of classical swine fever in wild boar. Front Microbiol. 2015;6:1211. http://dx.doi.org/10.3389/fmicb.2015.01211
3. Postel A, Schmeiser S, Bernau J, Meindl-Boehmer A, Pridotkas G, Dirbakova Z, et al. Improved strategy for phylogenetic analysis of classical swine fever virus based on full-length E2 encoding sequences. Vet Res (Faisalabad). 2012;43:50. http://dx.doi.org/10.1186/1297-9716-43-50
4. Lowings P, Ibata G, Needham J, Paton D. Classical swine fever virus diversity and evolution. J Gen Virol. 1996;77:1311–21. http://dx.doi.org/10.1099/0022-1317-77-6-1311
5. Postel A, Moennig V, Becher P. Classical swine fever in Europe—the current situation. Berl Munch Tierarztl Wochenschr. 2013;126:468–75.
6. Postel A, Schmeiser S, Zimmermann B, Becher P. The European classical swine fever virus database: blueprint for a pathogen-specific sequence database with integrated sequence analysis tools. Viruses. 2016;8: pii: E302. http://dx.doi.org/10.3390/v8110302
7. Nishi T, Kameyama KI, Kato T, Fukai K. Genome sequence of a classical swine fever virus of subgenotype 2.1, isolated from a pig

in Japan in 2018. Microbiol Resour Announc. 2019;8:pii: e01362-18. http://dx.doi.org/10.1128/MRA.01362-18
8. Hu D, Lv L, Gu J, Chen T, Xiao Y, Liu S. Genetic diversity and positive selection analysis of classical swine fever virus envelope protein gene E2 in east China under C-strain vaccination. Front Microbiol. 2016;7:85. http://dx.doi.org/10.3389/fmicb.2016.00085
9. Luo Y, Ji S, Liu Y, Lei JL, Xia SL, Wang Y, et al. Isolation and characterization of a moderately virulent classical swine fever virus emerging in China. Transbound Emerg Dis. 2017;64:1848–57. http://dx.doi.org/10.1111/tbed.12581

Address for correspondence: Paul Becher, EU and OIE Reference Laboratory for Classical Swine Fever, Institute for Virology, University of Veterinary Medicine, Buenteweg 17, 30559 Hannover, Germany; email: paul.becher@tiho-hannover.de; Katsuhiko Fukai, National and OIE Reference Laboratory for Classical Swine Fever, National Institute of Animal Health, National Agriculture and Food Research Organization, 6-20-1, Josui-honchyo, Kodaira, Tokyo 187-0022, Japan; email: fukai@affrc.go.jp

African Swine Fever Virus in Pork Brought into South Korea by Travelers from China, August 2018

Hyun-Joo Kim, Min-Jung Lee, Soo-Kyoung Lee, Da-young Kim, Sang-Ji Seo, Hae-Eun Kang, Hyang-Mi Nam

Author affiliation: Animal and Plant Quarantine Agency, Gimcheon, South Korea

DOI: https://doi.org/10.3201/eid2506.181684

We tested samples of pork products confiscated from travelers to South Korea for African swine fever virus (ASFV). We detected ASFV in 4 food items confiscated from travelers from Shenyang, China, in August 2018. Surveillance of pork products at country entry points is needed to mitigate the risk for ASFV introduction.

African swine fever (ASF) is a fatal viral disease that affects pigs of all ages and breeds. ASF virus (ASFV) is highly virulent and remains a global threat because of the lack of a vaccine and the ability of the virus to survive in various environmental conditions. Since 2007, ASFV has been spreading across Europe and Russia. In August 2018, China reported the first outbreak of ASF in Asia (*1*). Since then, ASFV has been reported in numerous provinces and continues to spread across China (*2*).

Although ASF has never occurred in the Republic of Korea (hereafter referred to as South Korea), ASFV could be introduced into this country through various routes. The risk for ASF introduction into South Korea increases with the continuous spread of the disease across China. Pork products contaminated with ASFV are among the main risk factors for spreading the disease (*3*). Hence, since 2015, we have been conducting surveillance on pork products confiscated at airports and ports from travelers coming from countries affected by ASF. Since the program started in 2015, an average of 6,200 products have been seized per month, and we tested an average of 10 (0.16%) products per month.

After the first ASF outbreak in China, South Korea enhanced quarantine inspections of travelers, especially those coming from China. A total of 4,064 pork products (3,374 sausages, 12 hams, and 678 other products containing pork) were seized from travelers from China in August 2018. Among these products, we randomly selected samples from 52 (1.28%) products for real-time PCR testing. We homogenized these samples and extracted nucleic acids using High Pure PCR Template Preparation Kit (Roche, https://www.roche.com) in a Biosafety Level 3 laboratory at the Animal and Plant Quarantine Agency in Gimcheon, South Korea. We used ASFV OURT88/3 virus as a positive control. To amplify the ASFV *B646L* gene, we performed TaqMan real-time PCR (Applied Biosystems, https://www.thermofisher.com) as recommended (*4*).

In total, 4 samples from China tested positive for ASFV: 2 blood sausages (identification [ID] no. 18083111, seized August 16, 2018, and ID no. 18081148, seized August 20, 2018), 1 dumpling (ID no. 18082721, seized August 18, 2018), and 1 commercial sausage product (ID no. JI 18080406, seized August 26, 2018). All ASFV-positive samples were from products seized at the Incheon and Jeju International Airports from passengers flying from Shenyang, China, where the first ASFV outbreak in China was reported.

We performed conventional PCR to further analyze the ASFV isolates detected. We amplified 3 independent regions of the ASFV genome: the *B646L* gene encoding p72, the *E183L* gene encoding p54, and a tandem-repeat sequence located between the *I73R* and *I329L* genes (*5–7*). All genes detected were ASFV genotype II (Figure). All positive samples had an intergenic region II variant with an additional tandem-repeat sequence (5′-GGAATATATA-3′) between the *I73R* and *I329L* genes (*5*). The intergenic region II variant we observed was identical to those reported in isolates Ukr12/Zapo, Bel13/Grodno, Lt14/1490, Lt14/1482, Pol14/Sz, and Pol14/Krus (*6*). The same tandem-repeat sequence insertion was also observed in China isolates ASFV SY18 and CN201801 (*1,2*).

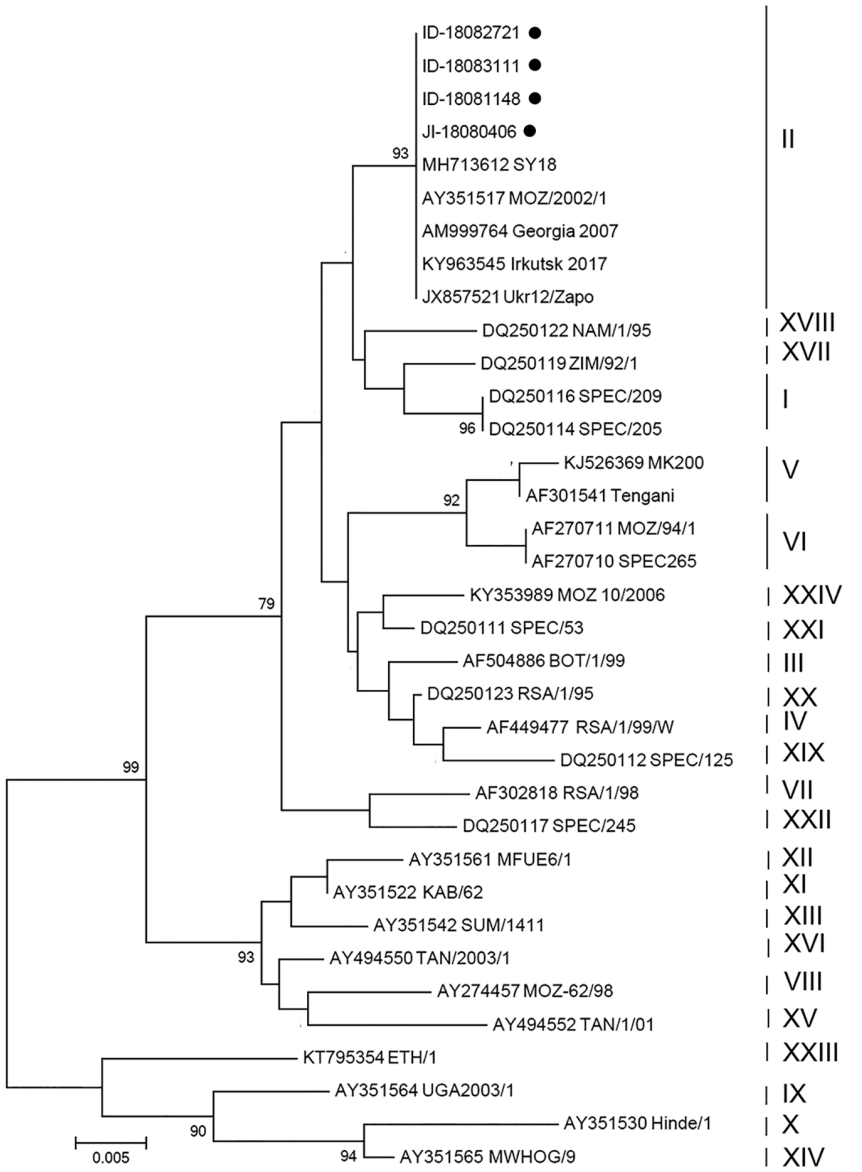

Figure. Phylogenic analysis of partial *B646L* gene sequence of African swine fever virus (ASFV) in samples of pork products brought into South Korea by travelers from Shunyang, China, August 2018, and reference sequences. Neighbor-joining phylogenic tree was constructed by using MEGA 6.0 (https://www.megasoftware.net). Black dots indicate genes of ASFV isolates detected in 3 food items containing pork and 1 commercial pork product confiscated from travelers. Vertical lines at right indicate ASFV genotypes I–XXIV. GenBank accession numbers are provided for reference sequences. Scale bar indicates the number of base pair substitutions per nucleotide.

We compared the gene sequences of our samples with those of ASFV SY18 (GenBank accession nos. MH713612, MH717102, and MH717104). The genes detected in the blood sausage samples (ID nos. 18083111 and 18082721) were 100% identical to those of ASFV SY18. However, the *E183L* gene and *I73R–I329L* intergenic spacer were not detectable in the other 2 samples (ID nos. 18081148 and JI 18080406), suggesting that only part of the ASFV genome remained intact and preventing more thorough genomic comparisons. We also attempted to culture virus from the 4 samples in primary pig alveolar macrophage cells using the procedure established by the Center for Animal Health Research (http://asf-referencelab.info/asf/en/procedures-diagnosis/sops), the European Union Reference Laboratory for ASF in Madrid, Spain, but the virus did not propagate.

Our results indicate that the ASFV isolates detected in South Korea in August 2018 were identical to those reported in China. Also, the detection of ASFV genes in commercial sausage products from China indicates that pigs infected with ASFV might have been slaughtered and distributed in markets throughout China.

The Food and Agriculture Organization of the United Nations reported the possibility of ASFV spread from China to other parts of Asia, including the Korean Peninsula and Japan (*8*). Table and kitchen scraps containing pork contaminated with ASFV was reported to be a potential source of the infection in China (*9*). Contaminated pork products fed to pigs have often been the source of ASFV outbreaks and introduction into previously unaffected areas (*10*). Thus, detection of ASFV in these confiscated products highlights the

importance of surveillance at points of entry to mitigate the risk for ASFV introduction through illegal imports.

Acknowledgments

The authors thank staff from the Pirbright Institute for providing the ASFV OURT88/3 strain.

This project was supported financially by a grant (no. B-1543085-2017-18-02) from the Animal and Plant Quarantine Agency, the Ministry of Agriculture, Food and Rural Affairs, South Korea.

About the Author

Dr. Kim is a veterinary researcher working for the Foreign Animal Disease Research Division, Animal and Plant Quarantine Agency, Gimcheon, South Korea. Her research interests are diagnostics and the prevention of disease in animals from emerging pathogens.

References

1. Zhou X, Li N, Luo Y, Liu Y, Miao F, Chen T, et al. Emergence of African swine fever in China, 2018. Transbound Emerg Dis. 2018;65:1482–4. http://dx.doi.org/10.1111/tbed.12989
2. Ge S, Li J, Fan X, Liu F, Li L, Wang Q, et al. Molecular characterization of African swine fever virus, China, 2018. Emerg Infect Dis. 2018;24:2131–3. http://dx.doi.org/10.3201/eid2411.181274
3. Kolbasov D, Titov I, Tsybanov S, Gogin A, Malogolovkin A. African swine fever virus, Siberia, Russia, 2017. Emerg Infect Dis. 2018;24:796–8. http://dx.doi.org/10.3201/eid2404.171238
4. World Organisation for Animal Health. African swine fever. In: Manual of diagnostic tests and vaccines for terrestrial animals. Paris: The Organisation; 2012.
5. Bastos ADS, Penrith ML, Crucière C, Edrich JL, Hutchings G, Roger F, et al. Genotyping field strains of African swine fever virus by partial *p72* gene characterisation. Arch Virol. 2003;148:693–706. http://dx.doi.org/10.1007/s00705-002-0946-8
6. Gallardo C, Fernández-Pinero J, Pelayo V, Gazaev I, Markowska-Daniel I, Pridotkas G, et al. Genetic variation among African swine fever genotype II viruses, eastern and central Europe. Emerg Infect Dis. 2014;20:1544–7. http://dx.doi.org/10.3201/eid2009.140554
7. Gallardo C, Mwaengo DM, Macharia JM, Arias M, Taracha EA, Soler A, et al. Enhanced discrimination of African swine fever virus isolates through nucleotide sequencing of the *p54*, *p72*, and *pB602L* (CVR) genes. Virus Genes. 2009;38:85–95. http://dx.doi.org/10.1007/s11262-008-0293-2
8. Food and Agriculture Organization of the United Nations. African swine fever threatens People's Republic of China: a rapid risk assessment of ASF introduction. Animal health risk analysis. Assessment no. 05. 2018 Mar 6 [cited 2018 Oct 31]. http://www.fao.org/3/i8805en/I8805EN.pdf
9. Li X, Tian K. African swine fever in China. Vet Rec. 2018; 183:300–1. http://dx.doi.org/10.1136/vr.k3774
10. Penrith ML, Vosloo W. Review of African swine fever: transmission, spread and control. J S Afr Vet Assoc. 2009;80:58–62. http://dx.doi.org/10.4102/jsava.v80i2.172

Address for correspondence: Hyang-Mi Nam, Animal and Plant Quarantine Agency, 177, Hyeoksin 8-ro Gimcheon 39660, South Korea; email: namhm@korea.kr

Hepatitis E Virus Infection in European Brown Hares, Germany, 2007–2014

Victor Max Corman, Laura Hilgensloh, Ulrich Voigt, Marco Marklewitz, Ursula Siebert, Christian Drosten, Jan Felix Drexler

Author affiliations: Charité-Universitätsmedizin Berlin, Berlin, Germany (V.M. Corman, M. Marklewitz, C. Drosten, J.F. Drexler); German Centre for Infection Research (DZIF), Berlin (V.M. Corman, C. Drosten, J.F. Drexler); University of Bonn Medical Centre, Bonn, Germany (L. Hilgensloh); University of Veterinary Medicine Hannover Foundation, Hannover, Germany (U. Voigt, U. Siebert)

DOI: https://doi.org/10.3201/eid2506.181618

Rabbit-associated hepatitis E viruses (HEVs) cause zoonotic infections. We investigated 2,389 hares in Germany during 2007–2014. Complete genome characterization of a hare-associated HEV strain revealed close genomic relatedness to rabbit-associated HEV strains. Although hare-specific HEV seroprevalence was low, at 2.6%, hares represent a potential source of sporadic HEV infections.

Hepatitis E virus (HEV; family Hepeviridae, genus *Orthohepevirus*) is a major cause of acute hepatitis in humans worldwide. Large outbreaks have included waterborne HEV in the tropics and zoonotic infections in temperate climates (*1*). In 2017, researchers identified human infection with HEV strains associated with rabbits (raHEV) in France (*2*,*3*).

In Germany, rabbits (family Leporidae, genus *Oryctolagus*) are common in the wild but are also popular pets, potentially explaining human exposure to raHEV. Hares (family Leporidae, genus *Lepus*), although genetically related, are physically larger and are primarily hunted as food in large parts of Europe (>5 million hares annually) (*4*). HEV associated with hares (haHEV) had been previously unknown (*5*). For this study, we tested for HEV in 2,389 European brown hares (*L. europaeus*) hunted in Germany during 2007–2014, across an area of ≈30,000 km^2 (Appendix Figure 1, http://wwwnc.cdc.gov/EID/article/25/6/18-1618-App1.pdf). One animal (0.04% of all samples; 95% CI 0.03%–0.05%) tested positive in a broadly reactive reverse transcription PCR assay; 25 (2.6%; 95% CI 1.6%–3.5%) animals were identified as seropositive.

RNA concentration was 5.4×10^4 IU/mL in the serum of the animal that tested positive, comparable to viral loads observed in rabbits and in human blood donors (*3*,*6*). After we determined its complete viral genome (GenBank accession

no. MK050463), the haHEV isolate showed the typical genome organization of *Orthohepevirus* A, including 3 predicted open reading frames (ORF). We found a 93-nt insertion in the X-domain of ORF1 that is thought to be typical of raHEV strains and absent in other HEV strains (*2*,*3*). This finding may reflect a common origin of raHEV and haHEV strains or a host-associated virus adaptation. We found no evidence for recombination of haHEV with other *Orthohepevirus* species or subtypes.

When averaged over the complete genome, the haHEV isolate we obtained shared 86% nucleotide identity with the most closely related raHEV strain (GenBank accession no. KY436898), from a rabbit sampled in Germany in 2016 (*5*). Average translated amino acid identity of the haHEV with raHEV strains was high at 88.5%–97.5% for ORF1, 90.2%–98.5% for ORF2, and 88.6%–95.1% for ORF3. In phylogenetic reconstructions, the haHEV clustered with raHEV strains, further suggesting a common origin for haHEV and raHEV, and suggesting an origin of haHEV in ancestors carried by rabbits and distinct from the greater HEV diversity existing in swine (*7*) (Figure; Appendix Figure 2). This interpretation is consistent with sporadic sharing of habitats between wild rabbits and hares in the study area.

To determine seroprevalence, we expressed the capsid protein of haHEV and used it for indirect immunofluorescence assays (Appendix). In total, serum samples from 944 hares, covering all sampling regions and years, were available in sufficient quality and quantity for serological testing (Appendix Table 2). HEV seroprevalence for hares was 2.6% (95% CI 1.6%–3.5%), similar to values in a previous serologic study of 669 European brown hares that used a capsid fragment from a human HEV genotype 1 strain as antigen and yielded a seroprevalence of 1.6%–4.3% (*5*). The sampling sites from that study were up to 400 km from those in our study, suggesting geographically widespread HEV infection of hares. That study also found wild rabbits to be seropositive at rates >35% (*5*). The lower HEV seroprevalence in hares than in rabbits might be explained by the fact that hares live solitarily and have low-density populations, ≈12–20 animals/100 ha in the sampling region; wild rabbits live in groups of ≈15 that are also proximal to other groups.

We found no statistically significant differences in seroprevalence for hares <1 versus >1 year of age (χ^2 0.08; p = 0.78), which is unlike the age-dependent increase of seropositivity observed in pigs and humans (*8*,*9*). Explanations may include a lack of statistical power in this study or differential pathogenesis of HEV in hares. Although the data

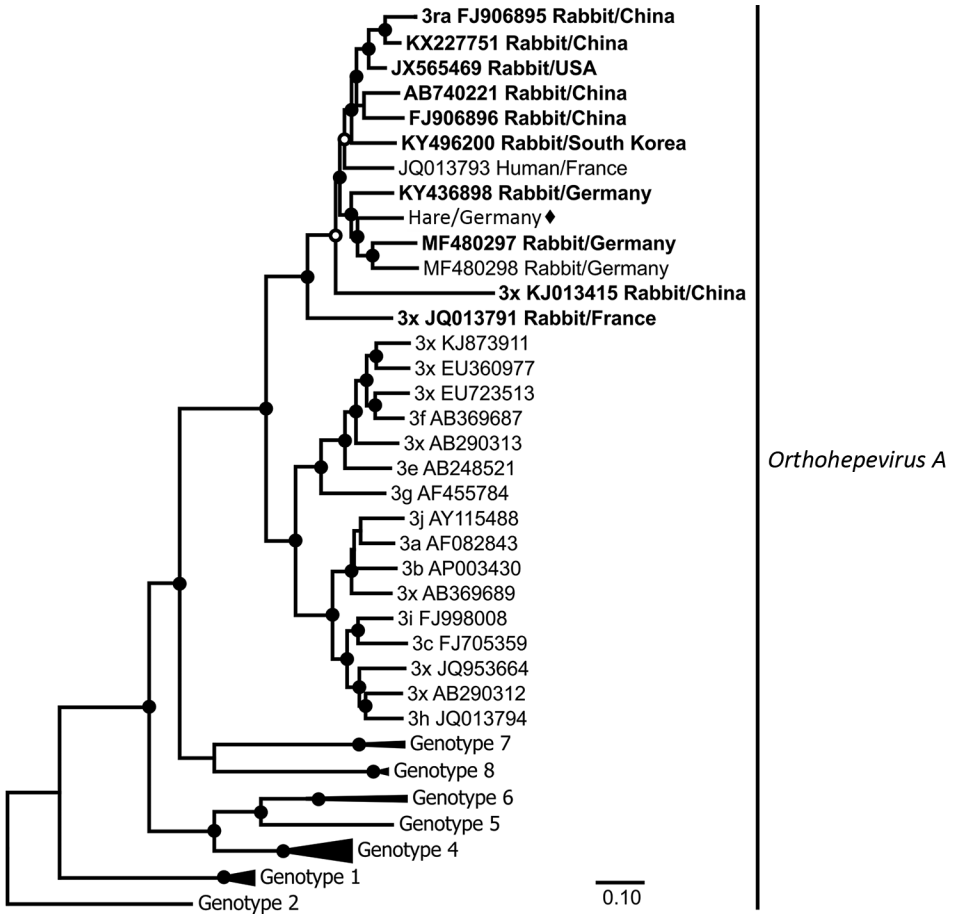

Figure. Maximum-likelihood phylogeny of the concatenated open reading frame 1 and 2 nucleotide sequences of hare hepatitis E virus (HEV) strain from Germany (black diamond), related strains from rabbits (bold) and humans, and reference *Orthohepevirus A* strains, as defined by Smith et al. (*7*). Taxon names of all reference sequences include genotype, subtype (x if not available), and GenBank accession number. Black circles at nodes indicate bootstrap supports of >90% and white circles >75% (1,000 replicates). The clades comprising sequences other than HEV genotype 3 were collapsed for graphical reasons. Scale bar indicates nucleotide substitutions per site.

on HEV pathogenesis in rabbits are in part controversial, occurrence of HEV in apparently healthy laboratory rabbits suggests that rabbits frequently survive HEV infection (*10*). Whether the apparently low seroprevalence in hares compared with rabbits is thus due to infrequent infection, differential antibody responses, or other host- or virus-associated factors remains to determined.

We detected no statistically significant differences in seroprevalence rates, either between sexes (χ^2 0.01; p = 0.92) or across the 8 sampling years (Yates χ^2 0.6; p = 0.96) and the 5 individual sampling regions (Yates χ^2 1.945; p = 0.96). These findings suggested constant low levels of HEV transmission in hares irrespective of sex and geographic region.

The infection of hares with HEV strains that are closely related to raHEV strains suggests that hares may act as sporadic sources of zoonotic HEV infections. Although the low RNA detection rate and seroprevalence speak against a prominent role of hares in the epidemiology of zoonotic HEV, hunters and persons handling hare-derived products could represent risk groups. Awareness about hare-derived HEV infections may be particularly relevant for immunocompromised persons, in whom chronic HEV infections are most common.

Acknowledgments

We thank all hunters for their help during fieldwork, Joerg Roesner for help with immunofluorescence microscopy, and Sarah Schulz for providing HEV antibody reference material.

This research was supported by a grant from the German Federal Ministry of Health (grant ZMVI1-2518FSB705) to V.M.C.

About the Author

Dr. Corman is a physician and virologist at the Institute of Virology, Charité-Universitätsmedizin Berlin. His current research is dedicated to characterization of novel human and zoonotic viruses and development of diagnostic tools.

References

1. Aggarwal R. The global prevalence of hepatitis E virus infection and susceptibility: a systematic review. Geneva: World Health Organization; 2010.
2. Abravanel F, Lhomme S, El Costa H, Schvartz B, Peron JM, Kamar N, et al. Rabbit hepatitis E virus infections in humans, France. Emerg Infect Dis. 2017;23:1191–3. http://dx.doi.org/10.3201/eid2307.170318
3. Izopet J, Dubois M, Bertagnoli S, Lhomme S, Marchandeau S, Boucher S, et al. Hepatitis E virus strains in rabbits and evidence of a closely related strain in humans, France. Emerg Infect Dis. 2012;18:1274–81. http://dx.doi.org/10.3201/eid1808.120057
4. Chapman JA, Flux JEC; International Union for Conservation of Nature and Natural Resources. Lagomorph Specialist Group. Rabbits, hares, and pikas: status survey and conservation action plan. Gland (Switzerland): International Union for Conservation of Nature and Natural Resources; 1990.
5. Hammerschmidt F, Schwaiger K, Dähnert L, Vina-Rodriguez A, Höper D, Gareis M, et al. Hepatitis E virus in wild rabbits and European brown hares in Germany. Zoonoses Public Health. 2017;64:612–22. http://dx.doi.org/10.1111/zph.12355
6. Hewitt PE, Ijaz S, Brailsford SR, Brett R, Dicks S, Haywood B, et al. Hepatitis E virus in blood components: a prevalence and transmission study in southeast England. Lancet. 2014;384:1766–73. http://dx.doi.org/10.1016/S0140-6736(14)61034-5
7. Smith DB, Simmonds P, Izopet J, Oliveira-Filho EF, Ulrich RG, Johne R, et al. Proposed reference sequences for hepatitis E virus subtypes. J Gen Virol. 2016;97:537–42. http://dx.doi.org/10.1099/jgv.0.000393
8. Krumbholz A, Joel S, Neubert A, Dremsek P, Dürrwald R, Johne R, et al. Age-related and regional differences in the prevalence of hepatitis E virus-specific antibodies in pigs in Germany. Vet Microbiol. 2013;167:394–402. http://dx.doi.org/10.1016/j.vetmic.2013.10.001
9. Faber MS, Wenzel JJ, Jilg W, Thamm M, Höhle M, Stark K. Hepatitis E virus seroprevalence among adults, Germany. Emerg Infect Dis. 2012;18:1654–7. http://dx.doi.org/10.3201/eid1810.111756
10. Han SH, Park BJ, Ahn HS, Kim YH, Go HJ, Kim DH, et al. Evidence of hepatitis E virus infection in specific pathogen-free rabbits in Korea. Virus Genes. 2018;54:587–90. http://dx.doi.org/10.1007/s11262-018-1562-3

Address for correspondence: Victor Max Corman, Institute of Virology, Charité-Universitätsmedizin Berlin, 10117 Berlin, Germany, email: victor.corman@charite.de

Sarcoptic Mange of Fox Origin in Multiple Farm Animals and Scabies in Humans, Switzerland, 2018

Simone R.R. Pisano, Marie-Pierre Ryser-Degiorgis, Luca Rossi, Andrea Peano, Karin Keckeis, Petra Roosje

Author affiliations: University of Bern, Bern, Switzerland (S.R.R. Pisano, M.-P. Ryser-Degiorgis, P. Roosje); University of Turin, Grugliasco, Italy (L. Rossi, A. Peano); consulting veterinarian, Wabern, Switzerland (K. Keckeis)

DOI: https://doi.org/10.3201/eid2506.181891

Fox-derived *Sarcoptes scabiei* mites caused an outbreak of mange on a farm in Switzerland in 2018. Pruritic skin lesions suggestive of *S. scabiei* mite infestation developed in 4 humans who had direct contact with affected farm animals but not foxes. Sarcoptic mange is continuously spreading; such outbreaks affecting humans could start occurring more frequently.

The *Sarcoptes scabiei* mite is the causative agent of scabies in humans and sarcoptic mange in animals (*1*). Scabies is considered a neglected reemerging disease of public health concern (*2*). Sarcoptic mange causes distress in livestock, economic loss in the livestock industry, and disease and death in wildlife (*3*). The degrees of host specificity and cross-infectivity of *S. scabiei* mites are still debated (*3*).

In January 2018, sarcoptic mange was suspected on a farm in the Jura Mountains, Switzerland. The outdoor loose housing system of this farm hosting 2 oxen (*Bos taurus*), 2 horses (*Equus caballus*), 5 goats (*Capra hircus*), 4 alpacas (*Vicugna pacos*), 8 fallow deer (*Dama dama*), and 15 sheep (*Ovis aries*) was separated from a stable housing 3 pigs (*Sus scrofa domesticus*). Six dogs (*Canis lupus familiaris*) and 17 cats (*Felis catus*) had access to all stables. Pruritic skin lesions developed in several species 2–3 weeks after repeated episodes of mangy red foxes (*Vulpes vulpes*) sleeping in the stables and making partial body contact with the livestock (Figure, panels A, B). Pruritic skin lesions also developed in 4 persons who had direct contact with the domestic animals but not the foxes. A fox with mange was found dead nearby and a necropsy was performed. Oxen, dogs, and pigs were treated with avermectins before diagnostic investigations were carried out.

Clinical examination revealed papules, erythema, excoriations, hyperkeratosis, and hypotrichosis with variable severity in 2 pigs, 2 goats, 2 dogs, all horses, and all oxen (Figure, panels C, D). The 3 sheep and 1 cat examined did not have lesions suggestive of mange. Close examination of the fallow deer and alpacas was impracticable. Humans had pruritic erythematous papules and excoriations on their neck, legs, or arms (Figure, panel E). Health authorities temporarily prohibited 1 affected person (a teenager) from attending school because of suspected scabies. Pruritus and skin lesions disappeared in the affected animals and humans within 6 weeks after ≥2 treatments with avermectins, topical neem oil, or both.

We identified *S. scabiei* mites by light microscopy in the skin scrapings from 2 pigs, 1 horse, 1 ox, 1 goat, and 1 fox but none of the scrapings from 3 sheep, 5 dogs, and 1 cat sampled. A few mites but no eggs, eggshells, or gravid females were observed on livestock, whereas all stages were present and numerous on the fox. Skin scrapings were not obtained from the affected humans. We confirmed *S. scabiei* mite mitochondrial 16S rDNA by TaqMan real-time PCR (*4*) in the sampled horse, ox, goat, and fox but not in the sampled sheep, cat, dogs, or pigs. Analyses with a panel of 9 microsatellites (sarms 33, 35–38, 40, 41, 44, and 45) (*5*) confirmed that foxes were the source of the mites (Figure, panel F); the mites on the outbreak farm were similar to each other and to mites previously collected from foxes in Switzerland (*6*) but different from those collected from wild ungulates in Spain, Switzerland, France, and Italy (*5*,*7*,*8*).

Genetic investigations suggest that multiple *S. scabiei* mite subpopulations can infect the same host and that mite subpopulations can differ from host to host. Different subpopulations undergo varying degrees of gene flow depending on the geographic distances among infested hosts and cluster in animals that share a taxonomic classification above the species level (*1,9*). In Europe, wildlife herbivore-, carnivore- and omnivore-derived *S. scabiei* mites have been described as distinct groups, and intraspecies and interspecies transmission have been proposed to occur among hosts of the same taxon but not among different taxa under natural conditions (*8*). However, prey-to-predator transmission was demonstrated in Africa (*10*). Thus, direct contact between affected hosts or fomites and susceptible hosts (*1*) rather than mite host specificity might determine whether *S. scabiei* mites are transmitted to different taxonomic groups.

Our investigation unambiguously identified wild carnivore–derived *S. scabiei* mites as the cause of a point-like outbreak involving different domestic herbivores and omnivores. However, we found no evidence of mite reproduction, which suggests that the mites that transmitted from foxes to other species were not able to actively replicate. Yet, persistence of clinical signs despite treatment and suspected subsequent transmission from domestic animals to humans is not fully consistent with the self-limiting pattern described for zoonotic scabies, although reinfection of domestic animals by other foxes with mange could have occurred.

Increased fox abundance, reemergence, and continuous spread of sarcoptic mange in foxes could lead to its emergence in other wild and domestic animal species. Although mites or their DNA could not be demonstrated in the affected humans, their clinical signs were highly suggestive of scabies, highlighting the zoonotic potential of *S. scabiei* mites. The propensity of foxes with mange to live close to human settlements, the increase in green farming, and increased density and size of domestic animal populations augment the risk for contacts between foxes, domestic animals, and humans. Therefore, such outbreaks might become more frequent in the future.

Acknowledgments

We thank the owners of the animal refuge, Tante Martha, and the game warden, Thierry Studer, for their contributions to sample collection.

About the Author

Mr. Pisano is a veterinary resident in the Wildlife Population Health specialty of the European College of Zoological Medicine at the Centre for Fish and Wildlife Health, University of Bern, Bern, Switzerland. He has a special interest in infectious diseases in free-ranging wildlife and researches various aspects of sarcoptic mange in Swiss wildlife.

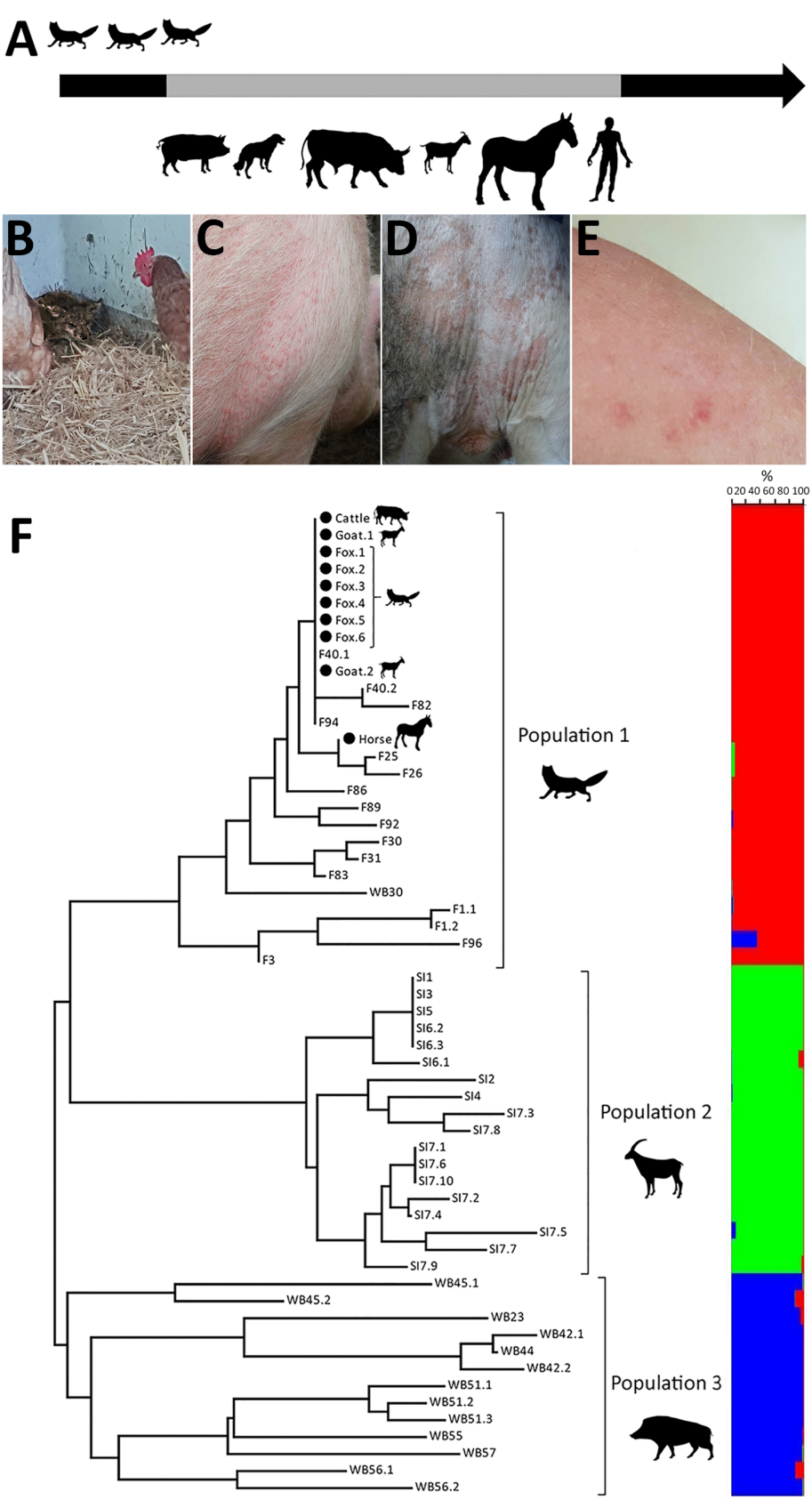

Figure. Clinical and molecular characterization of an outbreak of fox-derived *Sarcoptes scabiei* mites in multiple mammal species on a farm in Switzerland, 2018. A) Outbreak timeline displaying animal species (pigs [*Sus scrofa domesticus*], oxen [*Bos taurus*], dogs [*Canis lupus familiaris*], goats [*Capra hircus*], horses [*Equus caballus*], and red foxes [*Vulpes vulpes*]) showing clinical signs compatible with sarcoptic mange and humans with signs of zoonotic scabies, in order of appearance. Gray portion of arrow indicates the period during which clinical signs were observed in domestic animals and humans. Foxes with mange were observed in stables up to 3 weeks before the beginning of clinical signs in livestock. B–E) Clinical signs observed in a red fox (B; lethargy, severe hyperkeratosis), a pig (C; erythematous papules on shoulder and thorax), an ox (D; alopecia and erythema in the perineal region), and a teenage girl (E; erythematous papules on an arm). F) Multilocus microsatellite analysis demonstrating the genetic relationship of 10 individual mites isolated from a horse, an ox, a goat, and a fox at the farm where the outbreak occurred (black dots) and 48 additional mites from red foxes from the same region of Switzerland (population 1); Iberian ibex (*Capra pyrenaica*) from southern Spain (population 2); and wild boars (*Sus scrofa*) from Switzerland, nearby areas of France, and northern Italy (population 3). Neighbor-joining tree (left) constructed by using distance matrices with Populations version 1.2.28 (http://bioinformatics.org/populations) and displayed by using MEGA4 (http://www.megasoftware.net). Tree branch lengths are proportional to the percent genetic distance. Bar plot (right) obtained with Structure 2.3.4 (https://web.stanford.edu/group/pritchardlab/structure.html) represents the cluster membership according to the analyses of 9 markers for K = 3 with the probability (0%–100%) for each mite to belong to a different population. Medium gray indicates population 1, light gray indicates population 2, and dark gray indicates population 3. The 3 populations are the same as those in the distance tree. F, red fox; SI, Iberian ibex; WB, wild boar.

References

1. Arlian LG, Morgan MS. A review of *Sarcoptes scabiei*: past, present and future. Parasit Vectors. 2017;10:297. http://dx.doi.org/10.1186/s13071-017-2234-1
2. Karimkhani C, Colombara DV, Drucker AM, Norton SA, Hay R, Engelman D, et al. The global burden of scabies: a cross-sectional analysis from the Global Burden of Disease Study 2015. Lancet Infect Dis. 2017;17:1247–54. http://dx.doi.org/10.1016/S1473-3099(17)30483-8
3. Fraser TA, Charleston M, Martin A, Polkinghorne A, Carver S. The emergence of sarcoptic mange in Australian wildlife: an unresolved debate. Parasit Vectors. 2016;9:316. http://dx.doi.org/10.1186/s13071-016-1578-2
4. Angelone-Alasaad S, Molinar Min A, Pasquetti M, Alagaili AN, D'Amelio S, Berrilli F, et al. Universal conventional and real-time PCR diagnosis tools for *Sarcoptes scabiei* [published erratum in Parasit Vectors. 2015;8:622]. Parasit Vectors. 2015;8:587. http://dx.doi.org/10.1186/s13071-015-1204-8
5. Alasaad S, Oleaga Á, Casais R, Rossi L, Min AM, Soriguer RC, et al. Temporal stability in the genetic structure of *Sarcoptes scabiei* under the host-taxon law: empirical evidences from wildlife-derived *Sarcoptes* mite in Asturias, Spain. Parasit Vectors. 2011;4:151. http://dx.doi.org/10.1186/1756-3305-4-151
6. Nimmervoll H, Hoby S, Robert N, Lommano E, Welle M, Ryser-Degiorgis M-P. Pathology of sarcoptic mange in red foxes (*Vulpes vulpes*): macroscopic and histologic characterization of three disease stages. J Wildl Dis. 2013;49:91–102. http://dx.doi.org/10.7589/2010-11-316
7. Haas C, Origgi FC, Rossi S, López-Olvera JR, Rossi L, Castillo-Contreras R, et al. Serological survey in wild boar (*Sus scrofa*) in Switzerland and other European countries: *Sarcoptes scabiei* may be more widely distributed than previously thought. BMC Vet Res. 2018;14:117. http://dx.doi.org/10.1186/s12917-018-1430-3
8. Rasero R, Rossi L, Soglia D, Maione S, Sacchi P, Rambozzi L, et al. Host taxon-derived *Sarcoptes* mite in European wild animals revealed by microsatellite markers. Biol Conserv. 2010;143:1269–77. http://dx.doi.org/10.1016/j.biocon.2010.03.001
9. Andriantsoanirina V, Ariey F, Izri A, Bernigaud C, Fang F, Charrel R, et al. *Sarcoptes scabiei* mites in humans are distributed into three genetically distinct clades. Clin Microbiol Infect. 2015;21:1107–14. http://dx.doi.org/10.1016/j.cmi.2015.08.002
10. Gakuya F, Rossi L, Ombui J, Maingi N, Muchemi G, Ogara W, et al. The curse of the prey: *Sarcoptes* mite molecular analysis reveals potential prey-to-predator parasitic infestation in wild animals from Masai Mara, Kenya. Parasit Vectors. 2011;4:193. http://dx.doi.org/10.1186/1756-3305-4-193

Address for correspondence: Petra Roosje, Department of Clinical Veterinary Medicine, Division of Clinical Dermatology, Vetsuisse Faculty, University of Bern, Laenggassstrasse 128, PO Box 8466, 3001 Bern, Switzerland; email: petra.roosje@vetsuisse.unibe.ch

Suboptimal Handling of Piccolo Samples or Reagent Discs for Consideration in Ebola Response

Jessica R. Spengler, Stephen R. Welch, Sarah C. Genzer, JoAnn Coleman-McCray, Jessica R. Harmon, Stuart T. Nichol, Christina F. Spiropoulou

Author affiliation: Centers for Disease Control and Prevention, Atlanta, Georgia, USA

DOI: https://doi.org/10.3201/eid2506.181928

Operating clinical analyzers within recommended parameters can be challenging during outbreak response. Using the Piccolo Xpress point-of-care blood chemistry analyzer on guinea pig blood, we found that values of many analytes are still readily comparable when samples and reagent discs are handled at various conditions outside of manufacturers recommendations.

Blood chemistry analyses are useful for guiding patient care. However, following manufacturer-recommended handling and storage conditions can be challenging in areas with underdeveloped infrastructure, as experienced in past and ongoing Ebola outbreak response (*1*). To investigate the utility of data from samples or reagent discs handled under suboptimal conditions, we evaluated 14 conditions outside of manufacturers recommendations by using Strain 13/N guinea pig blood and plasma samples. Animal procedures were approved by the Centers for Disease Control and Prevention Institutional Animal Care and Use Committee and conducted at an AAALAC-International–accredited facility.

Samples were run on the Abaxis Piccolo Xpress Chemistry Analyzer (https://www.abaxis.com; quality control with Abbot General Chemistry controls and verification sample, https://www.fishersci.com/shop/products/piclpd-pls-gen-chm-ct-2x6x1ml/07p0401a). This platform is a compact and portable Clinical Laboratory Improvement Amendments–approved automated point-of-care system for whole blood, serum, and plasma (*2*). This platform, together with the General Chemistry 13 reagent disc used here, is widely used in past and ongoing Ebola outbreak responses (*3*–*6*) and in laboratory research on viral pathogenesis, therapeutics, and vaccine efficacy (*7*–*9*). All samples were collected in the recommended lithium heparin (LiH) tubes, except as indicated.

We determined intrinsic variation of each analyte under recommended conditions by running 31 samples on 2

different machines simultaneously or on 1 machine sequentially (represented as mean percentage change ± SD). We then evaluated 2 blood collection anticoagulants, 8 sample storage conditions, and 4 reagent disc storage conditions. Overall, >200 samples from 93 guinea pigs (48 males, 45 females; 7 were <1 month of age, 24 were 1–3 months, 8 were 4–6 months, 16 were 7–12 months, 17 were 1–2 years, 11 were 2–3 years, and 10 were >3 years), from healthy animals or animals with noninfectious chronic disease (e.g., renal failure) were analyzed.

We first evaluated the effect of anticoagulants on sample analytes. Blood was collected and then partitioned from the syringe into paired samples stored in LiH (baseline), EDTA, or sodium citrate. Deviations from baseline were determined and expressed as mean percentage differences (Table). As expected, because of the chelating action of EDTA, assay reactions involving cationic substrates (Ca^{2+}, alkaline phosphatase) generated no values or were greatly altered, although values of several analytes remained closely comparable to baseline. Values from samples collected in sodium citrate were uniformly lower than those collected in LiH.

To assess effects of sample storage temperatures on data output, we conducted similar analyses on whole blood stored overnight at –20°C, –4°C, or room temperature (≈20°C–22°C) and on plasma stored overnight at -20°C, room temperature, or 32°C. In general, plasma was more resistant to suboptimal temperatures; values for most analytes were comparable with paired control. Although data from whole blood samples varied more, many analytes (creatinine, alanine aminotransferase, alkaline phosphatase, total bilirubin) remained within ± 1 SD of baseline values. This finding is useful in situations where centrifuging blood samples might not be possible. For application to high-containment studies, we also evaluated the utility of data from plasma stored overnight at –20°C and γ-irradiated (5×10^6 rads) before analysis. Under these conditions, 6 of 12 analytes varied by >1 SD from expected range, suggesting that samples should be processed before inactivation by γ-irradiation.

Table. Mean percentage change of clinical chemistry values obtained on the Piccolo Xpress Chemistry Analyzer from blood samples or reagent discs processed under various conditions that deviated from the manufacturer recommendations*

Condition	No. tested	Percentage change compared with baseline											
		GLU	BUN	CRE	CA	ALB	TP	ALT	AST	ALP	TBIL	GGT	AMY
Sample collection													
WB in EDTA†	15	–3.0	0.2	–0.8	ERR	4.1	–3.0	1.4	10.9	–93.2	–0.6	21.0	–1.7
WB in Na citrate†	18	–30.0	–23.3	–20.8	–59.1	–31.0	–34.4	–36.5	–23.6	–38.1	–6.9	–31.3	–0.5
Sample handling													
WB 4°C O/N†	13	–19.2	1.2	–9.4	–1.0	–2.3	0.0	1.6	20.1	–2.5	–1.9	227.3	0.0
WB RT O/N†	16	–76.4	1.7	–4.7	2.0	–4.2	4.9	–0.1	37.7	–9.3	0.6	572.3	1.2
WB 32°C O/N†	16	–92.6	8.9	6.4	0.7	–4.1	6.3	–0.2	64.0	–10.5	–1.8	489.0	2.8
WB –20°C O/N†	3‡	ERR	ERR	ERR	ERR	ERR	ERR	ERR	ERR	ERR	ERR	ERR	ERR
PL†	35	–0.4	1.1	13.2	1.2	1.1	0.1	2.8	–1.5	2.1	4.7	–11.1	–0.1
PL RT O/N§	15	0.4	2.9	–11.3	0.3	–4.1	1.9	–0.4	1.8	–3.3	–4.8	1.5	–0.5
PL 32°C O/N§	18	0.2	6.1	–12.2	0.1	–6.2	2.2	–5.5	2.1	–0.6	3.9	0.2	–0.5
PL –20°C O/N§	14	–1.1	0.4	–3.9	–2.4	–0.6	–1.6	2.5	4.0	–5.9	–3.6	0.0	–0.5
PL –20°C O/N + γ-irradiation§	16	0.3	3.4	11.3	2.5	0.0	–4.9	–12.3	–13.2	–15.8	1.6	–15.8	–0.5
Disc handling													
WB + disc RT 7 d†	15	–3.4	1.1	–3.6	–1.4	0.9	0.6	3.0	2.2	–2.9	2.2	36.6	1.2
WB + disc 32°C 5 d†	12	–4.3	0.5	56.7	0.3	1.3	0.8	–4.1	1.8	7.6	–7.5	22.0	1.7
WB + disc 32°C 14 d†¶	7‡	–0.9	ERR	ERR	–1.8	–8.0	–0.5	5.3	–0.2	ERR	0.0	0.5	–0.5
WB + disc 32°C 5 wk†	2‡	ERR	ERR	ERR	ERR	ERR	ERR	ERR	ERR	ERR	ERR	ERR	ERR
Intrinsic variation													
±1 SD		3.0	2.8	18.3	1.5	3.1	1.8	8.9	4.0	13.2	16.6	20.3	1.8
±2 SD		5.9	5.7	36.5	3.1	6.2	3.7	17.7	8.1	26.5	33.3	40.6	3.7
Reference values#		143 ± 16 mg/dL	20.5 ± 3.3 mg/dL	0.32 ± 0.2 mg/dL	11.4 ± 0.5 mg/dL	2.9 ± 0.2 g/dL	5.4 ± 0.3 g/dL	27 ± 6 U/L	46 ± 15 U/L	43 ± 15 U/L	0.3 ± 0.04 mg/dL	10 ± 3 U/L	1,149 ± 131 U/L

*All analytes were quantified with the Piccolo General Chemistry 13 reagent discs (https://www.abaxis.com). Baseline values were obtained from aliquots of the same samples run according to manufacturer's recommendations for comparison. Values in white cells varied by <1 SD; values in light gray cells, by 1–2 SD; and values in dark gray cells, by >2 SD from the determined % intrinsic variation derived from analysis of samples run either sequentially on the same machine or in parallel on different machines. γ indicates γ-irradiated at 5×10^6 rads. ALB, albumin; AMY, amylase; ALP, alkaline phosphatase; ALT, alanine aminotransferase; AST, aspartate aminotransferase; BUN, blood urea nitrogen; CA, calcium; CRE, creatinine; ERR, analyte, sample, or disc error; GGT, γ-glutamyltransferase; GLU, glucose; Na, sodium; O/N, overnight; PL, plasma; RT, room temperature; TBIL, total bilirubin; TP, total protein; WB, whole blood. An expanded version of this table is available online (https://wwwnc.cdc.gov/EID/article/25/6/18-1928-T1.htm).
†Baseline sample: WB.
§‡Smaller sample size tested because tests did not function at indicated condition.
‡§Baseline sample: PL.
¶Only subset of discs (7 of 10) generated values; remainder generated no values because of disc error.
#Reference values for strain 13/N guinea pigs 50–900 d of age, expressed as mean ± SD (*10*).

Finally, we assessed effects of storing reagent discs at room temperature or 32°C for varying lengths of time. Although discs must be refrigerated when stored >48 hours, all values obtained from discs stored at room temperature for a week were within ± 1 SD of controls, except glucose and γ-glutamyltransferase (± 1–2 SD). Data from discs stored at 32°C for 5 days were similarly comparable with baseline; we observed deviations in glucose, γ-glutamyltransferase, and creatinine. Discs stored at 32°C for 14 days were unreliable; many generated no values or a "disc error" message. However, values read from discs that did not result in an error message were all within expected limits. All discs stored at 32°C for 5 weeks generated error messages. These findings suggest that although extended storage at elevated temperatures substantially damages discs, discs stored at these conditions for up to 2 weeks might still yield clinically relevant data.

In summary, we found that under various suboptimal conditions, many analytes are still readily comparable (within ± 1 SD of intrinsic variation) to those from paired samples handled according to the manufacturer's recommendations. In addition, the pattern of values that deviate from baseline is often consistent (e.g., glucose decreases) and may be considered in clinical evaluation. Although we used SDs to highlight deviation here, the clinical implication of these findings will vary based on the analyte and condition being monitored. We believe these findings, based on guinea pig samples, enabling us to efficiently sample a large population and process under controlled conditions, are translatable to other species, including humans, because the equivalent veterinary point-of-care platform (VetScan VS2) is also disc-based and uses comparable assay chemistry. However, the possibility for some species differences remains and should be considered for future investigations.

Acknowledgments

We thank the staff of the Comparative Medicine Branch, Division of Scientific Resources, National Center for Emerging and Zoonotic Infectious Diseases, Centers for Disease Control and Prevention, for assistance with colony husbandry and maintenance, and Tatyana Klimova for assistance in editing the manuscript.

This study was supported in part by the CDC Emerging Infectious Disease Research Core funds.

About the Author

Dr. Spengler is a veterinary medical officer with the Viral Special Pathogens Branch, Division of High-Consequence Pathogens and Pathology, National Center for Emerging and Zoonotic Infectious Diseases, CDC. Her research interests include model development and translational research on pathogenesis and therapeutic interventions for diseases caused by hemorrhagic fever viruses.

References

1. Carazo Perez S, Folkesson E, Anglaret X, Beavogui A-H, Berbain E, Camara A-M, et al. Challenges in preparing and implementing a clinical trial at field level in an Ebola emergency: a case study in Guinea, West Africa. PLoS Negl Trop Dis. 2017;11:e0005545. http://dx.doi.org/10.1371/journal.pntd.0005545
2. Murata K, Glaser L, Nardiello M, Richardson S, Ramanathan LV, Carlow DC. Analytical performance of the Abaxis Piccolo Xpress® point of care analyzer in whole blood, serum, and plasma. Clin Biochem. 2015;48:1344–6. http://dx.doi.org/10.1016/j.clinbiochem.2015.08.002
3. de Wit E, Rosenke K, Fischer RJ, Marzi A, Prescott J, Bushmaker T, et al. Ebola laboratory response at the Eternal Love Winning Africa campus, Monrovia, Liberia, 2014–2015. J Infect Dis. 2016;214(suppl 3):S169–76. http://dx.doi.org/10.1093/infdis/jiw216
4. de Wit E, Kramer S, Prescott J, Rosenke K, Falzarano D, Marzi A, et al. Clinical chemistry of patients with Ebola in Monrovia, Liberia. J Infect Dis. 2016;214(suppl 3):S303–7. http://dx.doi.org/10.1093/infdis/jiw187
5. Sissoko D, Laouenan C, Folkesson E, M'Lebing A-B, Beavogui A-H, Baize S, et al.; JIKI Study Group. Experimental treatment with favipiravir for Ebola virus disease (the JIKI trial): a historically controlled, single-arm proof-of-concept trial in Guinea. PLoS Med. 2016;13:e1001967. 2 Errata in: PLoS Med. 2016. http://dx.doi.org/10.1371/journal.pmed.1001967
6. Hunt L, Gupta-Wright A, Simms V, Tamba F, Knott V, Tamba K, et al. Clinical presentation, biochemical, and haematological parameters and their association with outcome in patients with Ebola virus disease: an observational cohort study. Lancet Infect Dis. 2015;15:1292–9. http://dx.doi.org/10.1016/S1473-3099(15)00144-9
7. Bradfute SB, Swanson PE, Smith MA, Watanabe E, McDunn JE, Hotchkiss RS, et al. Mechanisms and consequences of ebolavirus-induced lymphocyte apoptosis. J Immunol. 2010;184:327–35. http://dx.doi.org/10.4049/jimmunol.0901231
8. Geisbert TW, Mire CE, Geisbert JB, Chan Y-P, Agans KN, Feldmann F, et al. Therapeutic treatment of Nipah virus infection in nonhuman primates with a neutralizing human monoclonal antibody. Sci Transl Med. 2014;6:242ra82. http://dx.doi.org/10.1126/scitranslmed.3008929
9. Geisbert TW, Jones S, Fritz EA, Shurtleff AC, Geisbert JB, Liebscher R, et al. Development of a new vaccine for the prevention of Lassa fever. PLoS Med. 2005;2:e183. http://dx.doi.org/10.1371/journal.pmed.0020183
10. Genzer SC, Huynh T, Coleman-McCray JD, Harmon JR, Welch SR, Spengler JR. Hematology and clinical chemistry reference intervals for inbred strain 13/N guinea pigs (*Cavia porcellus*). J Am Assoc Lab Anim Sci. 2019 Apr 22 [Epub ahead of print]. http://dx.doi.org/10.30802/AALAS-JAALAS-18-000118

Address for correspondence: Jessica R. Spengler, Centers for Disease Control and Prevention, 1600 Clifton Rd NE, Mailstop H18-SB, Atlanta, GA 30329-4027, USA; email: jspengler@cdc.gov

Infection with New York Orthohantavirus and Associated Respiratory Failure and Multiple Cerebral Complications

Rajeev Fernando, David Capone, Susan Elrich, Raymond Mantovani, Luther Quarles III, Alison D'Amato, Nathan Lowe, Ashwin Malhotra, Teresa Khoo, Sara Zufan, Maria Morales-Betoulle, Shelley M. Brown, Deborah Cannon, James C. Graziano, John D. Klena, Shannon Whitmer, Stuart T. Nichol, Paul Strachan, Bernard C. Camins, Luis A. Marcos

Author affiliations: Stony Brook Southampton Hospital, Southampton, New York, USA (R. Fernando, D. Capone, S. Elrich, R. Mantovani, L. Quarles III, A. D'Amato, N. Lowe); New York Presbyterian Hospital/Weill Cornell Medical Center, New York, New York, USA (A. Malhotra); Stony Brook University, Stony Brook, New York, USA (A. Malhotra, T. Khoo, P. Strachan, L.A. Marcos); Centers for Disease Control and Prevention, Atlanta, Georgia, USA (S. Zufan, M. Morales-Betoulle, S.M. Brown, D. Cannon, J.C. Graziano, J.D. Klena, S. Whitmer, S.T. Nichol); Icahn School of Medicine at Mount Sinai, New York (B.C. Camins)

DOI: https://doi.org/10.3201/eid2506.181966

We report a case of infection with New York orthohantavirus in a woman who showed renal impairment and hemorrhage, complicated by hydrocephalus, in Long Island, New York, USA. Phylogenetic analysis showed that this virus was genetically similar to a New York orthohantavirus isolated in the same region during 1993.

In the United States, New York orthohantavirus (NYV) is carried by the white-footed mouse (*Peromyscus leucopus*). During 1993–1995, human cases of NYV infection were reported in persons who visited or resided on Long Island, New York, USA (*1*). Since that time, no other cases have been reported on Long Island. We report an NYV infection with unusual clinical manifestations.

A 52-year-old woman from the east end of Long Island came to an emergency department in May 2017 because of fevers, headaches, myalgias, vomiting, somnolence, and lethargy for 3 days. She had a history of tick exposure and had recently cleaned her basement, where she reported observing mice droppings.

The patient had a core temperature of 102°F, a heart rate of 108 beats/min, a respiration rate of 20 breaths/min, and a blood pressure of 94/56 mm Hg. Her oxygen saturation was 95% on room air. Laboratory tests showed the following results: leukocytes 4,500 cells/mm^3, platelets 102,000 platelets/mm^3, aspartate aminotransferase 355 U/L, alanine aminotransferase 180 U/L, procalcitonin 4.3 ng/mL, erythrocyte sedimentation rate 2 mm/h, and C-reactive protein 4.7 mg/dL. A chest radiograph showed clear lung fields. A lumbar puncture showed an opening pressure of 45 cm of H_2O (reference range 8–15 cm H_2O), 1 nucleated cell (reference value <5/high-powered field), glucose 152 mg/dL, and protein 31 mg/dL.

On day 4 postonset, her condition rapidly deteriorated. A second chest radiograph showed developing pulmonary congestion, and she required intubation and mechanical ventilation. She also had severe thrombocytopenia (18,000/platelets mm^3), acute kidney injury, proteinuria and microhematuria (peak creatinine 2.3 mg/dL, urinary protein 30 mg/dL, 50 erythrocytes/high-powered field), worsening transaminitis (aspartate aminotransferase 329 U/L, alanine aminotransferase 258 U/L), and an increased lactate dehydrogenase (769 U/L). A computed tomography (CT) scan of the lungs showed bilateral pleural effusions (day 6 postonset). Because a CT scan of the head showed cerebral edema, the patient was transferred to a tertiary care hospital (day 7 postonset).

Serologic test results were negative for Powassan virus, *Ehrlichia* spp., *Anaplasma* spp., Lyme disease, and Rocky Mountain spotted fever. Results of a hantavirus IgM and IgG ELISA (recognizing the nucleocapsid protein common to all hantaviruses) were positive (Associated Regional and University Pathologists Laboratories, https://www.aruplab.com). An acute hantavirus infection was confirmed by the Centers for Disease Control and Prevention (Atlanta, GA, USA) by ELISA and identified antibodies that cross-reacted with Sin Nombre virus antigens (serum titers: IgM 1:6,400 and IgG 1:400). Orthohantavirus RNA was also detected by using reverse transcription PCR specific for the large RNA segment (*2*).

Although the patient's condition improved on day 14 postonset, she had 3 episodes of witnessed tonic–clonic seizures. A CT scan of the head showed an acute intraparenchymal hemorrhage (platelet count range 37,000/μL–57,000/μL) in the left basal ganglia with intraventricular extension into the left lateral and third ventricles and hydrocephalus that required placement of an emergent external ventricular drain. Blood and cerebrospinal fluid (CSF) collected at day 15 postonset had undetectable levels of virus RNA but IgM (serum 1:6,400, CSF 1:20) and IgG (serum 1:6,400, CSF 1:20) antibody titers had increased. She was discharged on day 26 postonset and given anticonvulsant therapy. One year later, the patient was asymptomatic.

We sequenced hantavirus RNA isolated from the initial blood specimen by using Sanger and unbiased next-generation sequencing (Figure). Phylogenetic analysis of

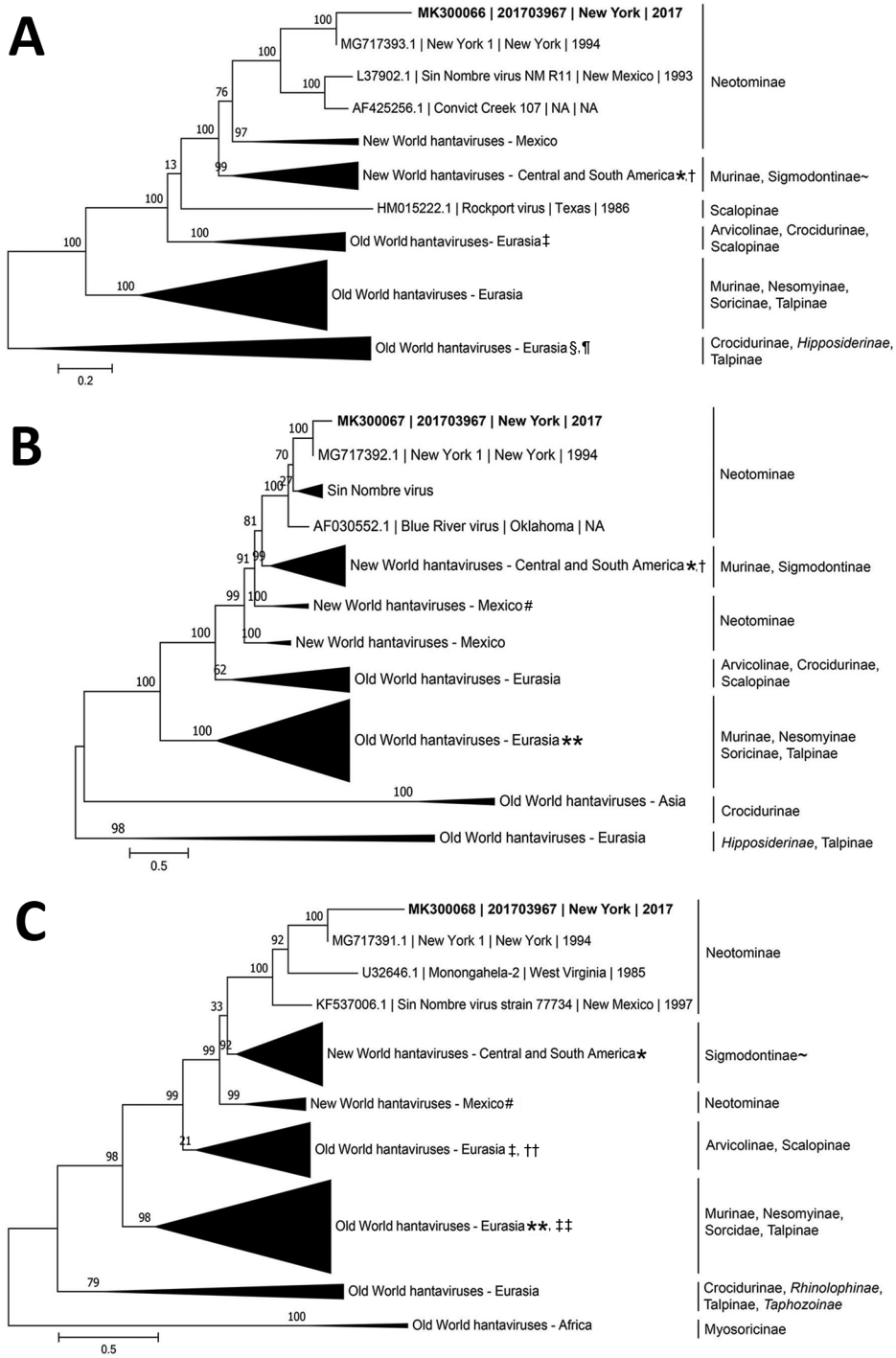

Figure. Inference of phylogenetic relationships for A) large, B) medium, and C) small RNA segments of orthohantaviruses by using representative full-genome sequences in study of infection with New York orthohantavirus and associated respiratory failure and multiple cerebral complications. Partial sequences from the case in New York during 2017 (specimen no. 201703967), are indicated in bold (GenBank accession no. MK300066–8). Genome coverage for the 201703967 small, medium, and large RNA segments are 12%, 30%, and 5%, respectively. Evolutionary history was inferred by using a maximum-likelihood method based on the subtree pruning and regrafting model with the general time-reversible plus gamma (n = 4) nucleotide substitution model, and branch support was calculated by using the approximate likelihood ratio test method. Branch lengths are measured in number of nucleotide substitutions per site (scale bars). Clades are collapsed by region for clarity, and clades of interest are annotated with reservoir subfamily. Clades with incomplete reservoir information are annotated with ~, and bat subfamilies are shown in italics. Sequences collected outside a specified geographic region are denoted by a symbol. *Black Creek Canal virus, USA; †Bayou virus, USA; ‡Prospect Hill virus, USA; §Kilimanjaro virus, Tanzania; ¶Uluguru virus, Tanzania; #Limestone Canyon virus, USA; **Sangoussa virus, Guinea; ††Rockport virus, USA; ‡‡Jemez Springs virus, USA.

a partial genome inferred that the virus had a most recent common ancestor with an NYV collected in 1994 from a white-footed mouse from Shelter Island, NY (*3*). Given the inferred evolutionary relationship, our data are consistent with disease transmission likely occurring after contact with excreta from a local rodent. It is unclear if NYV (formerly classified as a distinct species) might have caused the neurologic complications (hydrocephalus and intracranial bleeding) for this case. Neurologic signs and symptoms did not develop for previous cases of infection with NYV (*1*).

Hantavirus pulmonary syndrome is a severe respiratory illness caused by infection with New World hantaviruses (*4*). During 1993–2015, a total of 688 cases of hantavirus pulmonary syndrome were reported in the United States (case-fatality rate 36%) (*5*). We report an orthohantavirus infection that progressed to respiratory failure and renal impairment

on day 4 postonset, which preceded cerebral complications on day 14 postonset. Brain complications, including subarachnoid (*6*), pituitary hemorrhage (*7*), and encephalitis (*8*), with orthohantavirus infections have been reported. The direct effect of the virus into the brain has been demonstrated in an animal model (*9*), which raises the question whether intracranial bleeding for this case-patient was associated with endothelial damage directly from the virus infection.

In conclusion, we report an orthohantavirus infection in New York that caused intracranial bleeding and hydrocephalus that required an emergent surgical intervention. Because orthohantaviruses are endemic to North America and several strains/species have not been fully characterized, it is essential that clinicians recognize and be aware of other clinical manifestations of these infections (e.g., kidney injury), which are often indicators of subsequent complications.

About the Author

Dr. Fernando is an infectious diseases specialist at Stony Brook Southampton Hospital, Southampton, NY. His primary research interest is tropical medicine.

References

1. Nuovo GJ, Simsir A, Steigbigel RT, Kuschner M. Analysis of fatal pulmonary hantaviral infection in New York by reverse transcriptase in situ polymerase chain reaction. Am J Pathol. 1996;148:685–92.
2. Woods C, Palekar R, Kim P, Blythe D, de Senarclens O, Feldman K, et al. Domestically acquired Seoul virus causing hemorrhagic fever with renal syndrome, Maryland, 2008. Clin Infect Dis. 2009;49:e109–12. http://dx.doi.org/10.1086/644742
3. McMullan LK, Albariño CG, Ksiazek TG, Nichol ST, Spiropoulou CF. Complete genome sequences of a hantavirus isolate from New York. Genome Announc. 2018;6:e00188–18. http://dx.doi.org/10.1128/genomeA.00188-18
4. Nichol ST, Spiropoulou CF, Morzunov S, Rollin PE, Ksiazek TG, Feldmann H, et al. Genetic identification of a hantavirus associated with an outbreak of acute respiratory illness. Science. 1993;262:914–7. http://dx.doi.org/10.1126/science.8235615
5. Centers for Disease Control and Prevention. Annual US hantavirus disease and HPS case fatality, 1993–2016 [cited 2018 Nov 30]. https://www.cdc.gov/hantavirus/surveillance/annual-cases.html
6. Xu Z, Xu P, Lei X, Xu Z, Wu Q, Zhang J. Subarachnoid hemorrhage associated with epidemic hemorrhagic fever: a rare case report. Int J Med Sci. 2011;8:640–2. http://dx.doi.org/10.7150/ijms.8.640
7. Hautala T, Hautala N, Mähönen SM, Sironen T, Pääkkö E, Karttunen A, et al. Young male patients are at elevated risk of developing serious central nervous system complications during acute Puumala hantavirus infection. BMC Infect Dis. 2011;11:217. http://dx.doi.org/10.1186/1471-2334-11-217
8. Talamonti L, Padula PJ, Canteli MS, Posner F, Marczeski FP, Weller C. Hantavirus pulmonary syndrome: encephalitis caused by virus Andes. J Neurovirol. 2011;17:189–92. http://dx.doi.org/10.1007/s13365-010-0011-4
9. Shin OS, Song GS, Kumar M, Yanagihara R, Lee HW, Song JW. Hantaviruses induce antiviral and pro-inflammatory innate immune responses in astrocytic cells and the brain. Viral Immunol. 2014;27:256–66. http://dx.doi.org/10.1089/vim.2014.0019

Address for correspondence: Luis A. Marcos, Stony Brook University Health Sciences Center School of Medicine, Internal Medicine, Division of Infectious Disease, 101 Nicolls Rd, Health Science Center T16, Rm 027J, Stony Brook, NY 11794, USA; email: luis.marcos@stonybrookmedicine.edu

Rickettsia japonica Infection after Land Leech Bite, Japan

Eiichiro Sando, Motoi Suzuki, Mitsuya Katayama, Masakatsu Taira, Hiromi Fujita, Koya Ariyoshi

Author affiliations: Kameda Medical Center, Kamogawa, Japan (E. Sando, M. Katayama); Nagasaki University, Nagasaki, Japan (E. Sando, M. Suzuki, K. Ariyoshi); Chiba Prefectural Institute of Public Health, Chiba, Japan (M. Taira); Mahara Institute of Medical Acarology, Anan, Japan (H. Fujita)

DOI: https://doi.org/10.3201/eid2506.181985

We report a case of *Rickettsia japonica* infection in an 81-year-old man in central Japan. The patient had fever, rash, and an eschar but no evidence of a tick bite. His symptoms began 8 days after a land leech bite. The land leech is a potential vector of *R. japonica*.

Japanese spotted fever, a tickborne disease caused by *Rickettsia japonica*, has been reported in Japan, Korea, and China (*1*–*3*). We describe a case of Japanese spotted fever after a land leech (*Haemadipsa zeylanica japonica*) bite.

On August 3, 2016, an 81-year-old man was transported to an emergency department with a 2-day history of fever (temperature of 38°C), staggering, appetite loss, and general malaise. He was undergoing hormonal therapy for prostate cancer and had an indwelling urinary catheter. However, he was fully independent and walked 2 km every day as a tour guide to a mountain road in the southern Boso area of Japan. At admission, he was alert and oriented, with no apparent fever (temperature of 36.8°C). Clinicians observed a nonpruritic, painless rash on his torso and extremities (Figure, panels A, B), including his palms and the soles of his feet. The attending physician thoroughly searched for an eschar and noted only a single nonpruritic, painless lesion on the man's lower abdomen (Figure, panel C). The patient and his family reported that the eschar appeared at the site where a land leech had been attached on July 24, 10

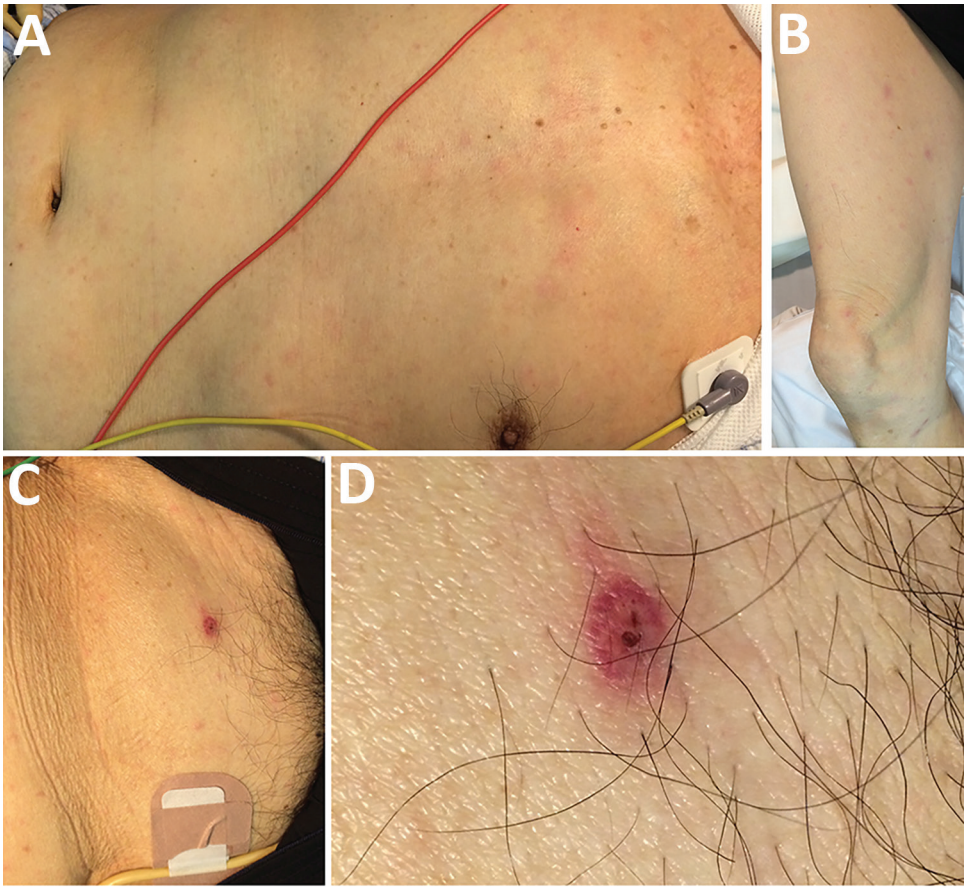

Figure. Patient with *Rickettsia japonica* infection after being bitten by a land leech, Japan. A, B) Erythematous macular rash on the patient's torso (A) and extremities (B); C, D) eschar on the lower abdomen showing an atypical appearance with a relatively well-demarcated boundary of erythema with a tiny scab.

days before admission, and that the site bled when the leech was removed. They denied any tick bite.

Notable laboratory data included low platelet count (102,000/μL), slightly elevated aspartate aminotransferase (52 IU/L), elevated lactate dehydrogenase (468 IU/L), and elevated C-reactive protein (5.37 mg/dL). Urinalysis was positive for protein and occult blood. Chest radiograph and electrocardiogram findings were unremarkable.

We suspected rickettsial disease because the patient had typical symptoms, including fever, rash, and eschar, and a history of walking in the mountains. We sent his blood samples and the crust of the eschar to the Chiba Prefectural Institute of Public Health (Chiba, Japan) for indirect immunofluorescence and PCR assays (Appendix, https://wwwnc.cdc.gov/EID/article/25/6/18-1985-App1.pdf). In addition, the blood samples were tested at the Mahara Institute of Medical Acarology (Anan, Japan) with indirect immunoperoxidase assay to identify 6 *Orientia tsutsugamushi* serotypes: Kato, Karp, Gilliam, Irie/Kawasaki, Hirano/Kuroki, and Shimokoshi.

The patient received 100 mg of minocycline intravenously every 12 hours for 7 days and received the same dose orally for 1 day after he was discharged. His symptoms promptly resolved without any complications.

Paired serum antibody titers against *R. japonica* in the acute phase (day 1 of treatment) were IgM <1:20 and IgG <1:20 but increased to IgM 1:1,280 and IgG 1:10,240 in the convalescent phase (day 21 of treatment). The samples tested for *O. tsutsugamushi* were negative for all serology except IgG titer against serotypes Karp (1:160) and Hirano/Kuroki (1:80) in both acute and convalescent phases, indicating past infection with *O. tsutsugamushi*. Target genes obtained from the eschar were identical with *R. japonica*; the 17-kDa protein had 100% sequence homology and *gltA* 99.5% (Appendix Figures 1, 2).

We detected *R. japonica* from the eschar formed after a land leech bite in a patient without evidence of a tick bite. Most patients with rickettsial diseases, such as Japanese spotted fever and scrub typhus, do not notice a tick or mite bite (*4*), but a leech bite is easy to detect because the site bleeds for an extended time due to hirudin in leech saliva. We conducted a thorough physical examination to check for tick bites but found no additional eschar on this patient. In our experience (*4*), a typical eschar caused by a tick or mite bite appears as a circular crater with a scab, red flare with an indistinct border, and desquamation. However, the eschar in this case was atypical because of a relatively well-

demarcated boundary of erythema with a tiny scab (Figure, panel D).

A new species of *Rickettsia* was detected from leeches in Japan (*5*,*6*). Furthermore, certain leech species, parasitizing frogs or fish, can complete the vertical transmission of *Rickettsia* spp. with possible horizontal transmission (*6*). The leech is reported to be a potential vector for human rickettsial infections (*7*,*8*). Slesak et al. described the case of a 39-year-old woman with *R. felis* infection confirmed by eschar PCR after a leech bite in northern Laos (*7*). Balcells et al. reported the case of a 54-year-old man with scrub typhus–like illness after a leech bite in southern Chile (*8*). In our previous study (*4*), 13% (4/31) of patients with Japanese spotted fever and 2% (4/188) of patients with scrub typhus diagnosed by serologic tests had a history of land leech bite before the symptom onset.

Our report is limited because we did not have the land leech for testing by PCR. The patient might have had rickettsia on his skin and then been inoculated by the leech bite or by scratching after the bite (*7*). Further investigations, including an experimental model, are needed to support the potential role of leeches in the transmission of *R. japonica* and other *Rickettsia* spp.

Acknowledgments

We thank the patient, who provided written consent for publishing this case report and the accompanying images; Satoshi Kobayashi for the patient's care and his assistance in collecting samples; and Shuji Ando for critical comments.

This study was supported by the Japan Agency for Medical Research and Development under grant no. JP18fk0108068.

About the Author

Dr. Sando is a general physician at the Kameda Medical Center, Kamogawa, Japan, and an assistant professor at the Institute of Tropical Medicine, Nagasaki University, Nagasaki, Japan. His primary research interest is rickettsial diseases.

References

1. National Institute of Infectious Disease–Japan. Scrub typhus and Japanese spotted fever in Japan 2007–2016. Infectious Agent Surveillance Report. Tokyo: The Institute; 2017.
2. Chung M-H, Lee S-H, Kim M-J, Lee J-H, Kim E-S, Lee J-S, et al. Japanese spotted fever, South Korea. Emerg Infect Dis. 2006;12:1122–4. http://dx.doi.org/10.3201/eid1207.051372
3. Lu Q, Yu J, Yu L, Zhang Y, Chen Y, Lin M, et al. *Rickettsia japonica* infections in humans, Zhejiang Province, China, 2015. Emerg Infect Dis. 2018;24:2077–9. http://dx.doi.org/10.3201/eid2411.170044
4. Sando E, Suzuki M, Katoh S, Fujita H, Taira M, Yaegashi M, et al. Distinguishing Japanese spotted fever and scrub typhus, Central Japan, 2004–2015. Emerg Infect Dis. 2018;24:1633–41. http://dx.doi.org/10.3201/eid2409.171436
5. Kikuchi Y, Sameshima S, Kitade O, Kojima J, Fukatsu T. Novel clade of *Rickettsia* spp. from leeches. Appl Environ Microbiol. 2002;68:999–1004. http://dx.doi.org/10.1128/AEM.68.2.999-1004.2002
6. Kikuchi Y, Fukatsu T. *Rickettsia* infection in natural leech populations. Microb Ecol. 2005;49:265–71. http://dx.doi.org/10.1007/s00248-004-0140-5
7. Slesak G, Inthalath S, Dittrich S, Paris DH, Newton PN. Leeches as further potential vectors for rickettsial infections. Proc Natl Acad Sci U S A. 2015;112:E6593–4. http://dx.doi.org/10.1073/pnas.1515229112
8. Balcells ME, Rabagliati R, García P, Poggi H, Oddó D, Concha M, et al. Endemic scrub typhus-like illness, Chile. Emerg Infect Dis. 2011;17:1659–63. http://dx.doi.org/10.3201/eid1709.100960

Address for correspondence: Eiichiro Sando, Department of Clinical Medicine, Institute of Tropical Medicine, Nagasaki University, Nagasaki, Japan; email: eiichiro-ymn@umin.ac.jp

Schistosome Interactions within the *Schistosoma haematobium* Group, Malawi

Bonnie L. Webster, Mohammad H. Alharbi, Sekeleghe Kayuni, Peter Makaula, Fenella Halstead, Rosie Christiansen, Lazarus Juziwelo, Michelle C. Stanton, E. James LaCourse, David Rollinson, Khumbo Kalua, J. Russell Stothard

Author affiliations: Natural History Museum, London, UK (B.L. Webster, D. Rollinson); Ministry of Health, Qassim, Saudi Arabia (M.H. Alharbi); Liverpool School of Tropical Medicine, Liverpool, UK (M.H. Alharbi, S. Kayuni, F. Halstead, R. Christiansen, E.J. LaCourse, J.R. Stothard); Medical Aid Society of Malawi, Blantyre, Malawi (S. Kayuni); Research for Health Environment and Development, Mangochi, Malawi (P. Makaula); Ministry of Health, Lilongwe, Malawi (L. Juziwelo); Lancaster University Medical School, Lancaster, UK (M.C. Stanton); Lions Sight First Eye Hospital, Blantyre (K. Kalua)

DOI: https://doi.org/10.3201/eid2506.190020

Molecular analysis of atypical schistosome eggs retrieved from children in Malawi revealed genetic interactions occurring between human (*Schistosoma haematobium*) and livestock (*S. mattheei* and *S. bovis*) schistosome species. Detection of hybrid schistosomes adds a notable new perspective to the epidemiology and control of urogenital schistosomiasis in central Africa.

Urogenital schistosomiasis is a waterborne disease transmitted by certain freshwater snails that occurs throughout much of sub-Saharan Africa. Until recently, this disease was attributed solely to *Schistosoma haematobium*, which was considered to have limited zoonotic potential (*1*). However, genetic analysis of natural infections with noninvasive larval sampling (*2*) has provided new evidence. In West Africa, for example, species interactions with hybrid combinations of *S. haematobium* and the bovine or ovine species of *S. bovis* and *S. curassoni* are commonly encountered in humans and snails (*3*). Although key biologic features of hybrids may not always be apparent, the risk for zoonotic transmission along with enhanced definitive and intermediate host compatibilities needs investigation (*2*,*3*). The recent emergence and persistent transmission of *S. haematobium–bovis* hybrids on the Mediterranean island of Corsica (*4*) demonstrates the public health impact of such genetic introgression.

Genetic analysis of *S. haematobium* group species in central and southern Africa is a high priority. Atypical egg morphologies suggest a capacity for natural hybridization of *S. haematobium* with the bovine species *S. mattheei*, later confirmed with biochemical markers and experimental infections demonstrating viable progeny (*3*). During ongoing surveillance of urogenital schistosomiasis in Chikhwawa District, Malawi, we encountered atypical *S. haematobium* eggs in urine samples from several infected children (*5*). We report the further genetic characterization of atypical eggs collected from epidemiologic surveys of children within Chikhawa, Nsanje, and Mangochi Districts (Figure, panel A).

Ethics approvals for the epidemiological surveys were granted by Liverpool School of Tropical Medicine, College of Medicine, Malawi, and Ministry of Health and Population, Malawi. All children found infected were treatment with praziquantel.

We filtered schistosome eggs from the urine of infected children, then photographed and measured them before storing them on Whatman FTA cards for molecular analysis (*2*). We alkaline-eluted and genotyped DNA from individual eggs using both the mitochondrial cytochrome oxidase subunit 1 (*cox*1) and the nuclear ribosomal internal transcribed spacer (rITS) DNA regions (*2*) (Appendix Table, https://wwwnc.cdc.gov/EID/article/25/6/19-0020-App1.pdf). In addition, for the samples from Mangochi District, we analyzed a partial region (300-bp) of the nuclear ribosomal 18S DNA to confirm the presence of *S. mattheei* nuclear DNA (*2*,*6*) (Appendix).

Of 6 atypical eggs from Chikhwawa, all had a pure *S. haematobium* genetic profile (Figure, panels B, C). Of 19 eggs from Nsanje, 18 had a pure *S. haematobium* genetic profile; 4 eggs had atypical morphology, but only 1 atypical egg had a discordant genetic profile (i.e., *cox*1 *S. bovis* and rITS *S. haematobium*). Of 20 eggs from Mangochi, 16 typical *S. haematobium* eggs had a pure *S. haematobium* genetic profile, whereas the 4 atypical eggs had the same discordant genetic profiles (*cox*1 *S. mattheei* and rITS *S. haematobium-mattheei*). Inspection of the partial 18S gene

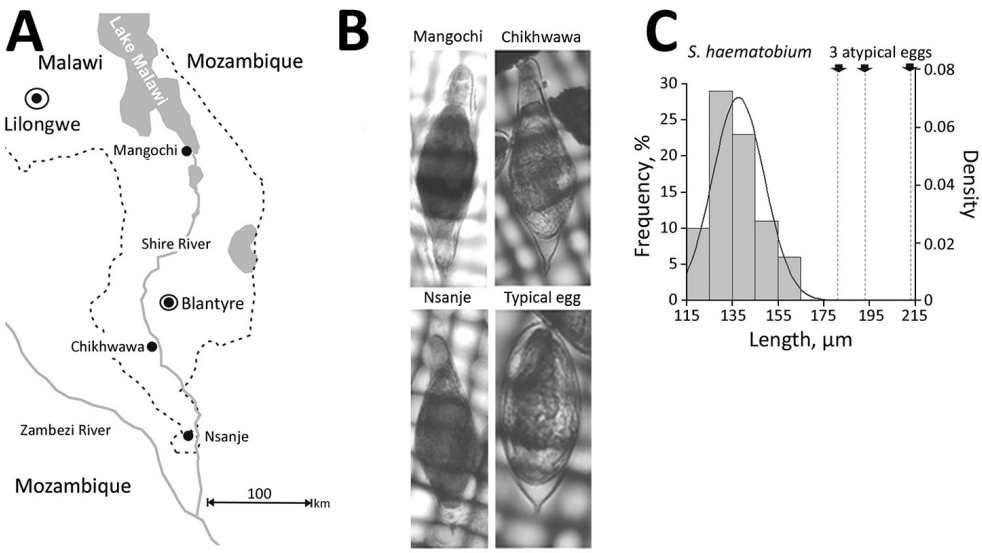

Figure. Investigation of atypical schistosome eggs retrieved from children in Malawi. A) Locations where urine samples containing *Schistosoma haematobium* eggs were collected from children in Mangochi (Samama village, 14°41′74.65″S, 35°21′75.80″E), Chikhwawa (Mpangani village, 16°03′62.99″S, 34°84′10.63″E), and Nsanje (Kastiano village, 16°90′63.98″S, 35°26′65.78″E) districts. Of the children sampled, ≈10% had atypical eggs in their urine, in an approximate atypical:typical ratio of 1:25. Note that the Shire River flows southward from Lake Malawi, linking the 3 sampled locations within the same drainage basin. B) Photomicrographs of a representative atypical egg from each location. Corresponding genotypes assigned for the mitochondrial *cox*1 and nuclear rITS loci: Mangochi, *cox*1 *S. mattheei* and rITS *S. haematobium-mattheei*; Chikhwawa, *cox*1 and rITS *S. haematobium*; Nsanje, *cox*1 *S. bovis* and rITS *S. haematobium*. A typical *S. haematobium* egg is shown for comparison. Sizes are not to scale. C) Histogram of length measurements for 83 typical *S. haematobium* eggs collected from Nsanje. Solid line indicates the associated density distribution. The mean length of this sample of typical eggs was 135 ± 28 µm (1 SD), with minimum 86 µm and maximum 180 µm. Arrows with dashed lines at right indicate the length of the 3 atypical eggs, which fall well outside the range of length variation of the 83 typical eggs as measured.

sequence confirmed *S. haematobium–mattheei* hybrids (Appendix). We deposited all sequence data into GenBank (accession nos. MK358841–MK358858).

Our genetic analysis demonstrated the presence of *S. haematobium* group hybrids in Malawi as introgressed forms of *S. haematobium–mattheei* and *S. haematobium–bovis*. Of note, an unusual egg morphology may not always correspond with the ability to detect introgression with the current combination of genetic markers used (*6*; Appendix). As described by Boon et al., successive backcrossings of hybrid progeny may obscure our ability to detect ancestral introgression, and the development of a wider panel of nuclear genetic markers is needed (*6*). Nonetheless, detection of these 2 hybrid schistosomes strongly suggests interactions of *S. haematobium* with the ungulate schistosomes *S. mattheei* and *S. bovis*. That *S. bovis* has not been reported in Malawi implies a changing species dynamic with possible zoonotic transmission along the drainage basin of Lake Malawi, adding a new dimension to the epidemiology and control of urogenital schistosomiasis in Malawi (*7*).

Because we did not attempt miracidial hatching during this study, we cannot confirm that these hybrids or introgressed forms are fully viable in autochthonous natural transmission. However, the process of ancestral introgression with subsequent natural selection may help explain unexpected shifts in local snail–schistosome relationships (e.g., the changing compatibility of *Bulinus nyassanus* snails in Lake Malawi with *S. haematobium* schistosomes) (*8*). Further studies are needed to better characterize schistosomes involved in human infection, investigate more thoroughly any zoonotic potential, and assess all possible combinations of interspecies introgressions.

Molecular evidence for ancestral hybridization between *S. haematobium* and *S. mansoni* schistosomes was presented recently (*9*); given autochthonous transmission of intestinal schistosomiasis in Lake Malawi (*10*), there may be sufficient epidemiologic opportunity for other introgression events to occur with the hybrids we report. We therefore advise heightened concurrent surveillance of urogenital and intestinal schistosomiasis, entailing a One-Health approach with molecular vigilance for interspecies interactions along with phenotypic assessments for any altered host pathogenicity or susceptibility to praziquantel treatment. Detection of the hybrid schistosomes we report adds a new perspective to the epidemiology and control of urogenital schistosomiasis in central Africa.

Acknowledgments

We are particularly grateful to the local health and education authorities of Malawi, district teachers, and community health workers involved in schistosome surveys in Chikhwawa, Nsanje, and Mangochi. We thank Jahashi Nzalawahe for assistance with measurements and analysis of schistosome egg morphology. M.H.A. is funded by a PhD scholarship from the Ministry of Health, Kingdom of Saudi Arabia. S.K. received a scholarship from Commonwealth Scholarship Commission and a research fellowship from the African Research Network for Neglected Tropical Diseases (ARNTD).

About the Author

Dr. Webster is a researcher with the Natural History Museum, London, UK. She has specific expertise in medical helminthology and a longstanding interest in studies of schistosome hybridization in both natural and experimental settings.

References

1. Rollinson D. A wake-up call for urinary schistosomiasis: reconciling research effort with public health importance. Parasitology. 2009;136:1593–610. http://dx.doi.org/10.1017/S0031182009990552
2. Huyse T, Webster BL, Geldof S, Stothard JR, Diaw OT, Polman K, et al. Bidirectional introgressive hybridization between a cattle and human schistosome species. PLoS Pathog. 2009;5:e1000571. http://dx.doi.org/10.1371/journal.ppat.1000571
3. Leger E, Webster JP. Hybridizations within the genus *Schistosoma*: implications for evolution, epidemiology and control. Parasitology. 2017;144:65–80. http://dx.doi.org/10.1017/S0031182016001190
4. Boissier J, Grech-Angelini S, Webster BL, Allienne JF, Huyse T, Mas-Coma S, et al. Outbreak of urogenital schistosomiasis in Corsica (France): an epidemiological case study. Lancet Infect Dis. 2016;16:971–9. http://dx.doi.org/10.1016/S1473-3099(16)00175-4
5. Poole H, Terlouw DJ, Naunje A, Mzembe K, Stanton M, Betson M, et al. Schistosomiasis in pre-school-age children and their mothers in Chikhwawa district, Malawi with notes on characterization of schistosomes and snails. Parasit Vectors. 2014; 7:153. http://dx.doi.org/10.1186/1756-3305-7-153
6. Boon NAM, Fannes W, Rombouts S, Polman K, Volckaert FAM, Huyse T. Detecting hybridization in African schistosome species: does egg morphology complement molecular species identification? Parasitology. 2017;144:954–64. http://dx.doi.org/10.1017/S0031182017000087
7. Makaula P, Sadalaki JR, Muula AS, Kayuni S, Jemu S, Bloch P. Schistosomiasis in Malawi: a systematic review. Parasit Vectors. 2014;7:570. http://dx.doi.org/10.1186/s13071-014-0570-y
8. Stauffer JR Jr, Madsen H, Webster B, Black K, Rollinson D, Konings A. *Schistosoma haematobium* in Lake Malaŵi: susceptibility and molecular diversity of the snail hosts *Bulinus globosus* and *B. nyassanus.* J Helminthol. 2008;82:377–82. http://dx.doi.org/10.1017/S0022149X08056290
9. Le Govic Y, Kincaid-Smith J, Allienne JF, Rey O, de Gentile L, Boissier J. *Schistosoma haematobium–Schistosoma mansoni* hybrid parasite in migrant boy, France, 2017. Emerg Infect Dis. 2019;25:365–7. http://dx.doi.org/10.3201/eid2502.172028
10. Alharbi MH, Condemine C, Christiansen R, LaCourse EJ, Makaula P, Stanton MC, et al. *Biomphalaria pfeifferi* snails and intestinal schistosomiasis in Lake Malawi, Africa, 2017–2018. Emerg Infect Dis. 2019;25:613–5. http://dx.doi.org/10.3201/eid2503.181601

Address for correspondence: J. Russell Stothard, Liverpool School of Tropical Medicine, Pembroke Pl, Liverpool, Merseyside L3 5QA UK; email: russell.stothard@lstmed.ac.uk

Hepatitis Rebound after Infection with Yellow Fever Virus

Blandine Denis, David Chirio, Diane Ponscarme, Ségolène Brichler, Nathalie Colin de Verdière, François Simon, Jean-Michel Molina

Author affiliations: Hôpital Saint Louis, Paris, France (B. Denis, D. Chirio, D. Ponscarme, N. Colin de Verdière, F. Simon, J.-M. Molina); Hôpital Avicenne, Bobigny, France (S. Brichler); Université Paris Diderot, Sorbonne Cité, Paris (F. Simon, J.-M. Molina)

DOI: https://doi.org/10.3201/eid2506.190096

In 2018, yellow fever with hepatitis was diagnosed for 2 unvaccinated travelers returning to France from Brazil. Hepatitis persisted for >6 months; liver enzyme levels again increased 2 months after disease onset with no detection of yellow fever virus RNA or other pathogens. Persistent hepatitis with hepatic cytolysis rebound probably resulted from immune response.

Although most cases of yellow fever are asymptomatic, some lead to severe liver disease, caused by liver cell cytolysis. In February 2018, yellow fever with hepatitis was diagnosed for 2 patients returning to France after travel to Brazil (Rio de Janeiro coastal area, including the island of Ilha Grande). Both were previously healthy, HIV-negative men, 38 (patient A) and 28 (patient B) years of age; neither had been vaccinated against yellow fever. Their first signs and symptoms occurred 7 (patient B) and 8 (patient A) days after arrival in Brazil, and they sought care in France on day 7 of symptom onset.

Each patient had fever, jaundice, asthenia, thrombocytopenia (57,000 [patient A] and 61,000 [patient B] platelets/mm^3; reference range >150,000 platelets/mm^3), and hepatitis (alanine aminotransferase [ALT] >5,000 IU/L and aspartate aminotransferase [AST] >3,400 IU/L; reference range <40 IU/L). One patient also had acute renal failure (serum creatinine 170 µmol/L). For both patients, malaria blood smear was negative, IgM against yellow fever virus was detected on 3 evaluations by IgM capture ELISA, and seroconversion was confirmed by detection of yellow fever virus IgG by indirect ELISA at the National Reference Center for Arboviruses (HIA Laveran, Marseille, France). Results of testing for other viruses (dengue [4 serotypes]; chikungunya; Zika; hepatitis A, B, C, E; cytomegalovirus; and Epstein-Barr) were negative. The patients showed no sign of bleeding and were discharged 2 (patient B) and 3 (patient A) days after admission, after thrombocytopenia and liver enzyme elevations had improved.

The patients remained asthenic for ≈1 month with no other symptoms. Elevated bilirubin levels persisted 6 weeks after discharge for patient A and 8 weeks for patient B; levels even increased in patient A (up to 164 µmol/L on day 14 of symptom onset). Within 3 weeks, liver cytolysis decreased to ≤4 times the upper limit of the reference range. However, ≈2 months after symptom onset, liver enzyme levels again increased (ALT >1,000 IU/L) (Figure). For each patient, rebound ALT levels were higher than rebound AST levels (patient A: ALT 1,046, AST 301 IU/L; patient B: ALT 1,410, AST 483 IU/L). During the rebound period, yellow fever RNA detection by PCR remained negative. Conversely, for each patient, yellow fever virus neutralizing activities were detected in plasma by a recently developed highly specific test based on a pseudoviral vector releasing pseudotype yellow fever virus–like particles (*1*). Serum from each patient exhibited 100% inhibitory activity against yellow fever virus particles (*1*). Deep sequencing performed on plasma and urine remained negative for eukaryotic pathogens (*2*). Also negative were serum autoimmune antibodies (antinuclear, anti–smooth muscle, anti–liver-kidney microsomal type 1, and antimitochondrial) and anti–soluble liver antigen. For patient B, liver enzyme levels returned to reference range

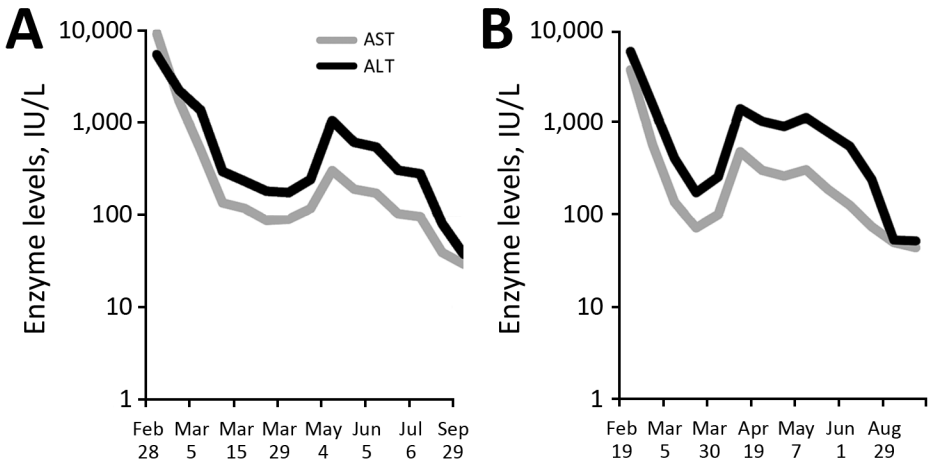

Figure. Time course for liver enzyme levels in 2 patients with yellow fever, France, 2018. A) Patient A; B) patient B. AST, aspartate aminotransferase; ALT, alanine aminotransferase.

within 6 months; for patient A, AST returned to reference range within 6 months and ALT within 7 months (Figure). Because the patients were asymptomatic at the time of rebound, we did not perform liver biopsies.

Each patient had acquired yellow fever in Ilha Grande, Brazil, as had 11 other nonvaccinated travelers to Brazil in 2018 (*3*), before vaccination against yellow fever was recommended for travelers to the states of São Paulo and Rio de Janeiro. For each of the 2 patients reported here, illness was similar: relatively mild disease despite jaundice and severe cytolysis (AST >1,200 IU/L, ALT >1,500 IU/L at diagnosis), known risk factors associated with higher mortality rates (*4*). For each patient, hepatic cytolysis rebounded ≈2 months after the initial peak, with no clinical signs or symptoms and no detection of other pathogens. Previous reports have described liver cytolysis during yellow fever as being acute, decreasing rapidly on days 9–15, then reaching the upper limits of the reference range on day 16, and some persisting up to 2 months (*5*). Liver biopsy results have shown that liver lesions can persist up to 2 months (*6*).

We report persistent hepatitis over 6 months with a rebound of hepatic cytolysis after 2 months. In comparison, relapse has been described for ≈3% of patients with hepatitis A (*7*) with a biphasic peak of ALT (*7,8*) and detection of hepatitis A virus RNA in plasma (*9*), both 4–8 weeks after the first peak.

In terms of the cause of the hepatic cytolysis rebound in the 2 patients reported here, neither had taken a hepatotoxic drug during the rebound period, and results of deep sequencing for eukaryotic pathogens and autoimmune antibodies were negative. However, major yellow fever virus neutralizing activities were detected. Thus, the rebound could be attributed to host immune response to yellow fever virus rather than to another pathogen or to direct effects of the virus itself. In summary, our results show that yellow fever can induce persistent hepatitis with a rebound of liver cytolysis, probably an immune response to the yellow fever virus.

About the Author

Dr. Denis is an infectious diseases clinician working in the tropical and infectious diseases department at St. Louis Hospital, Paris, France. Her research interests focus on epidemiology and infections in immunocompromised patients.

References

1. Mercier-Delarue S, Durier C, Colin de Verdière N, Poveda JD, Meiffrédy V, Fernandez Garcia MD, et al. Screening test for neutralizing antibodies against yellow fever virus, based on a flavivirus pseudotype. PLoS One. 2017;12:e0177882. http://dx.doi.org/10.1371/journal.pone.0177882
2. Naccache SN, Federman S, Veeraraghavan N, Zaharia M, Lee D, Samayoa E, et al. A cloud-compatible bioinformatics pipeline for ultrarapid pathogen identification from next-generation sequencing of clinical samples. Genome Res. 2014;24:1180–92. 10.1101/gr.171934.113 http://dx.doi.org/10.1101/gr.171934.113
3. Oliosi E, Serero Corcos C, Barroso PF, Bleibtreu A, Grard G, De Filippis BAM, et al. Yellow fever in two unvaccinated French tourists to Brazil, January and March, 2018. Euro Surveill. 2018;23. http://dx.doi.org/10.2807/1560-7917.ES.2018.23.21.1800240
4. Tuboi SH, Costa ZG, da Costa Vasconcelos PF, Hatch D. Clinical and epidemiological characteristics of yellow fever in Brazil: analysis of reported cases 1998-2002. Trans R Soc Trop Med Hyg. 2007;101:169–75. http://dx.doi.org/10.1016/j.trstmh.2006.04.001
5. Oudart JL, Rey M. Proteinuria, proteinaemia, and serum transaminase activity in 23 confirmed cases of yellow fever [in French]. Bull World Health Organ. 1970;42:95–102.
6. Francis TI, Moore DL, Edington GM, Smith JA. A clinicopathological study of human yellow fever. Bull World Health Organ. 1972;46:659–67.
7. Jelić O, Fornet-Sapcevski J, Kovacevíc L, Pandak N, Jelić D. Recurrences of viral hepatitis A [in Croatian]. Acta Med Iugosl. 1990;44:565–76.
8. Sook-Hyang Jeong Hyo-Suk Lee. Hepatitis A: clinical manifestations and management. Intervirology. 2010;53:15–19.
9. Sagnelli E, Coppola N, Marrocco C, Onofrio M, Scarano F, Marotta A, et al. HAV replication in acute hepatitis with typical and atypical clinical course. J Med Virol. 2003;71:1–6. http://dx.doi.org/10.1002/jmv.10455

Address for correspondence: Blandine Denis, Hôpital Saint Louis, Service de Maladies Infectieuses et Tropicales, 1 Ave Claude Vellefaux, Paris 75010, France; email: blandine.denis@aphp.fr

Comparative Analysis of Whole-Genome Sequence of African Swine Fever Virus Belgium 2018/1

Jan H. Forth, Marylène Tignon, Ann Brigitte Cay, Leonie F. Forth, Dirk Höper, Sandra Blome, Martin Beer

Author affiliations: Friedrich-Loeffler-Institut, Greifswald, Germany (J.H. Forth, L.F. Forth, D. Höper, S. Blome, M. Beer); Sciensano, Brussels, Belgium (M. Tignon, A.B. Cay)

DOI: https://doi.org/10.3201/eid2506.190286

We analyzed the whole-genome sequence of African swine fever virus Belgium 2018/1. The strain fits into the European genotype II (>99.98% identity). The high-coverage sequence revealed 15 differences compared with an improved African swine fever virus Georgia 2007/1 sequence. However, in the absence of genetic markers, no spatial or temporal correlations could be defined.

African swine fever (ASF) is one of the most pathogenic viral diseases of swine leading to clinical and pathomorphological signs of a viral hemorrhagic fever (*1*). In 2007, ASF was introduced into Georgia (*2*) and thereafter into numerous eastern European and European Union (EU) countries (*3*), as well as Asia (China, Mongolia, and Vietnam) (World Organization for Animal Health–World Animal Health Information database, http://www.oie.int/wahis_2/public/wahid.php/Wahidhome/Home/indexcontent, 2019 Feb 21).

In September 2018, the African swine fever virus (ASFV) was introduced into Belgium (*3*,*4*); as of April 28, 2019, 719 cases have been reported by Belgium's Federal Agency for the Safety of the Food Chain (http://www.afsca.be/ppa/actualite/belgique).

Samples from the first 2 cases were taken for analysis to the Belgium National Reference Laboratory for ASF at Sciensano, Brussels, and were later confirmed by the ASF EU Reference Laboratory (EURL) in Valdeolmos, Spain. Partial sequencing at the EURL revealed a p72 genotype II with CVR-1, IGR-2, and MGF1 variants. Initial assessments of virus type and epidemiology were published by Gariglianey et al. (*4*) to share the data without delay. Subsequently, samples were transferred to the Friedrich-Loeffler-Institut, Greifswald, Germany, for whole-genome sequencing.

We prepared samples and sequenced them on an Illumina MiSeq (https://www.illumina.com), as previously described (*5*). In addition, we enriched DNA libraries for Illumina sequencing for ASFV specific target sequences using an ASFV-specific myBaits kit (Arbor Biosciences, https://arborbiosci.com). We analyzed the resulting sequence data by mapping against an improved ASFV Georgia 2007/1 sequence (International Nucleotide Sequence Database Collaboration accession no. FR682468.2) using Newbler 3.0 software (*6*); we assembled the identified ASFV-specific reads using SPAdes 3.13.0 (*7*).

For the assembly of the inverted terminal repeat (ITR) regions, we mapped the reads against the individual ASFV Georgia 2007/1 ITR regions using Newbler and manually assembled them with the ASFV Belgium 2018/1 sequence in Geneious 11.1.5 (Biomatters, https://www.geneious.com). For validation, we mapped all reads along the final contig using Newbler; the result was a median unique depth of 292 with an interquartile range of 42. We annotated the sequence according to the improved ASFV Georgia 2007/1 sequence, using Glimmer3 in Geneious. We aligned different available ASFV whole-genome sequences using MAFFT 7.388, and we performed a phylogenetic analysis using IQ-TREE v1.6.5 (*8,9*). The whole-genome sequence is available from the International Nucleotide Sequence Database Collaboration databases under study accession no. PRJEB31287 and sequence accession no. LR536725.

The ASFV Belgium 2018/1 whole-genome sequence has a length of 190,599 bp. Comparison with the improved ASFV Georgia 2007/1 sequence revealed 15 differences, for an overall sequence identity of 99.98% at the nucleotide level. The detected differences included 4 nucleotide transitions, 5 nucleotide transversions, 5 changes in homopolymer regions, and 1 integration of a repeat into a previously described variable intergenic region (*10*) (Table).

Altogether, 4 differences in annotated genes are nonsynonymous; 2 cause a frameshift, thereby truncating the MGF 110–1L gene and changing the amino acid sequence of the DP60R protein; and 9 differences were identified in noncoding regions (Table). The differences in the ITR regions must be viewed carefully because of the low coverage in these particular parts of the genome, but the differences in the core regions are well supported by the sequencing data (Table). The differences at the specific positions 7,061; 44,586; 134,524; and 170,827 were also identified in the ASFV-SY2018 (China), Estonia 2014, Kashino 04/13 (Russia), and Pol 16/17 (Poland) sequences, and position 170,827 also in ASFV strain Odintsovo_02/14 (Russia). Further genetic differences could be identified in 7 so-called poly G/C regions. Whether these are artifacts originating from sequencing any of the analyzed genomes or pose real differences remains to be determined by the analysis of further sequences from Belgium and other countries, which is in progress.

Finally, the alignment of all publicly available eastern European whole-genome sequences, as well as ASFV-China, shows that all these genomes are nearly identical with identities of more than 99.9% (Appendix Figure, http://wwwnc.cdc.gov/EID/article/25/6/19-0286-App1.pdf).

In conclusion, we provide a whole-genome analysis of ASFV from Belgium, which could show a high overall identity to recent ASFV strains from eastern Europe and China. We also identified locations showing differences from ASFV Georgia 2007/1 in single nucleotides, as well as a previously described repeat insertion. However, because the low mutation rate and the corresponding high genetic stability of the eastern European ASFV strains have hindered the definition of reliable genetic markers thus far, the currently available whole-genome information does not allow for further statements regarding correlations in space and time, and does not provide enough evidence for a more detailed mapping of strain origin.

Although MGF110 was assigned a possible function in preparing the endoplasmic reticulum for viral morphogenesis (*11*), in the absence of any observations regarding virus attenuation in the field, no conclusion can be drawn on the effect of the observed differences. Therefore, further in vitro and in vivo characterizations using the ASFV Belgium 2018/1 isolate are needed.

In the future, more high-quality whole-genome ASFV sequences might allow identification of genetic markers that could aid high-resolution molecular epidemiology. Coordinated efforts to improve data sharing, together

Table. Differences in the whole-genome sequence of ASFV Belgium2018/1 and the improved ASFV Georgia2007/1 reference genome*

Position	Type	Difference	ASFV Georgia 2007/1†	ASFV Belgium 2018/1†	Coverage	Gene	Synonymous/ nonsynonymous	ORF change
121	Transversion	G121C	AAGAT	AA**C**AT	44	ITR	NA	NA
129	Transversion	A129T	AAATA	AA**T**TA	47	ITR	NA	NA
479	Variation	+T	9 × T	10 × T	767	ITR	NA	NA
1393	Variation	+C	9 × C	10 × C	1375	NA	NA	NA
6786	Variation	–T	9 × T	8 × T	1755	NA	NA	NA
7061	Transition	C7061T	CCCAG	CC**T**AG	1556	MGF 110–1L	Trp197Stop	Shortened by 18 codons
15688	Variation	+3C	17 × C	20 × C	127	MGF 110–13Lb	Frameshift	Enlarged by 1 codon
17640	Variation	+2G	10 × G	12 × G	1117	NA	NA	NA
17854	Variation	+G	9 × G	10 × G	1304	NA	NA	NA
19807	Variation	–G	7 × G	6 × G	1238	NA	NA	NA
20017	Variation	–2G	16 x G	14 × G	832	ASFV G ACD 00350	Frameshift	Truncation
21815	Variation	+2G	9 × G	11 × G	1184	NA	NA	NA
27439	Variation	–T	10 × T	9 × T	1895	NA	NA	NA
44586	Transition	A44586G	TGAAA	TG**G**AA	1292	MGF 505–9R	Lys323Glu	NA
73282	Variation	–T	9 × T	8 × T	1241	NA	NA	NA
134524	Transition	T134524C	CATTT	CA**C**TT	1665	NP419L	Asp414Ser	NA
145080	Transition	G145080A	GAGGC	GA**A**GC	1266	D117L	Pro84Leu	NA
170827	Transversion	T170827A	GATGG	GA**A**GG	1263	I267L	Ile195Phe	NA
190138	Variation	+A	9 × A	10 × A	3021	DP60R	Frameshift	22 changed codons
173402	Repeat integration	+TATATAG GAA	NA	+TATATAGG AA	1731	NA	NA	NA
190478	Transversion	T190478A	TATTT	TA**A**TT	49	ITR	NA	NA
190486	Transversion	C190486G	ATCTT	AT**G**TT	49	ITR	NA	NA

*Differences are show in bold and underlined. ASFV, African swine fever virus; ITR, inverted terminal repeat; NA, not applicable; ORF, open reading frame.
†International Nucleotide Sequence Database Collaboration accession nos: ASFV Georgia 2007/1, FR682468.2; ASFV Belgium 2018/1, LR536725.

with harmonized protocols under quality assurance, are of utmost importance to interpret results correctly and aid the fight against ASF.

Acknowledgments

The authors thank Patrick Zitzow for excellent technical assistance. The rapid and efficient support from the EURL (M. Arias, Valdeolmos, Spain) was highly appreciated. The authors from Belgium also thank the excellent collaboration with the Walloon Region.

Dr. Forth is a biologist and postdoctoral researcher at the Friedrich-Loeffler-Institut, Greifswald, Germany. His work focuses mainly on ASFV whole-genome sequencing, molecular epidemiology, and virus evolution.

References

1. Alonso C, Borca M, Dixon L, Revilla Y, Rodriguez F, Escribano JM; ICTV Report Consortium. ICTV virus taxonomy profile: Asfarviridae. J Gen Virol. 2018;99:613–4. http://dx.doi.org/10.1099/jgv.0.001049
2. Beltran-Alcrudo D, Lubroth J, Depner K, De La Rocque S. African swine fever in the Caucasus. FAO EMPRES Watch. 2008:1–8 [cited 2019 Mar 22]. http://www.fao.org/docs/eims/upload/242232/ew_caucasus_apr08.pdf</eref>
3. Linden A, Licoppe A, Volpe R, Paternostre J, Lesenfants C, Cassart D, et al. Summer 2018: African swine fever virus hits north-western Europe. Transbound Emerg Dis. 2019;66:54–5. http://dx.doi.org/10.1111/tbed.13047
4. Garigliany M, Desmecht D, Tignon M, Cassart D, Lesenfant C, Paternostre J, et al. Phylogeographic analysis of African swine fever virus, Western Europe, 2018. Emerg Infect Dis. 2019;25:184–6. http://dx.doi.org/10.3201/eid2501.181535
5. Wylezich C, Papa A, Beer M, Höper D. A Versatile sample processing workflow for metagenomic pathogen detection. Sci Rep. 2018;8:13108. http://dx.doi.org/10.1038/s41598-018-31496-1
6. Margulies M, Egholm M, Altman WE, Attiya S, Bader JS, Bemben LA, et al. Genome sequencing in microfabricated high-density picolitre reactors. Nature. 2005;437:376–80. http://dx.doi.org/10.1038/nature03959
7. Antipov D, Korobeynikov A, McLean JS, Pevzner PA. hybridSPAdes: an algorithm for hybrid assembly of short and long reads. Bioinformatics. 2016;32:1009–15. http://dx.doi.org/10.1093/bioinformatics/btv688
8. Nguyen L-T, Schmidt HA, von Haeseler A, Minh BQ. IQ-TREE: a fast and effective stochastic algorithm for estimating maximum-likelihood phylogenies. Mol Biol Evol. 2015;32:268–74. http://dx.doi.org/10.1093/molbev/msu300
9. Kalyaanamoorthy S, Minh BQ, Wong TKF, von Haeseler A, Jermiin LS. ModelFinder: fast model selection for accurate phylogenetic estimates. Nat Methods. 2017;14:587–9. http://dx.doi.org/10.1038/nmeth.4285
10. Goller KV, Malogolovkin AS, Katorkin S, Kolbasov D, Titov I, Höper D, et al. Tandem repeat insertion in African swine fever virus, Russia, 2012. Emerg Infect Dis. 2015;21:731–2. http://dx.doi.org/10.3201/eid2104.141792
11. Netherton C, Rouiller I, Wileman T. The subcellular distribution of multigene family 110 proteins of African swine fever virus is

determined by differences in C-terminal KDEL endoplasmic reticulum retention motifs. J Virol. 2004;78:3710–21. http://dx.doi.org/10.1128/JVI.78.7.3710-3721.2004

Address for correspondence: Martin Beer, Institute of Diagnostic Virology, Friedrich-Loeffler-Institut, Südufer 10, 17489 Greifswald, Germany; email: martin.beer@fli.de

Highly Pathogenic Swine Getah Virus in Blue Foxes, Eastern China, 2017

Ning Shi, Li-Xia Li, Rong-Guang Lu, Xi-Jun Yan, Hao Liu

Author affiliations: Foshan University, Foshan, China (N. Shi, H. Liu); Jilin Wildlife Rescue and Rehabilitation Center, Forestry Department of Jilin Province, Changchun, China (L.-X. Li); Chinese Academy of Agricultural Sciences, Changchun (R.-G. Lu, X.-J. Yan)

DOI: https://doi.org/10.3201/eid2506.181983

We isolated Getah virus from infected foxes in Shandong Province, eastern China. We sequenced the complete Getah virus genome, and phylogenetic analysis revealed a close relationship with a highly pathogenic swine epidemic strain in China. Epidemiologic investigation showed that pigs might play a pivotal role in disease transmission to foxes.

Getah virus (GETV; genus *Alphavirus*, family *Togaviridae*) is a mosquitoborne RNA virus that causes death in young piglets, miscarriage in pregnant sows, and mild illness in horses (*1–3*). Serologic surveys show that the infection might occur in cattle, ducks, and chickens (*4*); some evidence suggests that GETV can infect humans and cause mild fever (*5,6*).

In September 2017, twenty-five 5-month-old blue foxes at a farm in Shandong Province in eastern China showed symptoms of sudden fever, anorexia, and depression; 6 of the 25 animals had onset of neurologic symptoms and died on the third day of illness. We collected blood samples from 45 healthy and 25 ill foxes. We subjected the tissue samples from dead animals, including the brains, lungs, spleens, kidneys, livers, intestines, hearts, and stomachs, to hematoxylin and eosin staining. Microscopic examination confirmed the presence of typical lesions in cerebral cortices with mild neuronal degeneration and inflammatory cell infiltration in vessels, as well as severe hemorrhagic pneumonia, congestion, and hemorrhage with a large number of erythrocytes in the alveolar space (Figure) (*1*). No obvious lesions were found in other organs.

We used supernatants of homogenized brain and lung tissues from each dead fox to inoculate Vero cells, as described previously (*7*). We observed a cytopathogenic effect within 72 hours. We observed numerous spherical, enveloped viral particles, ≈70 nm in diameter, after negative staining in a transmission electron microscope. To identify potential viral pathogens, we performed reverse transcription PCR (RT-PCR) to detect a panel of viruses, including canine distemper virus, canine parvovirus, canine coronavirus, and canine adenovirus. However, we detected none of these classical endemic viruses.

During the investigation, farmers reported that the foxes had been fed on organs from symptomatic pigs. We therefore tested for the presence of African swine fever virus, pseudorabies virus, porcine reproductive and respiratory syndrome virus, classical swine fever virus, Japanese encephalitis virus, porcine circovirus type 2, porcine circovirus type 3, porcine cytomegalovirus, and alphavirus by using the primers for those viruses (Appendix Table 2, https://wwwnc.cdc.gov/EID/article/25/6/18-1983-App1.pdf). RT-PCR using universal primers for alphavirus (M2w-cMw3) produced a 434-bp amplicon when we tested all samples from dead foxes. Sanger sequencing of the amplicon and a BLAST search (https://blast.ncbi.nlm.nih.gov/Blast.cgi) identified the sequence as that of GETV.

To further investigate the epidemic GETV infection, we performed quantitative RT-PCR by using RNA from all fox samples, as described elsewhere (*7*). Lung samples from all 6 dead foxes were positive, whereas only 2 samples from the remaining 19 ill foxes were also positive. None of the samples from healthy foxes were positive (Appendix Tables 1, 3). We measured serologic neutralizing antibodies by using a GETV isolate from a symptomatic fox, as previously described (*8,9*). Results showed no neutralizing antibody (<1:2) in healthy blue foxes (group 1) and variable levels of neutralizing antibodies (1:2 to 1:256) in ill foxes (groups 2–4) (Appendix Table 3). Samples from ill foxes with lower antibody titers had higher copies of RNA (groups 2–4). Spearman correlation analysis revealed a significant negative correlation between antibody titers and viral RNA copy numbers ($r^2 = 0.952$; $p<0.01$).

We obtained the complete genome of the novel GETV SD1709 strain (GenBank accession no. MH106780) by using a conventional RT-PCR method (*10*). SD1709 genome sequence comparisons showed high identity with the porcine GETV strain (HuN1) at the nucleotide (99.6%) and deduced amino acid (99.7%–99.8%) sequences (Appendix Table 4). Furthermore, phylogenetic analysis of the

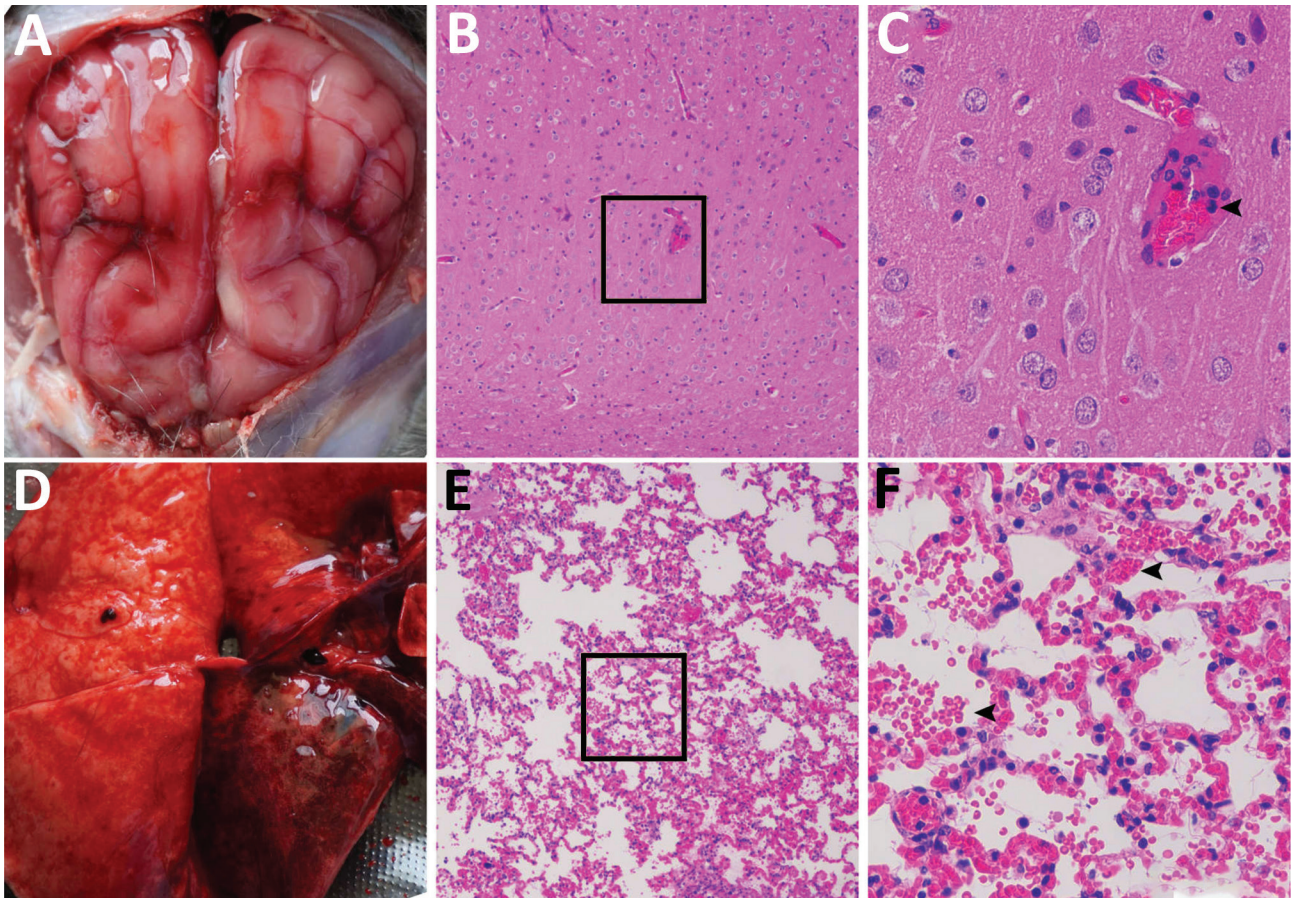

Figure. Dissected brain and lung of a dead fox, collected in 2017 in Shandong Province, eastern China, and histopathologic examination of samples using hematoxylin and eosin staining. A) Brain, showing congestion in the meninx. B) Histologic view of meninx, showing mild neuronal degeneration and inflammatory cell infiltration in vessels. Original magnification ×100. Box indicates area enlarged in panel C. C) A higher magnification view (original magnification ×400) of lesions in panel B, showing inflammatory cell infiltration in a vessel (arrow). D) Lung tissue, showing extensive congestion and hemorrhage. E) Histologic view of lung tissue, showing congestion, hemorrhage, or both, with many erythrocytes in the alveolar space. Original magnification ×100. Box indicates area enlarged in panel F. F) A higher magnification view (original magnification ×400) of tissue lesions in panel E, showing erythrocytes in the alveolar space (arrows).

complete genome and structural protein E2 gene indicated that the SD1709 strain was most similar to the recent epidemic HuN1 strain, which had caused large numbers of piglet deaths, stillbirths, and fetal mummies in southern China in 2017 (*1*) (Appendix Figures 1, 2).

We also detected GETV infection in pig serum samples and in mosquitoes (*Culex tritaeniorhynchus*, *Anopheles sinensis*, and *Armigeres subalbatus*) collected in the same region. The infection rate in pigs detected by quantitative RT-PCR was 20.0% (4/20) and by serum neutralization was 75.0% (15/20). The minimum infection rate in mosquitoes was ≈1.09%; *C. tritaeniorhynchus* mosquitoes had a higher minimum infection rate (2.31%) compared with other mosquito species (0–0.80%). These results suggest that pigs and *C. tritaeniorhynchus* mosquitoes might play a role in transmitting highly pathogenic GETV to captive foxes in this region (Appendix Tables 5, 6).

In China, the disease caused by GETV has only been reported in pigs in Hunan Province, although the virus has been detected in mosquitoes in >10 provinces (*1,4*). Our study provides evidence that GETV can cause lethal infection in blue foxes. Investigation of transmission routes for GETV in animals might help to prevent outbreaks of GETV disease in China.

Acknowledgments

We thank Ningyi Jin and Quan Liu for their discussions and suggestions.

This work was supported by the National Key Research and Development Program of China (grant no. 2017YFD0500104), the National Natural Sciences Foundation of China (grant no. 31802199), and the Key Laboratory for Preventive Research of Emerging Animal Diseases in Foshan University (grant no. KLPREAD201801-07).

About the Author

Dr. Shi is a researcher at the School of Life Sciences and Engineering, Foshan University, Foshan, Guangdong Province, China. His research interests include emerging mosquitoborne infectious diseases.

References

1. Yang T, Li R, Hu Y, Yang L, Zhao D, Du L, et al. An outbreak of Getah virus infection among pigs in China, 2017. Transbound Emerg Dis. 2018;65:632–7. http://dx.doi.org/10.1111/tbed.12867
2. Yago K, Hagiwara S, Kawamura H, Narita M. A fatal case in newborn piglets with Getah virus infection: isolation of the virus. Nippon Juigaku Zasshi. 1987;49:989–94. http://dx.doi.org/10.1292/jvms1939.49.989
3. Nemoto M, Bannai H, Tsujimura K, Kobayashi M, Kikuchi T, Yamanaka T, et al. Getah virus infection among racehorses, Japan, 2014. Emerg Infect Dis. 2015;21:883–5. http://dx.doi.org/10.3201/eid2105.141975
4. Li Y, Fu S, Guo X, Li X, Li M, Wang L, et al. Serological survey of Getah virus in domestic animals in Yunnan Province, China. Vector Borne Zoonotic Dis. 2019;19:59–61. http://dx.doi.org/10.1089/vbz.2018.2273
5. Li XD, Qiu FX, Yang H, Rao YN, Calisher CH, Calisher CH. Isolation of Getah virus from mosquitos collected on Hainan Island, China, and results of a serosurvey. Southeast Asian J Trop Med Public Health. 1992;23:730–4.
6. Marchette NJ, Rudnick A, Garcia R. Alphaviruses in peninsular Malaysia: II. Serological evidence of human infection. Southeast Asian J Trop Med Public Health. 1980;11:14–23.
7. Shi N, Liu H, Li LX, Hu B, Zhang L, Zhao CF, et al. Development of a TaqMan probe-based quantitative reverse transcription PCR assay for detection of Getah virus RNA. Arch Virol. 2018;163:2877–81. http://dx.doi.org/10.1007/s00705-018-3927-2
8. Kuwata R, Shimoda H, Phichitraslip T, Prasertsincharoen N, Noguchi K, Yonemitsu K, et al. Getah virus epizootic among wild boars in Japan around 2012. Arch Virol. 2018;163:2817–21. http://dx.doi.org/10.1007/s00705-018-3897-4
9. Bannai H, Nemoto M, Niwa H, Murakami S, Tsujimura K, Yamanaka T, et al. Geospatial and temporal associations of Getah virus circulation among pigs and horses around the perimeter of outbreaks in Japanese racehorses in 2014 and 2015. BMC Vet Res. 2017;13:187. http://dx.doi.org/10.1186/s12917-017-1112-6
10. Li YY, Liu H, Fu SH, Li XL, Guo XF, Li MH, et al. From discovery to spread: the evolution and phylogeny of Getah virus. Infect Genet Evol. 2017;55:48–55. http://dx.doi.org/10.1016/j.meegid.2017.08.016

Address for correspondence: Hao Liu, Foshan University, School of Life Sciences and Engineering, 18 Jiangwan First Rd, Chancheng District, Foshan, Guangdong 528000, China; email: liuhao_lh@hotmail.com

Correction: Vol. 25, No. 5

The affiliation for Marie E. Killerby was listed incorrectly in Risk Factors for MERS-CoV Seropositivity among Animal Market and Slaughterhouse Workers, Abu Dhabi, United Arab Emirates, 2014–2017 (A. Khudhair et al.). Dr. Killerby is affiliated only with the Centers for Disease Control and Prevention (Atlanta, GA, USA). The article has been corrected online (https://wwwnc.cdc.gov/eid/article/25/5/18-1728_article).

Get the content you want delivered to your inbox.

- Table of Contents
- Podcasts
- Ahead of Print articles
- CME
- Specialized Content

Online subscription: wwwnc.cdc.gov/eid/subscribe/htm

Correction: Vol. 25, No. 3

Figures 2 and 4 were incomplete in Donor-Derived Genotype 4 Hepatitis E Virus Infection, Hong Kong, China, 2018 (S. Sridhar et al.). The corrected figures are reproduced here, and the article has been corrected online (https://wwwnc.cdc.gov/eid/article/25/3/18-1563_article).

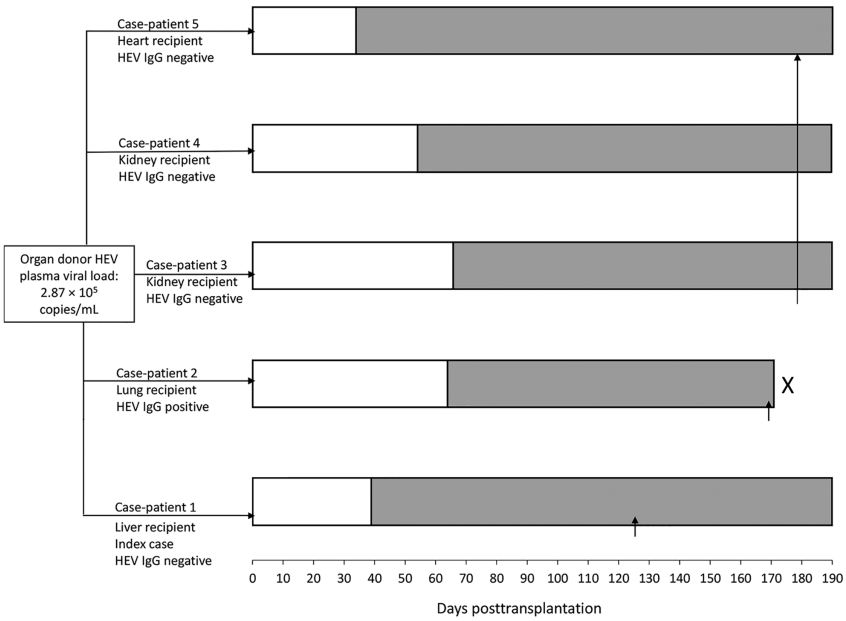

Figure 2. Timeline of outbreak in study of donor-derived genotype 4 HEV infection, Hong Kong, China, 2018, showing baseline HEV IgG status of each organ recipient. White bars indicate incubation period during which liver function test results were within reference range. Gray bars indicate timeline of alanine aminotransferase derangement after transplantation. X indicates patient death. Vertical arrows (↑) indicate time of hepatitis E diagnosis. HEV, hepatitis E virus.

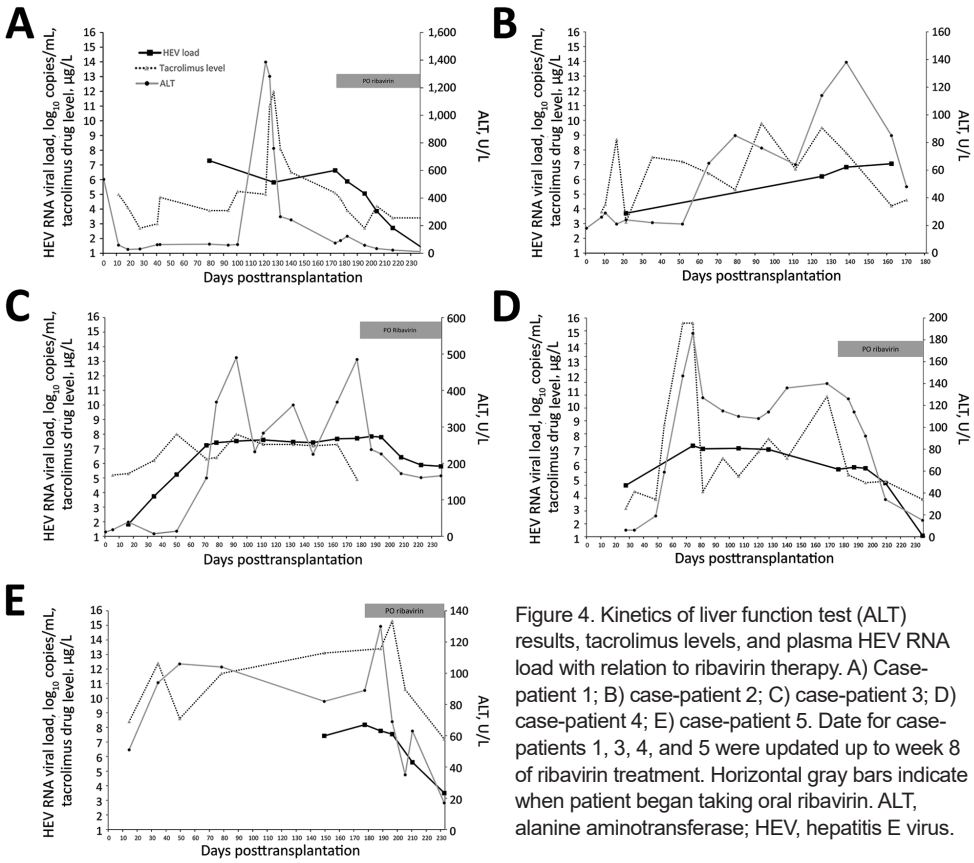

Figure 4. Kinetics of liver function test (ALT) results, tacrolimus levels, and plasma HEV RNA load with relation to ribavirin therapy. A) Case-patient 1; B) case-patient 2; C) case-patient 3; D) case-patient 4; E) case-patient 5. Date for case-patients 1, 3, 4, and 5 were updated up to week 8 of ribavirin treatment. Horizontal gray bars indicate when patient began taking oral ribavirin. ALT, alanine aminotransferase; HEV, hepatitis E virus.

Francisco de Goya y Lucientes (1746–1828). ***Don Manuel Osorio Manrique de Zuniga*** **(1784–1792)** (detail). Oil on canvas, 50 in x 40 in/127 cm x 101.6 cm. The Metropolitan Museum of Art, New York, NY, USA; The Jules Bache Collection, 1949 (49.7.41). Image copyright © The Metropolitan Museum of Art. Image source: Art Resource, NY.

The Red Boy, the Black Cat

Byron Breedlove

"Portraits of children accompanied by animals have a long tradition in Spanish painting," notes the Metropolitan Museum of Art. Francisco de Goya contributed to that tradition with his "Portrait of Manuel Osorio Manrique de Zuniga." But Goya also subverted tradition in this popular painting, commonly dubbed "The Red Boy," by instilling a sense of discomfort and darkness to what could have been a simple proclamation of youthful innocence.

Such tension appears in many of Goya's portraits. Art critic and historian Laura Cumming notes "That Francisco de Goya . . . was a portrait painter first to last is a truth often neglected," but she also observes a "strain of weirdness"

Author affiliation: Centers for Disease Control and Prevention, Atlanta, Georgia, USA

DOI: https://doi.org/10.3201/eid2506.AC2506

in his portraits. Whether one agrees fully with her assessment, Goya's art, which includes nearly 1,800 paintings, cartoons, murals, and etchings, defies convenient codification: he garners mentions as being among the last of the great masters and among the vanguard of modern artists.

Goya painted four portraits of members of the aristocratic Altamira family; of those, "The Red Boy" is the best known and most discussed. He completed those works nearly a decade before he suffered the debilitating, mysterious illness that caused headaches, vertigo, and delusions and is believed to have been triggered by his exposure to lead-based paints.

The Metropolitan Museum of Art Portraits offers this arm's length description of this portrait: "Outfitted in a splendid red costume, the young boy, the son of the Count and Countess of Altamira, is shown with a pet magpie (which holds the painter's calling card in its beak), a cage full of finches, and three wide-eyed cats. Although they add an engaging element for the viewer, Goya may have intended them as a reminder of the frail boundaries that separate the child's world from the forces of evil, or as a commentary on the fleeting nature of innocence and youth. Manuel died at the tender age of eight."

Manuel, resplendently dressed, dark eyes and hair, cuts a bold figure for one so young. He walks his magpie on a string while a trio of cats sizes up his pet, which grasps Goya's calling card in its tilted beak. To the boy's side, captive finches cluster near the bars of their green gazebo-like cage. Goya's juxtaposition of cats and birds and of shadow and light creates a sense of latent unease and interjects an atmosphere of fidgeting discomfiture into the portrait. The black cat cloaked in shadows, nearly invisible save for its eyes, amplifies the undercurrent of menace. (This cat is so deep in the shadows that some critical assessments and many reproductions overlook it.)

Essayist and critic Morgan Meis observes that Goya portrays a child who, because of his social standing, is not allowed to dress or play like a child. Meis notes "The boy is trapped in layers of refinement that he cannot possibly understand," and that "he knows nothing about court intrigues, just as he is unaware that the cats behind him are eagerly sizing up his pet bird."

Cumming echoes those sentiments. She writes "the 'Boy in Red' may be a much-loved treasure, but the moppet in his pool of light is surrounded by more nightmare critters in the shape of owl-eyed cats waiting to savage a magpie, while sharp-beaked finches chatter in the darkness."

Such elements of danger and tension in Goya's work find traction with modern viewers. The trio of cats, especially the spectral shadow cat, seem intent on menacing the tethered magpie and caged birds. Both felids and fowl could themselves be potential sources of zoonotic diseases or harbor zoonotic disease vectors.

More than 60% of known infectious diseases in people are spread from animals, and 75% of new or emerging infectious diseases in people are spread from animals. Among those who may be at greater risk of acquiring zoonotic infections are young children who may not have learned how to practice effective hygiene or who have close contacts with pets or domestic animals. Human infections associated with cats include rabies, cat-scratch disease, capnocytophagosis, pasteurellosis, ringworm, sporothrichosis, tularemia, plague, Q fever, campylobacterosis, salmonellosis, *Escherichia coli* infections, cryptosporidiosis, giardiasis, and toxoplasmosis. Influenza, psittacosis, and salmonellosis are among the diseases birds may transmit to humans.

The cause of young Manuel's death, if known, is not reported. Goya lived into his 80s and experienced a career that veered between triumph and torment. In the two centuries since Goya's death, our knowledge about infectious diseases etiology and treatment has coalesced into an impressive body of knowledge. Still, like the nearly invisible black cat in Goya's painting, some threats are harder than others to detect, and the need for constant vigilance remains a public health priority.

Bibliography

1. Centers for Disease Control and Prevention. One Health. Zoonotic diseases [cited 2019 Apr 15]. https://www.cdc.gov/onehealth/basics/zoonotic-diseases.html
2. Cumming L. Goya: the portraits review – the artist in an extraordinary new light [cited 2019 Apr 23]. https://www.theguardian.com/artanddesign/2015/oct/11/goya-the-portraits-review-national-gallery-astonishing-show-radical-truthfulness
3. Fuentes C. The buried mirror. Reflections on Spain and the New World. Boston: Houghton Mifflin Harcourt; 1999. p. 223–31.
4. Ives C, Stein SA. Goya in The Metropolitan Museum of Art [cited 2019 Apr 15]. http://resources.metmuseum.org/resources/metpublications/pdf/Goya_in_The_Metropolitan_Museum_of_Art.pdf
5. Meis M. Into the black [cited 2019 Apr 23]. https://thesmartset.com/article05211401
6. Metropolitan Museum of Art. Heilbrunn timeline of art history. Manuel Osorio Manrique de Zuñiga (1784–1792) [cited 2019 Apr 15]. https://www.metmuseum.org/toah/works-of-art/49.7.41
7. Metropolitan Museum of Art. Manuel Osorio Manrique de Zuñiga (1784–1792) [cited 2019 Apr 15]. https://www.metmuseum.org/art/collection/search/436545
8. Potter P. Francisco José de Goya y Lucientes (1746–1828). Cat fight (1786–1788). Emerg Infect Dis. 2003;9:1506–7. http://dx.doi.org/10.3201/eid0911.AC0911
9. Stull JW, Brophy J, Weese JS. Reducing the risk of pet-associated zoonotic infections. CMAJ. 2015;187:736–43. http://dx.doi.org/10.1503/cmaj.141020

Address for correspondence: Byron Breedlove, EID Journal, Centers for Disease Control and Prevention, 1600 Clifton Rd NE, Mailstop H16-2, Atlanta, GA 30329-4027, USA; email: wbb1@cdc.gov

EMERGING INFECTIOUS DISEASES®

Upcoming Issue

- Added Value of Comprehensive Program to Provide Universal Access to Care for Sputum Smear–Negative Drug-Resistant Tuberculosis, China
- *Bacillus cereus*–Attributable Primary Cutaneous Anthrax-Like Infection in Newborn Infants, India
- Essential Role of Interferon Response in Containing Human Pathogenic Bourbon Virus
- Environmental Hotspots for Azole Resistance Selection of *Aspergillus fumigatus*, the Netherlands
- High-Complexity *Plasmodium falciparum* Infection as a Result of Population Displacement in Northeastern Nigeria
- Asymptomatic Dengue Virus Infections, Cambodia, 2012–2013
- Hospital-Associated Multicenter Outbreak of Emerging Fungus *Candida auris*, Colombia, 2016
- Mitochondrial Junction Region as Genotyping Marker for *Cyclospora cayetanensis*
- Facility-Associated Release of Polioviruses into Communities: Risks for the Post-Eradication Era
- *Salmonella enterica* I 4,[5],12:i:- Associated with Lesions Typical of Swine Enteric Salmonellosis
- Dengue Outbreak during Ongoing Civil War, Taiz, Yemen
- Respiratory Syncytial Virus Infection in Homeless Population, Washington, USA
- Low Circulation of Subclade A1 Enterovirus D68 Strains in Senegal during 2014 North American Outbreak
- Diagnosis of Chagasic Encephalitis by Sequencing of 28S rRNA Gene
- Oropharyngeal Gonorrhea in Absence of Urogenital Gonorrhea in a Sex Network Including Men and Women, Australia, 2018
- Whole-Blood Testing for Diagnosis of Acute Zika Virus Infections in Routine Diagnostic Setting
- Microbiome and Antimicrobial Resistance Gene Dynamics in International Travelers
- Molecular Epidemiology of Human Parechovirus Type 3 Upsurge in 2 Hospitals, Freiburg, Germany, 2018
- Nontuberculous Mycobacteria, Botswana, 2011–2014

Complete list of articles in the July issue at http://www.cdc.gov/eid/upcoming.htm

Upcoming Infectious Disease Activities

June 20–24, 2019
ASM Microbe 2019
San Francisco, CA, USA
https://www.asm.org/index.php/asm-microbe-2018

June 23–28, 2019
Biology of Vector-borne Diseases Six-Day Training Course
Moscow, ID, USA
https://www.uidaho.edu/cals/center-for-health-in-the-human-ecosystem/education/vector-borne-diseases

July 14–17, 2019
STI and HIV 2019 World Congress
Vancouver, Canada
stihiv2019vancouver.com

July 20–24, 2019
American Society for Virology
Minneapolis, MN, USA
https://www.asv.org

July 21–24, 2019
International AIDS Society 2019
Mexico City, Mexico
https:// www.ias2019.org

August 12–23, 2019
16th International Course on Dengue, Zika and other Emergent Arboviruses
Havana, Cuba
http://instituciones.sld.cu/ipk/16th-international-course-on-dengue-zika-and-other-emergent-arboviruses/

August 28–September 1, 2019
OPTIONS X for the Control of Influenza
Suntec, Singapore
https://www.isirv.org/site/

November 20–24, 2019
American Society of Tropical Medicine and Hygiene
68th Annual Meeting
National Harbor, MD, USA
https://www.astmh.org/

Announcements

Email announcements to EIDEditor (eideditor@cdc.gov). Incl ude the event's date, location, sponsoring organization, and a website. Some events may appear only on EID's website, depending on their dates.

Earning CME Credit

To obtain credit, you should first read the journal article. After reading the article, you should be able to answer the following, related, multiple-choice questions. To complete the questions (with a minimum 75% passing score) and earn continuing medical education (CME) credit, please go to http://www.medscape.org/journal/eid. Credit cannot be obtained for tests completed on paper, although you may use the worksheet below to keep a record of your answers.

You must be a registered user on http://www.medscape.org. If you are not registered on http://www.medscape.org, please click on the "Register" link on the right hand side of the website.

Only one answer is correct for each question. Once you successfully answer all post-test questions, you will be able to view and/or print your certificate. For questions regarding this activity, contact the accredited provider, CME@medscape.net. For technical assistance, contact CME@medscape.net. American Medical Association's Physician's Recognition Award (AMA PRA) credits are accepted in the US as evidence of participation in CME activities. For further information on this award, please go to https://www.ama-assn.org. The AMA has determined that physicians not licensed in the US who participate in this CME activity are eligible for AMA PRA Category 1 Credits™. Through agreements that the AMA has made with agencies in some countries, AMA PRA credit may be acceptable as evidence of participation in CME activities. If you are not licensed in the US, please complete the questions online, print the AMA PRA CME credit certificate, and present it to your national medical association for review.

Article Title

Epidemiologic and Clinical Features of Lassa Fever Outbreak in Nigeria, January 1–May 6, 2018

CME Questions

1. You are advising a public health department in Africa regarding detection and management of an outbreak of Lassa fever (LF). According to the report by Ilori and colleagues, which of the following statements about epidemiological characteristics of the LF outbreak between January 1, 2018, and May 6, 2018 in Nigeria is correct?

A. Median age of cases was 32 years, and two-thirds of laboratory-confirmed cases were in women
B. ≈25% of laboratory-confirmed cases were in healthcare workers
C. 80.6% of confirmed cases were reported from 3 states: Edo, Ondo, and Ebonyi
D. Lassa virus is primarily transmitted to humans through contact with body fluids of infected persons

2. According to the report by Ilori and colleagues, which of the following statements about clinical characteristics and mortality in the LF outbreak between January 1, 2018, and May 6, 2018 in Nigeria is correct?

A. Hemorrhaging occurred in more than half of laboratory-confirmed cases
B. Gastrointestinal symptoms, including vomiting, abdominal pain, and anorexia, occurred in >30% of laboratory-confirmed cases
C. The case fatality rate (CFR) among laboratory-confirmed cases was 12.2%
D. The highest CFR occurred in children age <10 years

3. According to the report by Ilori and colleagues, which of the following statements about factors associated with mortality in the LF outbreak between January 1, 2018, and May 6, 2018 in Nigeria is correct?

A. Fatal cases were significantly more likely than survivors to have cough ($p = 0.005$), hemorrhaging ($p<0.001$), and unconsciousness ($p = 0.0018$)
B. Delay in visiting a health facility was a statistically significant predictor for death
C. CFR was 30% in patients treated with ribavirin and 45% in patients who did not receive ribavirin
D. The findings do not support national guidelines for clinical management of LF

Earning CME Credit

To obtain credit, you should first read the journal article. After reading the article, you should be able to answer the following, related, multiple-choice questions. To complete the questions (with a minimum 75% passing score) and earn continuing medical education (CME) credit, please go to http://www.medscape.org/journal/eid. Credit cannot be obtained for tests completed on paper, although you may use the worksheet below to keep a record of your answers.

You must be a registered user on http://www.medscape.org. If you are not registered on http://www.medscape.org, please click on the "Register" link on the right hand side of the website.

Only one answer is correct for each question. Once you successfully answer all post-test questions, you will be able to view and/or print your certificate. For questions regarding this activity, contact the accredited provider, CME@medscape.net. For technical assistance, contact CME@medscape.net. American Medical Association's Physician's Recognition Award (AMA PRA) credits are accepted in the US as evidence of participation in CME activities. For further information on this award, please go to https://www.ama-assn.org. The AMA has determined that physicians not licensed in the US who participate in this CME activity are eligible for AMA PRA Category 1 Credits™. Through agreements that the AMA has made with agencies in some countries, AMA PRA credit may be acceptable as evidence of participation in CME activities. If you are not licensed in the US, please complete the questions online, print the AMA PRA CME credit certificate, and present it to your national medical association for review.

Article Title

Nontuberculous Mycobacterial Musculoskeletal Infection Cases from a Tertiary Referral Center, Colorado, USA

CME Questions

1. Your patient is a 47-year-old man with a prosthetic knee joint and suspected nontuberculous (NTM) musculoskeletal (MSK) prosthetic joint infection (PJI). According to the case series of 14 patients treated at the University of Colorado Hospital (UCH) over a 6-year period by Goldstein and colleagues, which of the following statements about clinical characteristics of patients with NTM nonspinal MSK infection is correct?

A. Two patients were immunosuppressed at presentation
B. All 14 patients developed NTM infections at the site of a prior invasive procedure, including 10 at the site of a previous MSK surgery, with 6 of these involving joint prostheses (4 knee, 2 hip)
C. In most of the surgery-associated cases, symptom onset was ≤1 month after the preceding surgical procedure
D. Ten patients had elevated white blood cell count at presentation

2. According to the case series of 14 patients treated at UCH over a 6-year period by Goldstein and colleagues, which of the following statements about medical and surgical management of patients with NTM nonspinal MSK infections is correct?

A. Most patients did not need multiple or prolonged antibiotics
B. Antibiotic therapy was well tolerated without adverse effects or need for discontinuation
C. Most patients required only a single, localized surgical procedure
D. All patients with PJI had removal of infected hardware and 2-stage revision with a temporary articulating prosthesis and antibiotic spacer, later replaced with a permanent prosthesis

3. According to the case series of 14 patients treated at UCH over a 6-year period by Goldstein and colleagues, which of the following statements about microbiological and histopathological findings and treatment outcomes of patients with NTM nonspinal MSK infections would be correct?

A. NTM species causing MSK infection was identified in each patient; 7 were rapidly growing and 7 slowly growing
B. Most patients with granuloma formation on intraoperative biopsy specimens had direct microscopy evidence of acid fast bacillus
C. 9 of 14 patients were cured without clinical or microbiological relapse during postoperative follow-up
D. Mycobacterium marinum was the responsible pathogen in cases requiring amputation

EMERGING INFECTIOUS DISEASES®

EDITOR-IN-CHIEF
D. Peter Drotman

ASSOCIATE EDITORS
Paul Arguin, Atlanta, Georgia, USA
Charles Ben Beard, Fort Collins, Colorado, USA
Ermias Belay, Atlanta, Georgia, USA
David Bell, Atlanta, Georgia, USA
Sharon Bloom, Atlanta, Georgia, USA
Richard Bradbury, Atlanta, Georgia, USA
Mary Brandt, Atlanta, Georgia, USA
Corrie Brown, Athens, Georgia, USA
Charles Calisher, Fort Collins, Colorado, USA
Benjamin J. Cowling, Hong Kong, China
Michel Drancourt, Marseille, France
Paul V. Effler, Perth, Australia
Anthony Fiore, Atlanta, Georgia, USA
David Freedman, Birmingham, Alabama, USA
Peter Gerner-Smidt, Atlanta, Georgia, USA
Stephen Hadler, Atlanta, Georgia, USA
Matthew Kuehnert, Edison, New Jersey, USA
Nina Marano, Atlanta, Georgia, USA
Martin I. Meltzer, Atlanta, Georgia, USA
David Morens, Bethesda, Maryland, USA
J. Glenn Morris, Gainesville, Florida, USA
Patrice Nordmann, Fribourg, Switzerland
Johann D.D. Pitout, Calgary, Alberta, Canada
Ann Powers, Fort Collins, Colorado, USA
Didier Raoult, Marseille, France
Pierre Rollin, Atlanta, Georgia, USA
Frank Sorvillo, Los Angeles, California, USA
David Walker, Galveston, Texas, USA
J. Todd Weber, Atlanta, Georgia, USA
Jeffrey Scott Weese, Guelph, Ontario, Canada

Managing Editor
Byron Breedlove, Atlanta, Georgia, USA

Copy Editors Kristina Clark, Dana Dolan, Karen Foster, Thomas Gryczan, Amy Guinn, Michelle Moran, Shannon O'Connor, Jude Rutledge, P. Lynne Stockton, Deborah Wenger

Production Thomas Eheman, William Hale, Barbara Segal, Reginald Tucker

Journal Administrator Susan Richardson

Editorial Assistants Kelly Crosby, Kristine Phillips

Communications/Social Media Sarah Logan Gregory, Tony Pearson-Clarke

Founding Editor
Joseph E. McDade, Rome, Georgia, USA

EDITORIAL BOARD
Timothy Barrett, Atlanta, Georgia, USA
Barry J. Beaty, Ft. Collins, Colorado, USA
Martin J. Blaser, New York, New York, USA
Christopher Braden, Atlanta, Georgia, USA
Arturo Casadevall, New York, New York, USA
Kenneth C. Castro, Atlanta, Georgia, USA
Vincent Deubel, Shanghai, China
Christian Drosten, Charité Berlin, Germany
Isaac Chun-Hai Fung, Statesboro, Georgia, USA
Kathleen Gensheimer, Silver Spring, Maryland, USA
Rachel Gorwitz, Atlanta, Georgia, USA
Duane J. Gubler, Singapore
Richard L. Guerrant, Charlottesville, Virginia, USA
Scott Halstead, Arlington, Virginia, USA
David L. Heymann, London, UK
Keith Klugman, Seattle, Washington, USA
Takeshi Kurata, Tokyo, Japan
S.K. Lam, Kuala Lumpur, Malaysia
Stuart Levy, Boston, Massachusetts, USA
John S. Mackenzie, Perth, Australia
John E. McGowan, Jr, Atlanta, Georgia, USA
Jennifer H. McQuiston, Atlanta, Georgia, USA
Tom Marrie, Halifax, Novia Scotia, Canada
Nkuchia M. M'ikanatha, Harrisburg, Pennsylvania, USA
Frederick A. Murphy, Bethesda, Maryland, USA
Barbara E. Murray, Houston, Texas, USA
Stephen M. Ostroff, Silver Spring, Maryland, USA
Ann Powers, Fort Collins, Colorado, USA
Mario Raviglione, Prévessin-Möens, France
David Relman, Palo Alto, California, USA
Guenael R. Rodier, Saône-et-Loire, France
Connie Schmaljohn, Frederick, Maryland, USA
Tom Schwan, Hamilton, Montana, USA
David Swayne, Athens, Georgia, USA
Rosemary Soave, New York, New York, USA
P. Frederick Sparling, Chapel Hill, North Carolina, USA
Robert Swanepoel, Pretoria, South Africa
David E. Swayne, Athens, Georgia, USA
Phillip Tarr, St. Louis, Missouri, USA
Duc Vugia, Richmond, California, USA
John W. Ward, Atlanta, Georgia, USA
Mary E. Wilson, Cambridge, Massachusetts, USA

Emerging Infectious Diseases is published monthly by the Centers for Disease Control and Prevention, 1600 Clifton Rd NE, Mailstop H16-2, Atlanta, GA 30329-4027, USA. Telephone 404-639-1960, fax 404-639-1954, email eideditor@cdc.gov.

The conclusions, findings, and opinions expressed by authors contributing to this journal do not necessarily reflect the official position of the U.S. Department of Health and Human Services, the Public Health Service, the Centers for Disease Control and Prevention, or the authors' affiliated institutions. Use of trade names is for identification only and does not imply endorsement by any of the groups named above.

All material published in Emerging Infectious Diseases is in the public domain and may be used and reprinted without special permission; proper citation, however, is required.

Use of trade names is for identification only and does not imply endorsement by the Public Health Service or by the U.S. Department of Health and Human Services.

EMERGING INFECTIOUS DISEASES is a registered service mark of the U.S. Department of Health & Human Services (HHS).

∞ Emerging Infectious Diseases is printed on acid-free paper that meets the requirements of ANSI/NISO 239.48-1992 (Permanence of Paper)

In This Issue

Perspectives

Using Big Data to Monitor the Introduction and Spread of Chikungunya, Europe 1041
West Nile and Usutu Virus Infections and Challenges to Blood Safety in the European Union 1050

Synopses

Immunopathology of Fatal Human Variegated Squirrel Bornavirus 1 Encephalitis, Germany, 2011–2013 1058
Epidemiologic and Clinical Features of Lassa Fever Outbreak in Nigeria, January–May 2018 1066
Nontuberculous Mycobacterial Musculoskeletal Infection Cases from a Tertiary Referral Center, Colorado, USA 1075

Research

Phenotypic and Genomic Analyses of *Burkholderia stabilis* Clinical Contamination, Switzerland 1084
Patterns of Abundance, Host Use, and Everglades Virus Infection in *Culex* (*Melanoconion*) *cedecei* Mosquitoes, Florida, USA 1093
Assessment of Economic Burden of Concurrent Measles and Rubella Outbreaks, Romania, 2011–2012 1101
Novel Orthobunyavirus Causing Severe Kidney Disease in Broiler Chickens, Malaysia, 2014–2017 1110
Joint Estimation of Relative Risk for Dengue and Zika Virus Infections, Colombia, 2015–2016 1118
Respiratory Syncytial Virus Seasonality, Beijing, China, 2007–2015 1127
Enhancement of Risk for Lyme Disease by Landscape Connectivity, New York, New York, USA 1136
Use of Single-Injection Recombinant Vesicular Stomatitis Virus Vaccine to Protect Nonhuman Primates Against Lethal Nipah Virus Disease 1144
Performance of 2 Commercial Serologic Tests for Diagnosis of Zika Virus Infection 1153
Sequential Emergence and Wide Spread of Neutralization Escape Middle East Respiratory Syndrome Coronavirus Mutants, South Korea, 2015 1161
Mass Die-Off of Saiga Antelopes, Kazakhstan, 2015 1169
Survey of Crimean-Congo Hemorrhagic Fever Enzootic Focus, Spain, 2011–2015 1177

Historical Review

Equine Influenza Virus—A Neglected, Reemergent Disease 1185

Dispatches

Outbreak of Vaccinia Virus Infection from Occupational Exposure, China, 2017 1192
Pertactin-Negative and Filamentous Hemagglutinin-Negative *Bordetella pertussis*, Australia, 2013–2017 1196
Increase in Enterovirus D68 Infections in Young Children, 2006–2016 1200
Multirecombinant Enterovirus A71 Subgenogroup C1 Isolates Associated with Neurologic Disease, France, 2016–2017 1204
New Delhi Metallo-β-Lactamase 5–Producing *Klebsiella pneumoniae* Sequence Type 258, Southwest China, 2017 1209
Scrub Typhus in Continental Chile, 2016–2018 1214

ISSN 1080-6040

DEPARTMENT OF HEALTH & HUMAN SERVICES
Public Health Service
Centers for Disease Control and Prevention (CDC)
Mailstop D61, Atlanta, GA 30329-4027

Official Business
Penalty for Private Use $300
Return Service Requested

MEDIA MAIL
POSTAGE & FEES PAID
PHS/CDC
Permit No. G 284